NASA/TM–2012-217577

Effect of Sweep on Cavity Flow Fields at Subsonic and Transonic Speeds

Maureen B. Tracy, Elizabeth B. Plentovich, Michael J. Hemsch, and Floyd J. Wilcox, Jr.
Langley Research Center, Hampton, Virginia

May 2012

NASA STI Program . . . in Profile

Since its founding, NASA has been dedicated to the advancement of aeronautics and space science. The NASA scientific and technical information (STI) program plays a key part in helping NASA maintain this important role.

The NASA STI program operates under the auspices of the Agency Chief Information Officer. It collects, organizes, provides for archiving, and disseminates NASA's STI. The NASA STI program provides access to the NASA Aeronautics and Space Database and its public interface, the NASA Technical Report Server, thus providing one of the largest collections of aeronautical and space science STI in the world. Results are published in both non-NASA channels and by NASA in the NASA STI Report Series, which includes the following report types:

- TECHNICAL PUBLICATION. Reports of completed research or a major significant phase of research that present the results of NASA programs and include extensive data or theoretical analysis. Includes compilations of significant scientific and technical data and information deemed to be of continuing reference value. NASA counterpart of peer-reviewed formal professional papers, but having less stringent limitations on manuscript length and extent of graphic presentations.

- TECHNICAL MEMORANDUM. Scientific and technical findings that are preliminary or of specialized interest, e.g., quick release reports, working papers, and bibliographies that contain minimal annotation. Does not contain extensive analysis.

- CONTRACTOR REPORT. Scientific and technical findings by NASA-sponsored contractors and grantees.

- CONFERENCE PUBLICATION. Collected papers from scientific and technical conferences, symposia, seminars, or other meetings sponsored or co-sponsored by NASA.

- SPECIAL PUBLICATION. Scientific, technical, or historical information from NASA programs, projects, and missions, often concerned with subjects having substantial public interest.

- TECHNICAL TRANSLATION. English-language translations of foreign scientific and technical material pertinent to NASA's mission.

Specialized services also include creating custom thesauri, building customized databases, and organizing and publishing research results.

For more information about the NASA STI program, see the following:

- Access the NASA STI program home page at *http://www.sti.nasa.gov*

- E-mail your question via the Internet to help@sti.nasa.gov

- Fax your question to the NASA STI Help Desk at 443-757-5803

- Phone the NASA STI Help Desk at 443-757-5802

- Write to:
  NASA STI Help Desk
  NASA Center for AeroSpace Information
  7115 Standard Drive
  Hanover, MD 21076-1320

NASA/TM–2012-217577

Effect of Sweep on Cavity Flow Fields at Subsonic and Transonic Speeds

Maureen B. Tracy, Elizabeth B. Plentovich, Michael J. Hemsch, and Floyd J. Wilcox, Jr.
Langley Research Center, Hampton, Virginia

National Aeronautics and
Space Administration

Langley Research Center
Hampton, Virginia 23681-2199

May 2012

Available from:

NASA Center for AeroSpace Information
7115 Standard Drive
Hanover, MD 21076-1320
443-757-5802

Preface

The initial draft of this paper was written in the early 1990s and was based upon wind tunnel tests, which were a part of a cavity flow research program. However, work reassignments of the authors prevented the timely publication of the paper. Because of the unique cavity configurations that were tested, the authors believe it is important to belatedly publish these data, although data analysis in the paper is limited.

In the time since this paper was drafted, researchers have continued to study cavity flows. Progress has been made experimentally, computationally and theoretically. Some recent results are reported in References 1–12. Of particular relevance to this paper, Lada and Kontis [2] report success in improving pressure gradients in closed cavity flows using leading edge and trailing edge swept inserts separately.

Table of Contents

List of Figures

List of Tables

Nomenclature

Acronyms

Config	Configuration number
AOA	Angle-of-attack, degrees
dB	Decibel
ESP	Electronically-Scanned Pressure
FPL	Fluctuating Pressure Level (root-mean-square of measured fluctuating-pressure normalized with respect to q_∞), dB
HST	High Speed Tunnel
NASA	National Aeronautics and Space Administration
SPL	Sound Pressure Level (root-mean-square of measured fluctuating-pressure normalized with respect to 2.9×10^{-9} psia), dB

Symbols

C_p	Pressure coefficient, $C_p = (p - p_\infty)/q_\infty$
f	Frequency of observed mode, Hz
f_m	Frequency of Rossiter mode, Hz
h	Cavity depth, inches
l	Cavity length, inches (measured in free-stream direction)
k	Empirical parameter, ratio of shear layer and free-stream velocities, a function of M
m	Rossiter mode number
M_∞	Free-stream Mach number
p	Measured surface static-pressure, psia
p'	Measured fluctuating-pressure, psid
p_∞	Free-stream static pressure, psia
$p_{t\infty}$	Free-stream total pressure, psia
q_∞	Free-stream dynamic pressure, psia
Re_∞	Free-stream unit Reynolds number, per foot
$T_{t\infty}$	Free-stream total temperature, K
U_∞	Free-stream velocity, fps
w	Cavity width, inches (see Figure 10)
x	Distance in streamwise direction, inches (see Figure 7)
x_{max}	Maximum length from leading edge of flat plate to leading edge of swept cavity, inches (see Figure 10)
x_{min}	Minimum length from leading edge of flat plate to leading edge of swept cavity, inches (see Figure 10)
x_p	Distance from flat plate leading edge to cavity leading edge, inches (see Figure 10)
y	Distance in spanwise direction, inches (see Figures 4 and 7)
y'	Distance in spanwise direction for the port side wall, used for estimation of δ_{ave}, inches (see Figure 10)
z	Distance normal to the flat plate, inches (see Figure 4)
α	Empirical parameter related to phase between instabilities in the shear layer and upstream traveling pressure waves, a function of l/h

β	$\sqrt{1 - M_\infty^2}$
δ	Calculated boundary layer thickness at cavity leading edge, inches
δ_{ave}	Averaged calculated boundary layer thickness across cavity leading edge, inches
δ_{max}	Maximum calculated boundary layer thickness at cavity leading edge, inches
γ	Ratio of specific heats
ψ	Sweep angle, degree (see Figures 6 and 10)

Summary

An experimental investigation was conducted in the 7 × 10-Foot High Speed Tunnel (HST) at the National Aeronautics and Space Administration (NASA) Langley Research Center to study the effect of leading- and trailing-edge sweep on cavity flow fields for a range of cavity length-to-depth (l/h) ratios. The study included two experiments designed to characterize the flow fields in rectangular and swept cavities, respectively. The free-stream Mach number (M_∞) range was from 0.2 to 0.8. The unit Reynolds number (Re_∞) varied between 1×10^6 and 4×10^6 per foot and the boundary layer approaching the cavity was turbulent with an estimated thickness of 0.25 inches. The cavity had a depth of 0.5 inches, a width of 2.5 inches, and a maximum length of 12.0 inches. The same model was used in both experiments. The leading- and trailing-edge sweep was adjusted using block inserts to achieve leading edge sweep angles of 65°, 55°, 45°, and 35°. (The fore and aft walls were always parallel.) The aft wall of the cavity was remotely positioned to achieve a range of length-to-depth ratios. (The maximum l/h depended on sweep angle.) Fluctuating- and static-pressure data were obtained on the floor of the cavity. The fluctuating pressure data were used to determine whether or not resonance occurred in the cavity rather than to provide a characterization of the fluctuating pressure field. Qualitative surface flow visualization was obtained using a technique in which colored water was introduced into the model through static-pressure orifices. A complete tabulation of the mean static-pressure data for the swept leading edge cavities is included.

Results for cavities with sweep angles of 35° and 45° showed that static pressures did not vary with lateral position and in general sustained pressure distributions similar to those observed in rectangular cavities. However, for cavities with sweep angles of 55° and 65°, static pressure varied with lateral position and a new type of pressure distribution was observed along the centerline in the streamwise direction. Sweep appeared to have a strong effect on the static-pressure gradients in the vicinity of reattachment of the shear layer and near the cavity aft wall. While no clear relationship appeared between sweep angle and the changes in the reattachment pressure gradient, the static-pressure approaching the aft wall decreased monotonically with increasing sweep. The effect of varying l/h and M_∞ in swept cavities was generally similar to those observed for rectangular cavities.

Fluctuating-pressure results indicate that rectangular cavities for which open and transitional flow existed supported resonances of the type described by a modified Rossiter equation. Although spectral peaks were apparent in some swept cavity data, they did not indicate a longitudinal Rossiter-type cavity resonance.

Flow-visualization results were consistent with the static-pressure data when a known flow field type was indicated. Furthermore, flow visualization for the swept cavities indicated the flow characteristics that follow. (Note that the port side of the cavity was always farther upstream.):

1) inflow on the port side and outflow on the starboard side;
2) a turning of incoming flow to approach a perpendicular with the swept leading edge of the cavity (more pronounced for higher M_∞);
3) a vortex appearing along the leading edge which appears to remain confined forward of the reattachment line;
4) a similar vortex along the starboard side for cavities with sweep angles of 65° and 55°; and
5) a third vortex along the aft wall for closed flow conditions.

Introduction

Carrying weapons internally has aerodynamic advantages in flight. Cavities in aerodynamic surfaces, however, can generate both steady and unsteady disturbances in otherwise uniform flow. Many investigations, both experimental (References 13−46) and computational (References 47−56) have been conducted to study the flow fields in rectangular cavities. Changes in the cavity flow field can result in large pressure gradients and in unsteady flows which can generate self-sustaining oscillations which, in turn, generate acoustic tones that radiate from the cavity. Both the steady and the unsteady flows can present difficulties for store separation from an internal weapons bay. The former can generate large nose-in pitching moments and the latter can induce structural vibration. To insure safe separation, it is necessary to devise methods to alleviate these problems. One simple approach is to modify the geometry of the rectangular cavity typically used.

The objective of the study described herein was to determine the effect of leading- and trailing-edge sweep on cavity flows for a range of *l/h* values. Two experiments were conducted in the 7×10-foot HST at free-stream Mach numbers (M_∞) of 0.2, 0.4, 0.6, and 0.8. The unit Re_∞ varied between 1×10^6 and 4×10^6 per foot and the boundary layer approaching the cavity was turbulent with an estimated thickness of 0.25 inches. The cavity had a depth of 0.5 inches, a width of 2.5 inches and a maximum length that depended on sweep angle. (The maximum length of the rectangular cavity was 12.0 inches) The first experiment was designed to study rectangular cavities and the second, swept cavities. The leading- and trailing-edge sweep angle was adjusted using block inserts to achieve sweep angles of 65°, 55°, 45°, and 35°. The aft wall of the cavity was remotely positioned to achieve a range of length-to-depth ratios. Fluctuating- and static-pressure levels within the cavity and colored-water flow visualization on the model surface were obtained.

Background

Flow field types for transonic speeds have been identified based on a detailed evaluation of static-pressure measurements [17] which reference established flow field types for cavities in supersonic flows [14, 36–38, 46]. The flow field types identified for supersonic speeds are defined below and are used for reference because off-surface flow visualization and extensive computational studies are available for validation. A description of the flow field types identified for subsonic and transonic flows will also be provided in a subsequent section.

Cavity Flow Field Types for Supersonic Speeds

The first cavity flow field type identified for supersonic speeds generally occurs when the cavity is 'deep' (with a small value of *l/h*), as is typical of bomber aircraft bays, and is termed *open* cavity flow (Figure 1). Open flow occurs in cavities with *l/h* values ≲10. For this regime, the flow essentially bridges the cavity and a shear layer is formed over the cavity. This produces a nearly uniform static-pressure distribution along the floor of the cavity which is desirable for safe store separation. However, when open-cavity flow occurs, a cavity resonance can be sustained. The mechanism that produces this resonance is understood to be the reinforcement between instabilities in the shear layer and upstream-traveling pressure waves generated at the aft wall by the time-varying impingement of the shear layer. These oscillations can generate high-intensity acoustic tones that can induce vibrations in the surrounding structure, including the separating store, and lead to structural fatigue [45, 57]. The frequencies at which these tones occur can be predicted using a semi-empirical equation known as the modified Rossiter Equation [24].

$$f_m \frac{l}{U_\infty} = \frac{m-\alpha}{M_\infty\left[1+\left(\frac{\gamma-1}{2}\right)M_\infty^2\right]^{-1/2} + \frac{1}{k}}$$

Here, f_m is the frequency of a given acoustic mode, l the cavity length, U_∞ the free-stream velocity, m the mode number, M_∞ the free-stream Mach number, and γ the ratio of specific heats. There are two empirical constants in the equation; α which is a function of l/h and is related to the phase between the instabilities in the shear layer and the upstream traveling pressure waves; and k which is a function of M_∞ and is understood to be the relative speed of the instabilities in the shear layer to free-stream velocity. The modification [24] of the Rossiter Equation [22], equates the cavity sound speed to the stagnation sound speed to accommodate high-speed flows.

The second type of cavity flow identified for supersonic speeds occurs for ‘shallow’ cavities (with large values of l/h), as is typical of missile bays on fighter aircraft, and is termed *closed*-cavity flow (Figure 1). Closed flow occurs for cavities with l/h values $\gtrsim$13. In this regime, the flow separates at the forward face of the cavity, reattaches at some point along the cavity floor and separates again before reaching the rear cavity face. This produces a mean static-pressure distribution with low pressure in the forward region, a plateau in the attached region and high pressure in the aft region. Impingement and exit shocks are observed. In closed-cavity flow the flow entering the cavity and impinging on the cavity floor can cause the separating store to experience large pitching moments that turn the store nose into the cavity. Acoustic tones do not occur for closed-cavity flow at supersonic speeds because there is no free shear layer traversing the cavity and supersonic flow in the cavity prevents pressure waves from traveling upstream.

The third and fourth cavity flow field types defined for supersonic speeds are termed *transitional* (*transitional-open* and *transitional-closed*) and are flow fields that occur for cavities that have values of l/h that fall between closed- and open-cavity flow, i.e., values of l/h between approximately 10 and 13. Transitional-closed cavity flow (Figure 1) occurs when l/h is decreased from a value corresponding to closed-cavity flow. The change in flow field type is signaled by the collapse of the impingement and exit shocks into a single shock and the disappearance of the plateau in the mean static-pressure distribution. The shock signifies that the flow has impinged on the floor. Similar to closed-cavity flow, large static-pressure gradients occur along the cavity floor and can contribute to large pitching moments that turn the store nose into the cavity. With a very small reduction in l/h from the value corresponding to the transitional-closed cavity flow, the impingement-exit shock wave abruptly changes to a series of compression wavelets, indicating that although the shear layer no longer impinges on the cavity floor, it does turn into the cavity. This type of flow is referred to as transitional-open cavity flow (Figure 1). For this type of flow field, longitudinal pressure gradients in the cavity are not as large as for transitional-closed cavity flow, and consequently, the problem of store nose-in pitching moment is not as severe as for closed-cavity flows. The acoustic fields for the transitional-closed and transitional-open flow fields have not been determined.

Cavity Flow Field Types for Subsonic/Transonic Speeds

Figure 2 gives the characteristic static-pressure distributions for the various flow field types defined for subsonic and transonic speeds. As with supersonic flow, open- and closed-cavity flows occur. For the range of l/h between those for open and closed flow, there is a gradual change from open to closed flow and thus a single transitional type flow is defined (rather than transitional-open and transitional-closed as for supersonic flow). In this regime, the flow turns into the cavity and may or may not impinge on the cavity floor before turning out and exiting. At transonic speeds, flows with static-pressure distributions similar to the supersonic transitional-open and transitional-closed bound the transitional flow regime as indicated in Figure 2. The characteristics of the static-pressure distributions used to define the flow types in Reference 13 are summarized and given below.

Open-cavity flow has a uniform pressure distribution ($C_p \cong 0$) for values of streamwise distance-to-length (x/l) up to approximately 0.6. Aft of that point, the pressure distribution increases with increasing x/l and has a concave up shape. Open-cavity flow at subsonic and transonic speeds can sustain a cavity resonance, as discussed in the previous section, Cavity Flow Field Types For Supersonic Speeds. For subsonic and transonic speeds the acoustic frequencies are estimated from the modified Rossiter equation using $\alpha \cong 0.25$ and $k \cong 0.57$, (values were obtained by Rossiter [22] for a range of conditions).

The change from open- to transitional-cavity flow (as l/h increases) is identified by a change in pressure distribution from concave up to concave down in the aft portion of the cavity. (This distribution is similar to that for supersonic transitional-open flow.) The concave down pressure distribution for $x/l \gtrsim 0.6$ is typical of transitional-cavity flow for transonic speeds. As l/h increases, the distribution gradually changes to one marked by a uniform increase from negative values near the front face to large positive values near the aft face (similar to the supersonic transitional-closed distribution). The flow becomes closed (with increasing l/h) when an inflection point occurs in the pressure distribution at $x/l \cong 0.5$. With further increase in l/h, the inflection point becomes a plateau (a distribution typical of closed-cavity flow observed at supersonic speeds). With still further increase in l/h, a dip in pressure develops aft of the region of level pressure and forward of the aft pressure rise. The maximum value of the closed pressure distribution remains approximately the same as that observed at the boundary with transitional flow. Again, it is noted that the boundaries between the flow types are approximate, limited by the spacing between measurement locations and the increments by which l/h was changed.

The occurrence of the various flow field types was found to depend on M_∞, cavity l/h and also cavity width-to-depth ratio (w/h). A sketch from Reference 13 showing this dependence is provided as Figure 3. The flow field types that occurred for each combination of M_∞ and l/h are indicated for four configurations each with different w/h values. Boundaries have been drawn delimiting the flow field types for each configuration. At transonic speeds, as seen in Figure 3, open flow occurs in cavities with l/h values up to a maximum value between 6 and 8 and closed flow occurs for cavities with l/h values down to a minimum value between 9 and 15. Consequently, transitional-cavity flow can occur for a range of l/h values as narrow as 1 ($w/h = 1$ and $M_\infty = 0.2$) and as broad as 7 ($w/h = 8$ and $M_\infty = 0.95$). The effect of these flow fields on the store carriage and separation characteristics is similar to that observed at supersonic speeds for like pressure distributions [39].

Experimental Method

Model Description

The model was originally designed and fabricated to study cavity flow fields at supersonic speeds [14]. Sketches and a photograph of the cavity model assembly are shown in Figure 4. The model consisted of a sting-mounted splitter plate 41.9 inches long and 34.0 inches wide that housed a cavity with a forward face being located 10.4 inches downstream of the flat-plate leading edge. Because the model was designed for supersonic speeds, the outboard leading edges were swept 30° to decrease the plate planform area and thus decrease the supersonic tunnel starting loads on the support sting. In addition, the outboard leading edge sweep positioned supersonic tip vortices downstream as far as possible to minimize their effect on the flat plate flow field. The impact of the supersonic model design on the flat plate at subsonic and transonic speeds is discussed in the Wind Tunnel and Test Conditions section. The effect on a rectangular cavity at subsonic and transonic speeds is addressed in the Discussion of Results section.

The rectangular cavity was constructed with slightly rounded forward corners (0.16-inch radius) to facilitate fabrication of the cavity box. In order to facilitate computational modeling of the cavity the forward cavity corners were squared using a small rectangular block mounted on the forward wall of the cavity as seen in Figure 5. The cavity had a width of 2.50 inches and a depth of 0.50 inches. Cavity length was remotely controlled with a sliding-block assembly that formed the rear face of the cavity (see Figure 4(a)). Cavity width and depth were fixed with $w/h = 5$ for all cavity configurations. The rectangular cavity had a maximum length of 12 inches and could be fully closed. A flat plate configuration could also be tested by positioning the cavity floor flush with the flat plate with the aft wall fully retracted.

As the sliding block moved forward, the space where the sliding-block drive screw was located was uncovered creating a second cavity downstream of the test cavity. At supersonic speeds, the second cavity was not a concern because disturbances do not feed forward; however, this was a concern for testing at subsonic and transonic speeds. To eliminate the cavity, a thin plate was mounted over the space that housed the drive screw for the sliding-block assembly. This plate can be seen in Figure 4.

Four sets of blocks were used to create sweep angles (ψ) of 65°, 55°, 45°, and 35°, configurations 1 through 4 respectively as shown in Figure 6. Blocks were placed in the forward and rearward sections of the cavity to create parallel leading- and trailing-edge swept surfaces with the sweep initiating on the port side of the cavity and the starboard side being downstream. (The insert used to square the rectangular cavity was removed for the swept geometries.) The rear block was attached to the aft wall of the cavity to allow the cavity length to be remotely controlled. An o-ring was placed between the blocks and the cavity floor and side walls to minimize flow under the blocks. The maximum lengths for the swept cavities were 6.64 inches, 8.43 inches, 9.5 inches, and 10.25 inches for ψ = 65°, 55°, 45°, and 35°, respectively.

The leading-edge block changed the position of the cavity leading edge relative to the plate leading edge, resulting in a change in the *x*-coordinate origin position for each swept leading edge cavity. The effect this had on the boundary-layer thickness approaching the cavity is described in the Wind Tunnel and Test Conditions section of this report. Cavity x/l was measured from the trailing edge of the forward block. (Since the forward and aft walls are always parallel, x/l could be measured from any lateral position.)

The model was instrumented with 84 static-pressure orifices and with three fluctuating pressure transducers. The majority of the static-pressure orifices were located along three longitudinal rows on the cavity floor since longitudinal pressure distributions are essential in characterizing flow fields. Three fluctuating-pressure transducers were expected to be sufficient as the intent of the experiment was to determine whether or not resonance occurs rather than obtain a detailed characterization of the fluctuating-pressure field throughout the cavities. A sketch of the static-pressure orifice and fluctuating-pressure transducer locations are shown in Figure 7. Tables 1 and 2 give the orifice and transducer coordinates, respectively, for each configuration. Some pressure orifices and pressure transducers were covered by the blocks used to shape the cavity for each configuration. The static and fluctuating pressure locations that are covered by the blocks are shown in Figure 7 and indicated in Tables 1 and 2. The data from the covered and partially-covered pressure orifices and transducers were considered invalid and are not included in the analysis.

Wind Tunnel and Test Conditions

The test was conducted in the NASA Langley Research Center 7 × 10-foot HST, which has since closed. The 7 × 10-foot HST was a closed-circuit, single-return continuous-flow atmospheric wind tunnel capable of testing from $M_\infty = 0.1$ to 0.94. Additional details on the tunnel can be found in References 58 and 59. The tests were conducted at $M_\infty = 0.2$, 0.4, 0.6, and 0.8 and at Re_∞ between 1×10^5 and 4×10^6 per foot.

The effect of the splitter plate planform on the flow in the region of the cavity at transonic speeds was assessed by a comparison of the pressure distributions of the three longitudinal rows of orifices for the model configured with the cavity floor positioned flush with the surface of the flat plate, i.e., no cavity. It was found that the pressure distributions on the three rows of pressure orifices compared well indicating that the flow over the cavity at transonic speeds is essentially uniform. Oil flow images that are not included in this report supported this conclusion.

A boundary-layer transition strip was applied near the leading edge of the splitter plate to ensure fully-developed turbulent flow on the plate surface entering the cavity for all test conditions. To fix transition, a strip of No. 60 grit was distributed over a width of 0.1 inches, approximately 1 inch aft of the leading edge, in accordance with the recommendations in References 60 and 61.

At the beginning of the test, a limited study was conducted to determine the effect of plate angle-of-attack (AOA) on the pressure gradient over the cavity region of the splitter plate. The instrumented cavity floor was positioned flush with the flat plate surface (no cavity) and static-pressure data were obtained for AOA equal to −1.2°, 0°, and 1.2°. In theory, the pressure coefficient (C_p) distribution along a flat plate at 0° AOA should be a straight line with a slope that does not necessarily have to be zero. This relationship is observed to be true in the data presented in Figure 8. (The effects of varying the plate AOA included changes in the slope and intercepts of the C_p curve as well as a slight deviation from linearity.) The static-pressure measurements at the three lateral positions on the flat plate at AOA = 0° are presented in Figure 9 to demonstrate the uniformity of the flow field across the cavity region (note that the scale of Figure 9 is much larger than the scale of Figure 8). Thus the test was conducted with the upper surface of the splitter plate positioned on the tunnel centerline, at 0° AOA and 0° yaw relative to the tunnel centerline. A correction has been applied to the static pressure data which will be discussed in the next section.

Measurements of the boundary layer profile were not obtained during this test. The boundary layer thickness was estimated from the following equation obtained from Reference 62.

$$\delta = 0.37 x_p \left(Re_\infty / 12(x_p) \right)^{-1/5}$$

This equation was derived for a turbulent boundary layer over a flat plate assuming incompressible flow. For this equation, δ is the estimated boundary layer thickness; x_p is the distance from the leading edge of the flat plate to the cavity leading edge; and Re_∞ is the free-stream unit Reynolds.

For the swept leading edge cavities, x_p varies from a minimum of 10.4 inches (x_{min}) to a maximum (x_{max}) that depends on the cavity sweep angle (see figure 10). An average boundary layer thickness was estimated as follows:

$$\delta_{avg} = 0.37 \frac{1}{w} \int_0^w \left(x_{\min} + y' \tan\psi \right) \left(\mathrm{Re}_\infty / 12 \left(x_{\min} + y' \tan\psi \right) \right)^{-1/5} dy'$$

Table 3 gives the average boundary layer thicknesses as well as the maximum boundary layer thickness approaching the cavity for each configuration over a range of free-stream Reynolds numbers from 1 to 4 million per foot.

Instrumentation, Measurements and Data Reduction

Surface Static Pressures

Each static-pressure orifice had a nominal inner diameter of 0.030 inches. Measurements of static pressure were made using electronically-scanned pressure (ESP) transducers. Each ESP had a full-scale range of ±5 psid and used the tunnel static pressure for reference. It is believed that the dominant source of uncertainty in C_p is due to the repeatability (and calibration) of the ESP modules. That uncertainty was estimated to be no more than 0.15-percent full-scale (the quoted accuracy of the ESP) or ±0.008 psi. Table 4 gives this uncertainty in terms of C_p values (uncertainty in C_p being equal to the uncertainty in the pressure measurement divided by q_∞).

ESP measurements were made at a rate of 20 times per second. Two seconds of data were averaged to obtain the mean static pressure at each orifice location. Since variations could exist in individual orifice characteristics, a (very small) correction, described in the next paragraph, was applied to the data. Potential sources of variation in orifice characteristics include: differences in orifice installation and fabrication; and differences in model contour and finish between locations [63, 64].

The correction to the static pressure data was determined by configuring the model as a flat plate (i.e., the cavity floor was moved level with the plate surface and no cavity was present). The pressure distributions for the flat plate at repeat 0° AOA points show that the measurements repeat well, but there are local perturbations in the pressure measurements. For a flat plate at 0° AOA, in theory, the C_p distribution should be a straight line with a slope that does not necessarily have to be zero and with minimal deviation about that line. It is known that orifice installation, orifice fabrication, model contour and model finish quality can induce errors in the measured pressure, [63, 64]. Because there are significant repeatable deviations from a straight line faired through the points, it was assumed that the orifices and/or the model had manufacturing imperfections that induced bias errors into the measurement. To correct the bias errors three values were taken at each M_∞ at 0° AOA for the model configured with no cavity. The three values were averaged for each pressure tap on the model. A least squares fit was applied to the averaged data to generate a straight line for each of the three longitudinal rows of orifices on the cavity floor.

The difference in C_p at each pressure tap, between the averaged data and the least squares generated curve, was calculated to be the correction to be applied to all measurements at a given tap and M_∞. The correction was then applied to each tap for each M_∞. The corrections applied to the data are very small relative to the scale to be used in data presentation; the corrected C_p plots are smoother than the uncorrected C_p plots.

Fluctuating-Pressures

The fluctuating-pressure measurements were made using miniature (0.15-inch diaphragm) flush mounted fluctuating-pressure transducers. The transducers were piezoresistive with a full-scale range of 5 psid and a resonant frequency of 85,000 Hz. In order to utilize the maximum sensitivity of the transducers, the static component of the pressure measurement was removed. This modification was accomplished by installing the transducers in a differential configuration with local static pressure as a reference (orifice 20 was connected to the back of the diaphragm with 10 feet of 0.020-inch flexible tubing) and by alternating current coupling the instrumentation. An antialiasing filter was applied at 5 kHz and data were digitized at 12.8 kHz using a workstation-based 24-channel parallel signal processor. The processor had 16-bit analog-to-digital conversion which gave a dynamic range of 90 dB (signal-to-noise). Analog data were also recorded as a backup on a 28-channel frequency modulation (FM) tape recorder using wide-band format at 7.5 in/sec (modulation band of 0 to 10 kHz with 50 dB dynamic range). A sine-wave calibration was applied to each fluctuating-pressure transducer several times throughout the test.

Digitized data were divided on-line into 52 blocks of 1024 points each. Blocks were Fourier analyzed using a Hanning window and the resulting spectra were averaged. This process produced spectra with an upper frequency of 5 kHz, resolution of 12.5 Hz, and a 95-percent confidence interval of less than 2.5 dB. This confidence estimation is based on a chi-square distribution which assumes an ergodic Gaussian random process and independence of the sample blocks (see Reference 65).

Data are presented in sound pressure level (*SPL*).

$$SPL = 20\log\left(\frac{p'_{rms}}{2.9\times10^{-9}\,\text{psia}}\right)$$

It is possible to convert *SPL* representation to one that uses q_∞ as a reference as follows:

$$FPL = SPL + 20\log\left(\frac{2.9\times10^{-9}\,\text{psia}}{q_\infty}\right)$$

Colored-Water Surface Flow Visualization

Unsteady surface flow visualization was achieved using a method in which colored water is passed through pressure orifice tubes to the model surface. Reference 66 gives details of this technique and describes the advantages over conventional oil flow and tuft methods: the low viscosity of the water allows imaging of rapidly varying flow phenomena and the availability of many orifices and different dyes allows tailoring the visualization to elucidate particular features of the flow including the origin of vortices and mixing flows.

Results and Discussions

Presentation of Data

The volume of data obtained in this study requires that only selected representative data be presented in this report. Selected surface static-pressure distributions and fluctuating-pressure spectra from one transducer are represented graphically and representative photographs and sketches of the flow visualization are included in the body of this report. A complete tabulation of static-pressure data and black and white photographs of flow visualization are provided in the appendices. Except where noted, static-pressure distributions are given along the center-line of the cavity floor and fluctuating pressure data are presented from a single transducer. Note that while static and fluctuating pressure data were acquired at the same time, they were recorded using different systems and there are instances (of l/h and ψ values) for which both types of data are not available.

After the static-pressure data, fluctuating pressure data, and the flow-visualization photographs are presented individually; an analysis of all the data considered together will be presented as “Summary of Results” at the end of this section. It should be noted that w/h = 5 for the model tested. For configurations where values of $l/h < w/h$ there is the potential for significant cross flow which should be factored into data analysis.

Effect of Lateral Cavity-Floor Position on Static Pressures

The data in this section are presented to show the effect of lateral cavity-floor position on static-pressures for swept cavities. Lateral static-pressure data for the rectangular cavities were consistent with that published in Reference 13, and are not shown in this report.

Three rows of orifices were spaced across the floor as seen in Figure 7. One row was located on the centerline (y = 0 inches) and one on either side of the centerline, positioned midway between the centerline and the sidewall ($y = \pm\frac{w}{4} = \pm 0.63$ inches). There were 46 orifices along the centerline and 16 each along the rows at $\pm\frac{w}{4}$.

For the rectangular cavity, no variation was observed in pressure gradients measured at y = 0 and $\pm\frac{w}{4}$.

Comparisons of the pressure distributions at the three lateral locations for a selected set of representative l/h values are given in Figures 11 through 14 for configurations 1 through 4 respectively. The data for ψ = 65° and ψ = 55°, Figures 11 and 12, show significant variation of the pressure distribution with lateral position. For ψ = 65°, this variation is consistent over the M_∞ range tested. For ψ = 55° the variation is consistent over the range M_∞ = 0.2 through 0.6 and decreases at M_∞ = 0.8. (One exception is for l/h = 9, which has reduced variation at M_∞ = 0.6.) For ψ = 45° and ψ =35°, Figures 13 and 14, the three pressure distributions are very similar.

Note that for ψ = 55° (Figure 12) there is a lower pressure in the front portion of the port side (y = –0.63 inches) of the cavity for all M_∞ and l/h than is seen at the other values of ψ. For ψ = 65° data were not available just downstream of the leading edge at positions off of the centerline. For ψ = 45° and ψ = 35°, the static pressure downstream of the leading edge is nearly constant across the width of the cavity.

Effect of Streamwise Location on Fluctuating Pressures

Figure 15 shows typical fluctuating-pressure data obtained at various locations in rectangular cavities. (Recall that Transducer 3 is the furthest upstream followed by 1 and then 2, as seen in Figure 7, and that transducer x/l depends on l/h.) Results for a resonant rectangular cavity, presented in Figure 15 (a) agree with results published in Reference 27: resonant peak amplitudes vary (depending on the location relative to mode wavelength) and broadband noise increases with x/l. Figures 15 (b), (c) and (d) give comparisons of spectra obtained at three locations in nonresonant rectangular cavities.

Figure 16 gives typical data obtained at two locations in swept cavities. In Figures 16(a), (b) and (c), there is evidence of sustained oscillations in the forward region that decay or disappear with increasing x/l. Also, broadband levels decrease with increasing x/l, which differs from the data shown in Figure 15(a) for a resonant rectangular cavity. As in Figure 15, Figure 16 (d) shows comparable broadband levels from transducers located in the regions of reattachment and separation near the aft wall.

In the following sections results for Transducer 1 will be presented whenever it is available. For cases when it was not exposed (for rectangular cavities with l/h values of 3, 4, and 5), data from Transducer 3 will be used.

Static-pressure Data Including New Flow Type

Effect of Sweep

The effect of sweep on centerline static-pressure distribution is shown in Figure 17 for each value of M_∞ and l/h up to 20. For many cases, the pressure distributions are similar to those sketched in Figure 2 suggesting that the flow types described for rectangular cavities in Reference 17 are applicable to swept cavities. In general, static-pressure distributions for swept cavities had lower C_p values in the forward portion of the cavity than those observed for rectangular cavities. For low cavity l/h values, distributions were often observed that indicated open-cavity flow (see Figure 17(c) for l/h = 3 and ψ = 65°, and Figure 17(e) for l/h = 5 and ψ = 35°,) and distributions varied with sweep angle. As cavity l/h was increased, the pressure distribution more closely resembles that of closed-cavity flow for a rectangular cavity (see Figure 17(o), l/h = 15 for ψ = 45°) and variability with sweep angle decreased.

For cavities with ψ = 35° for l/h from 4 to 7, (8 for M_∞ = 0.8) and with ψ = 45° for l/h = 5 and 6 (through 8 for M_∞ = 0.8), the distribution resembles that of a rectangular open-cavity flow and for l/h > 8, the pressure distribution for all values of sweep resemble that of a rectangular cavity with transition to closed flow. While no clear relationship appeared between sweep angle and the changes in the reattachment pressure gradient, the static-pressure approaching the aft wall decreased monotonically with increasing sweep. There was a new static-pressure distribution observed in some swept cavity configurations that was characterized by a distinct departure from the distributions observed in rectangular cavities. This new distribution could produce a store nose-in pitching moment at reduced l/h as compared to rectangular cavities. Specifically, this new pressure distribution was distinguished by a sharp decrease in pressure followed by a sharp increase in pressure in the forward portion of the cavity; it varied with M_∞, l/h and ψ, and it could influence pressure distributions that otherwise would suggest classical open-, transitional- or closed-flow types. Features of the 'new distribution' were observed for most cavities with ψ = 65° and 55°. Exceptions include ψ = 65° for l/h = 3 (with open flow as seen in

Figure 17(c)) and ψ = 55° for intermediate l/h values (l/h = 6–14 for M_∞ = 0.8, l/h = 7–11 for M_∞ = 0.8 and l/h = 8 for M_∞ = 0.4, with transitional flow as seen in Figures 17(f) through (n), (g) through (k), and (h), respectively). Dramatic examples of the 'new distribution' (with C_p increases over 0.425) were observed for cavities with ψ = 55° for l/h = 5, 6 and 7 (for M_∞ = 0.2–0.8, 0.2–0.6 and 0.2–0.4, respectively), with ψ = 45° for l/h = 3 and 4 (for M_∞ = 0.2–0.8, and 0.2–0.6, respectively), and with ψ = 35° for l/h = 3 (M_∞ = 0.2–0.6).

Effect of l/h in Swept Cavities

Rectangular cavity data were consistent with that published in Reference 17; the flow field gradually progressed from open flow for low values of l/h, through transitional flows, to closed flow for large values of l/h. Because these cavity data were consistent with previously published results, they are not shown here.

For swept cavities, the effect of varying the cavity length while holding cavity width and depth constant is shown in Figure 18. Selected data are presented to illustrate the change in pressure distribution over the range of l/h tested for each cavity shape. The tabulated data for all configurations tested can be found in Appendix A, Supplemental Static Pressure Tables.

Cavities with ψ = 65°, Figure 18(a), show a gradual change in pressure distribution. For l/h = 3, the flow appears to be open. For l/h = 4 and 5 (reference Figure 17) the flow becomes open with features of the new distribution. For l/h = 6 through 13, the flow appears transitional with features of the new distribution. Closed cavity flow is not obtained for ψ = 65° over the range of l/h tested.

The flow fields in cavities with ψ = 55° (Figure 18(b)) gradually progress from the new type flow (l/h = 3) through transitional flow or transitional flow with new features (for M_∞ = 0.2 - 0.4) to closed-cavity flow or closed-cavity flow with new features (for M_∞ = 0.2 - 0.6). The pressure rise in the forward cavity region for the ψ = 55° cavity appears to be one of the most dramatic (occurring over a very short range of x/l) and persistent (effecting flows that resemble open, transitional and closed types).

For ψ = 45° and ψ = 35° (Figures 18(c), and (d)), the pressure distributions are similar to those shown in Figure 2 for a rectangular cavity and show a gradual change from distributions representative of open- to closed-type flows with increasing l/h. Exceptions are noted in the previous section for low l/h values for which the new flow type occurs.

This new flow type behavior near the leading edge is reminiscent of leading-edge vortex development on delta wings, which is dependent on sweep angle, M_∞ and probably boundary layer thickness (References 67 and 68).

Effect of M_∞ in Swept Cavities

Results for the rectangular cavities were consistent with those published in Reference 17 and will not be shown here: increasing M_∞ had an effect similar to decreasing l/h.

A representative sampling of the data is provided in Figure 19 to illustrate the effect of M_∞ in swept cavities. While there is little change in static-pressure distribution with M_∞ for the range 0.2 through 0.6, there are consistent changes for all configurations as M_∞ is increased to 0.8. The pressure distributions observed for a given configuration at M_∞ = 0.8 are typical of distributions that would occur for lower values of l/h; the same result was observed for rectangular cavities.

Fluctuating Pressure Data

Fluctuating-pressure results are given in Figure 20 for each value of *l*/*h* and M_∞. For reference, Table 5 gives the nondimensional resonant frequencies ($f_m l / U_\infty$) predicted by the modified Rossiter Equation for longitudinal modes in rectangular cavities. Those frequencies are indicated on the plots in Figure 20 by the solid symbols. For rectangular cavities, the occurrence of resonance is seen to depend on *l*/*h* and M_∞ and is consistent with previously published results [27]. There is evidence of resonance (peaks in the spectra) for rectangular cavities with *l*/*h* values up to 11 for M_∞ = 0.8 (Figures 20(a)-(i)), for *l*/*h* values up to 10 for M_∞ = 0.6 (Figures 20(a)-(h)), and for *l*/*h* = 4 and 5 for M_∞ = 0.4 (Figure 20(b) and (c)). Figure 17 reveals transitional- and open-flow distributions for the rectangular cavity at these conditions. (The pressure distributions corresponding to the spectra in Figure 20 referred to above are: 17 (c)-(k), 17 (c)-(j), 17(d) and 17(e), respectively. The pressure distributions in figures 17(d) and (e) indicate open flow and those in figures 17(j) and (k) indicate transitional flow.) No resonant peaks were apparent for any configuration for M_∞ = 0.2, nor for any configuration for *l*/*h* = 3. Table 6 lists the observed nondimensional frequencies for rectangular cavities. There appears to be good agreement between the observed and predicted resonant frequencies. The small discrepancies may be because single values were used for $\alpha\left(\frac{l}{h}\right)$ and *k*(*M*).

Spectral peaks are also observed in the data from swept cavities. The most distinct peaks were observed for ψ = 55° and 65° and will be discussed here. Appendix B provides a listing of all the peak frequencies observed for swept cavities (including those with very low amplitudes). Several observations can be made:

1) While the frequencies observed for swept cavities appear to depend on M_∞, they do not depend on *l* as prescribed by Rossiter-type equation. This is illustrated in Figure 21 in which f/U_∞ is plotted against *l*/*h*. While nondimensionalizing the observed frequencies by *l* would introduce rather than remove trends in the data, a smaller length scale depending on ψ is suggested by the differences observed between the frequencies for ψ = 65° and the first mode (lower) frequencies for ψ = 55°. A length scale less than *l* could be associated with a local oscillatory phenomena in the vicinity of the transducer (forward portion of the cavity).

2) Only cavities with ψ = 55°, sustained two modes of oscillation. The ratio of the frequencies of the two modes was not constant for the range of *l*/*h* values studied.

3) Peaks observed in rectangular cavities generally have higher amplitudes than those observed in swept cavities: See Figure 20(d) to (g) (*l*/*h* from 6 through 9) for M_∞ = 0.6 and 0.8. There are cases, however, for which peak amplitudes in swept cavities can be comparable to or higher than those in rectangular cavities: See Figures 20(b) to (c) for *l*/*h* from 4 and 5 for M_∞ = 0.6 and 0.8.

4) At M_∞ = 0.2 through 0.6 for ψ = 55° and *l*/*h* from 10 to 17, cavities sustained oscillations whereas rectangular cavities with the same *l*/*h* values did not. Above *l*/*h* = 18, no large spectral peaks are seen.

It is important to remember that the position of the transducer relative to the length of the cavity varies inversely with *l*/*h*. The reader may wish to consider whether or not the transducer was located in a region of attached or separated flow. This can be determined by referring to Figure 17 and Table B-2, which lists transducer *x*/*l* for each ψ and *l*/*h* value.

Surface-Flow Visualization Data

A method to observe surface flow characteristics was developed by Floyd J. Wilcox, Jr. and is described in Reference 66. This technique used a pressure differential to draw water, colored with food coloring, through tubes connected to the model static-pressure orifices. The water is then introduced into the cavity through the static-pressure ports. Black and white photographs and sketches of surface flow visualization are presented in Figures 22−26 for cavities with l/h values of 4, 8, and 12 for the rectangular and all swept cavity configurations. Figure 27 provides photographs and sketches of surface flow visualizations for larger cavities (l/h = 11, 14, and 19). A complete set of black and white photographs obtained is provided in Appendix C, Supplemental Flow Visualization Figures.

Flow visualization for the rectangular cavities was consistent with the pressure data, indicating open-, transitional- and closed-type flows. Open flow is characterized by reverse flow throughout the cavity and closed flow is characterized by separated flow in the fore and aft cavity region with attached flow between. Figure 22(c) includes typical examples of open (l/h = 4), transitional (l/h = 8) and closed flow (l/h = 12).

Flow visualization for the swept cavities indicated the following:

1) inflow on the port side and outflow on the starboard side;
2) centerline incoming flow turns towards the perpendicular to the swept leading edge (more pronounced for higher M_∞);
3) a vortex appearing along the leading edge which appears to remain confined forward of the reattachment line;
4) a similar vortex along the starboard side for cavities with sweep angles of 65° and 55°; and
5) a third vortex along the aft wall for closed flow conditions.

Summary of Results

Considering the complementary flow visualization, static-pressure and fluctuating-pressure results together provides additional insight. For reference, Figure 28 has been compiled to summarize the suggested flow field types in swept cavities based on static-pressure distributions. It is important to note here that the pressure distributions in swept cavities often contained elements of multiple flow field types and the assignments made for Figure 28 depend on one set of criteria (open-to-transitional flow is signaled by a change in distribution from concave up to concave down and transitional-to-closed flow is signaled by the appearance of an inflection point as seen in Figure 2.) Different assignments could be made using different criteria (such as sign and magnitude of C_p values).

In the earlier discussion a new distribution was noted where a sharp decrease in pressure (velocity increase) in the forward region of the cavity was followed by a sharp increase in pressure (velocity decrease) as x/l increased. Depending on the length of the cavity, the pressure could plateau or experience a gradual decrease (velocity increase). To gain insight into these phenomena, it is first necessary to consider swept cavities that appear to sustain flow fields similar to rectangular cavities. Figure 26(c) provides flow visualization images for cavities with ψ = 35°, for l/h = 4, 8, and 12 at M_∞ = 0.6. These images correspond to static pressure distributions that suggest open, transitional and closed cavity flows, respectively. While not aligned with the free-stream flow, the surface flows in these swept cavities have characteristics similar to those observed in rectangular cavities: reverse flow throughout the cavity for open flow, flow out from a region of impingement for transitional flow and attached flow downstream of impingement for closed flow. One significant difference between the flow images for these swept cavities and those for rectangular cavities in Fig. 22(c), occurs at the base of the rearward facing step that forms the leading edge. In swept cavities, flow appears to be entrained and travels with an upstream component in this region, contributing to the formation of a vortex in the leading-edge corner (on the port side) of the swept cavity. In rectangular cavities, flow pools along the base of the leading edge and vortices occur on both sides of the centerline. In cavities that experience the new distribution, flow appears to be entrained along the base of the swept leading edge and travels with a downstream component. (If a vortex occurs in the leading edge corner, it is small and not fed by flow from across the cavity.) Examples are seen in Figure 23(c) (ψ = 65° and M_∞ = 0.6) for l/h = 4 (open flow with new features), 8 and 12 (transitional flow with new features) and in Figure 24(c) (ψ = 55° and M_∞ = 0.6) for l/h = 4 (new flow), and 12 (closed flow with new features). (Note l/h = 8 appears to sustain transitional flow with the flow along the leading edge traveling in both directions.)

The pressure distributions in swept cavities appear consistent with flow visualization. Flow observed along the base of the leading edge in swept cavities with downstream components (increased velocity) produce lower pressures than flows with upstream components (decreased velocity). In general, swept cavities appear to have higher velocity flows downstream of the leading edge and upstream of the trailing edge than rectangular cavities and thus lower pressure in these regions. Increases in pressure downstream of the leading edge in cavities experiencing the new distribution may be due to the swept leading edge impeding the reverse flow upstream of the impingement region on the cavity floor.

A possible explanation for the new distribution involves vortex formation and can be seen using Figure 24(d), l/h = 4 (ψ = 55°, M_∞ = 0.8) as an example. In this photograph, flow is seen to enter the cavity approximately normal to the swept leading edge and also from the port side. External flow is deflected near the leading edge on the starboard side indicating flow exiting from the cavity. A small vortex is observed to form in the leading-edge corner (on the port side) of the swept cavity. This vortex appears to be entrained along the base of the rearward facing step that forms the leading edge of the cavity. This again would show as a decrease in pressure or an accelerated region of flow. Downstream of the cavity leading-edge vortex the flow is attached (resulting in a decrease in velocity or increase in pressure) and indicates a direction toward the aft starboard corner. It appears that the majority of the flow rolls-up in this corner and flows out of the cavity and downstream. This vortex flow could be the source of the non-Rossiter type pressure oscillations discussed above. l/h = 5, ψ = 55° provides an example; non-Rossiter type double peaks are observed in Fig 20(c) and dramatic new pressure distributions are observed in Fig. 17(e). Corresponding photographs illustrating vortex flow near the leading edge are found in Appendix C: Figs. C9(c), C10(d), C11(a) and C12(d).

More insight can be gained from cavities that appear to demonstrate open-cavity flow. An example configuration from Figure 28 is ψ = 45° and l/h = 8 at M_∞ = 0.8 and the corresponding flow visualization photograph in Figure 25(d). For this flow there appears to still be a vortex on the forward left-hand corner of the cavity, but it does not drive the incoming flow. As can be seen in the photo, the incoming flow to the side of the cavity is not pulled into the cavity. Figure 13(d) also confirms that the pressures on the floor of the cavity for ψ = 45° and M_∞ = 0.8 are nearly constant across the leading edge of the cavity for the range of l/h values shown. The forward corner flow does appear to be driving the flow within the cavity; however, as can be seen in the photograph all the surface flow in the forward region of the cavity is turned upstream (toward the forward cavity wall) and appears to pool in the forward port corner. A small portion of the flow in the aft section of the cavity rolls-up in the aft starboard corner where it exits the cavity and flows downstream. For this flow condition the pressure gradient shows a C_p to be nearly zero over much of the cavity floor with a gradual rise at the aft end of the cavity.

Another point of interest for the swept-cavity flows that resemble closed-flow conditions is that as the cavity length is increased, the flow in the forward portion of the cavity does not change (see Figure 27). As the cavity length is increased a vortex forms in the aft region of the cavity, parallel to the aft wall, and serves to entrain the flow and direct it toward the aft starboard corner where the flow exits the cavity. The formation of this downstream vortex appears to coincide with changes in the pressure distribution to more closely resemble that of closed-flow observed in rectangular cavities (Figures 17 (k-s)).

For low enough sweep angles, the separation off the leading edge creates a weak roller that is essentially two dimensional. With increasing sweep, the roller becomes a vortex with origin roughly at the upstream corner, depending on boundary layer thickness, thereby changing the character of the inflow completely. The vortex probably grows in size and strength from the upstream corner of the leading edge to the downstream corner of the leading edge. This new flow type behavior near the leading edge is reminiscent of leading-edge vortex development on delta wings, which is dependent on sweep angle, M_∞ and probably boundary layer thickness (References 67 and 68).

In summary, the data obtained during this test suggest the following effects on store carriage in and separation from swept cavities:

1) A store is likely to experience a strong nose-in pitching moment due to the roller/vortex that can be generated at the leading edge
2) Unlike a rectangular cavity, there will be cross flow which may affect store roll and yaw moments.
3) Longitudinal cavity resonance, a source of potential damage to stores with rectangular cavities, does not appear to occur.
4) It may be possible to manipulate the various influencing factors (i.e., leading edge sweep, boundary layer thickness, M_∞, l/h, etc.) to obtain more benign cavity flows than with a rectangular design.

Concluding Remarks

An experimental investigation was conducted in the 7 × 10-foot High-Speed Tunnel (HST) at the NASA Langley Research Center to study the effect of leading- and trailing-edge sweep on cavity flow fields for a range of cavity length-to-depth (l/h) ratios. The study included two experiments designed to characterize the flow fields in rectangular and swept cavities, respectively. The M_∞ range was from 0.2 to 0.8. The unit Reynolds number varied between 1×10^6 and 4×10^6 per foot and the boundary layer approaching the cavity was turbulent with an estimated thickness of 0.25 inches. The cavity had a depth of 0.5 inches, a width of 2.5 inches, and a maximum length of 12.0 inches. The leading- and trailing-edge sweep was adjusted using block inserts to achieve sweep angles of 65°, 55°, 45°, and 35°. (The fore and aft walls were always parallel.) The aft wall of the cavity was remotely positioned to achieve a range of length-to-depth ratios. (The maximum l/h depended on sweep angle.) The width and depth were fixed and $w/h = 5$. Fluctuating- and static-pressure data were obtained on the floor of the cavity. Qualitative surface flow visualization was obtained using a technique in which colored water was introduced into the model through static-pressure orifices.

Static-pressure distributions exhibited by swept cavities often appeared similar to those observed in rectangular cavities. A ‘new pressure distribution’ was also observed which suggests the formation of a vortex parallel to the cavity leading edge that entrained the flow along the base of the rearward facing step that formed the leading edge of the cavity. The new distribution exhibited a sharp decrease in pressure in the most forward portion of the cavity, followed by a sharp increase in pressure caused by the vortex formed at the cavity leading edge, followed by the flow reattaching downstream of the vortex. The distribution was most consistently found at $\psi = 55°$ where strong lateral gradients were also observed.

The highest values of sweep tested, $\psi = 65°$, produced encouraging results. For these cavities, the pressure distribution was more benign, similar to a rectangular open- or a transitional-open-cavity flow; however, there were no cavity-induced resonant tones.

Fluctuating-pressure results indicated that rectangular cavities for which open and transitional flow existed supported longitudinal resonances of the type described by the modified Rossiter Equation.

Although spectral peaks were apparent in swept-cavity data, their frequencies were not dependent on l as prescribed by the modified Rossiter equation.

In summary, the data obtained during this test suggest the following effects on store carriage in and separation from swept cavities:

1) A store is likely to experience a strong nose-in pitching moment due to the roller/vortex that can be generated at the leading edge.
2) Unlike a rectangular cavity, there will be cross flow, which may affect store roll and yaw moments.
3) Longitudinal cavity resonance, a source of potential damage to stores with rectangular cavities, does not appear to occur.
4) It may be possible to manipulate the various influencing factors (i.e., leading edge sweep, boundary layer thickness, M_∞, l/h, etc.) to obtain more benign cavity flows than with a rectangular design.

References

1. Delprat, Nathalie: "Rossiter's formula: A simple spectral model for a complex amplitude modulation process?" *Physics of Fluids*, Vol. 18, 071703 (2009), DOI: 10.1063/1.2219767.

2. Lada, C.; and Kontis, K.: "Experimental Studies on Transitional and Closed Cavity Configurations Including Flow Control." *Journal of Aircraft*, Vol. 47, No. 2, March–April 2010, DOI: 10.2514/1.46027.

3. Lawrie, David: *Investigation of cavity flows at low and high Reynolds numbers using computational fluid dynamics*. PhD thesis, University of Glasgow, 2004.

4. Lee, B. H. K.; Orchard, D. M.; and Tang, F. C.: "Flow past a Yawed Rectangular Cavity in Transonic and Low Supersonic Flows." *Journal of Aircraft*, Vol. 46, No. 5, September–October 2009, DOI: 10.2514/1.40729.

5. Malone, J.; Debiasi, M.; Little, J.; and Samimy, M.: "Analysis of the spectral relationships of cavity tones in subsonic resonant cavity flows." *Physics of Fluids* Vol. 21, Issue 5, pp. 055103-055103-9 (2009), DOI: 10.1063/1.3139270.

6. Nayyar, P.; Barakos, G. N.; and Badcock, K. J.: "Numerical and Experimental Analysis of Transonic Cavity Flows." *Presented at the 2nd International Symposium on Integrating CFD and Experiments in Aerodynamics* hosted by Cranfield University (Shrivenham) September 5–6, 2005

7. Ritchie, S. A.; Knowles, R.; and Lawson, N. J.: "Characterization of a 3D l/h = 5 Rectangular Cavity Flowfield using Experimental and Numerical Techniques." *Presented at the 2nd International Symposium on Integrating CFD and Experiments in Aerodynamics* hosted by Cranfield University (Shrivenham) September 5–6, 2005.

8. Yang, D.; Li, J.; and Fan, Z.: "Aerodynamic Characteristics of Transonic and Supersonic Flow over Rectangular Cavities." *Flow, Turbulence and Combustion* Vol. 84, No. 4 (2010), 639-652, DOI: 10.1007/s10494-010-9246-7.

9. *Aerodynamics and Aero-Acoustics of Rectangular Planform Cavities. Part I: Time-Averaged Flow*. ESDU International, Item No. 02008, 2004.

10. *Aerodynamics and Aero-Acoustics of Rectangular Planform Cavities. Part II: Unsteady Flow and Aero-Acoustics*. ESDU International, Item No. 04023, 2005.

11. *Aerodynamics and Aero-Acoustics of Rectangular Planform Cavities. Part IIIA: Introduction*. ESDU International, Item No. 08011, 2009.

12. *Aerodynamics and Aero-Acoustics of Rectangular Planform Cavities. Part IIIB: Acoustic Suppression Using Passive Devices*. ESDU International, Item No. 08012, 2009.

13. Charwat, A.F.; Roos, J.N.; Dewey, F.C., Jr.; and Hitz, J.A.: "An Investigation of Separated Flows- Part I: The Pressure Field." *Journal of the Aerospace Sciences,* June 1961, pp. 457–470.

14. Stallings, Robert L., Jr.; and Wilcox, Floyd J., Jr.: *Experimental Cavity Pressure Distributions at Supersonic Speeds*. NASA TP-2683, June 1987.

15. Plentovich, E. B.: *Three-Dimensional Cavity Flow Fields at Subsonic and Transonic Speeds*. NASA TM-4209, September 1990.

16. Plentovich, E. B.; Chu, Julio; Tracy, M. B.: *Effects of Yaw Angle and Reynolds Number on Rectangular-Box Cavities at Subsonic and Transonic Speeds*. NASA TP-3099, July 1991.

17. Plentovich, E. B.; Stallings, Robert L. Jr.; and Tracy, M.B.: *Experimental Cavity Pressure Measurements at Subsonic and Transonic Speeds - Static-Pressure Results*. NASA TP-3358, December 1993.

18. Ruderich, R.; and Fernholz, H. H.: "An Experimental Investigation of a Turbulent Shear Flow with Separation, Reverse Flow, and Reattachment." *Journal of Fluid Mechanics* Vol. 163, 1986, pp. 283-12.

19. DiMiccok R. G.; Disimile, P. J.; Lueders, K.;Toy, N.; and Savory, E.: "Three Dimensional Flow in a Rectangular Cavity." *Twelfth Symposium on Turbulence*, September 1990, pp. A13-1–A13-8.

20. Maull, D. J.; and East, L. F.: "Three-dimensional Flow in Cavities." *Journal of Fluid Mechanics,* Vol. 16, Pt. 4, 1963, pp. 620–632.

21. Rockwell, D.; and Knisely, C.: "Observations of the Three-dimensional Nature of Unstable Flow Past a Cavity." *Physics of Fluids* Vol. 23, No. 3, March 1980, pp. 425–431.

22. Rossiter, J. E.: *Wind-Tunnel Experiments on the Flow over Rectangular Cavities at Subsonic and Transonic Speeds*. R. & M. No. 3438, British Aeronautical Research Council, October 1964.

23. Kaufman, Louis G. II; Maciulaitis, Algirdas; and Clark, Rodney L.: *Mach 0.6 to 3.0 Flows Over Rectangular Cavities*. AFWAL-TR-82-3112, U. S. Air Force, May 1983 (Available from DTIC as AD A134 579.)

24. Heller, H. H.; Holmes, G.; and Covert, E. E.: *Flow-Induced Pressure Oscillations in Shallow Cavities*. AFFDL-TR-70-104, U. S. Air Force, December 1970. (Available from DTIC as AD 880 496.)

25. Heller, Hanno H.; and Bliss, Donald B.: *Aerodynamically Induced Pressure Oscillations in Cavities - Physical Mechanisms and Suppression Concepts*. AFFDL-TR-74-133, U. S. Air Force, February 1975.

26. Tracy, M. B.; Plentovich, E. B.; and Chu, J.: *Unsteady Pressure Measurements in a Rectangular Cavity in High Reynolds Number Transonic Flows*. NASA TM-4363, 1992.

27. Tracy, M. B.; and Plentovich, E. B.: *Characterization of Cavity Flow Fields Using Pressure Data Obtained in the Langley 0.3-Meter Transonic Cryogenic Tunnel*. NASA TM-4436, March 1993.

28. Bartel, H. W.; and McAvoy, J. M.: *Cavity Oscillation in Cruise Missile Carrier Aircraft*. AFWAL-TR-81-3036, June 1981.

29. Shaw, L.; Clark, R.; and Talmadge, D.: "F-111 Generic Weapons Bay Acoustic Environment." AIAA-87-0168, January 1987.

30. Shaw, L. L.; and Reed, S. A.: *Supersonic Flow Induced Cavity Acoustics*. AFWAL-TM-85-210-FIBG, December 1985.

31. Rockwell, D.; and Naudascher, E.: "Review – Self-Sustaining Oscillations of Flow Past Cavities." *Transactions of the ASME*, Vol. 100, June 1978, pp. 152 - 165.

32. Smith, D. L.; and Shaw, L. L.: *Prediction of the Pressure Oscillations in Cavities Exposed to Aerodynamic Flow*. AFFDL-TR-75-34, October 1975.

33. Komerath, N. M.; Ahuja, K. K.; and Chambers, F. W.: "Prediction and Measurement of Flows Over Cavities - A Survey." AIAA-87-0166, January 1987.

34. Dix, Richard E.: "On Simulation Techniques for the Separation of Stores from Internal Installations." SAE 871799, October 1987.

35. Dix, R. E.; and Dobson, T. W., Jr.: *Database for Internal Store Carriage and Jettison, Volumes I and II*. AEDC-TR-90-23, November 1990.

36. Wilcox, Floyd J., Jr.: "Experimental Measurements of Internal Store Separation Characteristics at Supersonic Speeds." *Store Carriage, Integration, and Release*, Royal Aeronautical Soc., 1990, pp. 5.1–5.16.

37. Stallings, Robert L., Jr.; and Forrest, Dana K.: *Separation Characteristics on Internally Carried Stores at Supersonic Speeds*. NASA TP-2993, 1990.

38. Stallings, Robert L., Jr.; Wilcox, Floyd J., Jr.; and Forrest, Dana K.: *Measurements of Forces, Moments, and Pressures on a Generic Store Separating From a Box Cavity at Supersonic Speeds*. NASA TP-3110, September 1991.

39. Stallings, Robert L., Jr.; Plentovich, Elizabeth B.; Tracy, Maureen B.; and Hemsch, Michael J.: *Measurement of Store Forces and Moments and Cavity Pressures for a Generic Store Separating From a Box Cavity at Subsonic and Transonic Speeds*. NASA TM-4611, May 1995.

40. Block, Patricia J. W.: *Noise Response of Cavities of Varying Dimensions at Subsonic Speeds*. NASA TN D-8351, December 1976.

41. Block, Patricia J. W.; and Heller, Hanno: *Measurements of Farfield Sound Generation From a Flow-Excited Cavity*. NASA TM X-3292, December 1975.

42. Block, P. J. W.; Stallings, R. L., Jr.; and Blair, A. B., Jr.: *Fluctuating Pressure Measurements Inside a Shallow Cavity with Doors in a Supersonic Flow*. NASA TP-2849, 1988.

43. Scheiman, James: *Acoustic Measurements of a Large Cavity in a Wind Tunnel.* NASA TM-78658, May 1978.

44. Ahuja, K. K.; and Mendoza, J.: *Effects of Cavity Dimensions, Boundary Layer, and Temperature on Cavity Noise with Emphasis on Benchmark Data to Validate Computational Aeroacoustic Codes*. NASA CR-4653, April 1995. (Contract NAS1-19061)

45. Tracy, M. B.; and Stallings, R. L., Jr.: *The Effect of the Acoustic Environment on a Store During Separation from a Rectangular Cavity at Supersonic Speeds*. NASA TP-2986, June 1990.

46. Wilcox, Floyd J., Jr.: *Experimental Investigation of Porous-Floor Effects on Cavity Flow Fields at Supersonic Speeds*. NASA TP-3032, November 1990.

47. Baysal, O.; Srinivasan S.; and Stallings, R. L., Jr.: "Unsteady Viscous Calculations of Supersonic Flows Past Deep and Shallow Three-Dimensional Cavities." AIAA-88-0101, January 1988.

48. Catalano, George D.: *Turbulent Flow Over an Embedded Rectangular Cavity*. AFATL-TR-8673, U. S. Air Force, February 1987. (Available from DTIC as AD A177 928.)

49. Om, Deepak: "Navier-Stokes Simulation for Flow Past an Open Cavity." AIAA-86-2628, October 1986.

50. Baysal, O.; and Stallings, R. L., Jr.: "Computational and Experimental Investigation of Cavity Flowfields." AIAA-87-0114, January 1987.

51. Suhs, N. E.: "Computations of Three-Dimensional Cavity Flow at Subsonic and Supersonic Mach Numbers." AIAA-87-1208, June 1987.

52. Srinivasan, S.; Baysal, O.; and Plentovich, E. B.: "Navier-Stokes Calculations of Transonic Flows Past Deep and Transitional Cavities." *Advances and Applications in Computational Fluid Dynamics*, O. Baysal, ed., FED-Vol. 66, *American Soc. of Mechanical Engineers*, 1988, pp. 169–179.

53. Hardin, Jay C.; and Mason, Jean P.: "Broadband Noise Generation by a Vortex Model of Cavity Flow." *AIAA Journal*, Vol. 15, No. 5, May 1977, pp. 632–637.

54. Hardin, J. C.; and Pope, D. S.: "Sound Generated by a Stenosis in a Pipe." *AIAA Journal*, Vol. 30, No. 2, February 1992, pp. 312–317.

55. Hardin, J. C.; and Pope, D. S.: "Sound Generated by Flow Over a Two-Dimensional Cavity." AIAA-93-4327, October 1993.

56. Dix, R. E.; and Bauer, R. C.: "Engineering Model Predictions of Aeroacoustic Amplitudes In A Weapons Cavity." AIAA-93-0858, January 1993.

57. Shaw, L. L.; and Shimovetz, R. M.: "Weapons Bay Acoustic Environment. Impact of Acoustic Loads on Aircraft Structures." AGARD-CP-549, September 1994.

58. Fox, Charles H. Jr.; and Huffman, Jarrett K.: *Calibration and Test Capabilities of the Langley 7- by 10-Foot High Speed Tunnel*. NASA TM X-74027, 1977.

59. Schaefer, William T., Jr.: *Characteristics of Major Active Wind Tunnels at the Langley Research Cente*r. NASA TMX-1130, 1965.

60. Braslow, Albert L.; Hicks, Raymond M.; and Harris, Roy V., Jr.: *Use of Grit-Type Boundary Layer-Transition Trips on Wind-Tunnel Models*. NASA TN D-3579, 1966.

61. Braslow, Albert L.; and Knox, Eugene C.: *Simplified Method for Determination of Critical Height of Distributed Roughness Particles for Boundary-Layer Transition at Mach Numbers From 0 to 5*. NACA TN 4363, 1958.

62. White, Frank M.: *Viscous Fluid Flow*. McGraw-Hill, Inc., 1974, p. 493.

63. Gloss, Blair B.: *Some Aerodynamic Considerations Related to Wind-Tunnel Model Surface Definition*. NASA TM-81820, September 1980.

64. Rayle, R.E.: "Influence of Orifice Geometry on Static Pressure Measurements." ASME Paper No. 59-A-234, November–December 1959.

65. Bendat, Julius S.; and Piersol, Allan G.: *Random Data, Analysis and Measurement Procedures*. John Wiley & Sons, New York, 1986, pp. 284–286.

66. Wilcox, Floyd J., Jr.: "Use of a Colored Water Surface Flow Visualization Technique in A Supersonic Wind Tunnel to Investigate Cavity Flow Fields." *Sixth International Symposium on Flow Visualization*, Yokohama, Japan, October 5–9, 1992

67. Mendenhall, M. R.; and Nielsen, J. N.: *Effect of symmetrical vortex shedding on the longitudinal characteristics of wing-body-tail combinations*. NASA CR-2473, January 1975.

68. Hemsch, M. J.; and Luckring, J. M.: "Connection between leading-edge sweep, vortex lift, and vortex strength for delta wings." *Journal of Aircraft*, Vol. 27, No. 5, May 1990, pp. 473–475.

Table 1. Orifice locations. (See Figure 7.)

Orifice	*x*, in. ψ = 0°	*x*, in. Conf. 1 ψ = 65°	*x*, in. Conf. 2, ψ = 55°	*x*, in. Conf. 3, ψ = 45°	*x*, in. Conf. 4, ψ = 35°	*y*, in.
Orifices Forward of Cavity						
(1)[a]	−2.188	−4.6815	−3.786	−3.250	−2.877	0.000
(2)[a]	−1.688	−4.1815	−3.286	−2.750	−2.377	0.000
3	−1.188	−3.6815	−2.786	−2.250	−1.877	0.000
(4)[a]	−0.688	−3.1815	−2.286	−1.750	−1.377	0.000
Orifices on Cavity Floor Centerline						
11	0.063	covered	covered	covered	covered	0.000
(12)[a]	0.313	covered	covered	covered	covered	0.000
13	0.563	covered	covered	covered	covered	0.000
14	0.813	covered	covered	covered	0.125	0.000
(15)[a]	1.063	covered	covered	covered	0.375	0.000
16	1.313	covered	covered	0.250	0.625	0.000
17	1.563	covered	covered	0.500	0.875	0.000
(18)[a]	1.813	covered	0.215	0.750	1.125	0.000
19	2.063	covered	0.465	1.000	1.375	0.000
20	2.313	covered	0.715	1.250	1.625	0.000
21	2.563	0.069	0.965	1.500	1.875	0.000
22	2.813	0.320	1.215	1.750	2.125	0.000
(23)[a]	3.063	0.570	1.465	2.000	2.375	0.000
(24)[a]	3.313	0.820	1.715	2.250	2.625	0.000
25	3.563	1.070	1.965	2.500	2.875	0.000
26	3.813	1.320	2.215	2.750	3.125	0.000
(27)[a]	4.063	1.570	2.465	3.000	3.375	0.000
28	4.313	1.820	2.715	3.250	3.625	0.000
29	4.563	2.070	2.965	3.500	3.875	0.000
30	4.813	2.320	3.215	3.750	4.125	0.000

[a] Orifice pressure tap leaking or pinched, data not shown in Appendix A.

Table 1. Continued.

Orifice	*x*, in. ψ = 0°	*x*, in. Conf. 1 ψ = 65°	*x*, in. Conf. 2, ψ = 55°	*x*, in. Conf. 3, ψ = 45°	*x*, in. Conf. 4, ψ = 35°	*y*, in.
(31)[a]	5.063	2.570	3.465	4.000	4.375	0.000
32	5.313	2.820	3.715	4.250	4.625	0.000
33	5.563	3.070	3.965	4.500	4.875	0.000
34	5.813	3.320	4.215	4.750	5.125	0.000
35	6.063	3.570	5.032	5.000	5.375	0.000
36	6.313	3.820	4.715	5.250	5.625	0.000
37	6.563	4.070	4.965	5.500	5.875	0.000
38	6.813	4.320	5.215	5.750	6.125	0.000
39	7.063	4.570	5.465	6.000	6.375	0.000
40	7.313	4.820	5.715	6.250	6.625	0.000
41	7.563	5.070	5.965	6.500	6.875	0.000
42	7.813	5.320	6.215	6.750	7.125	0.000
43	8.063	5.570	6.465	7.000	7.375	0.000
44	8.313	5.820	6.715	7.250	7.625	0.000
45	8.563	6.070	6.965	7.500	7.875	0.000
46	8.813	6.320	7.215	7.750	8.125	0.000
47	9.063	6.570	7.465	8.000	8.375	0.000
48	9.313	covered	7.715	8.250	8.625	0.000
49	9.563	covered	7.965	8.500	8.875	0.000
50	9.813	covered	8.215	8.750	9.125	0.000
51	10.063	covered	covered	9.000	9.275	0.000
52	10.313	covered	covered	9.250	9.625	0.000
53	10.563	covered	covered	9.500	9.875	0.000
54	10.813	covered	covered	covered	10.125	0.000
55	11.063	covered	covered	covered	covered	0.000

[a] Orifice pressure tap leaking or pinched, data not shown in Appendix A.

Table 1. Continued.

Orifice	*x*, in. ψ = 0°	*x*, in. Conf. 1 ψ = 65°	*x*, in. Conf. 2, ψ = 55°	*x*, in. Conf. 3, ψ = 45°	*x*, in. Conf. 4, ψ = 35°	*y*, in.
(56)[a]	11.313	covered	covered	covered	covered	0.000
57	11.563	covered	covered	covered	covered	0.000
Orifices Left of Cavity Floor Centerline						
111	0.063	covered	covered	covered	covered	−0.625
114	0.813	covered	0.108	0.375	0.562	−0.625
117	1.563	0.410	0.858	1.125	1.312	−0.625
120	2.313	1.160	1.608	1.875	2.062	−0.625
123	3.063	1.910	2.358	2.625	2.812	−0.625
126	3.813	2.660	3.108	3.375	3.562	−0.625
129	4.563	3.410	3.858	4.125	4.312	−0.625
(132)[a]	5.313	4.160	4.608	4.875	5.062	−0.625
135	6.063	4.910	5.358	5.625	5.812	−0.625
138	6.813	5.660	6.108	6.375	6.562	−0.625
(141)[a]	7.563	6.410	6.858	7.125	7.312	−0.625
144	8.313	covered	7.608	7.875	8.062	−0.625
147	9.063	covered	covered	8.625	8.812	−0.625
150	9.813	covered	covered	9.375	9.562	−0.625
153	10.563	covered	covered	covered	covered	−0.625
156	11.313	covered	covered	covered	covered	−0.625
Orifices Right of Cavity Floor Centerline						
211	0.063	covered	covered	covered	covered	0.625

[a] Orifice pressure tap leaking or pinched, data not shown in Appendix A.

Table 1. Concluded.

Orifice	x, in. ψ = 0°	x, in. Conf. 1 ψ = 65°	x, in. Conf. 2, ψ = 55°	x, in. Conf. 3, ψ = 45°	x, in. Conf. 4, ψ = 35°	y, in.
(214)[a]	0.813	covered	covered	covered	covered	0.625
217	1.563	covered	covered	covered	0.437	0.625
220	2.313	covered	covered	0.625	1.187	0.625
(223)[a]	3.063	covered	0.572	1.375	1.937	0.625
226	3.813	covered	1.322	2.125	2.687	0.625
229	4.563	0.729	2.072	2.875	3.437	0.625
232	5.313	1.479	2.822	3.625	4.187	0.625
235	6.063	2.229	3.572	4.375	4.937	0.625
(238)[a]	6.813	2.979	4.322	5.125	5.687	0.625
(241)[a]	7.563	3.729	5.072	5.875	6.437	0.625
244	8.313	4.479	5.822	6.625	7.187	0.625
(247)[a]	9.063	5.229	6.572	7.375	7.937	0.625
250	9.813	5.979	7.322	8.125	8.687	0.625
253	10.563	covered	8.072	8.875	9.437	0.625
(256)[a]	11.313	covered	covered	covered	10.187	0.625

[a] Orifice pressure tap leaking or pinched, data not shown in Appendix A.

Table 2. Transducer locations.

Transducer	x, in. $\psi = 0^o$	x, in. Conf. 1 $\psi = 65^o$	x, in. Conf. 2, $\psi = 55^o$	x, in. Conf. 3, $\psi = 45^o$	x, in. Conf. 4, $\psi = 35^o$	y, in.
1	2.313	0.491	1.162	1.563	1.844	–0.313
2	5.813	3.991	4.662	5.063	5.344	–0.313
3	0.813	covered	covered	covered	0.344	–0.313

Table 3. Estimated boundary layer thickness (range $Re_\infty = 1 - 4 \times 10^6$ per foot).

Configuration	Sweep	x_{max} , in.	δ_{ave}, in.	δ_{max}, in.
1	65º	15.76	0.30 − 0.23	0.35 − 0.26
2	55º	13.97	0.28 − 0.22	0.32 − 0.24
3	45º	12.90	0.27 − 0.21	0.30 − 0.22
4	35º	12.15	0.27 − 0.20	0.28 − 0.21
rectangular	0º	10.59	0.25 − 0.19	0.25 − 0.19

Table 4. Accuracy of static-pressure measurements.

M_∞	C_p
0.20	±0.020
0.40	±0.005
0.60	±0.003
0.80	±0.002

Table 5. Nondimensional frequencies from modified Rossiter Equation [24].

M_∞	Predicted Nondimensional Frequencies ($f_m \frac{l}{U_\infty}$), for –				
	Mode 1	Mode 2	Mode 3	Mode 4	Mode 5
0.2	0.384	0.895	1.407	1.918	2.429
0.4	0.347	0.810	1.273	1.736	2.198
0.6	0.316	0.737	1.158	1.579	2.000
0.8	0.288	0.672	1.056	1.440	1.824

Table 6. Observed nondimensional resonant frequencies in rectangular cavities.

l/h	M_∞	Observed Nondimensional Resonant Frequencies ($f\frac{l}{U_\infty}$) in Rectangular Cavities, for				
		Mode 1	Mode 2	Mode 3	Mode 4	Mode 5
4.0	0.4		0.800			
5.0	0.4		0.790	1.222	1.654	
6.0	0.4			1.255		
7.0	0.4			1.226	1.663	
8.0	0.4			1.164		
3.0	0.6		0.730			
4.0	0.6		0.729			
5.0	0.6		0.711	1.127		
6.0	0.6	0.286	0.683			
7.0	0.6			1.071	1.501	
8.0	0.6			1.064	1.463	
9.0	0.6				1.466	
10.0	0.6		0.614		1.398	
3.0	0.8	0.300	0.703			
4.0	0.8	0.304	0.693			
5.0	0.8	0.284	0.684	1.067		
6.0	0.8	0.281	0.660	1.063		
7.0	0.8	0.250	0.646	1.051	1.452	
8.0	0.8		0.612	1.019		1.823
9.0	0.8		0.620	0.994	1.419	1.850
10.0	0.8		0.578		1.384	
11.0	0.8		0.572			

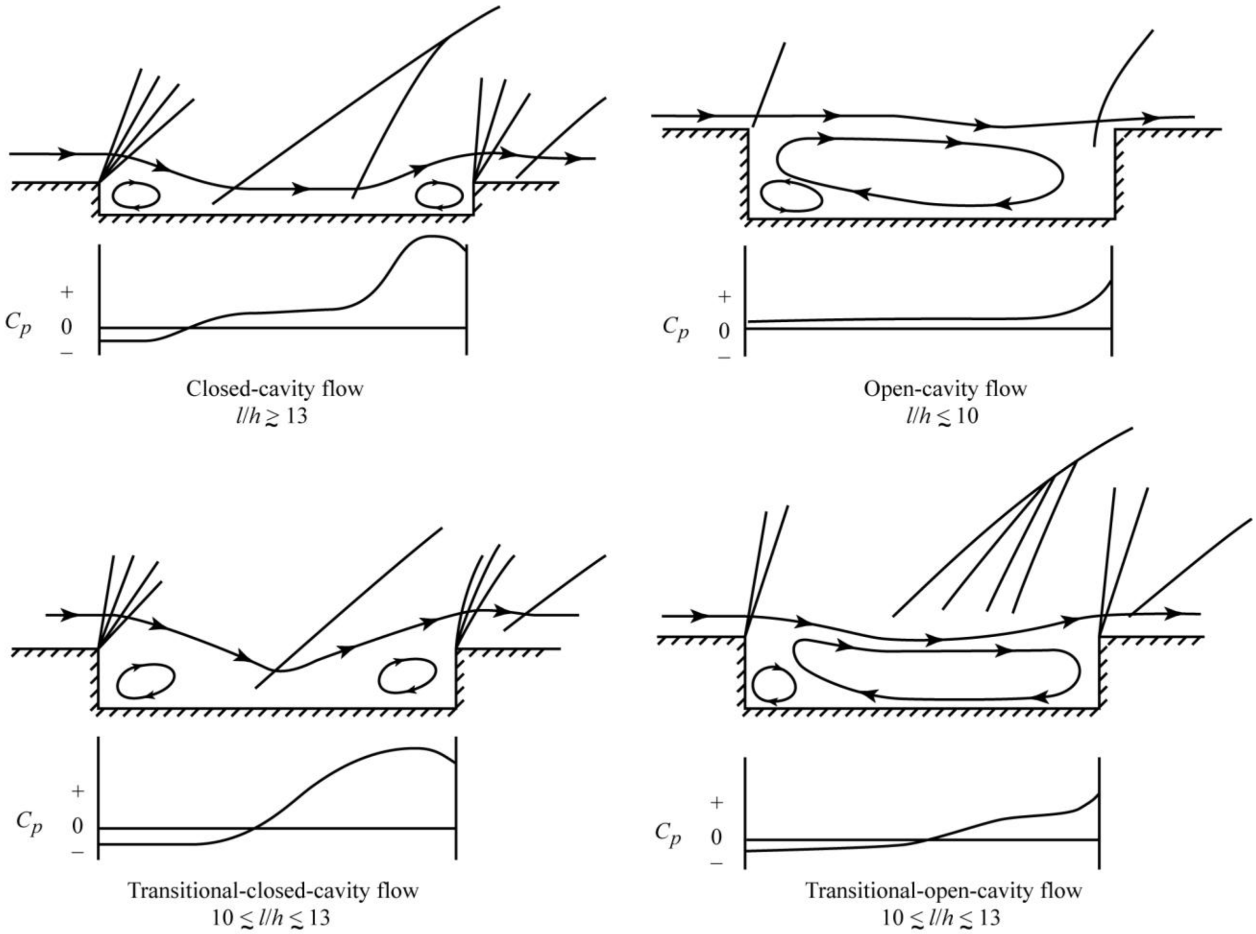

Figure 1. Typical cavity flow field sketches at supersonic speeds (adapted from References 38 and 46).

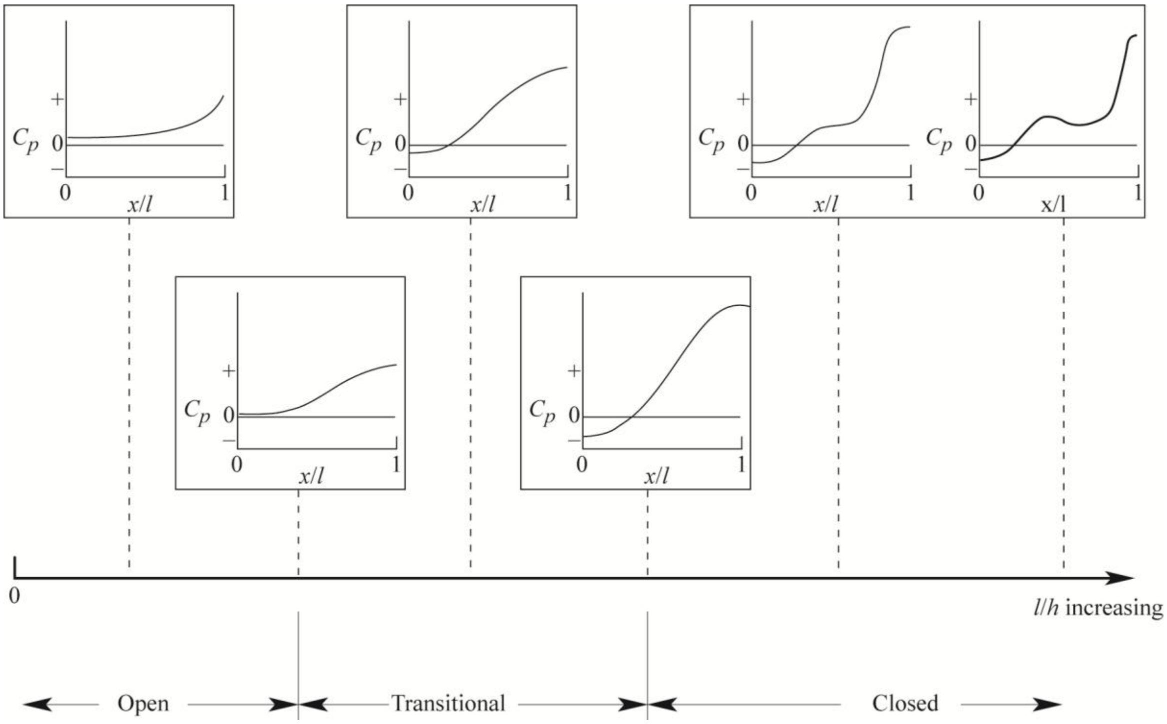

Figure 2. Representative cavity floor pressure distributions for flow field types at subsonic and transonic speeds [17].

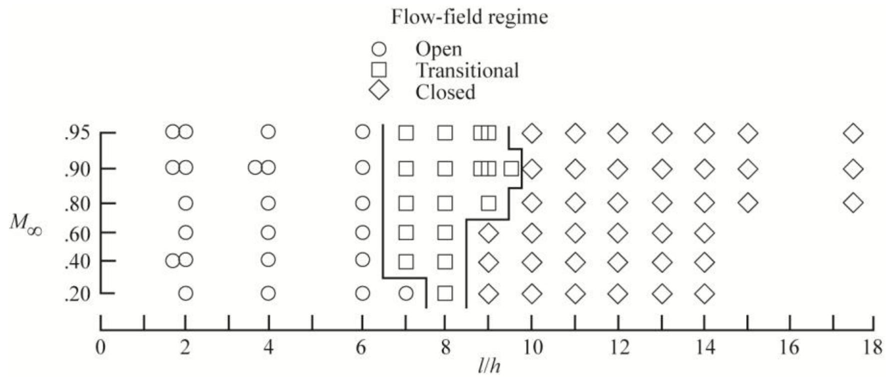

(a) w/h = 1.

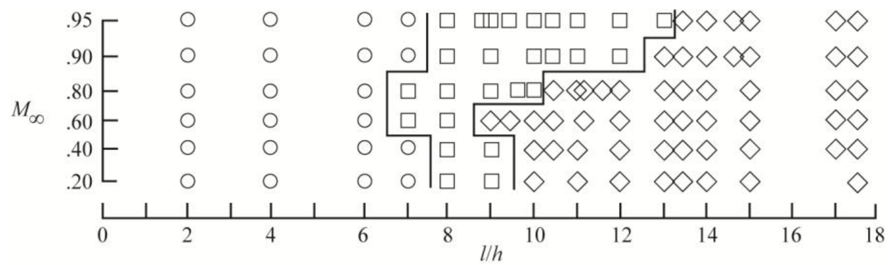

(b) w/h = 4.

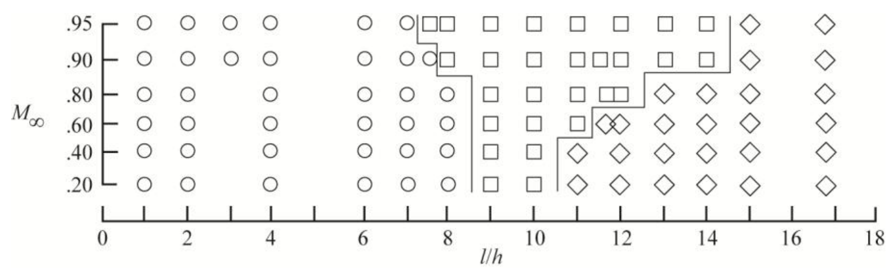

(c) w/h = 8.

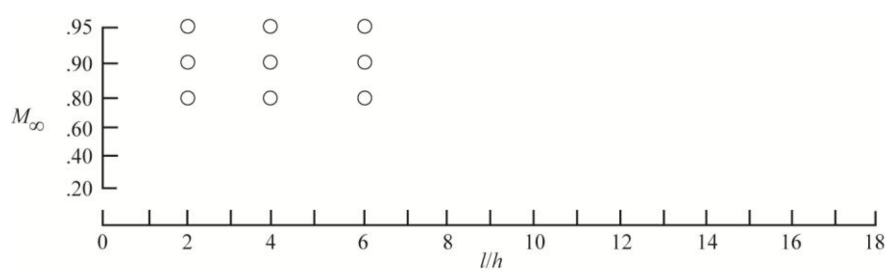

(d) w/h = 16.

Figure 3. Flow fields for rectangular cavities for a range of l/h and M_∞ [17].

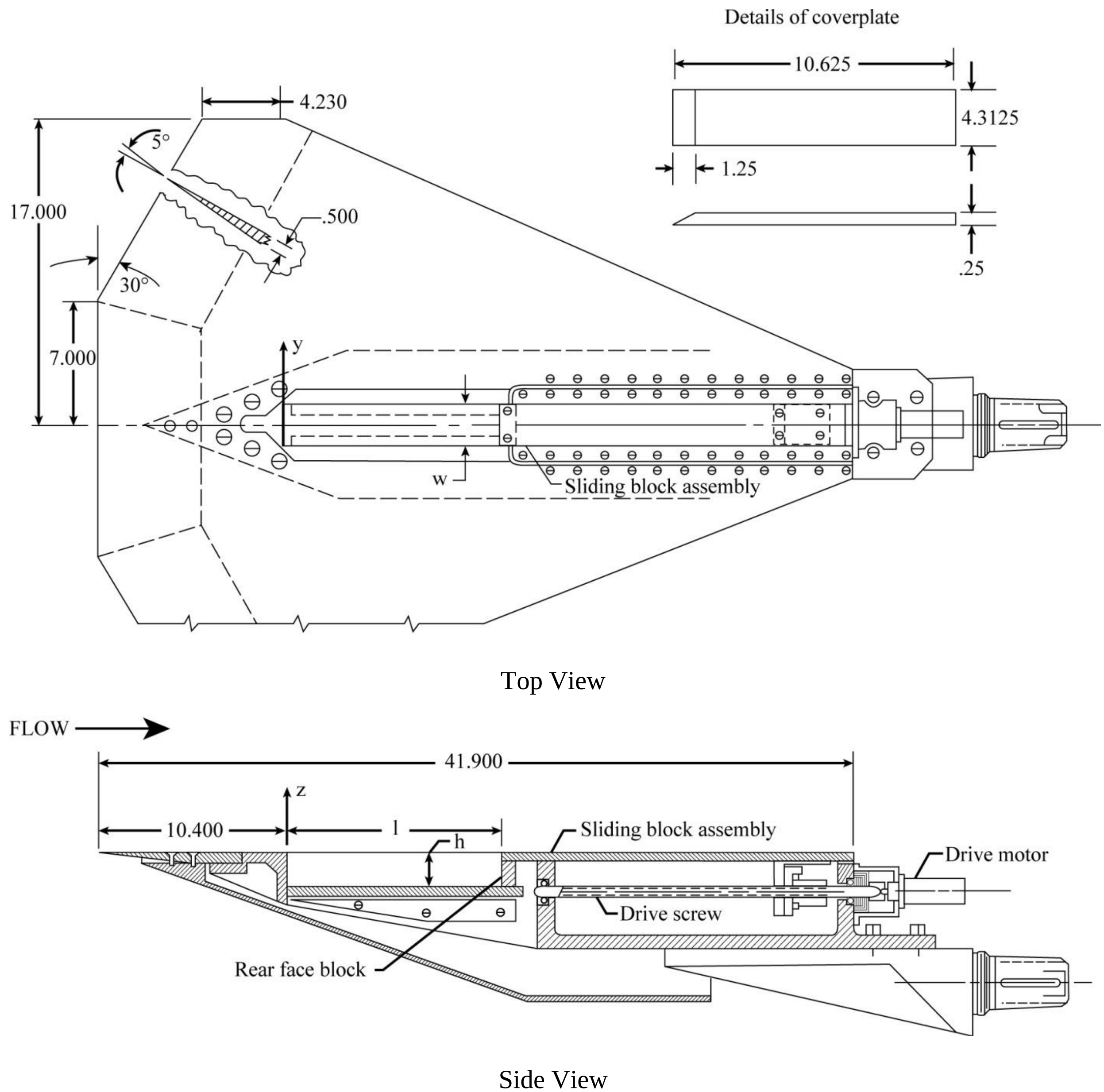

(a) Drawing. Linear dimensions are in inches.

Figure 4. Cavity model assembly.

(b) Photograph of model mounted in the LaRC 7 × 10-foot HST (92-08369).

Figure 4. Concluded.

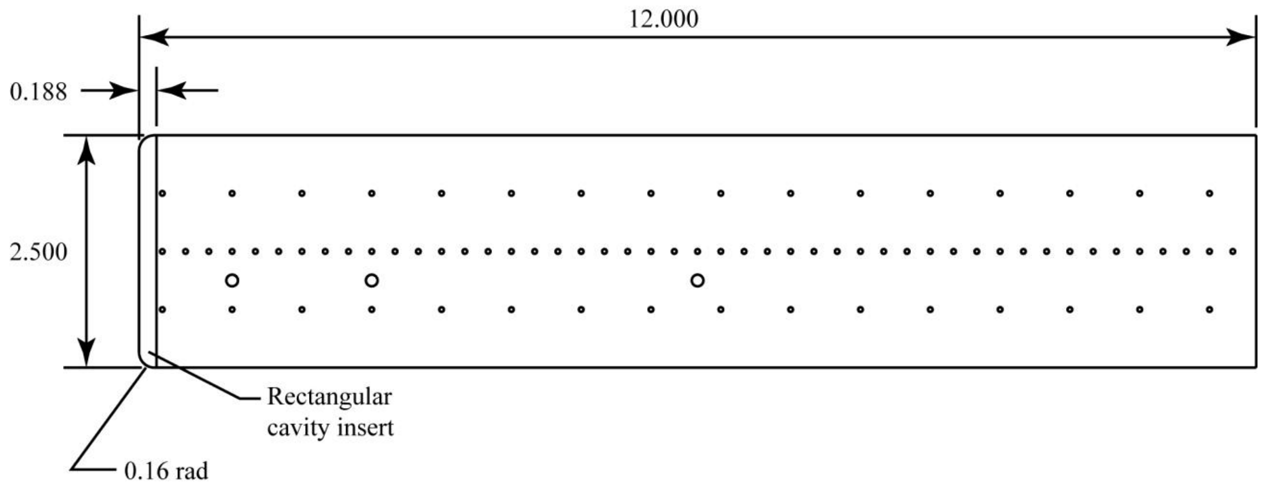

Top View

Figure 5. Rectangular cavity insert to square cavity leading-edge corners. Linear dimensions are in inches.

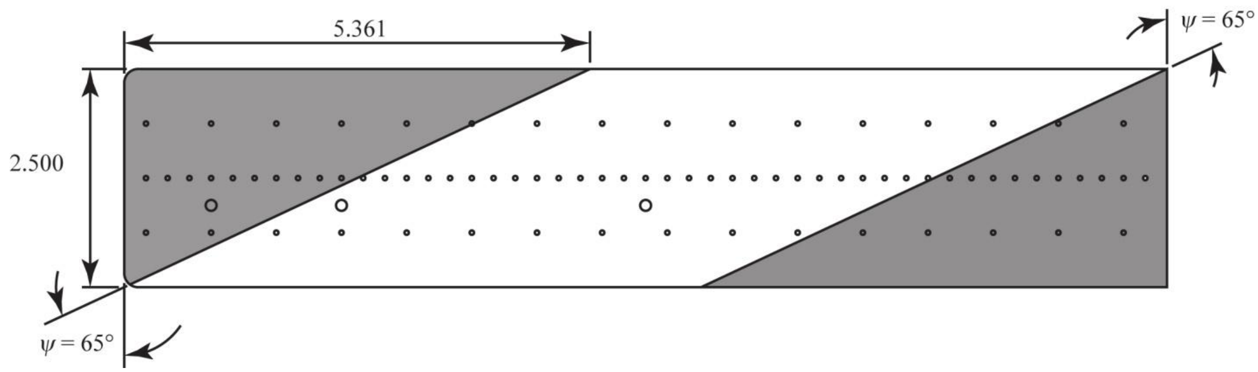

(a) $\psi = 65°$ (Config. 1).

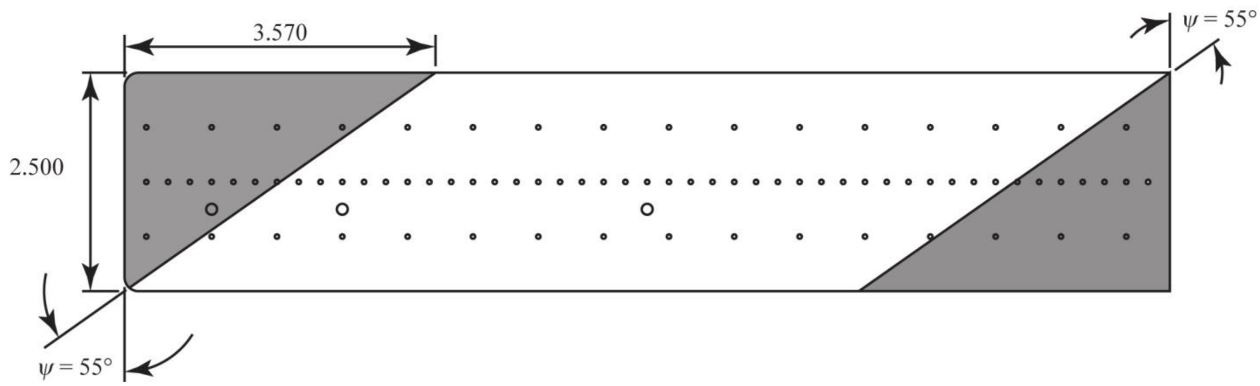

(b) $\psi = 55°$ (Config. 2).

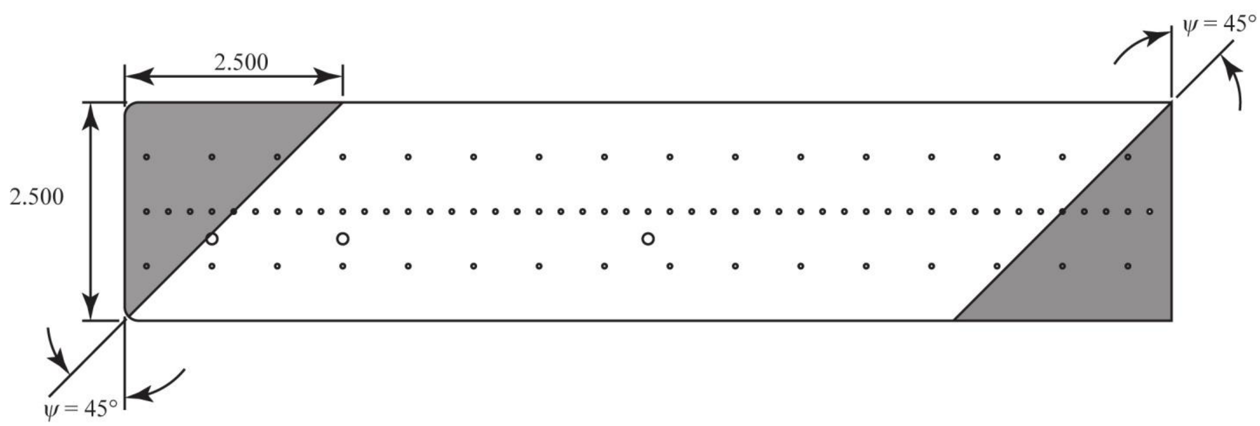

(c) $\psi = 45°$ (Config. 3).

Figure 6. Cavity block inserts. Linear dimensions are in inches.

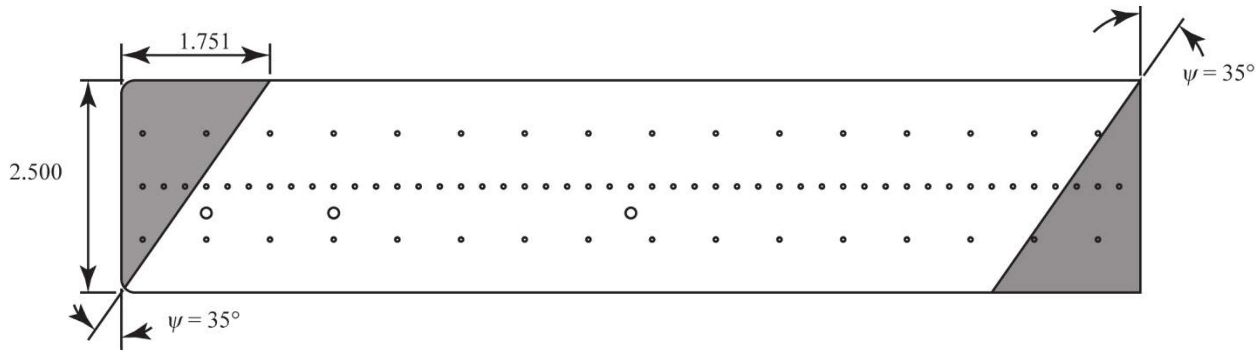

(d) ψ = 35° (Config. 4).

Figure 6. Concluded.

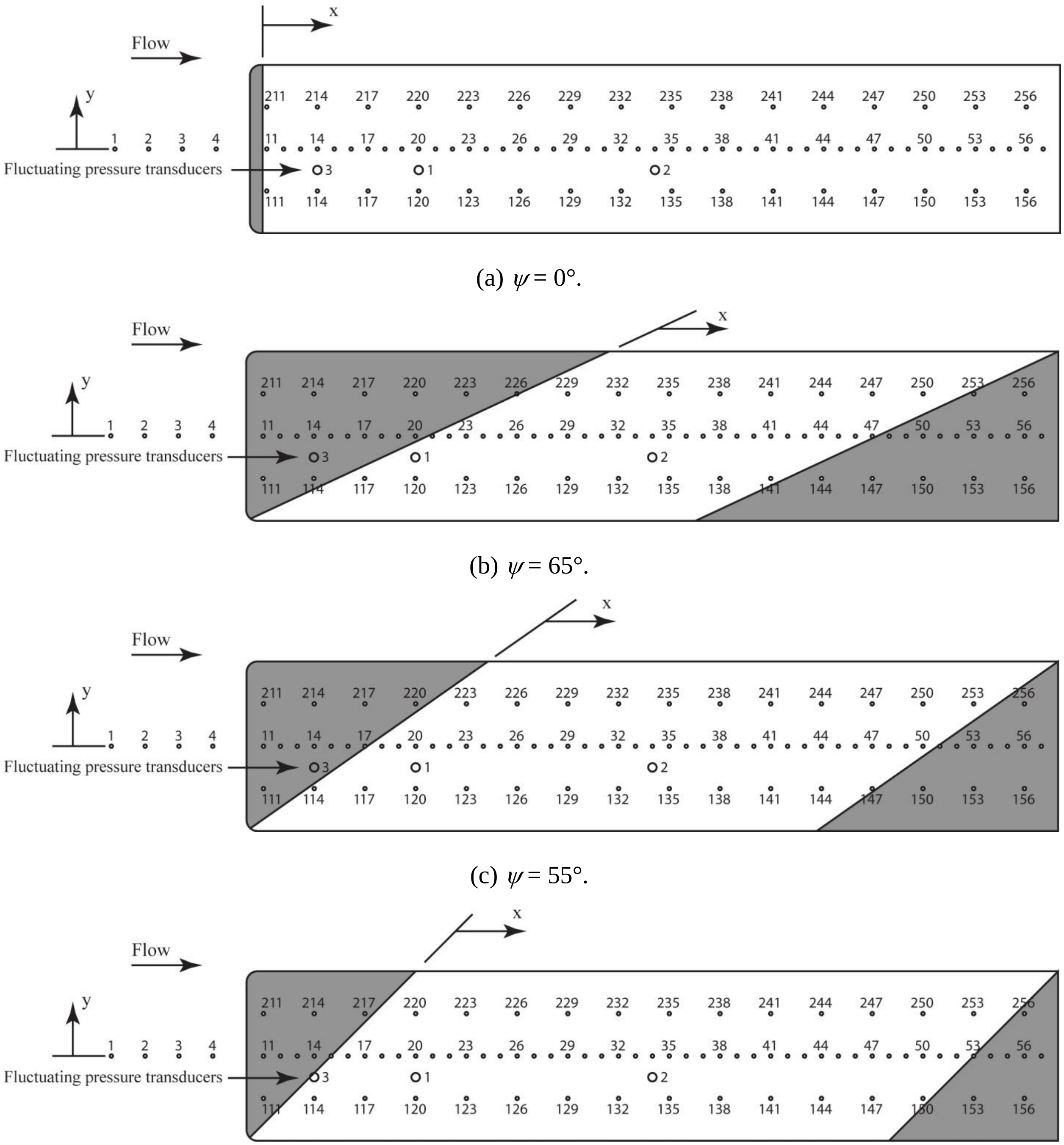

(a) $\psi = 0°$.

(b) $\psi = 65°$.

(c) $\psi = 55°$.

(d) $\psi = 45°$.

Figure 7. Layout of static pressure orifices and fluctuating pressure transducers. Coordinate locations are presented in Tables 1 and 2.

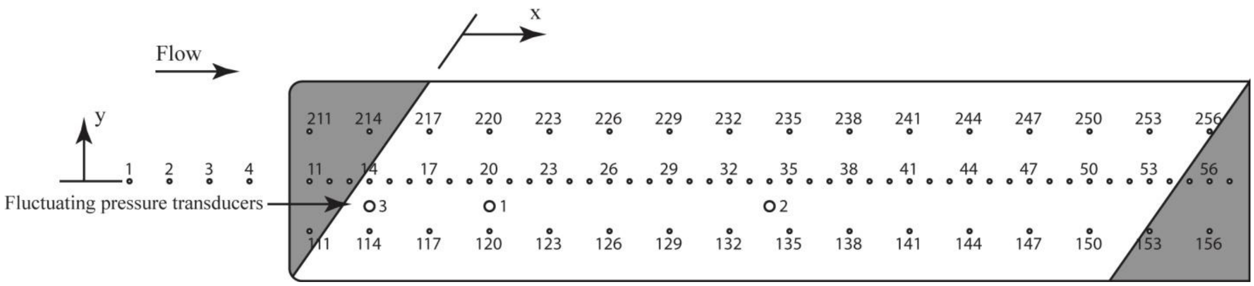

(e) $\psi = 35°$.

Figure 7. Concluded.

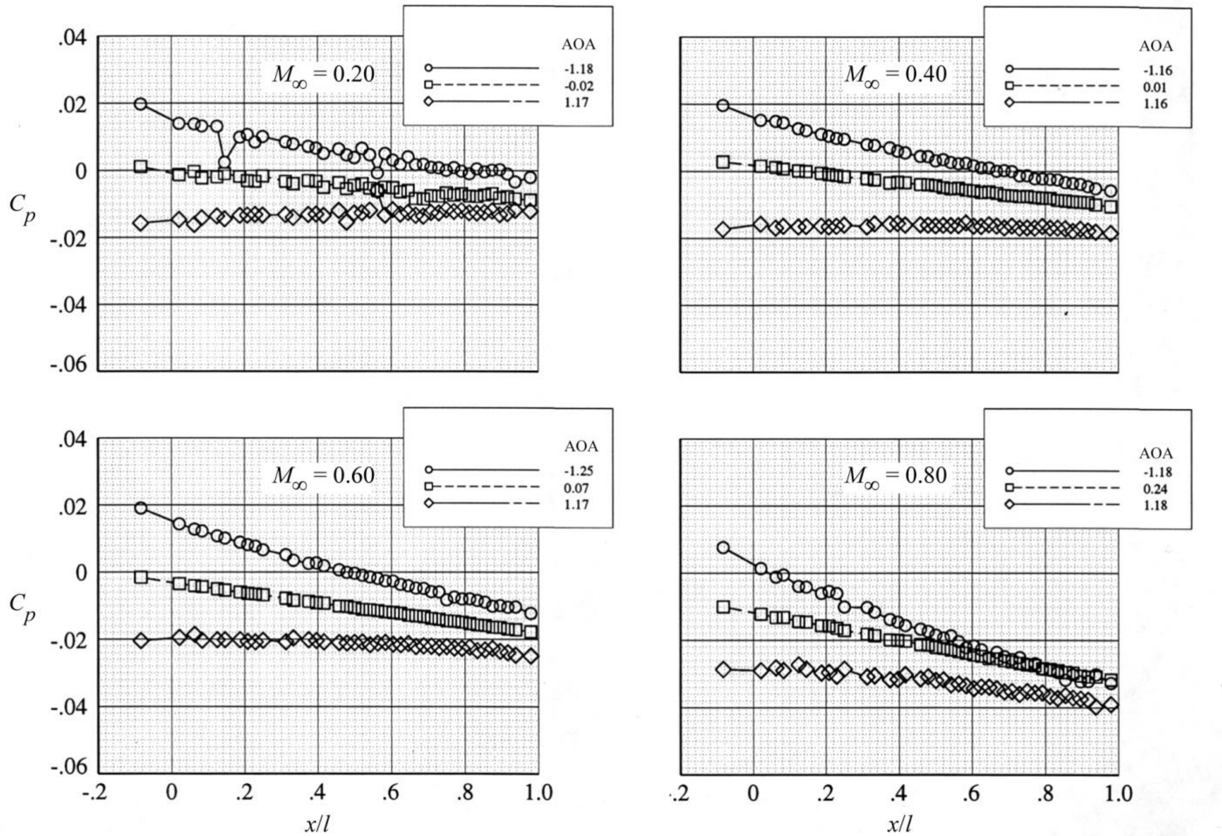

Figure 8. Effect of AOA on flat-plate pressure distributions.

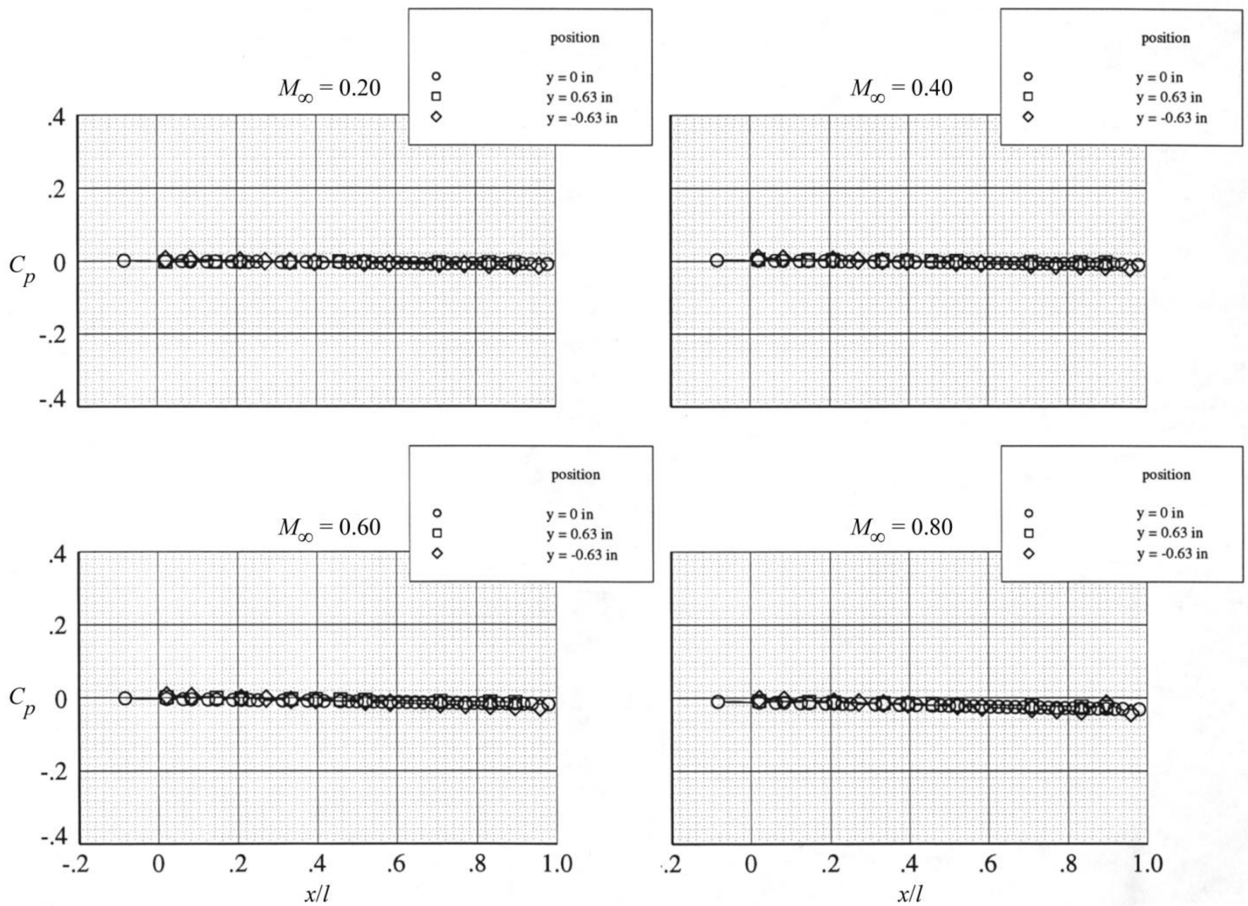

Figure 9. Static-pressure measurements at three lateral positions on the flat plate, AOA = 0º.

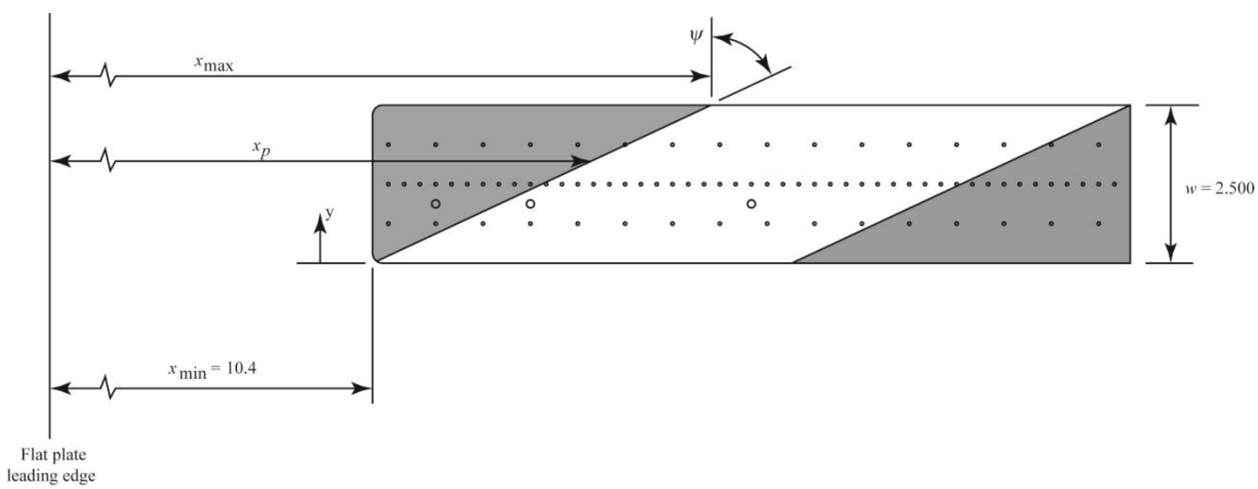

Figure 10. Nomenclature used for calculating average boundary layer height approaching swept leading edge cavities.

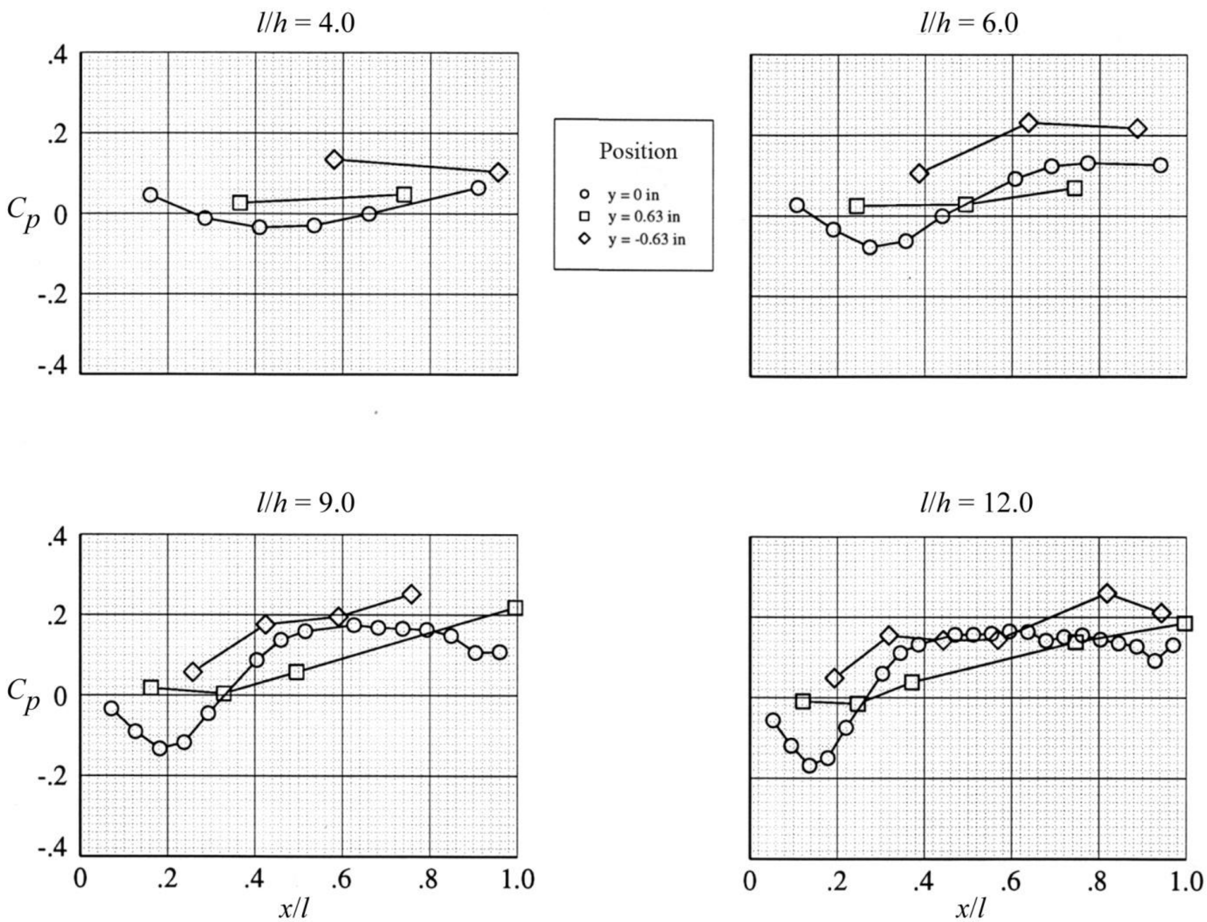

(a) $M_\infty = 0.2$.

Figure 11. Comparison of longitudinal pressure distributions along cavity floor at three lateral positions. Configuration 1, $\psi = 65°$.

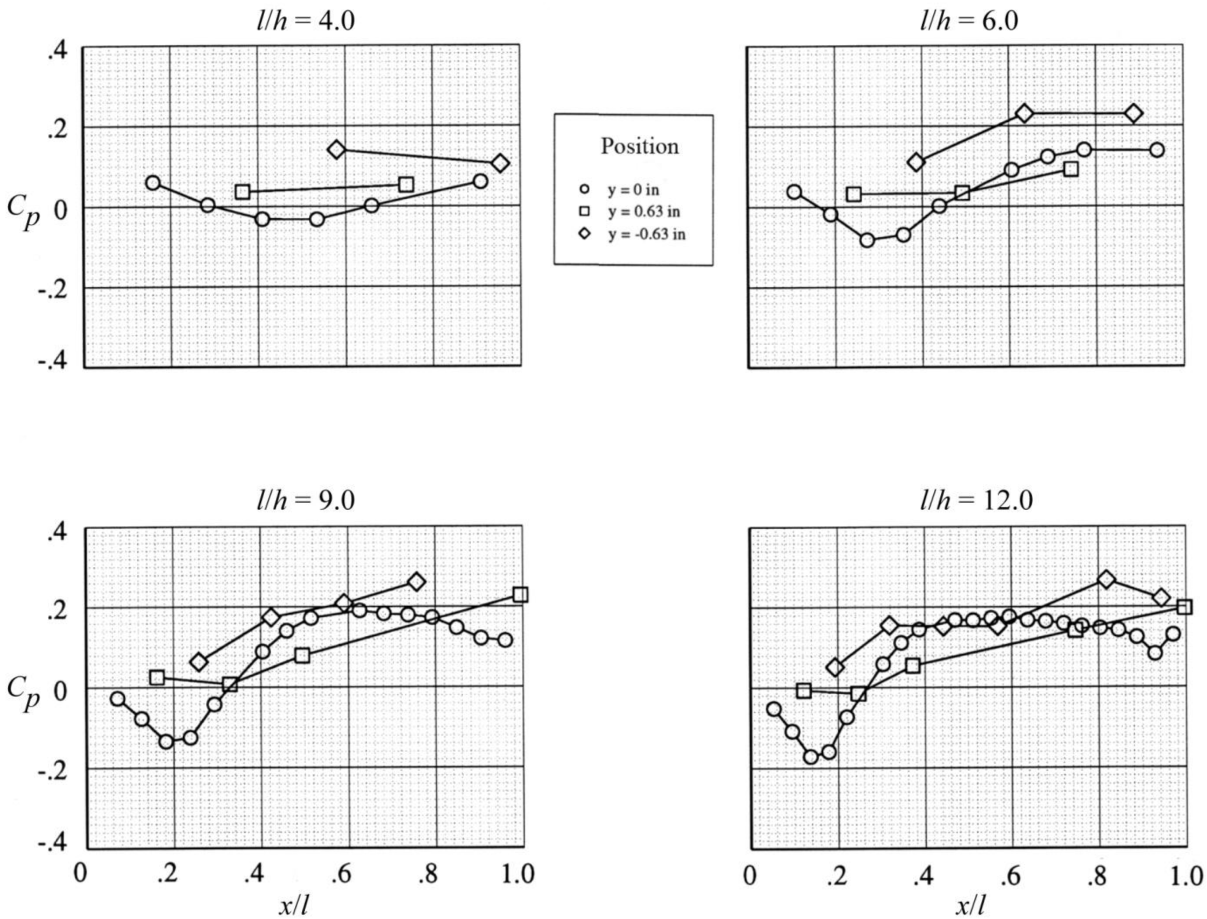

(b) $M_\infty = 0.4$.

Figure 11. Continued.

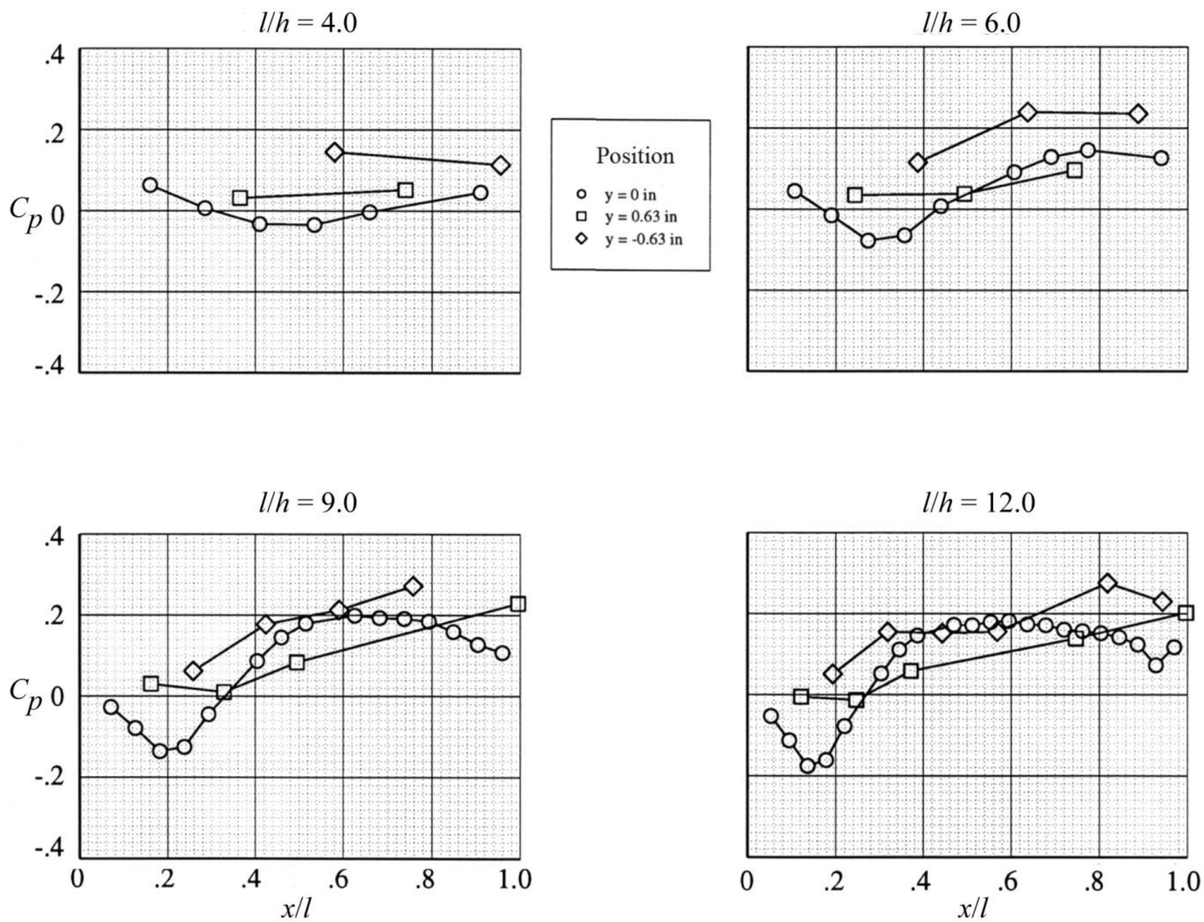

(c) $M_{\infty} = 0.6$.

Figure 11. Continued.

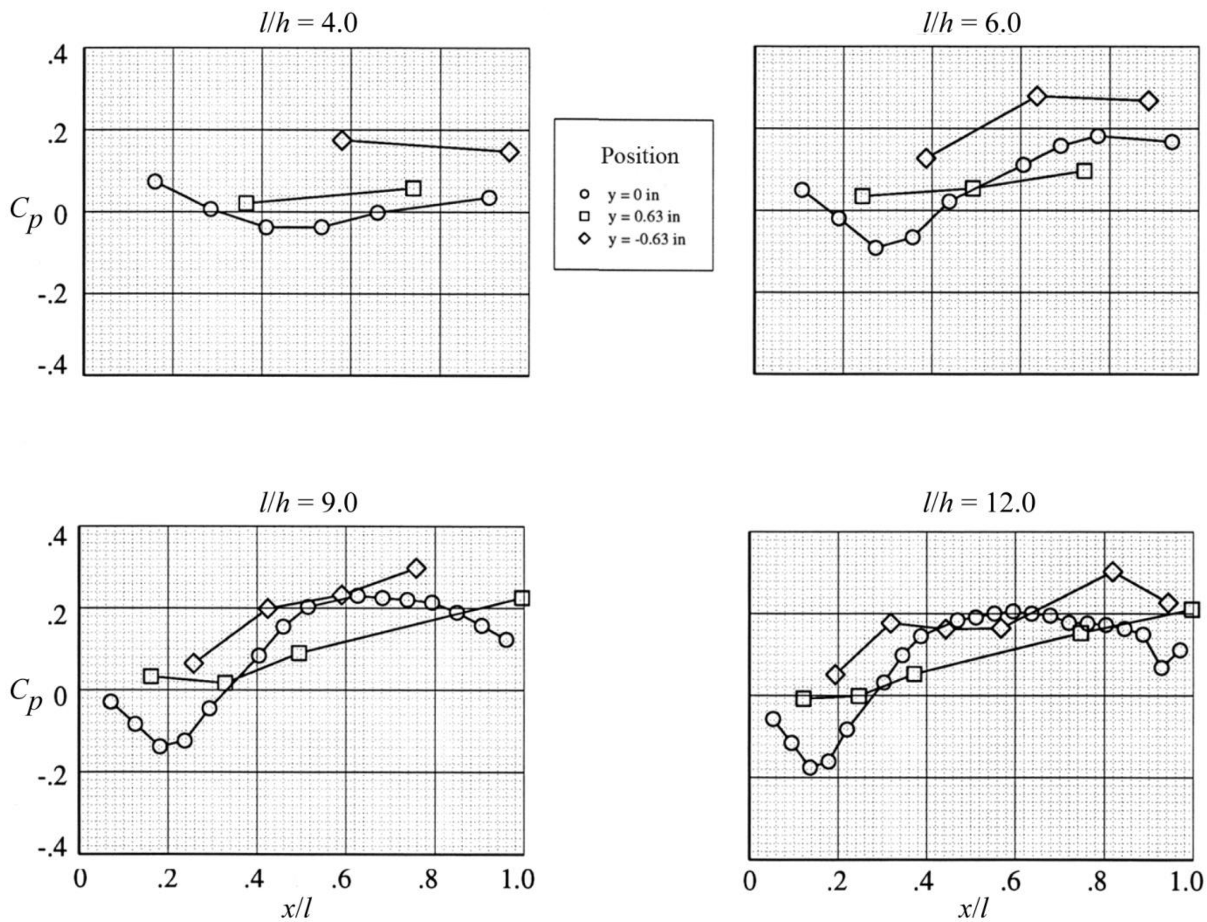

(d) $M_\infty = 0.8$.

Figure 11. Concluded.

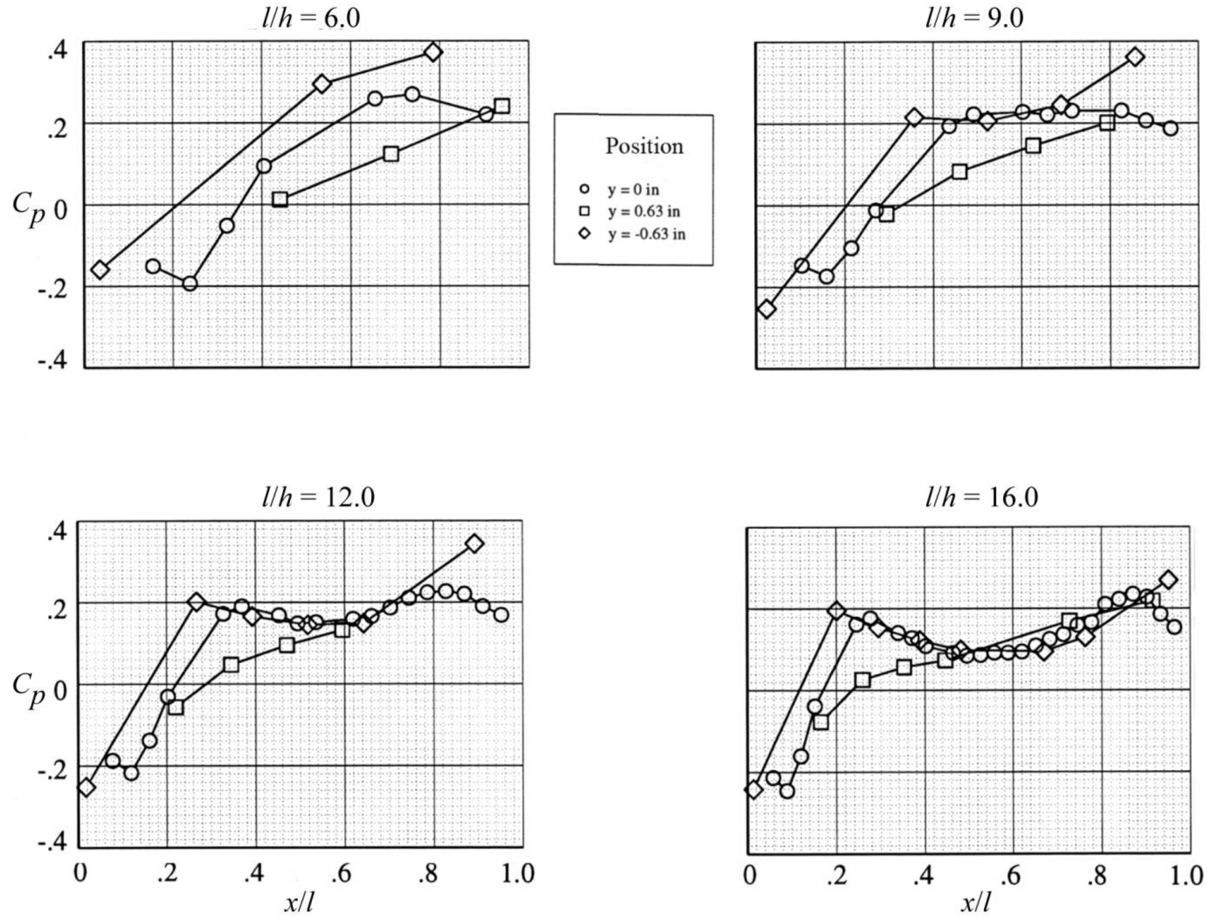

(a) $M_\infty = 0.2$.

Figure 12. Comparison of longitudinal pressure distributions along cavity floor at three lateral positions. Configuration 2, $\psi = 55°$.

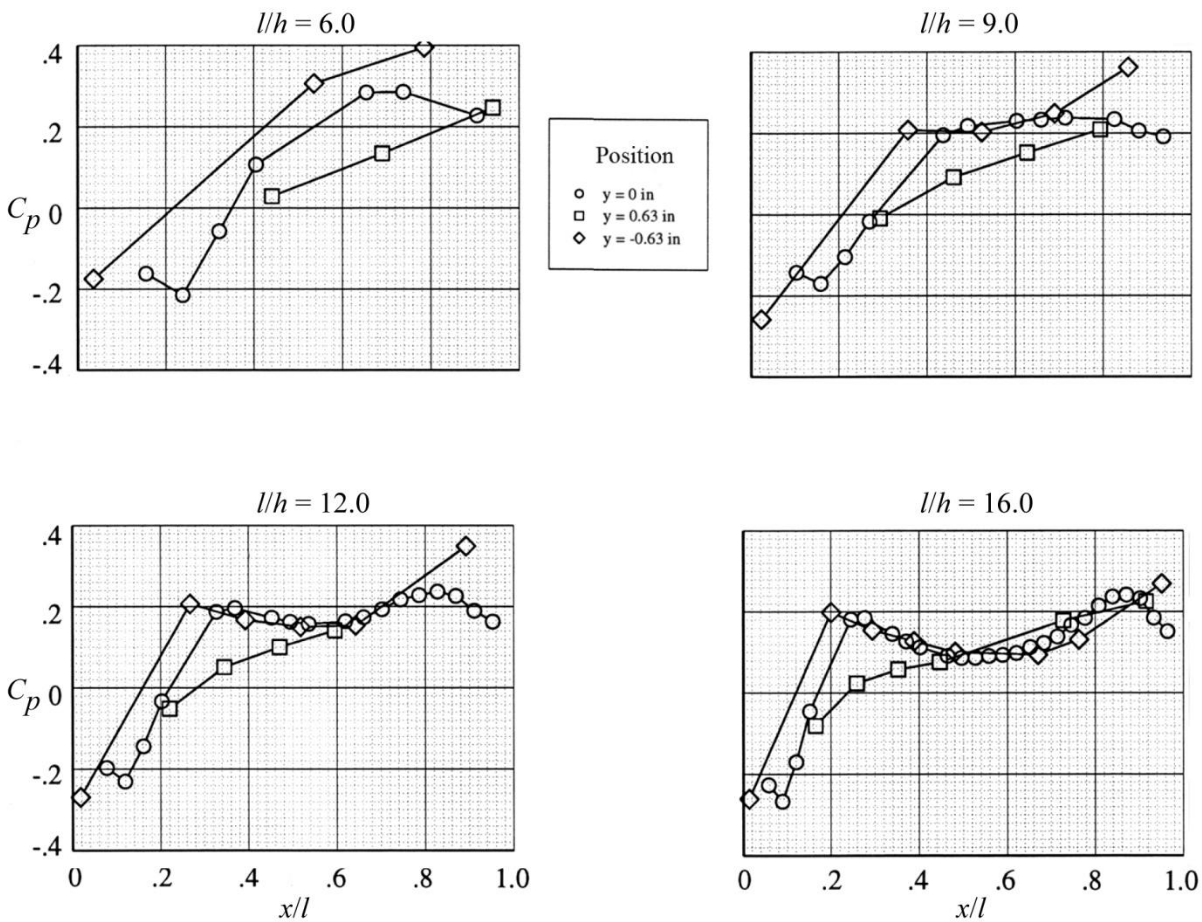

(b) $M_\infty = 0.4$.

Figure 12. Continued.

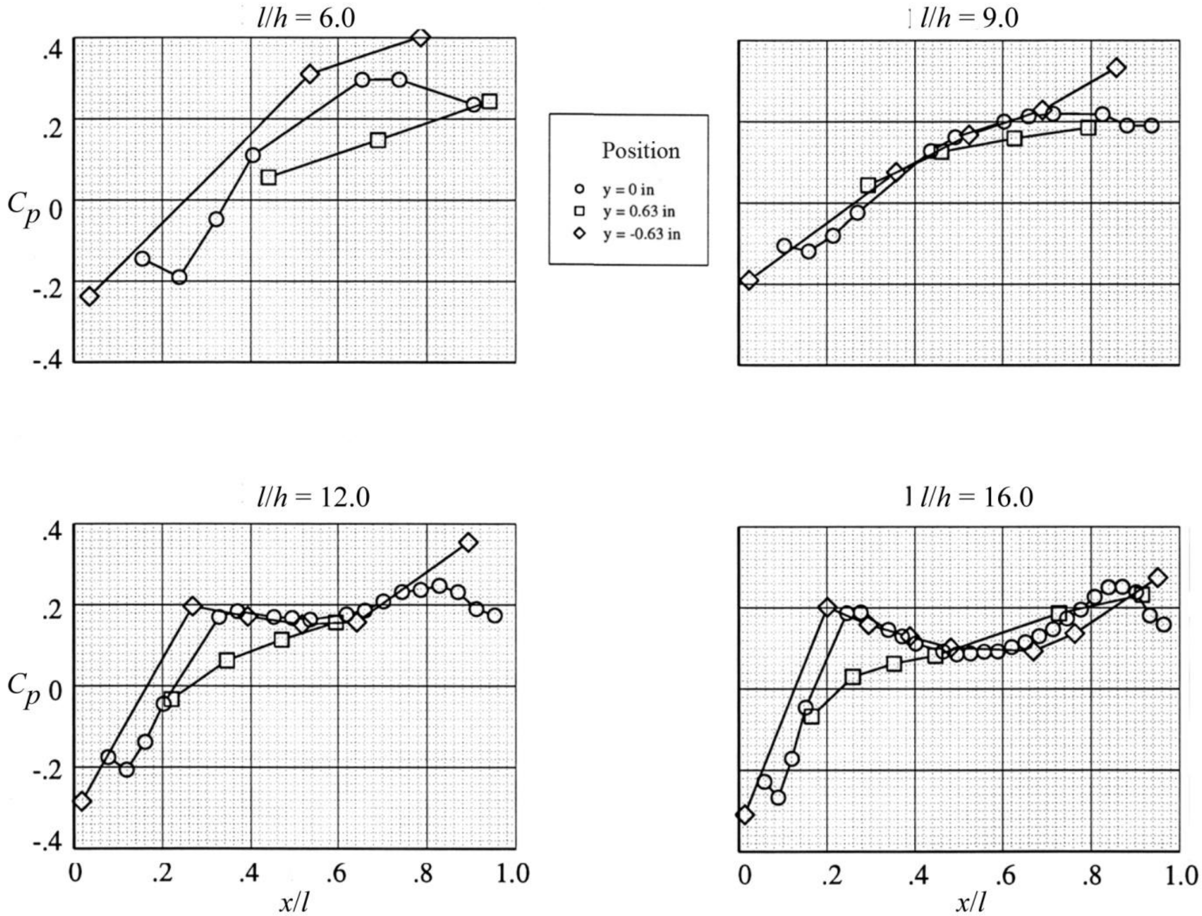

(c) $M_\infty = 0.6$.

Figure 12. Continued.

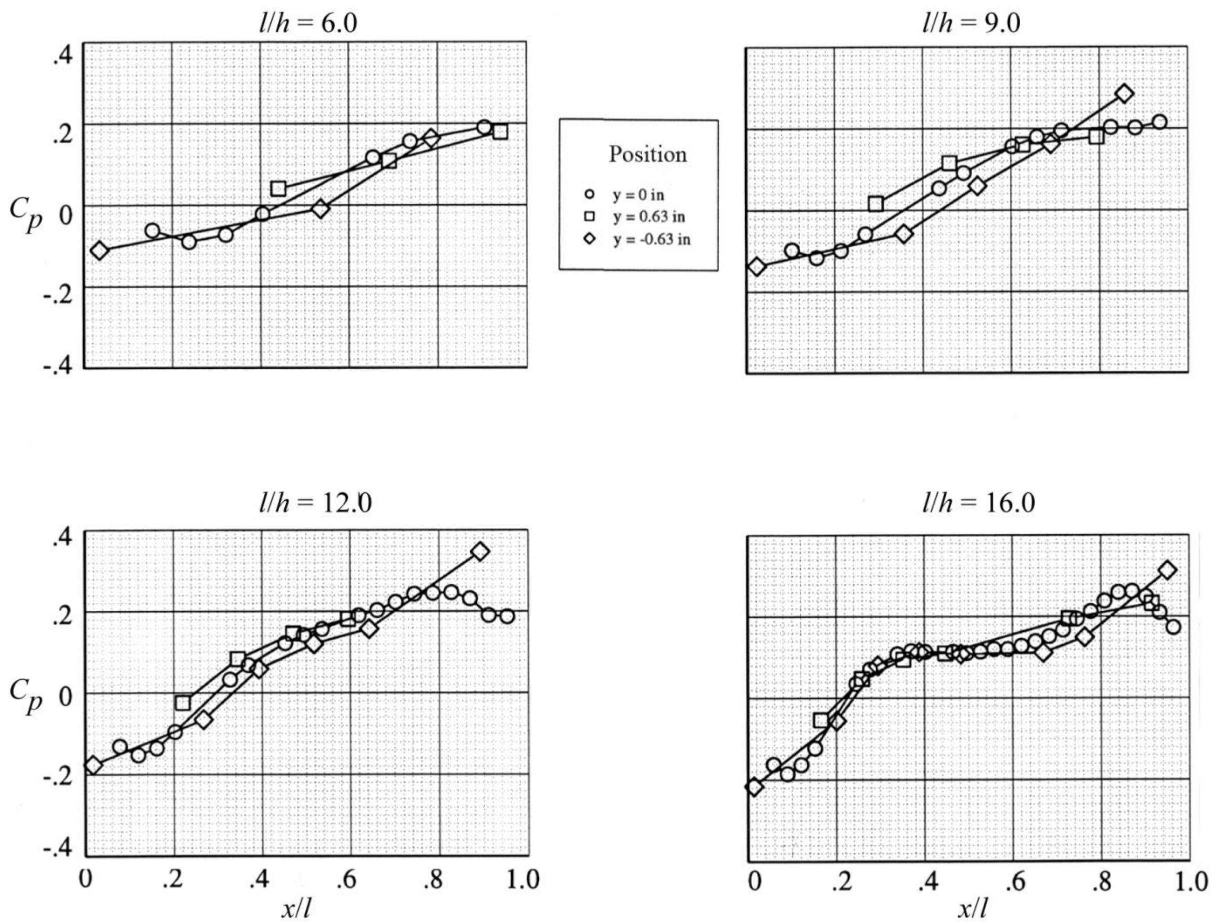

(d) $M_\infty = 0.8$.

Figure 12. Concluded.

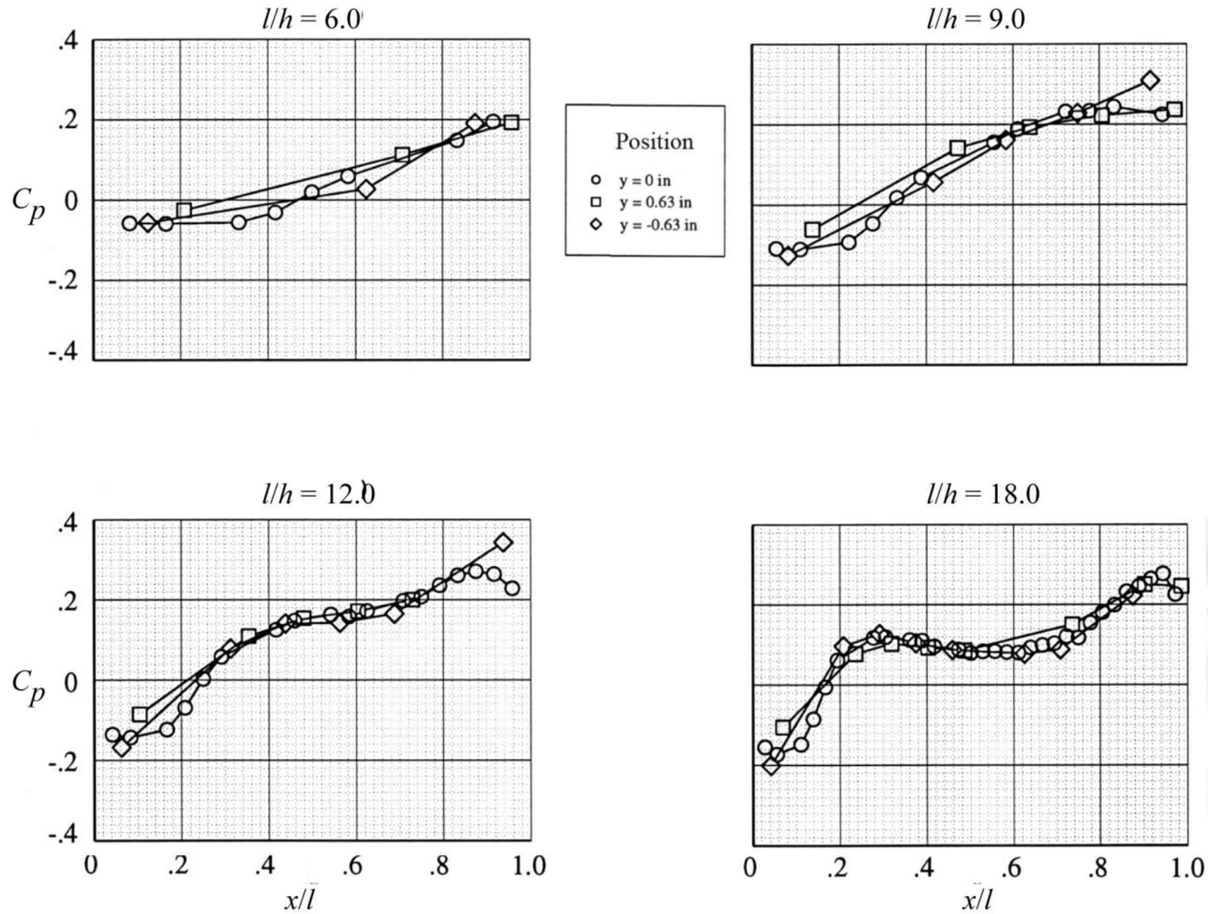

(a) $M_\infty = 0.2$.

Figure 13. Comparison of longitudinal pressure distribution along cavity floor at three lateral positions. Configuration 3, $\psi = 45°$.

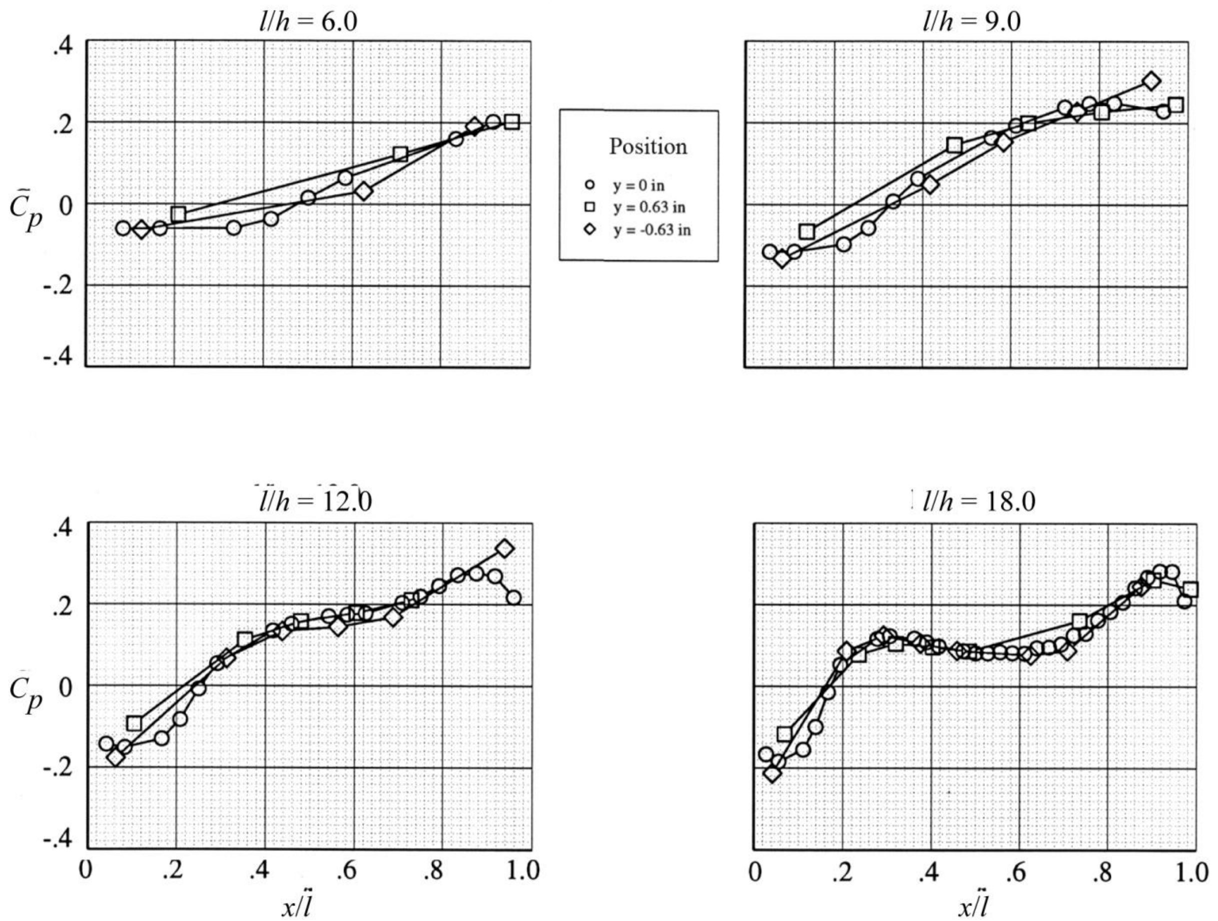

(b) $M_\infty = 0.4$.

Figure 13. Continued.

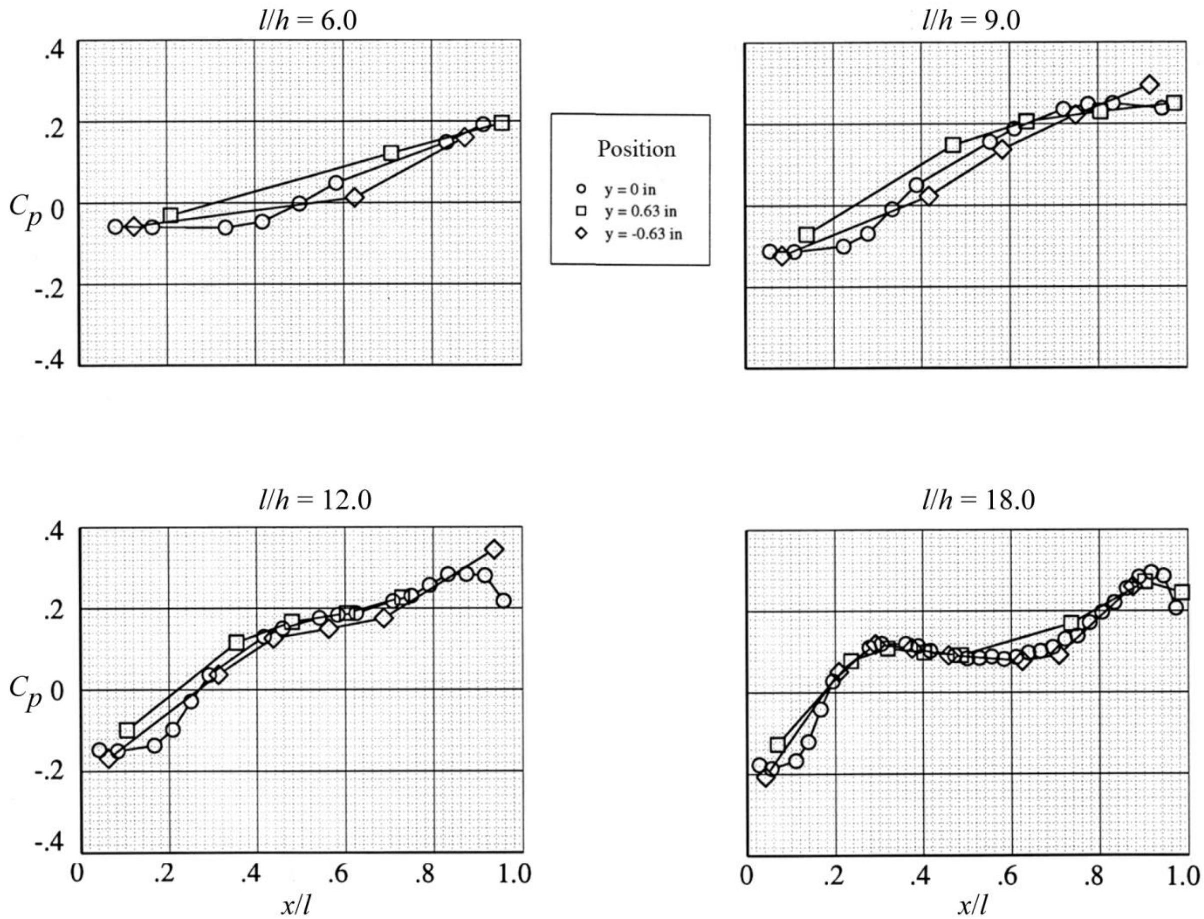

(c) $M_\infty = 0.6$.

Figure 13. Continued.

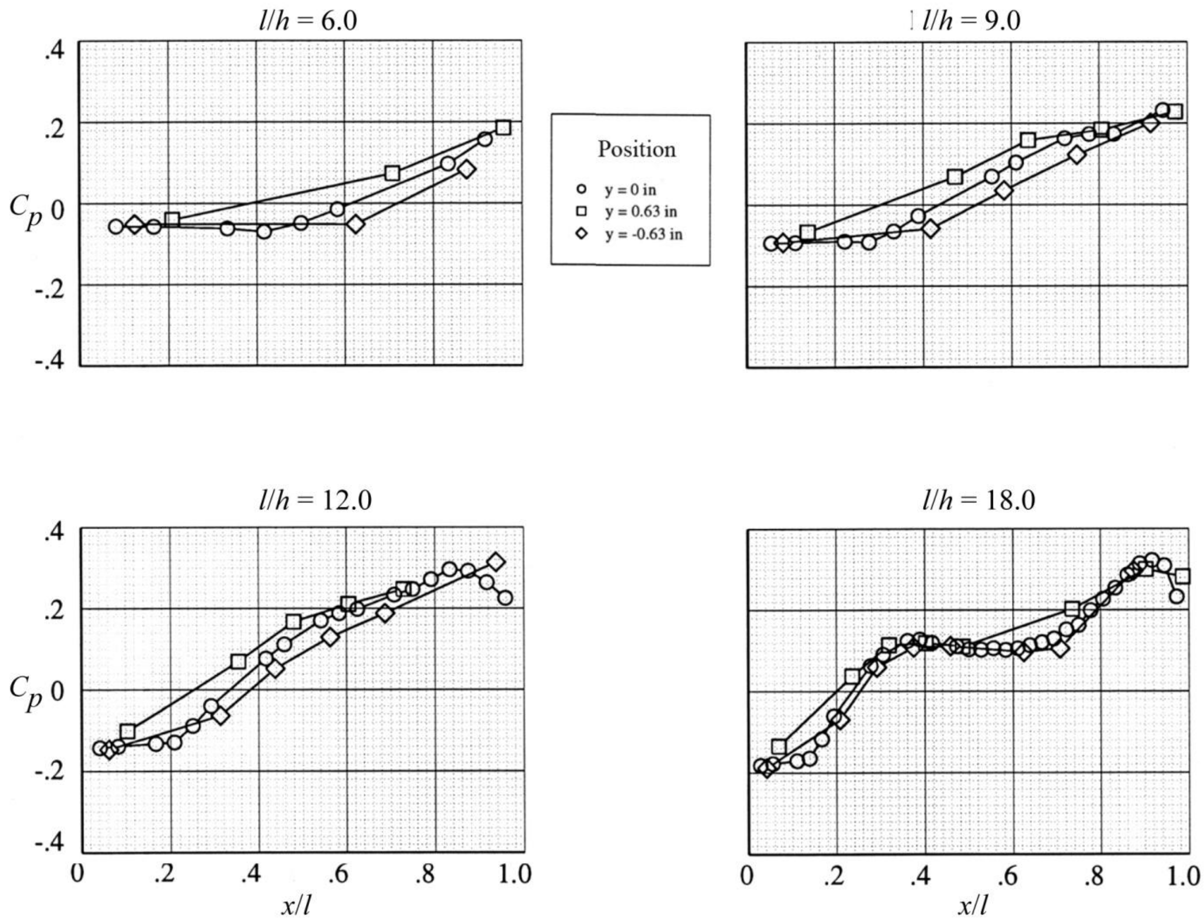

(d) $M_\infty = 0.8$.

Figure 13. Concluded.

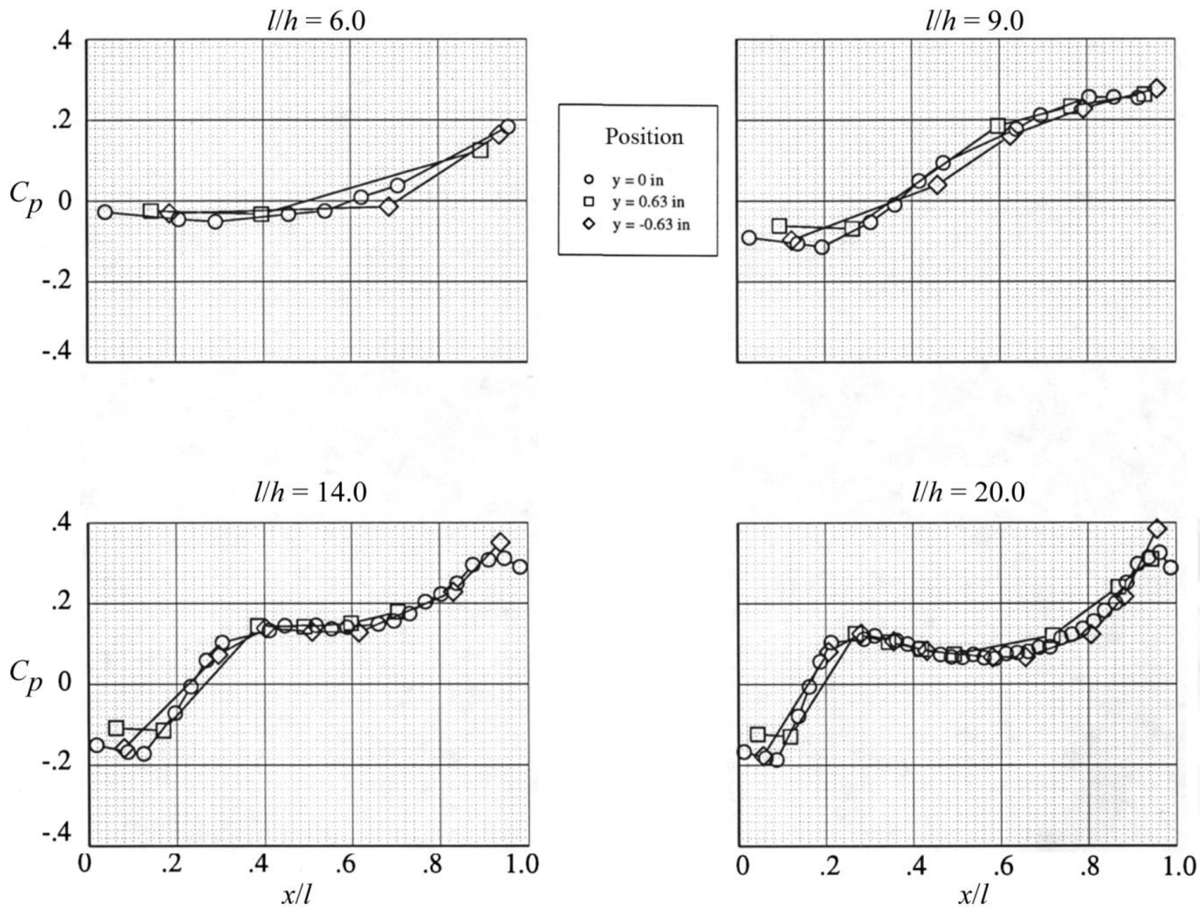

(a) $M_{\infty} = 0.2$.

Figure 14. Comparison of longitudinal pressure distribution along cavity floor at three lateral positions. Configuration 4, $\psi = 35°$.

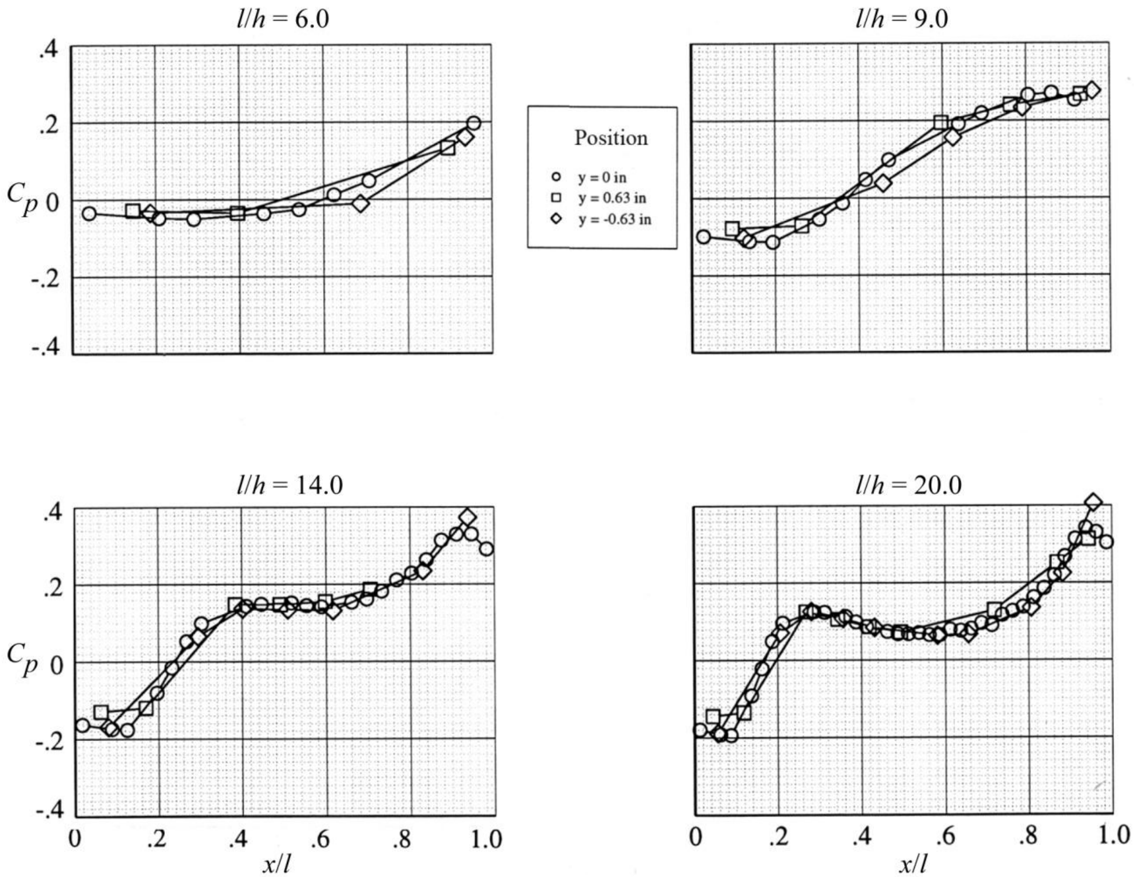

(b) $M_\infty = 0.4$.

Figure 14. Continued.

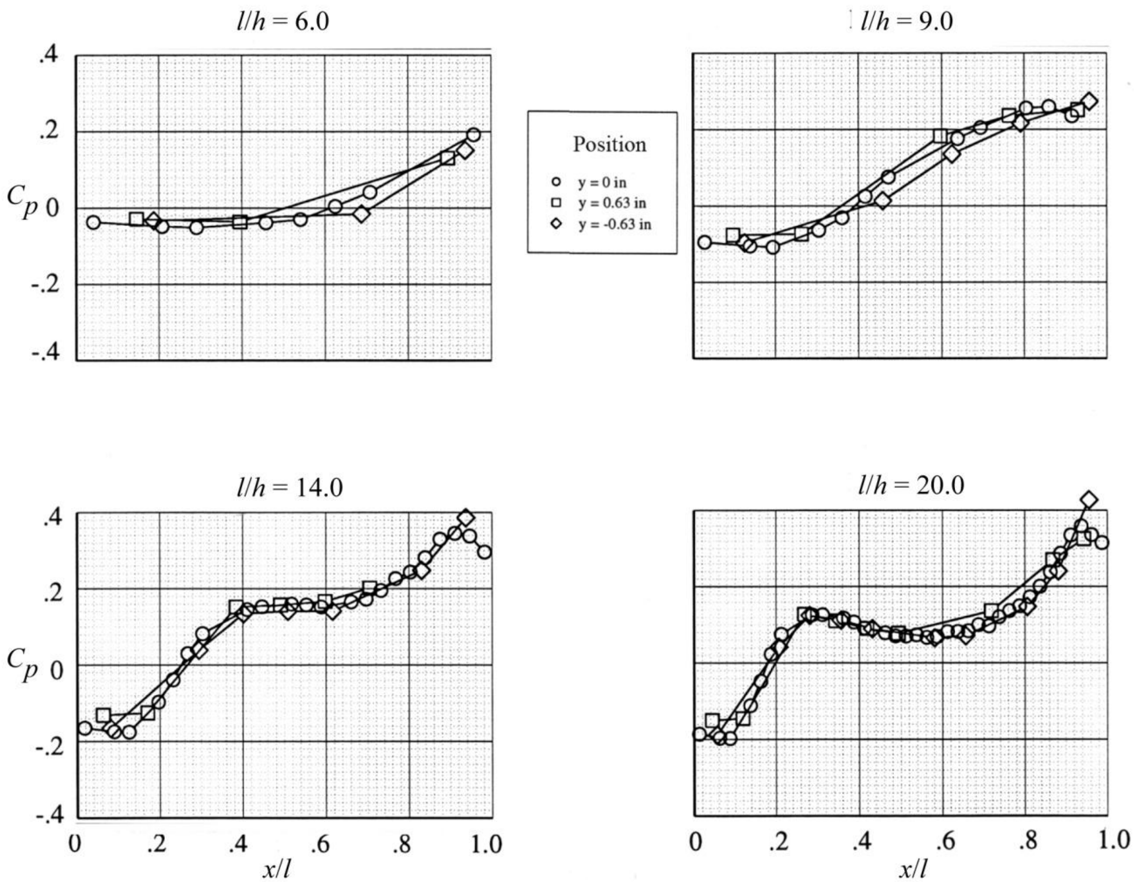

(c) $M_\infty = 0.6$.

Figure 14. Continued.

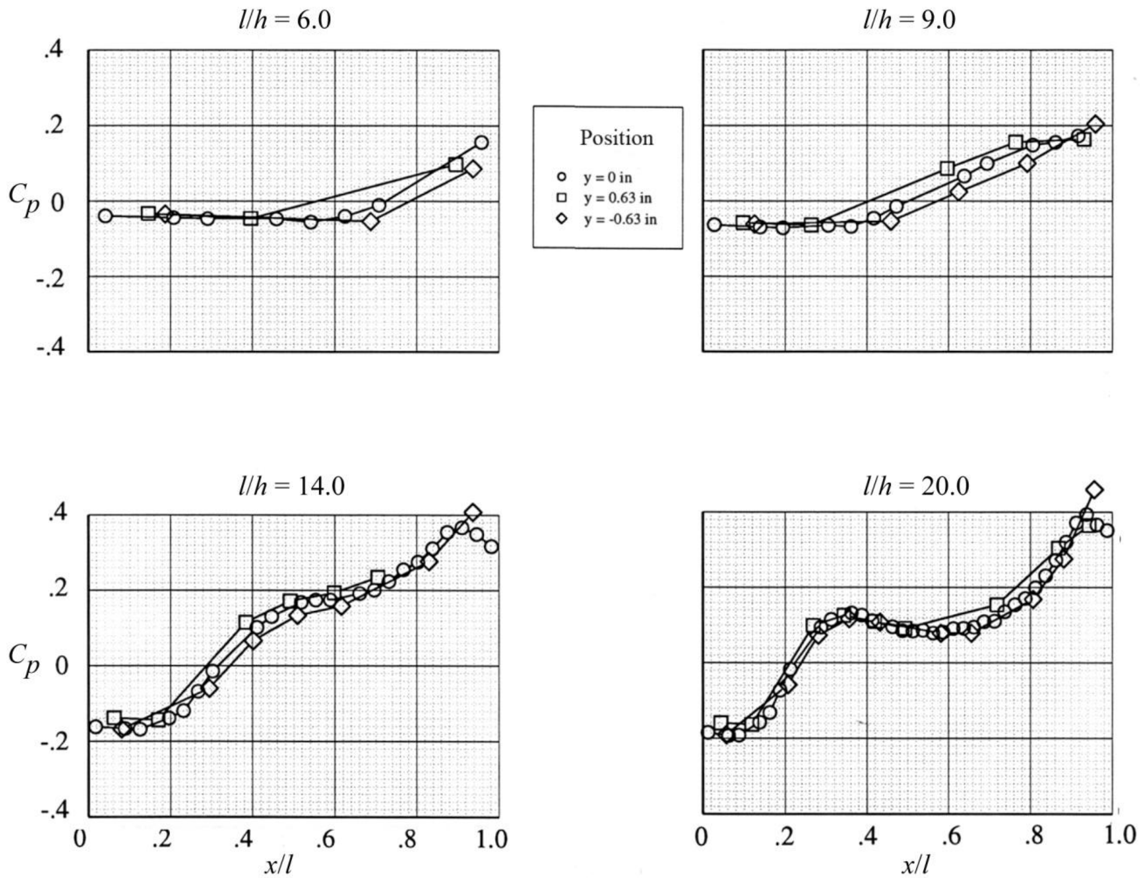

(d) $M_\infty = 0.8$.

Figure 14. Concluded.

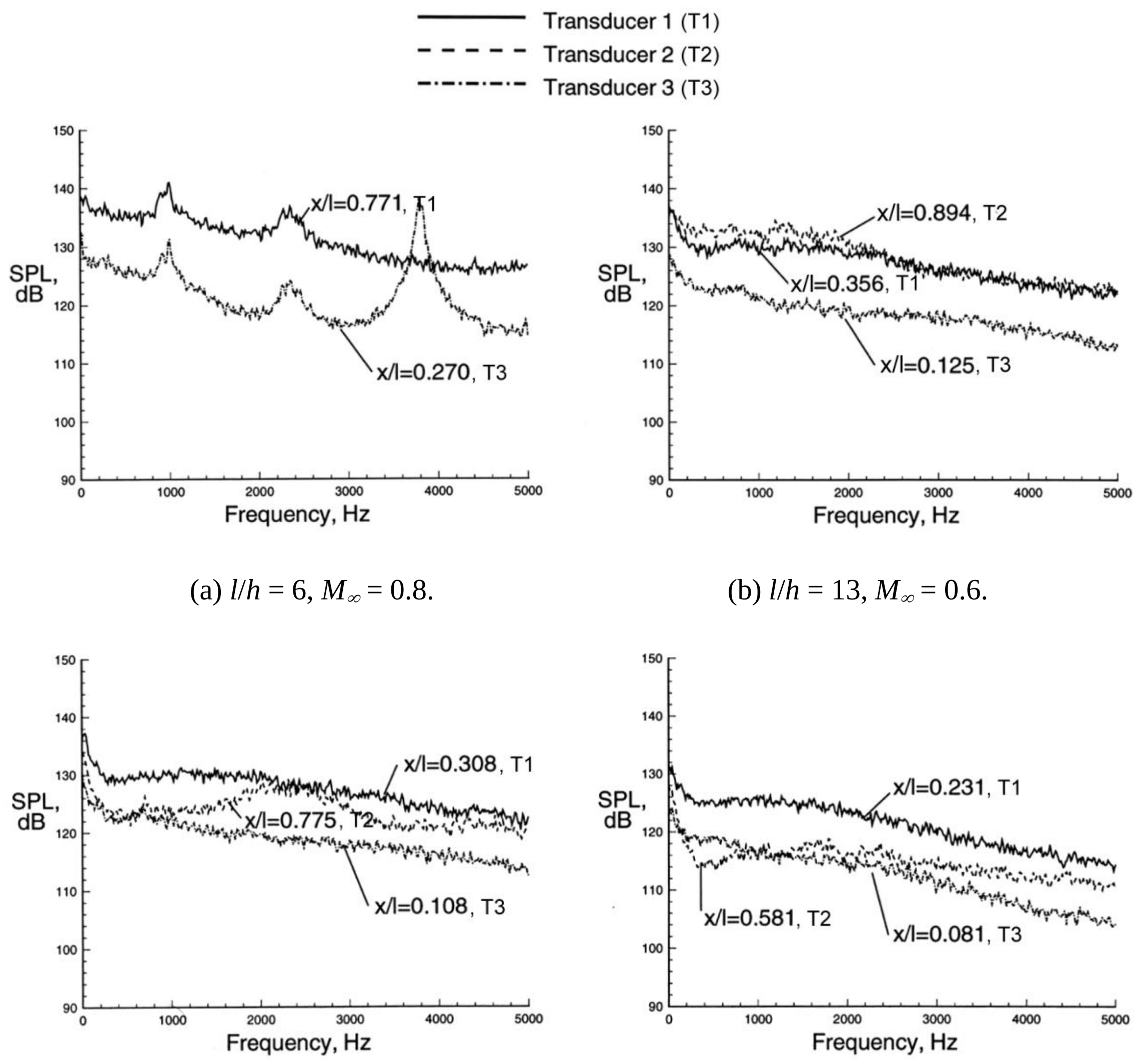

(a) $l/h = 6$, $M_\infty = 0.8$.

(b) $l/h = 13$, $M_\infty = 0.6$.

(c) $l/h = 15$, $M_\infty = 0.6$.

(d) $l/h = 20$, $M_\infty = 0.4$.

Figure 15. Effect of transducer location on fluctuating-pressure spectra in rectangular cavities.

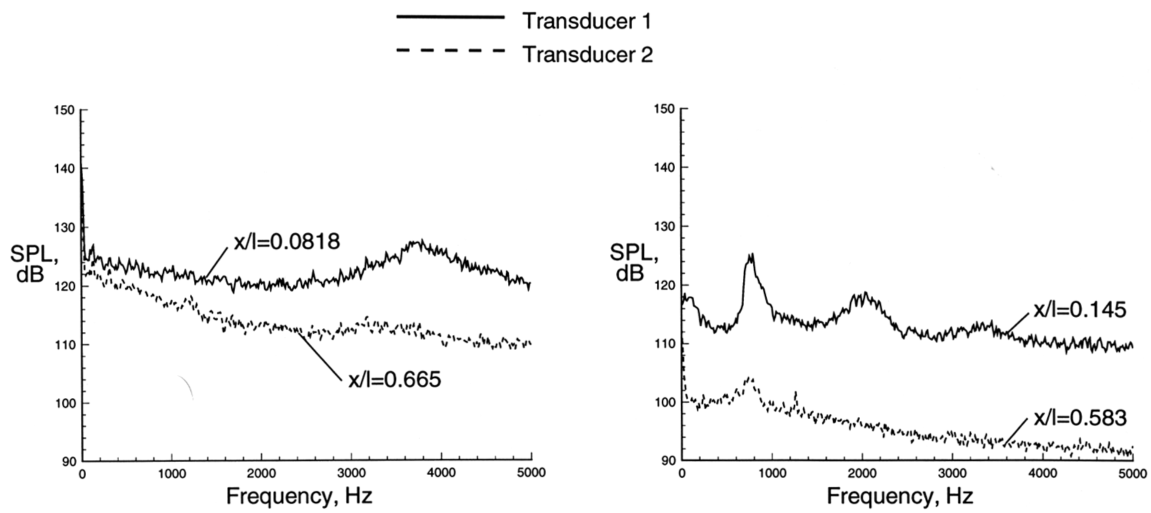

(a) $\psi = 65°$, $l/h = 12$, $M_\infty = 0.8$.

(b) $\psi = 55°$, $l/h = 16$, $M_\infty = 0.2$.

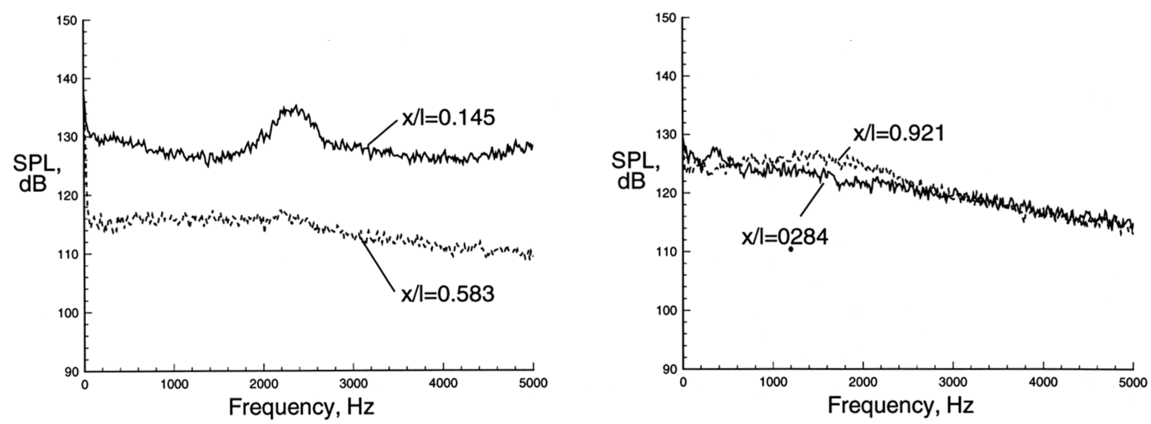

(c) $\psi = 55°$, $l/h = 16$, $M_\infty = 0.6$.

(d) $\psi = 45°$, $l/h = 11$, $M_\infty = 0.4$.

Figure 16. Effect of transducer location on fluctuating-pressure spectra in swept cavities.

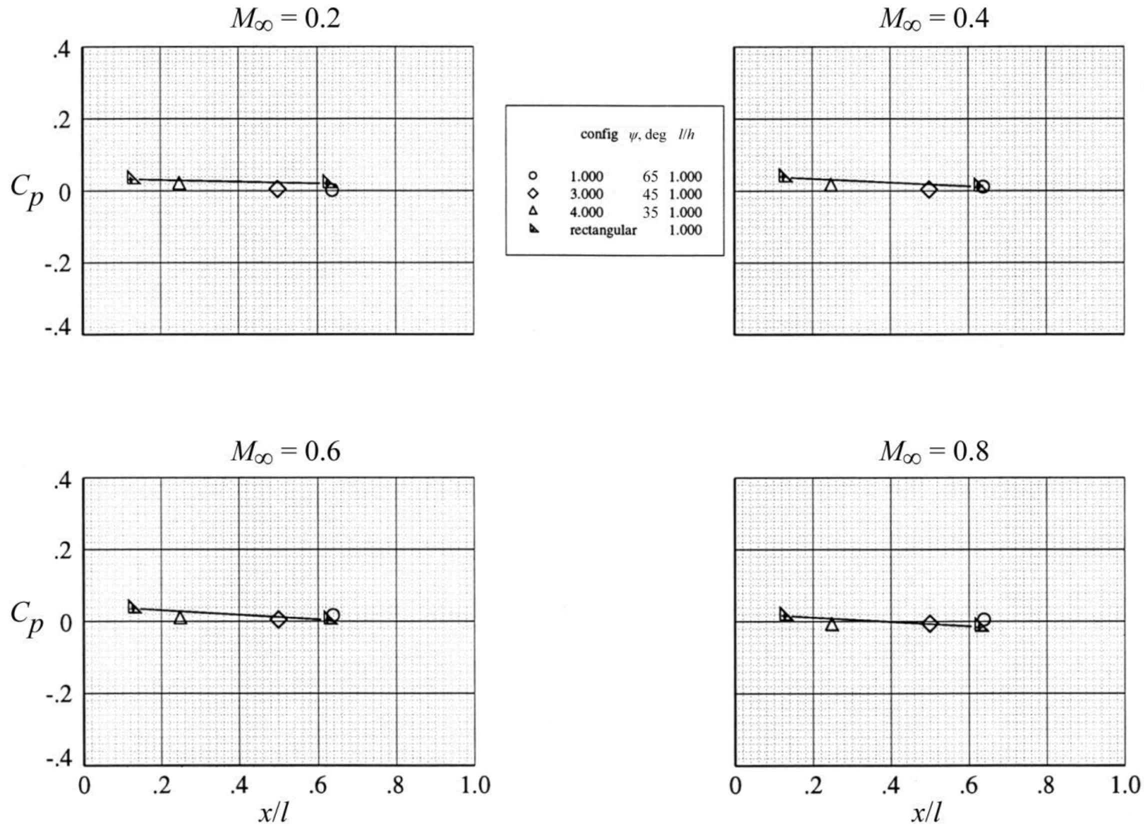

(a) $l/h = 1$.

Figure 17. Effect of sweep on cavity floor centerline pressure distributions.

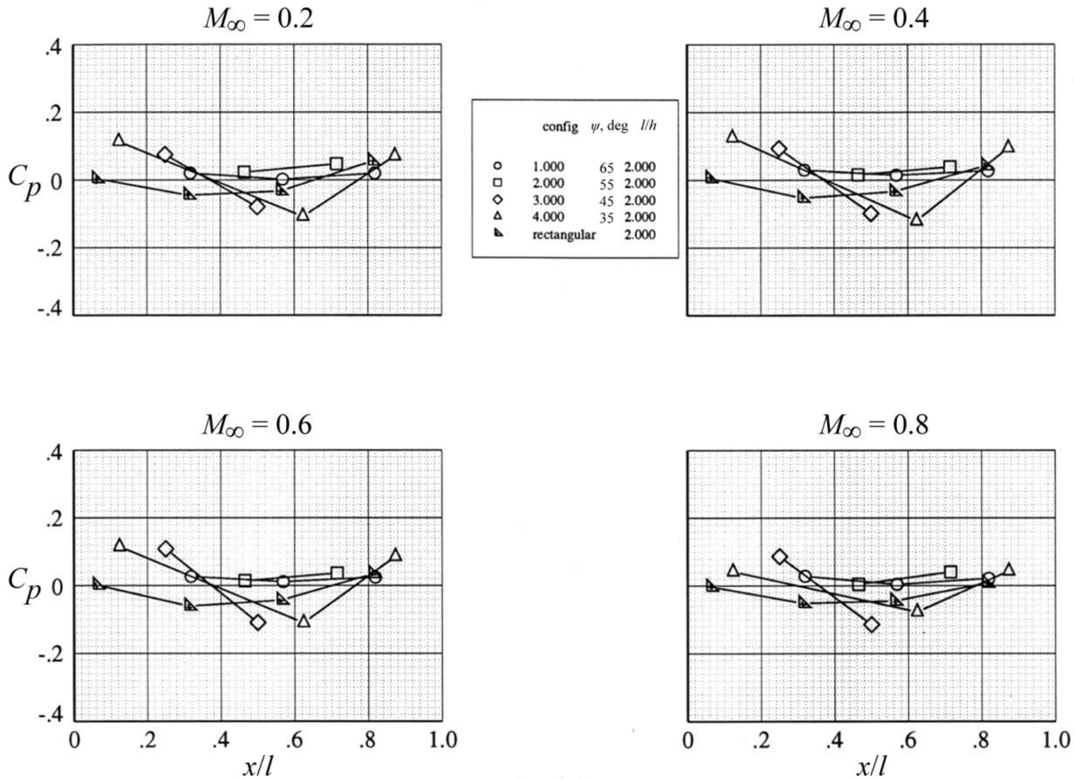

(b) $l/h = 2$.

Figure 17. Continued.

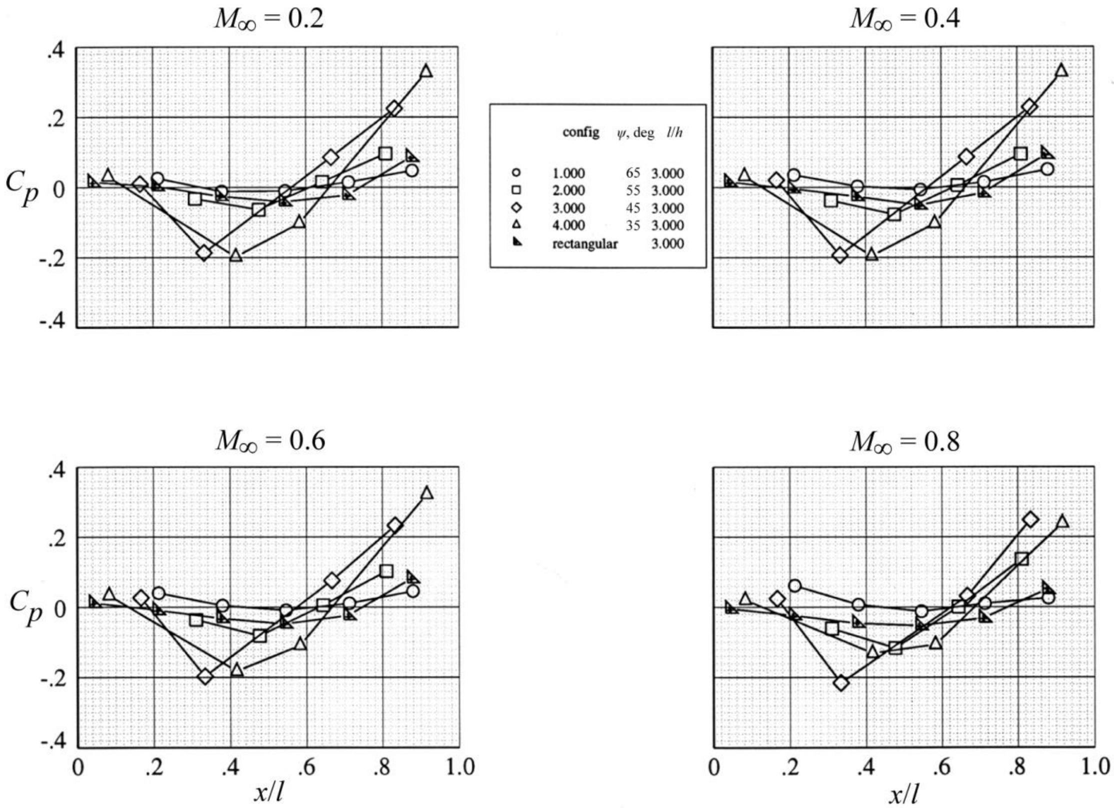

(c) $l/h = 3$.

Figure 17. Continued.

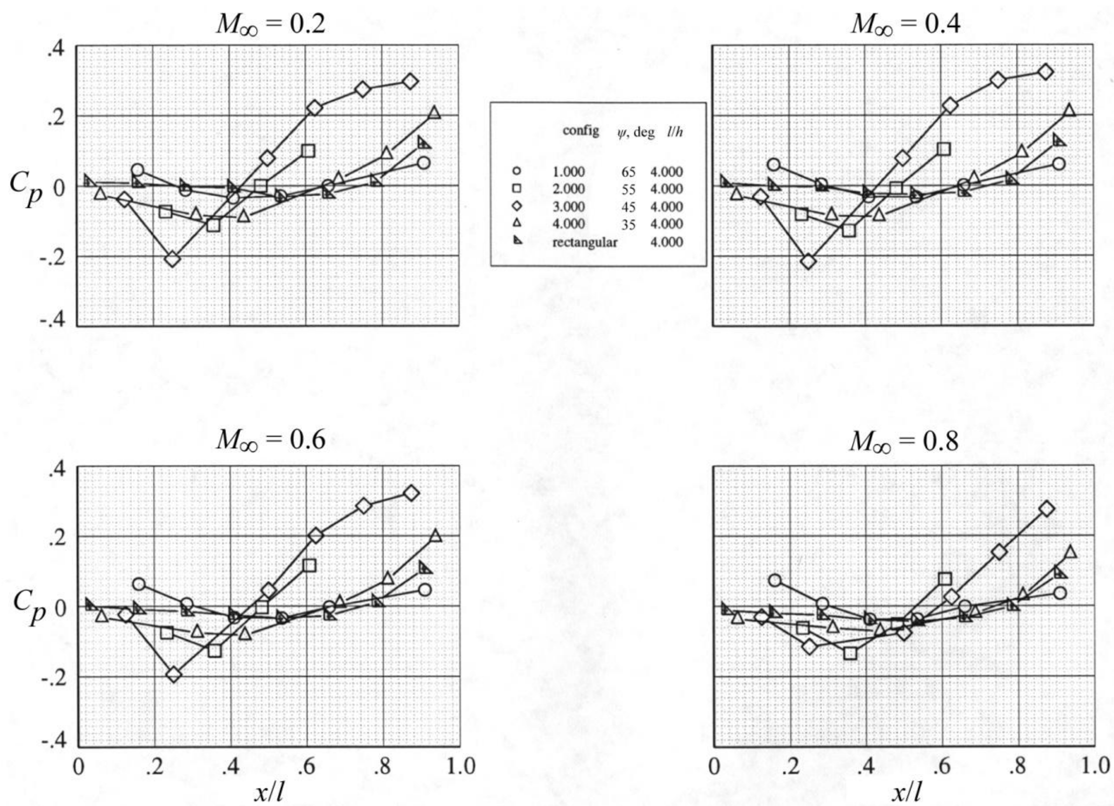

(d) $l/h = 4$.

Figure 17. Continued.

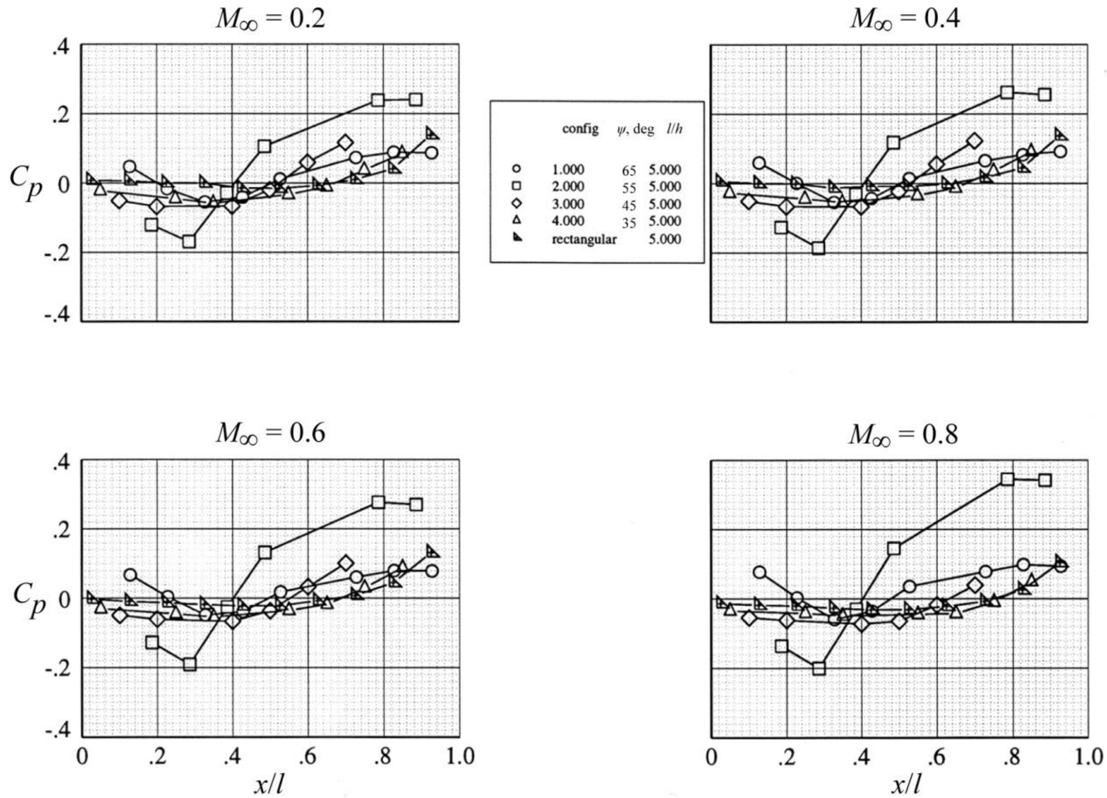

(e) $l/h = 5$.

Figure 17. Continued.

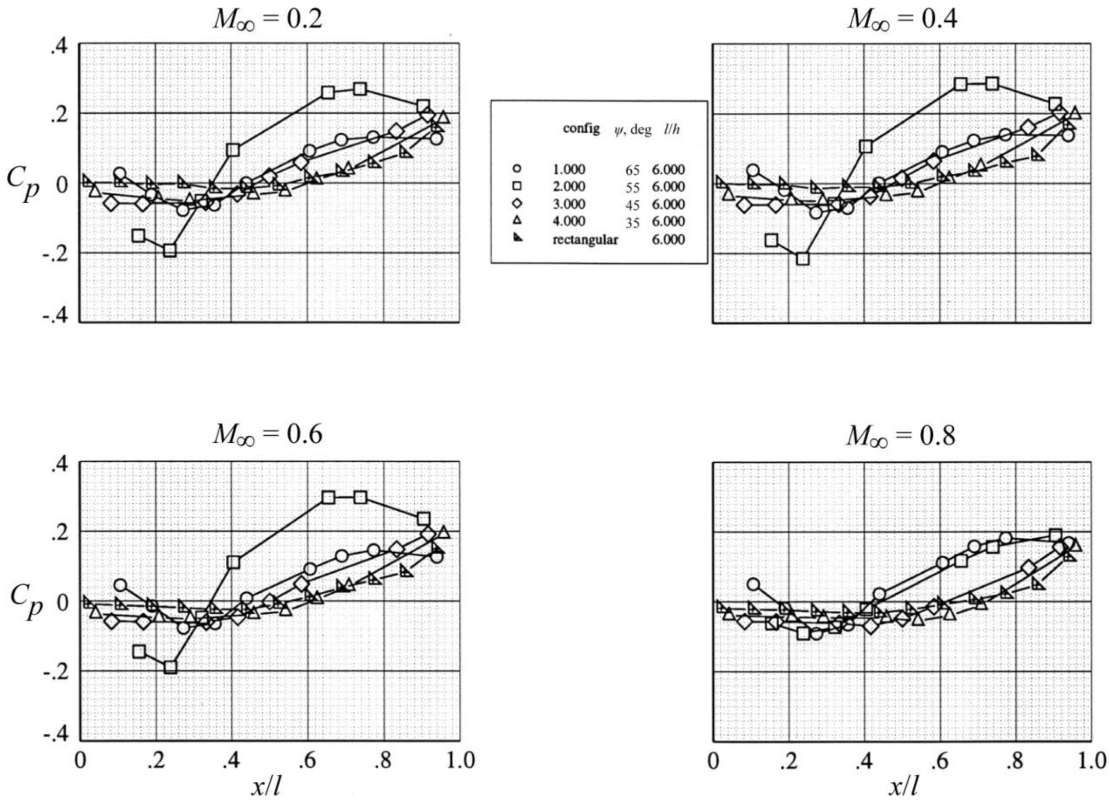

(f) $l/h = 6$.

Figure 17. Continued.

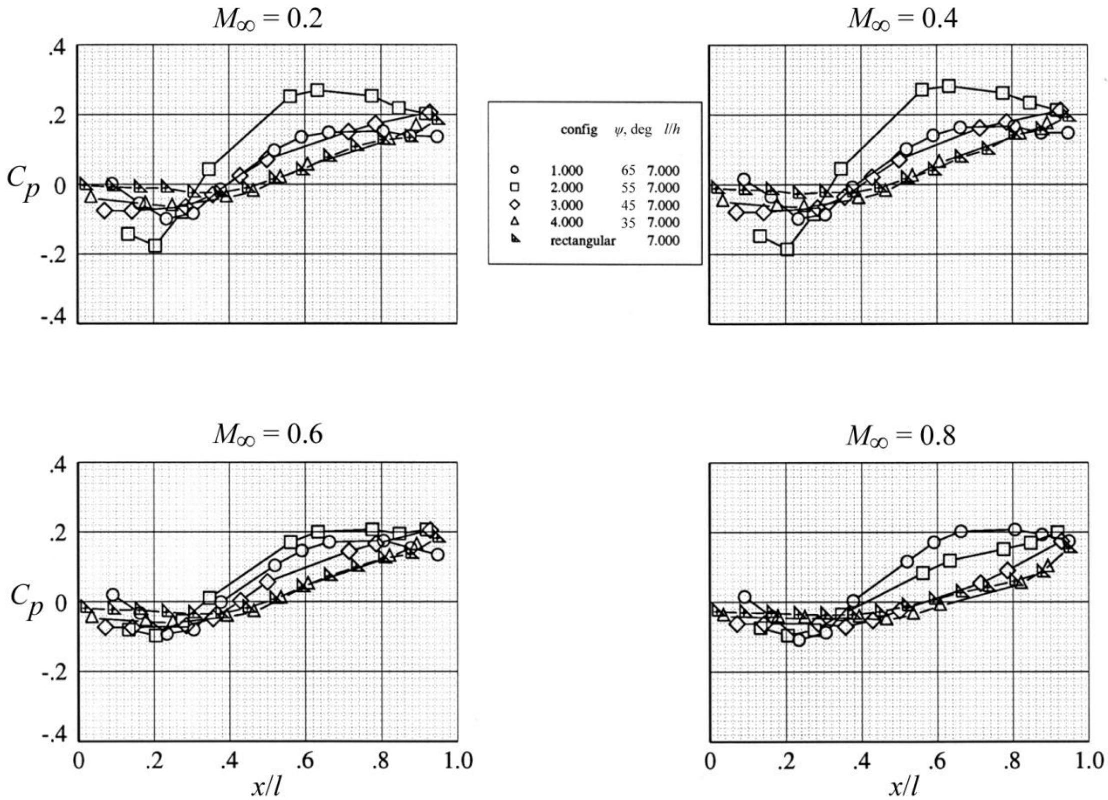

(g) l/h = 7.

Figure 17. Continued.

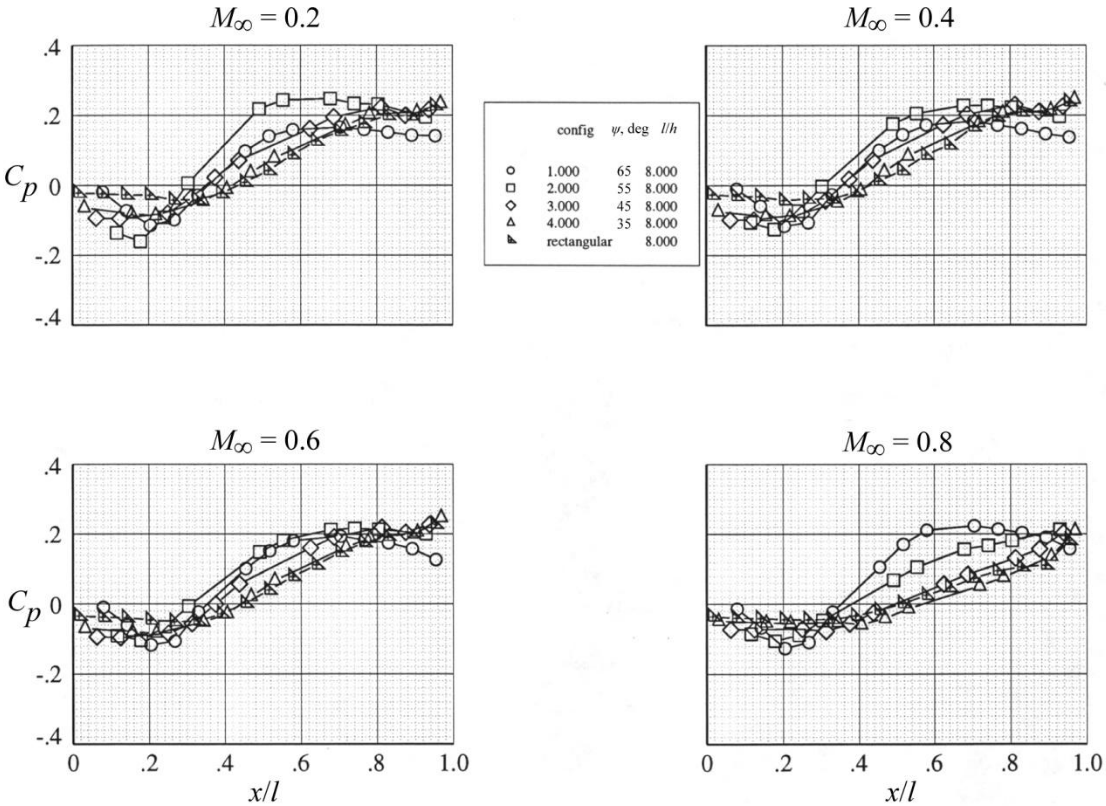

(h) $l/h = 8$.

Figure 17. Continued.

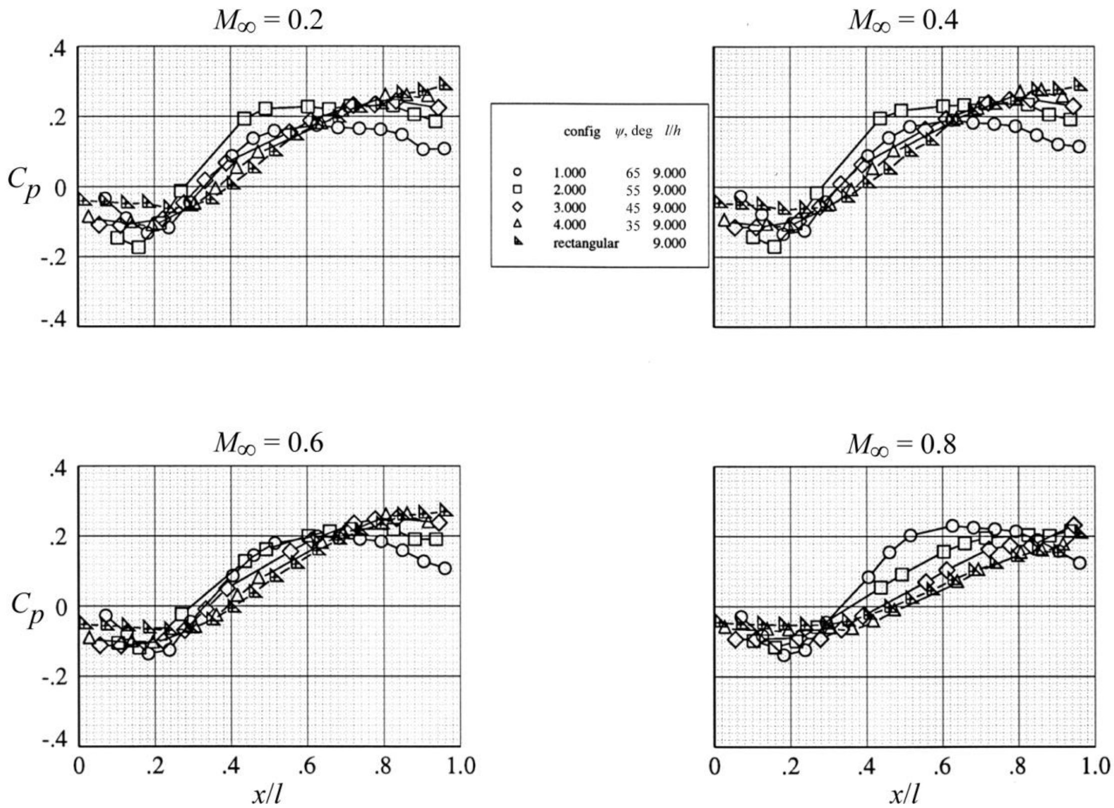

(i) $l/h = 9$.

Figure 17. Continued.

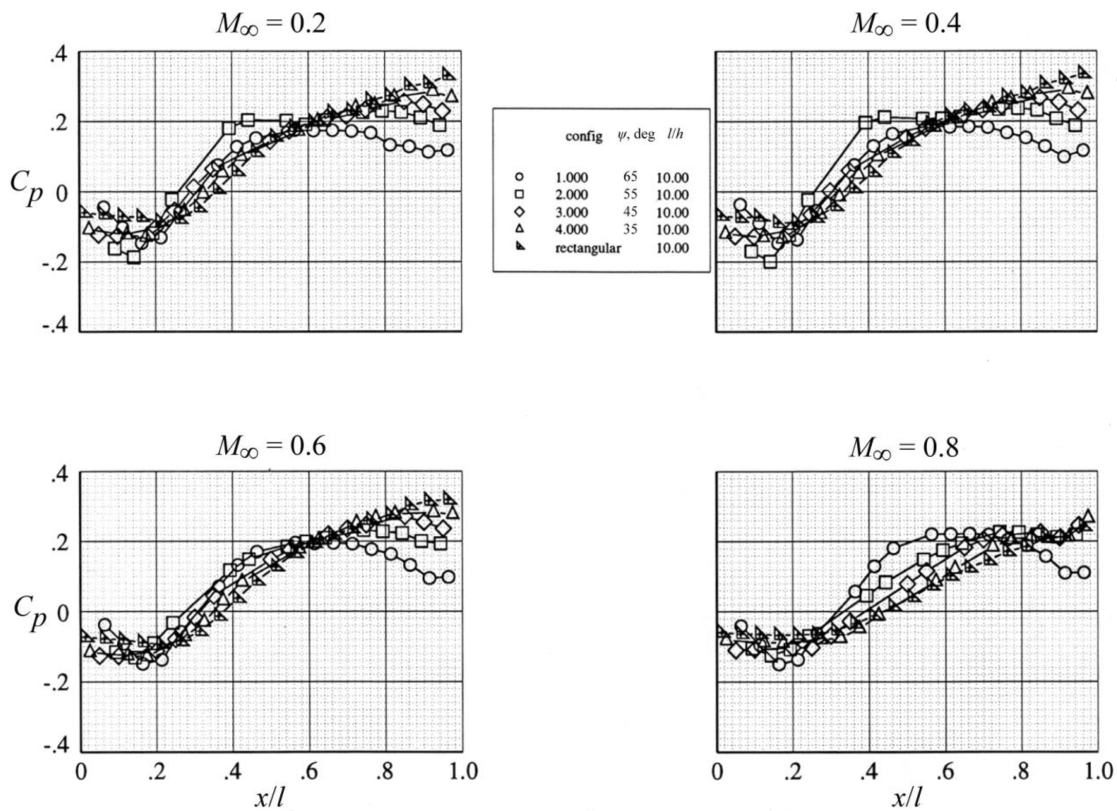

(j) *l*/*h* = 10.

Figure 17. Continued.

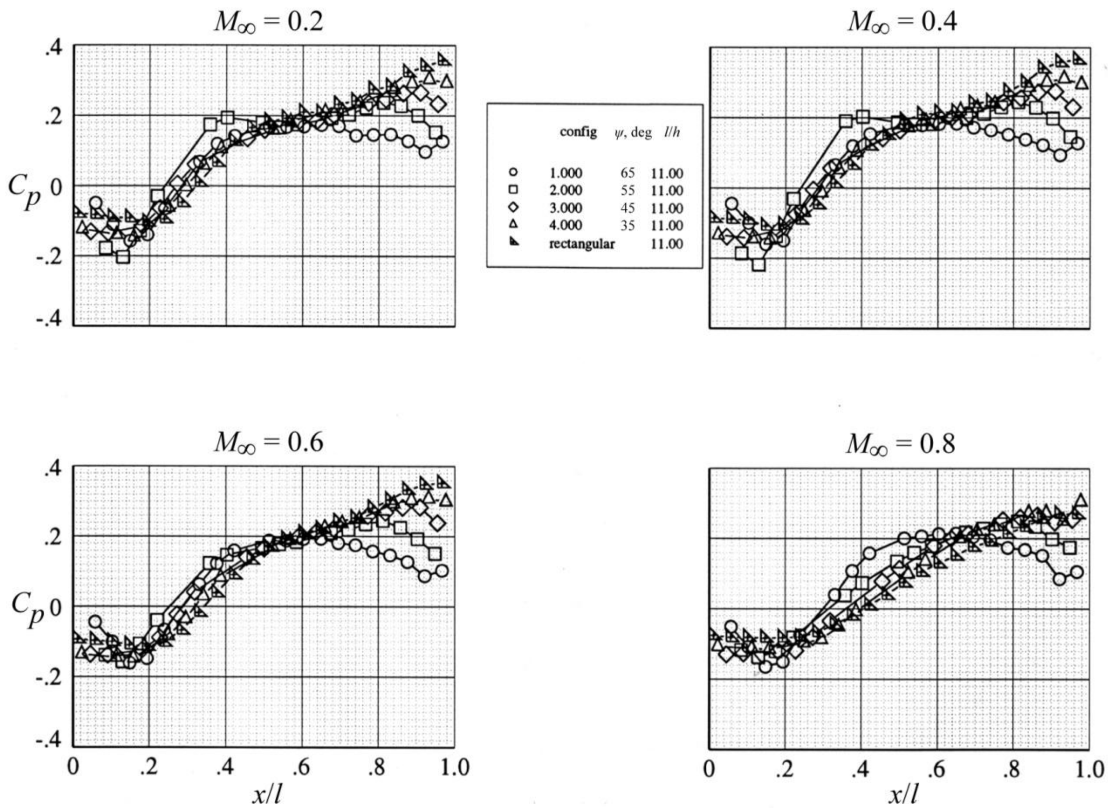

(k) $l/h = 11$.

Figure 17. Continued.

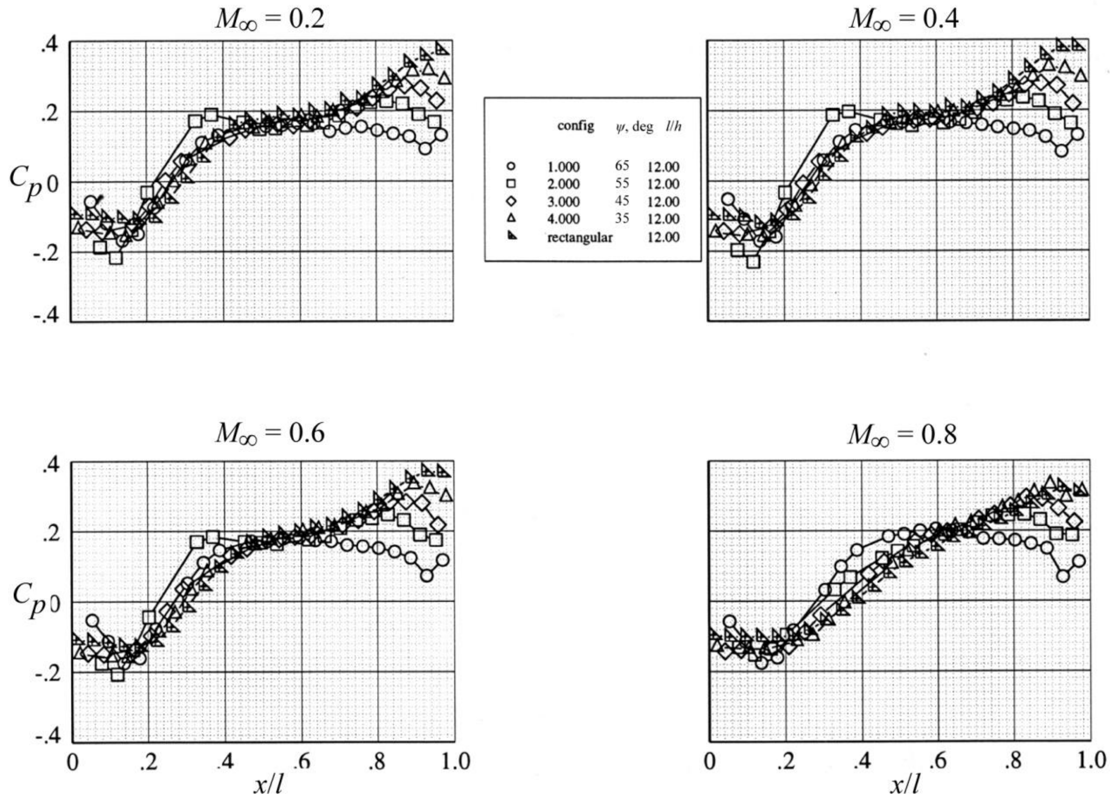

(l) l/h = 12.

Figure 17. Continued.

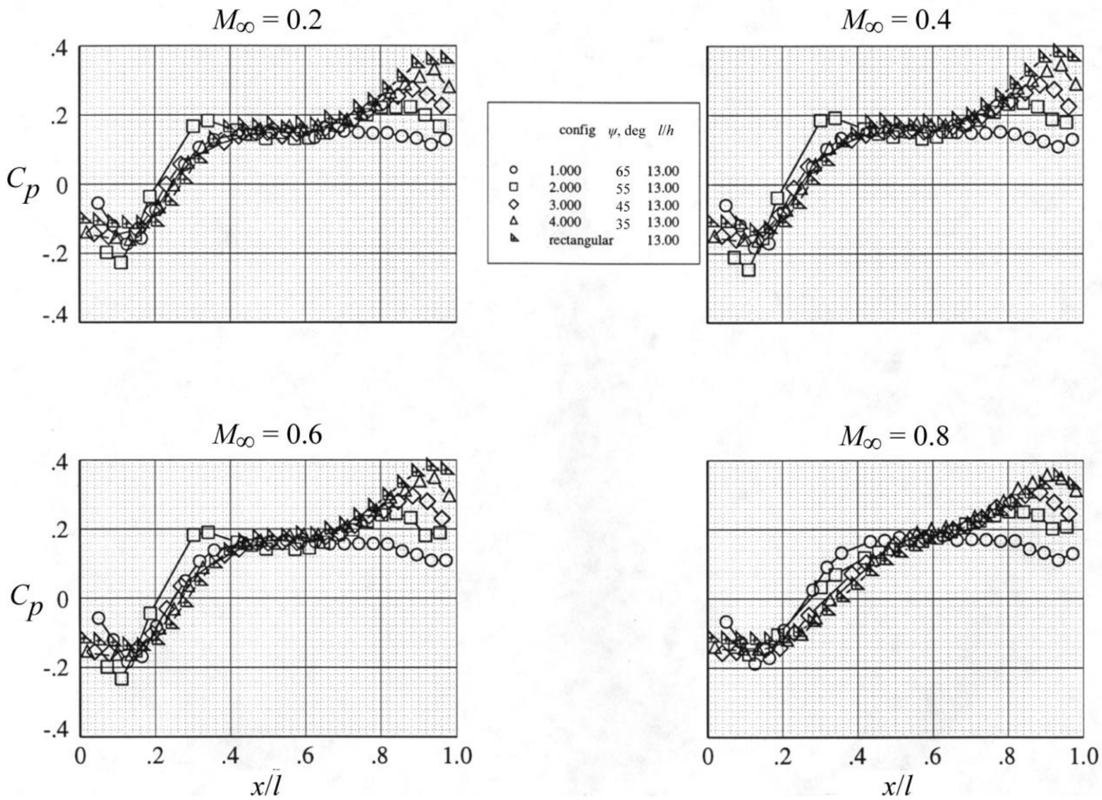

(m) l/h = 13.

Figure 17. Continued.

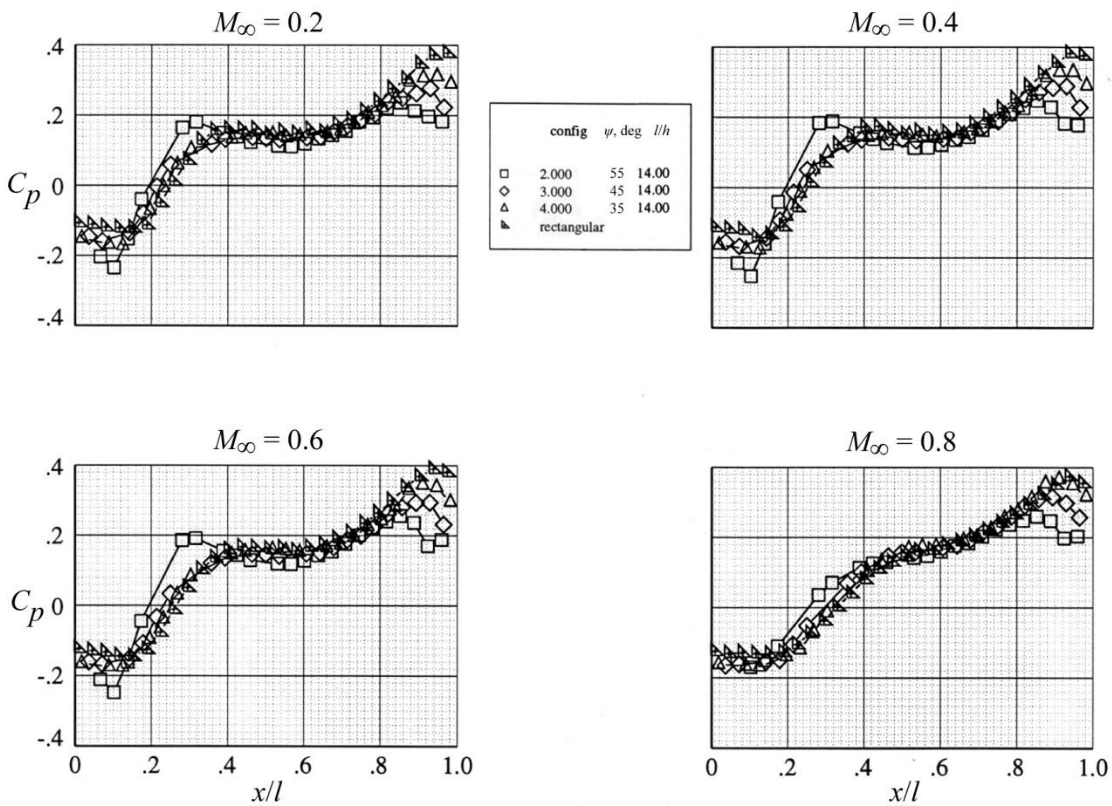

(n) $l/h = 14$.

Figure 17. Continued.

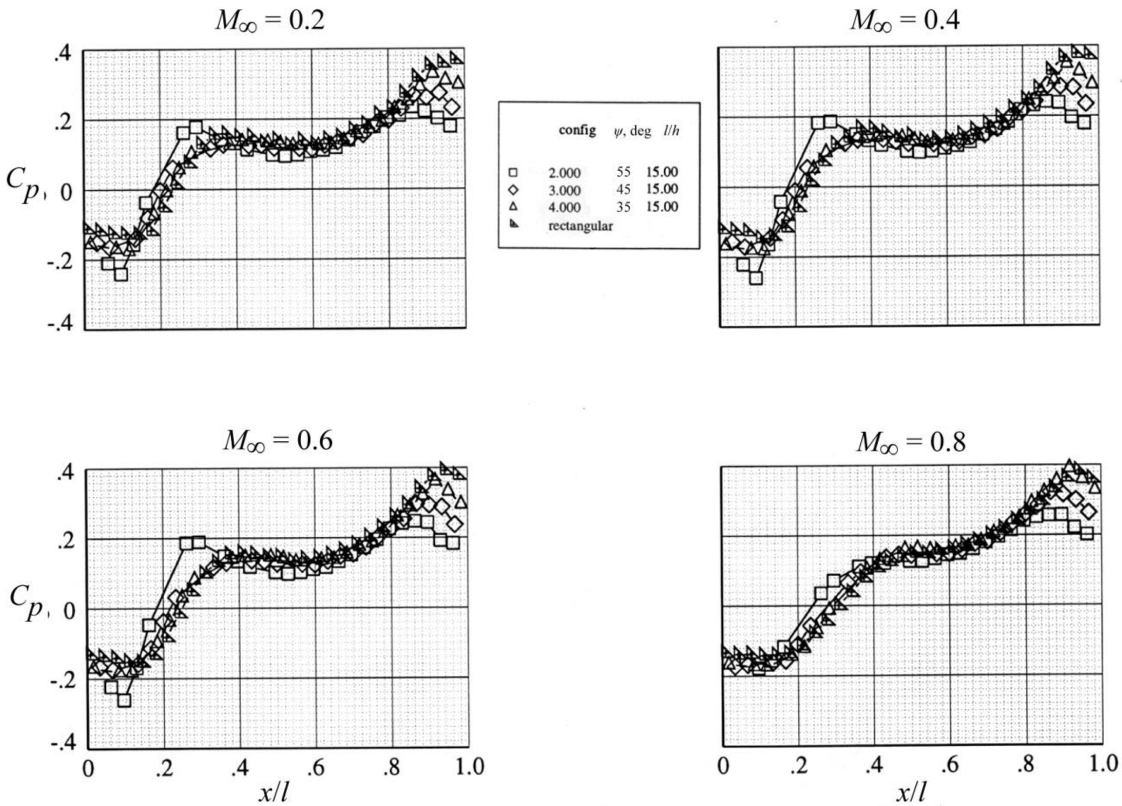

(o) $l/h = 15$.

Figure 17. Continued.

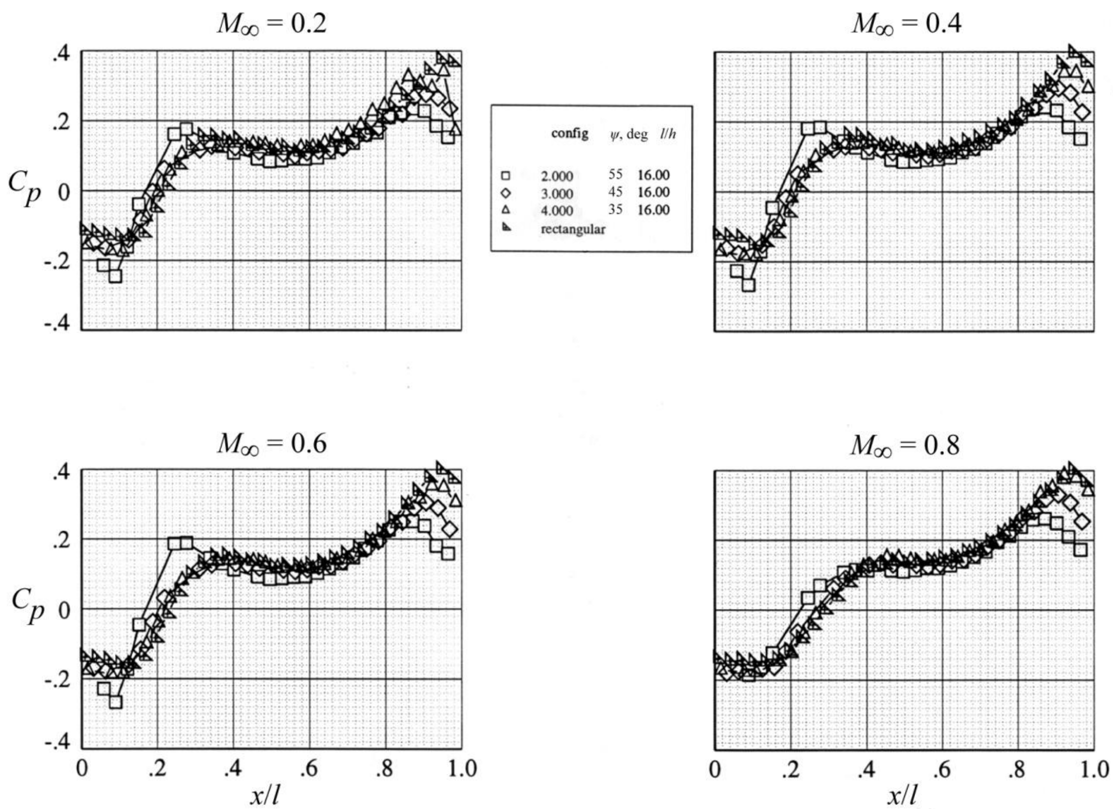

(p) $l/h = 16$.

Figure 17. Continued.

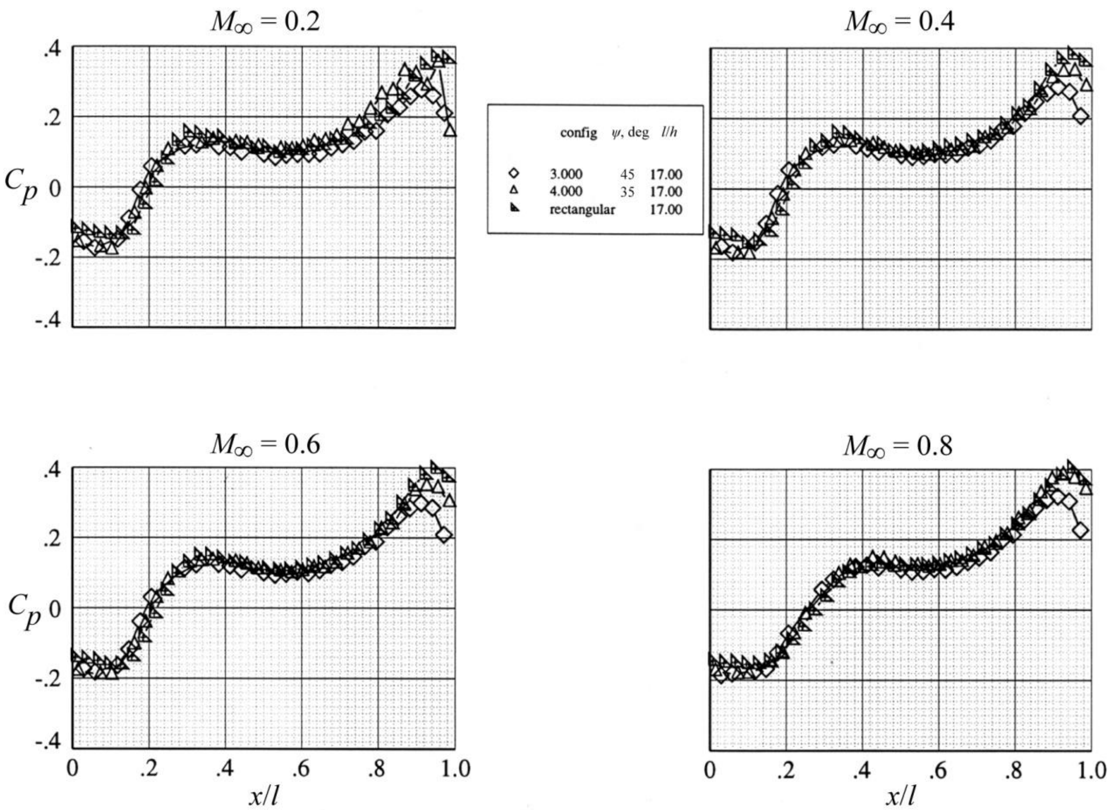

(q) $l/h = 17$.

Figure 17. Continued.

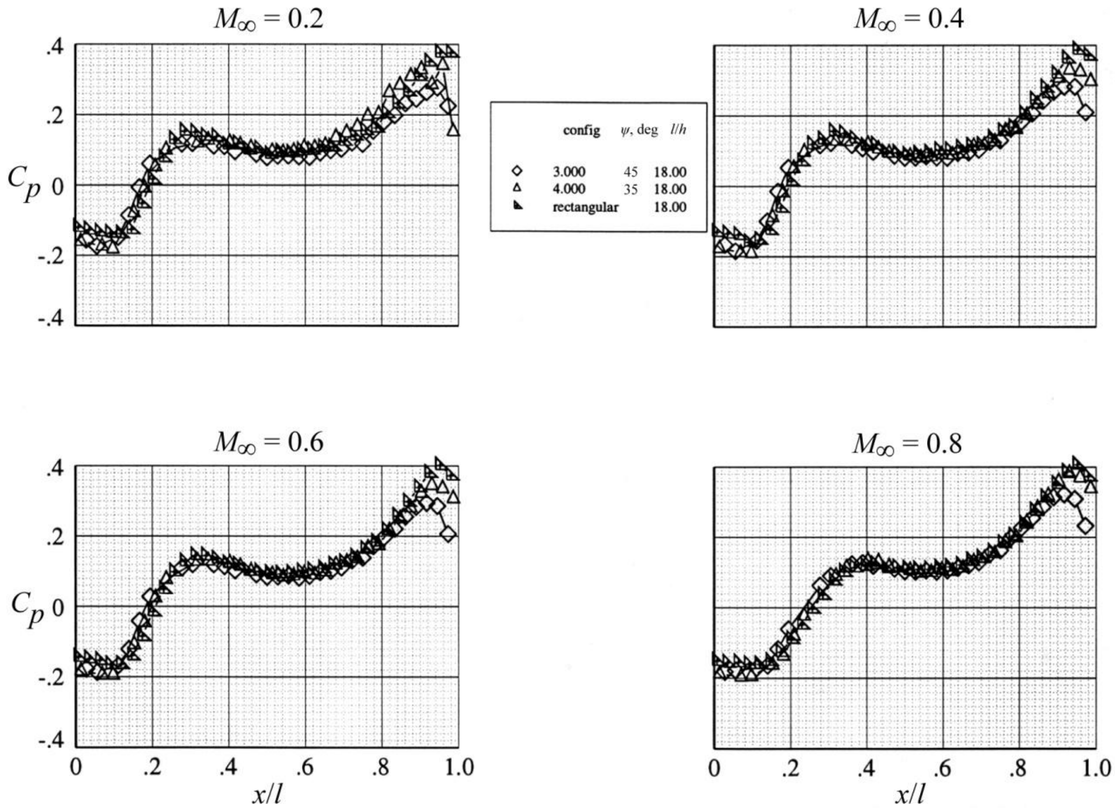

(r) $l/h = 18$.

Figure 17. Continued.

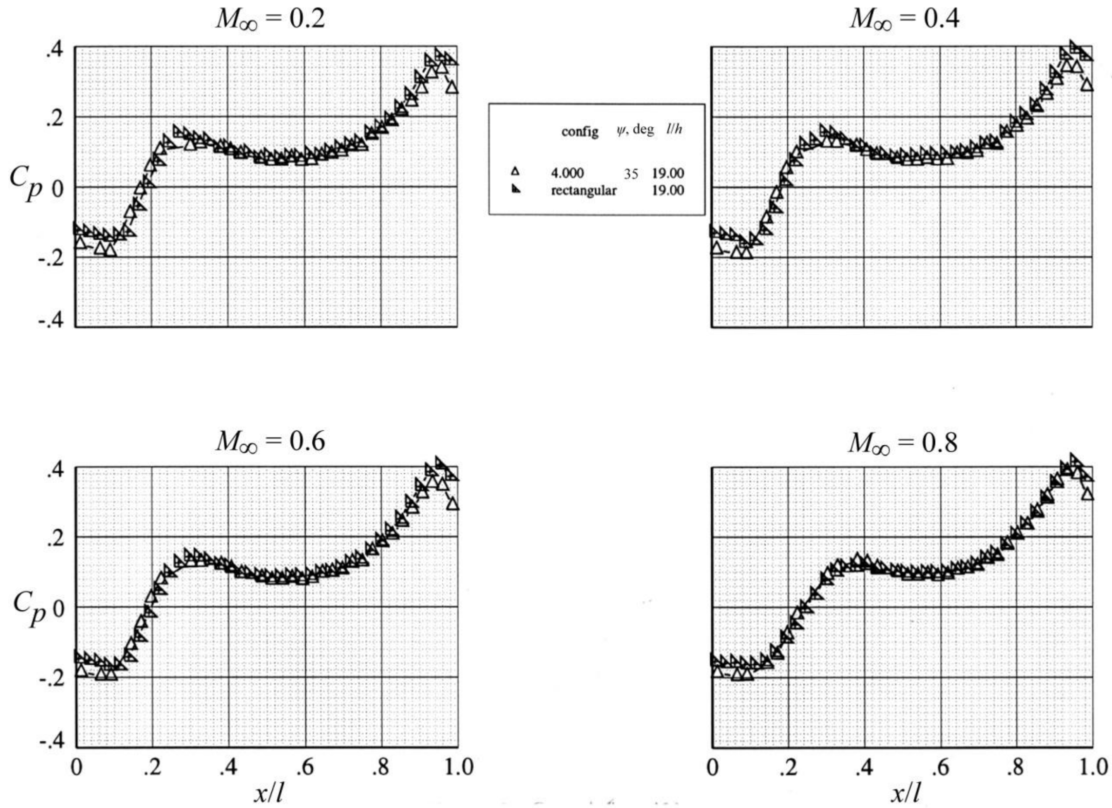

(s) $l/h = 19$.

Figure 17. Continued.

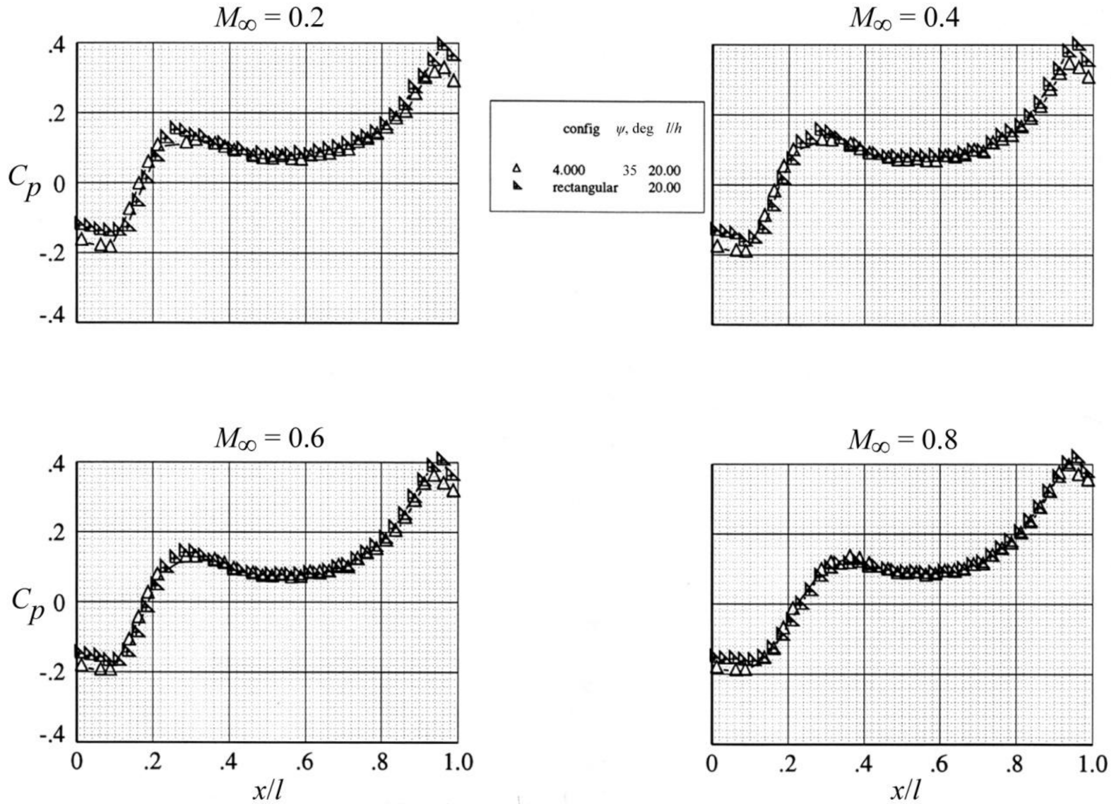

(t) $l/h = 20$.

Figure 17. Concluded

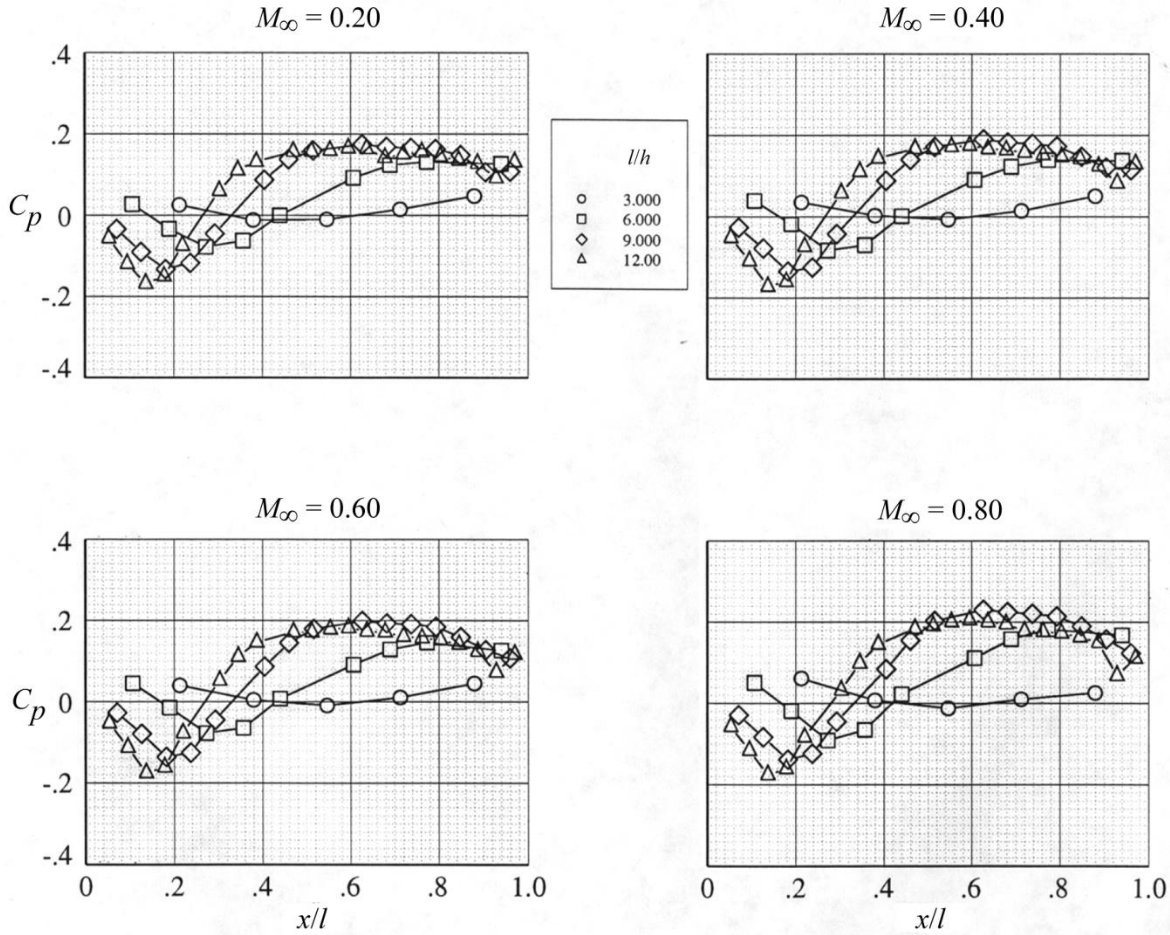

(a) Configuration 1, $\psi = 65°$, $l/h = 3, 6, 9, 12$.

Figure 18. Effect of l/h on cavity floor centerline pressure distributions.

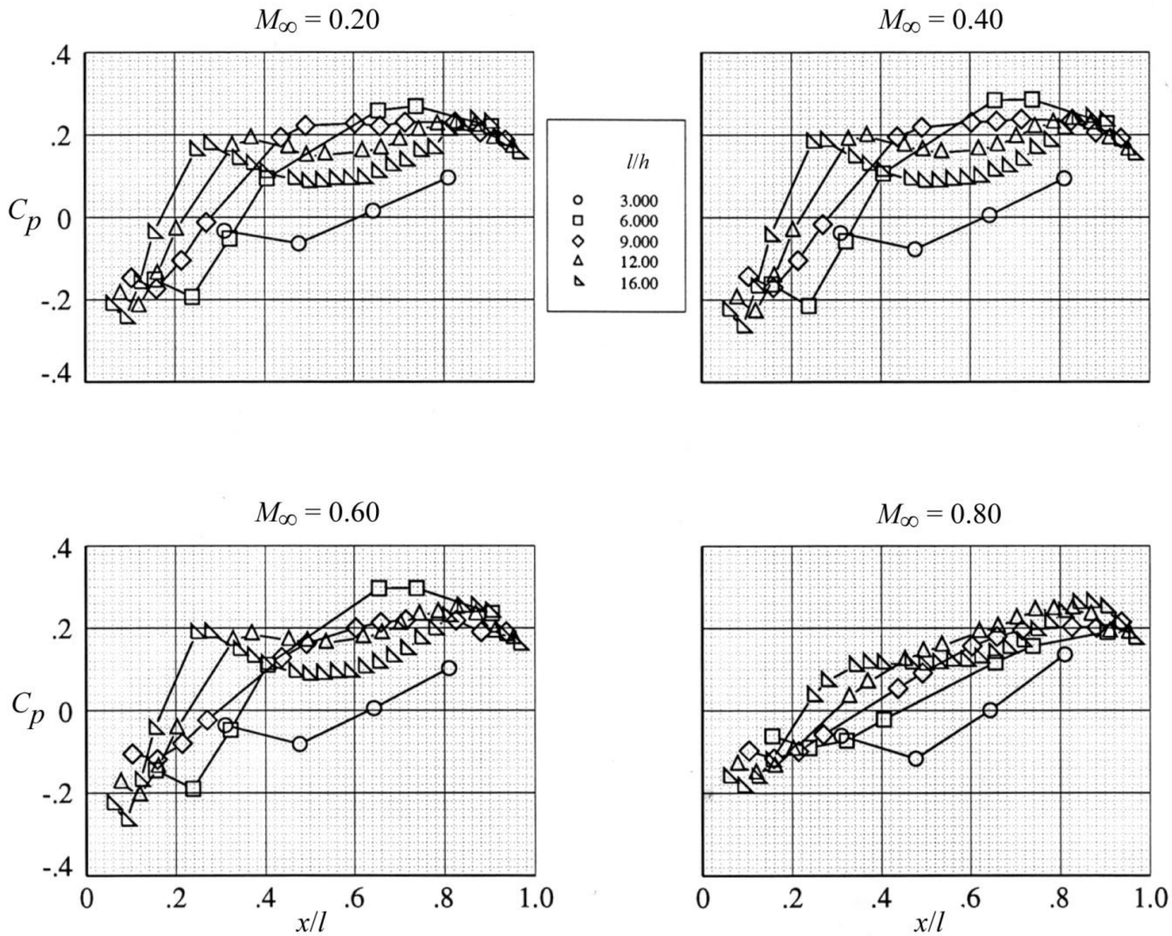

(b) Configuration 2, $\psi = 55°$, l/h = 3, 6, 9, 12, 16.

Figure 18. Continued.

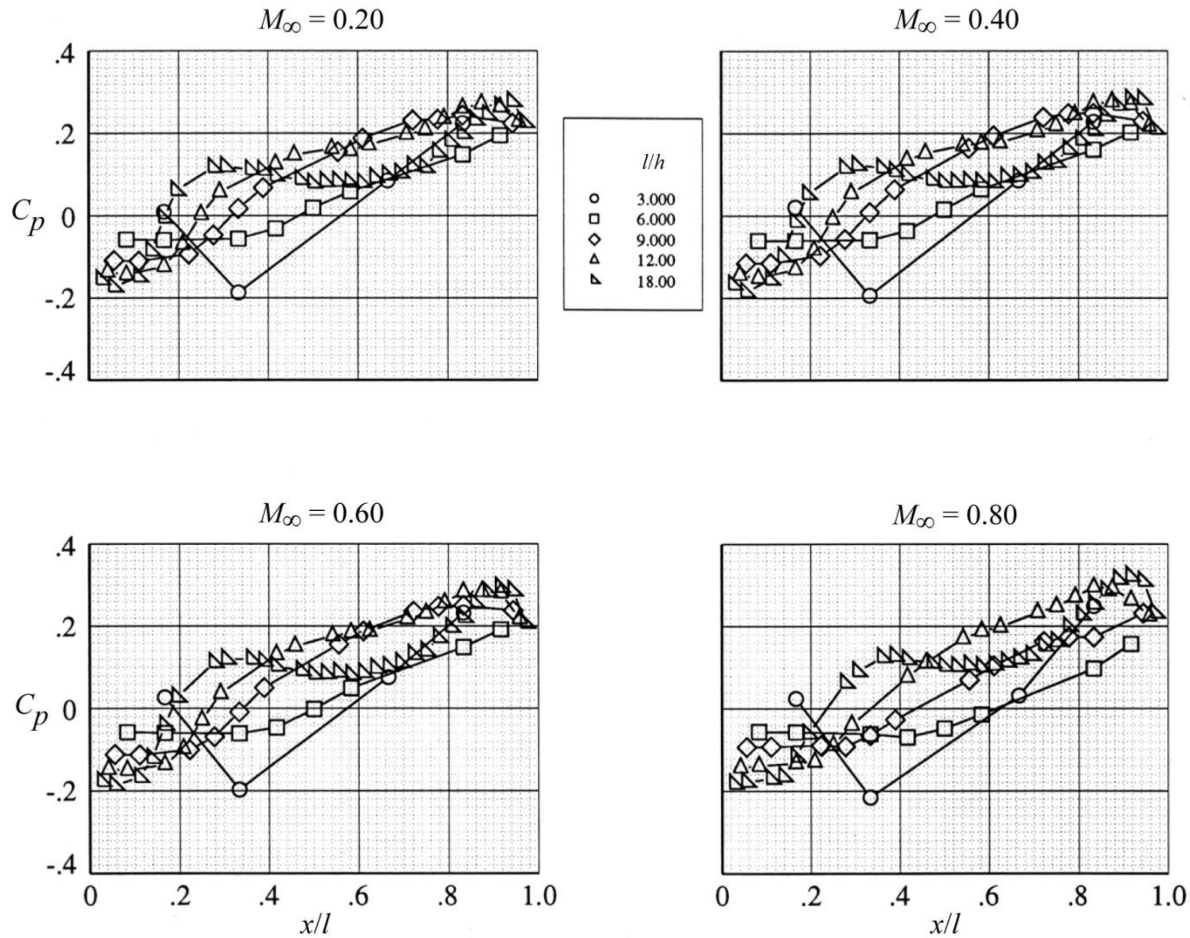

(c) Configuration 3, $\psi = 45°$, l/h = 3, 6, 9, 12, 18.

Figure 18. Continued.

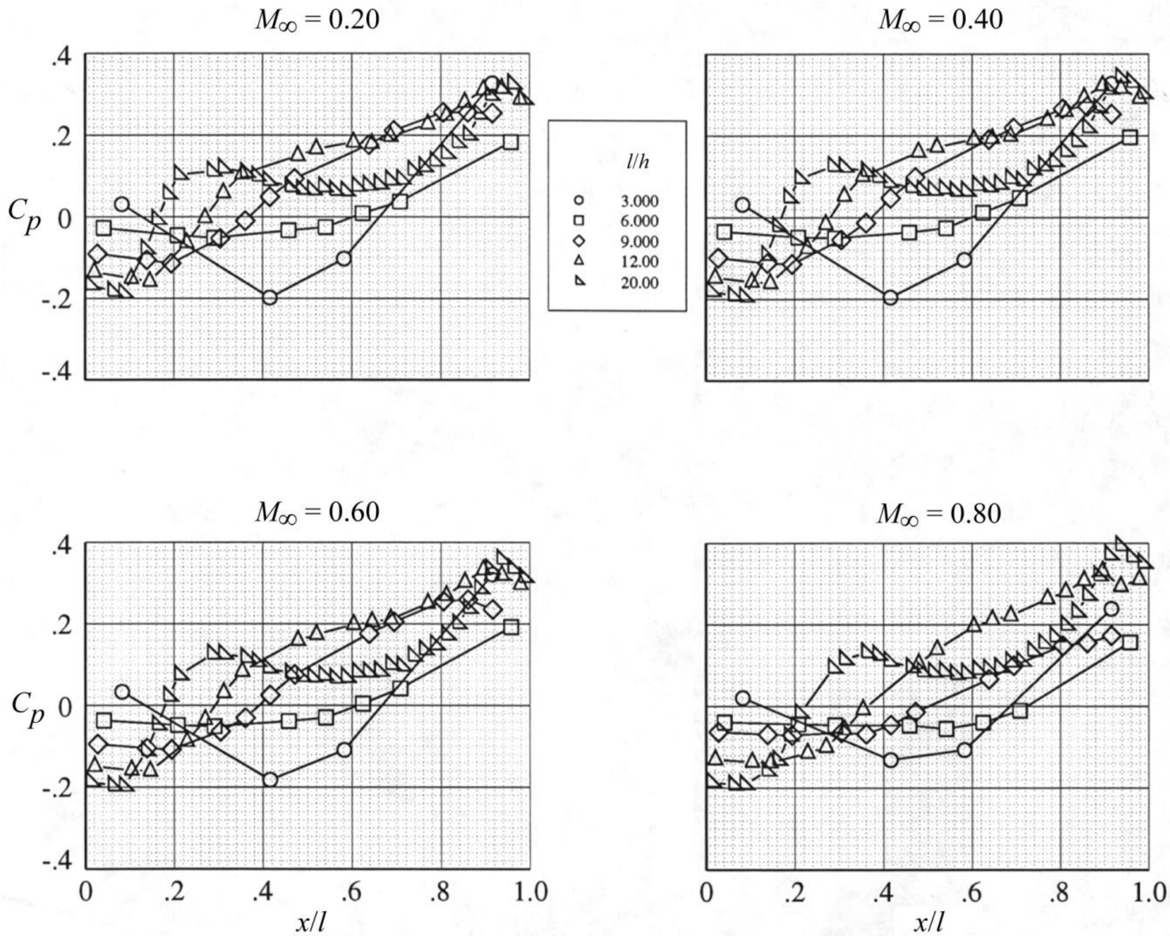

(d) Configuration 4, ψ = 35°, l/h = 3, 6, 9, 12, 20.

Figure 18. Concluded.

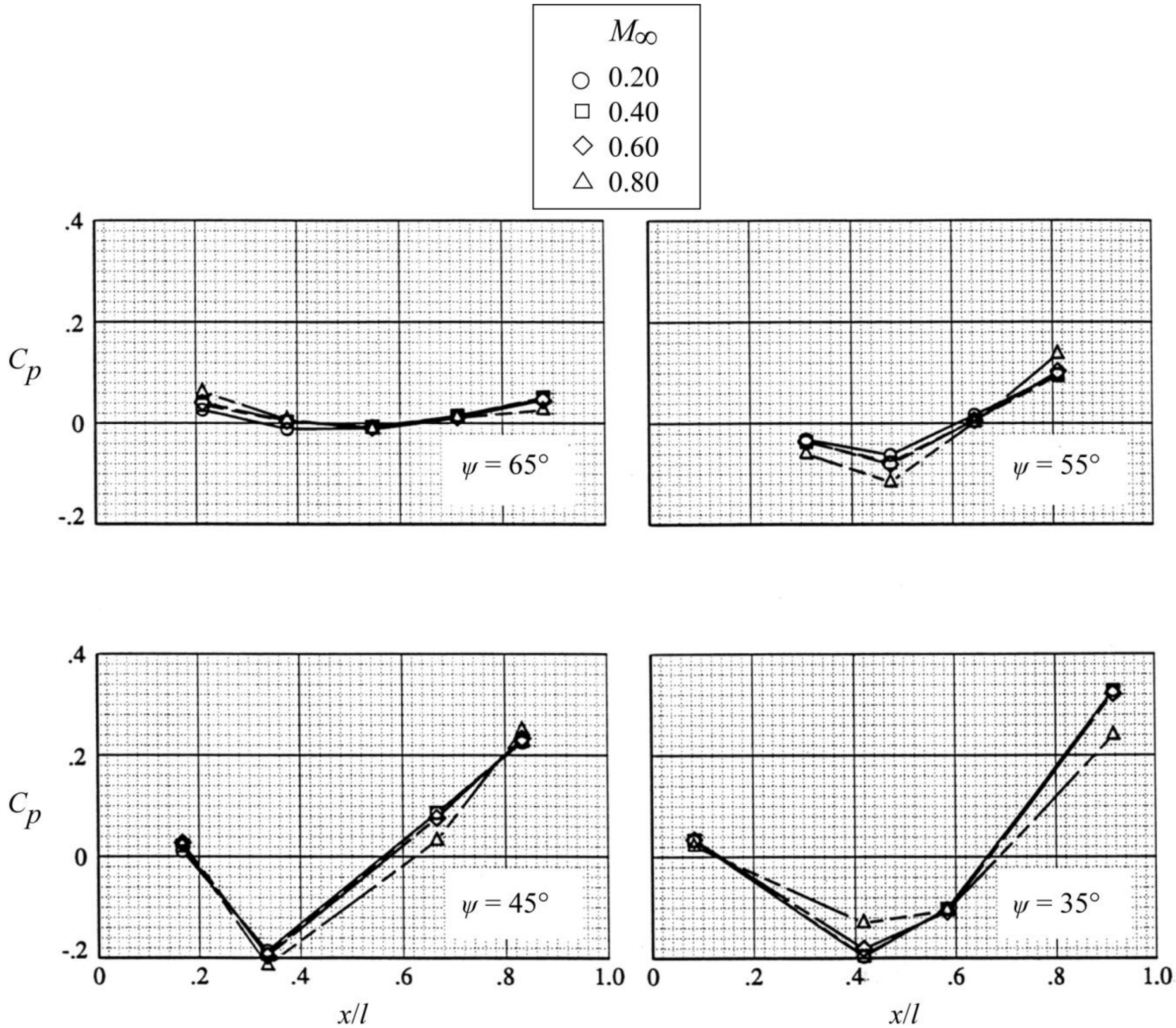

(a) l/h = 3.

Figure 19. Effect of M_∞ on cavity floor centerline pressure distributions.

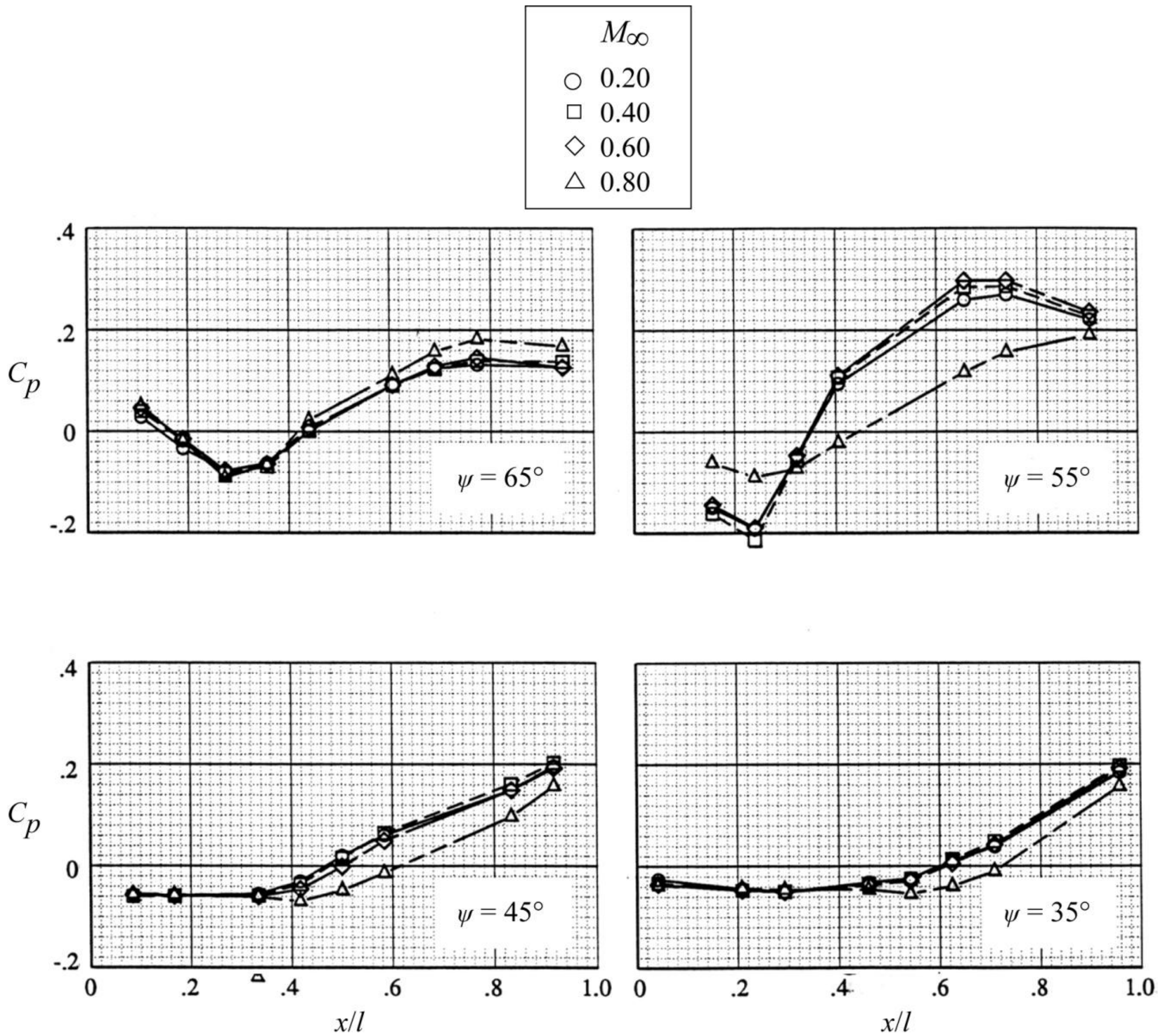

(b) l/h = 6.

Figure 19. Continued.

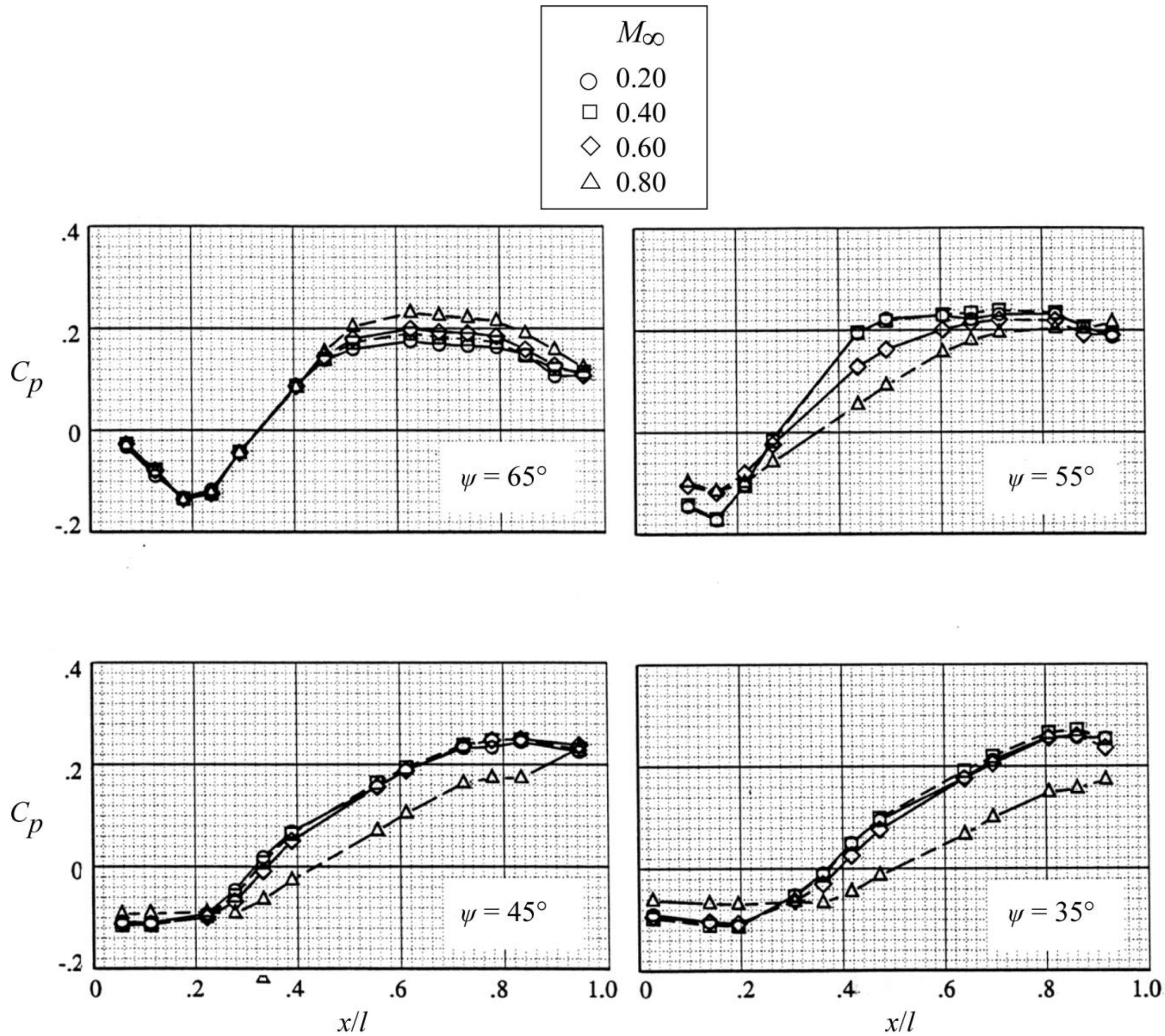

(c) $l/h = 9$.

Figure 19. Continued.

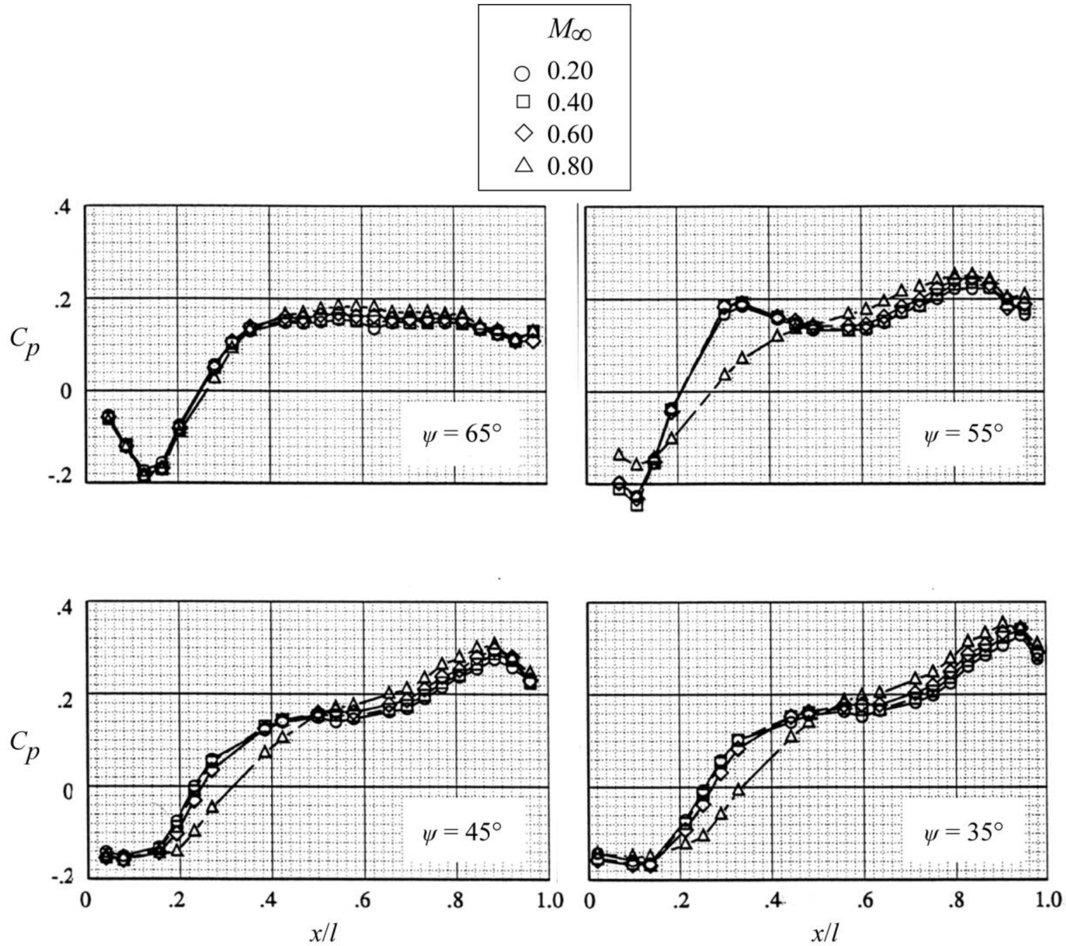

(d) l/h = 13.

Figure 19. Concluded.

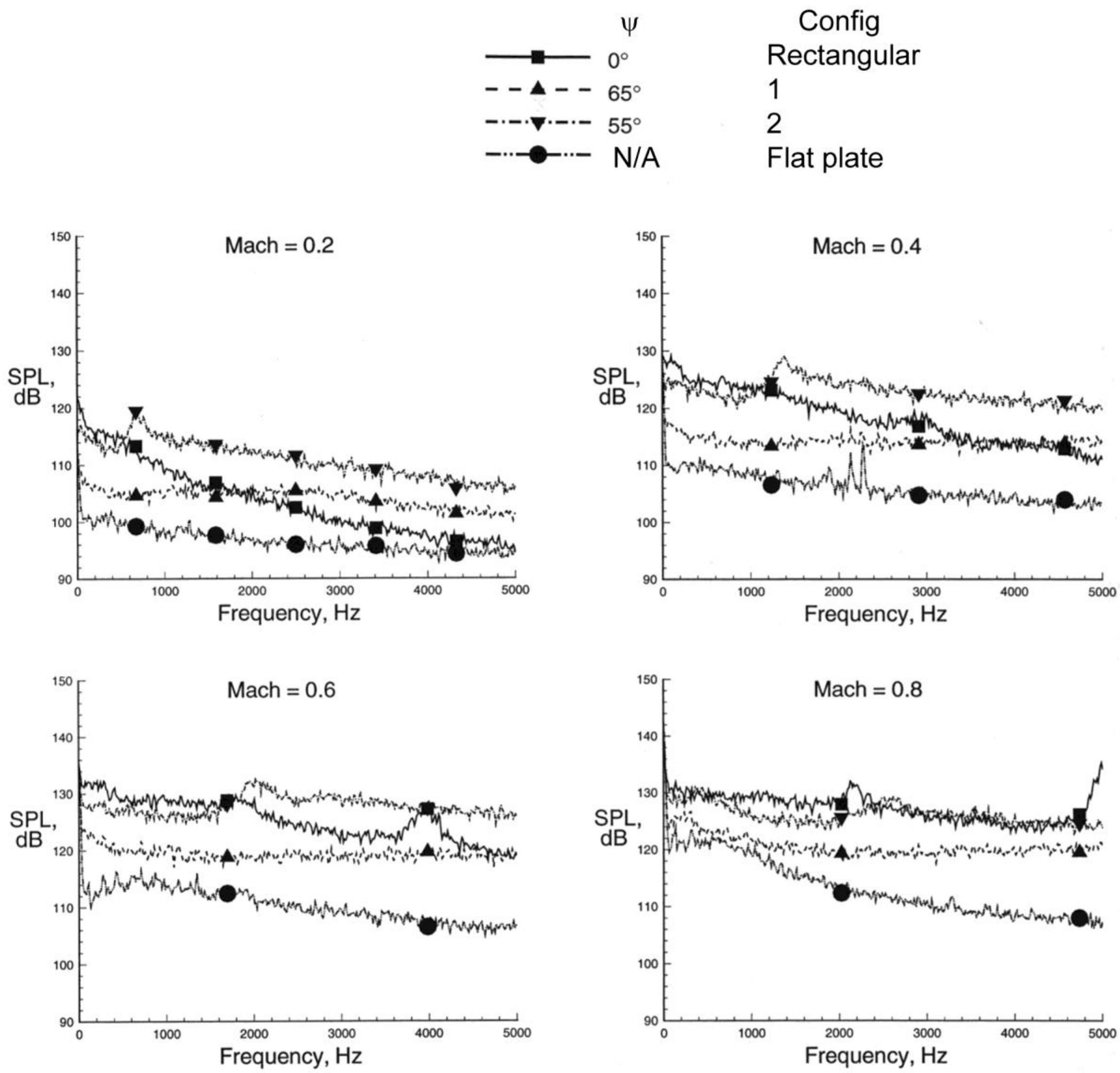

(a) $l/h = 3$. Transducer $x/l = 0.327$ ($\psi = 65^o$), 0.774 ($\psi = 55°$), 0.542 ($\psi = 0°$, Transducer 3).

Figure 20. Effect of sweep on fluctuating-pressure spectra from transducer 1. Symbols indicate predicted Rossiter frequencies for rectangular cavities.

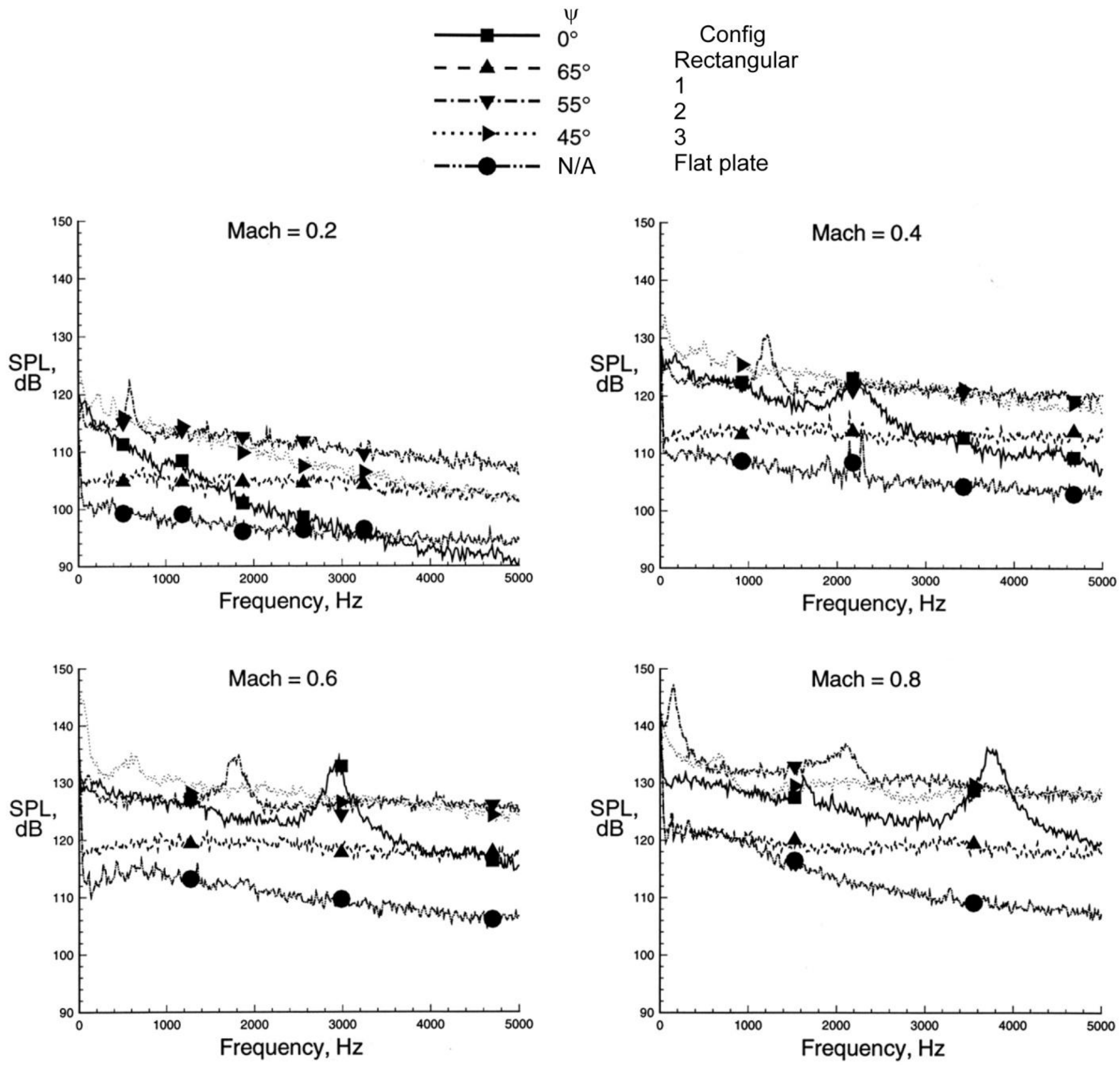

(b) l/h = 4. Transducer x/l = 0.246 (ψ = 65°), 0.581 (ψ = 55°), 0.782 (ψ = 45°), 0.407 (ψ = 0°, Transducer 3).

Figure 20. Continued.

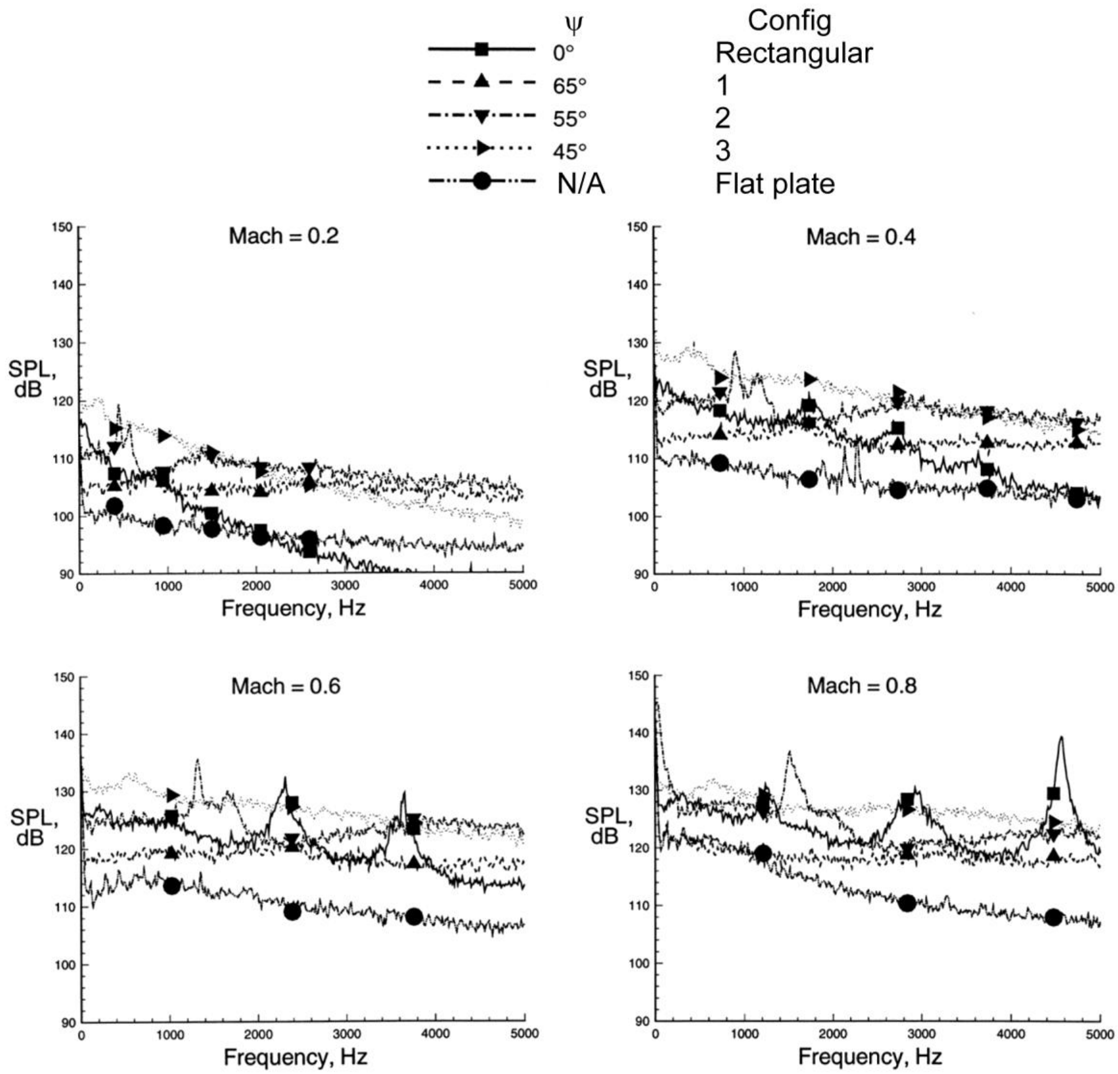

(c) l/h = 5. Transducer x/l = 0.196 (ψ = 65°), 0.465 (ψ = 55°), 0.625 (ψ = 45°), 0.325 (ψ = 0°, Transducer 3).

Figure 20. Continued.

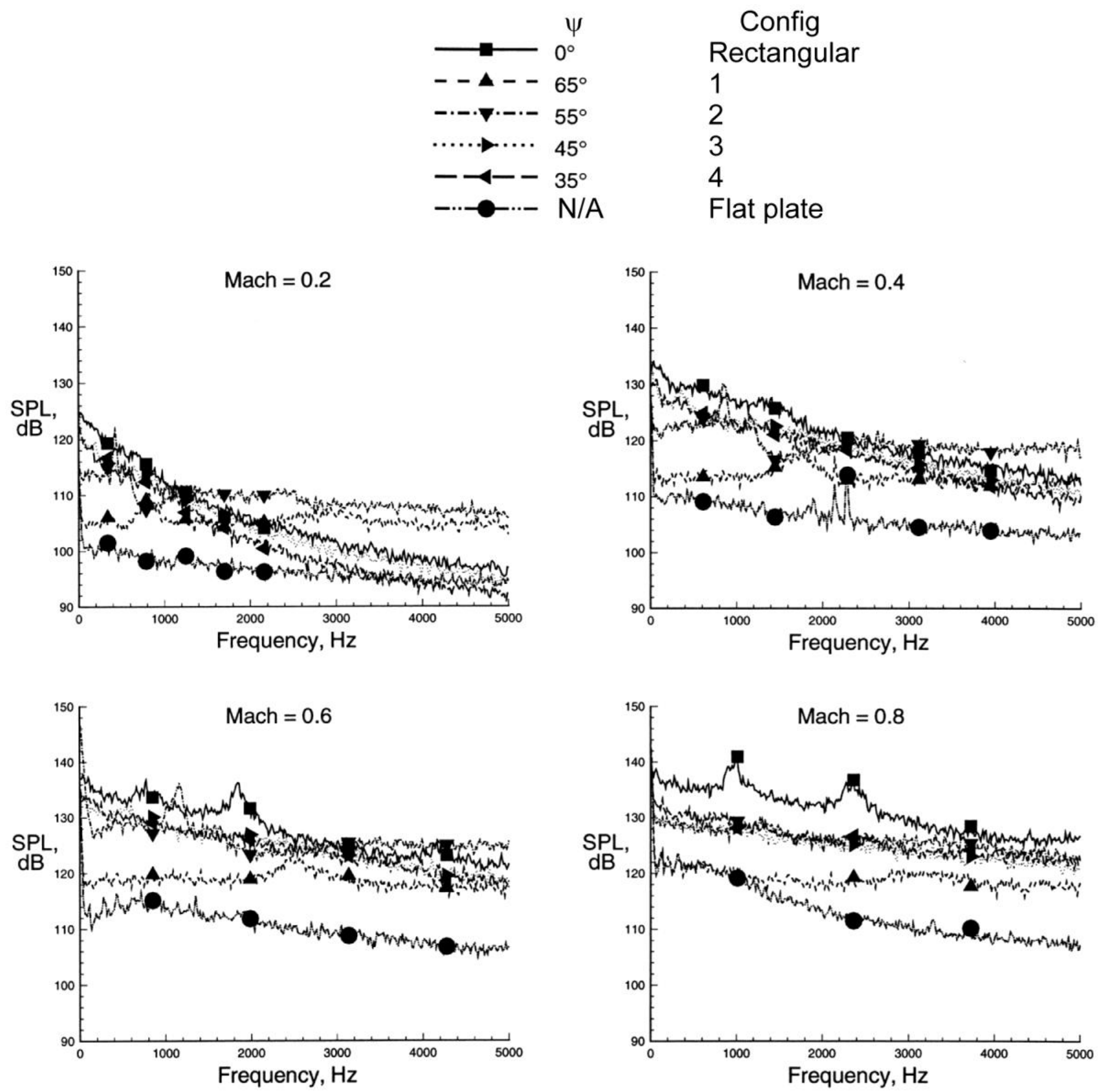

(d) *l/h* = 6. Transducer *x/l* = 0.163 ($\psi = 65°$), 0.387 ($\psi = 55°$), 0.521 ($\psi = 45°$), 0.614 ($\psi = 35°$), 0.771 ($\psi = 0°$).

Figure 20. Continued.

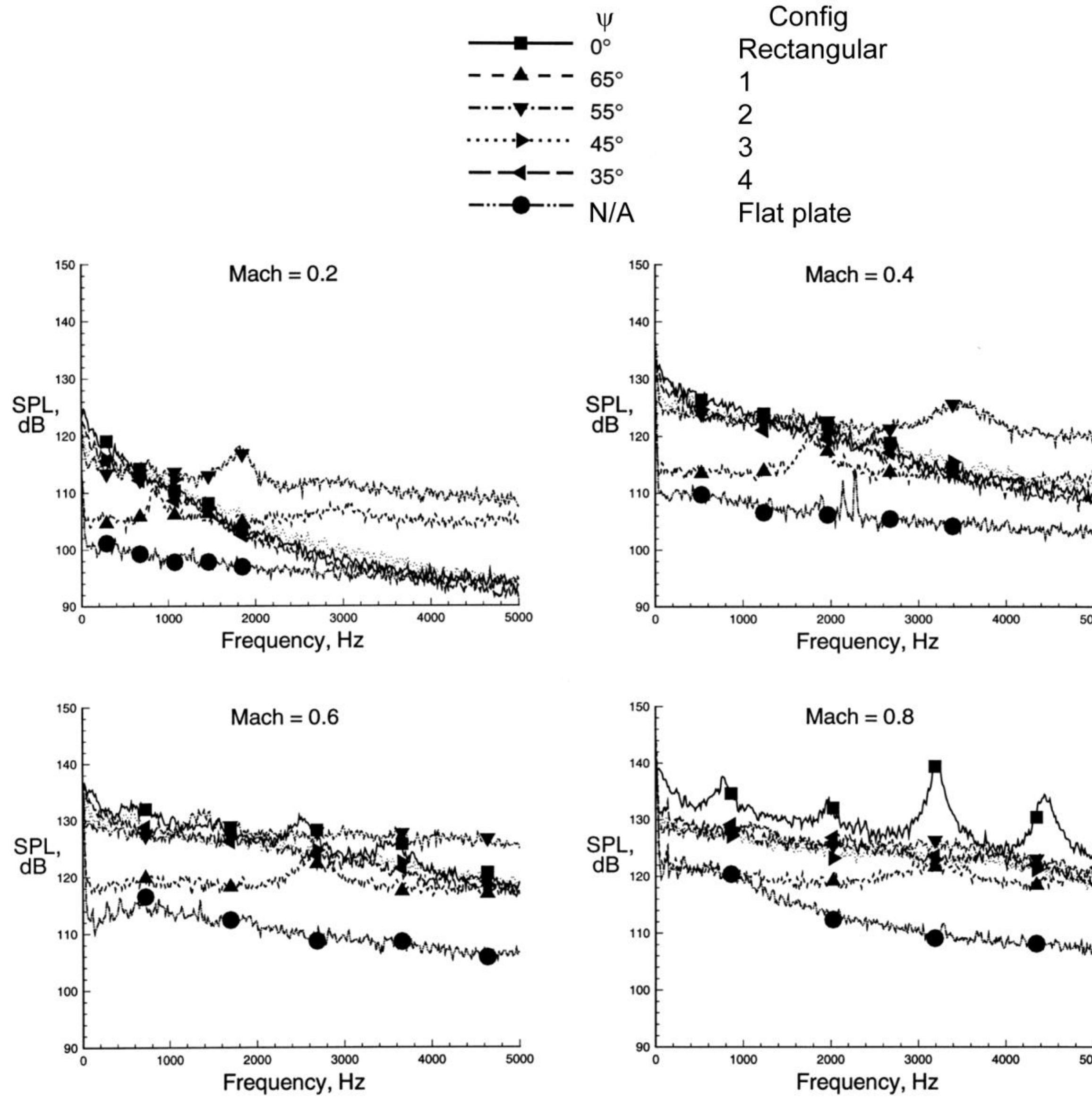

(e) *l/h* = 7. Transducer *x/l* = 0.140 (ψ = 65°), 0.332 (ψ = 55°), 0.447 (ψ = 45°), 0.527 (ψ = 35°), 0.661 (ψ = 0°).

Figure 20. Continued.

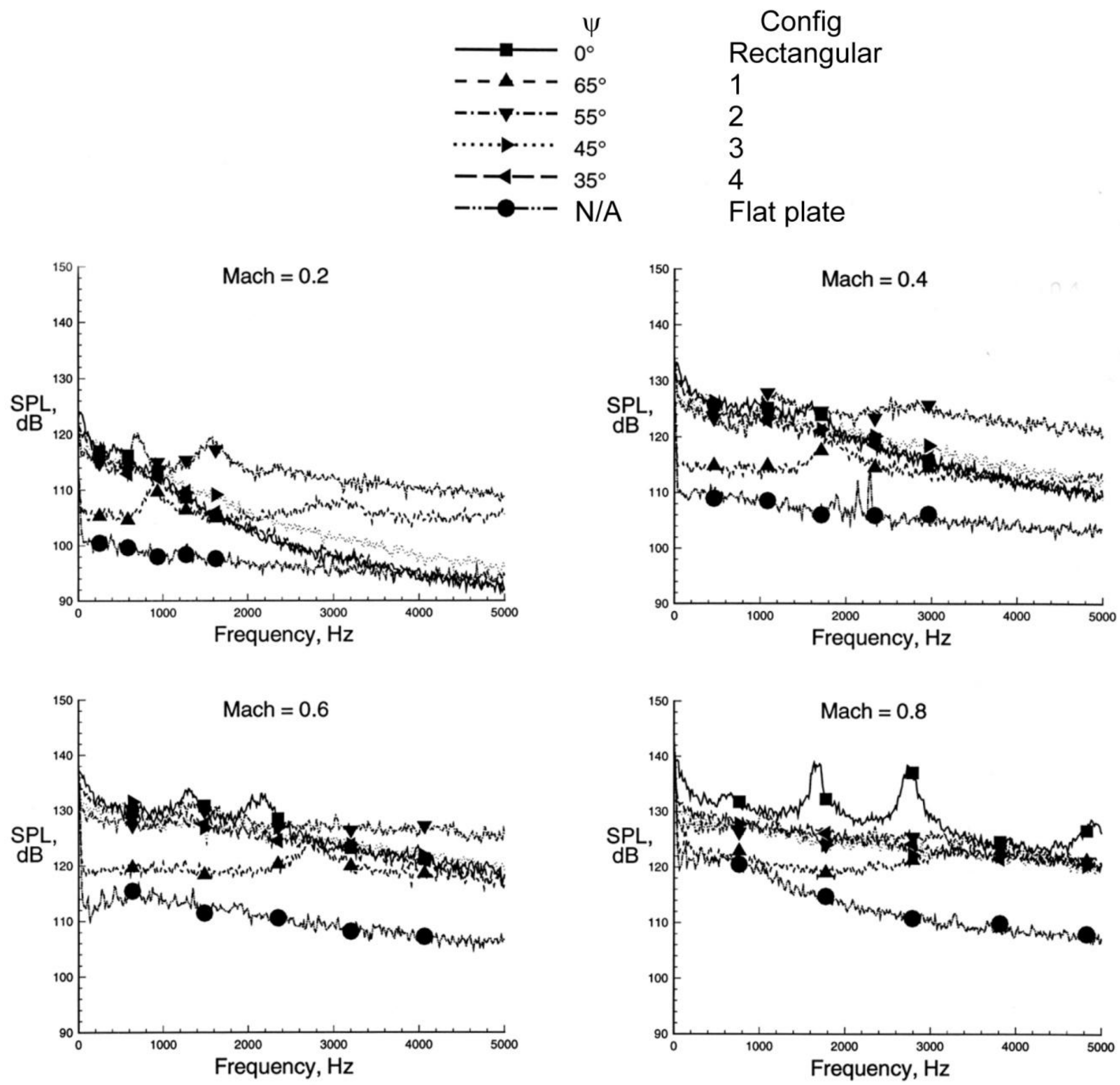

(f) *l/h* = 8. Transducer *x/l* = 0.123 (ψ = 65°), 0.291 (ψ = 55°), 0.391 (ψ = 45°), 0.461 (ψ = 35°), 0.578 (ψ = 0°).

Figure 20. Continued.

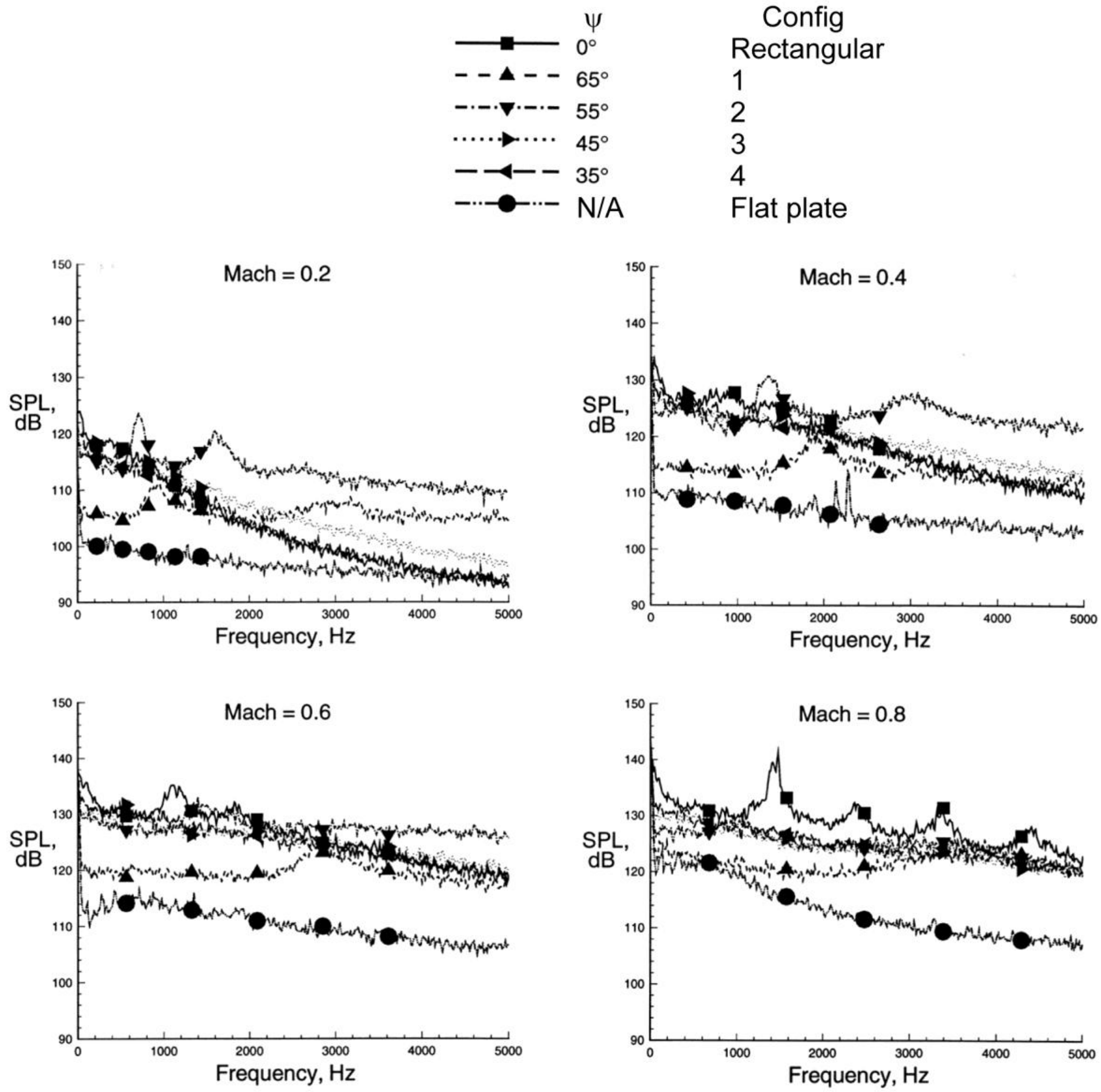

(g) *l/h* = 9. Transducer *x/l* = 0.109 ($\psi = 65°$), 0.258 ($\psi = 55°$), 0.347 ($\psi = 45°$), 0.410 ($\psi = 35°$), 0.514 ($\psi = 0°$).

Figure 20. Continued.

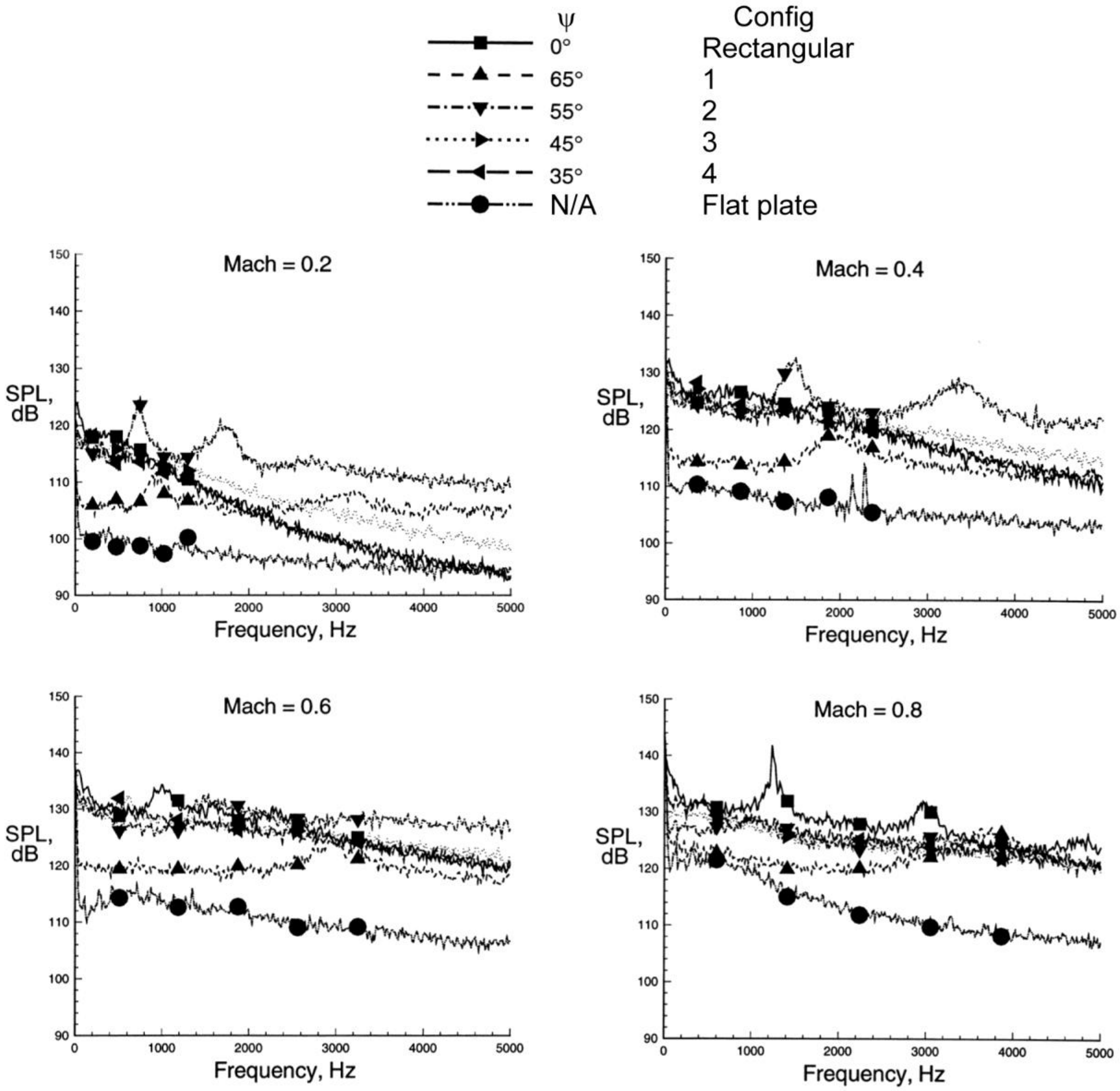

(h) *l*/*h* = 10. Transducer *x*/*l* = 0.098 ($\psi = 65°$), 0.232 ($\psi = 55°$), 0.313 ($\psi = 45°$), 0.369 ($\psi = 35°$), 0.463 ($\psi = 0°$).

Figure 20. Continued.

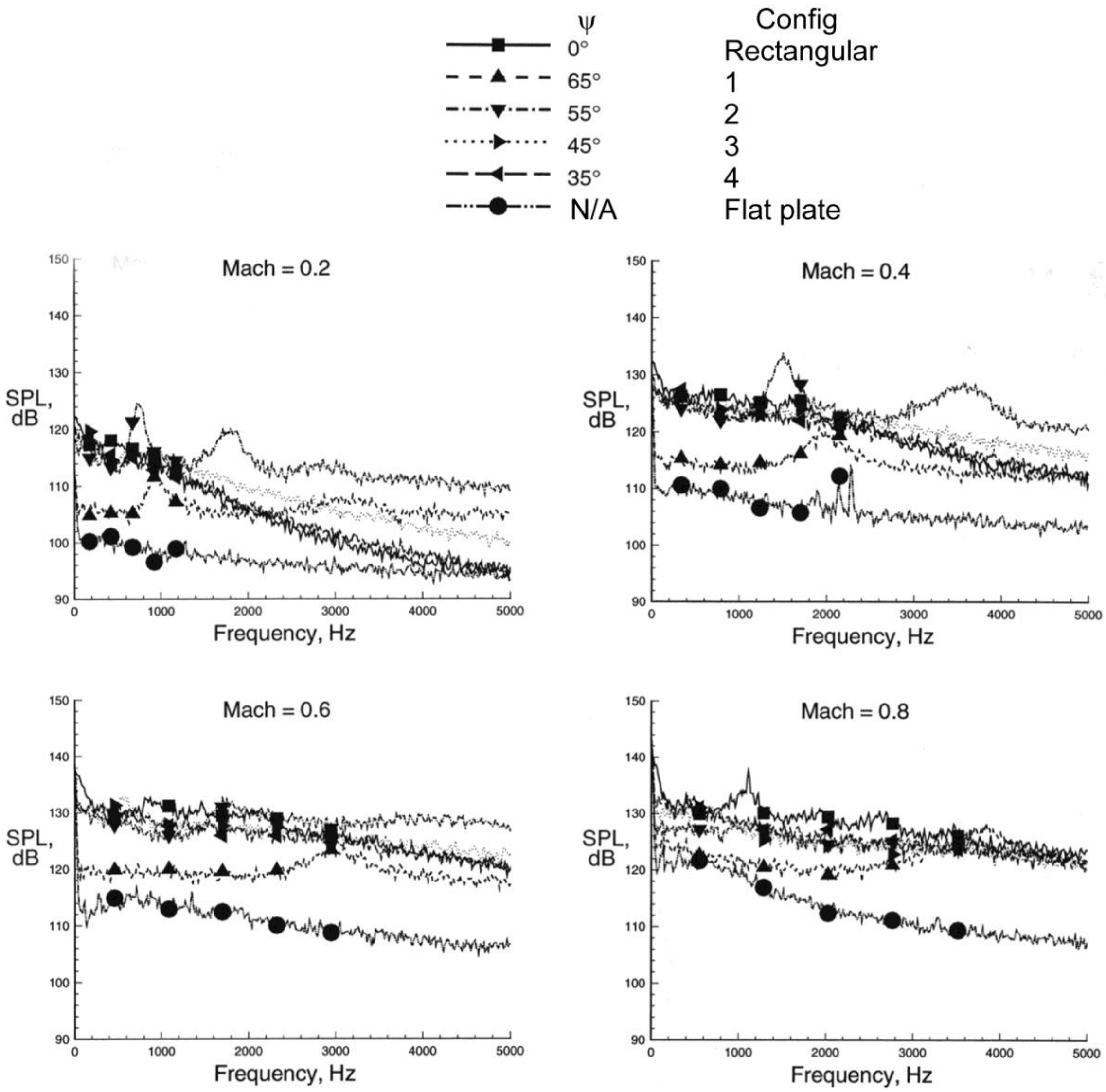

(i) l/h = 11. Transducer x/l = 0.089 (ψ = 65°), 0.211 (ψ = 55°), 0.284 (ψ = 45°), 0.335 (ψ = 35°), 0.421 (ψ = 0°).

Figure 20. Continued.

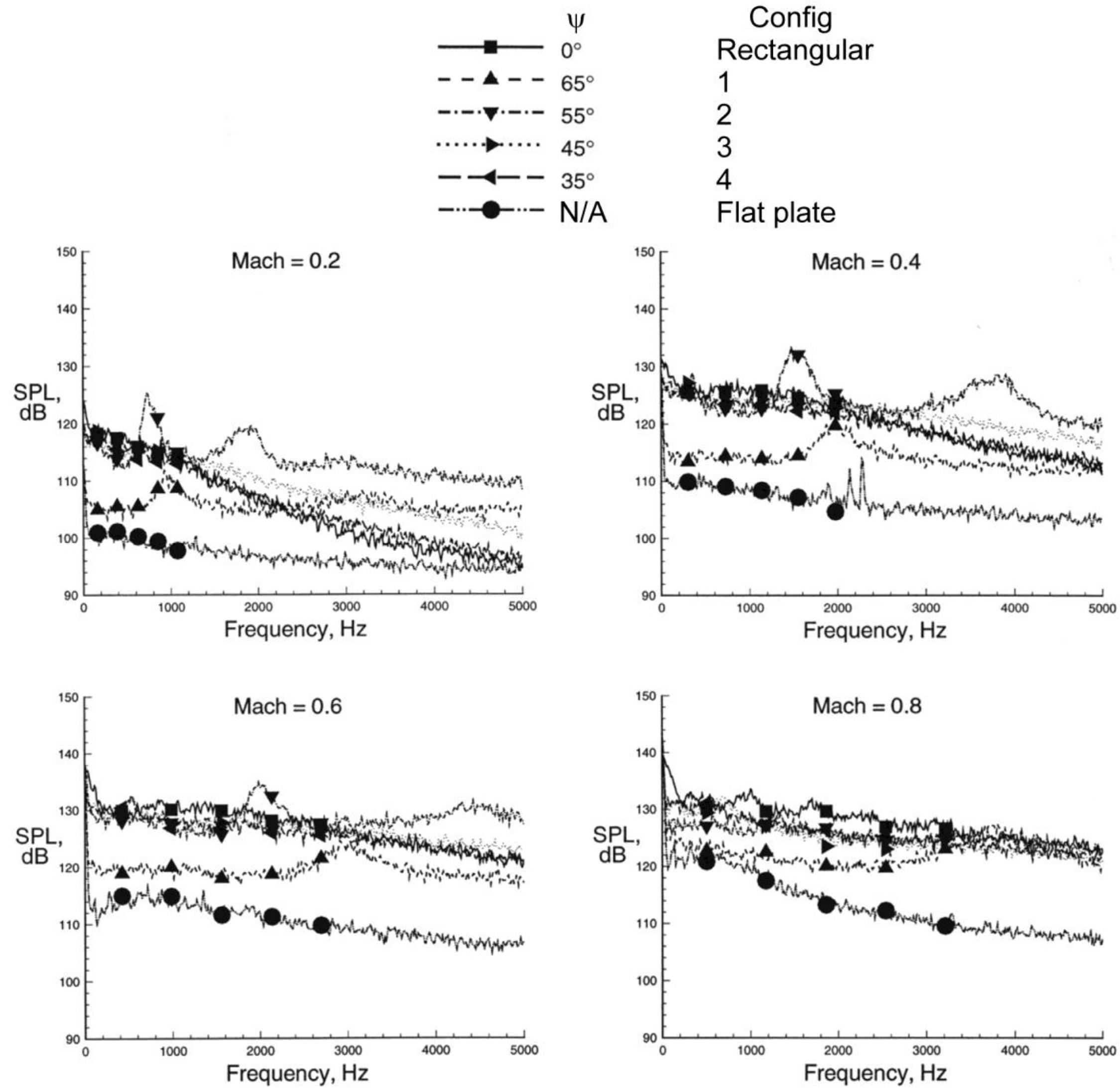

(j) *l*/*h* = 12. Transducer *x*/*l* = 0.082 ($\psi = 65°$), 0.193 ($\psi = 55°$), 0.261 ($\psi = 45°$), 0.307 ($\psi = 35°$), 0.386 ($\psi = 0°$).

Figure 20. Continued.

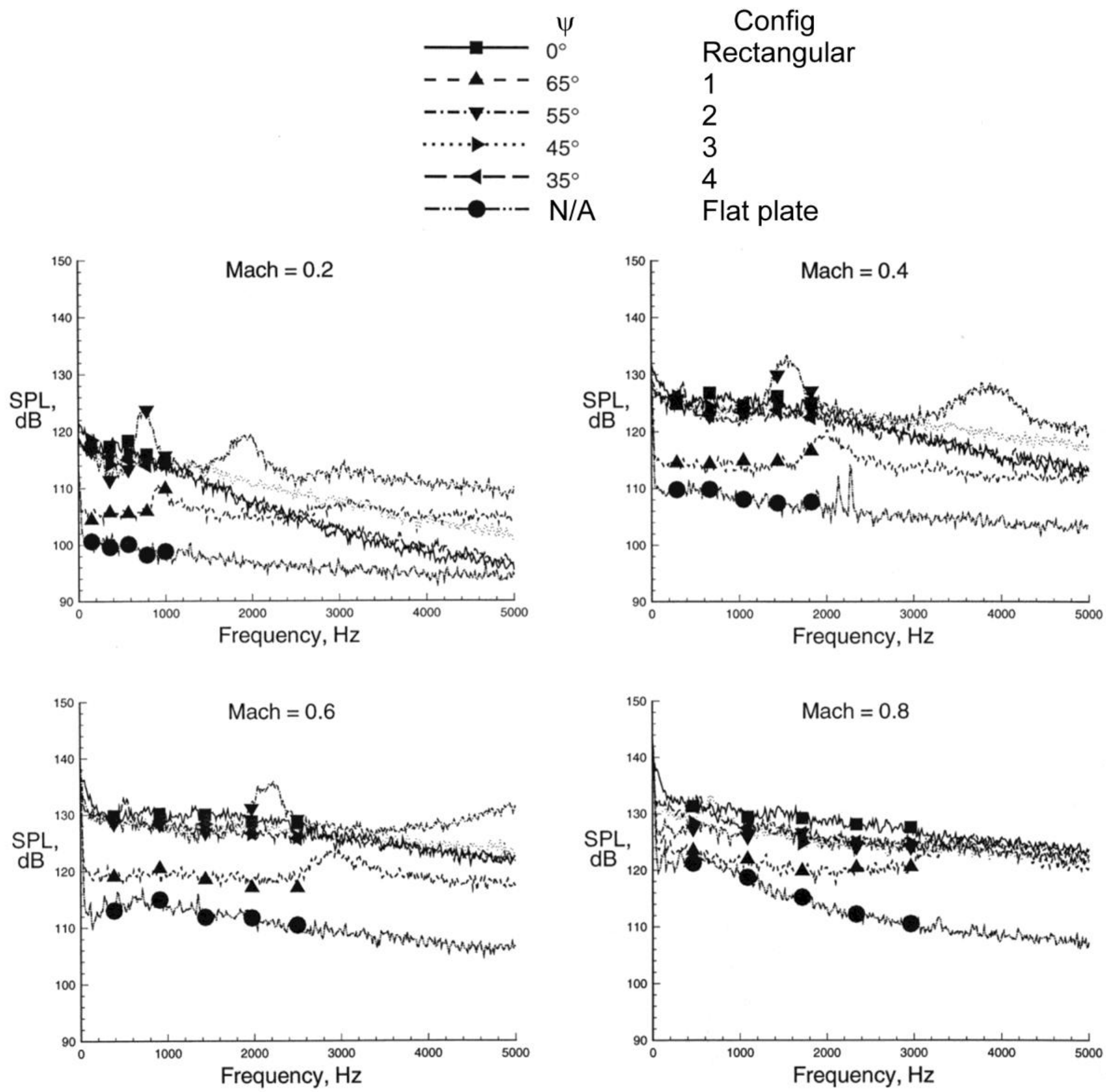

(k) l/h = 13. Transducer x/l = 0.076 (ψ = 65°), 0.179 (ψ = 55°), 0.240 (ψ = 45°), 0.284 (ψ = 35°), 0.356 (ψ = 0°).

Figure 20. Continued.

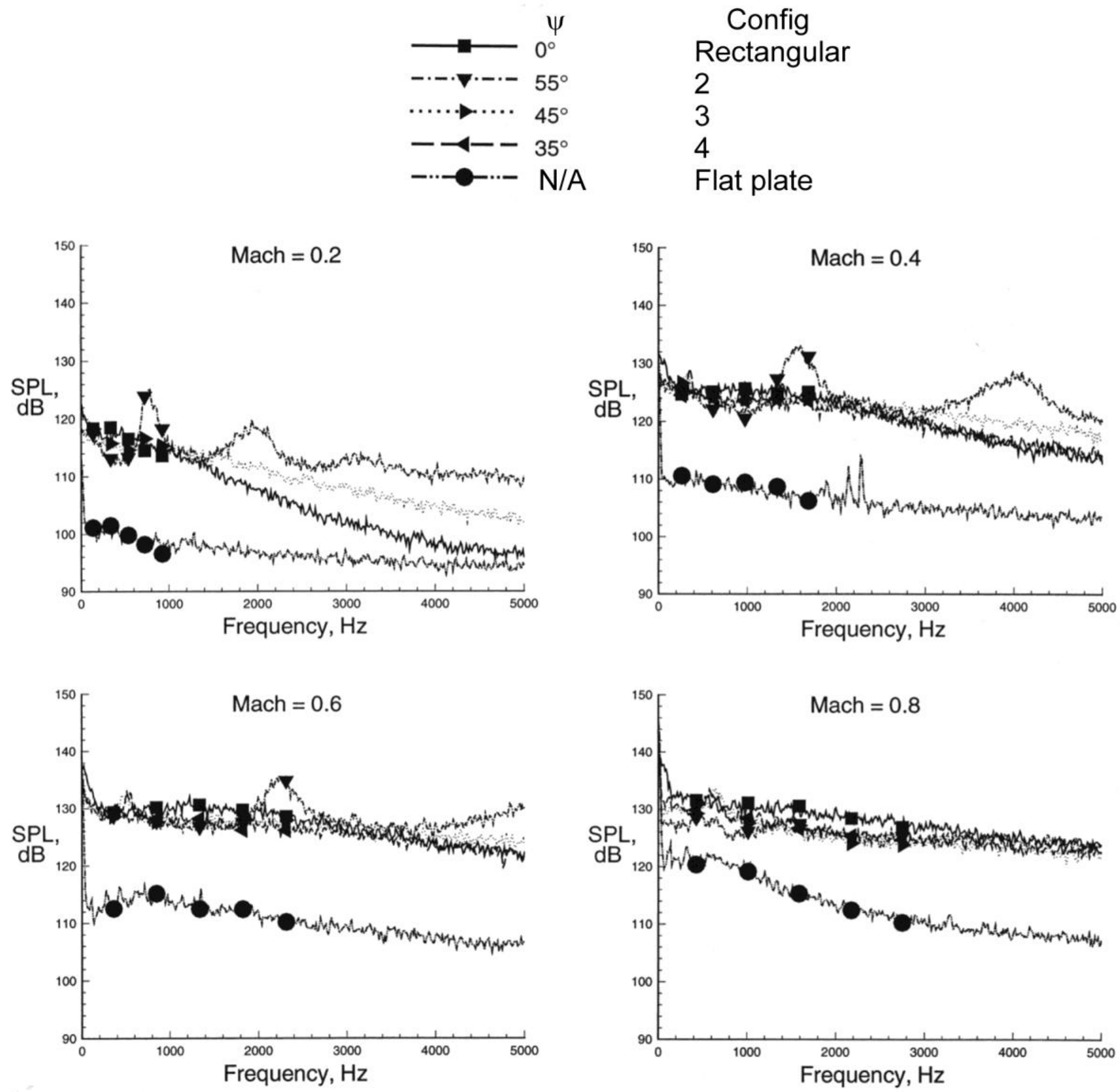

(l) l/h = 14. Transducer x/l = 0.166 (ψ = 55°), 0.223 (ψ = 45°), 0.263 (ψ = 35°), 0.330 (ψ = 0°).

Figure 20. Continued.

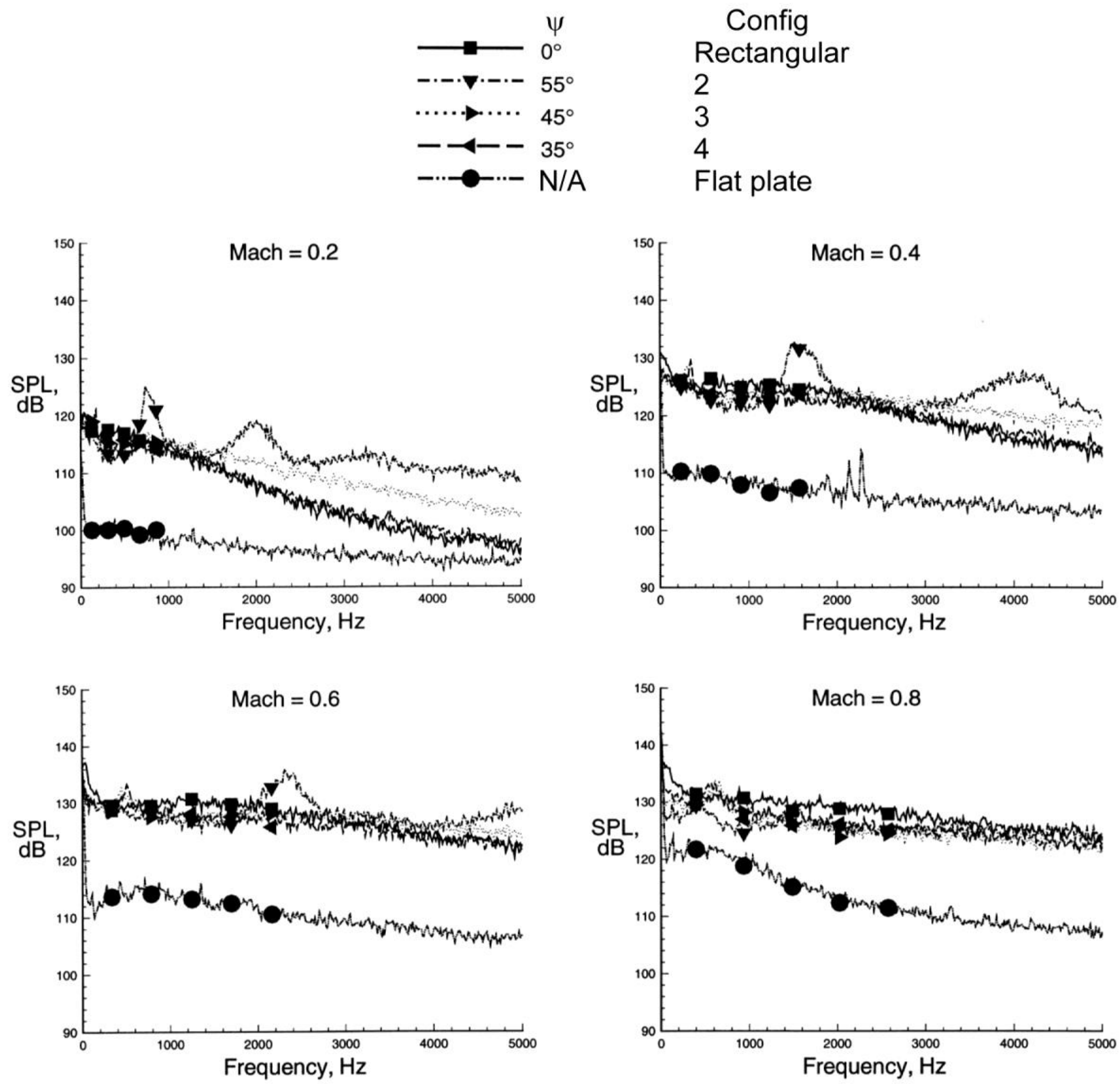

(m) l/h = 15. Transducer x/l = 0.155 (ψ = 55°), 0.208 (ψ = 45°), 0.246 (ψ = 35°), 0.308 (ψ = 0°).

Figure 20. Continued.

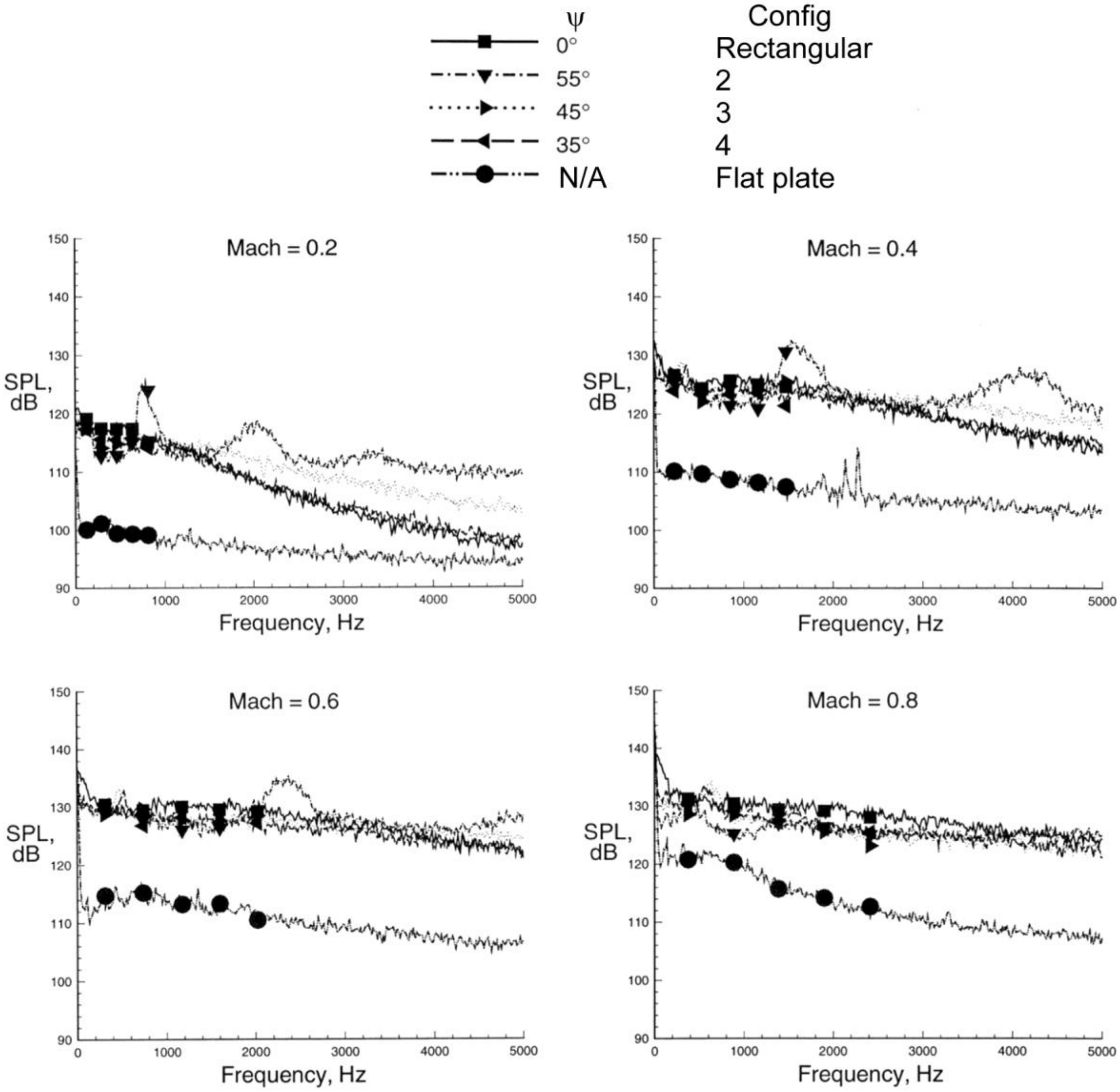

(n) l/h = 16. Transducer x/l = 0.145 (ψ = 55°), 0.195 (ψ = 45°), 0.231 (ψ = 35°), 0.289 (ψ = 0°).

Figure 20. Continued.

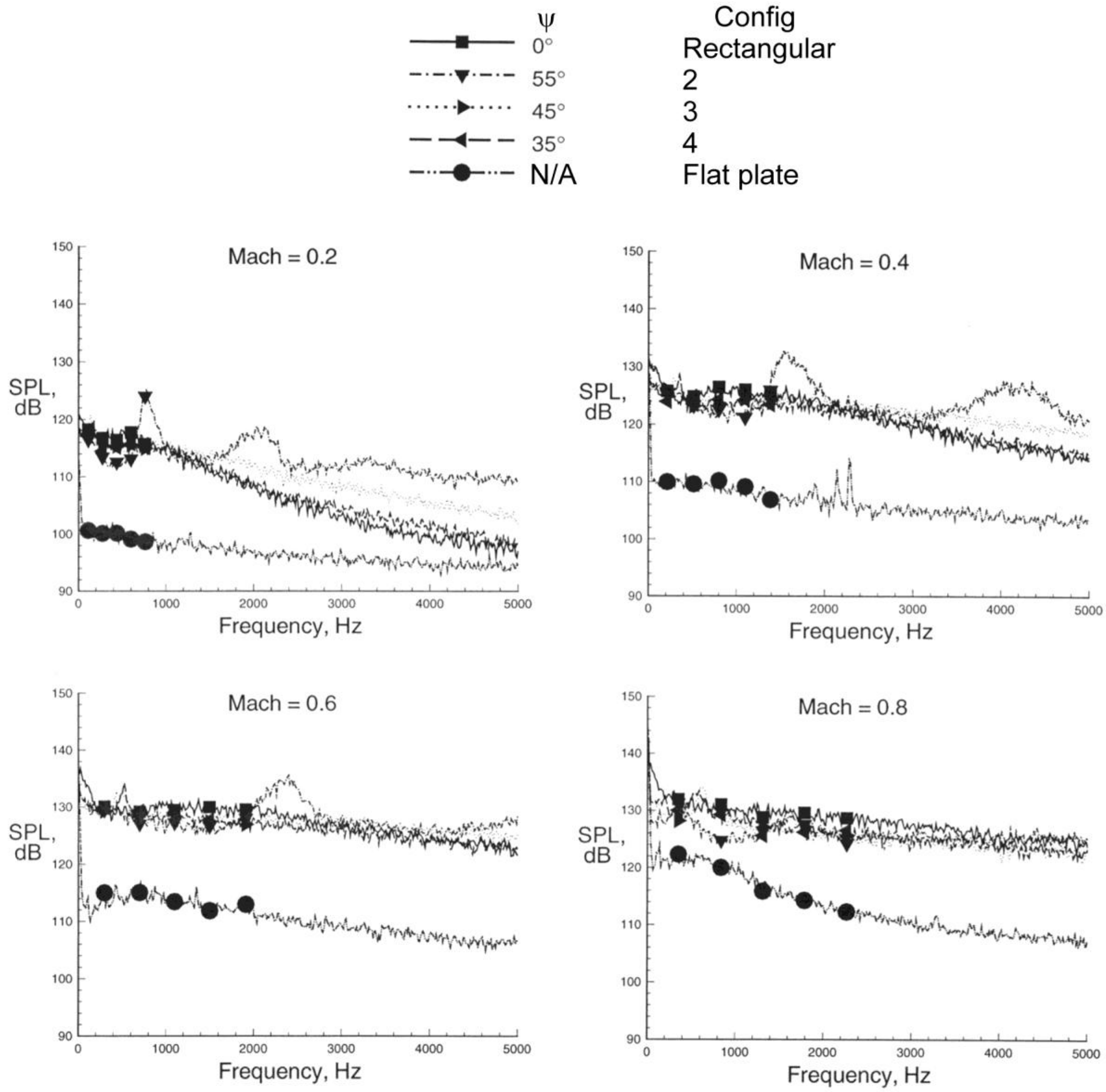

(o) l/h = 17. Transducer x/l = 0.137 (ψ = 55°), 0.184 (ψ = 45°), 0.217 (ψ = 35°), 0.272 (ψ = 0°).

Figure 20. Continued.

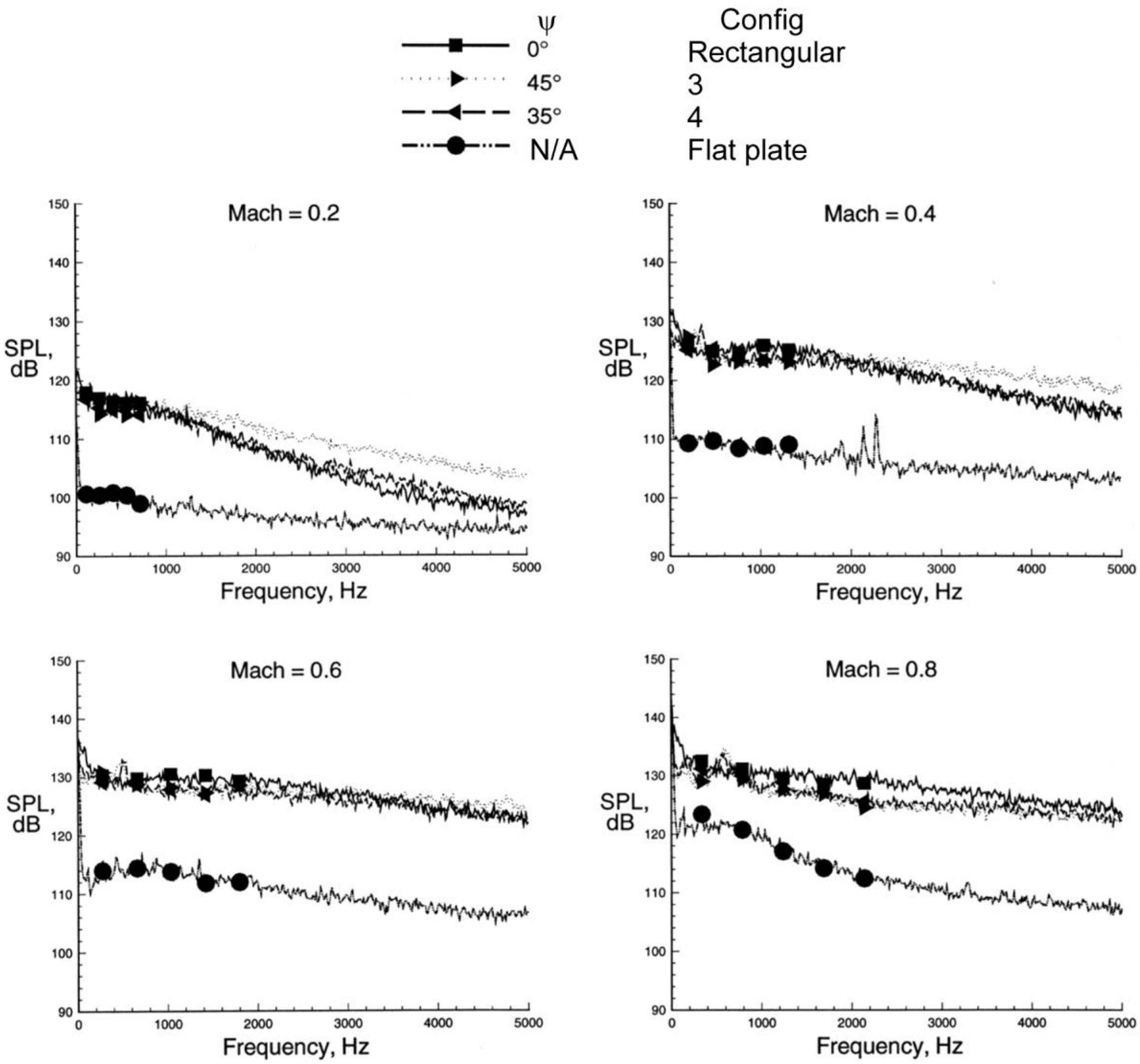

(p) l/h = 18. Transducer x/l = 0.173 (ψ = 45°), 0.205 (ψ = 35°), 0.257 (ψ = 0°).

Figure 20. Continued.

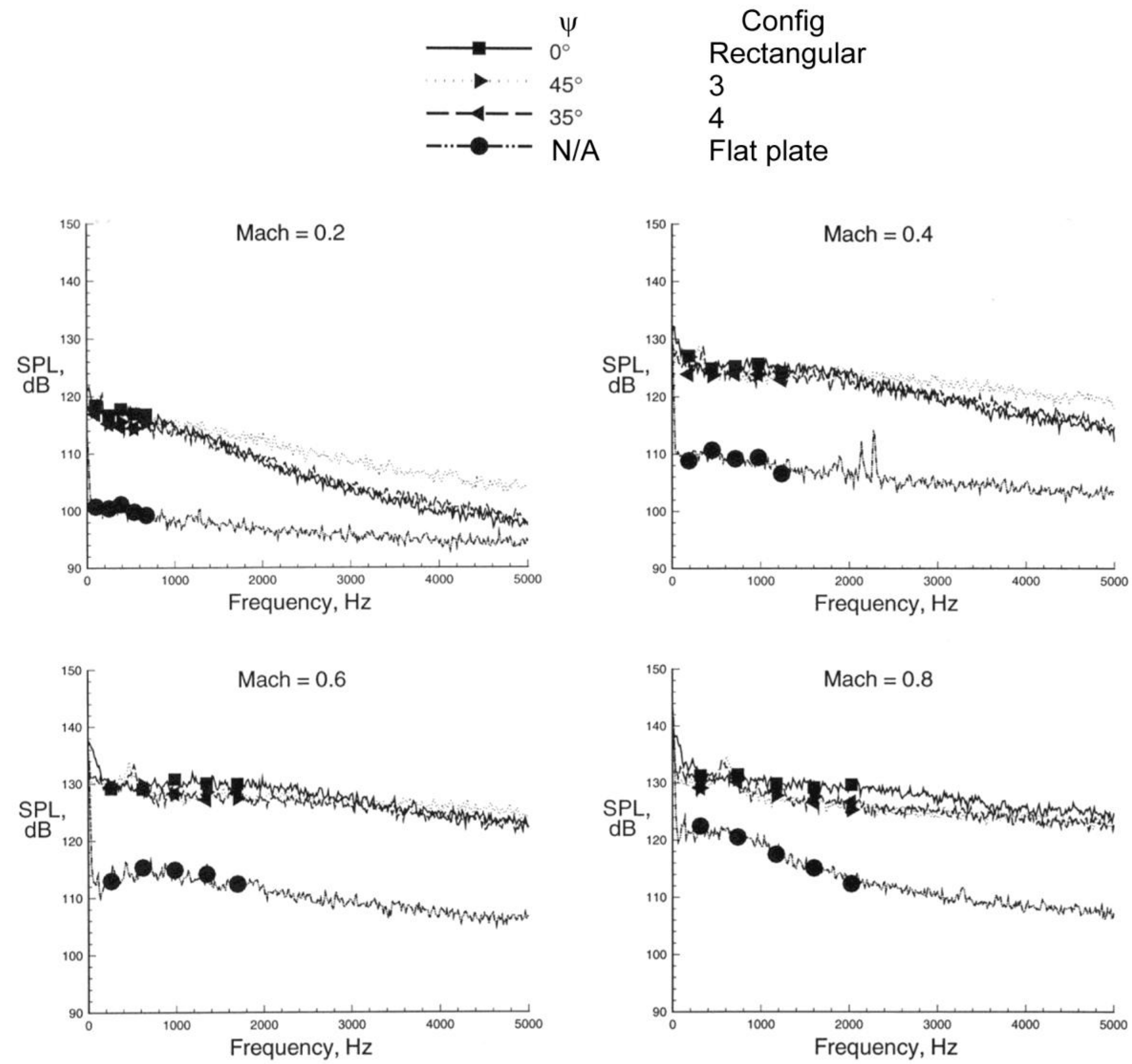

(q) l/h = 19. Transducer x/l = 0.165 (ψ = 45°), 0.194 (ψ = 35°), 0.243 (ψ = 0°).

Figure 20. Continued.

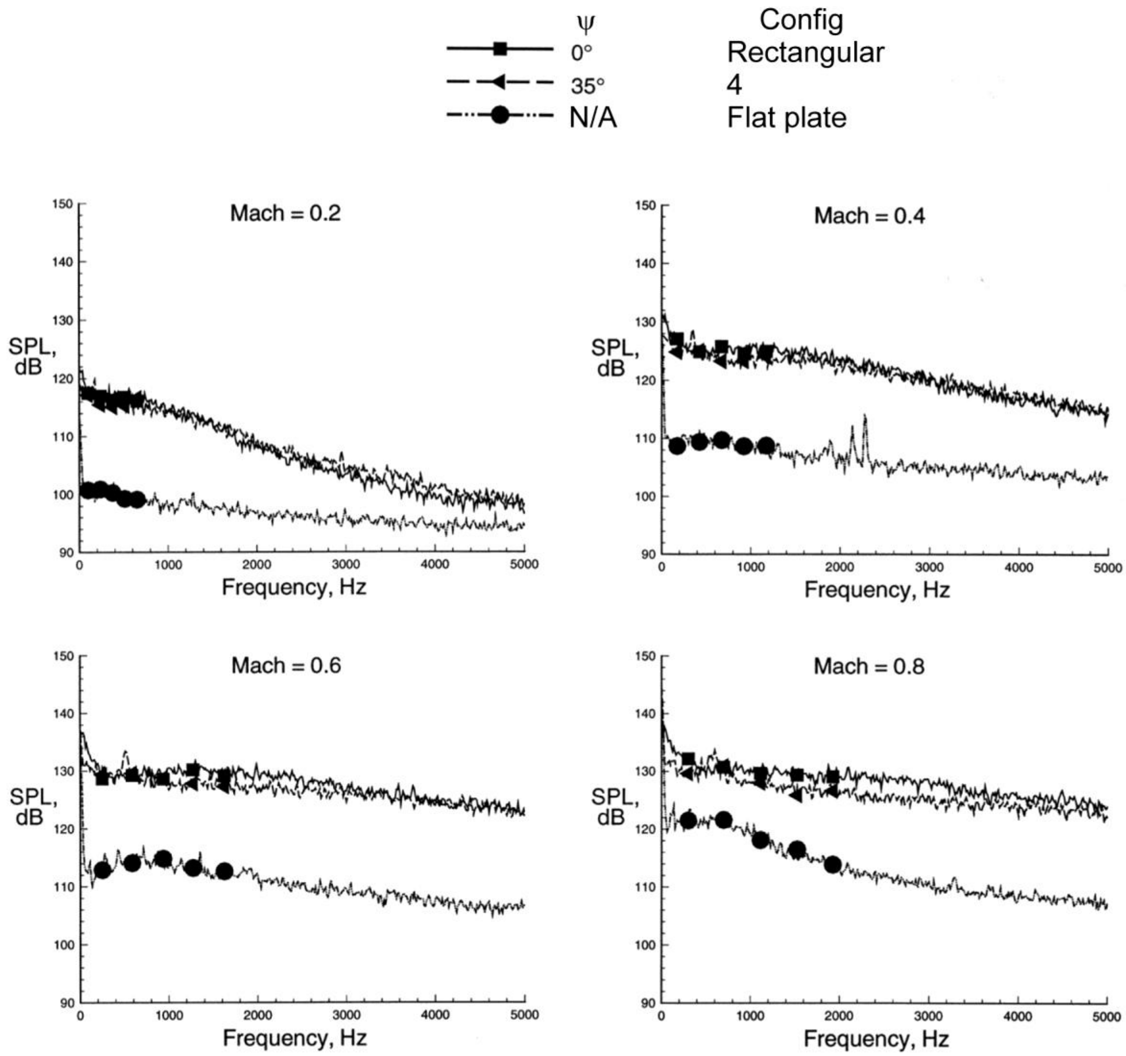

(r) *l*/*h* = 20. Transducer *x*/*l* = 0.184 (ψ = 35°), 0.231 (ψ = 0°).

Figure 20. Continued.

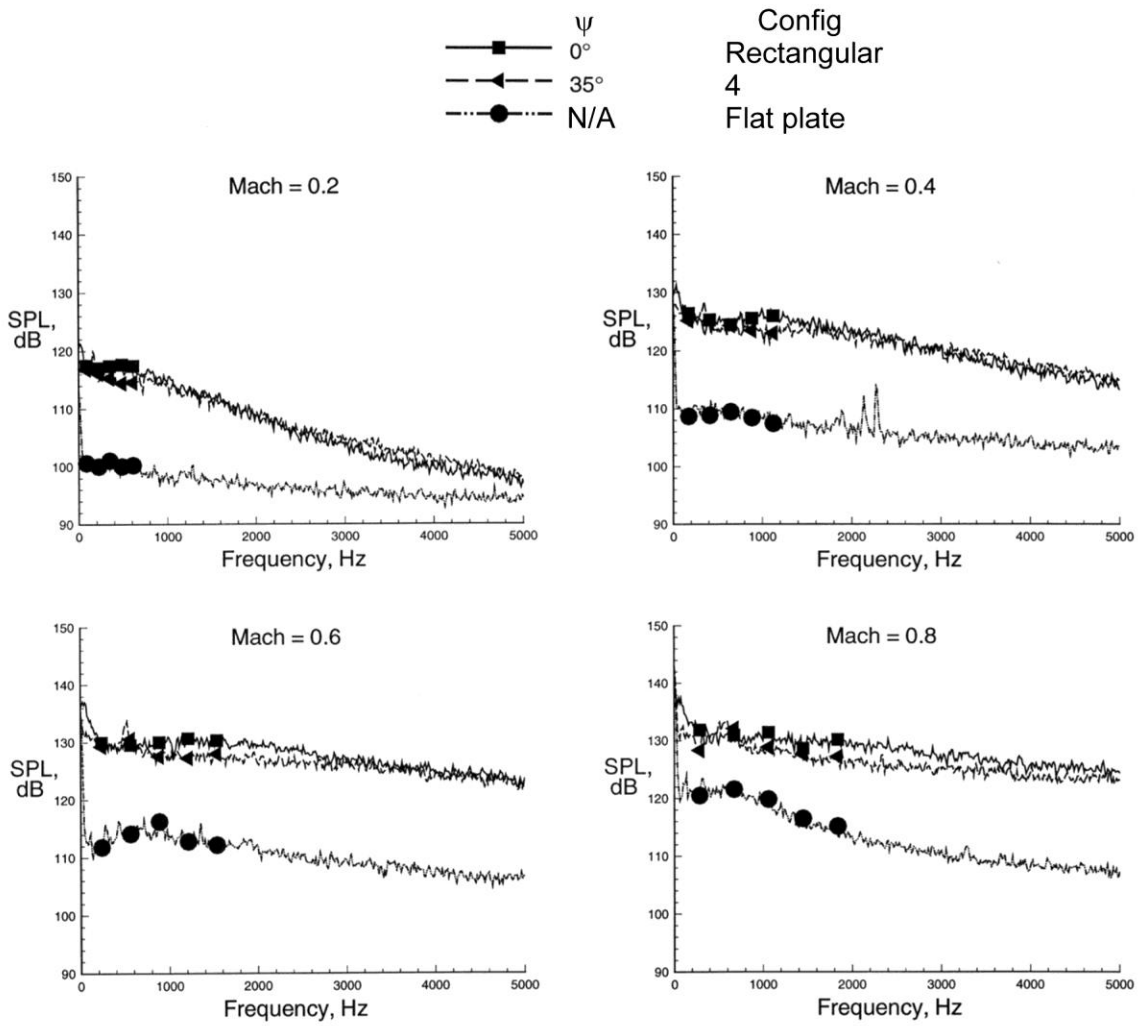

(s) *l*/*h* = 21. Transducer *x*/*l* 0.176 ($\psi = 35°$), 0.220 ($\psi = 0°$).

Figure 20. Concluded.

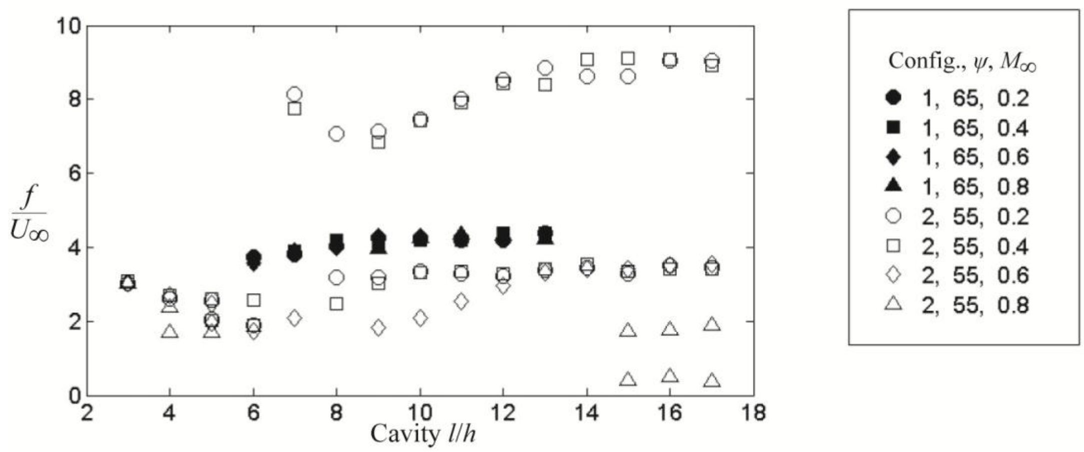

Figure 21. Spectral peak frequencies (divided by free-stream velocity) observed in cavities with $\psi = 65°$ and 55°.

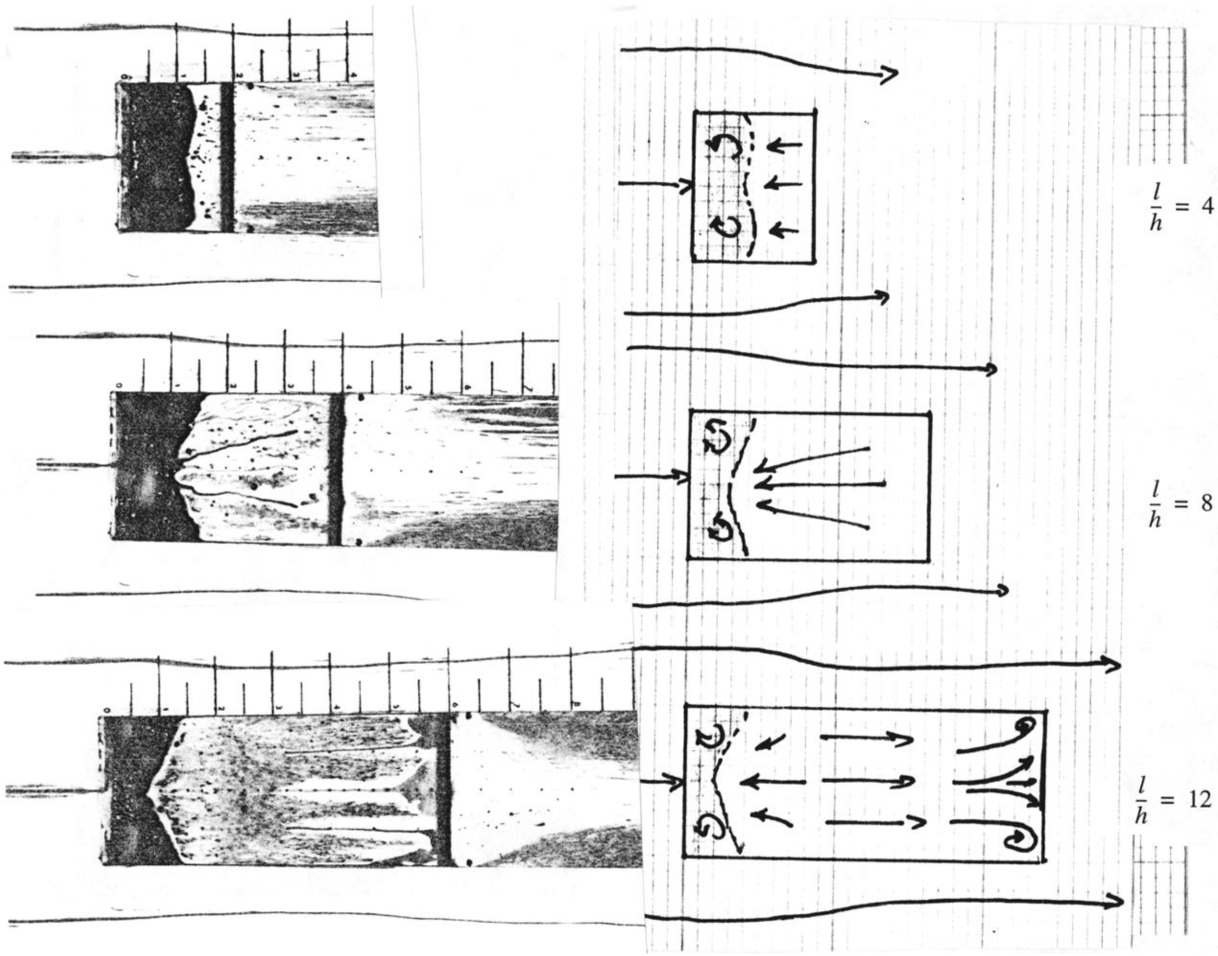

(a) $M_\infty = 0.2$.

Figure 22. Photographs and sketches of surface flow visualization, $\psi = 0°$.

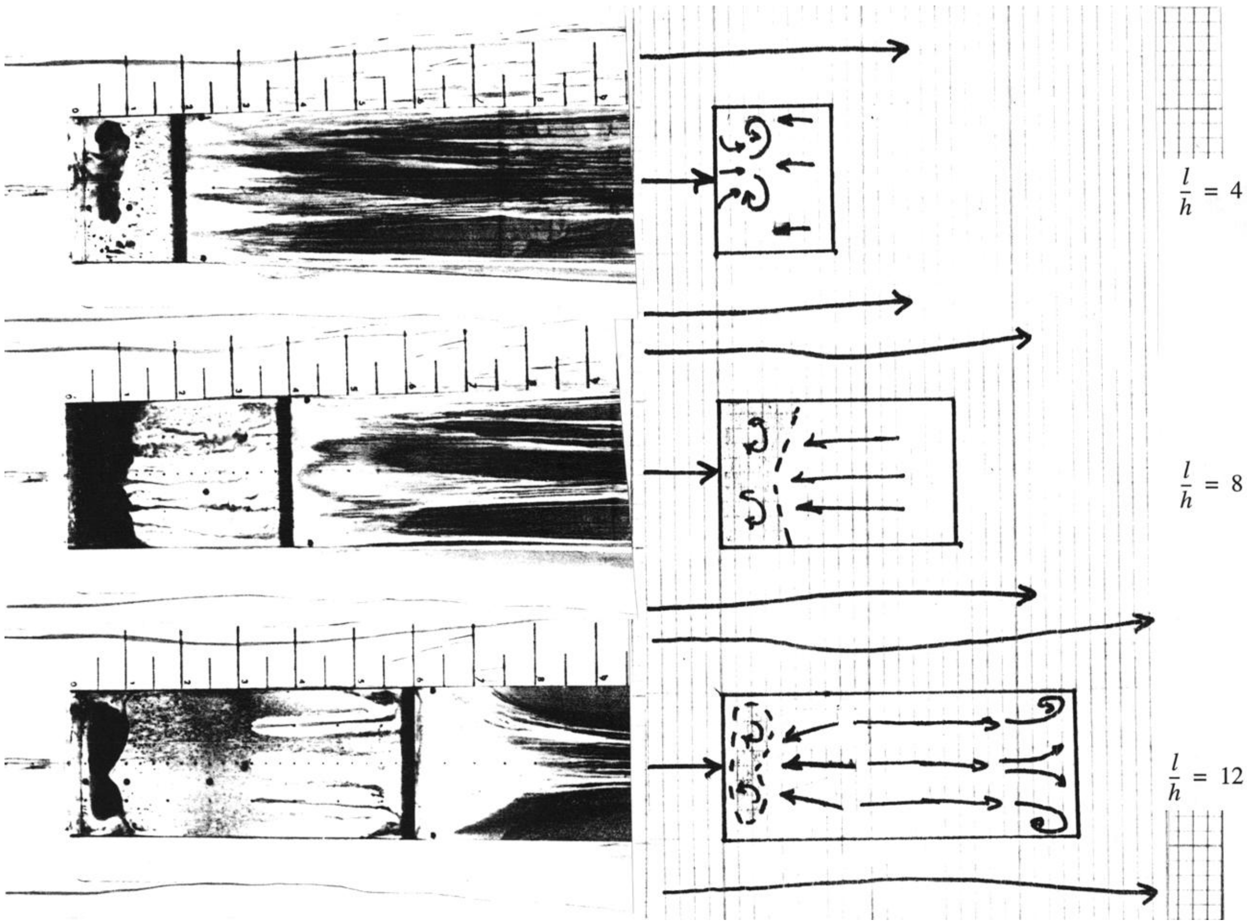

(b) $M_\infty = 0.4$.

Figure 22. Continued.

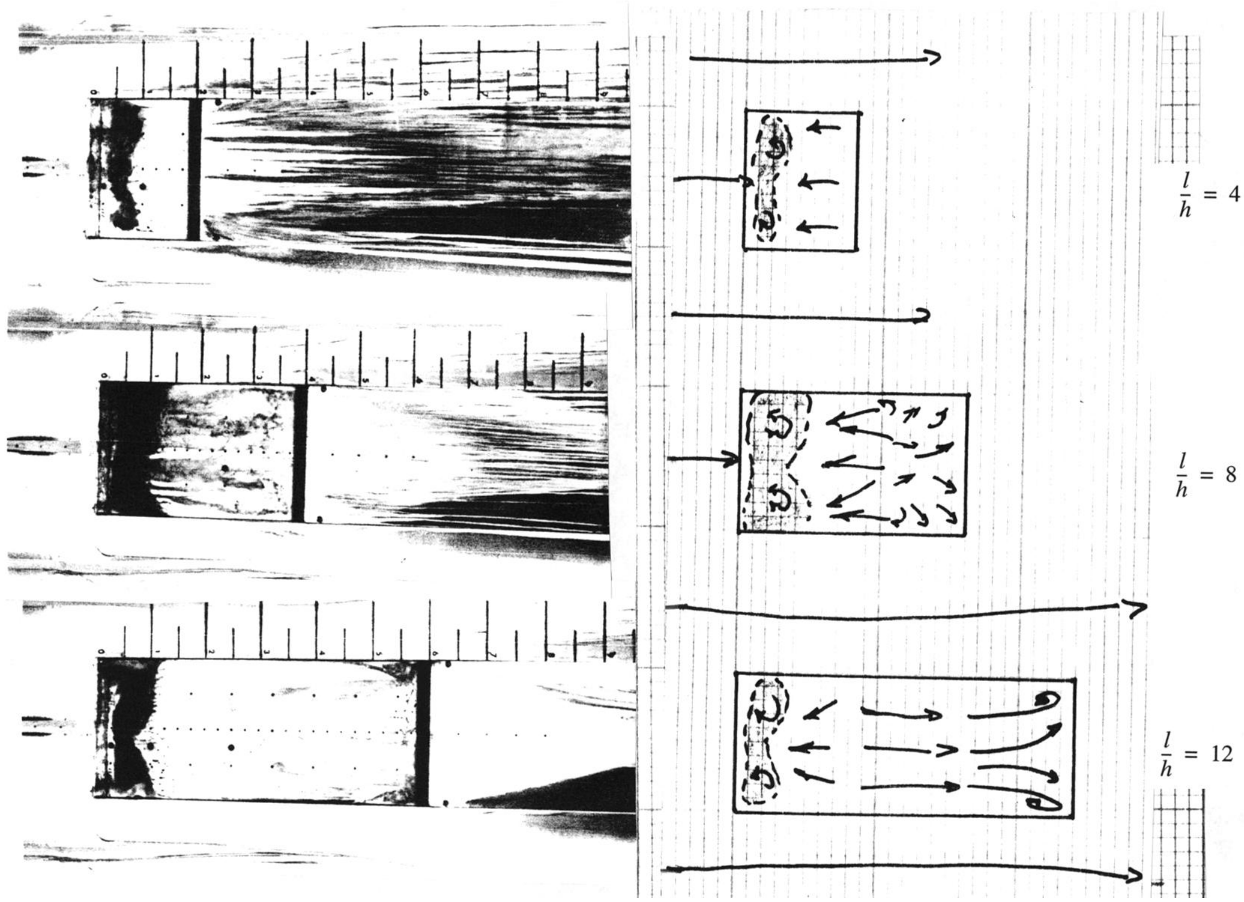

(c) $M_\infty = 0.6$.

Figure 22. Continued.

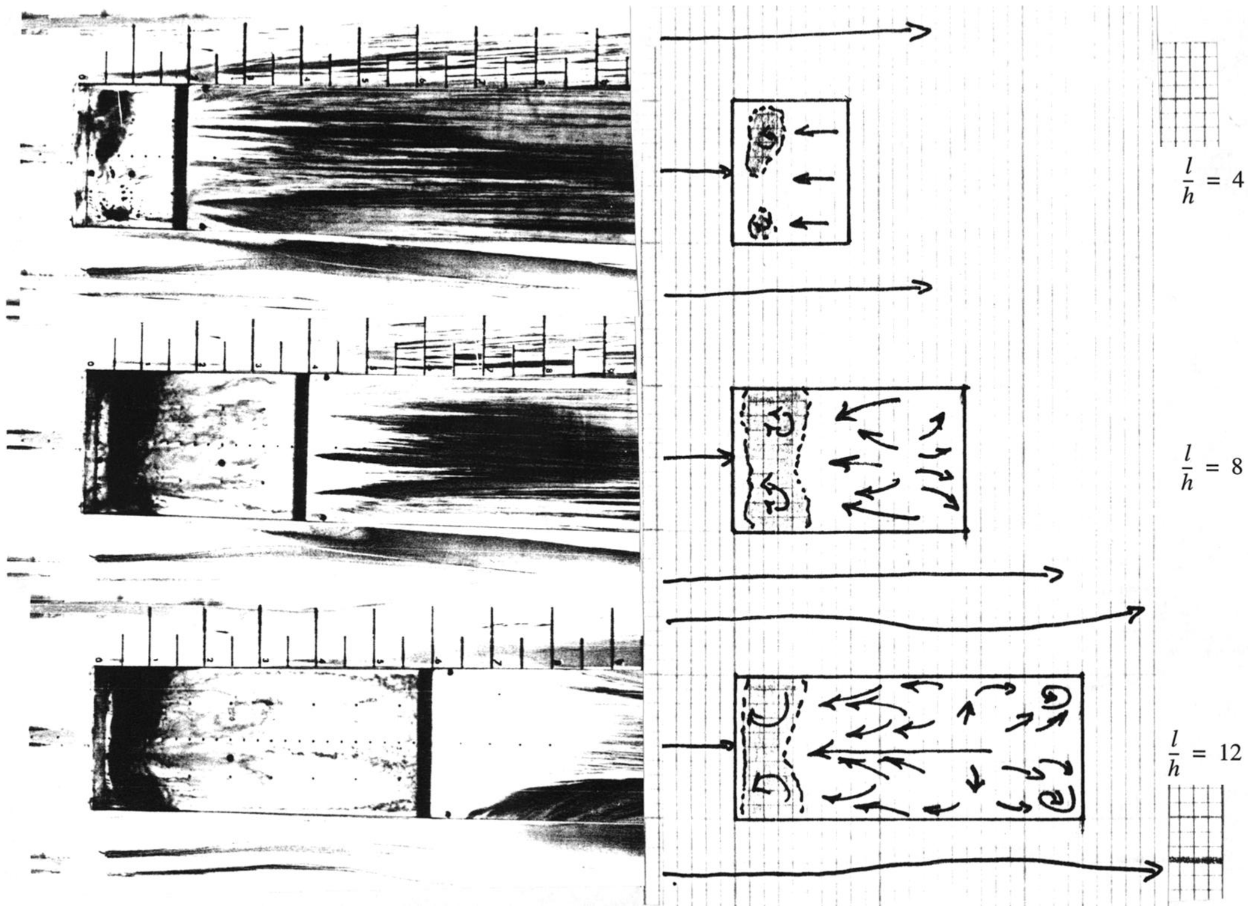

(d) $M_\infty = 0.8$.

Figure 22. Concluded.

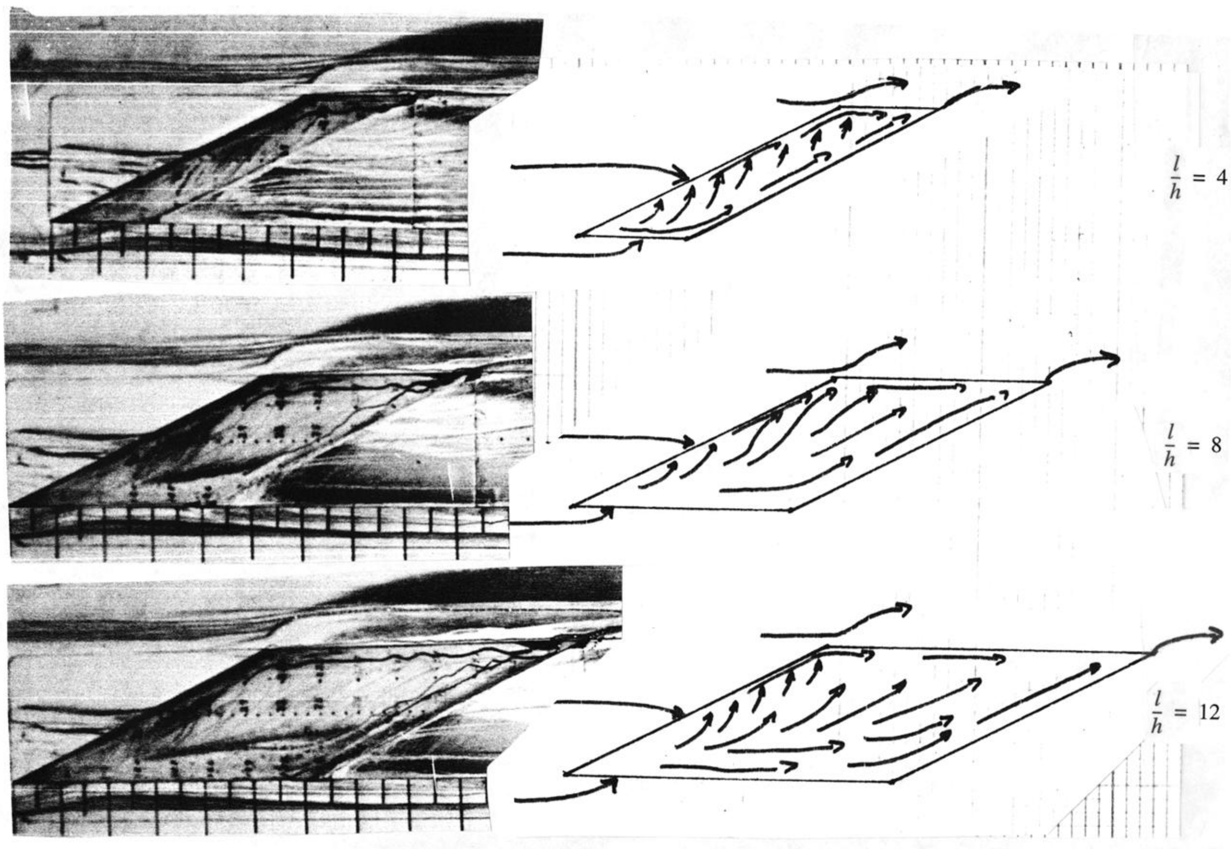

(a) $M_\infty = 0.2$.

Figure 23. Photographs and sketches of surface flow visualization, $\psi = 65°$.

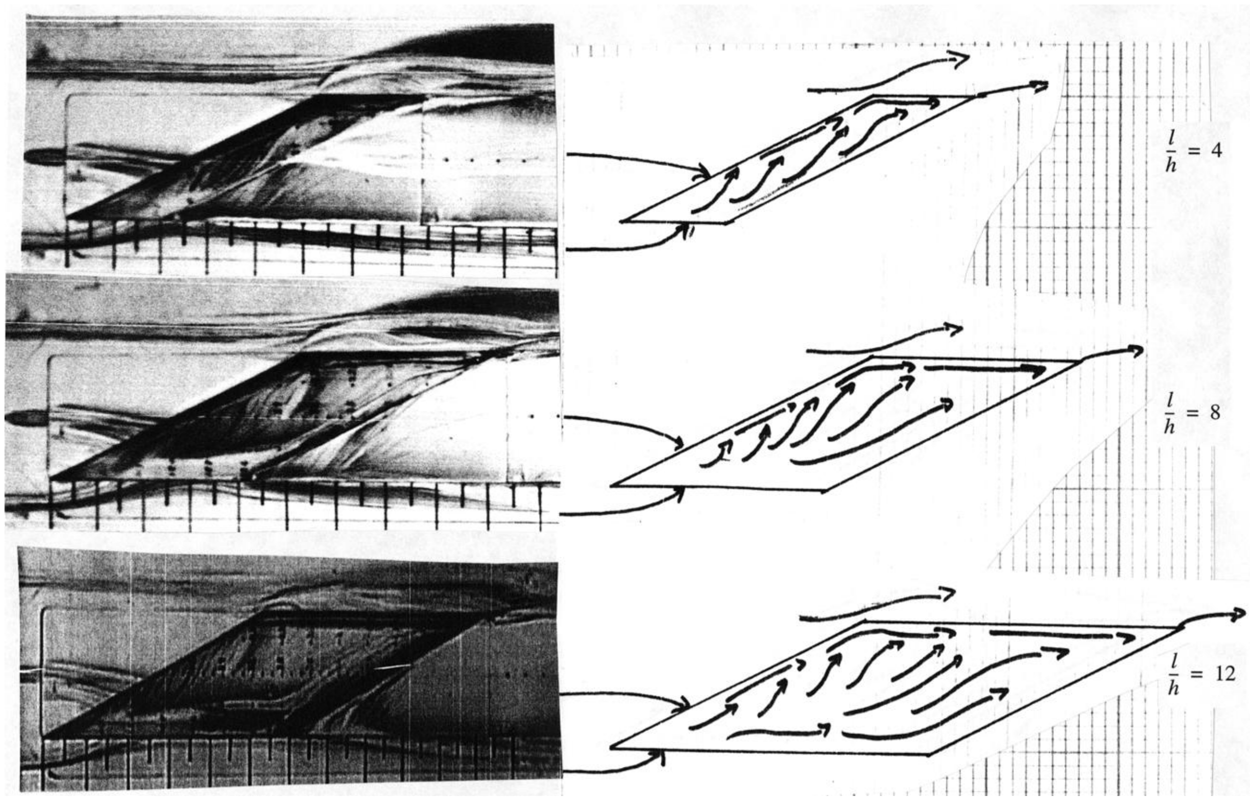

(b) $M_\infty = 0.4$.

Figure 23. Continued.

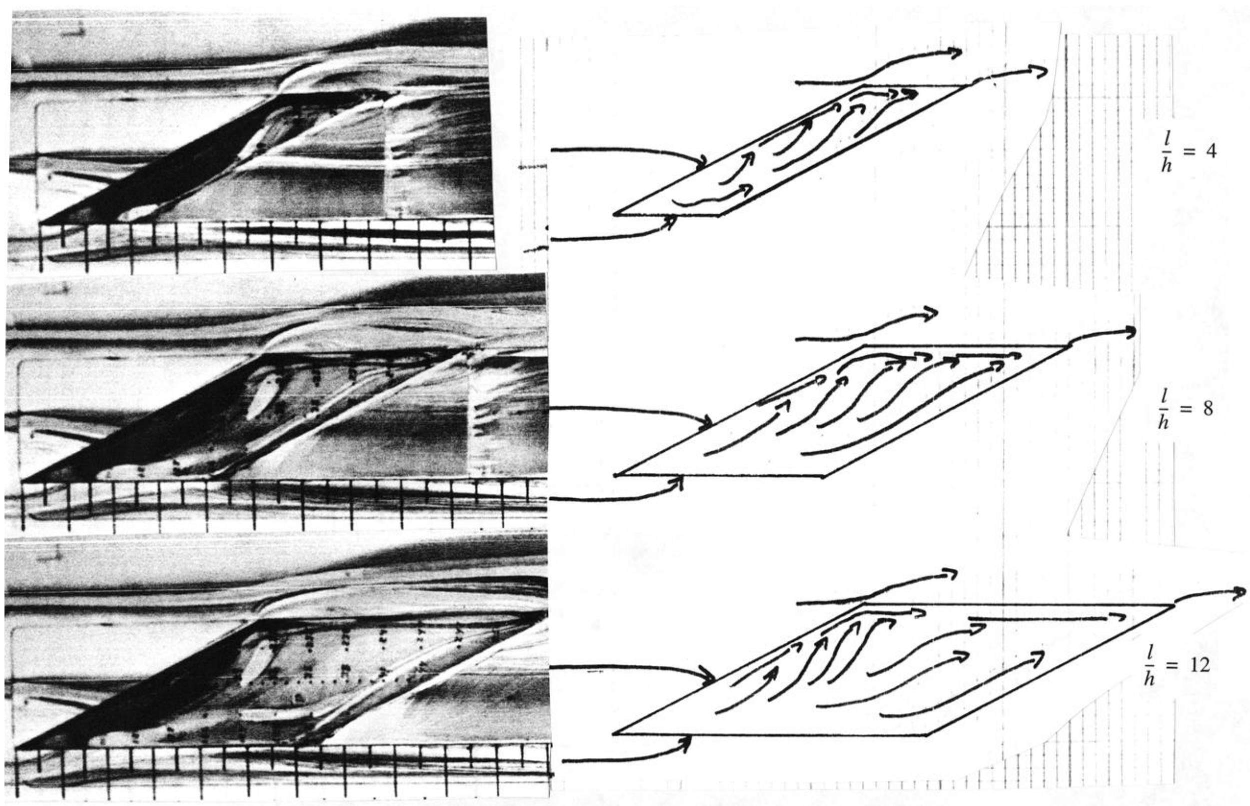

(c) $M_\infty = 0.6$.

Figure 23. Continued.

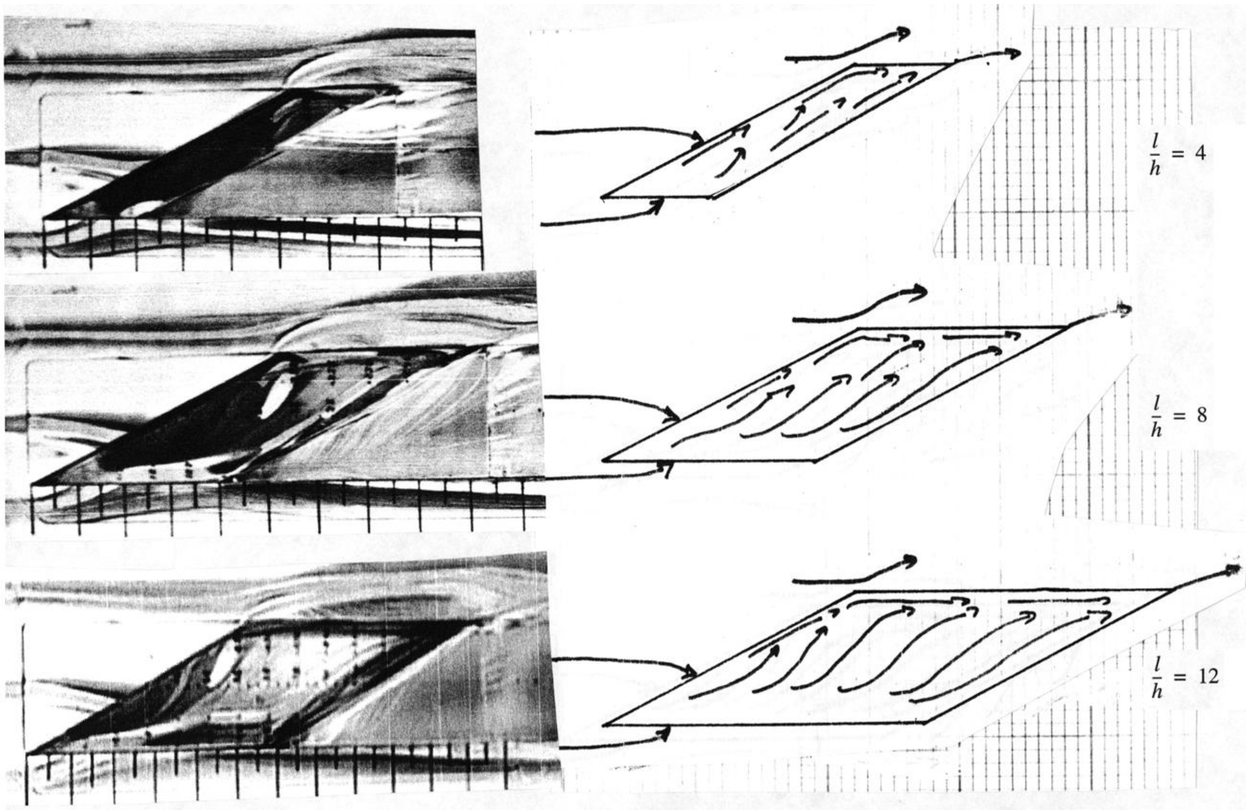

(d) $M_\infty = 0.8$.

Figure 23. Concluded.

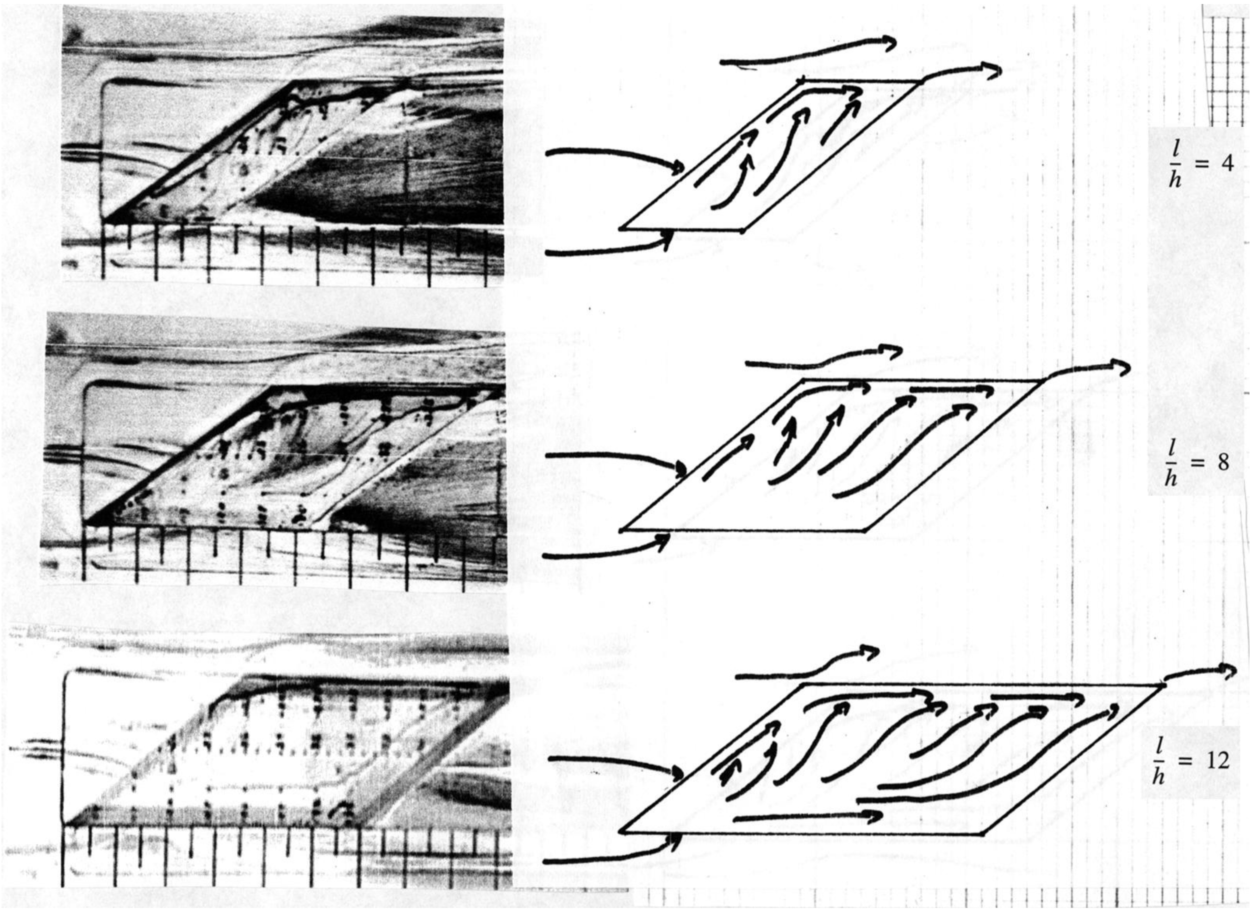

(a) $M_\infty = 0.2$.

Figure 24. Photographs and sketches of surface flow visualization, $\psi = 55°$.

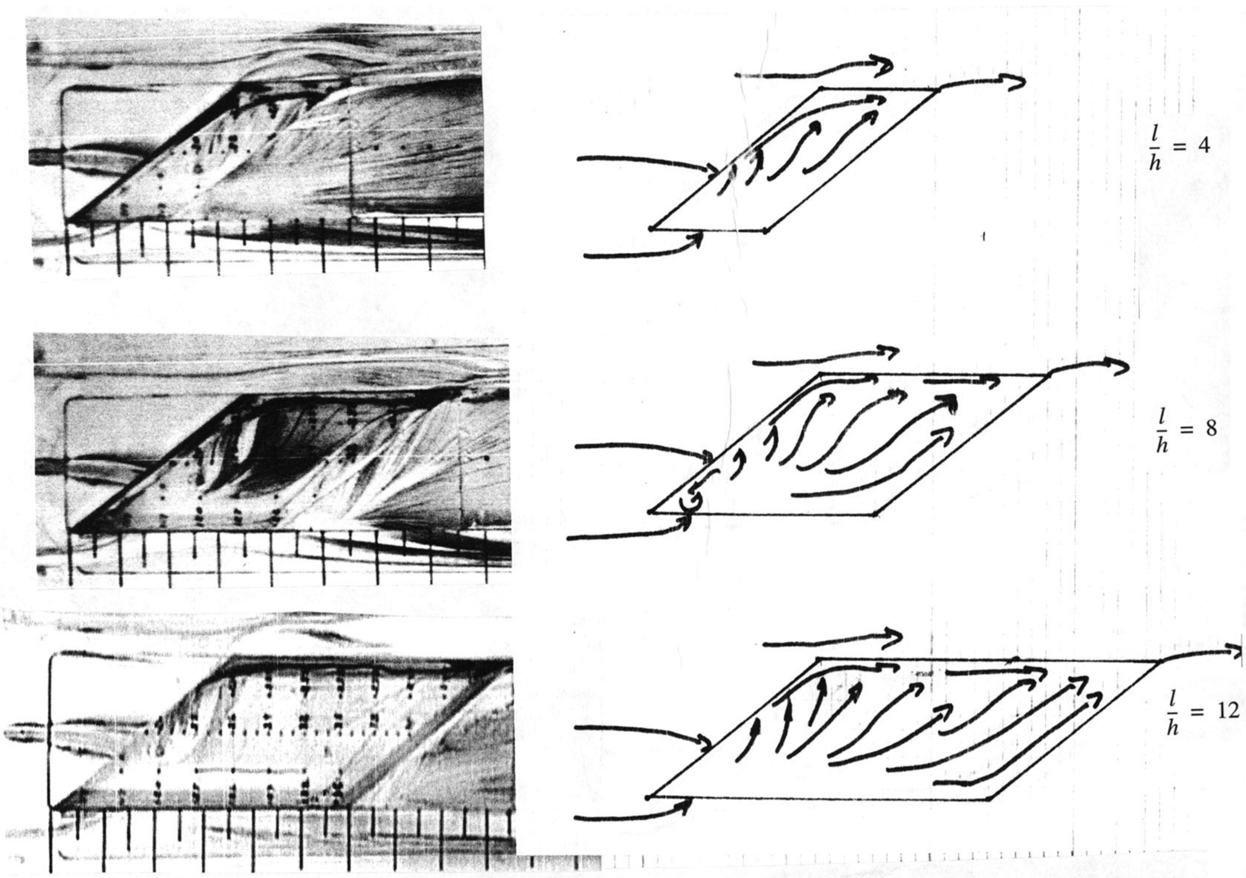

(b) $M_\infty = 0.4$.

Figure 24. Continued.

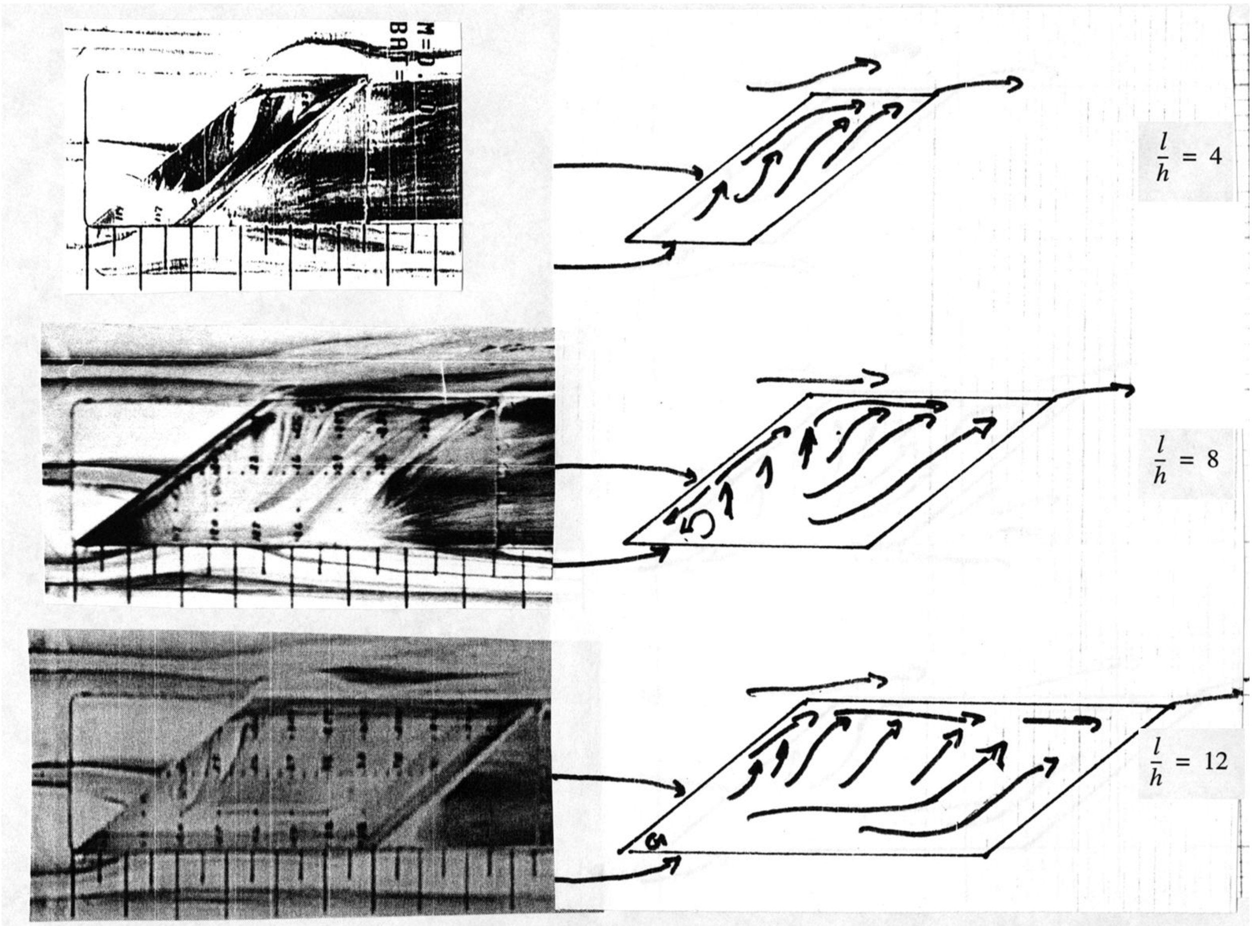

(c) $M_\infty = 0.6$.

Figure 24. Continued.

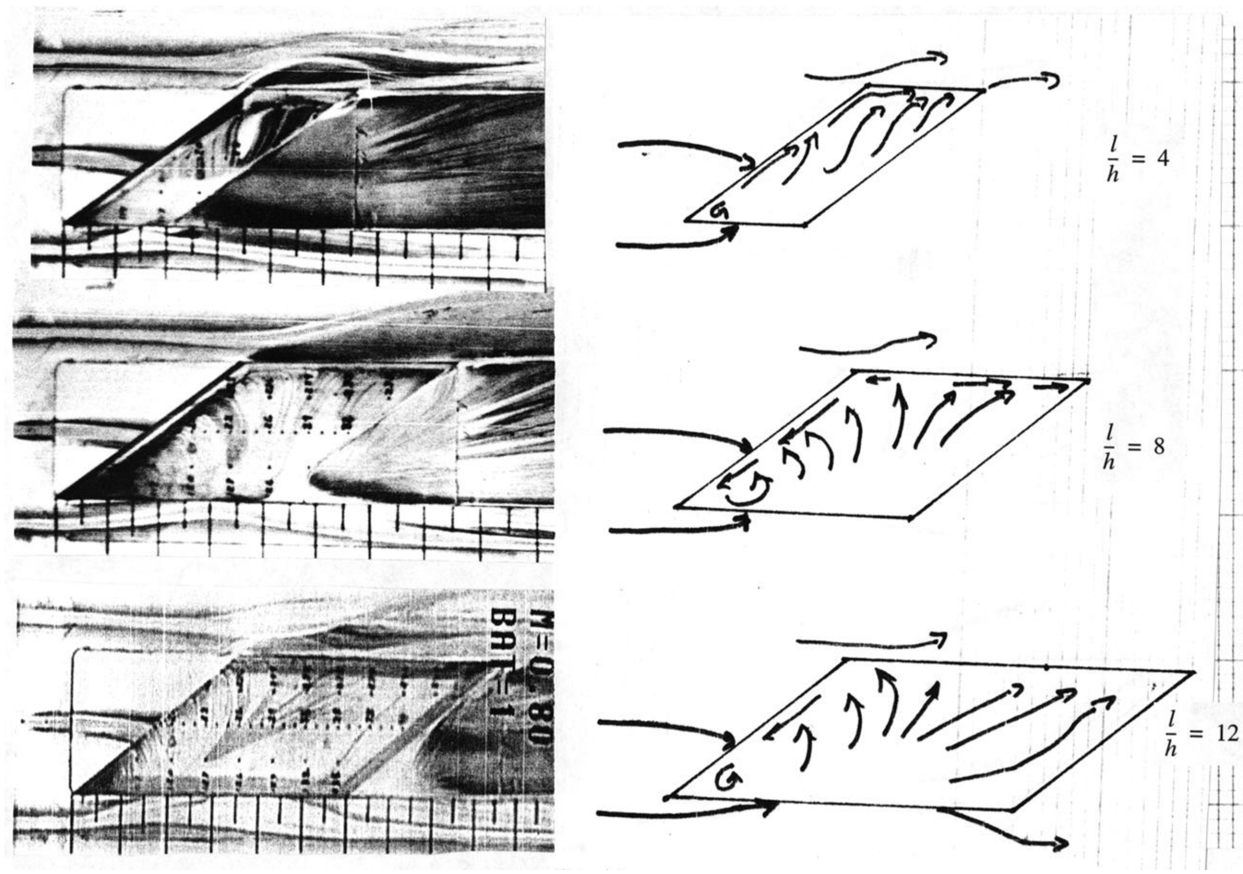

(d) $M_\infty = 0.8$.

Figure 24. Concluded.

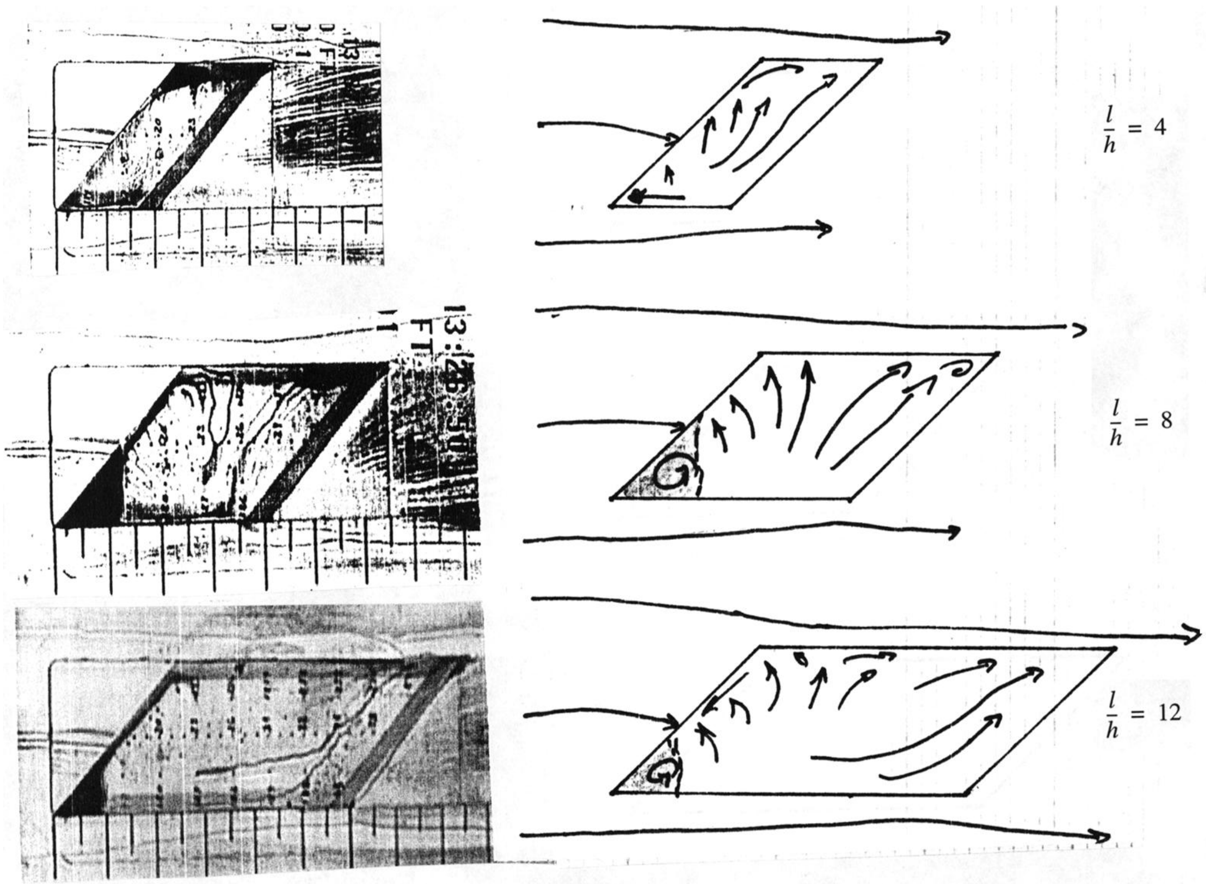

(a) $M_\infty = 0.2$.

Figure 25. Photographs and sketches of surface flow visualization, $\psi = 45°$.

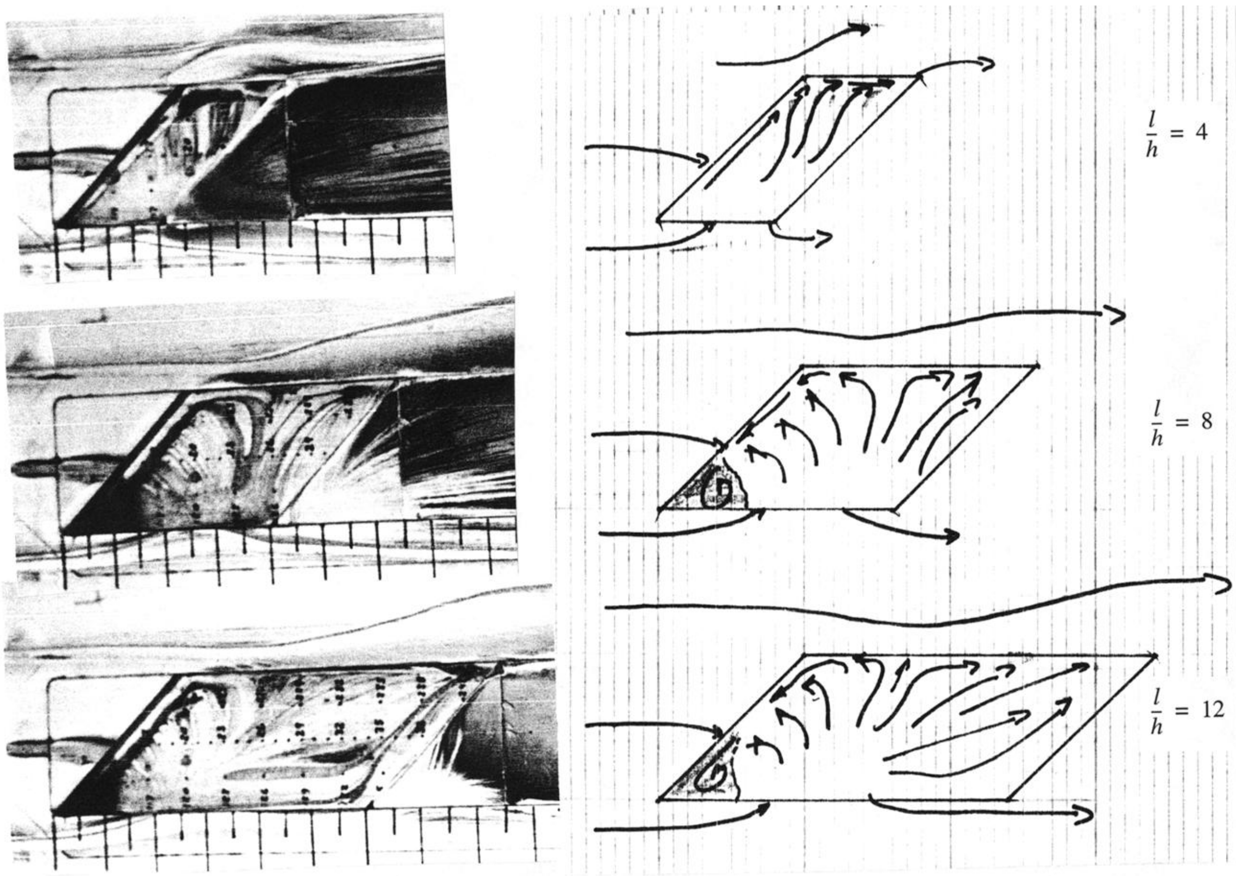

(b) $M_\infty = 0.4$.

Figure 25. Continued.

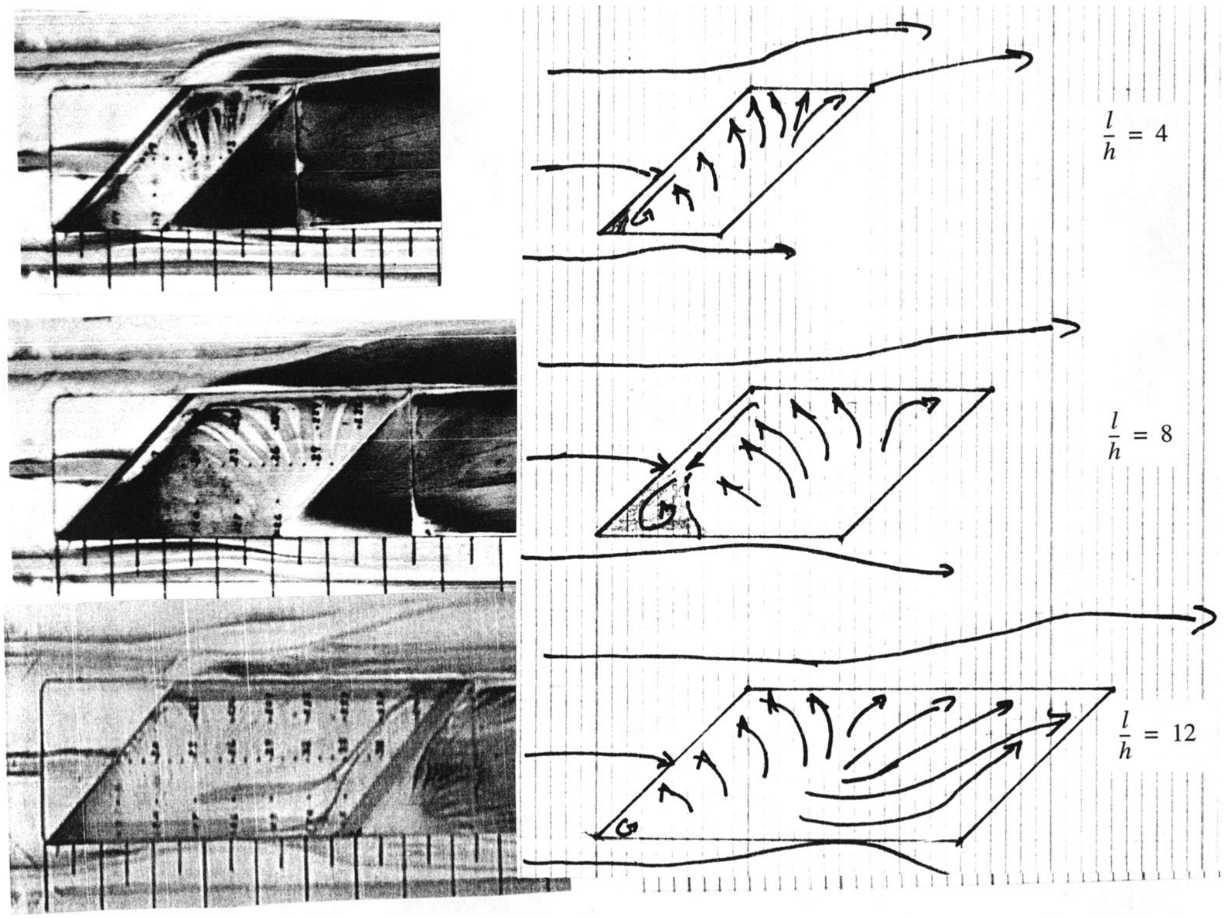

(c) $M_{\infty} = 0.6$.

Figure 25. Continued.

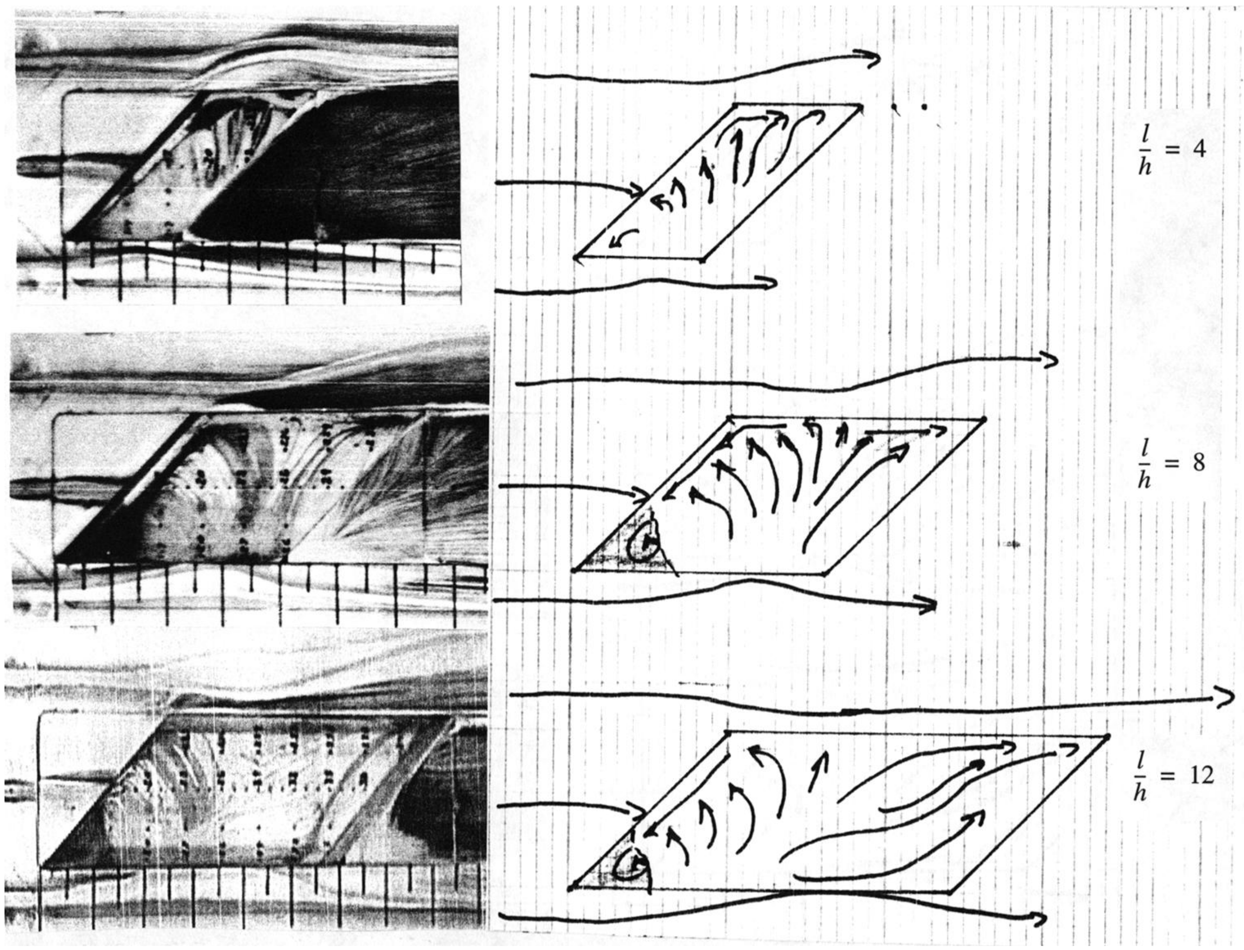

(d) $M_\infty = 0.8$.

Figure 25. Concluded.

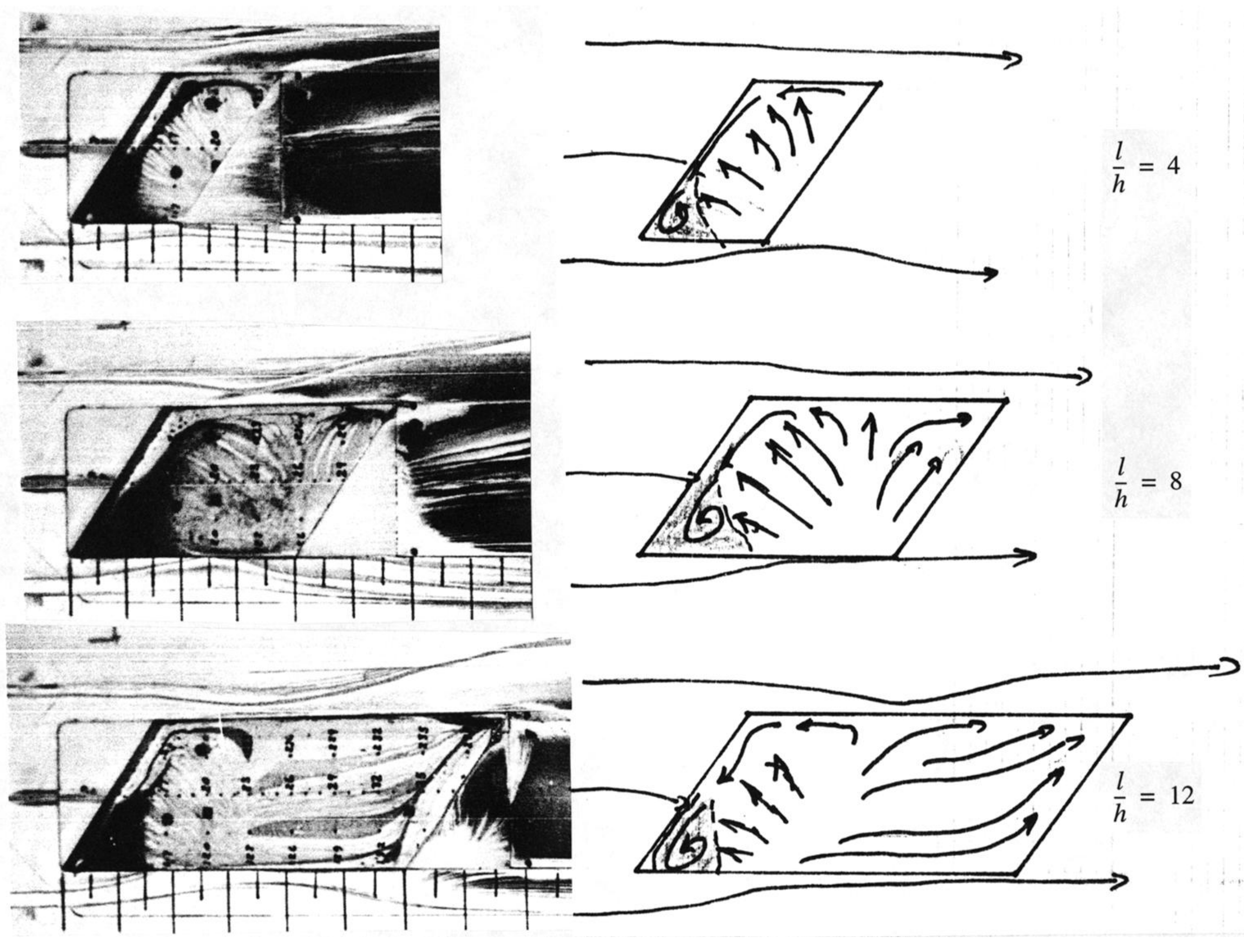

(a) $M_\infty = 0.2$.

Figure 26. Photographs and sketches of surface flow visualization, $\psi = 35°$.

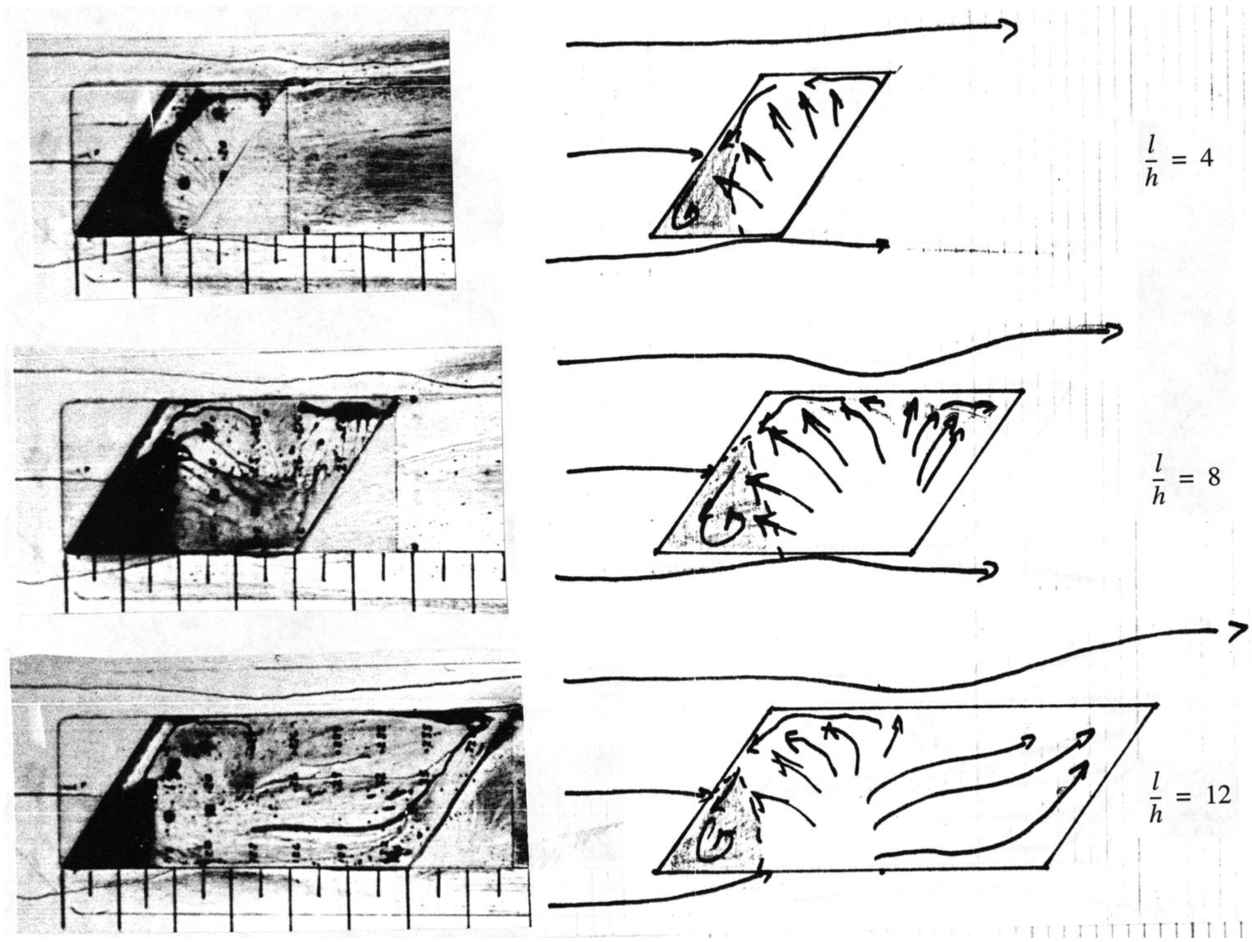

(b) $M_\infty = 0.4$.

Figure 26. Continued.

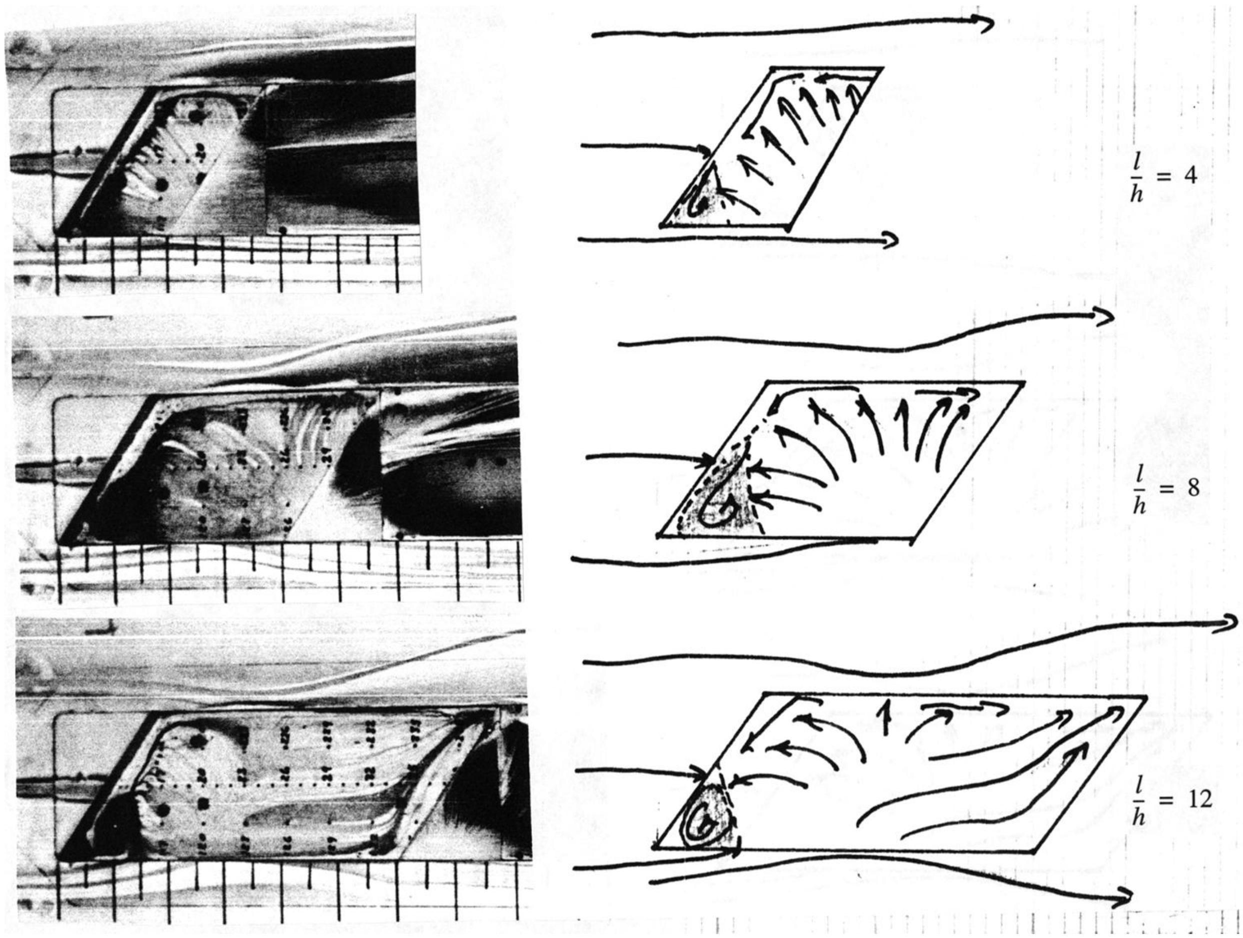

(c) $M_\infty = 0.6$.

Figure 26. Continued.

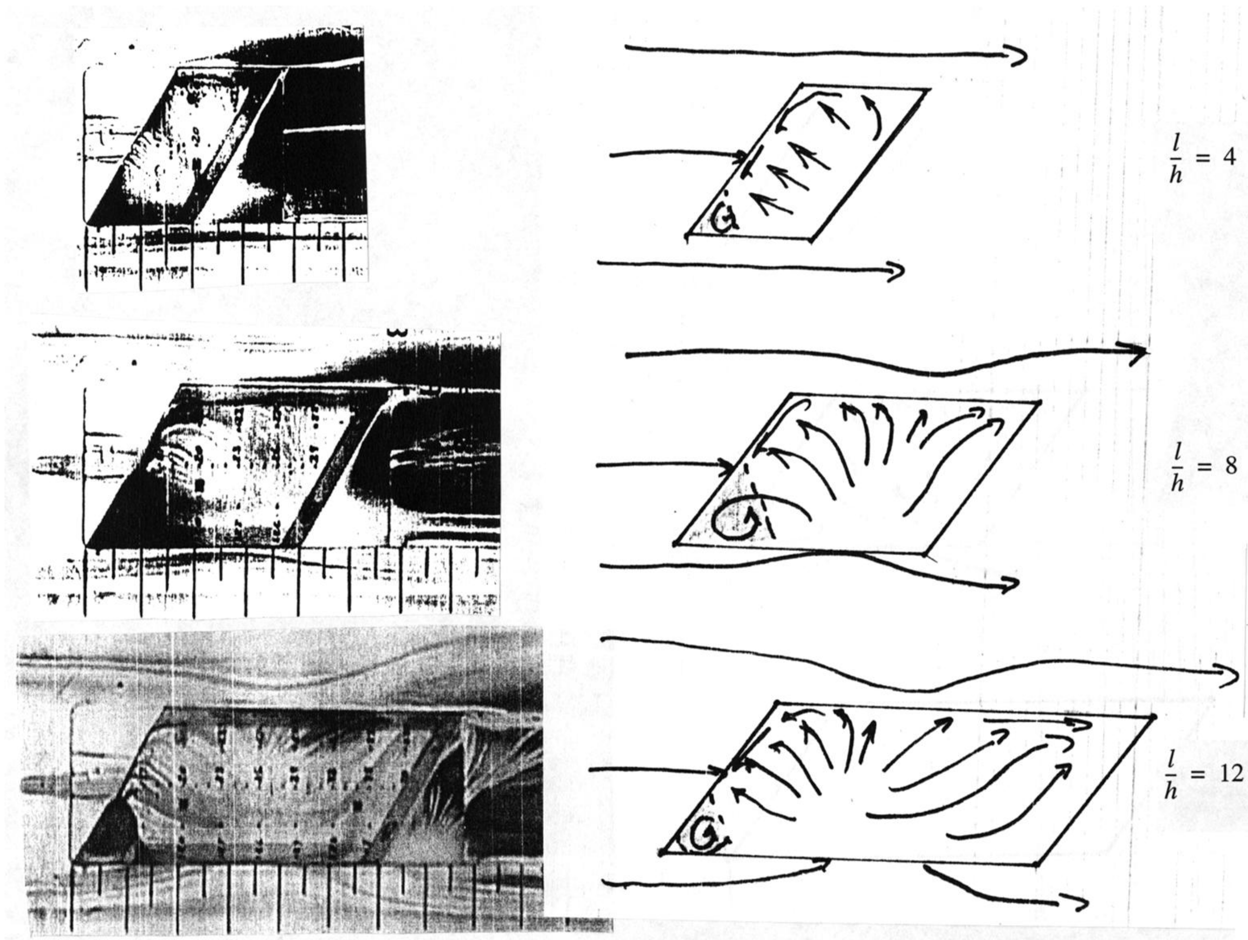

(d) $M_\infty = 0.8$.

Figure 26. Concluded.

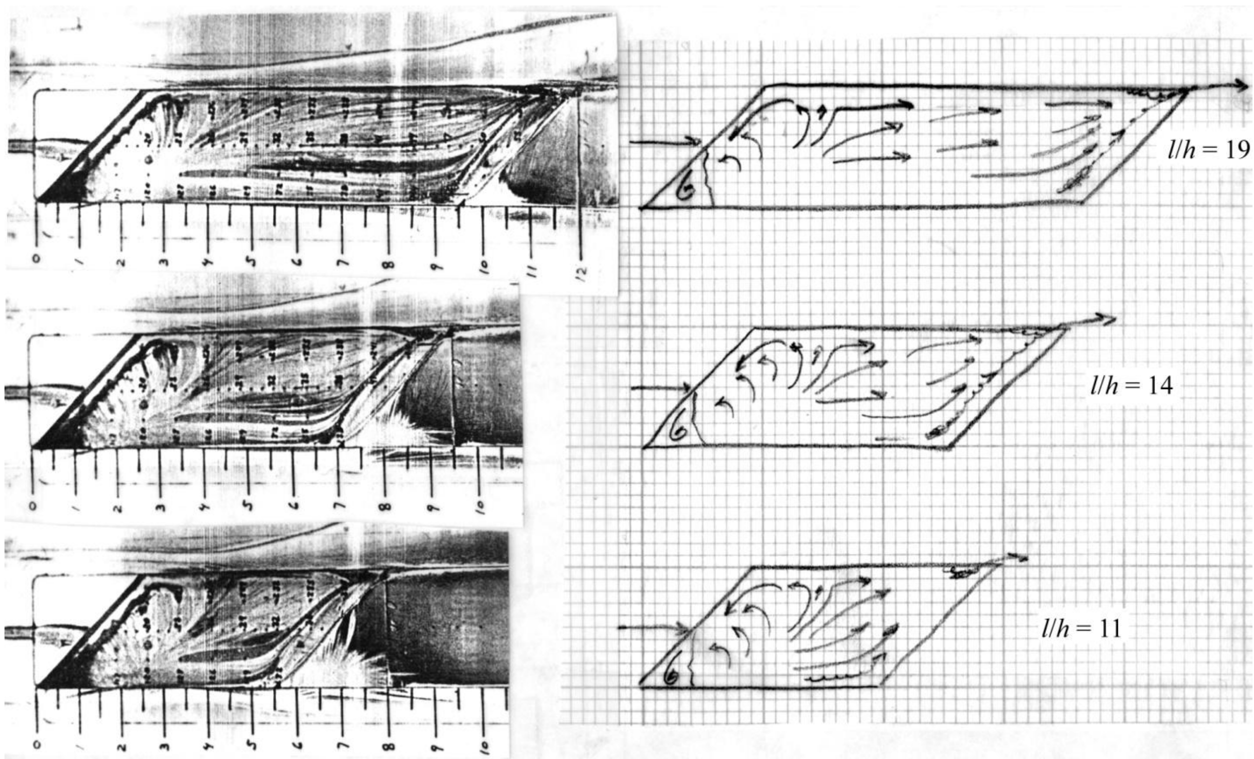

Figure 27. Photographs and sketches of surface flow visualization for longer cavities; $\psi = 45°$, $M_\infty = 0.4$.

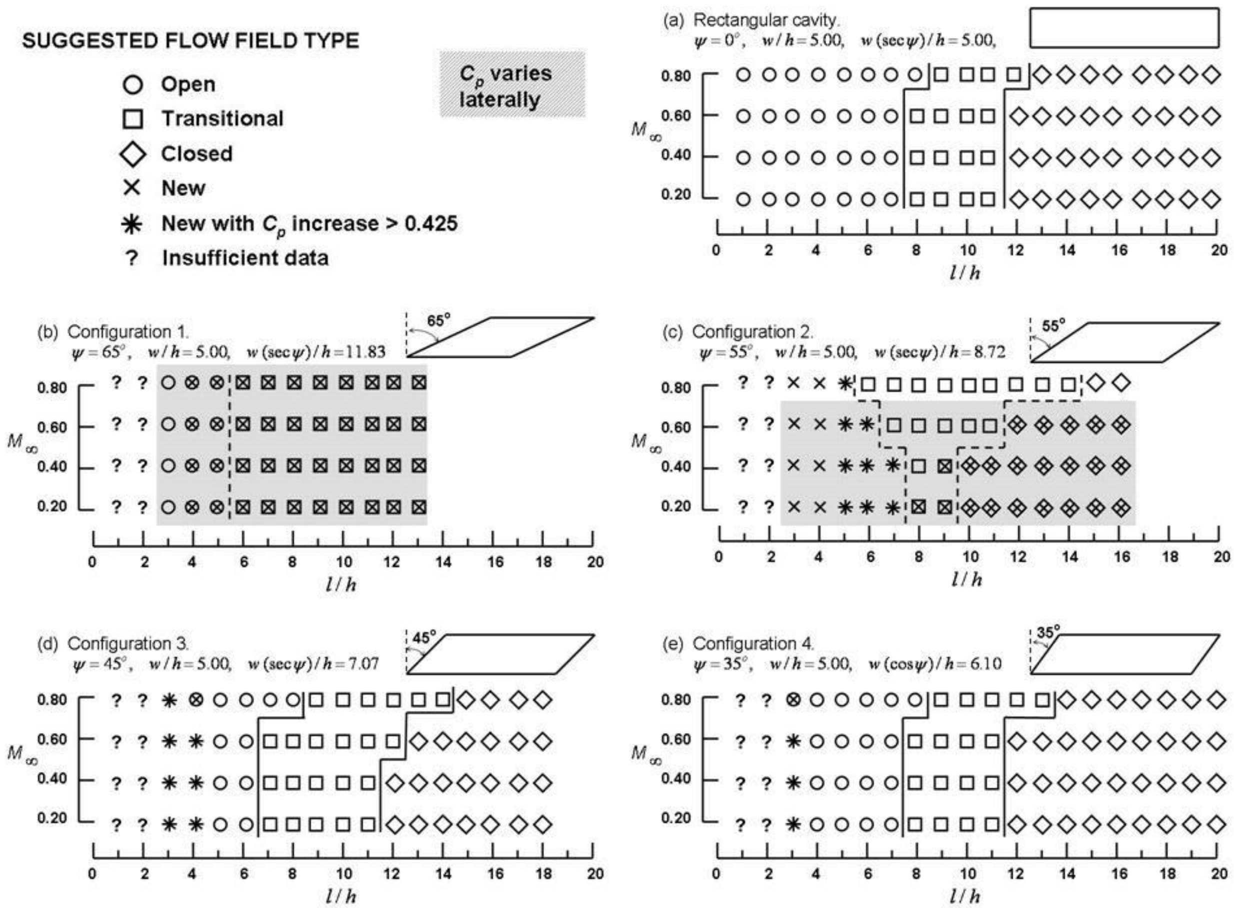

Figure 28. Summary of flowfield types suggested by static-pressure distributions shown in Figures 17 and 18. (Note: Characteristics of the new flow type are sometimes superimposed on otherwise known distribution types.)

Appendix A: Supplemental Static Pressure Tables

Tabulated static pressure coefficients for the swept (leading and trailing edge) cavities are presented in this Appendix. Table A-1 contains an index for the tabulated data. Table A-2 defines the nomenclature used in Tables A-3 through A-18. Pressure coefficient values in the tables are set to 9.9999 when the pressure orifice was covered.

Table A-1. Table numbers for corresponding Mach number.

Cavity Sweep, ψ	Table for $M_\infty = 0.2$	Table for $M_\infty = 0.4$	Table for $M_\infty = 0.6$	Table for $M_\infty = 0.8$
65°	A-3	A-4	A-5	A-6
55°	A-7	A-8	A-9	A-10
45°	A-11	A-12	A-13	A-14
35°	A-15	A-16	A-17	A-18

Table A-2. The nomenclature used in the data tables.

Run	run number
Point	point number
ψ	sweep angle, deg (see Figure 6)
Config.	configuration number (see Figure 6)
M	free-stream mach number
R	free-stream unit Reynolds number, per foot
p_∞	free-stream static pressure, psia
$p_{t,\infty}$	free-stream stagnation pressure, psia
q_∞	free-stream dynamic pressure, psia
$T_{t,\infty}$	free-stream stagnation temperature, degF
l/h	cavity length-to-depth ratio
cpX	pressure coefficient for orifice number X (orifice numbers are shown in Figure 7 and Table 1). Pressure coefficient values are set to 9.9999 when the pressure orifice was covered.

Table A-3. Pressure Coefficients at M = 0.2 for Cavity with sweep = 65 deg. (Config. 1).

Run	Point	Ψ deg	CONF	M	R×10^{-6} per ft	p_∞ psi	$p_{t,\infty}$ psi	q_∞ psi	$T_{t,\infty}$ °F	l/h	cp21	cp22	cp25	cp26	cp28	cp29	cp30	cp32	cp33	cp34
8	177	65	1	0.20	1.44	14.39	14.80	0.41	51.8	1	0.0395	0.0015	9.9999	9.9999	9.9999	9.9999	9.9999	9.9999	9.9999	9.9999
8	176	65	1	0.20	1.44	14.39	14.80	0.41	51.7	2	0.0898	0.0201	9.9999	9.9999	9.9999	9.9999	9.9999	9.9999	9.9999	9.9999
8	175	65	1	0.20	1.43	14.39	14.80	0.40	51.5	3	0.0818	0.0252	0.0209	0.0505	9.9999	9.9999	9.9999	9.9999	9.9999	9.9999
8	174	65	1	0.20	1.44	14.39	14.80	0.41	51.5	4	0.1101	0.0455	-0.0230	0.0025	0.0568	9.9999	9.9999	9.9999	9.9999	9.9999
8	173	65	1	0.20	1.44	14.38	14.80	0.41	51.4	5	0.0998	0.0471	-0.0347	0.0145	0.0653	0.0813	0.0894	9.9999	9.9999	9.9999
8	172	65	1	0.20	1.44	14.38	14.80	0.41	51.3	6	0.0714	0.0268	-0.0566	0.0025	0.0842	0.1163	0.1337	0.1289	9.9999	9.9999
8	171	65	1	0.20	1.44	14.39	14.80	0.41	51.2	7	0.0429	0.0014	-0.0771	-0.0112	0.0896	0.1283	0.1510	0.1545	0.1465	0.1422
8	170	65	1	0.20	1.44	14.39	14.80	0.41	51.2	8	0.0228	-0.0189	-0.0923	-0.0249	0.0896	0.1333	0.1613	0.1680	0.1669	0.1574
8	169	65	1	0.20	1.44	14.39	14.80	0.41	50.9	9	0.0077	-0.0343	-0.1111	-0.0421	0.0793	0.1301	0.1615	0.1767	0.1756	0.1711
8	168	65	1	0.20	1.44	14.39	14.80	0.40	50.8	10	-0.0008	-0.0445	-0.1248	-0.0558	0.0673	0.1202	0.1548	0.1769	0.1809	0.1796
8	167	65	1	0.20	1.44	14.39	14.80	0.41	50.8	11	-0.0075	-0.0496	-0.1332	-0.0626	0.0604	0.1118	0.1445	0.1700	0.1757	0.1745
8	166	65	1	0.20	1.44	14.39	14.80	0.40	50.6	12	-0.0143	-0.0566	-0.1437	-0.0714	0.0518	0.1036	0.1345	0.1585	0.1641	0.1647
8	165	65	1	0.20	1.44	14.39	14.80	0.40	49.9	13	-0.0194	-0.0549	-0.1506	-0.0715	0.0484	0.0986	0.1311	0.1501	0.1540	0.1547

Run	Point	cp35	cp36	cp37	cp38	cp39	cp40	cp41	cp42	cp43	cp44	cp45	cp46	cp117	cp120	cp123	cp126	cp129	cp135
8	177	9.9999	9.9999	9.9999	9.9999	9.9999	9.9999	9.9999	9.9999	9.9999	9.9999	9.9999	9.9999	0.1143	9.9999	9.9999	9.9999	9.9999	9.9999
8	176	9.9999	9.9999	9.9999	9.9999	9.9999	9.9999	9.9999	9.9999	9.9999	9.9999	9.9999	9.9999	0.1109	9.9999	9.9999	9.9999	9.9999	9.9999
8	175	9.9999	9.9999	9.9999	9.9999	9.9999	9.9999	9.9999	9.9999	9.9999	9.9999	9.9999	9.9999	0.0663	0.1000	9.9999	9.9999	9.9999	9.9999
8	174	9.9999	9.9999	9.9999	9.9999	9.9999	9.9999	9.9999	9.9999	9.9999	9.9999	9.9999	9.9999	-0.0101	0.1409	0.1082	9.9999	9.9999	9.9999
8	173	9.9999	9.9999	9.9999	9.9999	9.9999	9.9999	9.9999	9.9999	9.9999	9.9999	9.9999	9.9999	-0.0670	0.1388	0.2032	9.9999	9.9999	9.9999
8	172	9.9999	9.9999	9.9999	9.9999	9.9999	9.9999	9.9999	9.9999	9.9999	9.9999	9.9999	9.9999	-0.1033	0.1119	0.2357	0.2272	9.9999	9.9999
8	171	9.9999	9.9999	9.9999	9.9999	9.9999	9.9999	9.9999	9.9999	9.9999	9.9999	9.9999	9.9999	-0.1227	0.0852	0.2259	0.2525	0.2377	9.9999
8	170	0.1350	0.1462	9.9999	9.9999	9.9999	9.9999	9.9999	9.9999	9.9999	9.9999	9.9999	9.9999	-0.1314	0.0727	0.1987	0.2420	0.2754	9.9999
8	169	0.1547	0.1531	0.1126	0.1020	9.9999	9.9999	9.9999	9.9999	9.9999	9.9999	9.9999	9.9999	-0.1403	0.0637	0.1802	0.2050	0.2596	9.9999
8	168	0.1638	0.1717	0.1393	0.1225	0.1086	0.1214	9.9999	9.9999	9.9999	9.9999	9.9999	9.9999	-0.1457	0.0602	0.1700	0.1785	0.2185	0.2621
8	167	0.1655	0.1750	0.1499	0.1394	0.1421	0.1314	0.0853	0.1357	9.9999	9.9999	9.9999	9.9999	-0.1473	0.0584	0.1631	0.1624	0.1771	0.2780
8	166	0.1569	0.1686	0.1484	0.1449	0.1508	0.1485	0.1230	0.1360	0.0792	0.1271	9.9999	9.9999	-0.1512	0.0548	0.1583	0.1520	0.1522	0.2607
8	165	0.1462	0.1569	0.1414	0.1415	0.1492	0.1536	0.1350	0.1566	0.1255	0.1289	0.1171	0.1293	-0.1513	0.0567	0.1567	0.1485	0.1397	0.1999

Table A-3. Concluded.

Run	Point	cp138	cp229	cp232	cp235	cp244	cp250	cp3
8	177	9.9999	9.9999	9.9999	9.9999	9.9999	9.9999	-0.0153
8	176	9.9999	0.0250	9.9999	9.9999	9.9999	9.9999	-0.0153
8	175	9.9999	0.0125	9.9999	9.9999	9.9999	9.9999	-0.0173
8	174	9.9999	0.0232	0.0502	9.9999	9.9999	9.9999	-0.0223
8	173	9.9999	0.0197	0.0396	0.0638	9.9999	9.9999	-0.0239
8	172	9.9999	0.0214	0.0309	0.0638	9.9999	9.9999	-0.0239
8	171	9.9999	0.0214	0.0204	0.0604	9.9999	9.9999	-0.0257
8	170	9.9999	0.0197	0.0134	0.0570	9.9999	9.9999	-0.0257
8	169	9.9999	0.0143	0.0063	0.0518	9.9999	9.9999	-0.0292
8	168	9.9999	0.0072	0.0011	0.0448	0.1537	9.9999	-0.0275
8	167	9.9999	-0.0035	-0.0024	0.0413	0.1396	9.9999	-0.0292
8	166	0.2147	-0.0125	-0.0131	0.0326	0.1293	9.9999	-0.0276
8	165	0.2638	-0.0179	-0.0201	0.0309	0.1188	0.1620	-0.0259

Table A-4. Pressure Coefficients at M = 0.4 for Cavity with sweep = 65 deg. (Config. 1).

Run	Point	Ψ deg	CONF	M	$R \times 10^{-6}$ per ft	p_∞ psi	$p_{t,\infty}$ psi	q_∞ psi	$T_{t,\infty}$ °F	l/h	cp21	cp22	cp25	cp26	cp28	cp29	cp30	cp32	cp33	cp34
7	161	65	1	0.40	2.43	13.19	14.73	1.48	95.8	1	0.0287	0.0137	9.9999	9.9999	9.9999	9.9999	9.9999	9.9999	9.9999	9.9999
7	160	65	1	0.40	2.43	13.19	14.73	1.48	96.4	2	0.0789	0.0323	9.9999	9.9999	9.9999	9.9999	9.9999	9.9999	9.9999	9.9999
7	159	65	1	0.40	2.43	13.19	14.73	1.48	96.8	3	0.0720	0.0379	0.0201	0.0526	9.9999	9.9999	9.9999	9.9999	9.9999	9.9999
7	158	65	1	0.40	2.43	13.18	14.73	1.48	97.2	4	0.1000	0.0629	-0.0267	0.0029	0.0500	9.9999	9.9999	9.9999	9.9999	9.9999
7	157	65	1	0.40	2.44	13.17	14.73	1.50	97.6	5	0.0875	0.0626	-0.0373	0.0161	0.0549	0.0742	0.0951	9.9999	9.9999	9.9999
7	156	65	1	0.40	2.43	13.18	14.73	1.49	98.1	6	0.0611	0.0414	-0.0641	0.0035	0.0799	0.1144	0.1423	0.1414	9.9999	9.9999
7	155	65	1	0.40	2.43	13.18	14.73	1.49	98.6	7	0.0355	0.0184	-0.0798	-0.0053	0.0916	0.1322	0.1664	0.1704	0.1579	0.1534
7	154	65	1	0.40	2.42	13.18	14.73	1.49	99.1	8	0.0112	-0.0076	-0.1008	-0.0245	0.0895	0.1361	0.1752	0.1870	0.1814	0.1675
7	153	65	1	0.40	2.41	13.19	14.73	1.48	100.1	9	-0.0031	-0.0244	-0.1193	-0.0406	0.0779	0.1315	0.1749	0.1941	0.1927	0.1846
7	152	65	1	0.40	2.41	13.19	14.73	1.48	100.8	10	-0.0114	-0.0338	-0.1310	-0.0519	0.0652	0.1215	0.1679	0.1923	0.1942	0.1907
7	151	65	1	0.40	2.40	13.18	14.73	1.48	101.4	11	-0.0178	-0.0421	-0.1438	-0.0635	0.0552	0.1108	0.1570	0.1847	0.1889	0.1882
7	150	65	1	0.40	2.40	13.18	14.73	1.49	103.1	12	-0.0246	-0.0493	-0.1536	-0.0713	0.0476	0.1024	0.1469	0.1714	0.1770	0.1778
7	149	65	1	0.40	2.39	13.18	14.73	1.49	103.9	13	-0.0311	-0.0573	-0.1643	-0.0793	0.0405	0.0938	0.1367	0.1567	0.1608	0.1604

Run	Point	cp35	cp36	cp37	cp38	cp39	cp40	cp41	cp42	cp43	cp44	cp45	cp46	cp117	cp120	cp123	cp126	cp129	cp135
7	161	9.9999	9.9999	9.9999	9.9999	9.9999	9.9999	9.9999	9.9999	9.9999	9.9999	9.9999	9.9999	0.1224	9.9999	9.9999	9.9999	9.9999	9.9999
7	160	9.9999	9.9999	9.9999	9.9999	9.9999	9.9999	9.9999	9.9999	9.9999	9.9999	9.9999	9.9999	0.1165	9.9999	9.9999	9.9999	9.9999	9.9999
7	159	9.9999	9.9999	9.9999	9.9999	9.9999	9.9999	9.9999	9.9999	9.9999	9.9999	9.9999	9.9999	0.0643	0.1080	9.9999	9.9999	9.9999	9.9999
7	158	9.9999	9.9999	9.9999	9.9999	9.9999	9.9999	9.9999	9.9999	9.9999	9.9999	9.9999	9.9999	-0.0146	0.1481	0.1081	9.9999	9.9999	9.9999
7	157	9.9999	9.9999	9.9999	9.9999	9.9999	9.9999	9.9999	9.9999	9.9999	9.9999	9.9999	9.9999	-0.0778	0.1456	0.1984	9.9999	9.9999	9.9999
7	156	9.9999	9.9999	9.9999	9.9999	9.9999	9.9999	9.9999	9.9999	9.9999	9.9999	9.9999	9.9999	-0.1149	0.1181	0.2338	0.2387	9.9999	9.9999
7	155	9.9999	9.9999	9.9999	9.9999	9.9999	9.9999	9.9999	9.9999	9.9999	9.9999	9.9999	9.9999	-0.1304	0.0960	0.2273	0.2677	0.2546	9.9999
7	154	0.1432	0.1424	9.9999	9.9999	9.9999	9.9999	9.9999	9.9999	9.9999	9.9999	9.9999	9.9999	-0.1437	0.0796	0.1970	0.2563	0.2866	9.9999
7	153	0.1685	0.1520	0.1272	0.1043	9.9999	9.9999	9.9999	9.9999	9.9999	9.9999	9.9999	9.9999	-0.1509	0.0709	0.1770	0.2177	0.2714	9.9999
7	152	0.1789	0.1724	0.1599	0.1183	0.0935	0.1182	9.9999	9.9999	9.9999	9.9999	9.9999	9.9999	-0.1539	0.0660	0.1668	0.1881	0.2288	0.2847
7	151	0.1797	0.1773	0.1714	0.1420	0.1334	0.1240	0.0763	0.1346	9.9999	9.9999	9.9999	9.9999	-0.1580	0.0620	0.1615	0.1719	0.1882	0.2927
7	150	0.1711	0.1719	0.1706	0.1482	0.1470	0.1480	0.1235	0.1311	0.0704	0.1228	9.9999	9.9999	-0.1595	0.0590	0.1575	0.1619	0.1624	0.2770
7	149	0.1536	0.1568	0.1580	0.1399	0.1429	0.1490	0.1338	0.1526	0.1221	0.1172	0.1117	0.1329	-0.1629	0.0546	0.1514	0.1527	0.1458	0.2103

Table A-4. Concluded.

Run	Point	cp138	cp229	cp232	cp235	cp244	cp250	cp3
7	161	9.9999	9.9999	9.9999	9.9999	9.9999	9.9999	-0.0046
7	160	9.9999	0.0316	9.9999	9.9999	9.9999	9.9999	-0.0045
7	159	9.9999	0.0164	9.9999	9.9999	9.9999	9.9999	-0.0092
7	158	9.9999	0.0340	0.0551	9.9999	9.9999	9.9999	-0.0101
7	157	9.9999	0.0291	0.0419	0.0847	9.9999	9.9999	-0.0145
7	156	9.9999	0.0296	0.0362	0.0900	9.9999	9.9999	-0.0183
7	155	9.9999	0.0315	0.0286	0.0910	9.9999	9.9999	-0.0155
7	154	9.9999	0.0286	0.0186	0.0840	9.9999	9.9999	-0.0189
7	153	9.9999	0.0228	0.0099	0.0771	9.9999	9.9999	-0.0209
7	152	9.9999	0.0144	0.0046	0.0705	0.1484	9.9999	-0.0200
7	151	9.9999	0.0032	-0.0035	0.0618	0.1348	9.9999	-0.0204
7	150	0.2247	-0.0089	-0.0126	0.0527	0.1260	9.9999	-0.0212
7	149	0.2709	-0.0211	-0.0246	0.0427	0.1159	0.1617	-0.0241

Table A-5. Pressure Coefficients at M = 0.6 for Cavity with sweep = 65 deg. (Config. 1).

Run	Point	Ψ deg	CONF	M	R×10^{-6} per ft	p_∞ psi	$p_{t,\infty}$ psi	q_∞ psi	$T_{t,\infty}$ °F	l/h	cp21	cp22	cp25	cp26	cp28	cp29	cp30	cp32	cp33	cp34
7	147	65	1	0.60	3.20	11.52	14.71	2.92	116.6	1	0.0311	0.0192	9.9999	9.9999	9.9999	9.9999	9.9999	9.9999	9.9999	9.9999
7	146	65	1	0.60	3.20	11.52	14.71	2.92	116.5	2	0.0716	0.0291	9.9999	9.9999	9.9999	9.9999	9.9999	9.9999	9.9999	9.9999
7	145	65	1	0.60	3.20	11.52	14.71	2.92	116.6	3	0.0725	0.0425	0.0162	0.0474	9.9999	9.9999	9.9999	9.9999	9.9999	9.9999
7	144	65	1	0.60	3.20	11.52	14.71	2.91	116.6	4	0.1021	0.0660	-0.0284	-0.0004	0.0362	9.9999	9.9999	9.9999	9.9999	9.9999
7	143	65	1	0.60	3.19	11.54	14.71	2.90	116.6	5	0.0918	0.0695	-0.0329	0.0203	0.0507	0.0704	0.0816	9.9999	9.9999	9.9999
7	142	65	1	0.60	3.20	11.52	14.71	2.91	116.6	6	0.0611	0.0475	-0.0588	0.0101	0.0817	0.1197	0.1490	0.1300	9.9999	9.9999
7	141	65	1	0.60	3.20	11.50	14.71	2.93	116.6	7	0.0343	0.0220	-0.0745	0.0011	0.0941	0.1373	0.1742	0.1784	0.1658	0.1402
7	140	65	1	0.60	3.20	11.51	14.71	2.93	116.5	8	0.0075	-0.0072	-0.1003	-0.0210	0.0910	0.1428	0.1841	0.1970	0.1943	0.1798
7	139	65	1	0.60	3.20	11.51	14.71	2.92	116.6	9	-0.0075	-0.0249	-0.1196	-0.0421	0.0767	0.1359	0.1828	0.2027	0.2048	0.1962
7	138	65	1	0.60	3.20	11.51	14.71	2.92	116.8	10	-0.0164	-0.0353	-0.1317	-0.0557	0.0621	0.1236	0.1736	0.2000	0.2051	0.2002
7	137	65	1	0.60	3.20	11.50	14.71	2.93	116.8	11	-0.0221	-0.0417	-0.1420	-0.0637	0.0529	0.1133	0.1628	0.1918	0.1987	0.1974
7	136	65	1	0.60	3.20	11.52	14.71	2.92	116.9	12	-0.0307	-0.0502	-0.1554	-0.0748	0.0424	0.1018	0.1493	0.1757	0.1831	0.1843
7	135	65	1	0.60	3.19	11.53	14.71	2.91	117.1	13	-0.0346	-0.0549	-0.1626	-0.0790	0.0398	0.0975	0.1422	0.1633	0.1690	0.1694

Run	Point	cp35	cp36	cp37	cp38	cp39	cp40	cp41	cp42	cp43	cp44	cp45	cp46	cp117	cp120	cp123	cp126	cp129	cp135
7	147	9.9999	9.9999	9.9999	9.9999	9.9999	9.9999	9.9999	9.9999	9.9999	9.9999	9.9999	9.9999	0.1321	9.9999	9.9999	9.9999	9.9999	9.9999
7	146	9.9999	9.9999	9.9999	9.9999	9.9999	9.9999	9.9999	9.9999	9.9999	9.9999	9.9999	9.9999	0.1110	9.9999	9.9999	9.9999	9.9999	9.9999
7	145	9.9999	9.9999	9.9999	9.9999	9.9999	9.9999	9.9999	9.9999	9.9999	9.9999	9.9999	9.9999	0.0474	0.1182	9.9999	9.9999	9.9999	9.9999
7	144	9.9999	9.9999	9.9999	9.9999	9.9999	9.9999	9.9999	9.9999	9.9999	9.9999	9.9999	9.9999	-0.0355	0.1534	0.1180	9.9999	9.9999	9.9999
7	143	9.9999	9.9999	9.9999	9.9999	9.9999	9.9999	9.9999	9.9999	9.9999	9.9999	9.9999	9.9999	-0.0923	0.1512	0.2057	9.9999	9.9999	9.9999
7	142	9.9999	9.9999	9.9999	9.9999	9.9999	9.9999	9.9999	9.9999	9.9999	9.9999	9.9999	9.9999	-0.1293	0.1231	0.2436	0.2460	9.9999	9.9999
7	141	9.9999	9.9999	9.9999	9.9999	9.9999	9.9999	9.9999	9.9999	9.9999	9.9999	9.9999	9.9999	-0.1441	0.0989	0.2351	0.2744	0.2662	9.9999
7	140	0.1539	0.1319	9.9999	9.9999	9.9999	9.9999	9.9999	9.9999	9.9999	9.9999	9.9999	9.9999	-0.1578	0.0803	0.2021	0.2656	0.2979	9.9999
7	139	0.1809	0.1646	0.1323	0.0969	9.9999	9.9999	9.9999	9.9999	9.9999	9.9999	9.9999	9.9999	-0.1654	0.0699	0.1816	0.2236	0.2843	9.9999
7	138	0.1893	0.1829	0.1686	0.1215	0.0882	0.0979	9.9999	9.9999	9.9999	9.9999	9.9999	9.9999	-0.1696	0.0651	0.1707	0.1916	0.2393	0.3014
7	137	0.1891	0.1862	0.1798	0.1467	0.1399	0.1271	0.0683	0.1096	9.9999	9.9999	9.9999	9.9999	-0.1712	0.0635	0.1656	0.1747	0.1960	0.3061
7	136	0.1784	0.1794	0.1762	0.1500	0.1502	0.1518	0.1224	0.1305	0.0605	0.1086	9.9999	9.9999	-0.1771	0.0587	0.1592	0.1624	0.1675	0.2897
7	135	0.1641	0.1677	0.1676	0.1462	0.1507	0.1574	0.1384	0.1628	0.1236	0.1167	0.1113	0.1131	-0.1789	0.0580	0.1569	0.1565	0.1530	0.2250

Table A-5. Concluded.

Run	Point	cp138	cp229	cp232	cp235	cp244	cp250	cp3
7	147	9.9999	9.9999	9.9999	9.9999	9.9999	9.9999	-0.0011
7	146	9.9999	0.0253	9.9999	9.9999	9.9999	9.9999	-0.0083
7	145	9.9999	0.0156	9.9999	9.9999	9.9999	9.9999	-0.0104
7	144	9.9999	0.0292	0.0559	9.9999	9.9999	9.9999	-0.0147
7	143	9.9999	0.0287	0.0445	0.0868	9.9999	9.9999	-0.0161
7	142	9.9999	0.0327	0.0417	0.0943	9.9999	9.9999	-0.0188
7	141	9.9999	0.0357	0.0351	0.0947	9.9999	9.9999	-0.0174
7	140	9.9999	0.0332	0.0232	0.0883	9.9999	9.9999	-0.0208
7	139	9.9999	0.0277	0.0137	0.0816	9.9999	9.9999	-0.0225
7	138	9.9999	0.0178	0.0083	0.0746	0.1467	9.9999	-0.0225
7	137	9.9999	0.0070	0.0030	0.0677	0.1350	9.9999	-0.0214
7	136	0.2324	-0.0075	-0.0090	0.0562	0.1237	9.9999	-0.0247
7	135	0.2825	-0.0178	-0.0181	0.0493	0.1190	0.1660	-0.0238

Table A-6. Pressure Coefficients at M = 0.8 for Cavity with sweep = 65 deg. (Config. 1).

Run	Point	Ψ deg	CONF	M	$R \times 10^{-6}$ per ft	p_∞ psi	$p_{t,\infty}$ psi	q_∞ psi	$T_{t,\infty}$ °F	l/h	cp21	cp22	cp25	cp26	cp28	cp29	cp30	cp32	cp33	cp34
7	133	65	1	0.80	3.71	9.66	14.70	4.31	126.0	1	0.0193	0.0094	9.9999	9.9999	9.9999	9.9999	9.9999	9.9999	9.9999	9.9999
7	132	65	1	0.80	3.73	9.65	14.70	4.31	124.4	2	0.0808	0.0322	9.9999	9.9999	9.9999	9.9999	9.9999	9.9999	9.9999	9.9999
7	131	65	1	0.80	3.74	9.65	14.70	4.32	123.3	3	0.0964	0.0654	0.0154	0.0283	9.9999	9.9999	9.9999	9.9999	9.9999	9.9999
7	130	65	1	0.80	3.75	9.64	14.70	4.32	121.8	4	0.1171	0.0779	-0.0317	0.0007	0.0249	9.9999	9.9999	9.9999	9.9999	9.9999
7	129	65	1	0.80	3.75	9.64	14.69	4.32	121.5	5	0.1023	0.0816	-0.0303	0.0381	0.0672	0.0888	0.0972	9.9999	9.9999	9.9999
7	128	65	1	0.80	3.78	9.64	14.70	4.32	119.2	6	0.0649	0.0545	-0.0600	0.0250	0.1008	0.1487	0.1858	0.1729	9.9999	9.9999
7	127	65	1	0.80	3.79	9.62	14.70	4.33	117.4	7	0.0279	0.0196	-0.0822	0.0061	0.1056	0.1618	0.2061	0.2127	0.2053	0.1812
7	126	65	1	0.80	3.80	9.65	14.70	4.31	115.3	8	0.0019	-0.0095	-0.1039	-0.0201	0.0950	0.1615	0.2146	0.2285	0.2262	0.2103
7	125	65	1	0.80	3.81	9.66	14.70	4.30	113.8	9	-0.0109	-0.0248	-0.1186	-0.0425	0.0730	0.1454	0.2068	0.2353	0.2373	0.2272
7	124	65	1	0.80	3.83	9.66	14.70	4.30	112.2	10	-0.0209	-0.0368	-0.1315	-0.0599	0.0462	0.1195	0.1841	0.2251	0.2333	0.2285
7	123	65	1	0.80	3.85	9.63	14.70	4.33	110.4	11	-0.0303	-0.0470	-0.1452	-0.0725	0.0290	0.0986	0.1618	0.2061	0.2192	0.2199
7	122	65	1	0.80	3.87	9.63	14.70	4.32	107.9	12	-0.0357	-0.0532	-0.1553	-0.0803	0.0212	0.0892	0.1486	0.1893	0.2033	0.2074
7	121	65	1	0.80	3.96	9.65	14.70	4.32	98.2	13	-0.0430	-0.0617	-0.1659	-0.0885	0.0150	0.0818	0.1359	0.1703	0.1810	0.1842

Run	Point	cp35	cp36	cp37	cp38	cp39	cp40	cp41	cp42	cp43	cp44	cp45	cp46	cp117	cp120	cp123	cp126	cp129	cp135
7	133	9.9999	9.9999	9.9999	9.9999	9.9999	9.9999	9.9999	9.9999	9.9999	9.9999	9.9999	9.9999	0.1225	9.9999	9.9999	9.9999	9.9999	9.9999
7	132	9.9999	9.9999	9.9999	9.9999	9.9999	9.9999	9.9999	9.9999	9.9999	9.9999	9.9999	9.9999	0.0855	9.9999	9.9999	9.9999	9.9999	9.9999
7	131	9.9999	9.9999	9.9999	9.9999	9.9999	9.9999	9.9999	9.9999	9.9999	9.9999	9.9999	9.9999	-0.0067	0.1666	9.9999	9.9999	9.9999	9.9999
7	130	9.9999	9.9999	9.9999	9.9999	9.9999	9.9999	9.9999	9.9999	9.9999	9.9999	9.9999	9.9999	-0.0947	0.1825	0.1499	9.9999	9.9999	9.9999
7	129	9.9999	9.9999	9.9999	9.9999	9.9999	9.9999	9.9999	9.9999	9.9999	9.9999	9.9999	9.9999	-0.1561	0.1735	0.2457	9.9999	9.9999	9.9999
7	128	9.9999	9.9999	9.9999	9.9999	9.9999	9.9999	9.9999	9.9999	9.9999	9.9999	9.9999	9.9999	-0.1982	0.1347	0.2813	0.2777	9.9999	9.9999
7	127	9.9999	9.9999	9.9999	9.9999	9.9999	9.9999	9.9999	9.9999	9.9999	9.9999	9.9999	9.9999	-0.2220	0.0997	0.2657	0.3014	0.2945	9.9999
7	126	0.1878	0.1625	9.9999	9.9999	9.9999	9.9999	9.9999	9.9999	9.9999	9.9999	9.9999	9.9999	-0.2328	0.0806	0.2258	0.2904	0.3233	9.9999
7	125	0.2110	0.1946	0.1609	0.1131	9.9999	9.9999	9.9999	9.9999	9.9999	9.9999	9.9999	9.9999	-0.2329	0.0721	0.2014	0.2418	0.3105	9.9999
7	124	0.2160	0.2089	0.1917	0.1472	0.1026	0.1103	9.9999	9.9999	9.9999	9.9999	9.9999	9.9999	-0.2376	0.0645	0.1897	0.2040	0.2613	0.3299
7	123	0.2116	0.2099	0.1996	0.1639	0.1611	0.1515	0.0663	0.1118	9.9999	9.9999	9.9999	9.9999	-0.2451	0.0595	0.1817	0.1815	0.2060	0.3253
7	122	0.2025	0.2049	0.1989	0.1676	0.1691	0.1721	0.1439	0.1557	0.0558	0.1017	9.9999	9.9999	-0.2449	0.0582	0.1793	0.1720	0.1767	0.3160
7	121	0.1808	0.1870	0.1846	0.1592	0.1644	0.1702	0.1471	0.1735	0.1305	0.1236	0.1133	0.1333	-0.2484	0.0543	0.1733	0.1631	0.1586	0.2445

Table A-6. Concluded.

Run	Point	cp138	cp229	cp232	cp235	cp244	cp250	cp3
7	133	9.9999	9.9999	9.9999	9.9999	9.9999	9.9999	-0.0121
7	132	9.9999	0.0148	9.9999	9.9999	9.9999	9.9999	-0.0164
7	131	9.9999	0.0034	9.9999	9.9999	9.9999	9.9999	-0.0192
7	130	9.9999	0.0197	0.0619	9.9999	9.9999	9.9999	-0.0251
7	129	9.9999	0.0307	0.0491	0.1240	9.9999	9.9999	-0.0250
7	128	9.9999	0.0337	0.0579	0.0972	9.9999	9.9999	-0.0272
7	127	9.9999	0.0312	0.0428	0.1042	9.9999	9.9999	-0.0302
7	126	9.9999	0.0317	0.0281	0.0995	9.9999	9.9999	-0.0319
7	125	9.9999	0.0315	0.0207	0.0900	9.9999	9.9999	-0.0299
7	124	9.9999	0.0194	0.0157	0.0746	0.1750	9.9999	-0.0310
7	123	9.9999	0.0023	0.0103	0.0609	0.1461	9.9999	-0.0330
7	122	0.2320	-0.0091	0.0024	0.0526	0.1358	9.9999	-0.0318
7	121	0.3054	-0.0212	-0.0091	0.0410	0.1261	0.1921	-0.0343

Table A-7. Pressure Coefficients at M = 0.2 for Cavity with sweep = 55 deg. (Config. 2).

Run	Point	Ψ deg	CONF	M	R×10^{-6} per ft	p_∞ psi	$p_{t,\infty}$ psi	q_∞ psi	$T_{t,\infty}$ °F	l/h	cp19	cp20	cp21	cp22	cp25	cp26	cp28	cp29	cp30	cp32
9	254	55	2	0.20	1.39	14.40	14.81	0.41	66.8	1	0.0049	9.9999	9.9999	9.9999	9.9999	9.9999	9.9999	9.9999	9.9999	9.9999
9	253	55	2	0.20	1.38	14.40	14.82	0.41	67.0	2	0.0149	0.0511	0.0594	9.9999	9.9999	9.9999	9.9999	9.9999	9.9999	9.9999
9	252	55	2	0.20	1.38	14.40	14.81	0.41	67.3	3	-0.0409	-0.0598	0.0225	0.0955	9.9999	9.9999	9.9999	9.9999	9.9999	9.9999
9	251	55	2	0.20	1.38	14.40	14.82	0.41	67.3	4	-0.0814	-0.1083	0.0075	0.0988	0.1889	9.9999	9.9999	9.9999	9.9999	9.9999
9	249	55	2	0.20	1.38	14.40	14.82	0.41	67.7	5	-0.1288	-0.1656	-0.0211	0.1056	0.2446	0.2434	9.9999	9.9999	9.9999	9.9999
9	248	55	2	0.20	1.38	14.40	14.82	0.41	68.0	6	-0.1590	-0.1897	-0.0445	0.0937	0.2646	0.2721	0.2121	0.2127	9.9999	9.9999
9	247	55	2	0.20	1.38	14.40	14.82	0.41	68.2	7	-0.1507	-0.1725	-0.0730	0.0431	0.2581	0.2724	0.2450	0.2113	0.2049	9.9999
9	246	55	2	0.20	1.38	14.40	14.82	0.41	68.4	8	-0.1440	-0.1569	-0.0848	0.0058	0.2244	0.2468	0.2398	0.2263	0.2339	0.1971
9	244	55	2	0.20	1.38	14.40	14.82	0.41	68.8	9	-0.1547	-0.1696	-0.0974	-0.0126	0.1997	0.2251	0.2197	0.2134	0.2326	0.2329
9	243	55	2	0.20	1.38	14.40	14.82	0.41	69.2	10	-0.1701	-0.1837	-0.1110	-0.0227	0.1865	0.2067	0.1943	0.1838	0.2058	0.2282
9	242	55	2	0.20	1.38	14.40	14.82	0.41	69.5	11	-0.1856	-0.1996	-0.1212	-0.0296	0.1801	0.1968	0.1723	0.1591	0.1772	0.1949
9	241	55	2	0.20	1.38	14.40	14.82	0.41	69.8	12	-0.1955	-0.2133	-0.1311	-0.0312	0.1782	0.1933	0.1601	0.1407	0.1533	0.1612
9	240	55	2	0.20	1.38	14.40	14.82	0.41	70.1	13	-0.2054	-0.2234	-0.1393	-0.0362	0.1730	0.1863	0.1480	0.1356	0.1345	0.1342
9	239	55	2	0.20	1.38	14.40	14.82	0.41	70.6	14	-0.2112	-0.2309	-0.1453	-0.0393	0.1707	0.1839	0.1423	0.1319	0.1256	0.1153
9	238	55	2	0.20	1.38	14.40	14.82	0.41	71.1	15	-0.2180	-0.2379	-0.1504	-0.0377	0.1674	0.1806	0.1339	0.1236	0.1155	0.1003
9	237	55	2	0.20	1.37	14.40	14.82	0.41	71.9	16	-0.2216	-0.2416	-0.1539	-0.0394	0.1676	0.1791	0.1323	0.1204	0.1105	0.0937

Run	Point	cp33	cp34	cp35	cp36	cp37	cp38	cp39	cp40	cp41	cp42	cp43	cp44	cp45	cp46	cp47	cp48	cp49	cp114
9	254	9.9999	9.9999	9.9999	9.9999	9.9999	9.9999	9.9999	9.9999	9.9999	9.9999	9.9999	9.9999	9.9999	9.9999	9.9999	9.9999	9.9999	0.1209
9	253	9.9999	9.9999	9.9999	9.9999	9.9999	9.9999	9.9999	9.9999	9.9999	9.9999	9.9999	9.9999	9.9999	9.9999	9.9999	9.9999	9.9999	0.0755
9	252	9.9999	9.9999	9.9999	9.9999	9.9999	9.9999	9.9999	9.9999	9.9999	9.9999	9.9999	9.9999	9.9999	9.9999	9.9999	9.9999	9.9999	-0.0286
9	251	9.9999	9.9999	9.9999	9.9999	9.9999	9.9999	9.9999	9.9999	9.9999	9.9999	9.9999	9.9999	9.9999	9.9999	9.9999	9.9999	9.9999	-0.0480
9	249	9.9999	9.9999	9.9999	9.9999	9.9999	9.9999	9.9999	9.9999	9.9999	9.9999	9.9999	9.9999	9.9999	9.9999	9.9999	9.9999	9.9999	-0.1081
9	248	9.9999	9.9999	9.9999	9.9999	9.9999	9.9999	9.9999	9.9999	9.9999	9.9999	9.9999	9.9999	9.9999	9.9999	9.9999	9.9999	9.9999	-0.1679
9	247	9.9999	9.9999	9.9999	9.9999	9.9999	9.9999	9.9999	9.9999	9.9999	9.9999	9.9999	9.9999	9.9999	9.9999	9.9999	9.9999	9.9999	-0.2457
9	246	0.2180	9.9999	9.9999	9.9999	9.9999	9.9999	9.9999	9.9999	9.9999	9.9999	9.9999	9.9999	9.9999	9.9999	9.9999	9.9999	9.9999	-0.2563
9	244	0.2134	0.1919	0.2125	9.9999	9.9999	9.9999	9.9999	9.9999	9.9999	9.9999	9.9999	9.9999	9.9999	9.9999	9.9999	9.9999	9.9999	-0.2616
9	243	0.2373	0.2322	0.2022	0.1937	0.2191	9.9999	9.9999	9.9999	9.9999	9.9999	9.9999	9.9999	9.9999	9.9999	9.9999	9.9999	9.9999	-0.2638
9	242	0.2107	0.2276	0.2291	0.2324	0.2071	0.1471	0.2010	9.9999	9.9999	9.9999	9.9999	9.9999	9.9999	9.9999	9.9999	9.9999	9.9999	-0.2643
9	241	0.1734	0.1923	0.2024	0.2289	0.2334	0.2146	0.1858	0.1722	0.2051	9.9999	9.9999	9.9999	9.9999	9.9999	9.9999	9.9999	9.9999	-0.2606
9	240	0.1412	0.1537	0.1615	0.1887	0.2068	0.2161	0.2174	0.2268	0.1881	0.1751	0.2082	9.9999	9.9999	9.9999	9.9999	9.9999	9.9999	-0.2603
9	239	0.1188	0.1248	0.1257	0.1481	0.1622	0.1766	0.1900	0.2243	0.2243	0.2216	0.1847	0.1787	0.2285	9.9999	9.9999	9.9999	9.9999	-0.2556
9	238	0.1021	0.1032	0.0994	0.1166	0.1254	0.1346	0.1585	0.1814	0.1925	0.2183	0.2215	0.2181	0.2048	0.1790	0.2094	9.9999	9.9999	-0.2557
9	237	0.0921	0.0917	0.0836	0.0967	0.1009	0.1027	0.1204	0.1402	0.1472	0.1746	0.1971	0.2183	0.2373	0.2284	0.1864	0.1556	0.2162	-0.2507

Table A-7. Concluded.

Run	Point	cp117	cp120	cp123	cp126	cp129	cp135	cp138	cp144	cp226	cp229	cp232	cp235	cp244	cp250	cp3
9	254	9.9999	9.9999	9.9999	9.9999	9.9999	9.9999	9.9999	9.9999	9.9999	9.9999	9.9999	9.9999	9.9999	9.9999	-0.0102
9	253	0.2087	9.9999	9.9999	9.9999	9.9999	9.9999	9.9999	9.9999	9.9999	9.9999	9.9999	9.9999	9.9999	9.9999	-0.0103
9	252	0.1327	9.9999	9.9999	9.9999	9.9999	9.9999	9.9999	9.9999	0.0809	9.9999	9.9999	9.9999	9.9999	9.9999	-0.0154
9	251	0.1654	0.3278	9.9999	9.9999	9.9999	9.9999	9.9999	9.9999	0.0383	9.9999	9.9999	9.9999	9.9999	9.9999	-0.0188
9	249	0.1361	0.3405	0.3679	9.9999	9.9999	9.9999	9.9999	9.9999	0.0205	0.1397	9.9999	9.9999	9.9999	9.9999	-0.0222
9	248	0.0980	0.3008	0.3761	9.9999	9.9999	9.9999	9.9999	9.9999	0.0152	0.1200	0.2424	9.9999	9.9999	9.9999	-0.0239
9	247	0.0031	0.2581	0.3082	0.3832	9.9999	9.9999	9.9999	9.9999	0.0045	0.1059	0.1989	9.9999	9.9999	9.9999	-0.0239
9	246	-0.0487	0.2295	0.2452	0.3372	0.3661	9.9999	9.9999	9.9999	-0.0079	0.0917	0.1674	0.2136	9.9999	9.9999	-0.0239
9	244	-0.0449	0.2211	0.2099	0.2543	0.3693	9.9999	9.9999	9.9999	-0.0183	0.0789	0.1474	0.1952	9.9999	9.9999	-0.0254
9	243	-0.0295	0.2142	0.1881	0.1983	0.2790	9.9999	9.9999	9.9999	-0.0307	0.0648	0.1302	0.1713	9.9999	9.9999	-0.0271
9	242	-0.0106	0.2110	0.1765	0.1686	0.2027	0.3622	9.9999	9.9999	-0.0432	0.0524	0.1112	0.1473	9.9999	9.9999	-0.0272
9	241	0.0014	0.2072	0.1696	0.1544	0.1562	0.3441	9.9999	9.9999	-0.0538	0.0436	0.0972	0.1265	0.2376	9.9999	-0.0272
9	240	0.0083	0.2053	0.1644	0.1437	0.1329	0.2606	0.2826	9.9999	-0.0608	0.0347	0.0832	0.1074	0.2304	9.9999	-0.0288
9	239	0.0135	0.2027	0.1621	0.1396	0.1201	0.1731	0.3047	9.9999	-0.0675	0.0293	0.0725	0.0915	0.2139	9.9999	-0.0286
9	238	0.0152	0.2010	0.1571	0.1327	0.1095	0.1202	0.2011	9.9999	-0.0728	0.0241	0.0639	0.0761	0.1863	0.2198	-0.0303
9	237	0.0204	0.2012	0.1572	0.1310	0.1060	0.0956	0.1331	0.2734	-0.0747	0.0223	0.0587	0.0675	0.1604	0.2217	-0.0304

Table A-8. Pressure Coefficients at M = 0.4 for Cavity with sweep = 55 deg. (Config. 2).

Run	Point	Ψ deg	CONF	M	R×10^-6 per ft	p_∞ psi	$p_{t,\infty}$ psi	q_∞ psi	$T_{t,\infty}$ °F	l/h	cp19	cp20	cp21	cp22	cp25	cp26	cp28	cp29	cp30	cp32
9	234	55	2	0.40	2.55	13.24	14.80	1.50	79.4	1	0.0024	9.9999	9.9999	9.9999	9.9999	9.9999	9.9999	9.9999	9.9999	9.9999
9	233	55	2	0.40	2.54	13.24	14.80	1.50	80.2	2	0.0111	0.0458	0.0583	9.9999	9.9999	9.9999	9.9999	9.9999	9.9999	9.9999
9	232	55	2	0.40	2.54	13.24	14.80	1.50	80.5	3	-0.0427	-0.0702	0.0096	0.0965	9.9999	9.9999	9.9999	9.9999	9.9999	9.9999
9	231	55	2	0.40	2.54	13.25	14.80	1.50	80.8	4	-0.0861	-0.1210	-0.0033	0.1058	0.2057	9.9999	9.9999	9.9999	9.9999	9.9999
9	230	55	2	0.40	2.53	13.25	14.80	1.49	81.1	5	-0.1312	-0.1787	-0.0270	0.1206	0.2679	0.2576	9.9999	9.9999	9.9999	9.9999
9	229	55	2	0.40	2.53	13.25	14.80	1.49	81.6	6	-0.1667	-0.2076	-0.0531	0.1091	0.2895	0.2874	0.2167	0.2296	9.9999	9.9999
9	228	55	2	0.40	2.53	13.24	14.80	1.50	81.8	7	-0.1519	-0.1777	-0.0807	0.0482	0.2773	0.2838	0.2511	0.2254	0.2157	9.9999
9	227	55	2	0.40	2.53	13.24	14.80	1.50	82.5	8	-0.1115	-0.1183	-0.0693	-0.0006	0.1815	0.2070	0.2175	0.2190	0.2254	0.2006
9	226	55	2	0.40	2.52	13.25	14.80	1.49	83.0	9	-0.1475	-0.1628	-0.1002	-0.0145	0.2009	0.2197	0.2196	0.2247	0.2410	0.2381
9	225	55	2	0.40	2.52	13.25	14.80	1.50	83.4	10	-0.1749	-0.1918	-0.1197	-0.0214	0.2020	0.2139	0.1973	0.1999	0.2161	0.2378
9	224	55	2	0.40	2.52	13.24	14.80	1.50	83.9	11	-0.1911	-0.2109	-0.1324	-0.0281	0.1964	0.2049	0.1766	0.1730	0.1849	0.2032
9	223	55	2	0.40	2.52	13.25	14.80	1.49	84.4	12	-0.2021	-0.2231	-0.1399	-0.0311	0.1925	0.1982	0.1617	0.1536	0.1600	0.1676
9	222	55	2	0.40	2.51	13.25	14.80	1.49	84.9	13	-0.2151	-0.2384	-0.1504	-0.0362	0.1912	0.1941	0.1505	0.1382	0.1410	0.1368
9	221	55	2	0.40	2.51	13.24	14.80	1.49	85.4	14	-0.2200	-0.2448	-0.1549	-0.0380	0.1892	0.1902	0.1439	0.1295	0.1294	0.1175
9	220	55	2	0.40	2.50	13.25	14.80	1.49	86.1	15	-0.2263	-0.2527	-0.1597	-0.0394	0.1885	0.1886	0.1394	0.1237	0.1216	0.1052
9	219	55	2	0.40	2.51	13.24	14.80	1.50	86.6	16	-0.2316	-0.2595	-0.1658	-0.0432	0.1865	0.1862	0.1344	0.1181	0.1150	0.0950

Run	Point	cp33	cp34	cp35	cp36	cp37	cp38	cp39	cp40	cp41	cp42	cp43	cp44	cp45	cp46	cp47	cp48	cp49	cp114
9	234	9.9999	9.9999	9.9999	9.9999	9.9999	9.9999	9.9999	9.9999	9.9999	9.9999	9.9999	9.9999	9.9999	9.9999	9.9999	9.9999	9.9999	0.1355
9	233	9.9999	9.9999	9.9999	9.9999	9.9999	9.9999	9.9999	9.9999	9.9999	9.9999	9.9999	9.9999	9.9999	9.9999	9.9999	9.9999	9.9999	0.0860
9	232	9.9999	9.9999	9.9999	9.9999	9.9999	9.9999	9.9999	9.9999	9.9999	9.9999	9.9999	9.9999	9.9999	9.9999	9.9999	9.9999	9.9999	-0.0301
9	231	9.9999	9.9999	9.9999	9.9999	9.9999	9.9999	9.9999	9.9999	9.9999	9.9999	9.9999	9.9999	9.9999	9.9999	9.9999	9.9999	9.9999	-0.0610
9	230	9.9999	9.9999	9.9999	9.9999	9.9999	9.9999	9.9999	9.9999	9.9999	9.9999	9.9999	9.9999	9.9999	9.9999	9.9999	9.9999	9.9999	-0.1149
9	229	9.9999	9.9999	9.9999	9.9999	9.9999	9.9999	9.9999	9.9999	9.9999	9.9999	9.9999	9.9999	9.9999	9.9999	9.9999	9.9999	9.9999	-0.1842
9	228	9.9999	9.9999	9.9999	9.9999	9.9999	9.9999	9.9999	9.9999	9.9999	9.9999	9.9999	9.9999	9.9999	9.9999	9.9999	9.9999	9.9999	-0.2585
9	227	0.2169	9.9999	9.9999	9.9999	9.9999	9.9999	9.9999	9.9999	9.9999	9.9999	9.9999	9.9999	9.9999	9.9999	9.9999	9.9999	9.9999	-0.2302
9	226	0.2162	0.1972	0.2208	9.9999	9.9999	9.9999	9.9999	9.9999	9.9999	9.9999	9.9999	9.9999	9.9999	9.9999	9.9999	9.9999	9.9999	-0.2677
9	225	0.2473	0.2376	0.2036	0.1927	0.2269	9.9999	9.9999	9.9999	9.9999	9.9999	9.9999	9.9999	9.9999	9.9999	9.9999	9.9999	9.9999	-0.2779
9	224	0.2217	0.2360	0.2406	0.2344	0.2051	0.1363	0.2103	9.9999	9.9999	9.9999	9.9999	9.9999	9.9999	9.9999	9.9999	9.9999	9.9999	-0.2816
9	223	0.1837	0.1989	0.2134	0.2329	0.2434	0.2158	0.1846	0.1635	0.2073	9.9999	9.9999	9.9999	9.9999	9.9999	9.9999	9.9999	9.9999	-0.2785
9	222	0.1483	0.1578	0.1685	0.1910	0.2155	0.2215	0.2303	0.2254	0.1700	0.1860	0.2067	9.9999	9.9999	9.9999	9.9999	9.9999	9.9999	-0.2786
9	221	0.1242	0.1275	0.1316	0.1489	0.1705	0.1797	0.2037	0.2276	0.2285	0.2355	0.1705	0.1703	0.2336	9.9999	9.9999	9.9999	9.9999	-0.2736
9	220	0.1081	0.1071	0.1056	0.1212	0.1335	0.1373	0.1587	0.1855	0.2001	0.2376	0.2289	0.2308	0.1992	0.1816	0.2297	9.9999	9.9999	-0.2726
9	219	0.0961	0.0920	0.0863	0.0978	0.1045	0.1021	0.1175	0.1392	0.1485	0.1906	0.2023	0.2295	0.2442	0.2353	0.1881	0.1551	0.2203	-0.2707

Table A-8. Concluded.

Run	Point	cp117	cp120	cp123	cp126	cp129	cp135	cp138	cp144	cp226	cp229	cp232	cp235	cp244	cp250	cp3
9	234	9.9999	9.9999	9.9999	9.9999	9.9999	9.9999	9.9999	9.9999	9.9999	9.9999	9.9999	9.9999	9.9999	9.9999	-0.0039
9	233	0.2127	9.9999	9.9999	9.9999	9.9999	9.9999	9.9999	9.9999	9.9999	9.9999	9.9999	9.9999	9.9999	9.9999	-0.0081
9	232	0.1351	9.9999	9.9999	9.9999	9.9999	9.9999	9.9999	9.9999	0.0937	9.9999	9.9999	9.9999	9.9999	9.9999	-0.0113
9	231	0.1678	0.3366	9.9999	9.9999	9.9999	9.9999	9.9999	9.9999	0.0522	9.9999	9.9999	9.9999	9.9999	9.9999	-0.0151
9	230	0.1377	0.3544	0.3864	9.9999	9.9999	9.9999	9.9999	9.9999	0.0406	0.1567	9.9999	9.9999	9.9999	9.9999	-0.0151
9	229	0.0968	0.3140	0.3981	9.9999	9.9999	9.9999	9.9999	9.9999	0.0338	0.1320	0.2489	9.9999	9.9999	9.9999	-0.0189
9	228	-0.0204	0.2668	0.3121	0.3870	9.9999	9.9999	9.9999	9.9999	0.0193	0.1158	0.2060	9.9999	9.9999	9.9999	-0.0192
9	227	-0.1196	0.1753	0.2268	0.3254	0.3480	9.9999	9.9999	9.9999	0.0285	0.1114	0.1656	0.2070	9.9999	9.9999	-0.0188
9	226	-0.0909	0.2154	0.2062	0.2584	0.3726	9.9999	9.9999	9.9999	-0.0040	0.0899	0.1546	0.2076	9.9999	9.9999	-0.0212
9	225	-0.0544	0.2195	0.1878	0.2050	0.2878	9.9999	9.9999	9.9999	-0.0223	0.0719	0.1359	0.1861	9.9999	9.9999	-0.0230
9	224	-0.0326	0.2165	0.1761	0.1755	0.2078	0.3767	9.9999	9.9999	-0.0367	0.0577	0.1179	0.1616	9.9999	9.9999	-0.0247
9	223	-0.0135	0.2143	0.1702	0.1597	0.1636	0.3597	9.9999	9.9999	-0.0466	0.0481	0.1026	0.1399	0.2362	9.9999	-0.0244
9	222	-0.0031	0.2109	0.1647	0.1492	0.1383	0.2759	0.2714	9.9999	-0.0587	0.0380	0.0874	0.1187	0.2335	9.9999	-0.0268
9	221	0.0044	0.2094	0.1614	0.1438	0.1246	0.1835	0.3185	9.9999	-0.0645	0.0317	0.0764	0.1011	0.2190	9.9999	-0.0268
9	220	0.0096	0.2091	0.1602	0.1401	0.1164	0.1332	0.2099	9.9999	-0.0699	0.0268	0.0683	0.0875	0.1940	0.2258	-0.0268
9	219	0.0111	0.2060	0.1574	0.1365	0.1105	0.1040	0.1358	0.2705	-0.0761	0.0210	0.0600	0.0744	0.1630	0.2298	-0.0284

Table A-9. Pressure Coefficients at M = 0.6 for Cavity with sweep = 55 deg. (Config. 2).

Run	Point	Ψ deg	CONF	M	R×10^{-6} per ft	p_∞ psi	$p_{t,\infty}$ psi	q_∞ psi	$T_{t,\infty}$ °F	l/h	cp19	cp20	cp21	cp22	cp25	cp26	cp28	cp29	cp30	cp32
9	215	55	2	0.60	3.34	11.58	14.79	2.93	99.5	1	0.0015	9.9999	9.9999	9.9999	9.9999	9.9999	9.9999	9.9999	9.9999	9.9999
9	214	55	2	0.60	3.34	11.58	14.79	2.93	99.7	2	0.0095	0.0458	0.0633	9.9999	9.9999	9.9999	9.9999	9.9999	9.9999	9.9999
9	213	55	2	0.60	3.34	11.58	14.79	2.93	99.9	3	-0.0405	-0.0722	0.0107	0.1047	9.9999	9.9999	9.9999	9.9999	9.9999	9.9999
9	212	55	2	0.60	3.34	11.56	14.79	2.95	100.0	4	-0.0794	-0.1171	0.0029	0.1179	0.2199	9.9999	9.9999	9.9999	9.9999	9.9999
9	211	55	2	0.60	3.34	11.57	14.78	2.94	100.2	5	-0.1325	-0.1814	-0.0195	0.1341	0.2824	0.2727	9.9999	9.9999	9.9999	9.9999
9	210	55	2	0.60	3.34	11.56	14.79	2.94	100.6	6	-0.1493	-0.1807	-0.0416	0.1130	0.3022	0.2993	0.2258	0.2386	9.9999	9.9999
9	209	55	2	0.60	3.33	11.57	14.78	2.94	100.8	7	-0.0849	-0.0878	-0.0496	0.0129	0.1758	0.2024	0.1972	0.1858	0.2099	9.9999
9	208	55	2	0.60	3.33	11.58	14.79	2.93	101.0	8	-0.0956	-0.0946	-0.0598	-0.0036	0.1540	0.1845	0.2025	0.2068	0.2164	0.2047
9	207	55	2	0.60	3.33	11.58	14.78	2.93	101.2	9	-0.1094	-0.1093	-0.0747	-0.0212	0.1338	0.1643	0.1907	0.2041	0.2232	0.2221
9	206	55	2	0.60	3.32	11.58	14.78	2.93	101.5	10	-0.1202	-0.1219	-0.0845	-0.0298	0.1233	0.1515	0.1750	0.1899	0.2132	0.2350
9	205	55	2	0.60	3.32	11.59	14.78	2.92	102.0	11	-0.1429	-0.1476	-0.1009	-0.0365	0.1285	0.1495	0.1577	0.1684	0.1868	0.2131
9	204	55	2	0.60	3.32	11.57	14.78	2.94	102.4	12	-0.1801	-0.1972	-0.1325	-0.0418	0.1754	0.1866	0.1602	0.1585	0.1667	0.1801
9	203	55	2	0.60	3.31	11.58	14.78	2.93	103.1	13	-0.2027	-0.2228	-0.1466	-0.0413	0.1884	0.1927	0.1519	0.1435	0.1453	0.1450
9	202	55	2	0.60	3.31	11.58	14.78	2.93	103.7	14	-0.2152	-0.2380	-0.1551	-0.0421	0.1921	0.1940	0.1464	0.1343	0.1325	0.1230
9	201	55	2	0.60	3.30	11.58	14.78	2.93	104.3	15	-0.2278	-0.2518	-0.1640	-0.0447	0.1921	0.1916	0.1391	0.1251	0.1212	0.1059
9	200	55	2	0.60	3.29	11.58	14.78	2.93	105.4	16	-0.2326	-0.2574	-0.1660	-0.0434	0.1925	0.1908	0.1357	0.1204	0.1152	0.0957

Run	Point	cp33	cp34	cp35	cp36	cp37	cp38	cp39	cp40	cp41	cp42	cp43	cp44	cp45	cp46	cp47	cp48	cp49	cp114
9	215	9.9999	9.9999	9.9999	9.9999	9.9999	9.9999	9.9999	9.9999	9.9999	9.9999	9.9999	9.9999	9.9999	9.9999	9.9999	9.9999	9.9999	0.1267
9	214	9.9999	9.9999	9.9999	9.9999	9.9999	9.9999	9.9999	9.9999	9.9999	9.9999	9.9999	9.9999	9.9999	9.9999	9.9999	9.9999	9.9999	0.0679
9	213	9.9999	9.9999	9.9999	9.9999	9.9999	9.9999	9.9999	9.9999	9.9999	9.9999	9.9999	9.9999	9.9999	9.9999	9.9999	9.9999	9.9999	-0.0538
9	212	9.9999	9.9999	9.9999	9.9999	9.9999	9.9999	9.9999	9.9999	9.9999	9.9999	9.9999	9.9999	9.9999	9.9999	9.9999	9.9999	9.9999	-0.0977
9	211	9.9999	9.9999	9.9999	9.9999	9.9999	9.9999	9.9999	9.9999	9.9999	9.9999	9.9999	9.9999	9.9999	9.9999	9.9999	9.9999	9.9999	-0.1788
9	210	9.9999	9.9999	9.9999	9.9999	9.9999	9.9999	9.9999	9.9999	9.9999	9.9999	9.9999	9.9999	9.9999	9.9999	9.9999	9.9999	9.9999	-0.2496
9	209	9.9999	9.9999	9.9999	9.9999	9.9999	9.9999	9.9999	9.9999	9.9999	9.9999	9.9999	9.9999	9.9999	9.9999	9.9999	9.9999	9.9999	-0.1776
9	208	0.2123	9.9999	9.9999	9.9999	9.9999	9.9999	9.9999	9.9999	9.9999	9.9999	9.9999	9.9999	9.9999	9.9999	9.9999	9.9999	9.9999	-0.1857
9	207	0.2026	0.1961	0.2056	9.9999	9.9999	9.9999	9.9999	9.9999	9.9999	9.9999	9.9999	9.9999	9.9999	9.9999	9.9999	9.9999	9.9999	-0.2022
9	206	0.2400	0.2287	0.1968	0.1991	0.2129	9.9999	9.9999	9.9999	9.9999	9.9999	9.9999	9.9999	9.9999	9.9999	9.9999	9.9999	9.9999	-0.2194
9	205	0.2305	0.2396	0.2412	0.2311	0.1974	0.1405	0.2032	9.9999	9.9999	9.9999	9.9999	9.9999	9.9999	9.9999	9.9999	9.9999	9.9999	-0.2527
9	204	0.1977	0.2138	0.2280	0.2430	0.2521	0.2210	0.1836	0.1740	0.2083	9.9999	9.9999	9.9999	9.9999	9.9999	9.9999	9.9999	9.9999	-0.2962
9	203	0.1569	0.1667	0.1794	0.2032	0.2266	0.2304	0.2392	0.2326	0.1616	0.1960	0.2097	9.9999	9.9999	9.9999	9.9999	9.9999	9.9999	-0.3100
9	202	0.1299	0.1334	0.1393	0.1596	0.1813	0.1898	0.2163	0.2406	0.2373	0.2436	0.1578	0.1794	0.2419	9.9999	9.9999	9.9999	9.9999	-0.3151
9	201	0.1094	0.1080	0.1075	0.1224	0.1379	0.1411	0.1662	0.1952	0.2070	0.2482	0.2356	0.2352	0.1942	0.1874	0.2343	9.9999	9.9999	-0.3206
9	200	0.0971	0.0926	0.0879	0.0981	0.1080	0.1043	0.1235	0.1468	0.1543	0.2019	0.2147	0.2418	0.2541	0.2418	0.1850	0.1613	0.2240	-0.3210

Table A-9. Concluded.

Run	Point	cp117	cp120	cp123	cp126	cp129	cp135	cp138	cp144	cp226	cp229	cp232	cp235	cp244	cp250	cp3
9	215	9.9999	9.9999	9.9999	9.9999	9.9999	9.9999	9.9999	9.9999	9.9999	9.9999	9.9999	9.9999	9.9999	9.9999	-0.0018
9	214	0.2220	9.9999	9.9999	9.9999	9.9999	9.9999	9.9999	9.9999	9.9999	9.9999	9.9999	9.9999	9.9999	9.9999	-0.0066
9	213	0.1277	9.9999	9.9999	9.9999	9.9999	9.9999	9.9999	9.9999	0.1073	9.9999	9.9999	9.9999	9.9999	9.9999	-0.0092
9	212	0.1617	0.3489	9.9999	9.9999	9.9999	9.9999	9.9999	9.9999	0.0669	9.9999	9.9999	9.9999	9.9999	9.9999	-0.0114
9	211	0.1233	0.3663	0.3987	9.9999	9.9999	9.9999	9.9999	9.9999	0.0577	0.1672	9.9999	9.9999	9.9999	9.9999	-0.0169
9	210	0.0025	0.3186	0.4062	9.9999	9.9999	9.9999	9.9999	9.9999	0.0598	0.1455	0.2476	9.9999	9.9999	9.9999	-0.0152
9	209	-0.1276	0.1019	0.2471	0.3358	9.9999	9.9999	9.9999	9.9999	0.0677	0.1281	0.1757	9.9999	9.9999	9.9999	-0.0140
9	208	-0.1343	0.0852	0.1997	0.3082	0.3455	9.9999	9.9999	9.9999	0.0649	0.1329	0.1675	0.1968	9.9999	9.9999	-0.0139
9	207	-0.1458	0.0836	0.1719	0.2395	0.3456	9.9999	9.9999	9.9999	0.0478	0.1239	0.1630	0.1832	9.9999	9.9999	-0.0177
9	206	-0.1526	0.1017	0.1649	0.1959	0.2833	9.9999	9.9999	9.9999	0.0313	0.1135	0.1589	0.1790	9.9999	9.9999	-0.0171
9	205	-0.1564	0.1422	0.1676	0.1692	0.2094	0.3667	9.9999	9.9999	0.0033	0.0888	0.1420	0.1685	9.9999	9.9999	-0.0214
9	204	-0.1278	0.2044	0.1756	0.1625	0.1694	0.3687	9.9999	9.9999	-0.0291	0.0604	0.1178	0.1544	0.2406	9.9999	-0.0233
9	203	-0.0989	0.2123	0.1705	0.1532	0.1432	0.2865	0.2783	9.9999	-0.0417	0.0474	0.0988	0.1309	0.2400	9.9999	-0.0263
9	202	-0.0787	0.2134	0.1681	0.1483	0.1298	0.1922	0.3312	9.9999	-0.0504	0.0397	0.0858	0.1114	0.2262	9.9999	-0.0264
9	201	-0.0667	0.2102	0.1637	0.1422	0.1189	0.1362	0.2174	9.9999	-0.0598	0.0308	0.0736	0.0926	0.1995	0.2272	-0.0297
9	200	-0.0561	0.2096	0.1622	0.1395	0.1136	0.1072	0.1390	0.2756	-0.0640	0.0274	0.0663	0.0800	0.1712	0.2362	-0.0292

Table A-10. Pressure Coefficients at M = 0.8 for Cavity with sweep = 55 deg. (Config. 2).

Run	Point	Ψ deg	CONF	M	$R \times 10^{-6}$ per ft	p_∞ psi	$p_{t,\infty}$ psi	q_∞ psi	$T_{t,\infty}$ °F	l/h	cp19	cp20	cp21	cp22	cp25	cp26	cp28	cp29	cp30	cp32
9	197	55	2	0.80	3.81	9.68	14.77	4.35	117.6	1	0.0020	9.9999	9.9999	9.9999	9.9999	9.9999	9.9999	9.9999	9.9999	9.9999
9	196	55	2	0.80	3.81	9.66	14.77	4.36	117.6	2	-0.0004	0.0492	0.0640	9.9999	9.9999	9.9999	9.9999	9.9999	9.9999	9.9999
9	195	55	2	0.80	3.81	9.66	14.77	4.36	117.7	3	-0.0659	-0.1078	0.0047	0.1405	9.9999	9.9999	9.9999	9.9999	9.9999	9.9999
9	194	55	2	0.80	3.81	9.67	14.77	4.35	117.9	4	-0.0669	-0.1255	-0.0464	0.0806	0.2526	9.9999	9.9999	9.9999	9.9999	9.9999
9	193	55	2	0.80	3.81	9.67	14.77	4.35	118.0	5	-0.1407	-0.1916	-0.0261	0.1495	0.3500	0.3446	9.9999	9.9999	9.9999	9.9999
9	192	55	2	0.80	3.80	9.69	14.77	4.34	118.7	6	-0.0665	-0.0811	-0.0687	-0.0176	0.1223	0.1590	0.1798	0.1991	9.9999	9.9999
9	191	55	2	0.80	3.79	9.66	14.77	4.36	120.1	7	-0.0786	-0.0867	-0.0759	-0.0309	0.0885	0.1210	0.1404	0.1600	0.2036	9.9999
9	190	55	2	0.80	3.73	9.67	14.76	4.34	126.7	8	-0.0904	-0.0963	-0.0847	-0.0423	0.0733	0.1078	0.1459	0.1580	0.1852	0.2181
9	189	55	2	0.80	3.75	9.70	14.76	4.32	123.4	9	-0.1025	-0.1072	-0.0949	-0.0543	0.0593	0.0940	0.1455	0.1704	0.1986	0.2081
9	188	55	2	0.80	3.76	9.68	14.76	4.33	122.0	10	-0.1099	-0.1152	-0.1040	-0.0646	0.0506	0.0856	0.1376	0.1656	0.1980	0.2317
9	187	55	2	0.80	3.78	9.67	14.76	4.35	120.1	11	-0.1223	-0.1287	-0.1175	-0.0774	0.0433	0.0760	0.1244	0.1503	0.1821	0.2230
9	186	55	2	0.80	3.79	9.69	14.76	4.33	118.7	12	-0.1362	-0.1437	-0.1318	-0.0914	0.0379	0.0704	0.1114	0.1331	0.1601	0.1952
9	185	55	2	0.80	3.81	9.67	14.76	4.35	117.2	13	-0.1437	-0.1519	-0.1397	-0.0998	0.0391	0.0722	0.1072	0.1253	0.1469	0.1719
9	184	55	2	0.80	3.84	9.70	14.75	4.32	112.5	14	-0.1518	-0.1603	-0.1458	-0.1059	0.0414	0.0740	0.1034	0.1172	0.1336	0.1477
9	183	55	2	0.80	3.87	9.68	14.75	4.34	109.4	15	-0.1602	-0.1682	-0.1524	-0.1127	0.0408	0.0739	0.1003	0.1116	0.1250	0.1319
9	182	55	2	0.80	3.89	9.69	14.75	4.33	107.0	16	-0.1676	-0.1764	-0.1591	-0.1187	0.0403	0.0731	0.0970	0.1061	0.1171	0.1186

Run	Point	cp33	cp34	cp35	cp36	cp37	cp38	cp39	cp40	cp41	cp42	cp43	cp44	cp45	cp46	cp47	cp48	cp49	cp114
9	197	9.9999	9.9999	9.9999	9.9999	9.9999	9.9999	9.9999	9.9999	9.9999	9.9999	9.9999	9.9999	9.9999	9.9999	9.9999	9.9999	9.9999	0.0569
9	196	9.9999	9.9999	9.9999	9.9999	9.9999	9.9999	9.9999	9.9999	9.9999	9.9999	9.9999	9.9999	9.9999	9.9999	9.9999	9.9999	9.9999	0.0250
9	195	9.9999	9.9999	9.9999	9.9999	9.9999	9.9999	9.9999	9.9999	9.9999	9.9999	9.9999	9.9999	9.9999	9.9999	9.9999	9.9999	9.9999	-0.0982
9	194	9.9999	9.9999	9.9999	9.9999	9.9999	9.9999	9.9999	9.9999	9.9999	9.9999	9.9999	9.9999	9.9999	9.9999	9.9999	9.9999	9.9999	-0.1454
9	193	9.9999	9.9999	9.9999	9.9999	9.9999	9.9999	9.9999	9.9999	9.9999	9.9999	9.9999	9.9999	9.9999	9.9999	9.9999	9.9999	9.9999	-0.2493
9	192	9.9999	9.9999	9.9999	9.9999	9.9999	9.9999	9.9999	9.9999	9.9999	9.9999	9.9999	9.9999	9.9999	9.9999	9.9999	9.9999	9.9999	-0.1218
9	191	9.9999	9.9999	9.9999	9.9999	9.9999	9.9999	9.9999	9.9999	9.9999	9.9999	9.9999	9.9999	9.9999	9.9999	9.9999	9.9999	9.9999	-0.1280
9	190	0.2262	9.9999	9.9999	9.9999	9.9999	9.9999	9.9999	9.9999	9.9999	9.9999	9.9999	9.9999	9.9999	9.9999	9.9999	9.9999	9.9999	-0.1371
9	189	0.2143	0.2219	0.2217	9.9999	9.9999	9.9999	9.9999	9.9999	9.9999	9.9999	9.9999	9.9999	9.9999	9.9999	9.9999	9.9999	9.9999	-0.1485
9	188	0.2383	0.2262	0.2096	0.2244	0.2275	9.9999	9.9999	9.9999	9.9999	9.9999	9.9999	9.9999	9.9999	9.9999	9.9999	9.9999	9.9999	-0.1570
9	187	0.2411	0.2484	0.2467	0.2388	0.2022	0.1650	0.2111	9.9999	9.9999	9.9999	9.9999	9.9999	9.9999	9.9999	9.9999	9.9999	9.9999	-0.1722
9	186	0.2154	0.2293	0.2398	0.2498	0.2501	0.2213	0.1834	0.1868	0.2045	9.9999	9.9999	9.9999	9.9999	9.9999	9.9999	9.9999	9.9999	-0.1881
9	185	0.1884	0.2002	0.2123	0.2294	0.2443	0.2409	0.2441	0.2414	0.1834	0.2146	0.2097	9.9999	9.9999	9.9999	9.9999	9.9999	9.9999	-0.1975
9	184	0.1603	0.1664	0.1734	0.1886	0.2064	0.2129	0.2301	0.2483	0.2413	0.2540	0.1855	0.1945	0.2454	9.9999	9.9999	9.9999	9.9999	-0.2076
9	183	0.1389	0.1404	0.1420	0.1530	0.1650	0.1702	0.1891	0.2144	0.2230	0.2584	0.2443	0.2483	0.2235	0.2049	0.2404	9.9999	9.9999	-0.2172
9	182	0.1230	0.1207	0.1171	0.1246	0.1311	0.1291	0.1442	0.1666	0.1750	0.2187	0.2257	0.2499	0.2635	0.2525	0.2135	0.1752	0.2266	-0.2277

Table A-10. Concluded.

Run	Point	cp117	cp120	cp123	cp126	cp129	cp135	cp138	cp144	cp226	cp229	cp232	cp235	cp244	cp250	cp3
9	197	9.9999	9.9999	9.9999	9.9999	9.9999	9.9999	9.9999	9.9999	9.9999	9.9999	9.9999	9.9999	9.9999	9.9999	-0.0059
9	196	0.2507	9.9999	9.9999	9.9999	9.9999	9.9999	9.9999	9.9999	9.9999	9.9999	9.9999	9.9999	9.9999	9.9999	-0.0104
9	195	0.0275	9.9999	9.9999	9.9999	9.9999	9.9999	9.9999	9.9999	0.1328	9.9999	9.9999	9.9999	9.9999	9.9999	-0.0154
9	194	0.0066	0.3484	9.9999	9.9999	9.9999	9.9999	9.9999	9.9999	0.0559	9.9999	9.9999	9.9999	9.9999	9.9999	-0.0183
9	193	0.0042	0.4027	0.4753	9.9999	9.9999	9.9999	9.9999	9.9999	0.0777	0.2177	9.9999	9.9999	9.9999	9.9999	-0.0185
9	192	-0.1044	-0.0013	0.1657	9.9999	9.9999	9.9999	9.9999	9.9999	0.0465	0.1067	0.1825	9.9999	9.9999	9.9999	-0.0163
9	191	-0.1065	-0.0264	0.1006	0.2783	9.9999	9.9999	9.9999	9.9999	0.0466	0.1071	0.1517	9.9999	9.9999	9.9999	-0.0184
9	190	-0.1135	-0.0409	0.0752	0.2130	0.3530	9.9999	9.9999	9.9999	0.0352	0.1132	0.1552	0.1831	9.9999	9.9999	-0.0181
9	189	-0.1239	-0.0497	0.0622	0.1721	0.2974	9.9999	9.9999	9.9999	0.0226	0.1140	0.1647	0.1795	9.9999	9.9999	-0.0200
9	188	-0.1318	-0.0519	0.0600	0.1513	0.2558	9.9999	9.9999	9.9999	0.0100	0.1105	0.1715	0.1917	9.9999	9.9999	-0.0179
9	187	-0.1458	-0.0560	0.0586	0.1382	0.2093	0.3815	9.9999	9.9999	-0.0040	0.0978	0.1646	0.1931	9.9999	9.9999	-0.0203
9	186	-0.1608	-0.0583	0.0610	0.1302	0.1699	0.3595	9.9999	9.9999	-0.0180	0.0813	0.1489	0.1815	0.2228	9.9999	-0.0253
9	185	-0.1689	-0.0555	0.0691	0.1291	0.1514	0.2995	0.3109	9.9999	-0.0260	0.0717	0.1373	0.1686	0.2265	9.9999	-0.0243
9	184	-0.1778	-0.0515	0.0755	0.1270	0.1371	0.2116	0.3363	9.9999	-0.0324	0.0615	0.1219	0.1468	0.2143	9.9999	-0.0263
9	183	-0.1857	-0.0500	0.0792	0.1252	0.1282	0.1571	0.2332	9.9999	-0.0393	0.0536	0.1102	0.1280	0.1998	0.2410	-0.0288
9	182	-0.1951	-0.0480	0.0818	0.1225	0.1205	0.1242	0.1544	0.3124	-0.0473	0.0460	0.0983	0.1096	0.1780	0.2370	-0.0321

Table A-11. Pressure Coefficients at M = 0.2 for Cavity with sweep = 45 deg. (Config. 3).

Run	Point	Ψ deg	CONF	M	R×10^{-6} per ft	p_∞ psi	$p_{t,\infty}$ psi	q_∞ psi	$T_{t,\infty}$ °F	l/h	cp16	cp17	cp19	cp20	cp21	cp22	cp25	cp26	cp28	cp29
10	336	45	3	0.20	1.32	14.37	14.79	0.41	88.7	1	0.0079	9.9999	9.9999	9.9999	9.9999	9.9999	9.9999	9.9999	9.9999	9.9999
10	335	45	3	0.20	1.32	14.38	14.79	0.41	89.1	2	0.0786	-0.0629	9.9999	9.9999	9.9999	9.9999	9.9999	9.9999	9.9999	9.9999
10	334	45	3	0.20	1.31	14.38	14.79	0.41	89.7	3	0.0129	-0.1705	0.0775	0.2281	9.9999	9.9999	9.9999	9.9999	9.9999	9.9999
10	333	45	3	0.20	1.31	14.38	14.79	0.41	89.9	4	-0.0345	-0.1916	0.0709	0.2253	0.2810	0.2956	9.9999	9.9999	9.9999	9.9999
10	332	45	3	0.20	1.31	14.38	14.79	0.41	90.2	5	-0.0480	-0.0512	-0.0742	-0.0155	0.0665	0.1163	9.9999	9.9999	9.9999	9.9999
10	331	45	3	0.20	1.31	14.38	14.79	0.41	90.8	6	-0.0547	-0.0426	-0.0641	-0.0276	0.0263	0.0589	0.1545	0.1979	9.9999	9.9999
10	330	45	3	0.20	1.31	14.38	14.79	0.41	91.2	7	-0.0718	-0.0599	-0.0728	-0.0260	0.0314	0.0709	0.1566	0.1762	0.1981	9.9999
10	329	45	3	0.20	1.31	14.38	14.79	0.41	91.6	8	-0.0902	-0.0786	-0.0878	-0.0328	0.0297	0.0708	0.1681	0.1980	0.2150	0.1923
10	328	45	3	0.20	1.30	14.38	14.79	0.41	92.1	9	-0.1056	-0.0941	-0.1014	-0.0433	0.0247	0.0674	0.1615	0.1914	0.2238	0.2259
10	327	45	3	0.20	1.30	14.38	14.79	0.41	92.6	10	-0.1191	-0.1095	-0.1115	-0.0502	0.0196	0.0640	0.1497	0.1760	0.2031	0.2075
10	326	45	3	0.20	1.30	14.38	14.79	0.41	93.0	11	-0.1272	-0.1178	-0.1230	-0.0604	0.0130	0.0606	0.1410	0.1621	0.1769	0.1771
10	325	45	3	0.20	1.30	14.38	14.79	0.41	93.5	12	-0.1327	-0.1267	-0.1319	-0.0659	0.0096	0.0573	0.1312	0.1505	0.1550	0.1508
10	324	45	3	0.20	1.30	14.38	14.79	0.41	94.0	13	-0.1390	-0.1348	-0.1398	-0.0725	0.0063	0.0572	0.1275	0.1416	0.1408	0.1321
10	323	45	3	0.20	1.30	14.38	14.79	0.41	94.7	14	-0.1426	-0.1419	-0.1435	-0.0761	0.0046	0.0589	0.1243	0.1350	0.1290	0.1273
10	322	45	3	0.20	1.30	14.38	14.79	0.41	95.1	15	-0.1479	-0.1489	-0.1487	-0.0780	0.0045	0.0606	0.1227	0.1300	0.1170	0.1190
10	321	45	3	0.20	1.29	14.38	14.79	0.41	95.8	16	-0.1465	-0.1476	-0.1490	-0.0799	0.0045	0.0624	0.1229	0.1302	0.1155	0.1142
10	320	45	3	0.20	1.29	14.38	14.79	0.41	96.3	17	-0.1515	-0.1561	-0.1557	-0.0850	-0.0005	0.0590	0.1229	0.1233	0.1068	0.1058
10	319	45	3	0.20	1.29	14.38	14.79	0.41	97.0	18	-0.1521	-0.1566	-0.1563	-0.0819	0.0011	0.0608	0.1232	0.1219	0.1037	0.1027

Run	Point	cp30	cp32	cp33	cp34	cp35	cp36	cp37	cp38	cp39	cp40	cp41	cp42	cp43	cp44	cp45	cp46	cp47	cp48
10	336	9.9999	9.9999	9.9999	9.9999	9.9999	9.9999	9.9999	9.9999	9.9999	9.9999	9.9999	9.9999	9.9999	9.9999	9.9999	9.9999	9.9999	9.9999
10	335	9.9999	9.9999	9.9999	9.9999	9.9999	9.9999	9.9999	9.9999	9.9999	9.9999	9.9999	9.9999	9.9999	9.9999	9.9999	9.9999	9.9999	9.9999
10	334	9.9999	9.9999	9.9999	9.9999	9.9999	9.9999	9.9999	9.9999	9.9999	9.9999	9.9999	9.9999	9.9999	9.9999	9.9999	9.9999	9.9999	9.9999
10	333	9.9999	9.9999	9.9999	9.9999	9.9999	9.9999	9.9999	9.9999	9.9999	9.9999	9.9999	9.9999	9.9999	9.9999	9.9999	9.9999	9.9999	9.9999
10	332	9.9999	9.9999	9.9999	9.9999	9.9999	9.9999	9.9999	9.9999	9.9999	9.9999	9.9999	9.9999	9.9999	9.9999	9.9999	9.9999	9.9999	9.9999
10	331	9.9999	9.9999	9.9999	9.9999	9.9999	9.9999	9.9999	9.9999	9.9999	9.9999	9.9999	9.9999	9.9999	9.9999	9.9999	9.9999	9.9999	9.9999
10	330	9.9999	9.9999	9.9999	9.9999	9.9999	9.9999	9.9999	9.9999	9.9999	9.9999	9.9999	9.9999	9.9999	9.9999	9.9999	9.9999	9.9999	9.9999
10	329	0.2185	9.9999	9.9999	9.9999	9.9999	9.9999	9.9999	9.9999	9.9999	9.9999	9.9999	9.9999	9.9999	9.9999	9.9999	9.9999	9.9999	9.9999
10	328	0.2460	0.2266	9.9999	9.9999	9.9999	9.9999	9.9999	9.9999	9.9999	9.9999	9.9999	9.9999	9.9999	9.9999	9.9999	9.9999	9.9999	9.9999
10	327	0.2358	0.2587	0.2560	0.2347	9.9999	9.9999	9.9999	9.9999	9.9999	9.9999	9.9999	9.9999	9.9999	9.9999	9.9999	9.9999	9.9999	9.9999
10	326	0.2029	0.2379	0.2537	0.2694	0.2578	0.2383	9.9999	9.9999	9.9999	9.9999	9.9999	9.9999	9.9999	9.9999	9.9999	9.9999	9.9999	9.9999
10	325	0.1744	0.1997	0.2154	0.2415	0.2531	0.2758	0.2704	0.2224	9.9999	9.9999	9.9999	9.9999	9.9999	9.9999	9.9999	9.9999	9.9999	9.9999
10	324	0.1484	0.1638	0.1759	0.1956	0.2063	0.2415	0.2608	0.2691	0.2529	0.2311	9.9999	9.9999	9.9999	9.9999	9.9999	9.9999	9.9999	9.9999
10	323	0.1333	0.1387	0.1457	0.1590	0.1623	0.1917	0.2099	0.2339	0.2450	0.2665	0.2657	0.2319	9.9999	9.9999	9.9999	9.9999	9.9999	9.9999
10	322	0.1198	0.1186	0.1221	0.1306	0.1269	0.1500	0.1623	0.1798	0.1916	0.2334	0.2557	0.2696	0.2610	0.2277	9.9999	9.9999	9.9999	9.9999
10	321	0.1131	0.1086	0.1070	0.1140	0.1058	0.1233	0.1289	0.1410	0.1583	0.1820	0.2018	0.2274	0.2544	0.2714	0.2685	0.2357	9.9999	9.9999
10	320	0.1029	0.0967	0.0934	0.0972	0.0862	0.0998	0.1022	0.1069	0.1180	0.1351	0.1457	0.1694	0.1943	0.2228	0.2615	0.2785	0.2622	0.2146
10	319	0.0980	0.0902	0.0869	0.0890	0.0757	0.0866	0.0865	0.0868	0.0948	0.1070	0.1086	0.1255	0.1417	0.1766	0.2020	0.2329	0.2462	0.2670

Table A-11. Concluded.

Run	Point	cp49	cp50	cp114	cp117	cp120	cp123	cp126	cp129	cp135	cp138	cp144	cp147	cp220	cp226	cp229	cp232	cp235	cp244
10	336	9.9999	9.9999	0.0997	9.9999	9.9999	9.9999	9.9999	9.9999	9.9999	9.9999	9.9999	9.9999	9.9999	9.9999	9.9999	9.9999	9.9999	9.9999
10	335	9.9999	9.9999	-0.1938	9.9999	9.9999	9.9999	9.9999	9.9999	9.9999	9.9999	9.9999	9.9999	-0.0455	9.9999	9.9999	9.9999	9.9999	9.9999
10	334	9.9999	9.9999	-0.2556	0.3002	9.9999	9.9999	9.9999	9.9999	9.9999	9.9999	9.9999	9.9999	-0.0630	9.9999	9.9999	9.9999	9.9999	9.9999
10	333	9.9999	9.9999	-0.3005	0.3079	0.4818	9.9999	9.9999	9.9999	9.9999	9.9999	9.9999	9.9999	-0.0281	9.9999	9.9999	9.9999	9.9999	9.9999
10	332	9.9999	9.9999	-0.0762	-0.0673	0.1073	9.9999	9.9999	9.9999	9.9999	9.9999	9.9999	9.9999	-0.0246	0.1242	9.9999	9.9999	9.9999	9.9999
10	331	9.9999	9.9999	-0.0656	-0.0655	0.0338	0.1952	9.9999	9.9999	9.9999	9.9999	9.9999	9.9999	-0.0211	0.1153	0.1893	9.9999	9.9999	9.9999
10	330	9.9999	9.9999	-0.0906	-0.0762	0.0482	0.1752	0.3406	9.9999	9.9999	9.9999	9.9999	9.9999	-0.0300	0.1351	0.1648	9.9999	9.9999	9.9999
10	329	9.9999	9.9999	-0.1133	-0.0881	0.0553	0.1732	0.2761	9.9999	9.9999	9.9999	9.9999	9.9999	-0.0440	0.1474	0.1895	0.2100	9.9999	9.9999
10	328	9.9999	9.9999	-0.1347	-0.0968	0.0625	0.1648	0.2374	0.3164	9.9999	9.9999	9.9999	9.9999	-0.0563	0.1439	0.1896	0.2242	0.2310	9.9999
10	327	9.9999	9.9999	-0.1523	-0.1038	0.0715	0.1545	0.2001	0.2842	9.9999	9.9999	9.9999	9.9999	-0.0669	0.1368	0.1790	0.2120	0.2344	9.9999
10	326	9.9999	9.9999	-0.1678	-0.1087	0.0768	0.1474	0.1713	0.2191	9.9999	9.9999	9.9999	9.9999	-0.0755	0.1223	0.1644	0.1940	0.2183	9.9999
10	325	9.9999	9.9999	-0.1772	-0.1125	0.0841	0.1444	0.1522	0.1731	0.3442	9.9999	9.9999	9.9999	-0.0810	0.1119	0.1505	0.1735	0.1945	9.9999
10	324	9.9999	9.9999	-0.1871	-0.1155	0.0893	0.1405	0.1394	0.1422	0.2880	0.3562	9.9999	9.9999	-0.0859	0.1028	0.1341	0.1503	0.1662	9.9999
10	323	9.9999	9.9999	-0.1928	-0.1158	0.0912	0.1373	0.1308	0.1245	0.2030	0.3315	9.9999	9.9999	-0.0897	0.0958	0.1236	0.1348	0.1422	0.2633
10	322	9.9999	9.9999	-0.2000	-0.1159	0.0966	0.1357	0.1238	0.1120	0.1461	0.2377	9.9999	9.9999	-0.0950	0.0887	0.1148	0.1209	0.1197	0.2495
10	321	9.9999	9.9999	-0.2005	-0.1161	0.1004	0.1360	0.1222	0.1050	0.1142	0.1656	0.3729	9.9999	-0.0953	0.0871	0.1096	0.1123	0.1042	0.2167
10	320	9.9999	9.9999	-0.2092	-0.1195	0.1003	0.1308	0.1150	0.0978	0.0909	0.1184	0.3227	9.9999	-0.1005	0.0799	0.1025	0.1000	0.0885	0.1762
10	319	0.2766	0.2224	-0.2100	-0.1165	0.1024	0.1311	0.1136	0.0945	0.0786	0.0915	0.2270	0.3223	-0.1009	0.0801	0.0991	0.0950	0.0800	0.1416

Run	Point	cp250	cp253	cp3
10	336	9.9999	9.9999	-0.0098
10	335	9.9999	9.9999	-0.0133
10	334	9.9999	9.9999	-0.0151
10	333	9.9999	9.9999	-0.0186
10	332	9.9999	9.9999	-0.0117
10	331	9.9999	9.9999	-0.0100
10	330	9.9999	9.9999	-0.0135
10	329	9.9999	9.9999	-0.0152
10	328	9.9999	9.9999	-0.0186
10	327	9.9999	9.9999	-0.0203
10	326	9.9999	9.9999	-0.0236
10	325	9.9999	9.9999	-0.0238
10	324	9.9999	9.9999	-0.0253
10	323	9.9999	9.9999	-0.0254
10	322	9.9999	9.9999	-0.0272
10	321	9.9999	9.9999	-0.0273
10	320	0.2598	9.9999	-0.0289
10	319	0.2535	0.2503	-0.0291

Table A-12. Pressure Coefficients at M = 0.4 for Cavity with sweep = 45 deg. (Config. 3).

Run	Point	Ψ deg	CONF	M	R×10^{-6} per ft	p_∞ psi	$p_{t,\infty}$ psi	q_∞ psi	$T_{t,\infty}$ °F	l/h	cp16	cp17	cp19	cp20	cp21	cp22	cp25	cp26	cp28	cp29
10	316	45	3	0.40	2.39	13.22	14.78	1.49	105.7	1	0.0107	9.9999	9.9999	9.9999	9.9999	9.9999	9.9999	9.9999	9.9999	9.9999
10	315	45	3	0.40	2.39	13.23	14.78	1.49	106.1	2	0.0997	-0.0915	9.9999	9.9999	9.9999	9.9999	9.9999	9.9999	9.9999	9.9999
10	314	45	3	0.40	2.38	13.23	14.78	1.49	106.7	3	0.0273	-0.1875	0.0808	0.2355	9.9999	9.9999	9.9999	9.9999	9.9999	9.9999
10	313	45	3	0.40	2.39	13.22	14.78	1.49	106.8	4	-0.0245	-0.2096	0.0733	0.2351	0.3033	0.3247	9.9999	9.9999	9.9999	9.9999
10	312	45	3	0.40	2.39	13.22	14.78	1.49	107.1	5	-0.0443	-0.0596	-0.0720	-0.0155	0.0598	0.1252	9.9999	9.9999	9.9999	9.9999
10	311	45	3	0.40	2.38	13.23	14.78	1.49	107.4	6	-0.0538	-0.0538	-0.0640	-0.0294	0.0196	0.0667	0.1661	0.2043	9.9999	9.9999
10	310	45	3	0.40	2.38	13.23	14.78	1.49	108.0	7	-0.0724	-0.0721	-0.0719	-0.0280	0.0255	0.0742	0.1671	0.1806	0.2010	9.9999
10	309	45	3	0.40	2.38	13.23	14.78	1.49	108.3	8	-0.0922	-0.0918	-0.0867	-0.0365	0.0219	0.0751	0.1790	0.2038	0.2197	0.2012
10	308	45	3	0.40	2.37	13.22	14.78	1.49	109.3	9	-0.1090	-0.1088	-0.1020	-0.0496	0.0122	0.0662	0.1698	0.1959	0.2281	0.2390
10	307	45	3	0.40	2.38	13.22	14.78	1.50	109.3	10	-0.1204	-0.1222	-0.1134	-0.0581	0.0058	0.0624	0.1599	0.1822	0.2095	0.2237
10	306	45	3	0.40	2.37	13.23	14.78	1.49	110.2	11	-0.1317	-0.1351	-0.1252	-0.0677	0.0003	0.0583	0.1473	0.1653	0.1817	0.1921
10	305	45	3	0.40	2.37	13.22	14.78	1.50	110.8	12	-0.1364	-0.1445	-0.1350	-0.0750	-0.0033	0.0569	0.1406	0.1538	0.1602	0.1658
10	304	45	3	0.40	2.36	13.23	14.78	1.49	111.1	13	-0.1416	-0.1531	-0.1411	-0.0801	-0.0061	0.0547	0.1350	0.1454	0.1437	0.1457
10	303	45	3	0.40	2.36	13.23	14.78	1.49	111.8	14	-0.1483	-0.1608	-0.1486	-0.0854	-0.0094	0.0538	0.1305	0.1380	0.1316	0.1298
10	302	45	3	0.40	2.36	13.23	14.78	1.49	112.3	15	-0.1492	-0.1640	-0.1500	-0.0856	-0.0065	0.0569	0.1297	0.1349	0.1247	0.1204
10	301	45	3	0.40	2.35	13.23	14.78	1.49	113.1	16	-0.1549	-0.1703	-0.1566	-0.0924	-0.0125	0.0533	0.1262	0.1308	0.1163	0.1123
10	300	45	3	0.40	2.35	13.23	14.78	1.49	113.9	17	-0.1563	-0.1741	-0.1576	-0.0908	-0.0089	0.0561	0.1246	0.1274	0.1119	0.1056
10	299	45	3	0.40	2.34	13.23	14.78	1.49	115.0	18	-0.1597	-0.1780	-0.1601	-0.0920	-0.0103	0.0551	0.1221	0.1249	0.1065	0.0996

Run	Point	cp30	cp32	cp33	cp34	cp35	cp36	cp37	cp38	cp39	cp40	cp41	cp42	cp43	cp44	cp45	cp46	cp47	cp48
10	316	9.9999	9.9999	9.9999	9.9999	9.9999	9.9999	9.9999	9.9999	9.9999	9.9999	9.9999	9.9999	9.9999	9.9999	9.9999	9.9999	9.9999	9.9999
10	315	9.9999	9.9999	9.9999	9.9999	9.9999	9.9999	9.9999	9.9999	9.9999	9.9999	9.9999	9.9999	9.9999	9.9999	9.9999	9.9999	9.9999	9.9999
10	314	9.9999	9.9999	9.9999	9.9999	9.9999	9.9999	9.9999	9.9999	9.9999	9.9999	9.9999	9.9999	9.9999	9.9999	9.9999	9.9999	9.9999	9.9999
10	313	9.9999	9.9999	9.9999	9.9999	9.9999	9.9999	9.9999	9.9999	9.9999	9.9999	9.9999	9.9999	9.9999	9.9999	9.9999	9.9999	9.9999	9.9999
10	312	9.9999	9.9999	9.9999	9.9999	9.9999	9.9999	9.9999	9.9999	9.9999	9.9999	9.9999	9.9999	9.9999	9.9999	9.9999	9.9999	9.9999	9.9999
10	311	9.9999	9.9999	9.9999	9.9999	9.9999	9.9999	9.9999	9.9999	9.9999	9.9999	9.9999	9.9999	9.9999	9.9999	9.9999	9.9999	9.9999	9.9999
10	310	9.9999	9.9999	9.9999	9.9999	9.9999	9.9999	9.9999	9.9999	9.9999	9.9999	9.9999	9.9999	9.9999	9.9999	9.9999	9.9999	9.9999	9.9999
10	309	0.2283	9.9999	9.9999	9.9999	9.9999	9.9999	9.9999	9.9999	9.9999	9.9999	9.9999	9.9999	9.9999	9.9999	9.9999	9.9999	9.9999	9.9999
10	308	0.2520	0.2334	9.9999	9.9999	9.9999	9.9999	9.9999	9.9999	9.9999	9.9999	9.9999	9.9999	9.9999	9.9999	9.9999	9.9999	9.9999	9.9999
10	307	0.2461	0.2709	0.2648	0.2366	9.9999	9.9999	9.9999	9.9999	9.9999	9.9999	9.9999	9.9999	9.9999	9.9999	9.9999	9.9999	9.9999	9.9999
10	306	0.2121	0.2483	0.2666	0.2774	0.2709	0.2354	9.9999	9.9999	9.9999	9.9999	9.9999	9.9999	9.9999	9.9999	9.9999	9.9999	9.9999	9.9999
10	305	0.1809	0.2082	0.2291	0.2507	0.2679	0.2811	0.2765	0.2070	9.9999	9.9999	9.9999	9.9999	9.9999	9.9999	9.9999	9.9999	9.9999	9.9999
10	304	0.1554	0.1714	0.1863	0.2028	0.2207	0.2457	0.2716	0.2773	0.2688	0.2252	9.9999	9.9999	9.9999	9.9999	9.9999	9.9999	9.9999	9.9999
10	303	0.1368	0.1429	0.1521	0.1626	0.1728	0.1932	0.2195	0.2408	0.2654	0.2848	0.2702	0.2345	9.9999	9.9999	9.9999	9.9999	9.9999	9.9999
10	302	0.1253	0.1251	0.1300	0.1343	0.1380	0.1515	0.1701	0.1855	0.2107	0.2435	0.2682	0.2901	0.2695	0.2272	9.9999	9.9999	9.9999	9.9999
10	301	0.1152	0.1104	0.1130	0.1137	0.1124	0.1242	0.1331	0.1402	0.1582	0.1858	0.2073	0.2467	0.2664	0.2884	0.2853	0.2307	9.9999	9.9999
10	300	0.1084	0.1000	0.1012	0.0988	0.0942	0.1024	0.1062	0.1070	0.1187	0.1387	0.1502	0.1853	0.2033	0.2408	0.2747	0.2924	0.2801	0.2118
10	299	0.1013	0.0911	0.0913	0.0872	0.0805	0.0867	0.0872	0.0837	0.0910	0.1047	0.1073	0.1367	0.1499	0.1766	0.2094	0.2446	0.2715	0.2867

Table A-12. Concluded.

Run	Point	cp49	cp50	cp114	cp117	cp120	cp123	cp126	cp129	cp135	cp138	cp144	cp147	cp220	cp226	cp229	cp232	cp235	cp244
10	316	9.9999	9.9999	0.0973	9.9999	9.9999	9.9999	9.9999	9.9999	9.9999	9.9999	9.9999	9.9999	9.9999	9.9999	9.9999	9.9999	9.9999	9.9999
10	315	9.9999	9.9999	-0.2204	9.9999	9.9999	9.9999	9.9999	9.9999	9.9999	9.9999	9.9999	9.9999	-0.0698	9.9999	9.9999	9.9999	9.9999	9.9999
10	314	9.9999	9.9999	-0.2670	0.3078	9.9999	9.9999	9.9999	9.9999	9.9999	9.9999	9.9999	9.9999	-0.0683	9.9999	9.9999	9.9999	9.9999	9.9999
10	313	9.9999	9.9999	-0.3095	0.3143	0.5021	9.9999	9.9999	9.9999	9.9999	9.9999	9.9999	9.9999	-0.0397	9.9999	9.9999	9.9999	9.9999	9.9999
10	312	9.9999	9.9999	-0.0821	-0.0664	0.1152	9.9999	9.9999	9.9999	9.9999	9.9999	9.9999	9.9999	-0.0262	0.1404	9.9999	9.9999	9.9999	9.9999
10	311	9.9999	9.9999	-0.0728	-0.0681	0.0399	0.1936	9.9999	9.9999	9.9999	9.9999	9.9999	9.9999	-0.0249	0.1276	0.2002	9.9999	9.9999	9.9999
10	310	9.9999	9.9999	-0.0976	-0.0781	0.0512	0.1726	0.3395	9.9999	9.9999	9.9999	9.9999	9.9999	-0.0365	0.1447	0.1739	9.9999	9.9999	9.9999
10	309	9.9999	9.9999	-0.1217	-0.0899	0.0556	0.1683	0.2776	9.9999	9.9999	9.9999	9.9999	9.9999	-0.0514	0.1549	0.1963	0.2176	9.9999	9.9999
10	308	9.9999	9.9999	-0.1421	-0.1014	0.0569	0.1572	0.2381	0.3145	9.9999	9.9999	9.9999	9.9999	-0.0646	0.1511	0.1977	0.2295	0.2447	9.9999
10	307	9.9999	9.9999	-0.1592	-0.1093	0.0652	0.1495	0.2016	0.2956	9.9999	9.9999	9.9999	9.9999	-0.0741	0.1422	0.1888	0.2216	0.2520	9.9999
10	306	9.9999	9.9999	-0.1750	-0.1152	0.0697	0.1414	0.1733	0.2261	9.9999	9.9999	9.9999	9.9999	-0.0849	0.1284	0.1716	0.2024	0.2330	9.9999
10	305	9.9999	9.9999	-0.1861	-0.1206	0.0755	0.1369	0.1541	0.1787	0.3485	9.9999	9.9999	9.9999	-0.0918	0.1174	0.1556	0.1809	0.2092	9.9999
10	304	9.9999	9.9999	-0.1956	-0.1234	0.0825	0.1359	0.1429	0.1493	0.3092	0.3733	9.9999	9.9999	-0.0970	0.1075	0.1410	0.1594	0.1814	9.9999
10	303	9.9999	9.9999	-0.2040	-0.1283	0.0841	0.1323	0.1338	0.1298	0.2167	0.3553	9.9999	9.9999	-0.1034	0.0993	0.1289	0.1399	0.1530	0.2671
10	302	9.9999	9.9999	-0.2073	-0.1260	0.0898	0.1324	0.1276	0.1197	0.1582	0.2525	9.9999	9.9999	-0.1040	0.0957	0.1213	0.1271	0.1308	0.2607
10	301	9.9999	9.9999	-0.2143	-0.1323	0.0894	0.1302	0.1219	0.1095	0.1228	0.1721	0.3925	9.9999	-0.1099	0.0880	0.1127	0.1143	0.1115	0.2255
10	300	9.9999	9.9999	-0.2169	-0.1299	0.0930	0.1291	0.1178	0.1038	0.1011	0.1223	0.3462	9.9999	-0.1118	0.0862	0.1075	0.1059	0.0970	0.1833
10	299	0.2803	0.2012	-0.2218	-0.1316	0.0938	0.1271	0.1148	0.0978	0.0868	0.0919	0.2465	0.3341	-0.1159	0.0827	0.1020	0.0986	0.0850	0.1457

Run	Point	cp250	cp253	cp3
10	316	9.9999	9.9999	-0.0018
10	315	9.9999	9.9999	-0.0066
10	314	9.9999	9.9999	-0.0051
10	313	9.9999	9.9999	-0.0069
10	312	9.9999	9.9999	-0.0036
10	311	9.9999	9.9999	-0.0042
10	310	9.9999	9.9999	-0.0075
10	309	9.9999	9.9999	-0.0107
10	308	9.9999	9.9999	-0.0130
10	307	9.9999	9.9999	-0.0148
10	306	9.9999	9.9999	-0.0181
10	305	9.9999	9.9999	-0.0194
10	304	9.9999	9.9999	-0.0205
10	303	9.9999	9.9999	-0.0229
10	302	9.9999	9.9999	-0.0214
10	301	9.9999	9.9999	-0.0242
10	300	0.2693	9.9999	-0.0243
10	299	0.2660	0.2444	-0.0257

Table A-13. Pressure Coefficients at M = 0.6 for Cavity with sweep = 45 deg. (Config. 3).

Run	Point	Ψ deg	CONF	M	R×10^{-6} per ft	p_∞ psi	$p_{t,\infty}$ psi	q_∞ psi	$T_{t,\infty}$ °F	l/h	cp16	cp17	cp19	cp20	cp21	cp22	cp25	cp26	cp28	cp29
10	296	45	3	0.60	3.12	11.57	14.76	2.92	128.2	1	0.0115	9.9999	9.9999	9.9999	9.9999	9.9999	9.9999	9.9999	9.9999	9.9999
10	295	45	3	0.60	3.13	11.56	14.76	2.92	128.0	2	0.1149	-0.1047	9.9999	9.9999	9.9999	9.9999	9.9999	9.9999	9.9999	9.9999
10	294	45	3	0.60	3.13	11.57	14.76	2.92	128.3	3	0.0333	-0.1921	0.0711	0.2418	9.9999	9.9999	9.9999	9.9999	9.9999	9.9999
10	293	45	3	0.60	3.12	11.58	14.76	2.91	128.1	4	-0.0172	-0.1889	0.0403	0.2101	0.2910	0.3249	9.9999	9.9999	9.9999	9.9999
10	292	45	3	0.60	3.12	11.57	14.76	2.92	128.4	5	-0.0428	-0.0565	-0.0713	-0.0264	0.0379	0.1032	9.9999	9.9999	9.9999	9.9999
10	291	45	3	0.60	3.12	11.56	14.76	2.93	128.7	6	-0.0511	-0.0549	-0.0652	-0.0370	0.0037	0.0514	0.1540	0.1943	9.9999	9.9999
10	290	45	3	0.60	3.12	11.57	14.76	2.92	128.7	7	-0.0666	-0.0698	-0.0736	-0.0390	0.0077	0.0588	0.1497	0.1686	0.1955	9.9999
10	289	45	3	0.60	3.12	11.57	14.76	2.92	128.5	8	-0.0878	-0.0910	-0.0888	-0.0469	0.0047	0.0595	0.1656	0.1934	0.2088	0.1956
10	288	45	3	0.60	3.12	11.56	14.76	2.93	128.8	9	-0.1056	-0.1084	-0.1047	-0.0597	-0.0035	0.0526	0.1613	0.1902	0.2259	0.2385
10	287	45	3	0.60	3.12	11.57	14.76	2.92	129.2	10	-0.1200	-0.1227	-0.1172	-0.0697	-0.0113	0.0470	0.1532	0.1783	0.2104	0.2267
10	286	45	3	0.60	3.12	11.57	14.76	2.92	129.2	11	-0.1296	-0.1334	-0.1282	-0.0789	-0.0166	0.0437	0.1461	0.1671	0.1901	0.2028
10	285	45	3	0.60	3.12	11.56	14.76	2.93	129.2	12	-0.1409	-0.1455	-0.1413	-0.0884	-0.0226	0.0387	0.1358	0.1531	0.1666	0.1746
10	284	45	3	0.60	3.11	11.58	14.76	2.91	129.5	13	-0.1480	-0.1547	-0.1481	-0.0929	-0.0253	0.0376	0.1305	0.1445	0.1495	0.1530
10	283	45	3	0.60	3.12	11.56	14.76	2.93	129.6	14	-0.1540	-0.1624	-0.1551	-0.0983	-0.0274	0.0358	0.1265	0.1380	0.1365	0.1370
10	282	45	3	0.60	3.11	11.57	14.76	2.92	129.9	15	-0.1612	-0.1704	-0.1625	-0.1049	-0.0317	0.0333	0.1224	0.1316	0.1261	0.1246
10	281	45	3	0.60	3.12	11.56	14.76	2.93	130.1	16	-0.1628	-0.1732	-0.1638	-0.1065	-0.0317	0.0337	0.1210	0.1282	0.1201	0.1167
10	280	45	3	0.60	3.11	11.56	14.76	2.93	130.3	17	-0.1666	-0.1773	-0.1679	-0.1087	-0.0329	0.0330	0.1194	0.1258	0.1148	0.1106
10	279	45	3	0.60	3.11	11.57	14.76	2.92	130.5	18	-0.1706	-0.1819	-0.1716	-0.1114	-0.0354	0.0302	0.1163	0.1220	0.1095	0.1048

Run	Point	cp30	cp32	cp33	cp34	cp35	cp36	cp37	cp38	cp39	cp40	cp41	cp42	cp43	cp44	cp45	cp46	cp47	cp48
10	296	9.9999	9.9999	9.9999	9.9999	9.9999	9.9999	9.9999	9.9999	9.9999	9.9999	9.9999	9.9999	9.9999	9.9999	9.9999	9.9999	9.9999	9.9999
10	295	9.9999	9.9999	9.9999	9.9999	9.9999	9.9999	9.9999	9.9999	9.9999	9.9999	9.9999	9.9999	9.9999	9.9999	9.9999	9.9999	9.9999	9.9999
10	294	9.9999	9.9999	9.9999	9.9999	9.9999	9.9999	9.9999	9.9999	9.9999	9.9999	9.9999	9.9999	9.9999	9.9999	9.9999	9.9999	9.9999	9.9999
10	293	9.9999	9.9999	9.9999	9.9999	9.9999	9.9999	9.9999	9.9999	9.9999	9.9999	9.9999	9.9999	9.9999	9.9999	9.9999	9.9999	9.9999	9.9999
10	292	9.9999	9.9999	9.9999	9.9999	9.9999	9.9999	9.9999	9.9999	9.9999	9.9999	9.9999	9.9999	9.9999	9.9999	9.9999	9.9999	9.9999	9.9999
10	291	9.9999	9.9999	9.9999	9.9999	9.9999	9.9999	9.9999	9.9999	9.9999	9.9999	9.9999	9.9999	9.9999	9.9999	9.9999	9.9999	9.9999	9.9999
10	290	9.9999	9.9999	9.9999	9.9999	9.9999	9.9999	9.9999	9.9999	9.9999	9.9999	9.9999	9.9999	9.9999	9.9999	9.9999	9.9999	9.9999	9.9999
10	289	0.2305	9.9999	9.9999	9.9999	9.9999	9.9999	9.9999	9.9999	9.9999	9.9999	9.9999	9.9999	9.9999	9.9999	9.9999	9.9999	9.9999	9.9999
10	288	0.2532	0.2416	9.9999	9.9999	9.9999	9.9999	9.9999	9.9999	9.9999	9.9999	9.9999	9.9999	9.9999	9.9999	9.9999	9.9999	9.9999	9.9999
10	287	0.2506	0.2748	0.2662	0.2420	9.9999	9.9999	9.9999	9.9999	9.9999	9.9999	9.9999	9.9999	9.9999	9.9999	9.9999	9.9999	9.9999	9.9999
10	286	0.2249	0.2620	0.2800	0.2878	0.2793	0.2439	9.9999	9.9999	9.9999	9.9999	9.9999	9.9999	9.9999	9.9999	9.9999	9.9999	9.9999	9.9999
10	285	0.1910	0.2212	0.2423	0.2623	0.2796	0.2895	0.2852	0.2070	9.9999	9.9999	9.9999	9.9999	9.9999	9.9999	9.9999	9.9999	9.9999	9.9999
10	284	0.1638	0.1812	0.1987	0.2155	0.2341	0.2579	0.2846	0.2857	0.2738	0.2299	9.9999	9.9999	9.9999	9.9999	9.9999	9.9999	9.9999	9.9999
10	283	0.1439	0.1514	0.1622	0.1713	0.1835	0.2047	0.2304	0.2522	0.2744	0.2936	0.2752	0.2386	9.9999	9.9999	9.9999	9.9999	9.9999	9.9999
10	282	0.1291	0.1294	0.1360	0.1393	0.1441	0.1593	0.1786	0.1933	0.2198	0.2542	0.2780	0.3007	0.2757	0.2285	9.9999	9.9999	9.9999	9.9999
10	281	0.1198	0.1150	0.1187	0.1178	0.1173	0.1272	0.1395	0.1455	0.1654	0.1939	0.2140	0.2562	0.2767	0.2961	0.2918	0.2323	9.9999	9.9999
10	280	0.1123	0.1042	0.1058	0.1021	0.0986	0.1043	0.1117	0.1115	0.1244	0.1460	0.1562	0.1956	0.2172	0.2526	0.2866	0.3026	0.2896	0.2122
10	279	0.1056	0.0952	0.0953	0.0899	0.0842	0.0874	0.0914	0.0866	0.0947	0.1105	0.1113	0.1455	0.1591	0.1879	0.2229	0.2589	0.2869	0.2970

Table A-13. Concluded.

Run	Point	cp49	cp50	cp114	cp117	cp120	cp123	cp126	cp129	cp135	cp138	cp144	cp147	cp220	cp226	cp229	cp232	cp235	cp244
10	296	9.9999	9.9999	0.0619	9.9999	9.9999	9.9999	9.9999	9.9999	9.9999	9.9999	9.9999	9.9999	9.9999	9.9999	9.9999	9.9999	9.9999	9.9999
10	295	9.9999	9.9999	-0.2310	9.9999	9.9999	9.9999	9.9999	9.9999	9.9999	9.9999	9.9999	9.9999	-0.0681	9.9999	9.9999	9.9999	9.9999	9.9999
10	294	9.9999	9.9999	-0.2561	0.2773	9.9999	9.9999	9.9999	9.9999	9.9999	9.9999	9.9999	9.9999	-0.0736	9.9999	9.9999	9.9999	9.9999	9.9999
10	293	9.9999	9.9999	-0.2722	0.2444	0.4851	9.9999	9.9999	9.9999	9.9999	9.9999	9.9999	9.9999	-0.0239	9.9999	9.9999	9.9999	9.9999	9.9999
10	292	9.9999	9.9999	-0.0690	-0.0670	0.0750	9.9999	9.9999	9.9999	9.9999	9.9999	9.9999	9.9999	-0.0286	0.1379	9.9999	9.9999	9.9999	9.9999
10	291	9.9999	9.9999	-0.0696	-0.0668	0.0209	0.1644	9.9999	9.9999	9.9999	9.9999	9.9999	9.9999	-0.0283	0.1253	0.1927	9.9999	9.9999	9.9999
10	290	9.9999	9.9999	-0.0902	-0.0752	0.0279	0.1429	0.3247	9.9999	9.9999	9.9999	9.9999	9.9999	-0.0379	0.1394	0.1714	9.9999	9.9999	9.9999
10	289	9.9999	9.9999	-0.1163	-0.0898	0.0314	0.1467	0.2623	9.9999	9.9999	9.9999	9.9999	9.9999	-0.0541	0.1520	0.1966	0.2145	9.9999	9.9999
10	288	9.9999	9.9999	-0.1351	-0.1037	0.0307	0.1411	0.2328	0.3073	9.9999	9.9999	9.9999	9.9999	-0.0685	0.1516	0.2032	0.2334	0.2477	9.9999
10	287	9.9999	9.9999	-0.1524	-0.1138	0.0360	0.1363	0.2041	0.2947	9.9999	9.9999	9.9999	9.9999	-0.0784	0.1421	0.1957	0.2286	0.2581	9.9999
10	286	9.9999	9.9999	-0.1658	-0.1217	0.0415	0.1345	0.1805	0.2356	9.9999	9.9999	9.9999	9.9999	-0.0870	0.1324	0.1830	0.2151	0.2474	9.9999
10	285	9.9999	9.9999	-0.1805	-0.1306	0.0454	0.1303	0.1605	0.1874	0.3581	9.9999	9.9999	9.9999	-0.0966	0.1193	0.1641	0.1918	0.2246	9.9999
10	284	9.9999	9.9999	-0.1911	-0.1349	0.0526	0.1297	0.1476	0.1572	0.3188	0.3753	9.9999	9.9999	-0.1032	0.1096	0.1487	0.1685	0.1939	9.9999
10	283	9.9999	9.9999	-0.1982	-0.1393	0.0539	0.1275	0.1386	0.1377	0.2257	0.3623	9.9999	9.9999	-0.1096	0.1014	0.1362	0.1485	0.1645	0.2739
10	282	9.9999	9.9999	-0.2068	-0.1455	0.0540	0.1251	0.1310	0.1239	0.1644	0.2610	9.9999	9.9999	-0.1156	0.0938	0.1247	0.1315	0.1379	0.2672
10	281	9.9999	9.9999	-0.2096	-0.1455	0.0579	0.1253	0.1267	0.1154	0.1286	0.1763	0.3939	9.9999	-0.1171	0.0889	0.1173	0.1195	0.1178	0.2339
10	280	9.9999	9.9999	-0.2136	-0.1480	0.0584	0.1244	0.1233	0.1097	0.1066	0.1257	0.3601	9.9999	-0.1209	0.0864	0.1121	0.1105	0.1024	0.1930
10	279	0.2837	0.1966	-0.2186	-0.1508	0.0585	0.1222	0.1191	0.1034	0.0911	0.0944	0.2612	0.3333	-0.1249	0.0813	0.1056	0.1019	0.0892	0.1541

Run	Point	cp250	cp253	cp3
10	296	9.9999	9.9999	-0.0026
10	295	9.9999	9.9999	-0.0007
10	294	9.9999	9.9999	-0.0040
10	293	9.9999	9.9999	-0.0084
10	292	9.9999	9.9999	-0.0026
10	291	9.9999	9.9999	-0.0044
10	290	9.9999	9.9999	-0.0062
10	289	9.9999	9.9999	-0.0102
10	288	9.9999	9.9999	-0.0130
10	287	9.9999	9.9999	-0.0145
10	286	9.9999	9.9999	-0.0147
10	285	9.9999	9.9999	-0.0192
10	284	9.9999	9.9999	-0.0204
10	283	9.9999	9.9999	-0.0222
10	282	9.9999	9.9999	-0.0250
10	281	9.9999	9.9999	-0.0244
10	280	0.2772	9.9999	-0.0253
10	279	0.2768	0.2496	-0.0281

Table A-14. Pressure Coefficients at M = 0.8 for Cavity with sweep = 45 deg. (Config. 3).

Run	Point	Ψ deg	CONF	M	R×10^{-6} per ft	p_∞ psi	$p_{t,\infty}$ psi	q_∞ psi	$T_{t,\infty}$ °F	l/h	cp16	cp17	cp19	cp20	cp21	cp22	cp25	cp26	cp28	cp29
10	276	45	3	0.80	3.62	9.69	14.75	4.33	140.3	1	0.0015	9.9999	9.9999	9.9999	9.9999	9.9999	9.9999	9.9999	9.9999	9.9999
10	275	45	3	0.80	3.62	9.68	14.75	4.33	139.3	2	0.0933	-0.1105	9.9999	9.9999	9.9999	9.9999	9.9999	9.9999	9.9999	9.9999
10	274	45	3	0.80	3.64	9.69	14.75	4.32	137.4	3	0.0316	-0.2113	0.0263	0.2580	9.9999	9.9999	9.9999	9.9999	9.9999	9.9999
10	273	45	3	0.80	3.66	9.66	14.75	4.34	135.9	4	-0.0235	-0.1115	-0.0813	0.0347	0.1565	0.2800	9.9999	9.9999	9.9999	9.9999
10	272	45	3	0.80	3.66	9.68	14.75	4.33	134.9	5	-0.0466	-0.0580	-0.0773	-0.0555	-0.0143	0.0433	9.9999	9.9999	9.9999	9.9999
10	271	45	3	0.80	3.67	9.68	14.75	4.33	133.4	6	-0.0489	-0.0531	-0.0668	-0.0608	-0.0442	-0.0100	0.1022	0.1594	9.9999	9.9999
10	270	45	3	0.80	3.68	9.67	14.75	4.34	132.3	7	-0.0547	-0.0581	-0.0667	-0.0617	-0.0482	-0.0202	0.0586	0.0926	0.1631	9.9999
10	269	45	3	0.80	3.69	9.68	14.75	4.33	130.8	8	-0.0657	-0.0684	-0.0760	-0.0689	-0.0528	-0.0211	0.0621	0.0866	0.1204	0.1477
10	268	45	3	0.80	3.71	9.66	14.75	4.35	129.4	9	-0.0862	-0.0884	-0.0944	-0.0834	-0.0609	-0.0229	0.0750	0.1065	0.1526	0.1641
10	267	45	3	0.80	3.73	9.70	14.75	4.32	124.8	10	-0.1031	-0.1038	-0.1082	-0.0940	-0.0655	-0.0236	0.0838	0.1174	0.1714	0.1952
10	266	45	3	0.80	3.74	9.71	14.75	4.31	123.8	11	-0.1221	-0.1225	-0.1253	-0.1098	-0.0764	-0.0301	0.0838	0.1170	0.1687	0.1908
10	265	45	3	0.80	3.76	9.69	14.75	4.33	121.9	12	-0.1355	-0.1349	-0.1375	-0.1203	-0.0848	-0.0358	0.0817	0.1141	0.1594	0.1789
10	264	45	3	0.80	3.78	9.68	14.75	4.33	119.6	13	-0.1494	-0.1498	-0.1510	-0.1331	-0.0949	-0.0433	0.0768	0.1064	0.1462	0.1608
10	263	45	3	0.80	3.80	9.68	14.75	4.33	117.7	14	-0.1579	-0.1578	-0.1594	-0.1404	-0.1004	-0.0476	0.0746	0.1035	0.1365	0.1479
10	262	45	3	0.80	3.82	9.69	14.75	4.33	114.7	15	-0.1651	-0.1643	-0.1664	-0.1469	-0.1065	-0.0524	0.0703	0.0981	0.1267	0.1359
10	261	45	3	0.80	3.84	9.70	14.75	4.32	112.5	16	-0.1722	-0.1715	-0.1733	-0.1536	-0.1131	-0.0577	0.0666	0.0932	0.1187	0.1258
10	260	45	3	0.80	3.87	9.68	14.75	4.33	109.4	17	-0.1789	-0.1770	-0.1792	-0.1589	-0.1182	-0.0625	0.0629	0.0896	0.1120	0.1183
10	259	45	3	0.80	3.90	9.69	14.75	4.33	106.2	18	-0.1745	-0.1736	-0.1755	-0.1551	-0.1129	-0.0567	0.0681	0.0930	0.1136	0.1183

Run	Point	cp30	cp32	cp33	cp34	cp35	cp36	cp37	cp38	cp39	cp40	cp41	cp42	cp43	cp44	cp45	cp46	cp47	cp48
10	276	9.9999	9.9999	9.9999	9.9999	9.9999	9.9999	9.9999	9.9999	9.9999	9.9999	9.9999	9.9999	9.9999	9.9999	9.9999	9.9999	9.9999	9.9999
10	275	9.9999	9.9999	9.9999	9.9999	9.9999	9.9999	9.9999	9.9999	9.9999	9.9999	9.9999	9.9999	9.9999	9.9999	9.9999	9.9999	9.9999	9.9999
10	274	9.9999	9.9999	9.9999	9.9999	9.9999	9.9999	9.9999	9.9999	9.9999	9.9999	9.9999	9.9999	9.9999	9.9999	9.9999	9.9999	9.9999	9.9999
10	273	9.9999	9.9999	9.9999	9.9999	9.9999	9.9999	9.9999	9.9999	9.9999	9.9999	9.9999	9.9999	9.9999	9.9999	9.9999	9.9999	9.9999	9.9999
10	272	9.9999	9.9999	9.9999	9.9999	9.9999	9.9999	9.9999	9.9999	9.9999	9.9999	9.9999	9.9999	9.9999	9.9999	9.9999	9.9999	9.9999	9.9999
10	271	9.9999	9.9999	9.9999	9.9999	9.9999	9.9999	9.9999	9.9999	9.9999	9.9999	9.9999	9.9999	9.9999	9.9999	9.9999	9.9999	9.9999	9.9999
10	270	9.9999	9.9999	9.9999	9.9999	9.9999	9.9999	9.9999	9.9999	9.9999	9.9999	9.9999	9.9999	9.9999	9.9999	9.9999	9.9999	9.9999	9.9999
10	269	0.2074	9.9999	9.9999	9.9999	9.9999	9.9999	9.9999	9.9999	9.9999	9.9999	9.9999	9.9999	9.9999	9.9999	9.9999	9.9999	9.9999	9.9999
10	268	0.1769	0.2370	9.9999	9.9999	9.9999	9.9999	9.9999	9.9999	9.9999	9.9999	9.9999	9.9999	9.9999	9.9999	9.9999	9.9999	9.9999	9.9999
10	267	0.2204	0.2311	0.2221	0.2531	9.9999	9.9999	9.9999	9.9999	9.9999	9.9999	9.9999	9.9999	9.9999	9.9999	9.9999	9.9999	9.9999	9.9999
10	266	0.2181	0.2580	0.2732	0.2736	0.2438	0.2590	9.9999	9.9999	9.9999	9.9999	9.9999	9.9999	9.9999	9.9999	9.9999	9.9999	9.9999	9.9999
10	265	0.2019	0.2387	0.2598	0.2784	0.2927	0.2970	0.2673	0.2150	9.9999	9.9999	9.9999	9.9999	9.9999	9.9999	9.9999	9.9999	9.9999	9.9999
10	264	0.1795	0.2049	0.2230	0.2404	0.2603	0.2835	0.3027	0.2969	0.2713	0.2452	9.9999	9.9999	9.9999	9.9999	9.9999	9.9999	9.9999	9.9999
10	263	0.1625	0.1768	0.1895	0.2004	0.2146	0.2373	0.2629	0.2811	0.3027	0.3149	0.2794	0.2638	9.9999	9.9999	9.9999	9.9999	9.9999	9.9999
10	262	0.1468	0.1520	0.1605	0.1653	0.1724	0.1880	0.2090	0.2256	0.2535	0.2859	0.3041	0.3229	0.2879	0.2546	9.9999	9.9999	9.9999	9.9999
10	261	0.1337	0.1338	0.1375	0.1372	0.1383	0.1491	0.1615	0.1703	0.1925	0.2231	0.2461	0.2881	0.3067	0.3209	0.3099	0.2574	9.9999	9.9999
10	260	0.1242	0.1198	0.1205	0.1164	0.1128	0.1193	0.1256	0.1256	0.1413	0.1636	0.1782	0.2199	0.2439	0.2803	0.3149	0.3268	0.3129	0.2304
10	259	0.1231	0.1161	0.1155	0.1092	0.1028	0.1065	0.1090	0.1031	0.1134	0.1291	0.1326	0.1691	0.1865	0.2175	0.2560	0.2899	0.3178	0.3249

Table A-14. Concluded.

Run	Point	cp49	cp50	cp114	cp117	cp120	cp123	cp126	cp129	cp135	cp138	cp144	cp147	cp220	cp226	cp229	cp232	cp235	cp244
10	276	9.9999	9.9999	0.0447	9.9999	9.9999	9.9999	9.9999	9.9999	9.9999	9.9999	9.9999	9.9999	9.9999	9.9999	9.9999	9.9999	9.9999	9.9999
10	275	9.9999	9.9999	-0.2187	9.9999	9.9999	9.9999	9.9999	9.9999	9.9999	9.9999	9.9999	9.9999	-0.0804	9.9999	9.9999	9.9999	9.9999	9.9999
10	274	9.9999	9.9999	-0.2503	0.1996	9.9999	9.9999	9.9999	9.9999	9.9999	9.9999	9.9999	9.9999	-0.1188	9.9999	9.9999	9.9999	9.9999	9.9999
10	273	9.9999	9.9999	-0.1204	-0.0727	0.4120	9.9999	9.9999	9.9999	9.9999	9.9999	9.9999	9.9999	-0.0896	9.9999	9.9999	9.9999	9.9999	9.9999
10	272	9.9999	9.9999	-0.0660	-0.0663	0.0041	9.9999	9.9999	9.9999	9.9999	9.9999	9.9999	9.9999	-0.0442	0.1097	9.9999	9.9999	9.9999	9.9999
10	271	9.9999	9.9999	-0.0629	-0.0524	-0.0438	0.0855	9.9999	9.9999	9.9999	9.9999	9.9999	9.9999	-0.0396	0.0801	0.1841	9.9999	9.9999	9.9999
10	270	9.9999	9.9999	-0.0677	-0.0535	-0.0469	0.0192	0.2394	9.9999	9.9999	9.9999	9.9999	9.9999	-0.0440	0.0637	0.1250	9.9999	9.9999	9.9999
10	269	9.9999	9.9999	-0.0791	-0.0634	-0.0467	0.0289	0.1057	9.9999	9.9999	9.9999	9.9999	9.9999	-0.0514	0.0664	0.1313	0.1706	9.9999	9.9999
10	268	9.9999	9.9999	-0.1040	-0.0832	-0.0511	0.0379	0.1320	0.2131	9.9999	9.9999	9.9999	9.9999	-0.0658	0.0751	0.1572	0.1876	0.2284	9.9999
10	267	9.9999	9.9999	-0.1236	-0.0984	-0.0498	0.0476	0.1440	0.2434	9.9999	9.9999	9.9999	9.9999	-0.0766	0.0834	0.1723	0.2190	0.2266	9.9999
10	266	9.9999	9.9999	-0.1450	-0.1166	-0.0549	0.0507	0.1427	0.2241	9.9999	9.9999	9.9999	9.9999	-0.0915	0.0806	0.1724	0.2232	0.2515	9.9999
10	265	9.9999	9.9999	-0.1586	-0.1280	-0.0561	0.0540	0.1390	0.2004	0.3267	9.9999	9.9999	9.9999	-0.1008	0.0753	0.1659	0.2142	0.2473	9.9999
10	264	9.9999	9.9999	-0.1738	-0.1422	-0.0611	0.0538	0.1315	0.1737	0.3393	0.4232	9.9999	9.9999	-0.1129	0.0659	0.1522	0.1933	0.2248	9.9999
10	263	9.9999	9.9999	-0.1829	-0.1499	-0.0616	0.0565	0.1282	0.1560	0.2568	0.3858	9.9999	9.9999	-0.1204	0.0601	0.1410	0.1743	0.1972	0.2966
10	262	9.9999	9.9999	-0.1904	-0.1567	-0.0639	0.0569	0.1233	0.1424	0.1925	0.2926	9.9999	9.9999	-0.1260	0.0529	0.1302	0.1547	0.1681	0.2938
10	261	9.9999	9.9999	-0.1980	-0.1636	-0.0660	0.0558	0.1186	0.1315	0.1485	0.2017	0.4494	9.9999	-0.1328	0.0459	0.1196	0.1380	0.1405	0.2638
10	260	9.9999	9.9999	-0.2035	-0.1690	-0.0680	0.0554	0.1149	0.1237	0.1204	0.1386	0.3879	9.9999	-0.1386	0.0419	0.1123	0.1252	0.1196	0.2221
10	259	0.3077	0.2217	-0.2004	-0.1655	-0.0618	0.0610	0.1179	0.1233	0.1094	0.1102	0.2969	0.3590	-0.1342	0.0434	0.1123	0.1221	0.1105	0.1855

Run	Point	cp250	cp253	cp3
10	276	9.9999	9.9999	-0.0108
10	275	9.9999	9.9999	-0.0139
10	274	9.9999	9.9999	-0.0182
10	273	9.9999	9.9999	-0.0125
10	272	9.9999	9.9999	-0.0134
10	271	9.9999	9.9999	-0.0128
10	270	9.9999	9.9999	-0.0132
10	269	9.9999	9.9999	-0.0140
10	268	9.9999	9.9999	-0.0182
10	267	9.9999	9.9999	-0.0178
10	266	9.9999	9.9999	-0.0212
10	265	9.9999	9.9999	-0.0218
10	264	9.9999	9.9999	-0.0264
10	263	9.9999	9.9999	-0.0270
10	262	9.9999	9.9999	-0.0293
10	261	9.9999	9.9999	-0.0320
10	260	0.3057	9.9999	-0.0342
10	259	0.3051	0.2858	-0.0291

Table A-15. Pressure Coefficients at M = 0.2 for Cavity with sweep = 35 deg. (Config. 4).

Run	Point	Ψ deg	CONF	M	R×10^{-6} per ft	p_∞ psi	$p_{t,\infty}$ psi	q_∞ psi	$T_{t,\infty}$ °F	l/h	cp14	cp16	cp17	cp19	cp20	cp21	cp22	cp25	cp26	cp28
11	429	35	4	0.20	1.38	14.38	14.80	0.41	68.8	1	0.0195	9.9999	9.9999	9.9999	9.9999	9.9999	9.9999	9.9999	9.9999	9.9999
11	428	35	4	0.20	1.38	14.38	14.80	0.41	69.0	2	0.1177	-0.1045	0.0875	9.9999	9.9999	9.9999	9.9999	9.9999	9.9999	9.9999
11	427	35	4	0.20	1.38	14.38	14.80	0.41	68.9	3	0.0350	-0.1950	-0.0861	0.3184	9.9999	9.9999	9.9999	9.9999	9.9999	9.9999
11	426	35	4	0.20	1.38	14.38	14.80	0.41	69.0	4	-0.0216	-0.0804	-0.0740	0.0091	0.0922	0.2104	9.9999	9.9999	9.9999	9.9999
11	425	35	4	0.20	1.38	14.38	14.80	0.41	68.9	5	-0.0183	-0.0420	-0.0419	-0.0413	-0.0076	0.0442	0.0843	9.9999	9.9999	9.9999
11	424	35	4	0.20	1.38	14.38	14.80	0.41	68.8	6	-0.0234	-0.0420	-0.0351	-0.0413	-0.0214	0.0159	0.0372	0.1893	9.9999	9.9999
11	423	35	4	0.20	1.37	14.39	14.80	0.41	68.8	7	-0.0360	-0.0528	-0.0477	-0.0471	-0.0184	0.0242	0.0527	0.1318	0.1679	9.9999
11	422	35	4	0.20	1.38	14.39	14.80	0.41	68.8	8	-0.0602	-0.0781	-0.0699	-0.0537	-0.0079	0.0427	0.0781	0.1756	0.2053	0.2009
11	421	35	4	0.20	1.37	14.39	14.80	0.40	68.5	9	-0.0865	-0.1022	-0.0976	-0.0608	-0.0062	0.0563	0.0936	0.1829	0.2144	0.2482
11	420	35	4	0.20	1.38	14.39	14.80	0.40	68.0	10	-0.1040	-0.1194	-0.1133	-0.0642	-0.0028	0.0614	0.1005	0.1779	0.2043	0.2311
11	419	35	4	0.20	1.39	14.39	14.80	0.41	68.0	11	-0.1191	-0.1356	-0.1298	-0.0696	0.0010	0.0657	0.1060	0.1655	0.1862	0.2022
11	418	35	4	0.20	1.39	14.39	14.80	0.41	68.1	12	-0.1312	-0.1474	-0.1418	-0.0713	0.0010	0.0657	0.1043	0.1555	0.1694	0.1750
11	417	35	4	0.20	1.38	14.39	14.80	0.41	68.3	13	-0.1398	-0.1559	-0.1486	-0.0797	-0.0041	0.0641	0.1010	0.1455	0.1576	0.1546
11	416	35	4	0.20	1.38	14.39	14.80	0.41	68.6	14	-0.1467	-0.1643	-0.1554	-0.0797	-0.0024	0.0658	0.1027	0.1388	0.1475	0.1375
11	415	35	4	0.20	1.38	14.39	14.80	0.41	68.7	15	-0.1504	-0.1662	-0.1591	-0.0816	-0.0042	0.0642	0.1011	0.1323	0.1392	0.1257
11	413	35	4	0.20	1.38	14.39	14.80	0.41	69.3	16	-0.1509	-0.1684	-0.1596	-0.0836	-0.0008	0.0626	0.1047	0.1326	0.1395	0.1260
11	412	35	4	0.20	1.38	14.39	14.80	0.41	69.5	17	-0.1540	-0.1698	-0.1627	-0.0851	-0.0042	0.0626	0.1029	0.1291	0.1360	0.1173
11	411	35	4	0.20	1.38	14.39	14.80	0.41	69.6	18	-0.1561	-0.1702	-0.1648	-0.0870	-0.0043	0.0593	0.0997	0.1259	0.1311	0.1124
11	410	35	4	0.20	1.38	14.39	14.80	0.41	70.2	19	-0.1594	-0.1751	-0.1680	-0.0835	-0.0042	0.0643	0.1047	0.1225	0.1259	0.1037
11	409	35	4	0.20	1.37	14.39	14.80	0.41	70.6	20	-0.1631	-0.1787	-0.1700	-0.0870	-0.0025	0.0626	0.1031	0.1176	0.1226	0.1004

Run	Point	cp29	cp30	cp32	cp33	cp34	cp35	cp36	cp37	cp38	cp39	cp40	cp41	cp42	cp43	cp44	cp45	cp46	cp47
11	429	9.9999	9.9999	9.9999	9.9999	9.9999	9.9999	9.9999	9.9999	9.9999	9.9999	9.9999	9.9999	9.9999	9.9999	9.9999	9.9999	9.9999	9.9999
11	428	9.9999	9.9999	9.9999	9.9999	9.9999	9.9999	9.9999	9.9999	9.9999	9.9999	9.9999	9.9999	9.9999	9.9999	9.9999	9.9999	9.9999	9.9999
11	427	9.9999	9.9999	9.9999	9.9999	9.9999	9.9999	9.9999	9.9999	9.9999	9.9999	9.9999	9.9999	9.9999	9.9999	9.9999	9.9999	9.9999	9.9999
11	426	9.9999	9.9999	9.9999	9.9999	9.9999	9.9999	9.9999	9.9999	9.9999	9.9999	9.9999	9.9999	9.9999	9.9999	9.9999	9.9999	9.9999	9.9999
11	425	9.9999	9.9999	9.9999	9.9999	9.9999	9.9999	9.9999	9.9999	9.9999	9.9999	9.9999	9.9999	9.9999	9.9999	9.9999	9.9999	9.9999	9.9999
11	424	9.9999	9.9999	9.9999	9.9999	9.9999	9.9999	9.9999	9.9999	9.9999	9.9999	9.9999	9.9999	9.9999	9.9999	9.9999	9.9999	9.9999	9.9999
11	423	9.9999	9.9999	9.9999	9.9999	9.9999	9.9999	9.9999	9.9999	9.9999	9.9999	9.9999	9.9999	9.9999	9.9999	9.9999	9.9999	9.9999	9.9999
11	422	0.2261	9.9999	9.9999	9.9999	9.9999	9.9999	9.9999	9.9999	9.9999	9.9999	9.9999	9.9999	9.9999	9.9999	9.9999	9.9999	9.9999	9.9999
11	421	0.2485	0.2565	9.9999	9.9999	9.9999	9.9999	9.9999	9.9999	9.9999	9.9999	9.9999	9.9999	9.9999	9.9999	9.9999	9.9999	9.9999	9.9999
11	420	0.2386	0.2704	0.2869	0.2750	9.9999	9.9999	9.9999	9.9999	9.9999	9.9999	9.9999	9.9999	9.9999	9.9999	9.9999	9.9999	9.9999	9.9999
11	419	0.2055	0.2378	0.2778	0.2996	0.3093	0.2854	9.9999	9.9999	9.9999	9.9999	9.9999	9.9999	9.9999	9.9999	9.9999	9.9999	9.9999	9.9999
11	418	0.1725	0.1990	0.2294	0.2560	0.2861	0.3031	0.3192	0.2944	9.9999	9.9999	9.9999	9.9999	9.9999	9.9999	9.9999	9.9999	9.9999	9.9999
11	417	0.1444	0.1670	0.1844	0.2057	0.2296	0.2521	0.2894	0.3121	0.3216	0.2722	9.9999	9.9999	9.9999	9.9999	9.9999	9.9999	9.9999	9.9999
11	416	0.1295	0.1433	0.1509	0.1637	0.1797	0.1957	0.2279	0.2559	0.2897	0.3037	0.3153	0.2781	9.9999	9.9999	9.9999	9.9999	9.9999	9.9999
11	415	0.1230	0.1265	0.1260	0.1336	0.1449	0.1518	0.1765	0.1964	0.2226	0.2459	0.2959	0.3172	0.3182	0.2848	9.9999	9.9999	9.9999	9.9999
11	413	0.1233	0.1268	0.1263	0.1322	0.1435	0.1504	0.1736	0.1934	0.2215	0.2398	0.2933	0.3146	0.3174	0.2820	0.3370	0.1736	9.9999	9.9999
11	412	0.1149	0.1165	0.1093	0.1135	0.1183	0.1202	0.1367	0.1491	0.1689	0.1779	0.2233	0.2518	0.2831	0.3168	0.3177	0.2911	0.3550	0.1588
11	411	0.1067	0.1082	0.0977	0.1002	0.1018	0.0991	0.1102	0.1193	0.1303	0.1448	0.1705	0.1847	0.2107	0.2505	0.2803	0.3122	0.3300	0.2872
11	410	0.0967	0.0962	0.0826	0.0816	0.0800	0.0743	0.0784	0.0822	0.0829	0.0897	0.1039	0.1019	0.1242	0.1343	0.1597	0.1889	0.2171	0.2420
11	409	0.0918	0.0912	0.0759	0.0749	0.0717	0.0655	0.0702	0.0700	0.0695	0.0731	0.0841	0.0783	0.1006	0.1010	0.1185	0.1395	0.1559	0.1825

Table A-15. Concluded.

Run	Point	cp48	cp49	cp50	cp51	cp52	cp53	cp114	cp117	cp120	cp123	cp126	cp129	cp135	cp138	cp144	cp147	cp150	cp217
11	429	9.9999	9.9999	9.9999	9.9999	9.9999	9.9999	9.9999	9.9999	9.9999	9.9999	9.9999	9.9999	9.9999	9.9999	9.9999	9.9999	9.9999	0.0207
11	428	9.9999	9.9999	9.9999	9.9999	9.9999	9.9999	-0.1223	9.9999	9.9999	9.9999	9.9999	9.9999	9.9999	9.9999	9.9999	9.9999	9.9999	-0.0543
11	427	9.9999	9.9999	9.9999	9.9999	9.9999	9.9999	-0.1957	0.3354	9.9999	9.9999	9.9999	9.9999	9.9999	9.9999	9.9999	9.9999	9.9999	-0.0434
11	426	9.9999	9.9999	9.9999	9.9999	9.9999	9.9999	-0.0586	-0.0321	9.9999	9.9999	9.9999	9.9999	9.9999	9.9999	9.9999	9.9999	9.9999	0.0047
11	425	9.9999	9.9999	9.9999	9.9999	9.9999	9.9999	-0.0360	-0.0494	0.0343	9.9999	9.9999	9.9999	9.9999	9.9999	9.9999	9.9999	9.9999	-0.0113
11	424	9.9999	9.9999	9.9999	9.9999	9.9999	9.9999	-0.0395	-0.0391	-0.0084	0.1679	9.9999	9.9999	9.9999	9.9999	9.9999	9.9999	9.9999	-0.0203
11	423	9.9999	9.9999	9.9999	9.9999	9.9999	9.9999	-0.0543	-0.0501	0.0093	0.1113	9.9999	9.9999	9.9999	9.9999	9.9999	9.9999	9.9999	-0.0207
11	422	9.9999	9.9999	9.9999	9.9999	9.9999	9.9999	-0.0790	-0.0691	0.0290	0.1488	0.2155	9.9999	9.9999	9.9999	9.9999	9.9999	9.9999	-0.0368
11	421	9.9999	9.9999	9.9999	9.9999	9.9999	9.9999	-0.1059	-0.0850	0.0453	0.1646	0.2374	0.2848	9.9999	9.9999	9.9999	9.9999	9.9999	-0.0568
11	420	9.9999	9.9999	9.9999	9.9999	9.9999	9.9999	-0.1238	-0.0921	0.0561	0.1630	0.2162	0.2940	9.9999	9.9999	9.9999	9.9999	9.9999	-0.0695
11	419	9.9999	9.9999	9.9999	9.9999	9.9999	9.9999	-0.1408	-0.0972	0.0680	0.1591	0.1904	0.2402	9.9999	9.9999	9.9999	9.9999	9.9999	-0.0823
11	418	9.9999	9.9999	9.9999	9.9999	9.9999	9.9999	-0.1513	-0.1023	0.0716	0.1541	0.1676	0.1924	0.3316	9.9999	9.9999	9.9999	9.9999	-0.0930
11	417	9.9999	9.9999	9.9999	9.9999	9.9999	9.9999	-0.1602	-0.1075	0.0716	0.1474	0.1519	0.1587	0.3123	9.9999	9.9999	9.9999	9.9999	-0.1020
11	416	9.9999	9.9999	9.9999	9.9999	9.9999	9.9999	-0.1672	-0.1075	0.0787	0.1423	0.1396	0.1357	0.2293	0.3545	9.9999	9.9999	9.9999	-0.1038
11	415	9.9999	9.9999	9.9999	9.9999	9.9999	9.9999	-0.1727	-0.1094	0.0788	0.1408	0.1345	0.1216	0.1695	0.2689	9.9999	9.9999	9.9999	-0.1075
11	413	9.9999	9.9999	9.9999	9.9999	9.9999	9.9999	-0.1732	-0.1098	0.0808	0.1394	0.1313	0.1201	0.1664	0.2642	9.9999	9.9999	9.9999	-0.1079
11	412	9.9999	9.9999	9.9999	9.9999	9.9999	9.9999	-0.1765	-0.1114	0.0825	0.1376	0.1276	0.1111	0.1272	0.1920	0.4543	9.9999	9.9999	-0.1113
11	411	0.3436	0.1524	9.9999	9.9999	9.9999	9.9999	-0.1804	-0.1116	0.0826	0.1344	0.1242	0.1041	0.1026	0.1401	0.3488	0.1977	9.9999	-0.1133
11	410	0.2817	0.3215	0.3322	0.2665	9.9999	9.9999	-0.1819	-0.1132	0.0861	0.1326	0.1189	0.0933	0.0759	0.0843	0.1820	0.2948	9.9999	-0.1167
11	409	0.2033	0.2507	0.2941	0.3021	0.3285	0.2804	-0.1857	-0.1134	0.0862	0.1294	0.1155	0.0899	0.0671	0.0700	0.1272	0.2200	0.3533	-0.1187

Run	Point	cp220	cp226	cp229	cp232	cp235	cp244	cp250	cp253	cp3
11	429	9.9999	9.9999	9.9999	9.9999	9.9999	9.9999	9.9999	9.9999	-0.0080
11	428	9.9999	9.9999	9.9999	9.9999	9.9999	9.9999	9.9999	9.9999	-0.0064
11	427	0.0120	9.9999	9.9999	9.9999	9.9999	9.9999	9.9999	9.9999	-0.0063
11	426	-0.0332	9.9999	9.9999	9.9999	9.9999	9.9999	9.9999	9.9999	-0.0079
11	425	-0.0263	9.9999	9.9999	9.9999	9.9999	9.9999	9.9999	9.9999	-0.0080
11	424	-0.0281	0.1276	9.9999	9.9999	9.9999	9.9999	9.9999	9.9999	-0.0080
11	423	-0.0357	0.1412	0.2135	9.9999	9.9999	9.9999	9.9999	9.9999	-0.0100
11	422	-0.0479	0.1767	0.2133	9.9999	9.9999	9.9999	9.9999	9.9999	-0.0117
11	421	-0.0640	0.1878	0.2299	0.2652	9.9999	9.9999	9.9999	9.9999	-0.0169
11	420	-0.0764	0.1880	0.2194	0.2707	0.2854	9.9999	9.9999	9.9999	-0.0186
11	419	-0.0871	0.1766	0.1987	0.2443	0.2882	9.9999	9.9999	9.9999	-0.0214
11	418	-0.0959	0.1661	0.1758	0.2115	0.2556	9.9999	9.9999	9.9999	-0.0248
11	417	-0.1029	0.1556	0.1548	0.1803	0.2126	9.9999	9.9999	9.9999	-0.0265
11	416	-0.1099	0.1468	0.1389	0.1526	0.1730	9.9999	9.9999	9.9999	-0.0282
11	415	-0.1118	0.1417	0.1285	0.1337	0.1422	0.3177	9.9999	9.9999	-0.0283
11	413	-0.1139	0.1420	0.1270	0.1323	0.1408	0.3168	9.9999	9.9999	-0.0301
11	412	-0.1172	0.1383	0.1198	0.1182	0.1165	0.2972	9.9999	9.9999	-0.0301
11	411	-0.1192	0.1350	0.1129	0.1079	0.0993	0.2403	0.3334	9.9999	-0.0284
11	410	-0.1209	0.1313	0.1039	0.0939	0.0768	0.1444	0.2997	0.3070	-0.0301
11	409	-0.1246	0.1279	0.1005	0.0888	0.0682	0.1114	0.2438	0.3145	-0.0302

Table A-16. Pressure Coefficients at M = 0.4 for Cavity with sweep = 35 deg. (Config. 4).

Run	Point	Ψ deg	CONF	M	$R\times10^{-6}$ per ft	p_∞ psi	$p_{t,\infty}$ psi	q_∞ psi	$T_{t,\infty}$ °F	l/h	cp14	cp16	cp17	cp19	cp20	cp21	cp22	cp25	cp26	cp28
11	406	35	4	0.40	2.56	13.23	14.79	1.50	77.2	1	0.0135	9.9999	9.9999	9.9999	9.9999	9.9999	9.9999	9.9999	9.9999	9.9999
11	405	35	4	0.40	2.56	13.23	14.79	1.50	77.2	2	0.1276	-0.1138	0.1010	9.9999	9.9999	9.9999	9.9999	9.9999	9.9999	9.9999
11	404	35	4	0.40	2.56	13.24	14.79	1.50	77.3	3	0.0341	-0.1891	-0.0971	0.3223	9.9999	9.9999	9.9999	9.9999	9.9999	9.9999
11	403	35	4	0.40	2.56	13.24	14.79	1.49	77.3	4	-0.0251	-0.0785	-0.0815	0.0130	0.0992	0.2122	9.9999	9.9999	9.9999	9.9999
11	402	35	4	0.40	2.56	13.24	14.79	1.50	77.4	5	-0.0251	-0.0374	-0.0478	-0.0394	-0.0061	0.0396	0.0938	9.9999	9.9999	9.9999
11	401	35	4	0.40	2.56	13.23	14.79	1.50	77.5	6	-0.0321	-0.0415	-0.0441	-0.0412	-0.0183	0.0164	0.0505	0.2020	9.9999	9.9999
11	400	35	4	0.40	2.56	13.24	14.79	1.49	77.6	7	-0.0473	-0.0560	-0.0587	-0.0464	-0.0137	0.0260	0.0639	0.1477	0.1734	9.9999
11	399	35	4	0.40	2.55	13.24	14.79	1.49	77.8	8	-0.0727	-0.0817	-0.0843	-0.0547	-0.0085	0.0433	0.0870	0.1844	0.2078	0.2033
11	398	35	4	0.40	2.55	13.24	14.79	1.49	78.1	9	-0.0963	-0.1049	-0.1073	-0.0594	-0.0057	0.0520	0.1009	0.1966	0.2210	0.2552
11	397	35	4	0.40	2.55	13.24	14.79	1.49	78.1	10	-0.1179	-0.1233	-0.1273	-0.0693	-0.0067	0.0539	0.1030	0.1892	0.2081	0.2389
11	396	35	4	0.40	2.55	13.24	14.79	1.49	78.3	11	-0.1312	-0.1368	-0.1404	-0.0737	-0.0057	0.0566	0.1051	0.1782	0.1918	0.2102
11	395	35	4	0.40	2.55	13.24	14.79	1.49	78.5	12	-0.1447	-0.1505	-0.1538	-0.0804	-0.0090	0.0567	0.1038	0.1661	0.1744	0.1809
11	394	35	4	0.40	2.55	13.24	14.79	1.49	78.7	13	-0.1521	-0.1582	-0.1611	-0.0832	-0.0084	0.0570	0.1035	0.1577	0.1622	0.1597
11	393	35	4	0.40	2.55	13.23	14.79	1.50	78.9	14	-0.1608	-0.1676	-0.1697	-0.0858	-0.0084	0.0560	0.1011	0.1488	0.1504	0.1413
11	392	35	4	0.40	2.55	13.24	14.79	1.49	79.1	15	-0.1649	-0.1725	-0.1747	-0.0883	-0.0089	0.0570	0.1013	0.1435	0.1432	0.1293
11	391	35	4	0.40	2.55	13.24	14.79	1.49	79.2	16	-0.1687	-0.1758	-0.1780	-0.0892	-0.0094	0.0584	0.1017	0.1399	0.1376	0.1209
11	390	35	4	0.40	2.54	13.24	14.79	1.49	79.4	17	-0.1710	-0.1781	-0.1803	-0.0927	-0.0119	0.0539	0.0982	0.1365	0.1342	0.1145
11	389	35	4	0.40	2.54	13.24	14.79	1.49	79.7	18	-0.1738	-0.1813	-0.1836	-0.0927	-0.0104	0.0557	0.1001	0.1341	0.1300	0.1089
11	388	35	4	0.40	2.54	13.24	14.79	1.49	80.0	19	-0.1755	-0.1835	-0.1848	-0.0945	-0.0113	0.0557	0.0986	0.1317	0.1276	0.1051
11	387	35	4	0.40	2.53	13.24	14.79	1.49	80.4	20	-0.1775	-0.1849	-0.1872	-0.0966	-0.0143	0.0530	0.0984	0.1311	0.1255	0.1024

Run	Point	cp29	cp30	cp32	cp33	cp34	cp35	cp36	cp37	cp38	cp39	cp40	cp41	cp42	cp43	cp44	cp45	cp46	cp47
11	406	9.9999	9.9999	9.9999	9.9999	9.9999	9.9999	9.9999	9.9999	9.9999	9.9999	9.9999	9.9999	9.9999	9.9999	9.9999	9.9999	9.9999	9.9999
11	405	9.9999	9.9999	9.9999	9.9999	9.9999	9.9999	9.9999	9.9999	9.9999	9.9999	9.9999	9.9999	9.9999	9.9999	9.9999	9.9999	9.9999	9.9999
11	404	9.9999	9.9999	9.9999	9.9999	9.9999	9.9999	9.9999	9.9999	9.9999	9.9999	9.9999	9.9999	9.9999	9.9999	9.9999	9.9999	9.9999	9.9999
11	403	9.9999	9.9999	9.9999	9.9999	9.9999	9.9999	9.9999	9.9999	9.9999	9.9999	9.9999	9.9999	9.9999	9.9999	9.9999	9.9999	9.9999	9.9999
11	402	9.9999	9.9999	9.9999	9.9999	9.9999	9.9999	9.9999	9.9999	9.9999	9.9999	9.9999	9.9999	9.9999	9.9999	9.9999	9.9999	9.9999	9.9999
11	401	9.9999	9.9999	9.9999	9.9999	9.9999	9.9999	9.9999	9.9999	9.9999	9.9999	9.9999	9.9999	9.9999	9.9999	9.9999	9.9999	9.9999	9.9999
11	400	9.9999	9.9999	9.9999	9.9999	9.9999	9.9999	9.9999	9.9999	9.9999	9.9999	9.9999	9.9999	9.9999	9.9999	9.9999	9.9999	9.9999	9.9999
11	399	0.2369	9.9999	9.9999	9.9999	9.9999	9.9999	9.9999	9.9999	9.9999	9.9999	9.9999	9.9999	9.9999	9.9999	9.9999	9.9999	9.9999	9.9999
11	398	0.2627	0.2562	9.9999	9.9999	9.9999	9.9999	9.9999	9.9999	9.9999	9.9999	9.9999	9.9999	9.9999	9.9999	9.9999	9.9999	9.9999	9.9999
11	397	0.2533	0.2783	0.2938	0.2864	9.9999	9.9999	9.9999	9.9999	9.9999	9.9999	9.9999	9.9999	9.9999	9.9999	9.9999	9.9999	9.9999	9.9999
11	396	0.2204	0.2433	0.2913	0.3130	0.3176	0.2917	9.9999	9.9999	9.9999	9.9999	9.9999	9.9999	9.9999	9.9999	9.9999	9.9999	9.9999	9.9999
11	395	0.1852	0.2027	0.2420	0.2700	0.2989	0.3189	0.3213	0.2979	9.9999	9.9999	9.9999	9.9999	9.9999	9.9999	9.9999	9.9999	9.9999	9.9999
11	394	0.1587	0.1704	0.1957	0.2174	0.2422	0.2690	0.3001	0.3297	0.3299	0.2791	9.9999	9.9999	9.9999	9.9999	9.9999	9.9999	9.9999	9.9999
11	393	0.1363	0.1443	0.1574	0.1716	0.1876	0.2064	0.2333	0.2696	0.3032	0.3239	0.3303	0.2724	9.9999	9.9999	9.9999	9.9999	9.9999	9.9999
11	392	0.1224	0.1269	0.1315	0.1409	0.1495	0.1598	0.1779	0.2054	0.2321	0.2632	0.3031	0.3300	0.3333	0.2769	9.9999	9.9999	9.9999	9.9999
11	391	0.1120	0.1144	0.1131	0.1188	0.1225	0.1264	0.1377	0.1572	0.1738	0.1967	0.2295	0.2645	0.3060	0.3279	0.3332	0.2986	9.9999	9.9999
11	390	0.1044	0.1057	0.1000	0.1037	0.1035	0.1034	0.1137	0.1232	0.1325	0.1468	0.1708	0.1929	0.2300	0.2621	0.3066	0.3354	0.3376	0.2947
11	389	0.0980	0.0983	0.0903	0.0922	0.0902	0.0864	0.0936	0.0995	0.1033	0.1116	0.1280	0.1392	0.1687	0.1894	0.2263	0.2664	0.3095	0.3334
11	388	0.0934	0.0931	0.0833	0.0842	0.0801	0.0752	0.0803	0.0830	0.0829	0.0877	0.0997	0.1026	0.1263	0.1411	0.1634	0.1932	0.2285	0.2648
11	387	0.0900	0.0896	0.0779	0.0779	0.0733	0.0666	0.0699	0.0715	0.0687	0.0710	0.0826	0.0773	0.0968	0.1047	0.1198	0.1401	0.1644	0.1897

Table A-16. Concluded.

Run	Point	cp48	cp49	cp50	cp51	cp52	cp53	cp114	cp117	cp120	cp123	cp126	cp129	cp135	cp138	cp144	cp147	cp150	cp217
11	406	9.9999	9.9999	9.9999	9.9999	9.9999	9.9999	9.9999	9.9999	9.9999	9.9999	9.9999	9.9999	9.9999	9.9999	9.9999	9.9999	9.9999	0.0190
11	405	9.9999	9.9999	9.9999	9.9999	9.9999	9.9999	-0.1480	9.9999	9.9999	9.9999	9.9999	9.9999	9.9999	9.9999	9.9999	9.9999	9.9999	-0.0824
11	404	9.9999	9.9999	9.9999	9.9999	9.9999	9.9999	-0.2003	0.3389	9.9999	9.9999	9.9999	9.9999	9.9999	9.9999	9.9999	9.9999	9.9999	-0.0512
11	403	9.9999	9.9999	9.9999	9.9999	9.9999	9.9999	-0.0685	-0.0317	9.9999	9.9999	9.9999	9.9999	9.9999	9.9999	9.9999	9.9999	9.9999	0.0088
11	402	9.9999	9.9999	9.9999	9.9999	9.9999	9.9999	-0.0391	-0.0528	0.0338	9.9999	9.9999	9.9999	9.9999	9.9999	9.9999	9.9999	9.9999	-0.0117
11	401	9.9999	9.9999	9.9999	9.9999	9.9999	9.9999	-0.0438	-0.0443	-0.0032	0.1636	9.9999	9.9999	9.9999	9.9999	9.9999	9.9999	9.9999	-0.0229
11	400	9.9999	9.9999	9.9999	9.9999	9.9999	9.9999	-0.0598	-0.0572	0.0129	0.1119	9.9999	9.9999	9.9999	9.9999	9.9999	9.9999	9.9999	-0.0357
11	399	9.9999	9.9999	9.9999	9.9999	9.9999	9.9999	-0.0873	-0.0750	0.0319	0.1462	0.2165	9.9999	9.9999	9.9999	9.9999	9.9999	9.9999	-0.0542
11	398	9.9999	9.9999	9.9999	9.9999	9.9999	9.9999	-0.1119	-0.0884	0.0456	0.1594	0.2438	0.2868	9.9999	9.9999	9.9999	9.9999	9.9999	-0.0724
11	397	9.9999	9.9999	9.9999	9.9999	9.9999	9.9999	-0.1336	-0.0991	0.0535	0.1570	0.2207	0.3047	9.9999	9.9999	9.9999	9.9999	9.9999	-0.0894
11	396	9.9999	9.9999	9.9999	9.9999	9.9999	9.9999	-0.1481	-0.1049	0.0608	0.1534	0.1951	0.2503	9.9999	9.9999	9.9999	9.9999	9.9999	-0.0994
11	395	9.9999	9.9999	9.9999	9.9999	9.9999	9.9999	-0.1615	-0.1113	0.0648	0.1480	0.1717	0.2008	0.3240	9.9999	9.9999	9.9999	9.9999	-0.1109
11	394	9.9999	9.9999	9.9999	9.9999	9.9999	9.9999	-0.1699	-0.1150	0.0700	0.1439	0.1571	0.1675	0.3331	9.9999	9.9999	9.9999	9.9999	-0.1167
11	393	9.9999	9.9999	9.9999	9.9999	9.9999	9.9999	-0.1788	-0.1172	0.0728	0.1395	0.1440	0.1420	0.2451	0.3775	9.9999	9.9999	9.9999	-0.1239
11	392	9.9999	9.9999	9.9999	9.9999	9.9999	9.9999	-0.1835	-0.1184	0.0754	0.1365	0.1355	0.1266	0.1795	0.2832	9.9999	9.9999	9.9999	-0.1266
11	391	9.9999	9.9999	9.9999	9.9999	9.9999	9.9999	-0.1878	-0.1203	0.0768	0.1346	0.1302	0.1159	0.1378	0.2010	9.9999	9.9999	9.9999	-0.1295
11	390	9.9999	9.9999	9.9999	9.9999	9.9999	9.9999	-0.1903	-0.1230	0.0755	0.1326	0.1261	0.1083	0.1118	0.1443	0.3709	9.9999	9.9999	-0.1323
11	389	0.3294	0.2965	9.9999	9.9999	9.9999	9.9999	-0.1931	-0.1230	0.0765	0.1302	0.1217	0.1019	0.0943	0.1087	0.2815	0.3087	9.9999	-0.1353
11	388	0.3076	0.3379	0.3281	0.2752	9.9999	9.9999	-0.1954	-0.1238	0.0779	0.1297	0.1192	0.0980	0.0821	0.0865	0.1963	0.3252	9.9999	-0.1361
11	387	0.2233	0.2667	0.3050	0.3320	0.3373	0.2941	-0.1979	-0.1265	0.0780	0.1290	0.1175	0.0947	0.0740	0.0718	0.1369	0.2313	0.3641	-0.1390

Run	Point	cp220	cp226	cp229	cp232	cp235	cp244	cp250	cp253	cp3
11	406	9.9999	9.9999	9.9999	9.9999	9.9999	9.9999	9.9999	9.9999	-0.0020
11	405	9.9999	9.9999	9.9999	9.9999	9.9999	9.9999	9.9999	9.9999	-0.0020
11	404	0.0008	9.9999	9.9999	9.9999	9.9999	9.9999	9.9999	9.9999	-0.0006
11	403	-0.0385	9.9999	9.9999	9.9999	9.9999	9.9999	9.9999	9.9999	-0.0012
11	402	-0.0317	9.9999	9.9999	9.9999	9.9999	9.9999	9.9999	9.9999	-0.0007
11	401	-0.0336	0.1376	9.9999	9.9999	9.9999	9.9999	9.9999	9.9999	-0.0030
11	400	-0.0414	0.1534	0.2192	9.9999	9.9999	9.9999	9.9999	9.9999	-0.0053
11	399	-0.0562	0.1858	0.2168	9.9999	9.9999	9.9999	9.9999	9.9999	-0.0095
11	398	-0.0702	0.1990	0.2383	0.2702	9.9999	9.9999	9.9999	9.9999	-0.0119
11	397	-0.0854	0.1952	0.2283	0.2781	0.3007	9.9999	9.9999	9.9999	-0.0162
11	396	-0.0947	0.1851	0.2079	0.2536	0.3061	9.9999	9.9999	9.9999	-0.0170
11	395	-0.1059	0.1732	0.1834	0.2186	0.2734	9.9999	9.9999	9.9999	-0.0208
11	394	-0.1121	0.1630	0.1630	0.1865	0.2295	9.9999	9.9999	9.9999	-0.0211
11	393	-0.1182	0.1527	0.1449	0.1573	0.1859	9.9999	9.9999	9.9999	-0.0243
11	392	-0.1227	0.1461	0.1330	0.1370	0.1511	0.3235	9.9999	9.9999	-0.0249
11	391	-0.1251	0.1413	0.1228	0.1208	0.1247	0.3083	9.9999	9.9999	-0.0258
11	390	-0.1279	0.1382	0.1163	0.1096	0.1050	0.2513	9.9999	9.9999	-0.0264
11	389	-0.1298	0.1338	0.1100	0.1000	0.0903	0.1940	0.3210	9.9999	-0.0273
11	388	-0.1321	0.1322	0.1060	0.0933	0.0798	0.1485	0.3130	0.3039	-0.0273
11	387	-0.1339	0.1301	0.1033	0.0887	0.0714	0.1139	0.2568	0.3188	-0.0283

Table A-17. Pressure Coefficients at M = 0.6 for Cavity with sweep = 35 deg. (Config. 4).

Run	Point	Ψ deg	CONF	M	R×10^-6 per ft	p_∞ psi	$p_{t,\infty}$ psi	q_∞ psi	$T_{t,\infty}$ °F	l/h	cp14	cp16	cp17	cp19	cp20	cp21	cp22	cp25	cp26	cp28
11	384	35	4	0.60	3.43	11.59	14.79	2.93	87.7	1	0.0074	9.9999	9.9999	9.9999	9.9999	9.9999	9.9999	9.9999	9.9999	9.9999
11	383	35	4	0.60	3.43	11.60	14.79	2.92	87.8	2	0.1173	-0.1035	0.0904	9.9999	9.9999	9.9999	9.9999	9.9999	9.9999	9.9999
11	382	35	4	0.60	3.43	11.60	14.79	2.92	87.6	3	0.0358	-0.1758	-0.1044	0.3168	9.9999	9.9999	9.9999	9.9999	9.9999	9.9999
11	381	35	4	0.60	3.43	11.59	14.79	2.93	87.6	4	-0.0290	-0.0691	-0.0780	0.0030	0.0842	0.2014	9.9999	9.9999	9.9999	9.9999
11	380	35	4	0.60	3.43	11.59	14.79	2.93	87.5	5	-0.0279	-0.0389	-0.0494	-0.0401	-0.0089	0.0351	0.0903	9.9999	9.9999	9.9999
11	379	35	4	0.60	3.43	11.60	14.79	2.92	87.6	6	-0.0344	-0.0418	-0.0466	-0.0430	-0.0205	0.0102	0.0442	0.1976	9.9999	9.9999
11	378	35	4	0.60	3.43	11.59	14.79	2.93	87.5	7	-0.0451	-0.0511	-0.0562	-0.0487	-0.0214	0.0135	0.0502	0.1330	0.1628	9.9999
11	377	35	4	0.60	3.44	11.58	14.79	2.93	87.5	8	-0.0673	-0.0733	-0.0786	-0.0566	-0.0187	0.0263	0.0690	0.1682	0.1903	0.1950
11	376	35	4	0.60	3.44	11.58	14.80	2.94	87.7	9	-0.0926	-0.0980	-0.1032	-0.0680	-0.0213	0.0307	0.0781	0.1819	0.2072	0.2458
11	375	35	4	0.60	3.44	11.58	14.79	2.94	87.8	10	-0.1138	-0.1193	-0.1236	-0.0756	-0.0200	0.0370	0.0868	0.1841	0.2057	0.2419
11	374	35	4	0.60	3.43	11.58	14.79	2.94	87.9	11	-0.1333	-0.1387	-0.1424	-0.0874	-0.0254	0.0358	0.0854	0.1742	0.1907	0.2144
11	373	35	4	0.60	3.43	11.58	14.79	2.94	87.9	12	-0.1467	-0.1521	-0.1555	-0.0928	-0.0254	0.0367	0.0859	0.1649	0.1765	0.1887
11	372	35	4	0.60	3.43	11.58	14.79	2.94	87.9	13	-0.1555	-0.1614	-0.1642	-0.0965	-0.0278	0.0367	0.0856	0.1578	0.1642	0.1669
11	371	35	4	0.60	3.43	11.59	14.79	2.93	88.0	14	-0.1625	-0.1680	-0.1709	-0.1014	-0.0295	0.0353	0.0845	0.1507	0.1547	0.1494
11	370	35	4	0.60	3.43	11.59	14.79	2.93	88.0	15	-0.1685	-0.1754	-0.1774	-0.1038	-0.0295	0.0363	0.0841	0.1449	0.1469	0.1361
11	369	35	4	0.60	3.43	11.59	14.79	2.93	88.0	16	-0.1726	-0.1793	-0.1814	-0.1045	-0.0305	0.0363	0.0848	0.1416	0.1412	0.1270
11	368	35	4	0.60	3.43	11.58	14.79	2.94	88.1	17	-0.1771	-0.1833	-0.1857	-0.1099	-0.0336	0.0321	0.0810	0.1375	0.1361	0.1197
11	367	35	4	0.60	3.43	11.59	14.79	2.93	88.0	18	-0.1808	-0.1876	-0.1898	-0.1129	-0.0364	0.0305	0.0792	0.1340	0.1321	0.1135
11	366	35	4	0.60	3.43	11.59	14.79	2.93	88.1	19	-0.1825	-0.1893	-0.1913	-0.1132	-0.0361	0.0309	0.0799	0.1328	0.1299	0.1098
11	365	35	4	0.60	3.43	11.58	14.79	2.93	88.1	20	-0.1835	-0.1903	-0.1927	-0.1159	-0.0384	0.0281	0.0770	0.1313	0.1284	0.1074

Run	Point	cp29	cp30	cp32	cp33	cp34	cp35	cp36	cp37	cp38	cp39	cp40	cp41	cp42	cp43	cp44	cp45	cp46	cp47
11	384	9.9999	9.9999	9.9999	9.9999	9.9999	9.9999	9.9999	9.9999	9.9999	9.9999	9.9999	9.9999	9.9999	9.9999	9.9999	9.9999	9.9999	9.9999
11	383	9.9999	9.9999	9.9999	9.9999	9.9999	9.9999	9.9999	9.9999	9.9999	9.9999	9.9999	9.9999	9.9999	9.9999	9.9999	9.9999	9.9999	9.9999
11	382	9.9999	9.9999	9.9999	9.9999	9.9999	9.9999	9.9999	9.9999	9.9999	9.9999	9.9999	9.9999	9.9999	9.9999	9.9999	9.9999	9.9999	9.9999
11	381	9.9999	9.9999	9.9999	9.9999	9.9999	9.9999	9.9999	9.9999	9.9999	9.9999	9.9999	9.9999	9.9999	9.9999	9.9999	9.9999	9.9999	9.9999
11	380	9.9999	9.9999	9.9999	9.9999	9.9999	9.9999	9.9999	9.9999	9.9999	9.9999	9.9999	9.9999	9.9999	9.9999	9.9999	9.9999	9.9999	9.9999
11	379	9.9999	9.9999	9.9999	9.9999	9.9999	9.9999	9.9999	9.9999	9.9999	9.9999	9.9999	9.9999	9.9999	9.9999	9.9999	9.9999	9.9999	9.9999
11	378	9.9999	9.9999	9.9999	9.9999	9.9999	9.9999	9.9999	9.9999	9.9999	9.9999	9.9999	9.9999	9.9999	9.9999	9.9999	9.9999	9.9999	9.9999
11	377	0.2376	9.9999	9.9999	9.9999	9.9999	9.9999	9.9999	9.9999	9.9999	9.9999	9.9999	9.9999	9.9999	9.9999	9.9999	9.9999	9.9999	9.9999
11	376	0.2504	0.2388	9.9999	9.9999	9.9999	9.9999	9.9999	9.9999	9.9999	9.9999	9.9999	9.9999	9.9999	9.9999	9.9999	9.9999	9.9999	9.9999
11	375	0.2572	0.2813	0.2859	0.2886	9.9999	9.9999	9.9999	9.9999	9.9999	9.9999	9.9999	9.9999	9.9999	9.9999	9.9999	9.9999	9.9999	9.9999
11	374	0.2280	0.2521	0.2980	0.3160	0.3133	0.2962	9.9999	9.9999	9.9999	9.9999	9.9999	9.9999	9.9999	9.9999	9.9999	9.9999	9.9999	9.9999
11	373	0.1961	0.2151	0.2543	0.2813	0.3080	0.3290	0.3253	0.3021	9.9999	9.9999	9.9999	9.9999	9.9999	9.9999	9.9999	9.9999	9.9999	9.9999
11	372	0.1691	0.1810	0.2070	0.2310	0.2547	0.2828	0.3126	0.3386	0.3326	0.2844	9.9999	9.9999	9.9999	9.9999	9.9999	9.9999	9.9999	9.9999
11	371	0.1483	0.1549	0.1689	0.1843	0.2003	0.2226	0.2490	0.2860	0.3192	0.3388	0.3382	0.2770	9.9999	9.9999	9.9999	9.9999	9.9999	9.9999
11	370	0.1321	0.1353	0.1404	0.1502	0.1586	0.1711	0.1910	0.2179	0.2483	0.2809	0.3202	0.3427	0.3394	0.2825	9.9999	9.9999	9.9999	9.9999
11	369	0.1205	0.1220	0.1202	0.1269	0.1297	0.1351	0.1484	0.1668	0.1851	0.2113	0.2449	0.2810	0.3228	0.3408	0.3404	0.3080	9.9999	9.9999
11	368	0.1120	0.1118	0.1056	0.1094	0.1087	0.1093	0.1178	0.1302	0.1405	0.1586	0.1830	0.2052	0.2450	0.2795	0.3237	0.3498	0.3452	0.3055
11	367	0.1048	0.1034	0.0943	0.0962	0.0928	0.0903	0.0956	0.1034	0.1080	0.1198	0.1368	0.1480	0.1805	0.2036	0.2416	0.2833	0.3265	0.3490
11	366	0.1003	0.0984	0.0872	0.0881	0.0827	0.0784	0.0816	0.0861	0.0862	0.0938	0.1057	0.1083	0.1350	0.1479	0.1753	0.2072	0.2453	0.2833
11	365	0.0975	0.0948	0.0822	0.0819	0.0754	0.0695	0.0725	0.0738	0.0711	0.0756	0.0836	0.0807	0.1030	0.1083	0.1279	0.1510	0.1759	0.2040

Table A-17. Concluded.

Run	Point	cp48	cp49	cp50	cp51	cp52	cp53	cp114	cp117	cp120	cp123	cp126	cp129	cp135	cp138	cp144	cp147	cp150	cp217
11	384	9.9999	9.9999	9.9999	9.9999	9.9999	9.9999	9.9999	9.9999	9.9999	9.9999	9.9999	9.9999	9.9999	9.9999	9.9999	9.9999	9.9999	0.0190
11	383	9.9999	9.9999	9.9999	9.9999	9.9999	9.9999	-0.1332	9.9999	9.9999	9.9999	9.9999	9.9999	9.9999	9.9999	9.9999	9.9999	9.9999	-0.0814
11	382	9.9999	9.9999	9.9999	9.9999	9.9999	9.9999	-0.1814	0.3036	9.9999	9.9999	9.9999	9.9999	9.9999	9.9999	9.9999	9.9999	9.9999	-0.0463
11	381	9.9999	9.9999	9.9999	9.9999	9.9999	9.9999	-0.0586	-0.0383	9.9999	9.9999	9.9999	9.9999	9.9999	9.9999	9.9999	9.9999	9.9999	0.0076
11	380	9.9999	9.9999	9.9999	9.9999	9.9999	9.9999	-0.0406	-0.0509	0.0262	9.9999	9.9999	9.9999	9.9999	9.9999	9.9999	9.9999	9.9999	-0.0137
11	379	9.9999	9.9999	9.9999	9.9999	9.9999	9.9999	-0.0456	-0.0445	-0.0075	0.1555	9.9999	9.9999	9.9999	9.9999	9.9999	9.9999	9.9999	-0.0255
11	378	9.9999	9.9999	9.9999	9.9999	9.9999	9.9999	-0.0577	-0.0530	0.0003	0.0931	9.9999	9.9999	9.9999	9.9999	9.9999	9.9999	9.9999	-0.0356
11	377	9.9999	9.9999	9.9999	9.9999	9.9999	9.9999	-0.0809	-0.0685	0.0133	0.1271	0.1924	9.9999	9.9999	9.9999	9.9999	9.9999	9.9999	-0.0519
11	376	9.9999	9.9999	9.9999	9.9999	9.9999	9.9999	-0.1082	-0.0859	0.0215	0.1398	0.2276	0.2857	9.9999	9.9999	9.9999	9.9999	9.9999	-0.0723
11	375	9.9999	9.9999	9.9999	9.9999	9.9999	9.9999	-0.1277	-0.0976	0.0314	0.1466	0.2184	0.3039	9.9999	9.9999	9.9999	9.9999	9.9999	-0.0879
11	374	9.9999	9.9999	9.9999	9.9999	9.9999	9.9999	-0.1479	-0.1099	0.0351	0.1446	0.1970	0.2572	9.9999	9.9999	9.9999	9.9999	9.9999	-0.1041
11	373	9.9999	9.9999	9.9999	9.9999	9.9999	9.9999	-0.1620	-0.1159	0.0411	0.1429	0.1771	0.2104	0.3255	9.9999	9.9999	9.9999	9.9999	-0.1149
11	372	9.9999	9.9999	9.9999	9.9999	9.9999	9.9999	-0.1707	-0.1212	0.0443	0.1405	0.1628	0.1769	0.3471	9.9999	9.9999	9.9999	9.9999	-0.1220
11	371	9.9999	9.9999	9.9999	9.9999	9.9999	9.9999	-0.1782	-0.1255	0.0466	0.1381	0.1517	0.1530	0.2619	0.3884	9.9999	9.9999	9.9999	-0.1280
11	370	9.9999	9.9999	9.9999	9.9999	9.9999	9.9999	-0.1843	-0.1284	0.0484	0.1357	0.1429	0.1362	0.1932	0.2997	9.9999	9.9999	9.9999	-0.1330
11	369	9.9999	9.9999	9.9999	9.9999	9.9999	9.9999	-0.1883	-0.1296	0.0508	0.1338	0.1362	0.1242	0.1485	0.2136	9.9999	9.9999	9.9999	-0.1368
11	368	9.9999	9.9999	9.9999	9.9999	9.9999	9.9999	-0.1934	-0.1332	0.0501	0.1318	0.1314	0.1157	0.1199	0.1518	0.3874	9.9999	9.9999	-0.1405
11	367	0.3390	0.3053	9.9999	9.9999	9.9999	9.9999	-0.1969	-0.1368	0.0484	0.1292	0.1273	0.1087	0.1003	0.1132	0.3018	0.3164	9.9999	-0.1442
11	366	0.3261	0.3506	0.3350	0.2770	9.9999	9.9999	-0.1979	-0.1381	0.0484	0.1284	0.1242	0.1041	0.0877	0.0892	0.2110	0.3450	9.9999	-0.1461
11	365	0.2410	0.2849	0.3249	0.3475	0.3447	0.3038	-0.2004	-0.1393	0.0491	0.1281	0.1227	0.1013	0.0794	0.0734	0.1486	0.2476	0.3811	-0.1469

Run	Point	cp220	cp226	cp229	cp232	cp235	cp244	cp250	cp253	cp3
11	384	9.9999	9.9999	9.9999	9.9999	9.9999	9.9999	9.9999	9.9999	-0.0023
11	383	9.9999	9.9999	9.9999	9.9999	9.9999	9.9999	9.9999	9.9999	-0.0014
11	382	-0.0033	9.9999	9.9999	9.9999	9.9999	9.9999	9.9999	9.9999	0.0009
11	381	-0.0349	9.9999	9.9999	9.9999	9.9999	9.9999	9.9999	9.9999	-0.0004
11	380	-0.0312	9.9999	9.9999	9.9999	9.9999	9.9999	9.9999	9.9999	-0.0005
11	379	-0.0339	0.1348	9.9999	9.9999	9.9999	9.9999	9.9999	9.9999	-0.0021
11	378	-0.0416	0.1403	0.2187	9.9999	9.9999	9.9999	9.9999	9.9999	-0.0030
11	377	-0.0544	0.1727	0.2064	9.9999	9.9999	9.9999	9.9999	9.9999	-0.0065
11	376	-0.0714	0.1866	0.2336	0.2555	9.9999	9.9999	9.9999	9.9999	-0.0110
11	375	-0.0847	0.1919	0.2337	0.2801	0.3007	9.9999	9.9999	9.9999	-0.0129
11	374	-0.0994	0.1832	0.2159	0.2616	0.3103	9.9999	9.9999	9.9999	-0.0176
11	373	-0.1094	0.1736	0.1920	0.2314	0.2839	9.9999	9.9999	9.9999	-0.0198
11	372	-0.1167	0.1642	0.1722	0.1984	0.2437	9.9999	9.9999	9.9999	-0.0205
11	371	-0.1233	0.1555	0.1547	0.1700	0.1997	9.9999	9.9999	9.9999	-0.0217
11	370	-0.1284	0.1484	0.1406	0.1462	0.1626	0.3324	9.9999	9.9999	-0.0234
11	369	-0.1311	0.1432	0.1297	0.1287	0.1335	0.3214	9.9999	9.9999	-0.0241
11	368	-0.1360	0.1381	0.1219	0.1157	0.1119	0.2683	9.9999	9.9999	-0.0257
11	367	-0.1398	0.1345	0.1155	0.1053	0.0952	0.2074	0.3304	9.9999	-0.0273
11	366	-0.1407	0.1321	0.1105	0.0977	0.0834	0.1582	0.3267	0.3131	-0.0274
11	365	-0.1432	0.1306	0.1079	0.0932	0.0751	0.1212	0.2740	0.3307	-0.0276

Table A-18. Pressure Coefficients at M = 0.8 for Cavity with sweep = 35 deg. (Config. 4).

Run	Point	Ψ deg	CONF	M	$R\times10^{-6}$ per ft	p_∞ psi	$p_{t,\infty}$ psi	q_∞ psi	$T_{t,\infty}$ °F	l/h	cp14	cp16	cp17	cp19	cp20	cp21	cp22	cp25	cp26	cp28
11	360	35	4	0.80	3.90	9.69	14.79	4.35	107.3	1	-0.0114	9.9999	9.9999	9.9999	9.9999	9.9999	9.9999	9.9999	9.9999	9.9999
11	359	35	4	0.80	3.89	9.70	14.79	4.34	108.0	2	0.0431	-0.0701	0.0471	9.9999	9.9999	9.9999	9.9999	9.9999	9.9999	9.9999
11	358	35	4	0.80	3.89	9.69	14.79	4.36	108.7	3	0.0221	-0.1236	-0.1026	0.2340	9.9999	9.9999	9.9999	9.9999	9.9999	9.9999
11	357	35	4	0.80	3.88	9.69	14.79	4.35	110.0	4	-0.0349	-0.0553	-0.0672	-0.0260	0.0370	0.1521	9.9999	9.9999	9.9999	9.9999
11	356	35	4	0.80	3.87	9.70	14.79	4.35	111.1	5	-0.0332	-0.0344	-0.0455	-0.0498	-0.0337	-0.0060	0.0533	9.9999	9.9999	9.9999
11	355	35	4	0.80	3.86	9.69	14.79	4.35	112.5	6	-0.0377	-0.0364	-0.0422	-0.0517	-0.0460	-0.0360	-0.0063	0.1617	9.9999	9.9999
11	354	35	4	0.80	3.84	9.67	14.78	4.36	114.9	7	-0.0396	-0.0383	-0.0436	-0.0508	-0.0433	-0.0328	-0.0076	0.0561	0.1007	9.9999
11	353	35	4	0.80	3.77	9.68	14.77	4.35	123.0	8	-0.0467	-0.0459	-0.0512	-0.0572	-0.0496	-0.0371	-0.0090	0.0561	0.0784	0.1253
11	352	35	4	0.80	3.69	9.69	14.75	4.33	131.3	9	-0.0617	-0.0614	-0.0665	-0.0697	-0.0585	-0.0419	-0.0097	0.0716	0.1022	0.1379
11	351	35	4	0.80	3.72	9.66	14.75	4.35	127.9	10	-0.0800	-0.0804	-0.0853	-0.0844	-0.0666	-0.0440	-0.0068	0.0903	0.1233	0.1736
11	350	35	4	0.80	3.73	9.66	14.75	4.34	126.8	11	-0.1053	-0.1052	-0.1103	-0.1016	-0.0776	-0.0468	-0.0030	0.1056	0.1388	0.1898
11	349	35	4	0.80	3.73	9.68	14.75	4.33	125.5	12	-0.1289	-0.1288	-0.1333	-0.1193	-0.0905	-0.0528	-0.0035	0.1099	0.1420	0.1851
11	348	35	4	0.80	3.74	9.67	14.75	4.33	124.3	13	-0.1429	-0.1423	-0.1469	-0.1290	-0.0977	-0.0557	-0.0037	0.1122	0.1410	0.1753
11	347	35	4	0.80	3.76	9.67	14.75	4.34	122.5	14	-0.1602	-0.1591	-0.1640	-0.1438	-0.1100	-0.0639	-0.0100	0.1069	0.1330	0.1574
11	346	35	4	0.80	3.77	9.68	14.75	4.33	121.0	15	-0.1650	-0.1646	-0.1688	-0.1476	-0.1119	-0.0640	-0.0080	0.1069	0.1309	0.1489
11	345	35	4	0.80	3.78	9.69	14.75	4.32	119.1	16	-0.1692	-0.1695	-0.1735	-0.1514	-0.1142	-0.0644	-0.0088	0.1059	0.1274	0.1404
11	344	35	4	0.80	3.82	9.65	14.75	4.35	116.5	17	-0.1738	-0.1752	-0.1778	-0.1550	-0.1164	-0.0655	-0.0099	0.1044	0.1256	0.1348
11	343	35	4	0.80	3.83	9.66	14.75	4.34	114.2	18	-0.1859	-0.1881	-0.1902	-0.1665	-0.1274	-0.0754	-0.0187	0.0961	0.1166	0.1235
11	342	35	4	0.80	3.85	9.67	14.75	4.34	112.2	19	-0.1859	-0.1880	-0.1902	-0.1660	-0.1257	-0.0730	-0.0165	0.0973	0.1165	0.1212
11	341	35	4	0.80	3.87	9.68	14.75	4.33	109.8	20	-0.1831	-0.1851	-0.1875	-0.1622	-0.1224	-0.0686	-0.0128	0.0995	0.1174	0.1210

Run	Point	cp29	cp30	cp32	cp33	cp34	cp35	cp36	cp37	cp38	cp39	cp40	cp41	cp42	cp43	cp44	cp45	cp46	cp47
11	360	9.9999	9.9999	9.9999	9.9999	9.9999	9.9999	9.9999	9.9999	9.9999	9.9999	9.9999	9.9999	9.9999	9.9999	9.9999	9.9999	9.9999	9.9999
11	359	9.9999	9.9999	9.9999	9.9999	9.9999	9.9999	9.9999	9.9999	9.9999	9.9999	9.9999	9.9999	9.9999	9.9999	9.9999	9.9999	9.9999	9.9999
11	358	9.9999	9.9999	9.9999	9.9999	9.9999	9.9999	9.9999	9.9999	9.9999	9.9999	9.9999	9.9999	9.9999	9.9999	9.9999	9.9999	9.9999	9.9999
11	357	9.9999	9.9999	9.9999	9.9999	9.9999	9.9999	9.9999	9.9999	9.9999	9.9999	9.9999	9.9999	9.9999	9.9999	9.9999	9.9999	9.9999	9.9999
11	356	9.9999	9.9999	9.9999	9.9999	9.9999	9.9999	9.9999	9.9999	9.9999	9.9999	9.9999	9.9999	9.9999	9.9999	9.9999	9.9999	9.9999	9.9999
11	355	9.9999	9.9999	9.9999	9.9999	9.9999	9.9999	9.9999	9.9999	9.9999	9.9999	9.9999	9.9999	9.9999	9.9999	9.9999	9.9999	9.9999	9.9999
11	354	9.9999	9.9999	9.9999	9.9999	9.9999	9.9999	9.9999	9.9999	9.9999	9.9999	9.9999	9.9999	9.9999	9.9999	9.9999	9.9999	9.9999	9.9999
11	353	0.1999	9.9999	9.9999	9.9999	9.9999	9.9999	9.9999	9.9999	9.9999	9.9999	9.9999	9.9999	9.9999	9.9999	9.9999	9.9999	9.9999	9.9999
11	352	0.1464	0.1765	9.9999	9.9999	9.9999	9.9999	9.9999	9.9999	9.9999	9.9999	9.9999	9.9999	9.9999	9.9999	9.9999	9.9999	9.9999	9.9999
11	351	0.1948	0.2164	0.2171	0.2788	9.9999	9.9999	9.9999	9.9999	9.9999	9.9999	9.9999	9.9999	9.9999	9.9999	9.9999	9.9999	9.9999	9.9999
11	350	0.2122	0.2387	0.2787	0.2869	0.2577	0.3029	9.9999	9.9999	9.9999	9.9999	9.9999	9.9999	9.9999	9.9999	9.9999	9.9999	9.9999	9.9999
11	349	0.2029	0.2258	0.2684	0.2935	0.3152	0.3287	0.2990	0.3145	9.9999	9.9999	9.9999	9.9999	9.9999	9.9999	9.9999	9.9999	9.9999	9.9999
11	348	0.1872	0.2055	0.2370	0.2593	0.2833	0.3099	0.3357	0.3557	0.3325	0.3006	9.9999	9.9999	9.9999	9.9999	9.9999	9.9999	9.9999	9.9999
11	347	0.1652	0.1783	0.1968	0.2133	0.2308	0.2521	0.2801	0.3145	0.3445	0.3598	0.3490	0.2982	9.9999	9.9999	9.9999	9.9999	9.9999	9.9999
11	346	0.1529	0.1614	0.1688	0.1793	0.1895	0.2027	0.2226	0.2515	0.2810	0.3148	0.3542	0.3724	0.3660	0.3161	9.9999	9.9999	9.9999	9.9999
11	345	0.1412	0.1463	0.1450	0.1511	0.1554	0.1620	0.1743	0.1941	0.2148	0.2418	0.2794	0.3147	0.3576	0.3754	0.3697	0.3420	9.9999	9.9999
11	344	0.1343	0.1357	0.1300	0.1317	0.1314	0.1325	0.1405	0.1530	0.1649	0.1834	0.2124	0.2386	0.2824	0.3188	0.3625	0.3865	0.3757	0.3449
11	343	0.1215	0.1212	0.1115	0.1111	0.1076	0.1047	0.1088	0.1163	0.1209	0.1329	0.1537	0.1676	0.2054	0.2306	0.2737	0.3196	0.3625	0.3861
11	342	0.1176	0.1163	0.1037	0.1016	0.0962	0.0910	0.0924	0.0960	0.0955	0.1024	0.1169	0.1201	0.1513	0.1665	0.1975	0.2356	0.2760	0.3194
11	341	0.1169	0.1153	0.1004	0.0975	0.0909	0.0834	0.0834	0.0845	0.0804	0.0845	0.0943	0.0898	0.1167	0.1231	0.1446	0.1721	0.2024	0.2342

Table A-18. Concluded.

Run	Point	cp48	cp49	cp50	cp51	cp52	cp53	cp114	cp117	cp120	cp123	cp126	cp129	cp135	cp138	cp144	cp147	cp150	cp217
11	360	9.9999	9.9999	9.9999	9.9999	9.9999	9.9999	9.9999	9.9999	9.9999	9.9999	9.9999	9.9999	9.9999	9.9999	9.9999	9.9999	9.9999	0.0179
11	359	9.9999	9.9999	9.9999	9.9999	9.9999	9.9999	-0.0798	9.9999	9.9999	9.9999	9.9999	9.9999	9.9999	9.9999	9.9999	9.9999	9.9999	-0.0642
11	358	9.9999	9.9999	9.9999	9.9999	9.9999	9.9999	-0.1319	0.1629	9.9999	9.9999	9.9999	9.9999	9.9999	9.9999	9.9999	9.9999	9.9999	-0.0574
11	357	9.9999	9.9999	9.9999	9.9999	9.9999	9.9999	-0.0502	-0.0448	9.9999	9.9999	9.9999	9.9999	9.9999	9.9999	9.9999	9.9999	9.9999	-0.0036
11	356	9.9999	9.9999	9.9999	9.9999	9.9999	9.9999	-0.0432	-0.0420	-0.0136	9.9999	9.9999	9.9999	9.9999	9.9999	9.9999	9.9999	9.9999	-0.0205
11	355	9.9999	9.9999	9.9999	9.9999	9.9999	9.9999	-0.0463	-0.0352	-0.0457	0.0889	9.9999	9.9999	9.9999	9.9999	9.9999	9.9999	9.9999	-0.0298
11	354	9.9999	9.9999	9.9999	9.9999	9.9999	9.9999	-0.0478	-0.0359	-0.0385	0.0064	9.9999	9.9999	9.9999	9.9999	9.9999	9.9999	9.9999	-0.0343
11	353	9.9999	9.9999	9.9999	9.9999	9.9999	9.9999	-0.0565	-0.0431	-0.0412	0.0137	0.0850	9.9999	9.9999	9.9999	9.9999	9.9999	9.9999	-0.0422
11	352	9.9999	9.9999	9.9999	9.9999	9.9999	9.9999	-0.0724	-0.0571	-0.0460	0.0267	0.1095	0.2171	9.9999	9.9999	9.9999	9.9999	9.9999	-0.0541
11	351	9.9999	9.9999	9.9999	9.9999	9.9999	9.9999	-0.0939	-0.0727	-0.0473	0.0421	0.1343	0.2111	9.9999	9.9999	9.9999	9.9999	9.9999	-0.0693
11	350	9.9999	9.9999	9.9999	9.9999	9.9999	9.9999	-0.1226	-0.0952	-0.0474	0.0552	0.1513	0.2287	9.9999	9.9999	9.9999	9.9999	9.9999	-0.0896
11	349	9.9999	9.9999	9.9999	9.9999	9.9999	9.9999	-0.1470	-0.1144	-0.0478	0.0639	0.1543	0.2176	0.3246	9.9999	9.9999	9.9999	9.9999	-0.1078
11	348	9.9999	9.9999	9.9999	9.9999	9.9999	9.9999	-0.1614	-0.1256	-0.0475	0.0699	0.1529	0.1978	0.3643	9.9999	9.9999	9.9999	9.9999	-0.1194
11	347	9.9999	9.9999	9.9999	9.9999	9.9999	9.9999	-0.1794	-0.1409	-0.0525	0.0689	0.1435	0.1710	0.2899	0.4127	9.9999	9.9999	9.9999	-0.1348
11	346	9.9999	9.9999	9.9999	9.9999	9.9999	9.9999	-0.1844	-0.1452	-0.0508	0.0733	0.1411	0.1570	0.2239	0.3333	9.9999	9.9999	9.9999	-0.1393
11	345	9.9999	9.9999	9.9999	9.9999	9.9999	9.9999	-0.1881	-0.1479	-0.0495	0.0753	0.1375	0.1448	0.1729	0.2456	9.9999	9.9999	9.9999	-0.1425
11	344	9.9999	9.9999	9.9999	9.9999	9.9999	9.9999	-0.1928	-0.1517	-0.0489	0.0768	0.1356	0.1376	0.1413	0.1801	0.4241	9.9999	9.9999	-0.1468
11	343	0.3724	0.3376	9.9999	9.9999	9.9999	9.9999	-0.2053	-0.1628	-0.0581	0.0697	0.1260	0.1245	0.1126	0.1272	0.3378	0.3551	9.9999	-0.1587
11	342	0.3628	0.3860	0.3675	0.3076	9.9999	9.9999	-0.2047	-0.1627	-0.0556	0.0711	0.1249	0.1207	0.0990	0.0996	0.2399	0.3817	9.9999	-0.1586
11	341	0.2746	0.3184	0.3605	0.3838	0.3755	0.3413	-0.2024	-0.1597	-0.0507	0.0754	0.1262	0.1201	0.0915	0.0835	0.1685	0.2827	0.4151	-0.1557

Run	Point	cp220	cp226	cp229	cp232	cp235	cp244	cp250	cp253	cp3
11	360	9.9999	9.9999	9.9999	9.9999	9.9999	9.9999	9.9999	9.9999	-0.0091
11	359	9.9999	9.9999	9.9999	9.9999	9.9999	9.9999	9.9999	9.9999	-0.0098
11	358	-0.0230	9.9999	9.9999	9.9999	9.9999	9.9999	9.9999	9.9999	-0.0102
11	357	-0.0420	9.9999	9.9999	9.9999	9.9999	9.9999	9.9999	9.9999	-0.0070
11	356	-0.0441	9.9999	9.9999	9.9999	9.9999	9.9999	9.9999	9.9999	-0.0069
11	355	-0.0450	0.1039	9.9999	9.9999	9.9999	9.9999	9.9999	9.9999	-0.0093
11	354	-0.0469	0.0771	0.2050	9.9999	9.9999	9.9999	9.9999	9.9999	-0.0077
11	353	-0.0524	0.0823	0.1183	9.9999	9.9999	9.9999	9.9999	9.9999	-0.0089
11	352	-0.0627	0.0924	0.1549	0.1678	9.9999	9.9999	9.9999	9.9999	-0.0122
11	351	-0.0767	0.1096	0.1834	0.2278	0.2750	9.9999	9.9999	9.9999	-0.0131
11	350	-0.0965	0.1254	0.2003	0.2528	0.2904	9.9999	9.9999	9.9999	-0.0170
11	349	-0.1146	0.1295	0.1981	0.2476	0.2998	9.9999	9.9999	9.9999	-0.0223
11	348	-0.1258	0.1304	0.1888	0.2284	0.2776	9.9999	9.9999	9.9999	-0.0225
11	347	-0.1427	0.1213	0.1706	0.1976	0.2350	9.9999	9.9999	9.9999	-0.0294
11	346	-0.1471	0.1200	0.1602	0.1755	0.1975	0.3612	9.9999	9.9999	-0.0283
11	345	-0.1507	0.1166	0.1489	0.1546	0.1631	0.3528	9.9999	9.9999	-0.0282
11	344	-0.1541	0.1135	0.1412	0.1412	0.1382	0.3045	9.9999	9.9999	-0.0283
11	343	-0.1656	0.1040	0.1288	0.1237	0.1122	0.2363	0.3653	9.9999	-0.0364
11	342	-0.1656	0.1042	0.1255	0.1165	0.0992	0.1805	0.3631	0.3508	-0.0352
11	341	-0.1623	0.1047	0.1242	0.1133	0.0916	0.1371	0.3088	0.3688	-0.0314

Appendix B: Supplemental Fluctuating Pressure Data

A complete listing of all spectral peaks (including those with very low amplitudes) is provided in Table B-1. Figure B-1 illustrates all f/U_∞ values plotted with respect to M_∞ and cavity l/h. The raw frequencies are proportional to M_∞ and appear to depend on ψ rather than on cavity length (as is the case for oscillations described by the Modified Rossiter Equation). Dividing by U_∞ largely removes the M_∞ dependence. Several attempts were made to find a characteristic length with which to nondimensionalize the frequency without success.

To allow comparisons between static pressure plots and fluctuating pressure data, Table B-2 provides a listing of the transducer x/l for each ψ and l/h value.

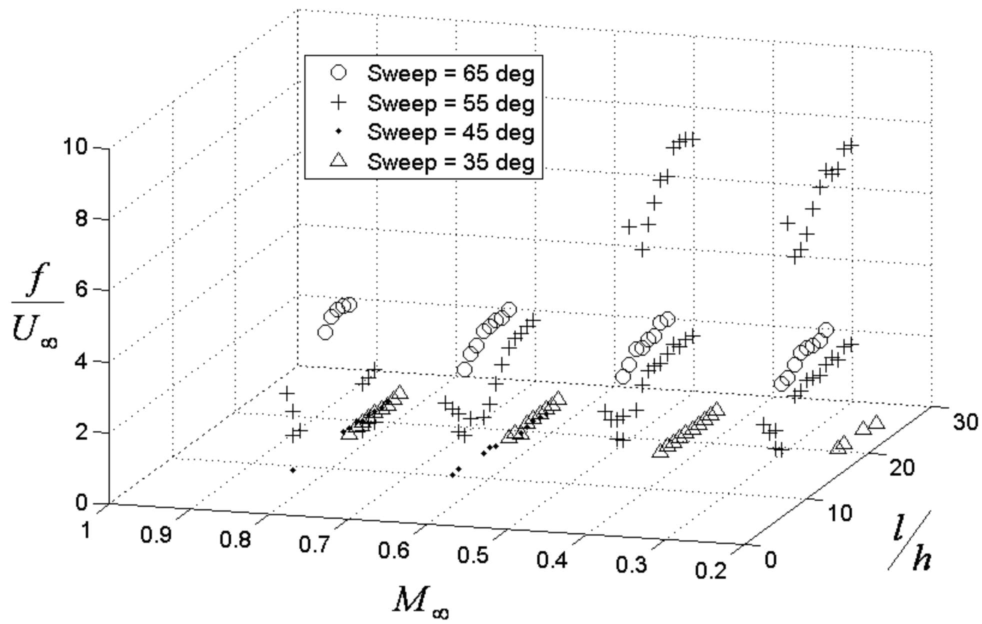

Figure B-1. Oscillation frequencies (divided by free-stream velocity) observed in swept cavities.

Table B-1. Observed oscillation frequencies in swept cavities.

ψ	l/h	M_∞	U_∞, fps	Frequency (f), Hz	$f\frac{l}{U_\infty}$	$\frac{f}{U_\infty}$
65º	6.0	0.2	220.7	825.0	0.934	3.738
65º	7.0	0.2	220.7	837.5	1.107	3.795
65º	8.0	0.2	220.7	887.5	1.341	4.022
65º	9.0	0.2	220.6	937.5	1.593	4.249
65º	10.0	0.2	220.6	937.5	1.771	4.250
65º	11.0	0.2	220.6	925.0	1.922	4.193
65º	12.0	0.2	220.6	925.0	2.097	4.194
65º	13.0	0.2	220.4	962.5	2.366	4.367
55º	3.0	0.2	224.1	675.0	0.376	3.012
55º	4.0	0.2	224.1	587.5	0.437	2.621
55º	5.0	0.2	224.2	450.0 , 575.0	0.418, 0.534	2.070,2.565
55º	6.0	0.2	224.3	425.0	0.474	1.895
55º	7.0	0.2	224.3	1825.0	2.373	8.136
55º	8.0	0.2	224.4	712.5, 1587.5	1.059, 2.359	3.176, 7.076
55º	9.0	0.2	224.4	712.5, 1600.0	1.190, 2.673	3.175, 7.129
55º	10.0	0.2	224.5	750.0, 1675.0	1.392, 3.108	3.340, 7.460
55º	11.0	0.2	224.6	737.5, 1800.0	1.505, 3.673	3.284, 8.015
55º	12.0	0.2	224.6	725.0, 1912.50	1.613, 4.257	3.227, 8.513
55º	13.0	0.2	224.7	762.5, 1987.50	1.838, 4.791	3.393, 8.845
55º	14.0	0.2	224.8	775.0, 1937.50	2.011, 5.027	3.447, 8.618
55º	15.0	0.2	224.9	737.5, 1937.50	2.049, 5.384	3.279, 8.615
55º	16.0	0.2	225.1	787.5, 2037.50	2.332, 6.034	3.498, 9.052
55º	17.0	0.2	225.3	775.0, 2037.50	2.437, 6.407	3.440, 9.045

Table B-1. Continued.

ψ	l/h	M_∞	U_∞, fps	Frequency (f), Hz	$f\frac{l}{U_\infty}$	$\frac{f}{U_\infty}$
35º	15.0	0.2	224.4	175.0	0.487	0.780
35º	16.0	0.2	224.6	175.0	0.519	0.779
35º	19.0	0.2	224.7	175.0	0.617	0.779
35º	21.0	0.2	225.0	162.5	0.632	0.722
65º	6.0	0.4	455.7	1675.0	0.919	3.676
65º	7.0	0.4	455.8	1775.0	1.136	3.894
65º	8.0	0.4	456.1	1912.50	1.398	4.193
65º	9.0	0.4	456.5	1862.50	1.530	4.080
65º	10.0	0.4	456.8	1912.50	1.744	4.187
65º	11.0	0.4	457.1	1912.50	1.918	4.184
65º	12.0	0.4	457.8	2012.50	2.198	4.396
65º	13.0	0.4	458.1	2012.50	2.380	4.393
55º	3.0	0.4	448.5	1387.50	0.387	3.094
55º	4.0	0.4	448.6	1212.50	0.451	2.703
55º	5.0	0.4	448.7	912.5	0.424	2.034
				1162.50	0.540	2.591
55º	6.0	0.4	448.9	850.0	0.473	1.894
				1150.0	0.640	2.562
55º	7.0	0.4	449.0	3475.0	2.257	7.739
55º	8.0	0.4	449.3	1112.50	0.825	2.476
55º	9.0	0.4	449.5	1350.0	1.126	3.036
				3075.0	2.566	6.841

Table B-1. Continued.

ψ	l/h	M_∞	U_∞, fps	Frequency (f), Hz	$f\frac{l}{U_\infty}$	$\frac{f}{U_\infty}$
55º	10.0	0.4	449.6	1487.50	1.378	3.308
				3337.50	3.093	7.423
55º	11.0	0.4	449.8	1500.0	1.528	3.335
				3562.50	3.630	7.920
55º	12.0	0.4	450.0	1475.0	1.639	3.277
				3787.50	4.208	8.416
55º	13.0	0.4	450.3	1537.50	1.849	3.414
				3775.0	4.541	8.383
55º	14.0	0.4	450.5	1600.0	2.072	3.552
				4087.50	5.293	9.074
55º	15.0	0.4	450.7	1512.50	2.097	3.356
				4100.0	5.685	9.096
55º	16.0	0.4	451.0	1537.5, 4087.5	2.273, 6.043	3.409, 9.064
55º	17.0	0.4	451.3	1537.5, 4025.0	2.413, 6.318	3.407, 8.919
35º	12.0	0.4	447.6	350.0	0.391	0.782
35º	13.0	0.4	447.7	362.5	0.439	0.810
35º	14.0	0.4	447.8	350.0	0.456	0.782
35º	15.0	0.4	447.84	350.0	0.488	0.782
35º	16.0	0.4	447.9	362.5	0.540	0.810
35º	17.0	0.4	448.0	350.0	0.553	0.781
35º	18.0	0.4	448.1	350.0	0.586	0.781
35º	19.0	0.4	448.2	350.0	0.618	0.781
35º	20.0	0.4	448.4	350.0	0.650	0.781
35º	21.0	0.4	448.6	350.0	0.683	0.780

Table B-1. Continued.

ψ	l/h	M_∞	U_∞, fps	Frequency (f), Hz	$f\,\frac{l}{U_\infty}$	$\frac{f}{U_\infty}$
65º	6.0	0.6	681.8	2450.0	0.898	3.593
65º	7.0	0.6	681.8	2650.0	1.134	3.886
65º	8.0	0.6	681.8	2725.0	1.332	3.997
65º	9.0	0.6	681.8	2925.0	1.609	4.290
65º	10.0	0.6	682.0	2925.0	1.787	4.289
65º	11.0	0.6	682.0	2950.0	1.983	4.326
65º	12.0	0.6	682.0	2912.50	2.135	4.270
65º	13.0	0.6	682.1	2975.0	2.362	4.361
55º	3.0	0.6	671.8	2025.0	0.377	3.014
55º	4.0	0.6	671.8	1825.0	0.453	2.716
55º	5.0	0.6	672.0	1325.0, 1662.5	0.411, 0.515	1.972, 2.474
55º	6.0	0.6	672.1	1162.50	0.432	1.730
55º	7.0	0.6	672.3	1400.0	0.607	2.082
55º	9.0	0.6	672.6	1237.50	0.690	1.840
55º	10.0	0.6	672.7	1400.0	0.867	2.081
55º	11.0	0.6	673.0	1700.0	1.158	2.526
55º	12.0	0.6	673.3	1987.50	1.476	2.952
55º	13.0	0.6	673.7	2225.0	1.789	3.303
55º	14.0	0.6	674.1	2312.50	2.001	3.430
55º	15.0	0.6	674.5	2312.50	2.143	3.429
55º	16.0	0.6	675.1	2375.0	2.345	3.518
55º	17.0	0.6	675.7	2400.0	2.516	3.552
45º	4.0	0.6	688.7	600.0	0.145	0.871
45º	5.0	0.6	688.8	625.0	0.189	0.907

Table B-1. Continued.

ψ	l/h	M_∞	U_∞, fps	Frequency (f), Hz	$f\frac{l}{U_\infty}$	$\frac{f}{U_\infty}$
45º	9.0	0.6	689.1	587.5	0.320	0.853
45º	10.0	0.6	689.4	600.0	0.363	0.870
45º	11.0	0.6	689.4	550.0	0.366	0.798
45º	15.0	0.6	689.8	450.0	0.408	0.6524
45º	16.0	0.6	690.0	475.0	0.459	0.689
45º	17.0	0.6	690.0	500.0	0.513	0.725
45º	18.0	0.6	690.1	475.0	0.516	0.688
45º	19.0	0.6	690.6	462.0	0.530	0.669
35º	13.0	0.6	664.4	500.0	0.408	0.753
35º	14.0	0.6	664.5	512.5	0.450	0.771
35º	15.0	0.6	664.5	412.5	0.388	0.621
35º	16.0	0.6	664.5	525.0	0.527	0.790
35º	17.0	0.6	664.5	525.0	0.560	0.790
35º	18.0	0.6	664.5	525.0	0.593	0.790
35º	19.0	0.6	664.6	525.0	0.625	0.790
35º	20.0	0.6	664.5	512.5	0.643	0.771
35º	21.0	0.6	664.5	525.0	0.691	0.790
65º	9.0	0.8	884.1	3512.50	1.490	3.973
65º	10.0	0.8	882.9	3750.0	1.770	4.247
65º	11.0	0.8	881.5	3837.50	1.995	4.353
65º	12.0	0.8	879.5	3800.0	2.160	4.321
65º	13.0	0.8	871.8	3687.0	2.291	4.229

Table B-1. Concluded.

ψ	l/h	M_∞	U_∞, fps	Frequency (f), Hz	$f\frac{l}{U_\infty}$	$\frac{f}{U_\infty}$
55º	3.0	0.8	887.4	2675.0	0.377	3.015
55º	4.0	0.8	887.4	150.0, 2100.0	0.282, 0.394	1.690, 2.367
55º	5.0	0.8	887.4	1512.50	0.355	1.704
55º	15.0	0.8	880.7	362.5, 1512.5	0.257, 1.073	0.412, 1.717
55º	16.0	0.8	878.7	437.5,1562.5	0.332, 1.185	0.498, 1.778
55º	17.0	0.8	876.8	337.5, 1650.0	0.273, 1.333	0.385, 1.882
45º	4.0	0.8	901.1	662.5	0.123	0.735
45º	12.0	0.8	890.4	687.5	0.386	0.772
45º	13.0	0.8	888.7	650.0	0.396	0.731
45º	14.0	0.8	887.2	687.5	0.452	0.775
45º	15.0	0.8	884.8	612.5	0.433	0.692
45º	16.0	0.8	883.1	637.5	0.481	0.722
45º	17.0	0.8	880.6	612.5	0.493	0.696
45º	18.0	0.8	878.2	587.5	0.502	0.669
45º	19.0	0.8	875.8	612.5	0.554	0.699
55º	13.0	0.8	892.3	500.0	0.304	0.560
55º	14.0	0.8	891.0	575.0	0.377	0.645
55º	15.0	0.8	889.7	575.0	0.404	0.646
55º	16.0	0.8	888.3	575.0	0.432	0.647
55º	17.0	0.8	886.2	587.5	0.470	0.663
55º	18.0	0.8	884.4	562.5	0.477	0.636
55º	19.0	0.8	882.9	550.0	0.493	0.623
55º	20.0	0.8	881.0	562.5	0.532	0.639
55º	21.0	0.8	878.9	600.0	0.5973	0.683

Table B-2. Transducer 1 x/l values.

l/h	ψ				Rectangular Cavity
	65º	55º	45º	35º	
3.000	0.327	0.775	1.042	1.229	0.542*
4.000	0.246	0.581	0.782	0.922	0.407*
5.000	0.196	0.465	0.625	0.738	0.325*
6.000	0.164	0.387	0.521	0.615	0.771
7.000	0.140	0.332	0.447	0.527	0.661
8.000	0.123	0.291	0.391	0.461	0.578
9.000	0.109	0.258	0.347	0.410	0.514
10.000	0.098	0.232	0.313	0.369	0.463
11.000	0.089	0.211	0.284	0.335	0.421
12.000	0.082	0.194	0.261	0.307	0.386
13.000	0.076	0.179	0.240	0.284	0.356
14.000	0.070	0.166	0.223	0.263	0.330
15.000	0.065	0.155	0.208	0.246	0.308
16.000	0.061	0.145	0.195	0.231	0.289
17.000	0.058	0.137	0.184	0.217	0.272
18.000	0.055	0.129	0.174	0.205	0.257
19.000	0.052	0.122	0.165	0.194	0.243
20.000	0.049	0.116	0.156	0.184	0.231
21.000	0.047	0.111	0.149	0.176	0.220

* Transducer 3 used since transducer 1 was covered

Appendix C: Supplemental Flow Visualization Figures

Colored water surface flow visualization photographs for the rectangular cavity and the swept cavities are contained in this Appendix as Figures C-1 through C-18. Table C-1 contains an index for the images.

Table C-1. Figure numbers for corresponding Mach number.

Cavity Sweep, ψ	Figure for $M_\infty = 0.2$	Figure for $M_\infty = 0.4$	Figure for $M_\infty = 0.6$	Figure for $M_\infty = 0.8$
65°	C-5	C-6	C-7	C-8
55°	C-9	C-10	C-11	C-12
45°		C-13	C-14	C-15
35°	C-16	C-17	C-18	
0°	C-1	C-2	C-3	C-4

Although the surface flow visualization technique used colored water, the photographs of the flow fields are presented as black and white images.

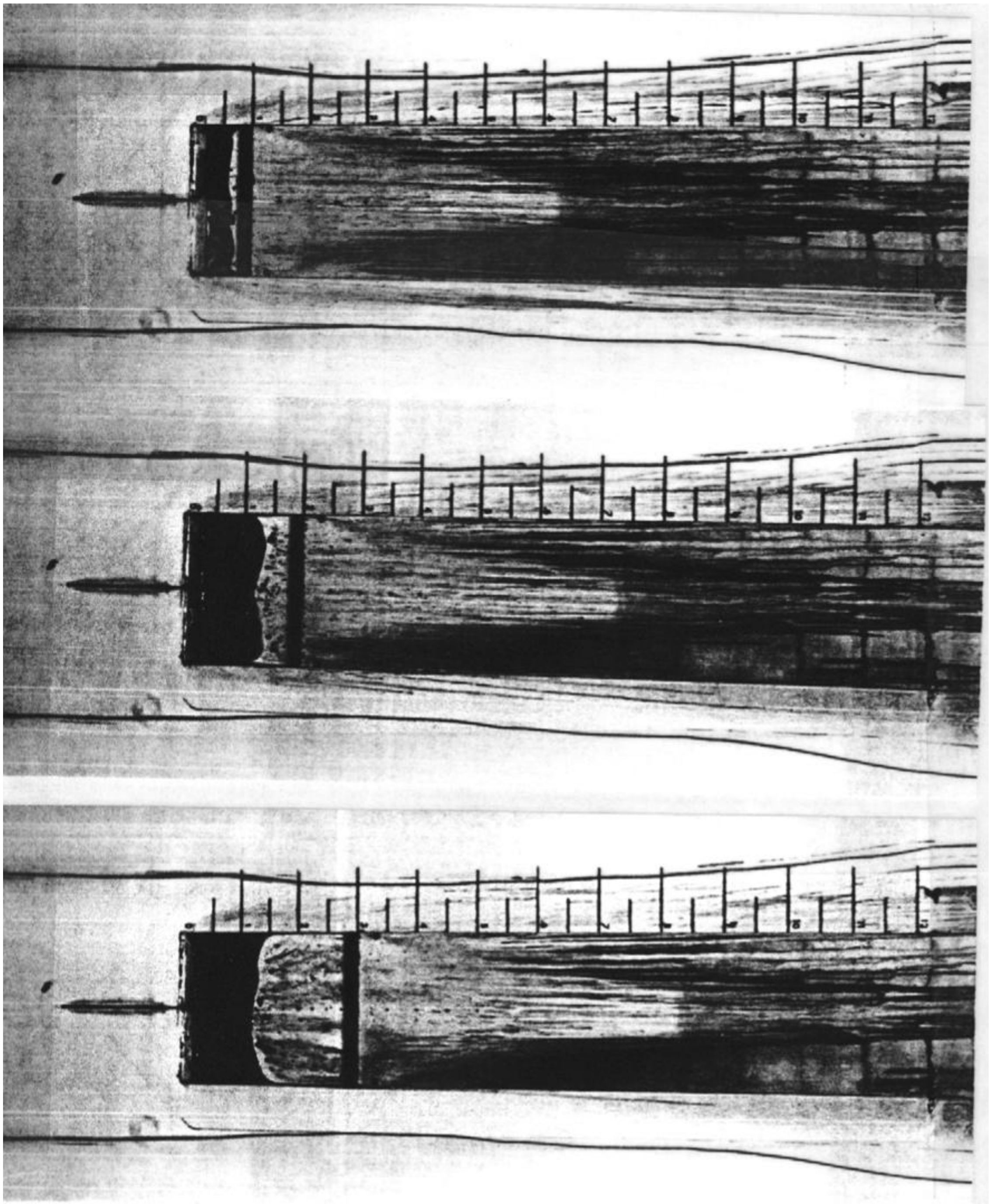

(a) l/h = 2.

(b) l/h = 4.

(c) l/h = 6.

Figure C-1. Surface water flow-visualization photographs for the rectangular cavity, $\psi = 0°$, $M_\infty = 0.2$.

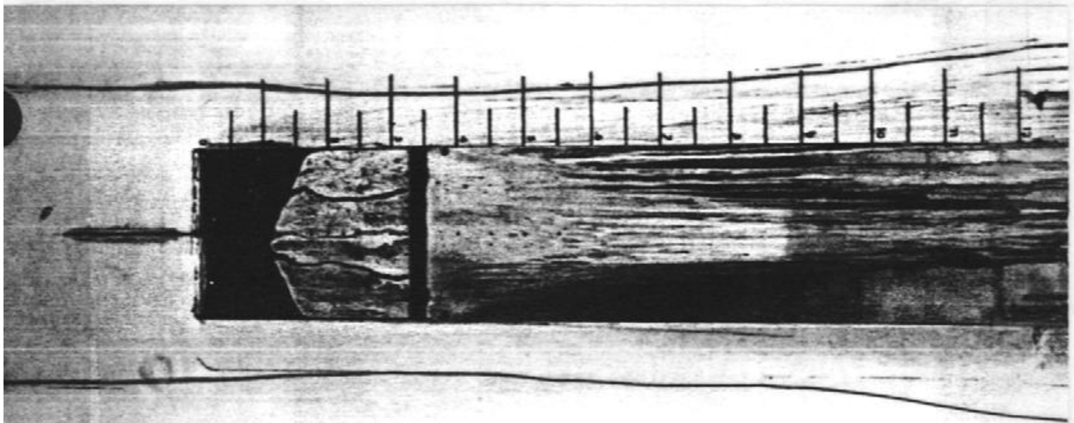

(d) l/h = 7.

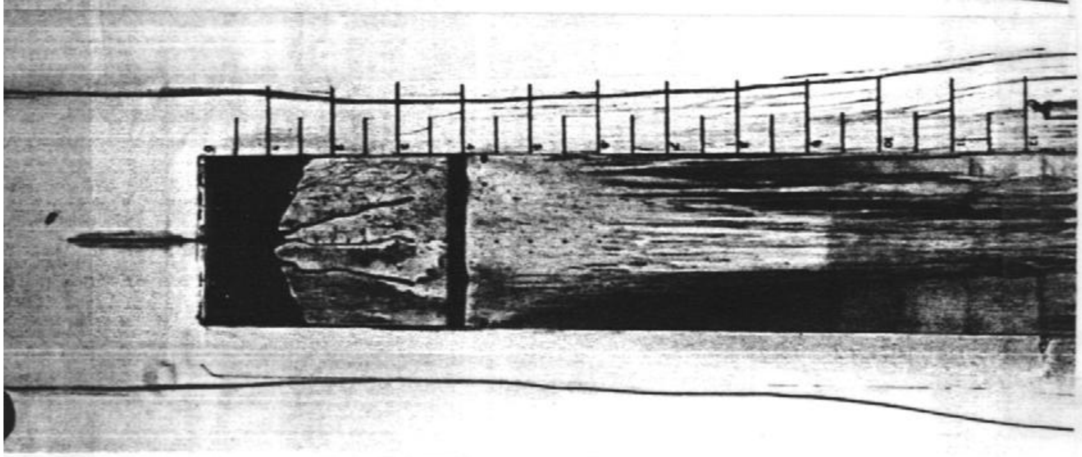

(e) l/h = 8.

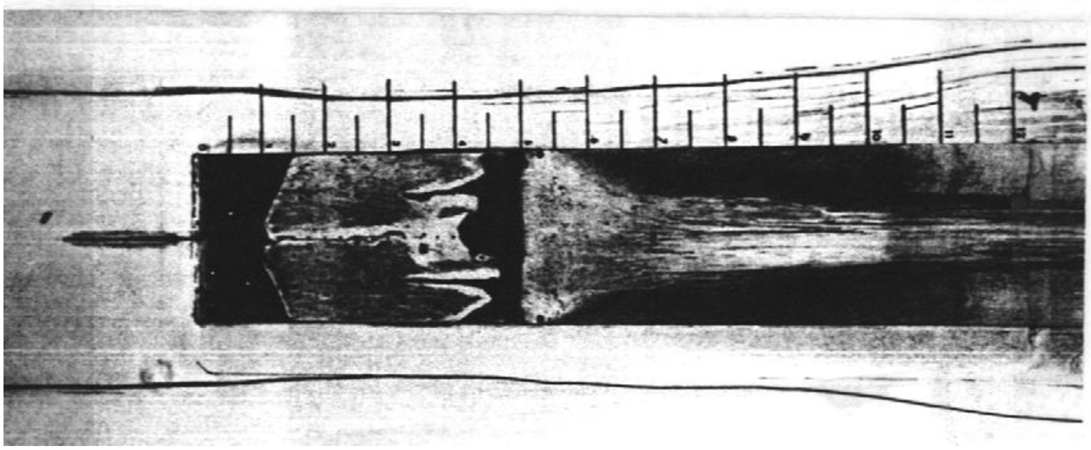

(f) l/h = 10.

Figure C-1. Continued.

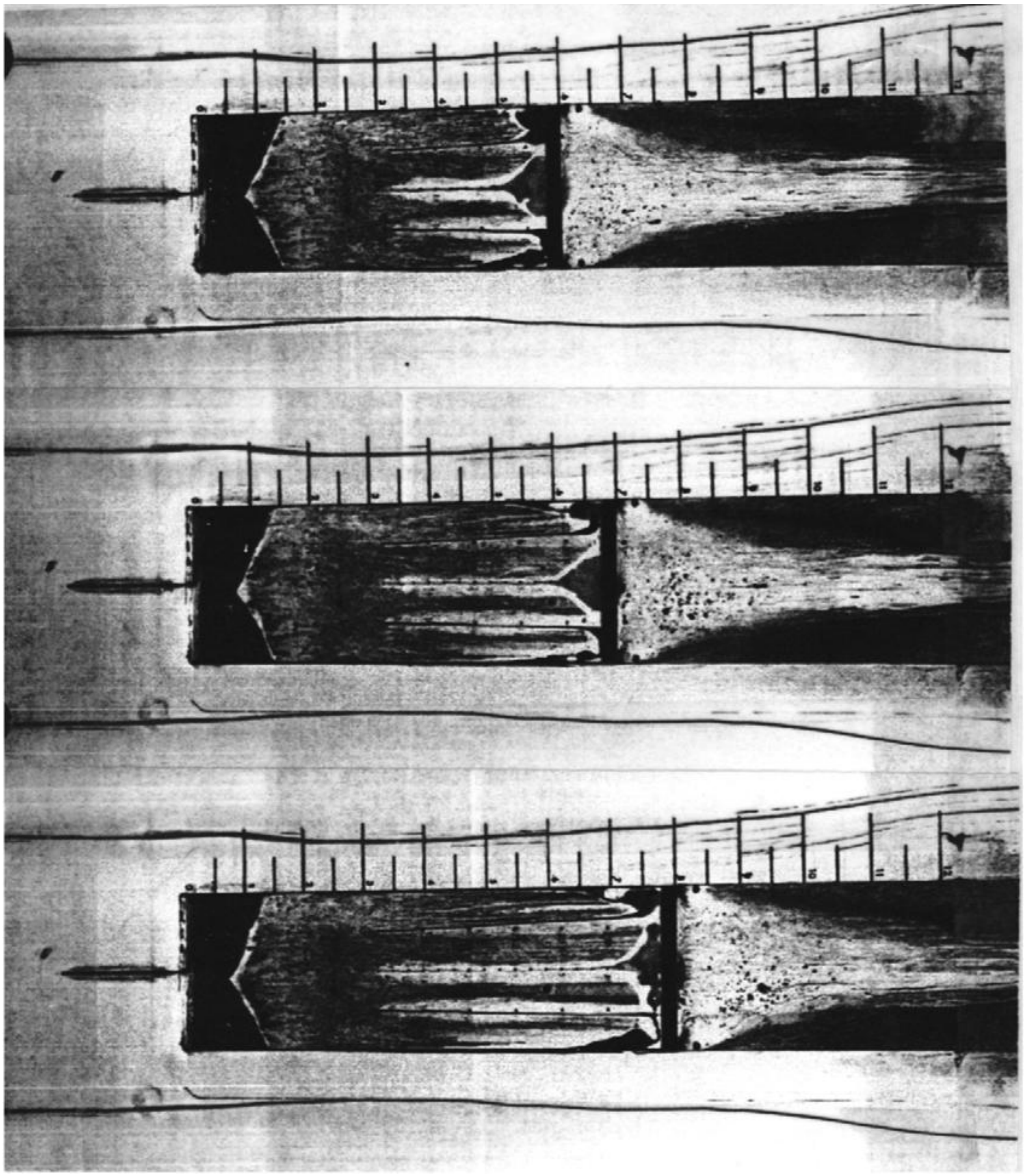

(g) $l/h = 12$.

(h) $l/h = 14$.

(i) $l/h = 16$.

Figure C-1. Continued.

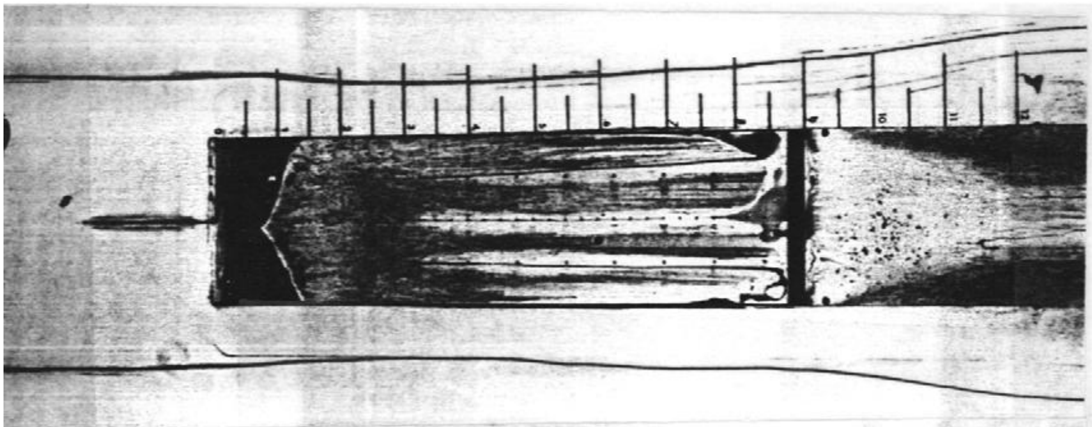

(j) $l/h = 18$.

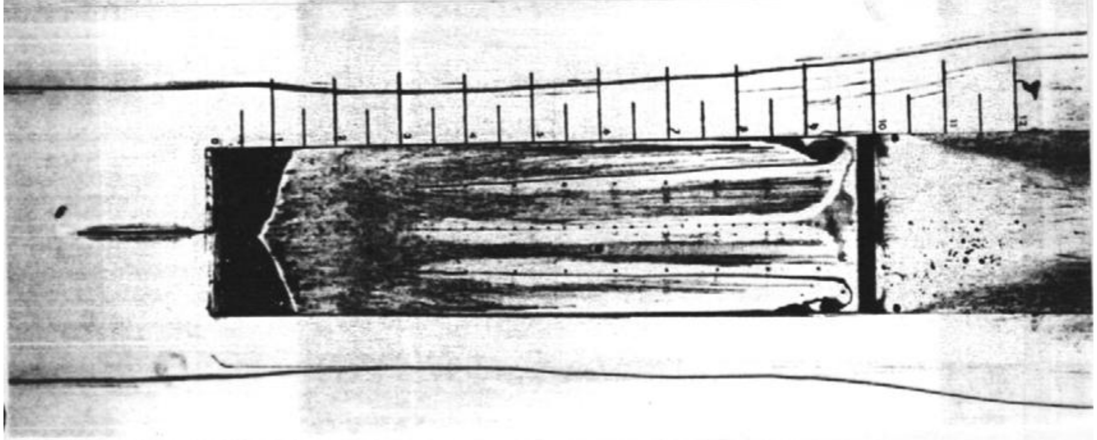

(k) $l/h = 20$.

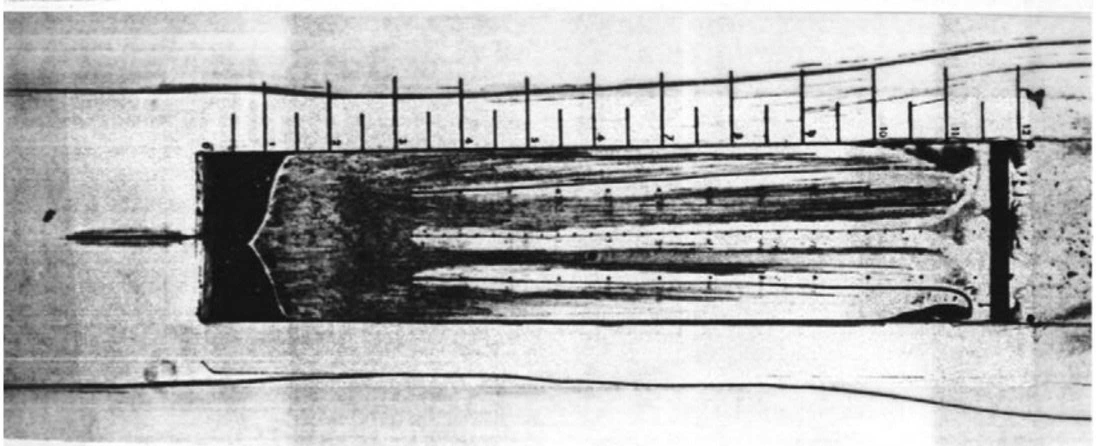

(l) $l/h = 24$.

Figure C-1. Concluded.

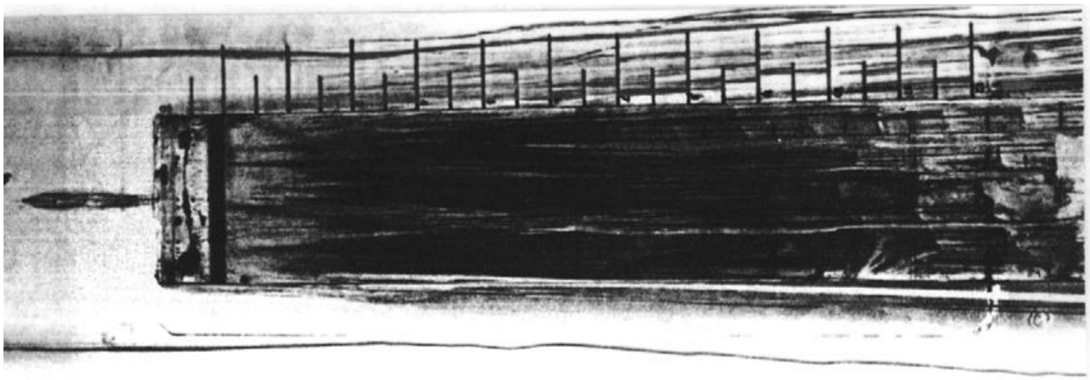

(a) l/h = 2.

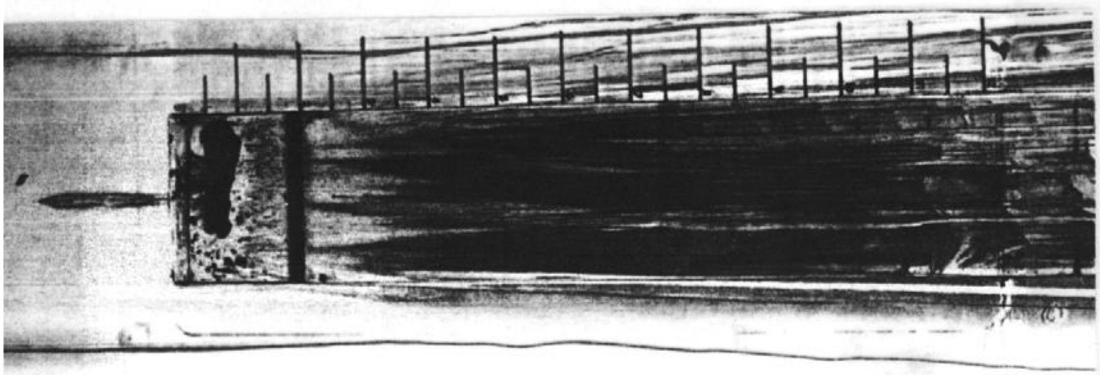

(b) l/h = 4.

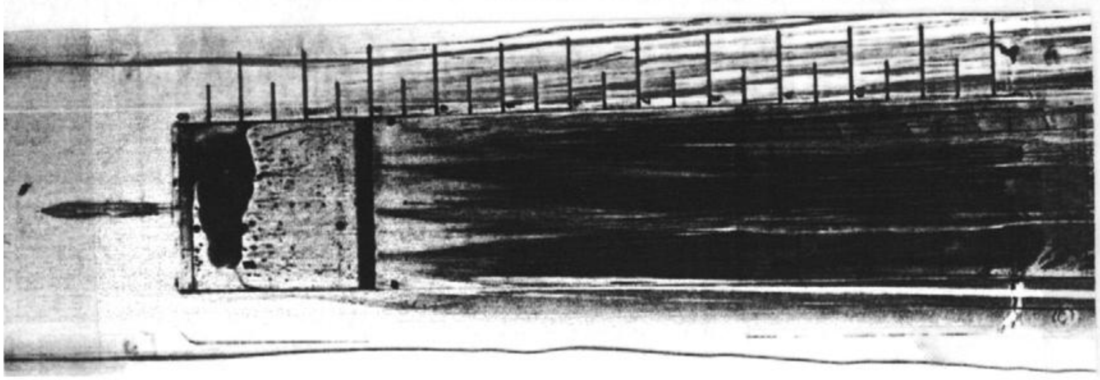

(c) l/h = 6.

Figure C-2. Surface water flow-visualization photographs for the rectangular cavity, $\psi = 0°$, $M_\infty = 0.4$.

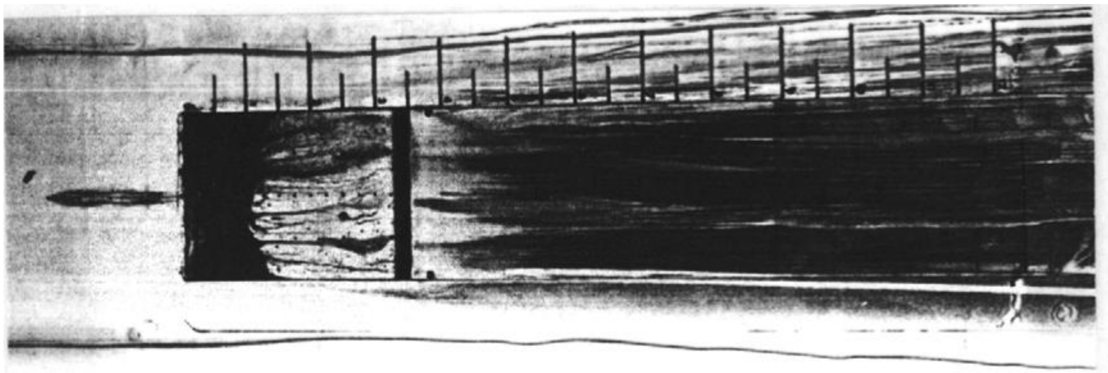

(d) l/h = 7.

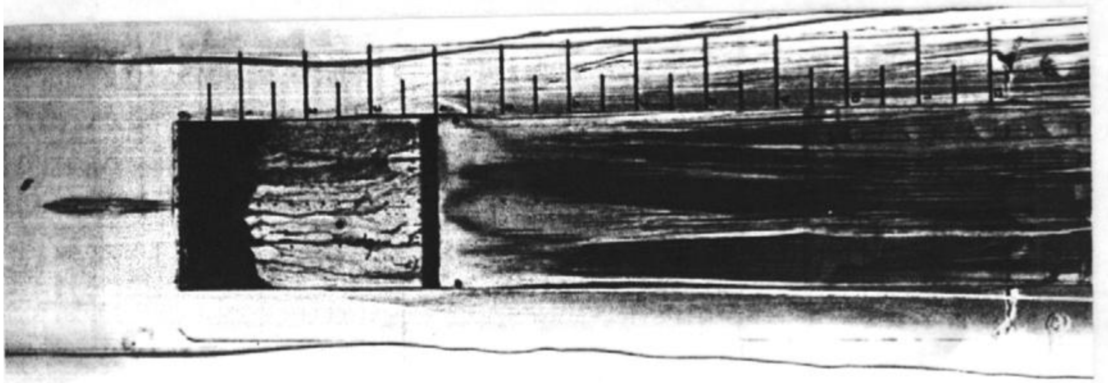

(e) l/h = 8.

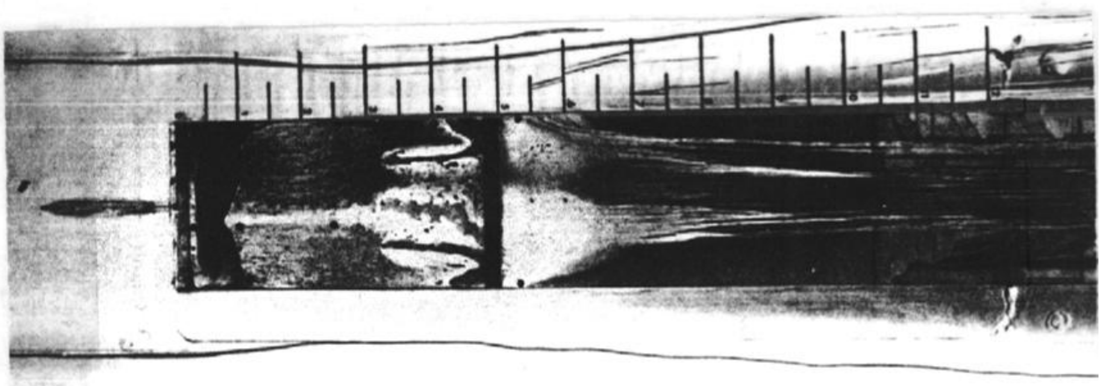

(f) l/h = 10.

Figure C-2. Continued.

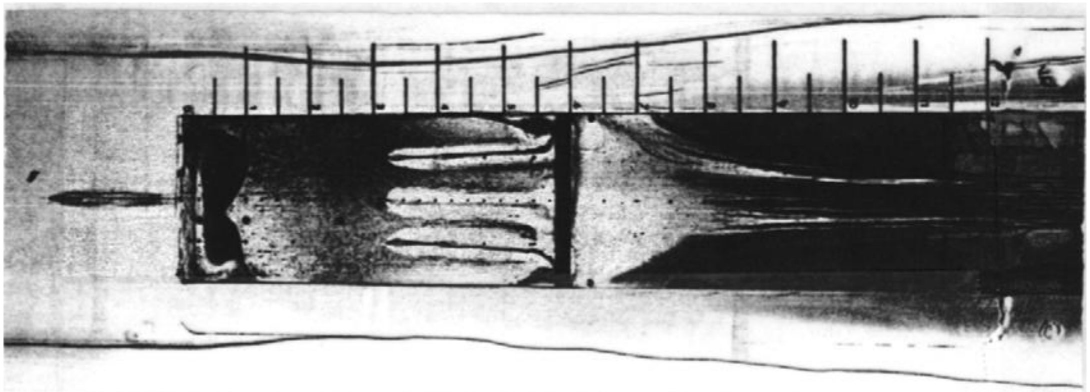

(g) l/h = 12.

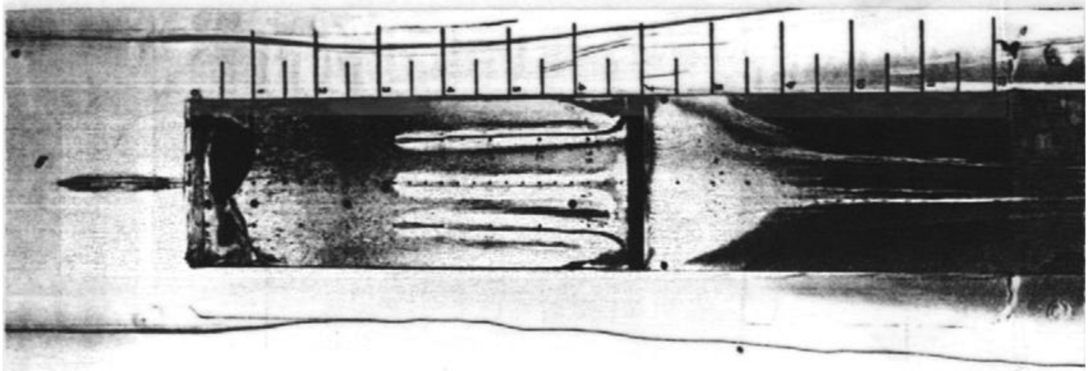

(h) l/h = 14.

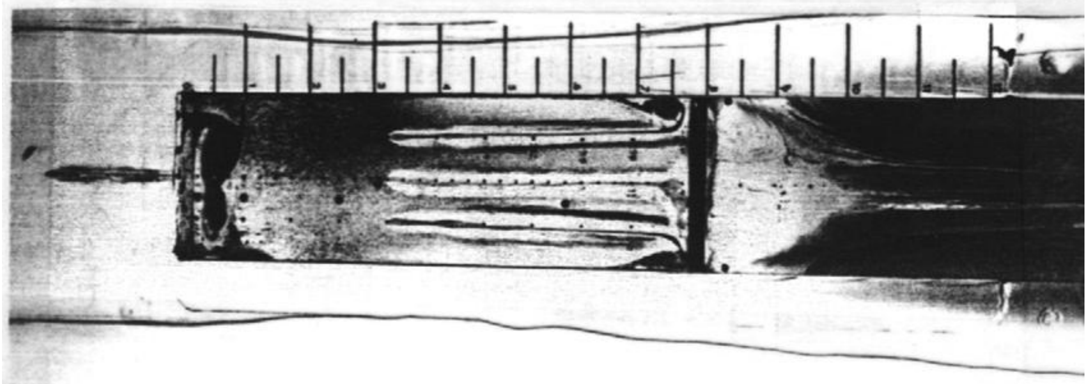

(i) l/h = 16.

Figure C-2. Continued.

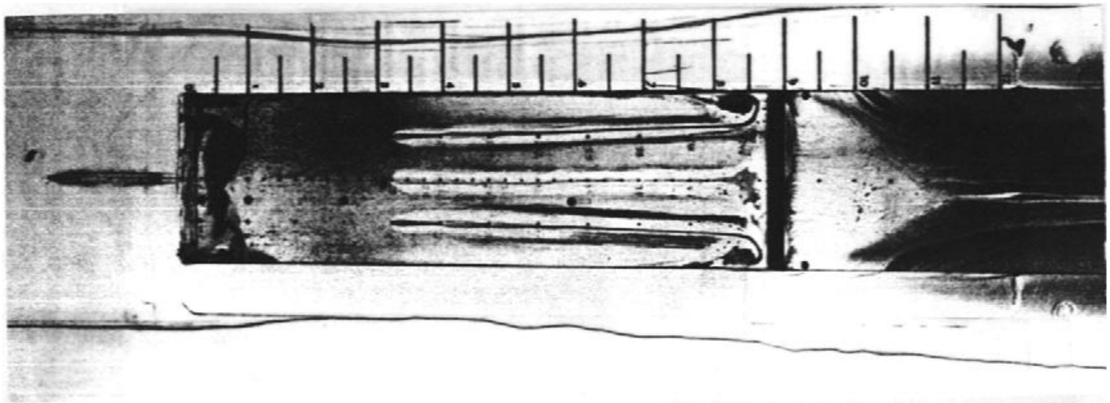

(j) l/h = 18.

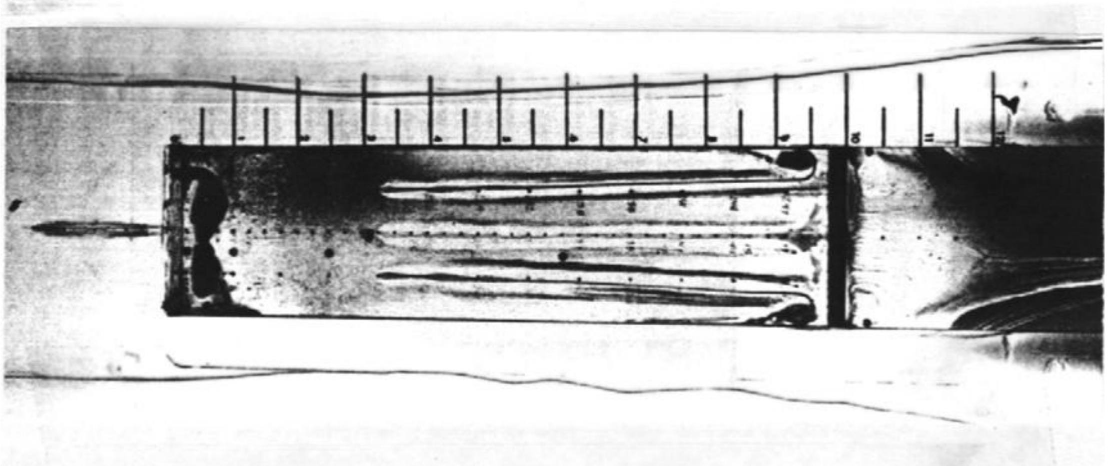

(k) l/h = 20.

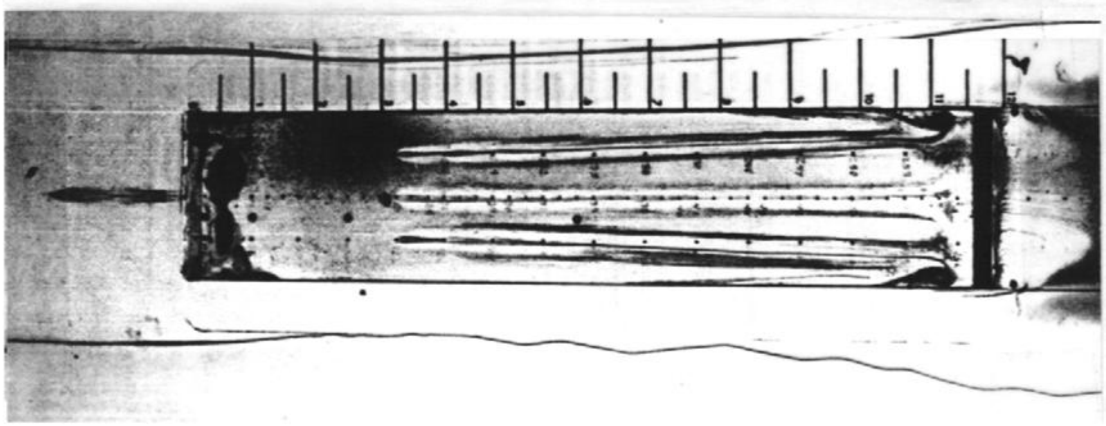

(l) l/h = 24.

Figure C-2. Concluded.

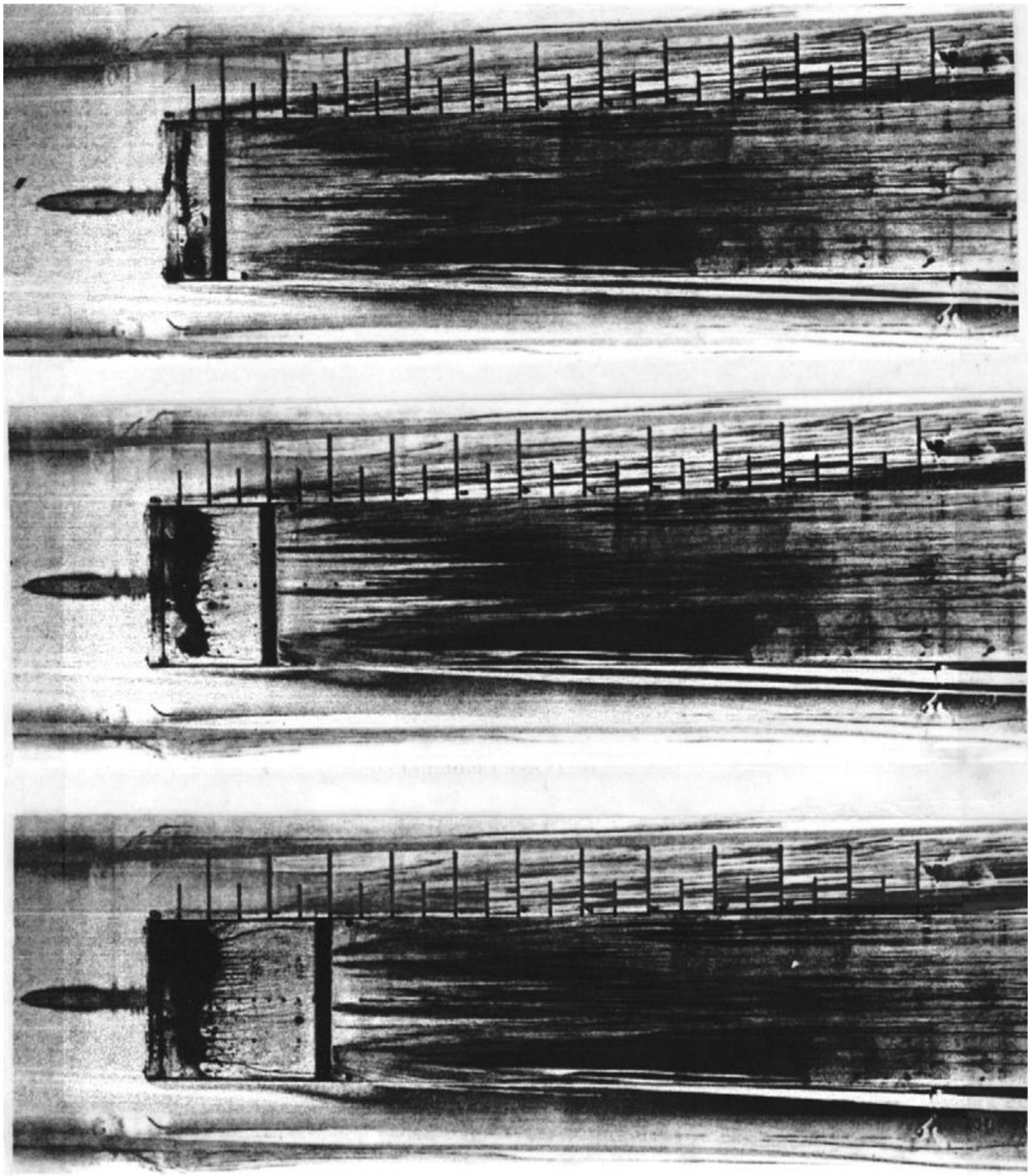

(a) l/h = 2.

(b) l/h = 4.

(c) l/h = 6.

Figure C-3. Surface water flow-visualization photographs for the rectangular cavity, $\psi = 0°$, $M_\infty = 06$.

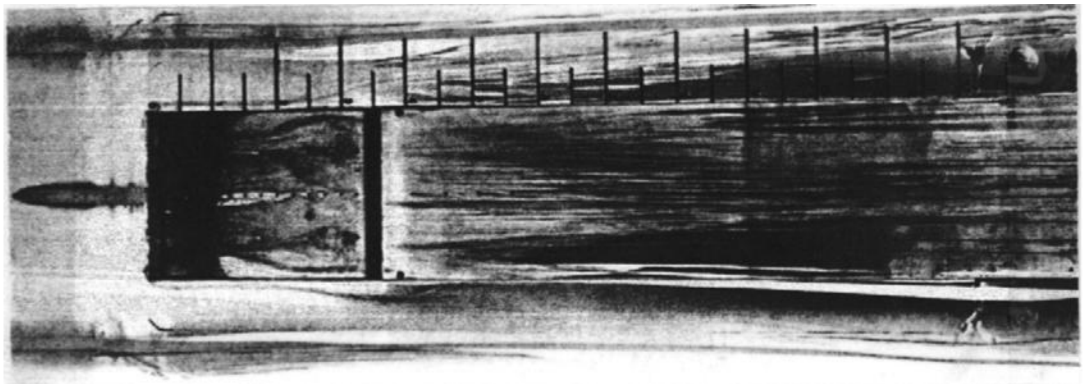

(d) l/h = 7.

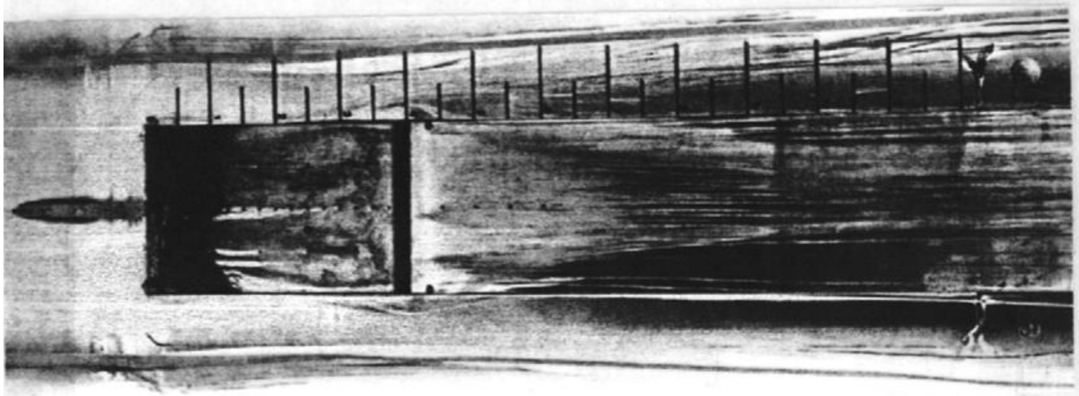

(e) l/h = 8.

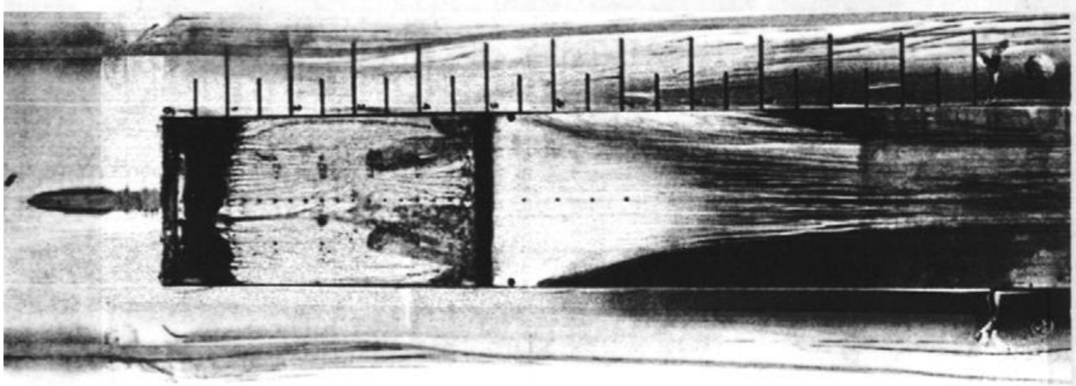

(f) l/h = 10.

Figure C-3. Continued.

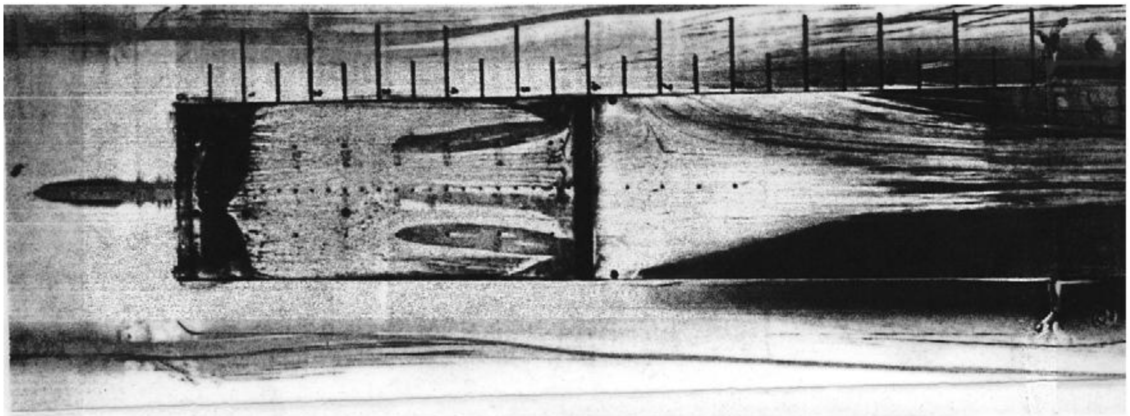

(g) $l/h = 12$.

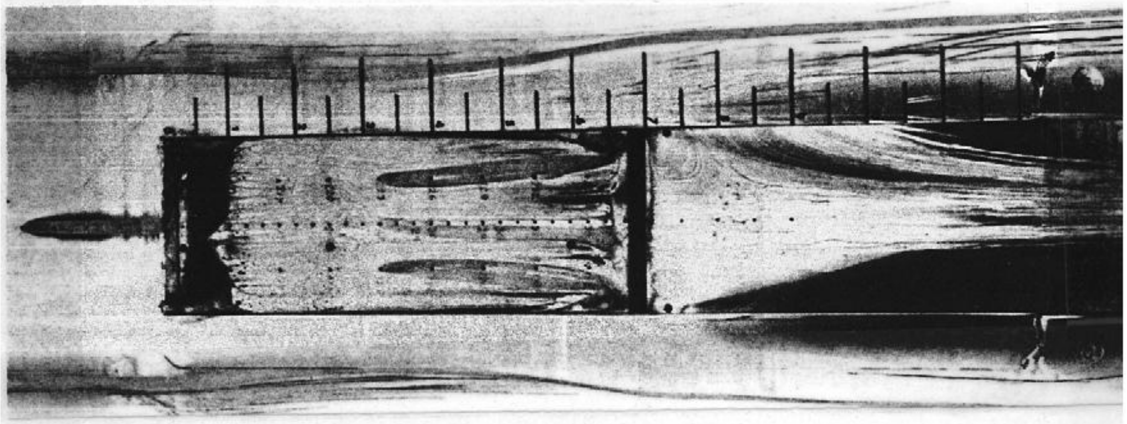

(h) $l/h = 14$.

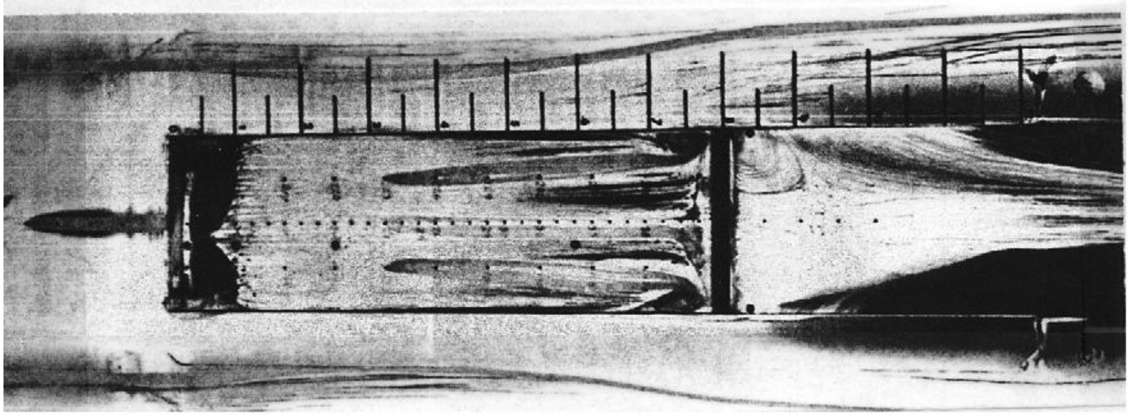

(i) $l/h = 16$.

Figure C-3. Continued.

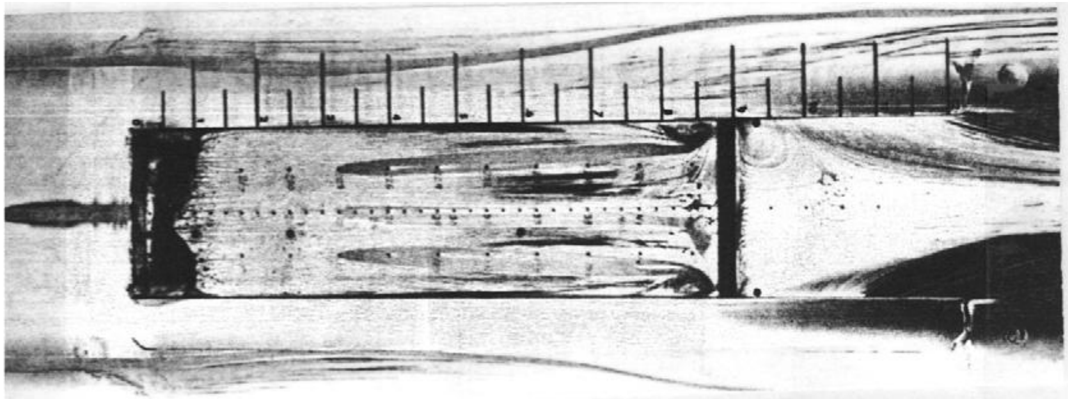

(j) l/h = 18.

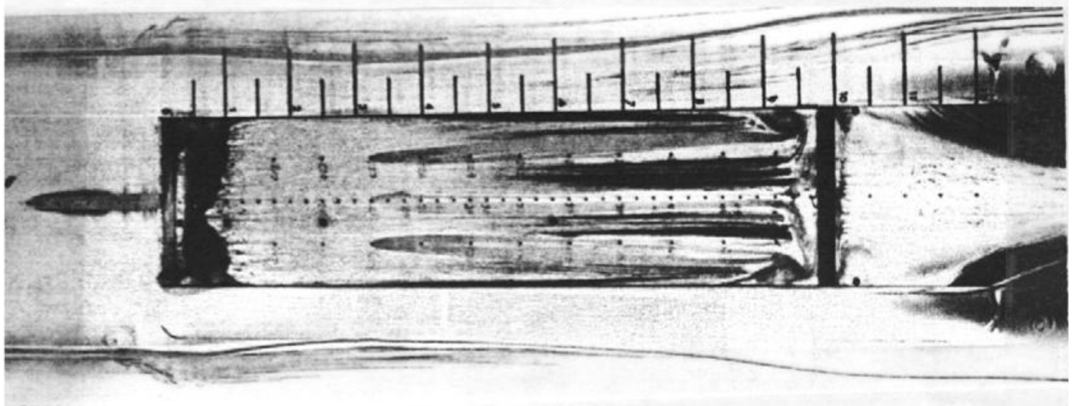

(k) l/h = 20.

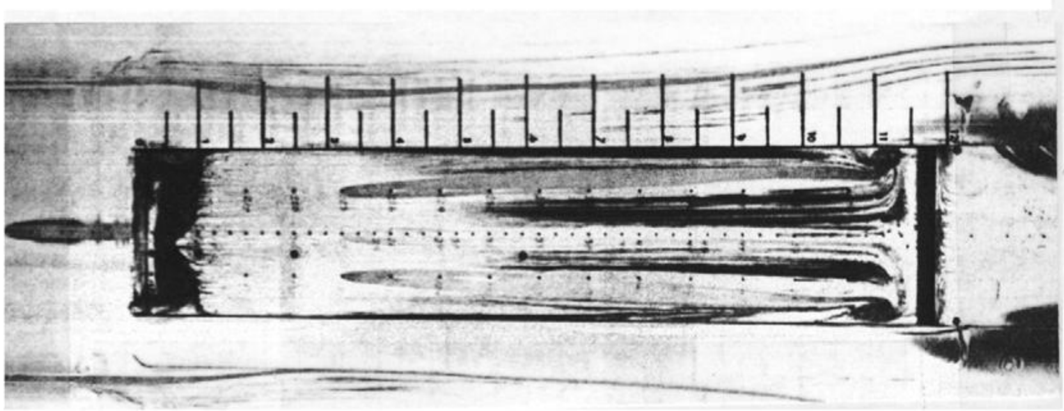

(l) l/h = 24.

Figure C-3. Concluded.

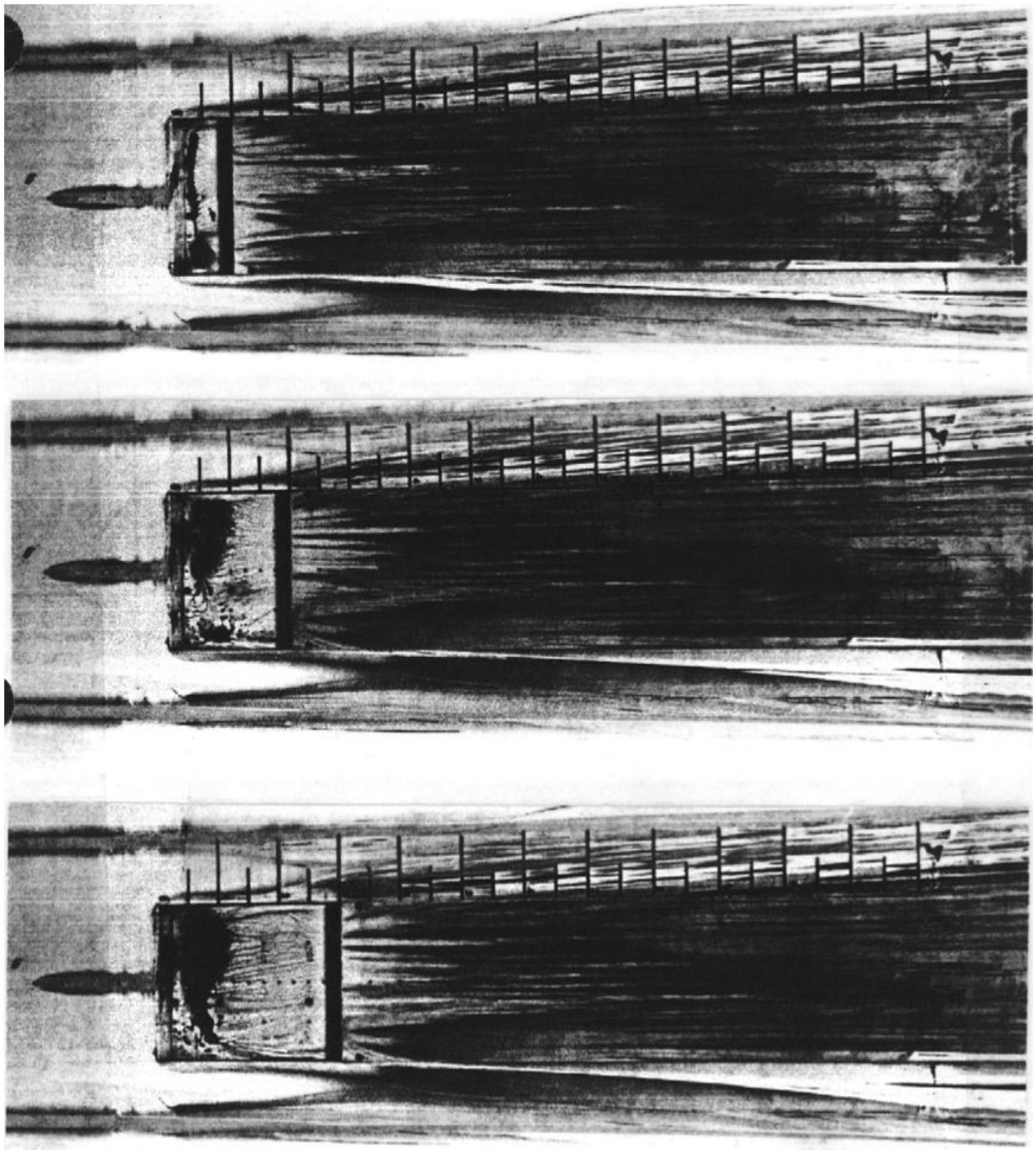

(a) l/h = 2.

(b) l/h = 4.

(c) l/h = 6.

Figure C-4. Surface water flow-visualization photographs for the rectangular cavity, $\psi = 0°$, $M_\infty = 0.8$.

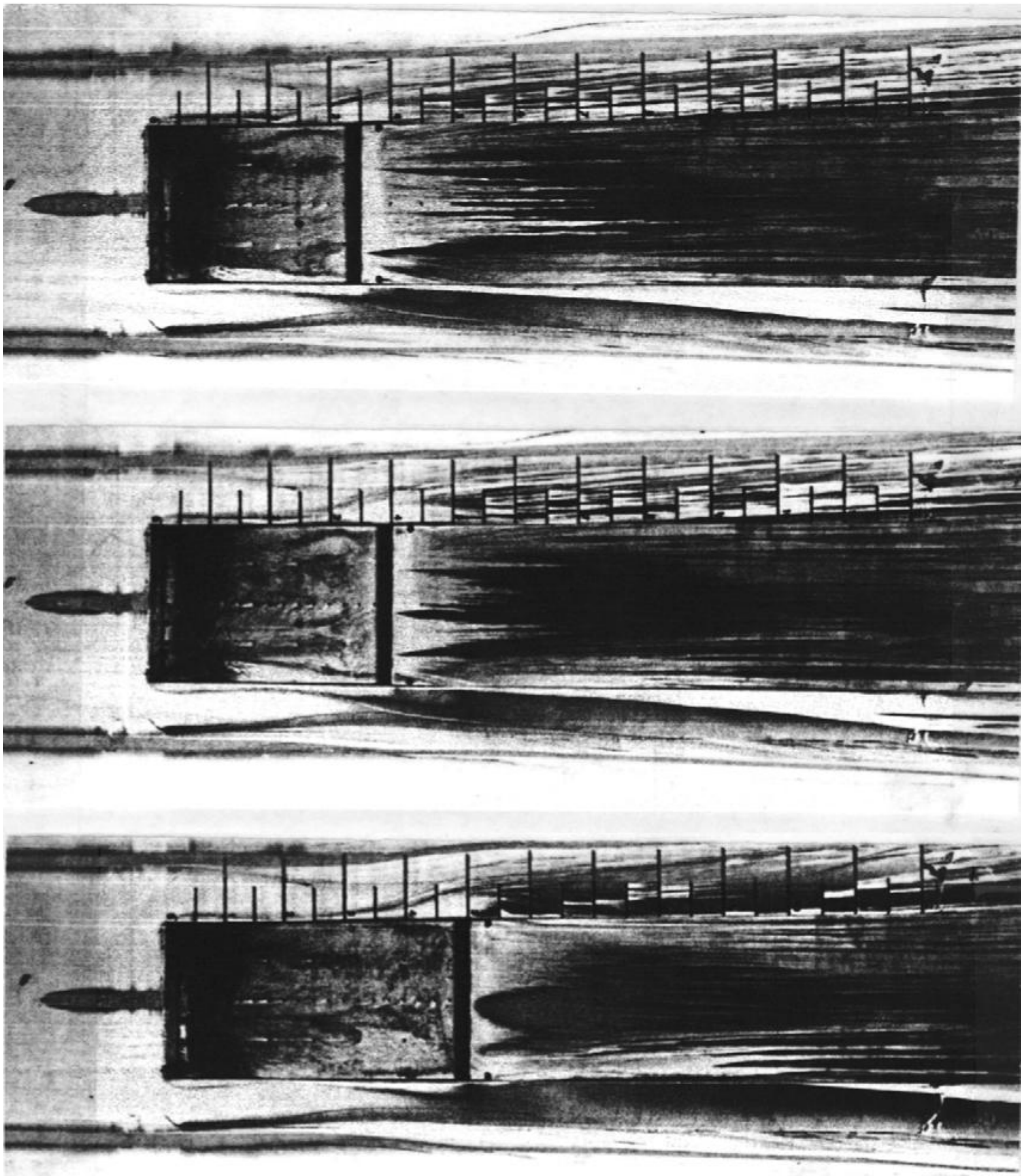

(d) l/h = 7.

(e) l/h = 8.

(f) l/h = 10.

Figure C-4. Continued.

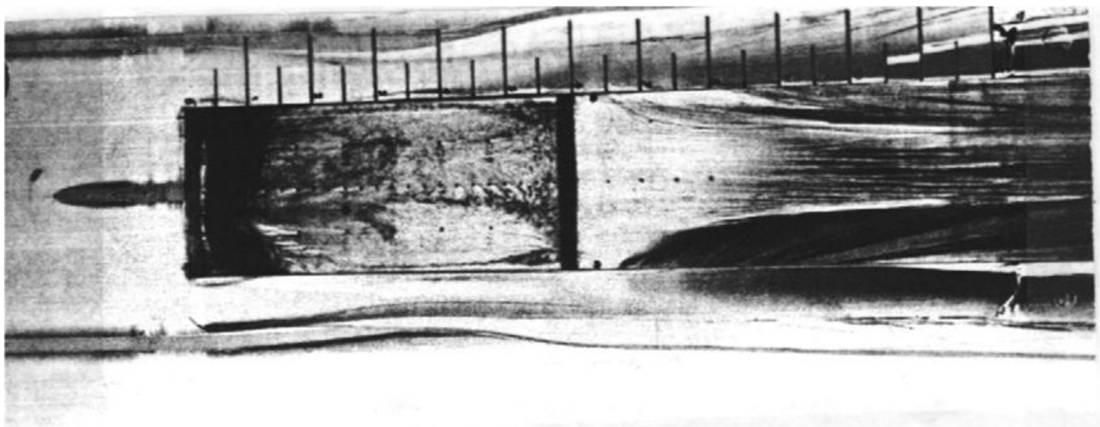

(g) l/h = 12.

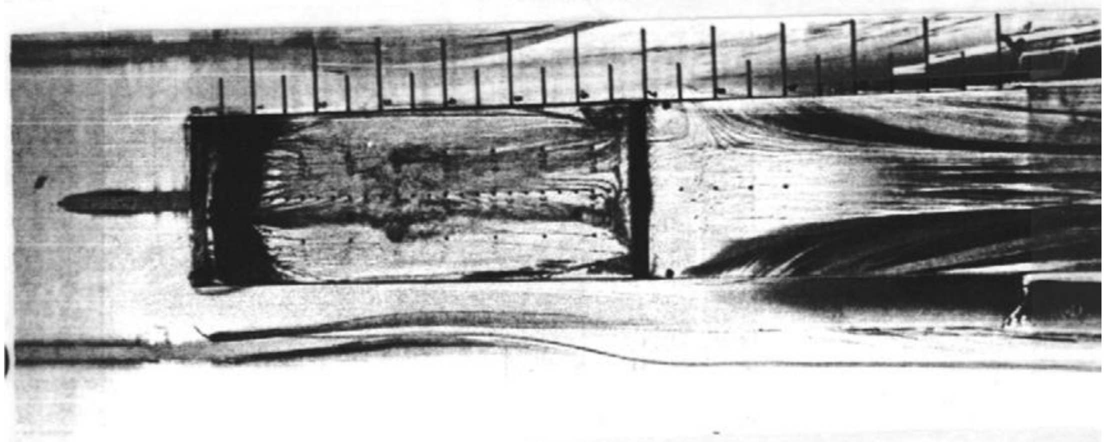

(h) l/h = 14.

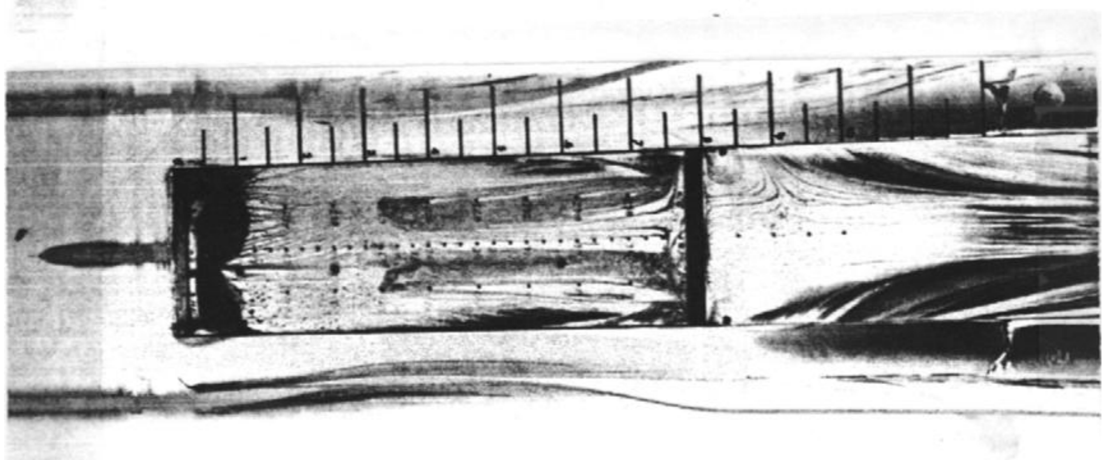

(i) l/h = 16.

Figure C-4. Continued.

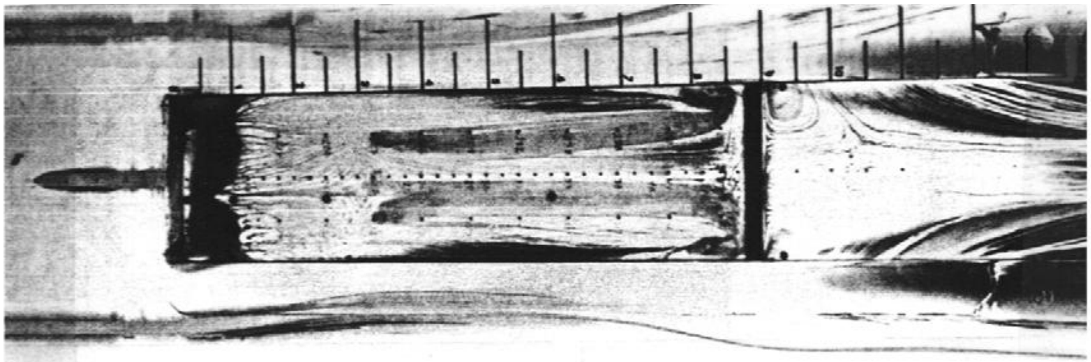

(j) l/h = 18.

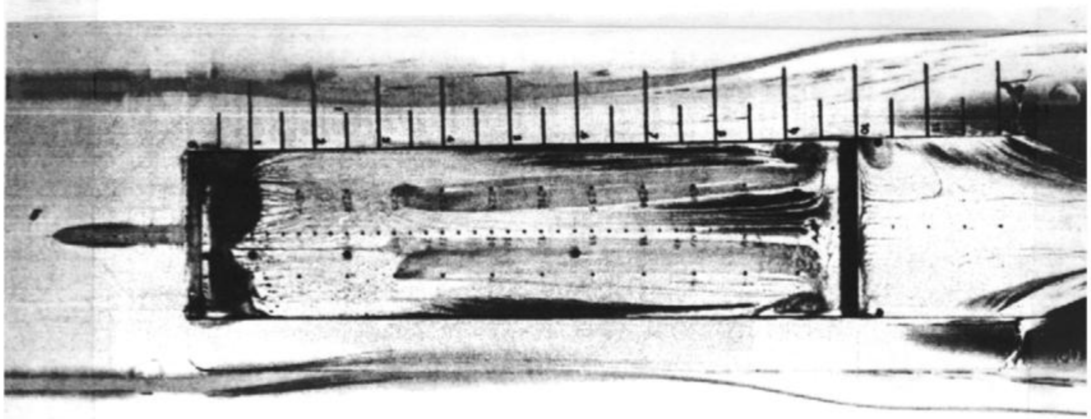

(k) l/h = 20.

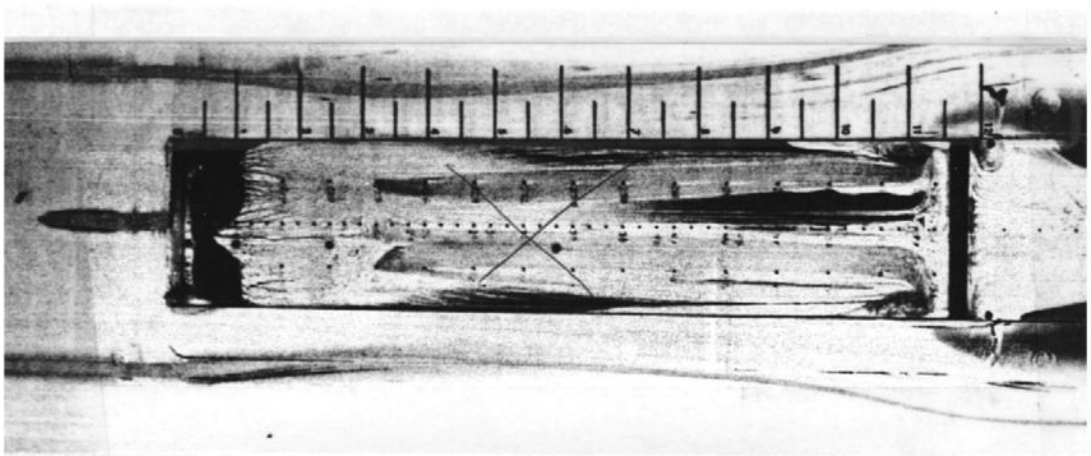

(l) l/h = 24.

Figure C-4. Concluded.

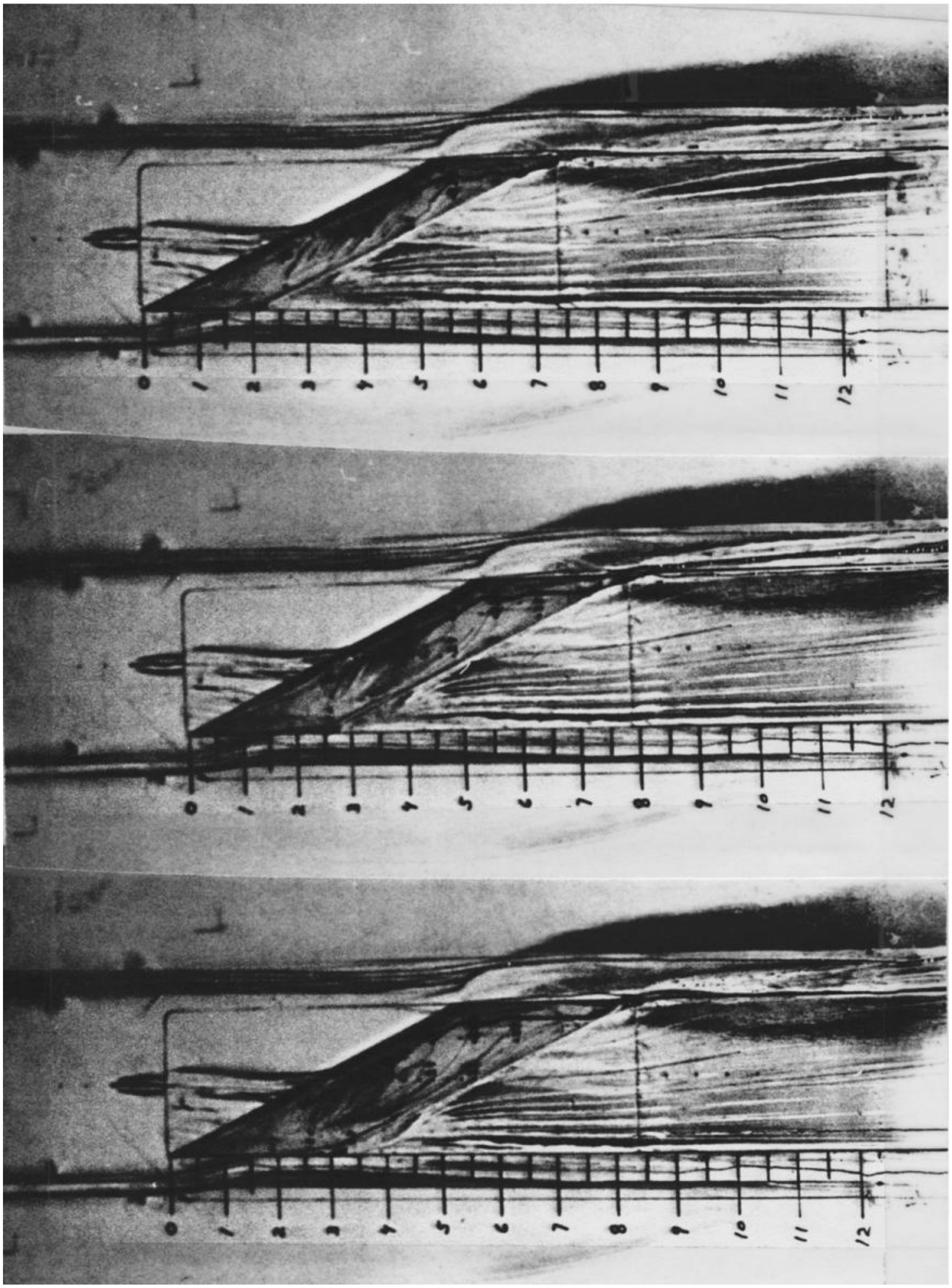

(a) $l/h = 4$.

(b) $l/h = 5$.

(c) $l/h = 6$.

Figure C-5. Surface water flow-visualization photographs for $\psi = 65°$ (configuration 1), $M = 0.2$.

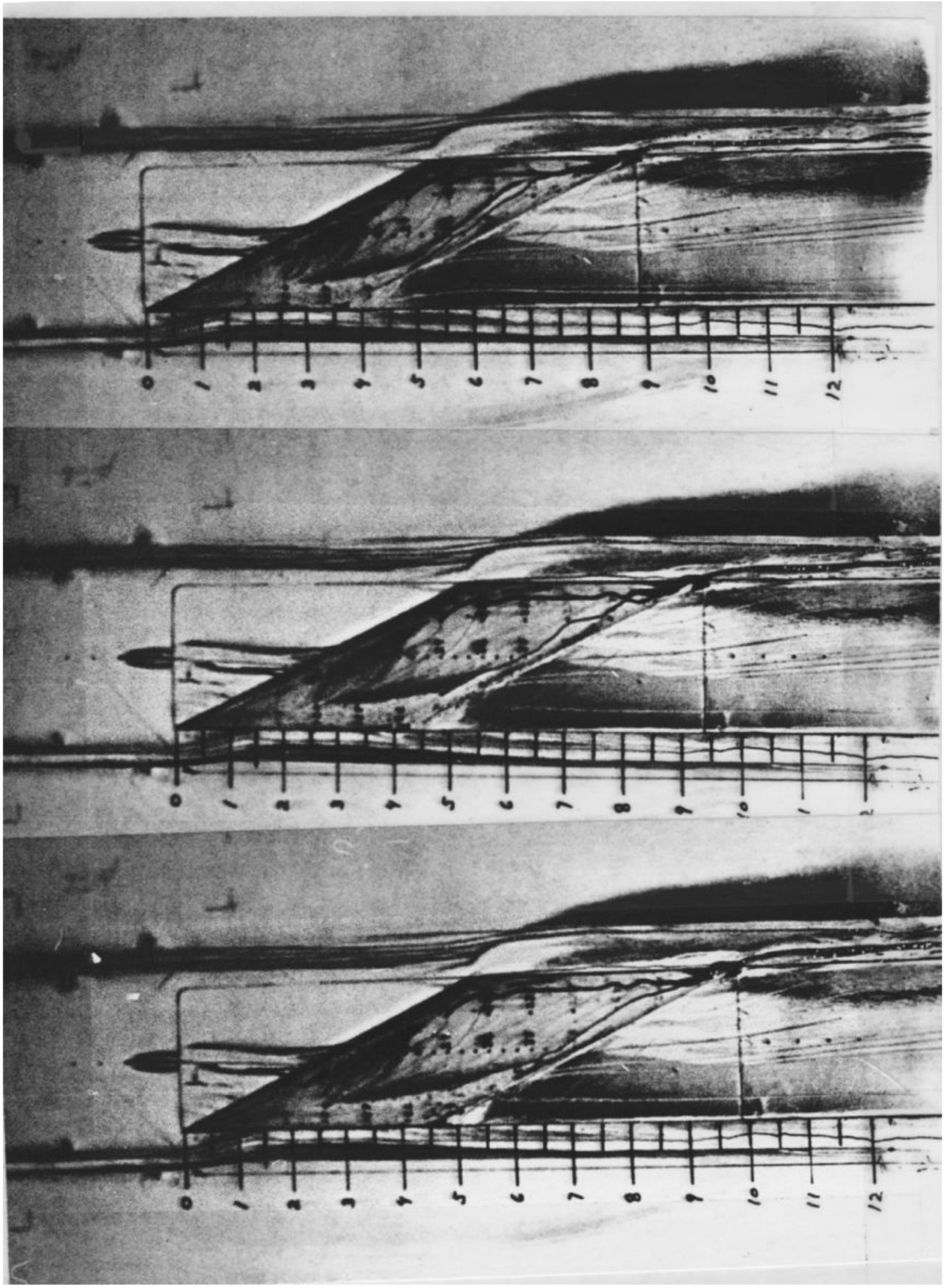

(d) $l/h = 7$.

(e) $l/h = 8$.

(f) $l/h = 9$.

Figure C-5. Continued.

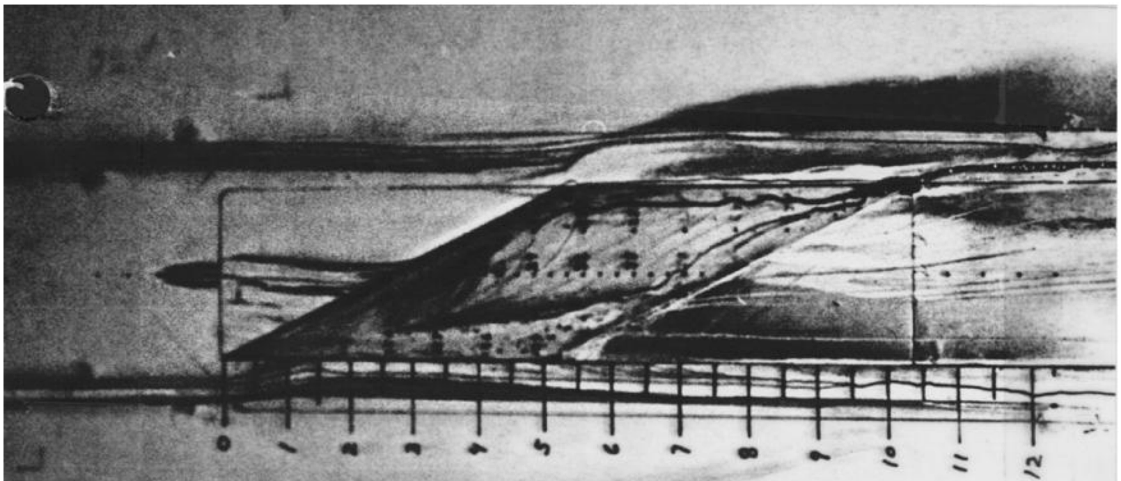

(g) $l/h = 10$.

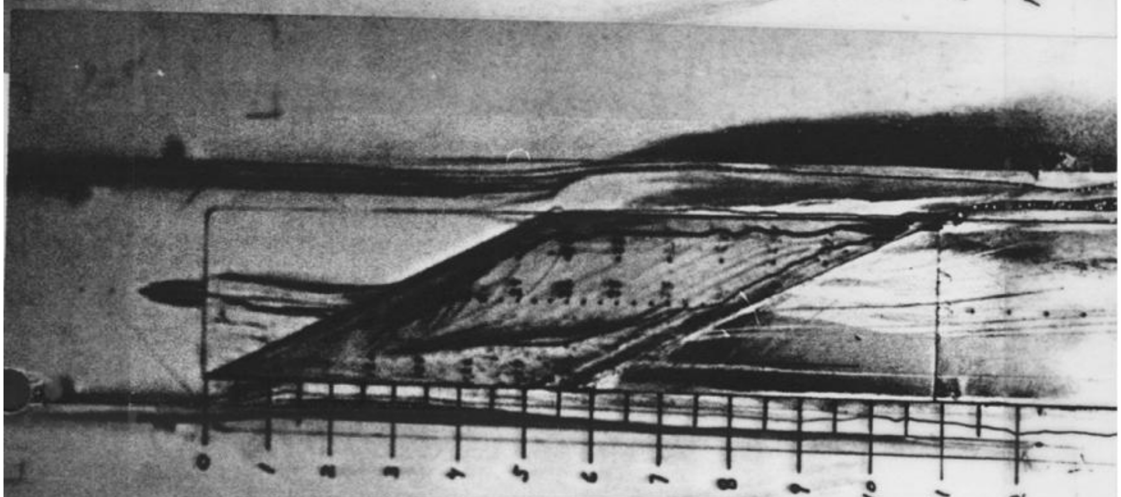

(h) $l/h = 11$.

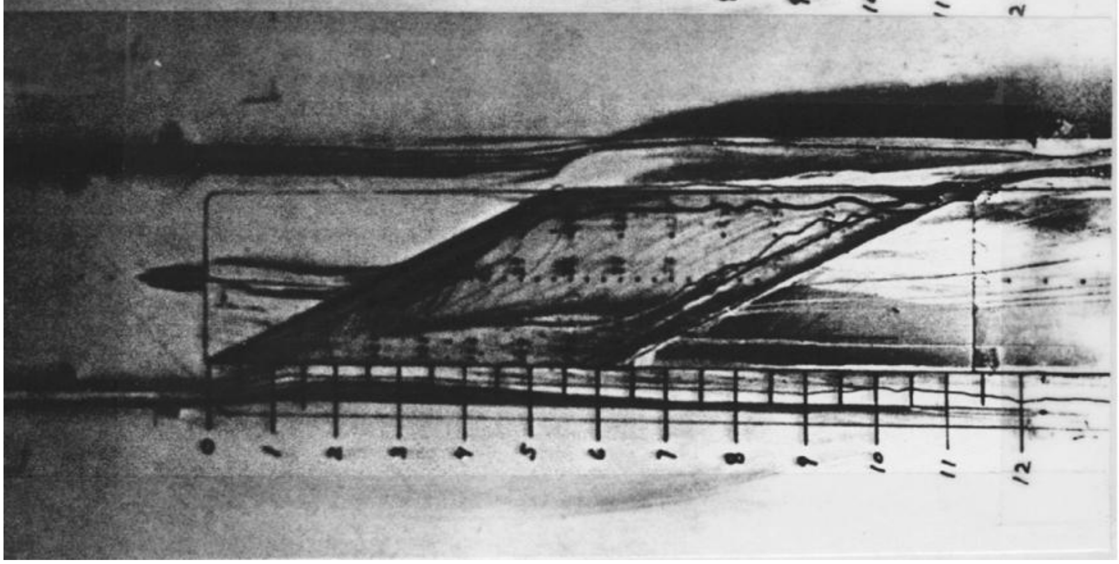

(i) $l/h = 12$.

Figure C-5. Continued.

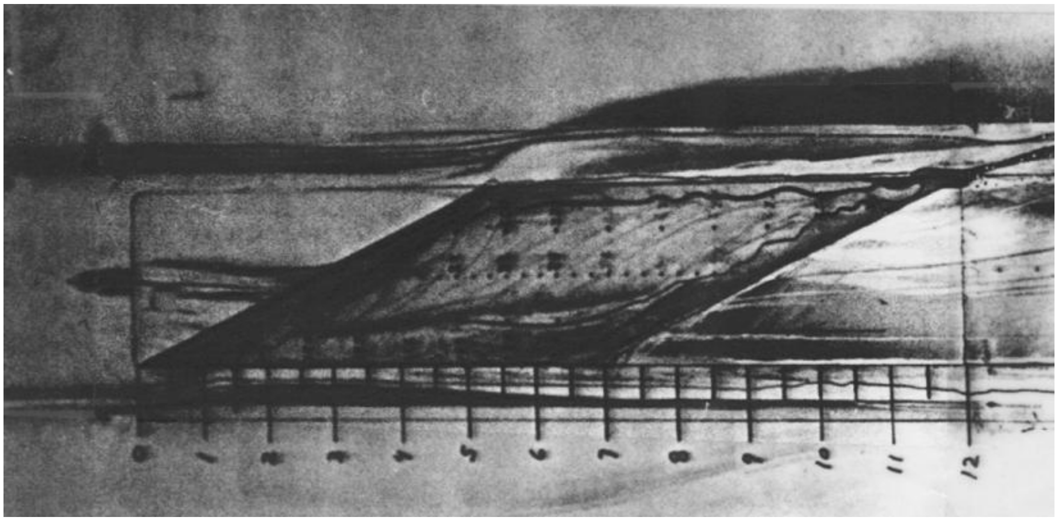

(j) l/h = 13.

Figure C-5. Concluded.

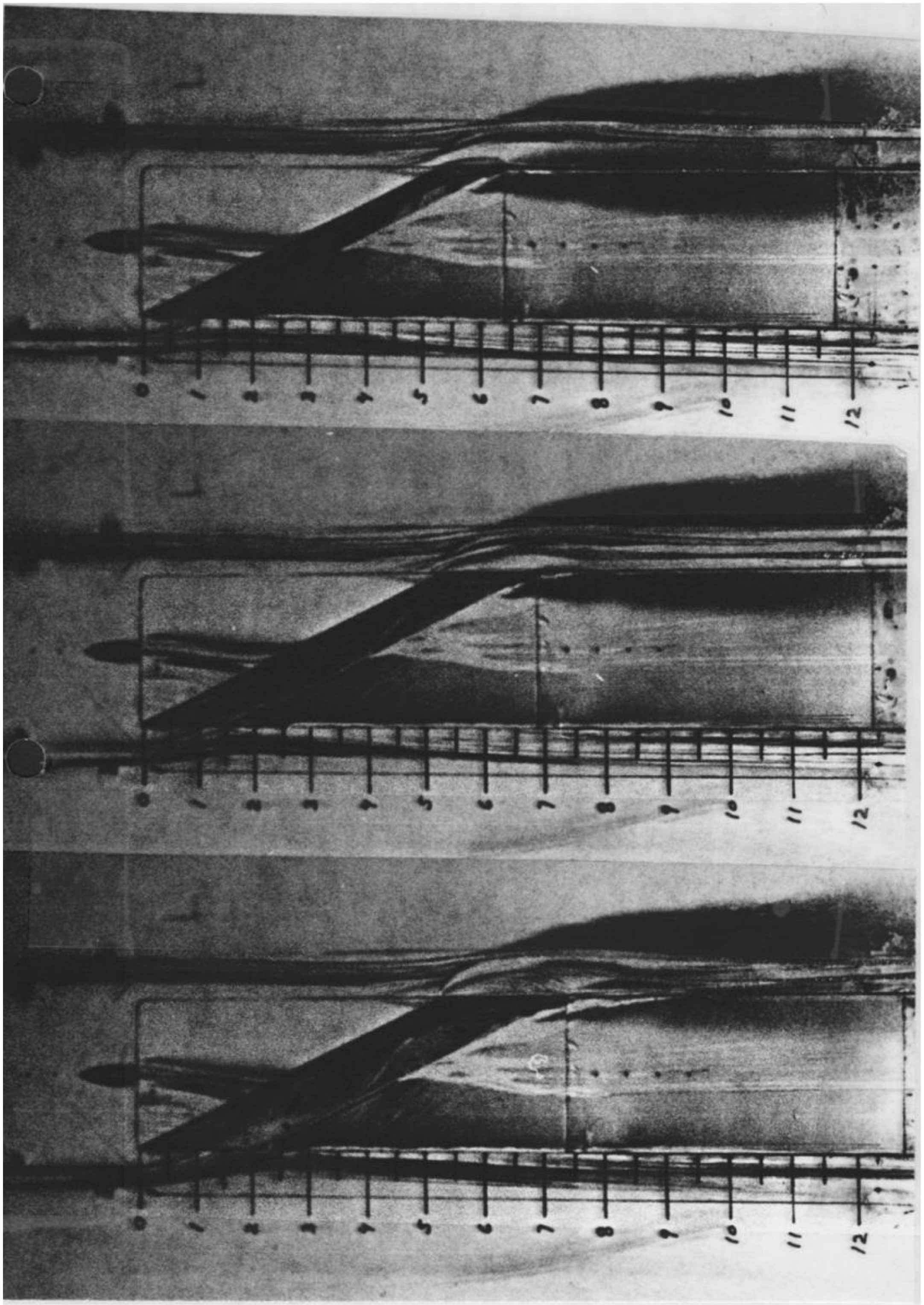

(a) l/h = 2.

(b) l/h = 3.

(c) l/h = 4.

Figure C-6. Surface water flow-visualization photographs for ψ = 65° (configuration 1), M = 0.4.

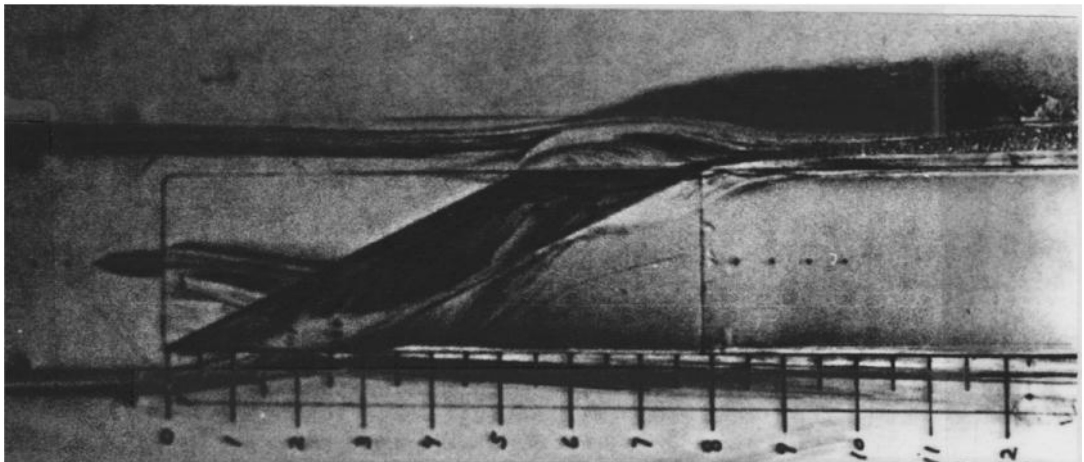

(d) l/h = 5.

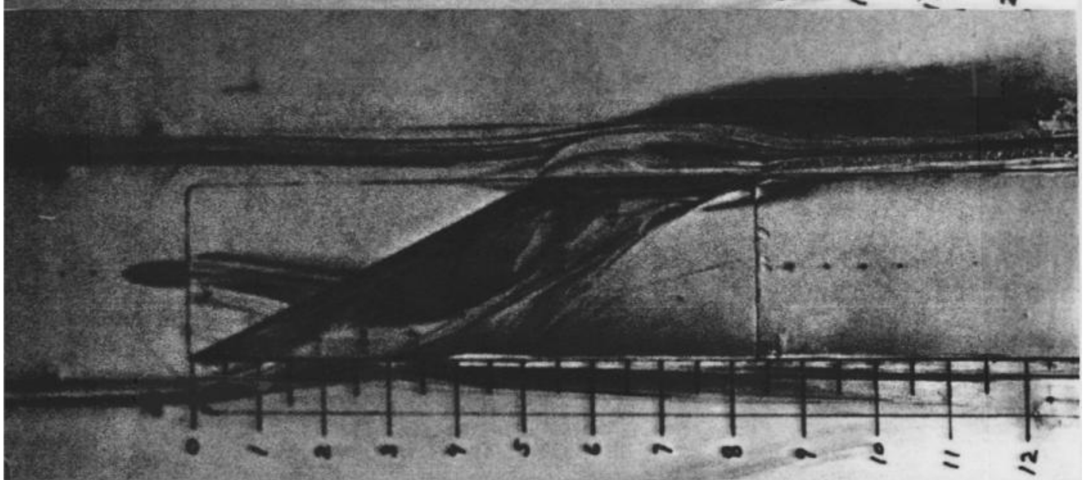

(e) l/h = 6.

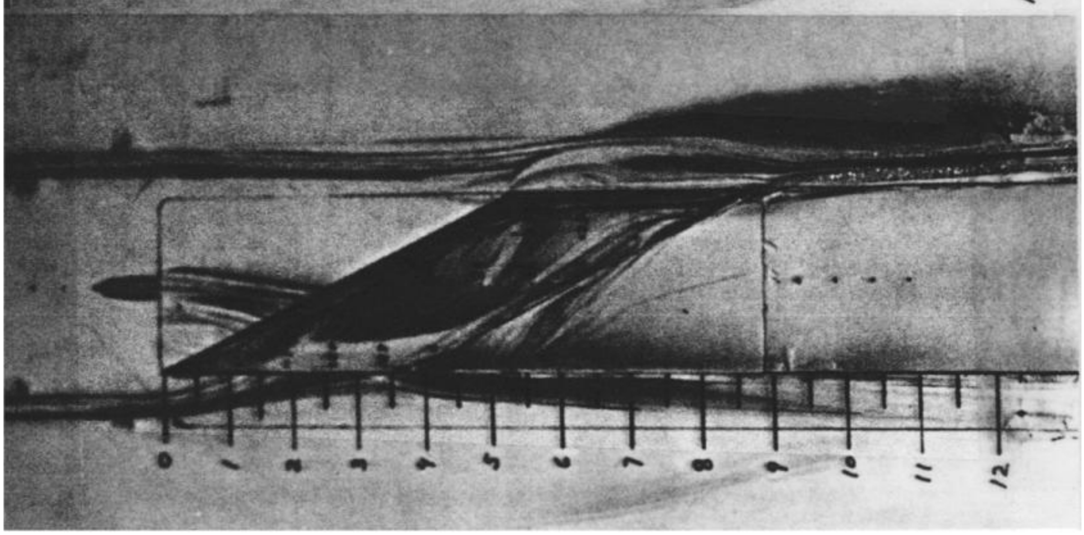

(f) l/h = 7.

Figure C-6. Continued.

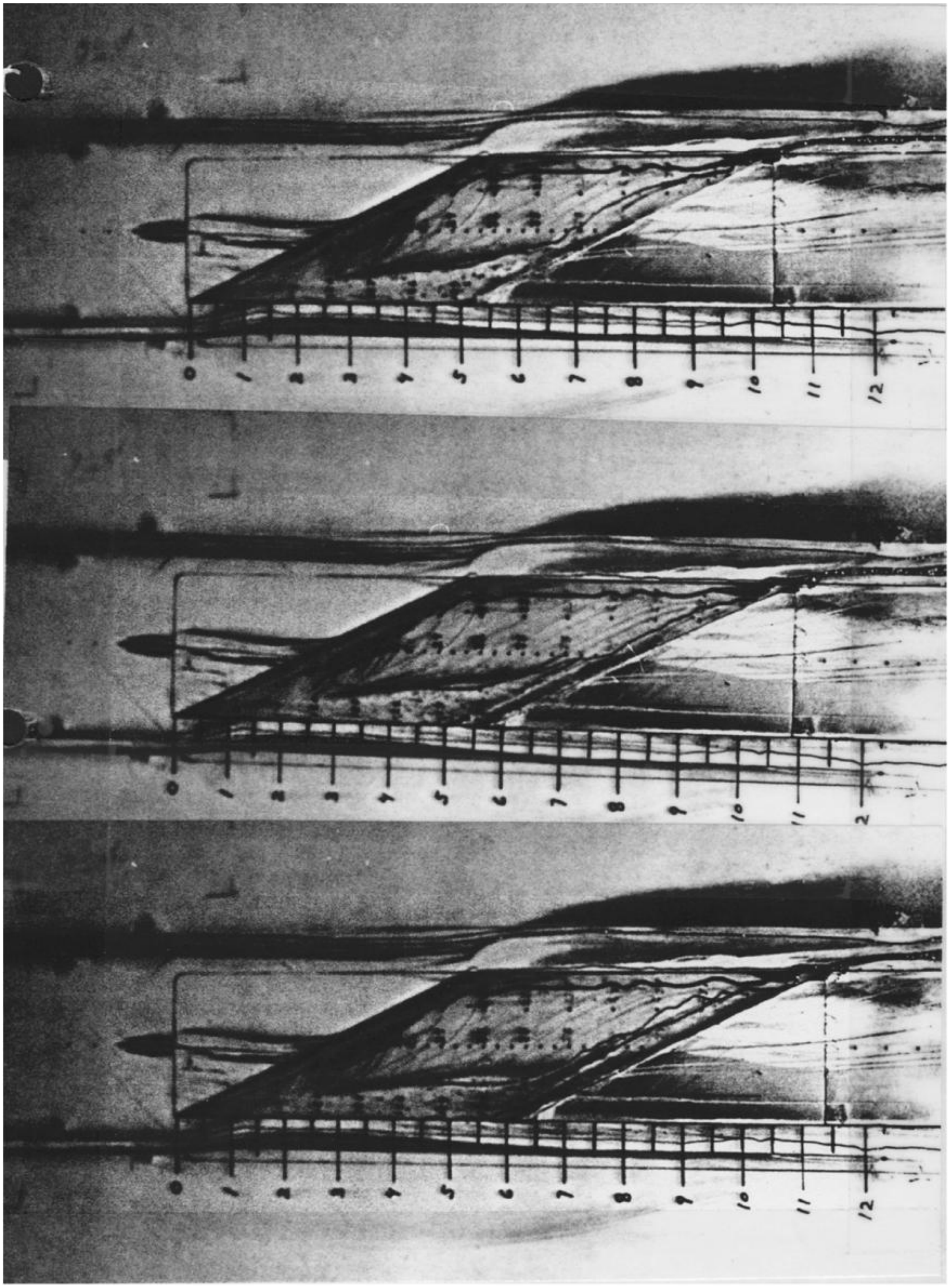

(g) l/h = 8.

(h) l/h = 9.

(i) l/h = 10.

Figure C-6. Concluded.

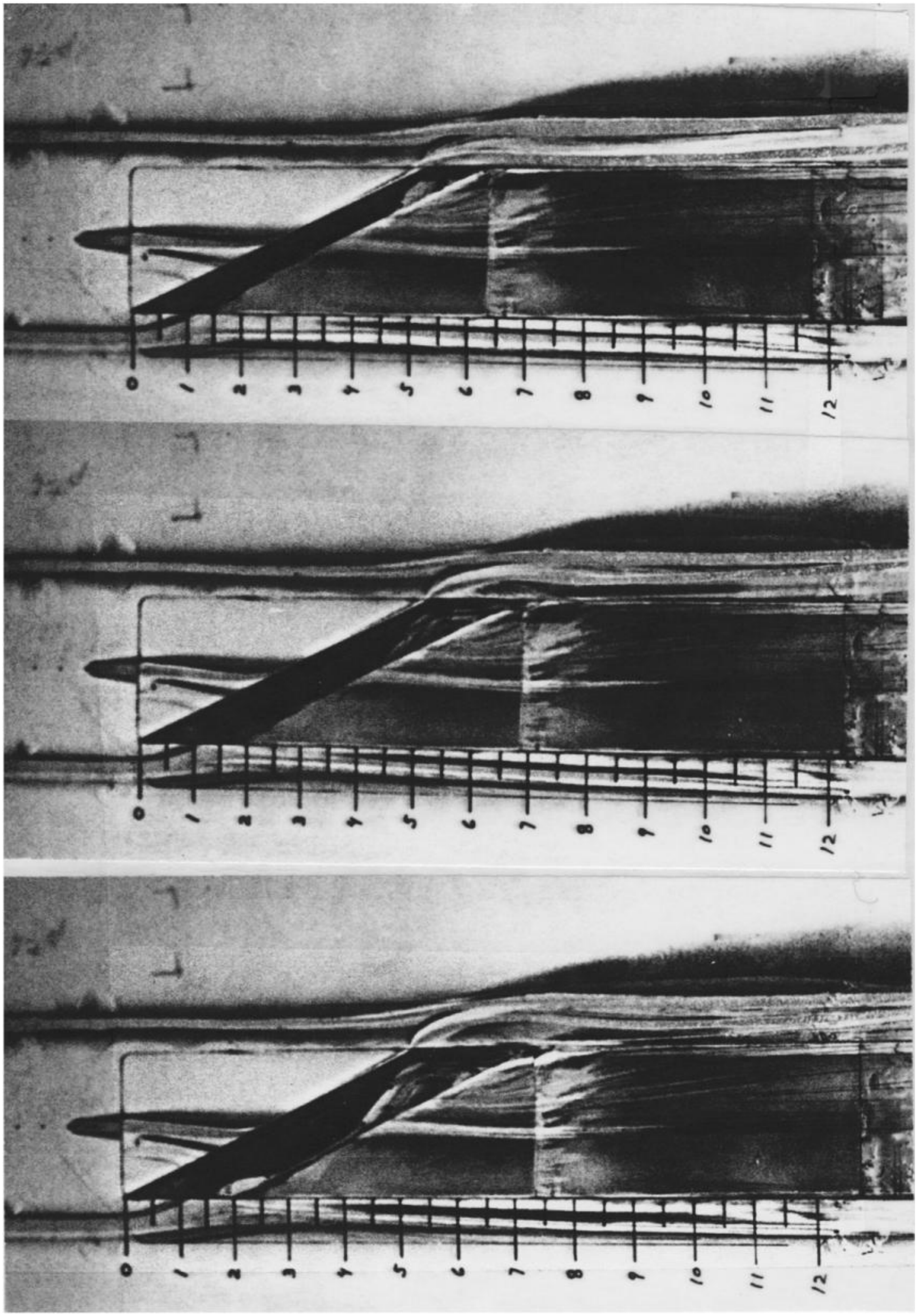

(a) $l/h = 2$.

(b) $l/h = 3$.

(c) $l/h = 4$.

Figure C-7. Surface water flow-visualization photographs for $\psi = 65°$ (configuration 1), $M = 0.6$.

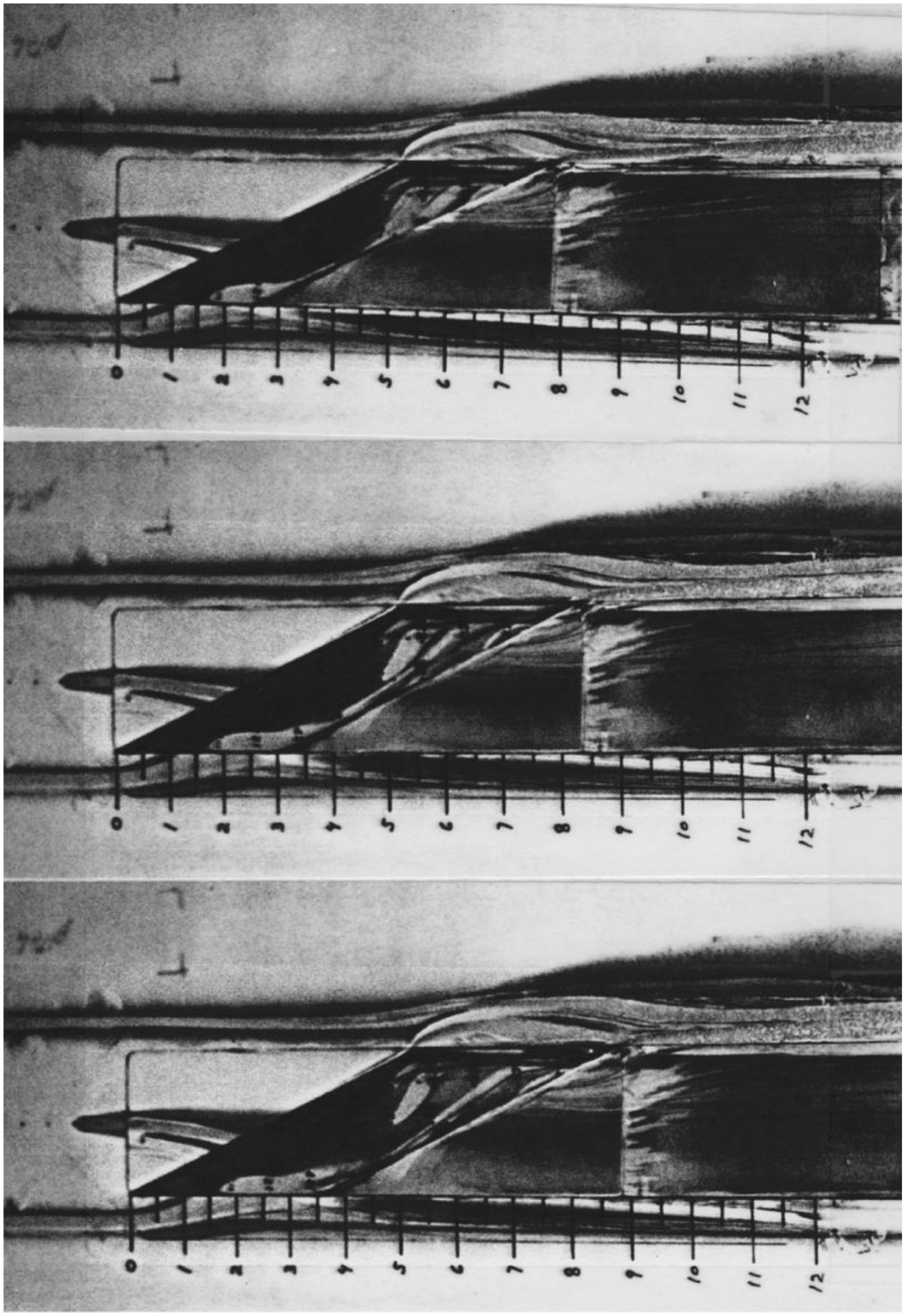

(d) $l/h = 5$.

(e) $l/h = 6$.

(f) $l/h = 7$.

Figure C-7. Continued.

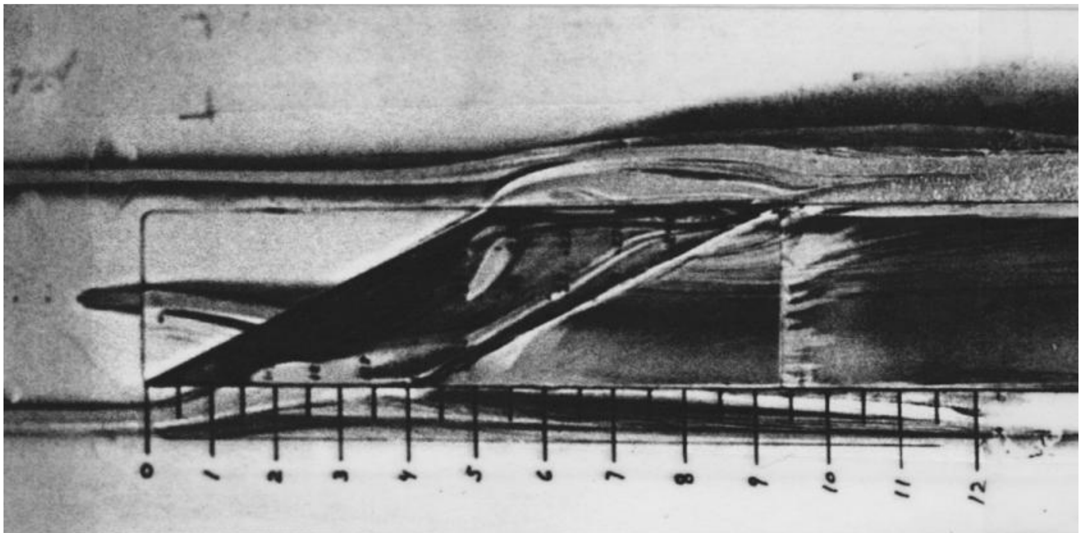

(g) l/h = 8.

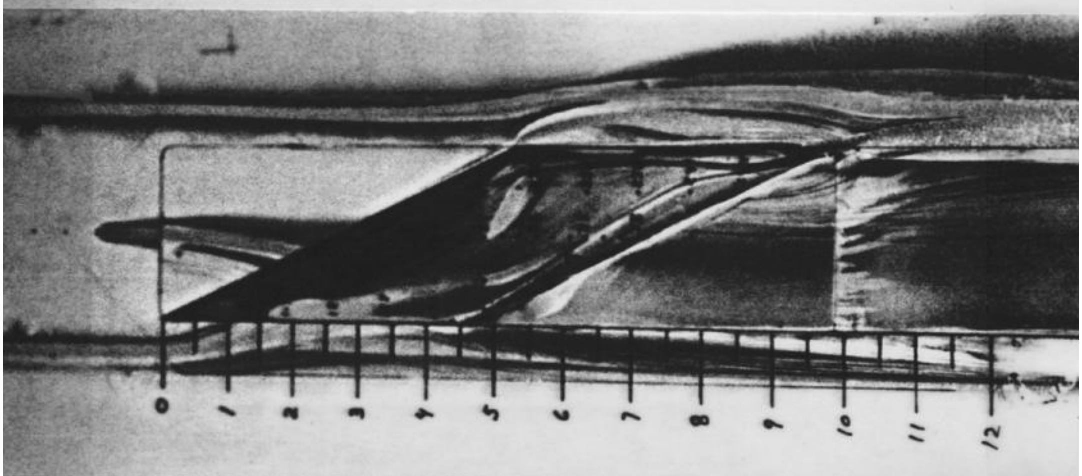

(h) l/h = 9.

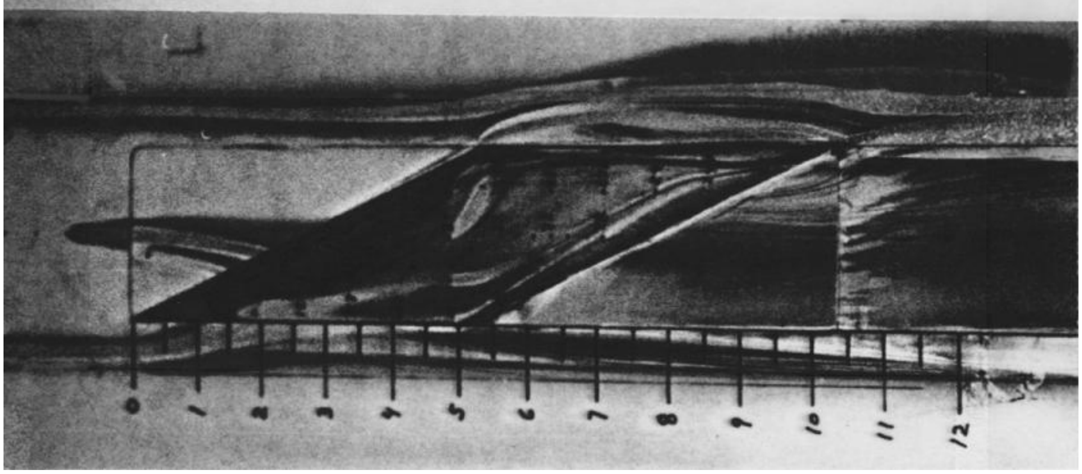

(i) l/h = 10.

Figure C-7. Continued.

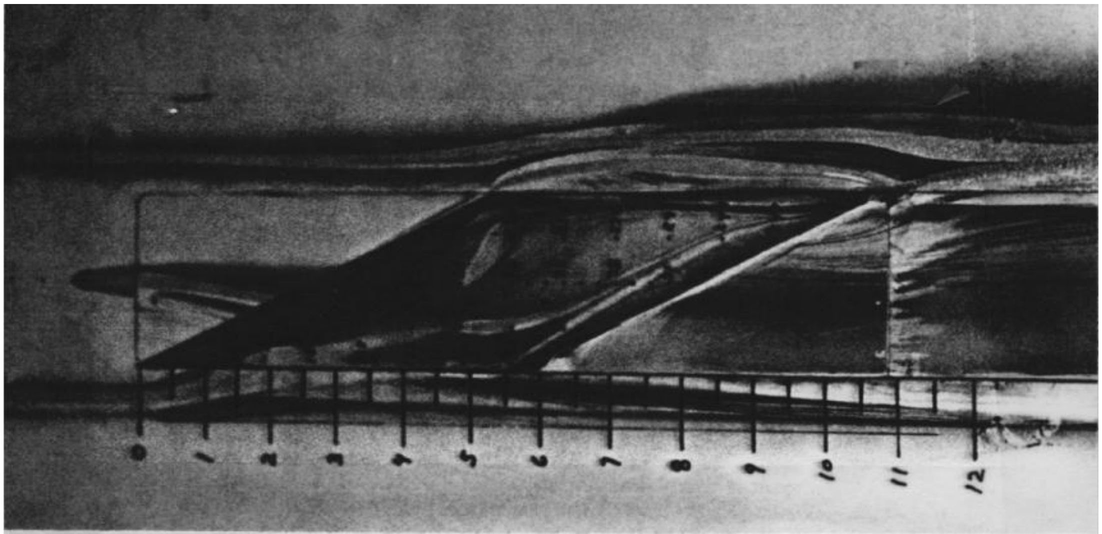

(j) $l/h = 11$.

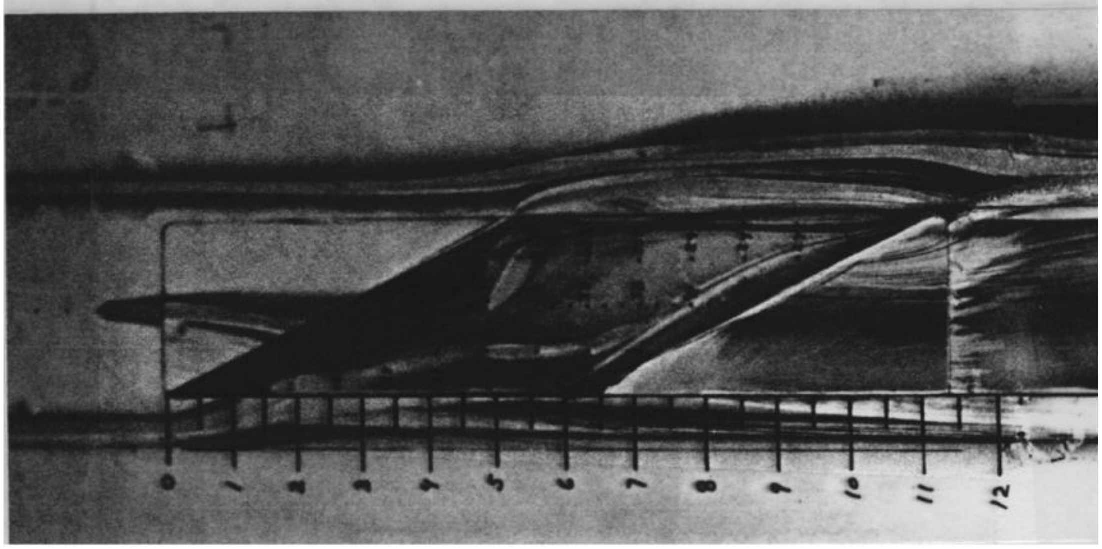

(k) $l/h = 12$.

Figure C-7. Concluded.

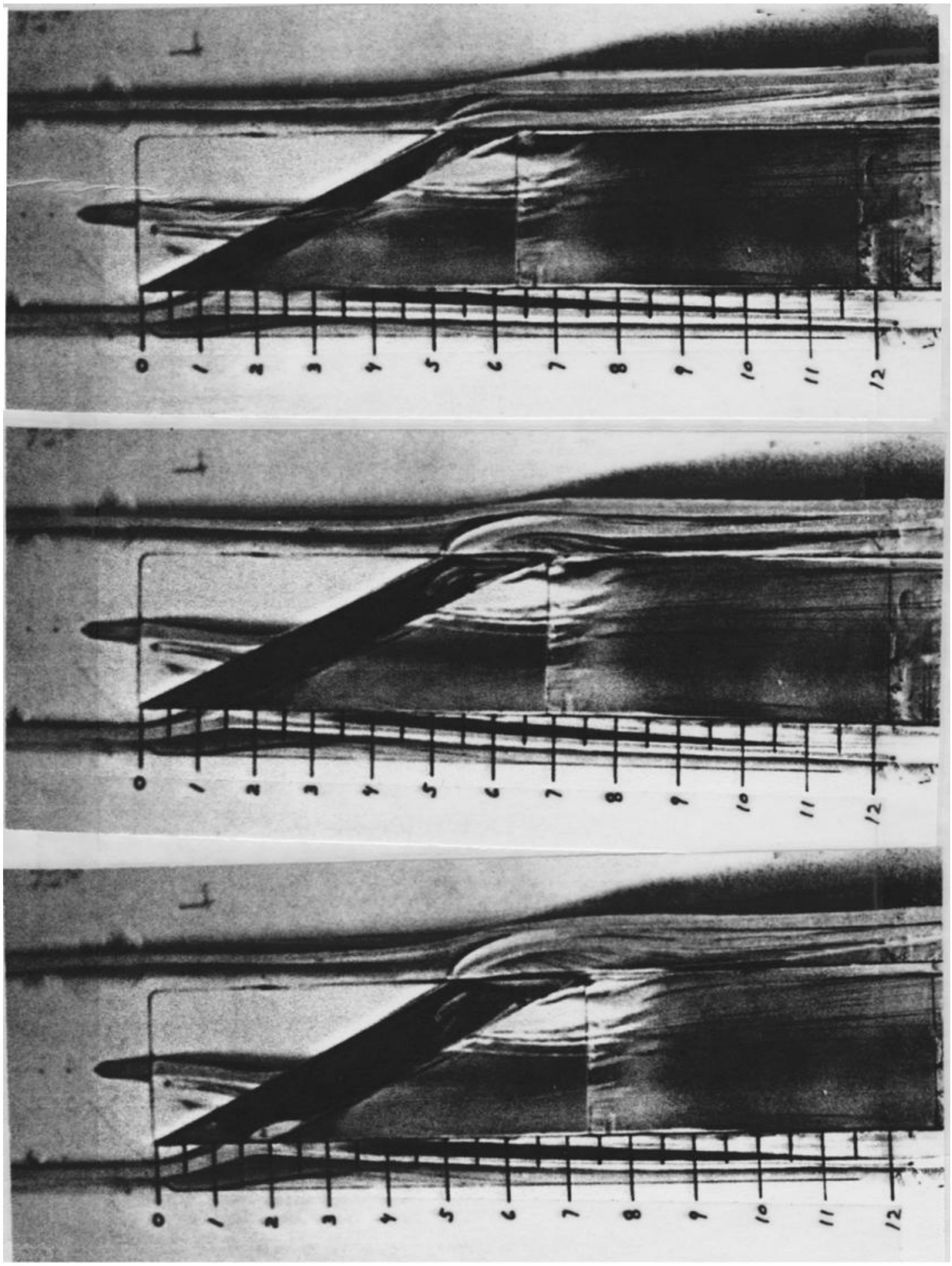

(a) l/h = 2.

(b) l/h = 3.

(c) l/h = 4.

Figure C-8. Surface water flow-visualization photographs for $\psi = 65°$ (configuration 1), $M = 0.8$.

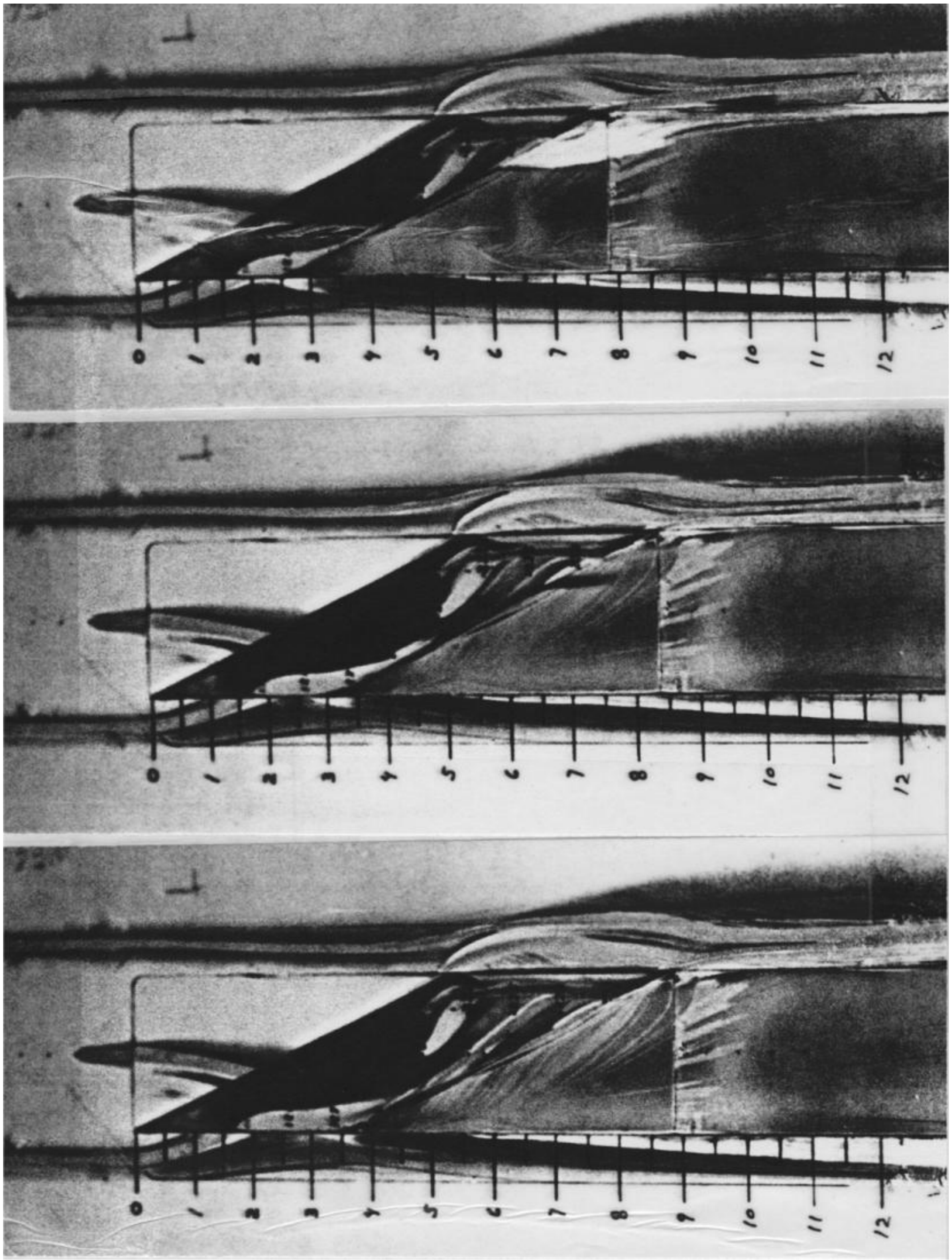

(d) l/h = 5.

(e) l/h = 6.

(f) l/h = 7.

Figure C-8. Continued.

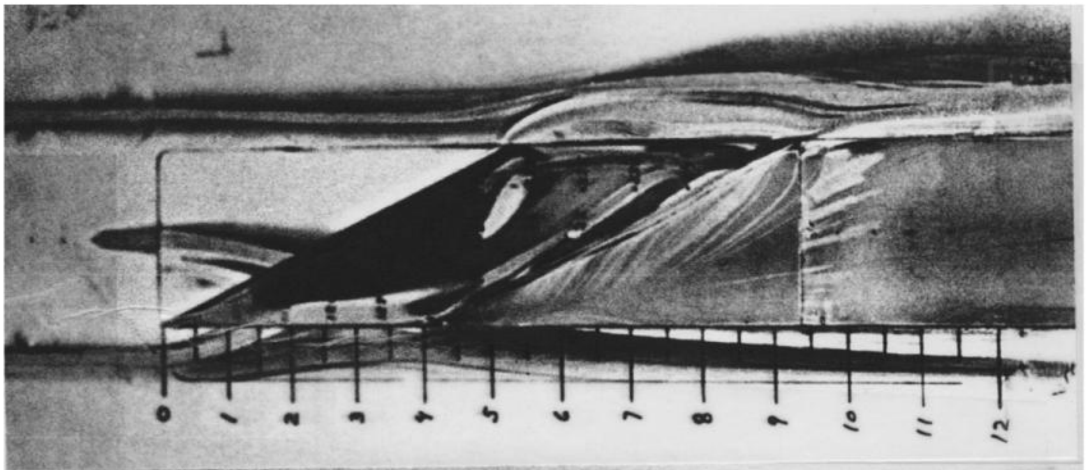

(g) l/h = 8.

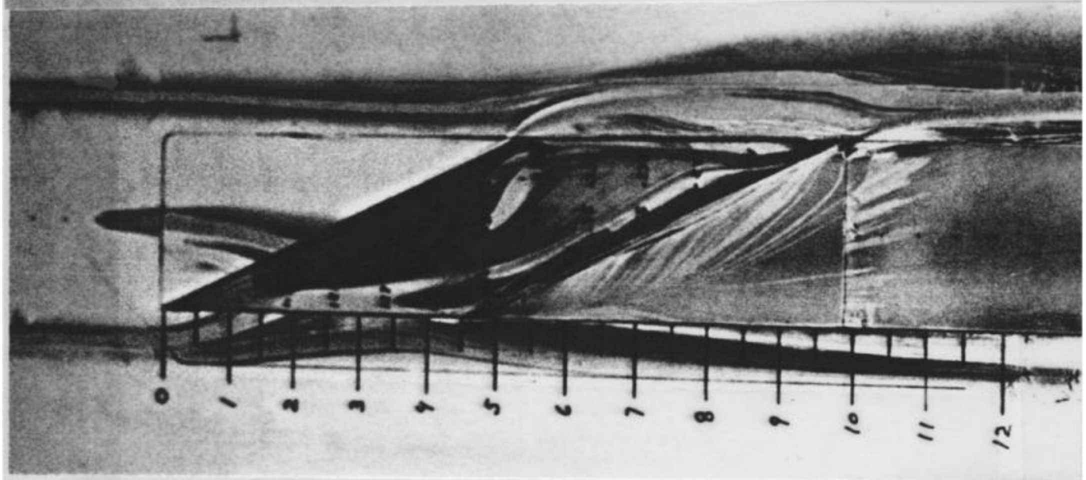

(h) l/h = 9.

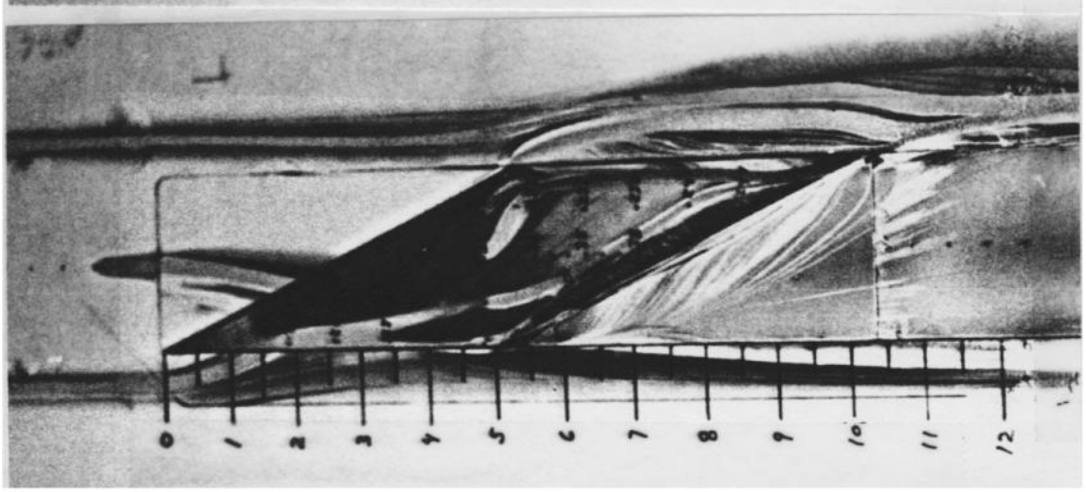

(i) l/h = 10.

Figure C-8. Continued.

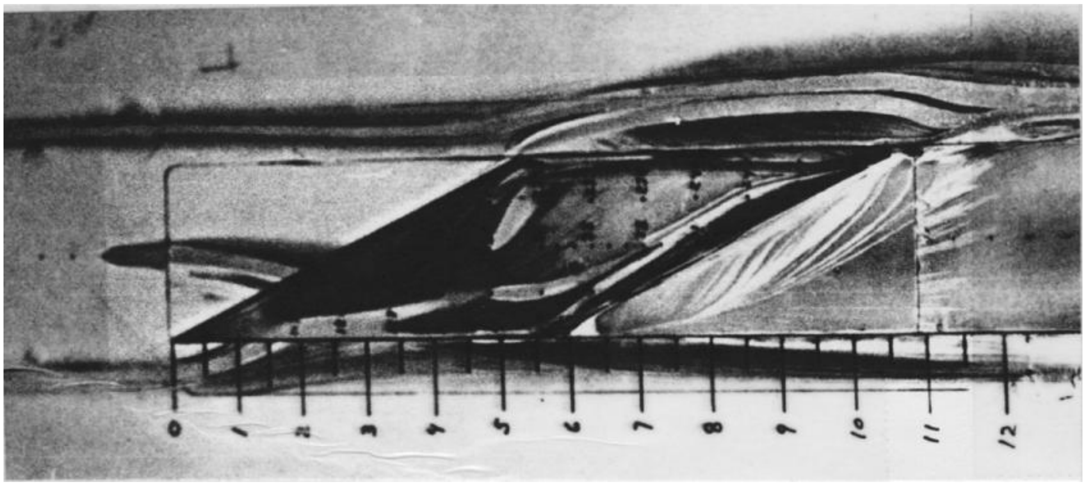

(j) l/h = 11.

Figure C-8. Concluded.

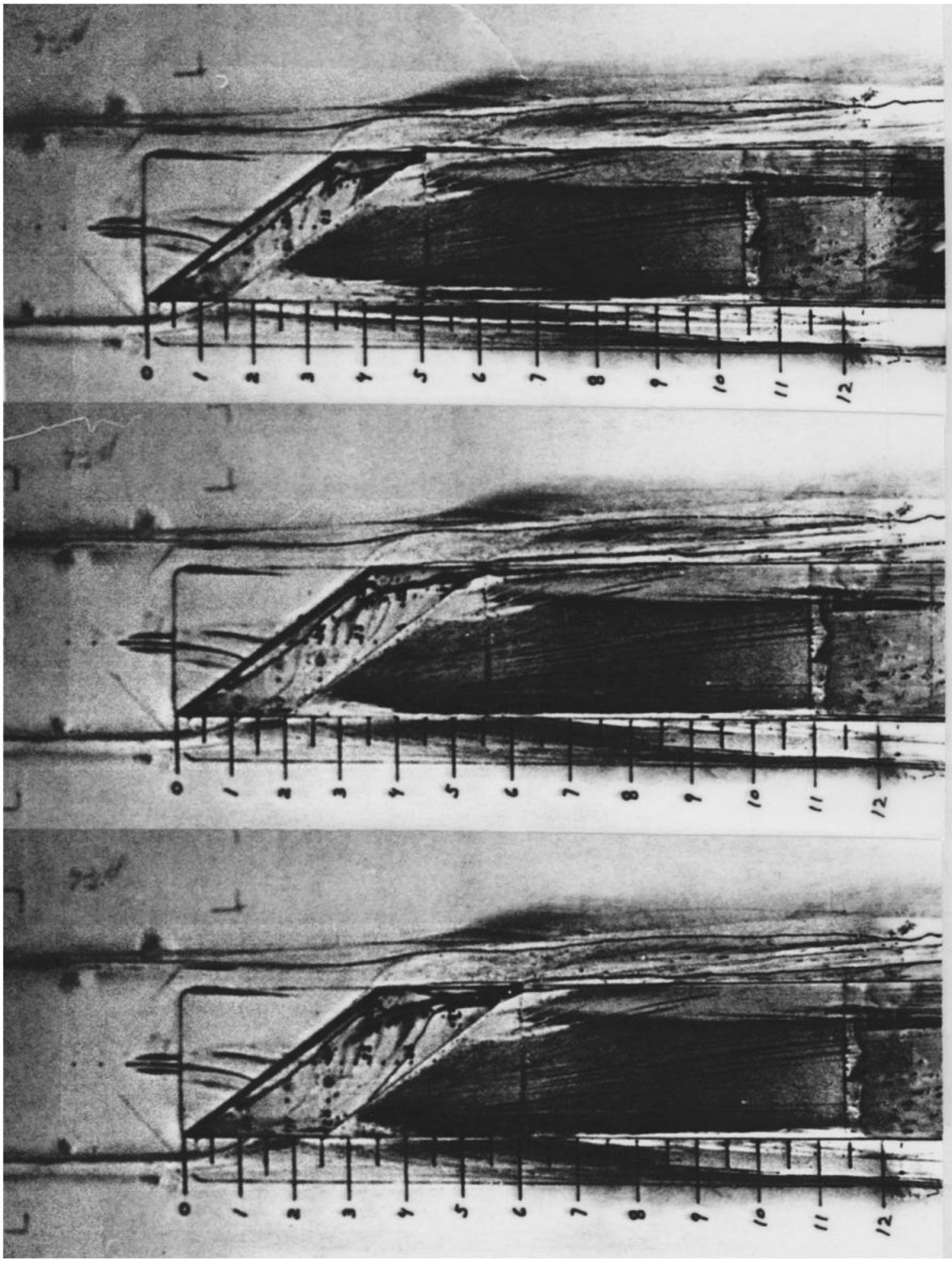

(a) l/h = 3.

(b) l/h = 4.

(c) l/h = 5.

Figure C-9. Surface water flow-visualization photographs for $\psi = 55°$ (configuration 2), $M = 0.2$.

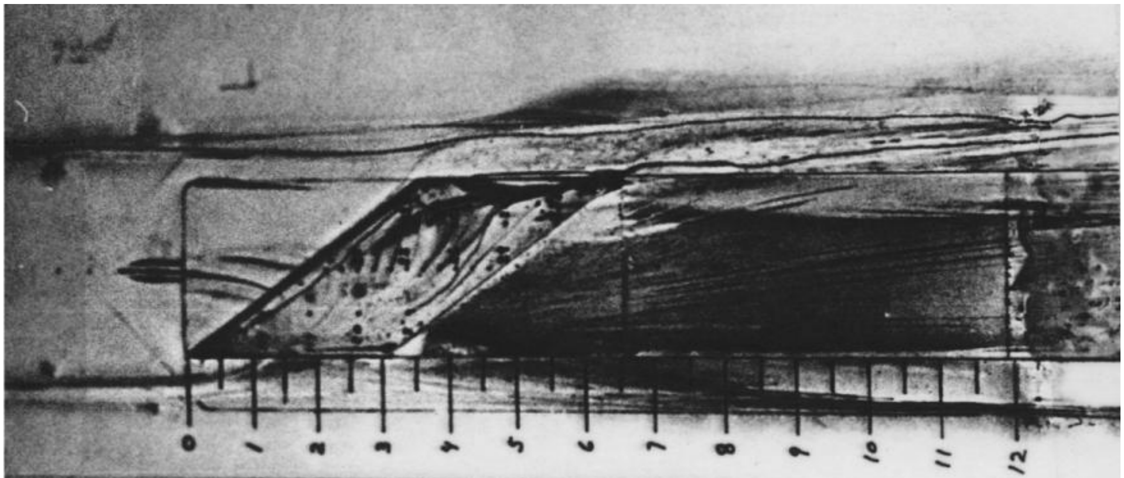

(d) $l/h = 6$.

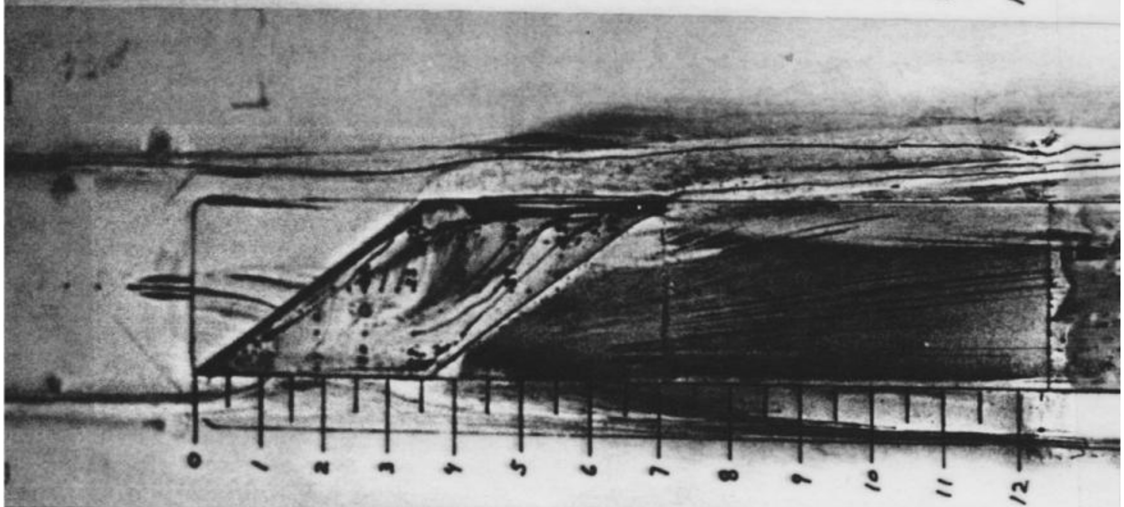

(e) $l/h = 7$.

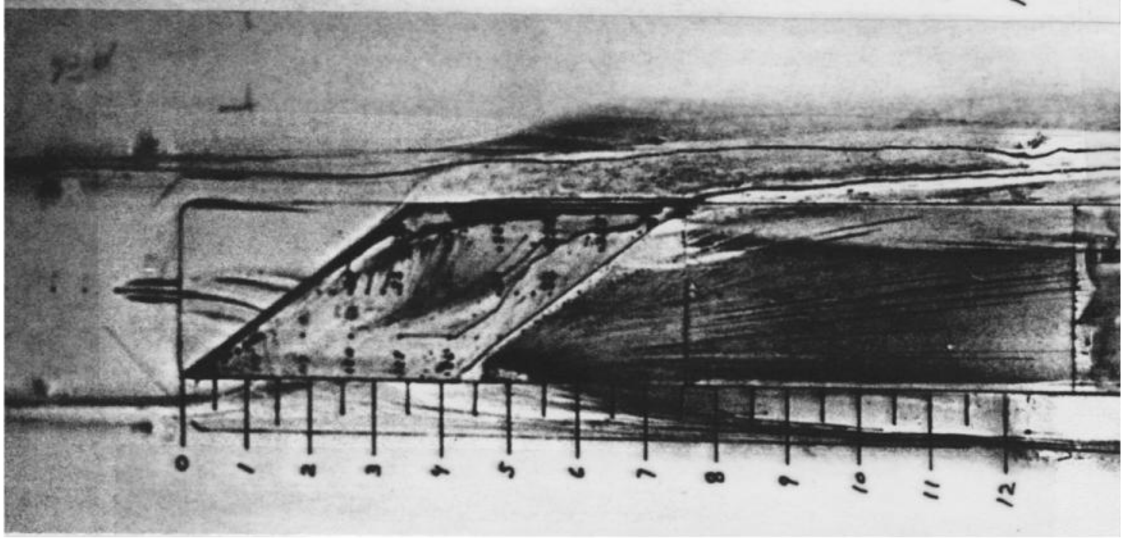

(f) $l/h = 8$.

Figure C-9. Continued.

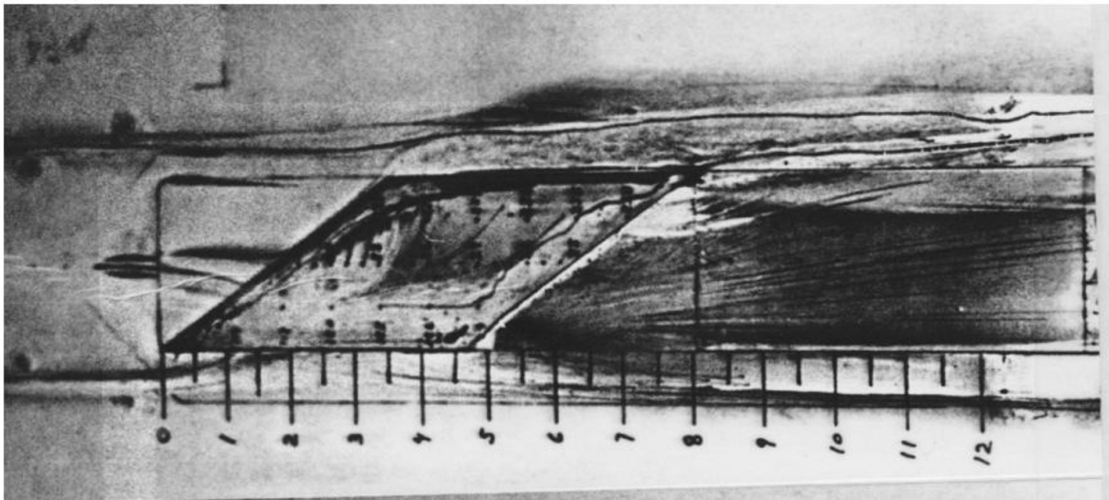

(g) *l*/*h* = 9.

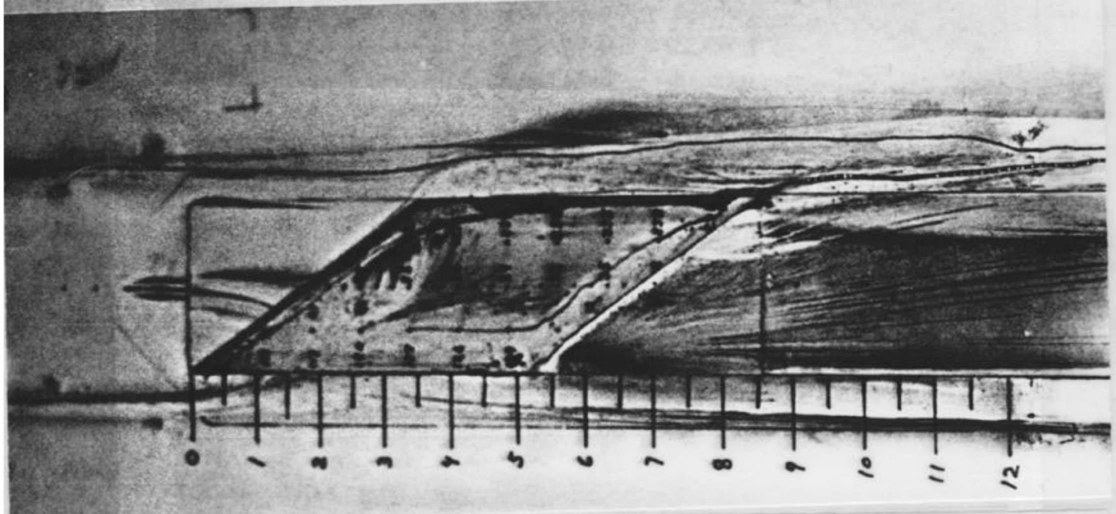

(h) *l*/*h* = 10.

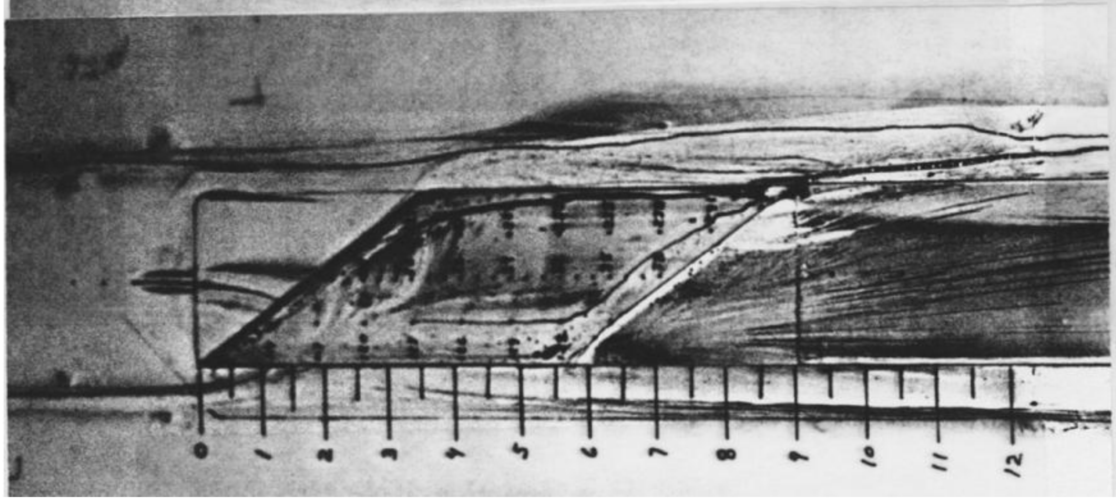

(i) *l*/*h* = 11.

Figure C-9. Continued.

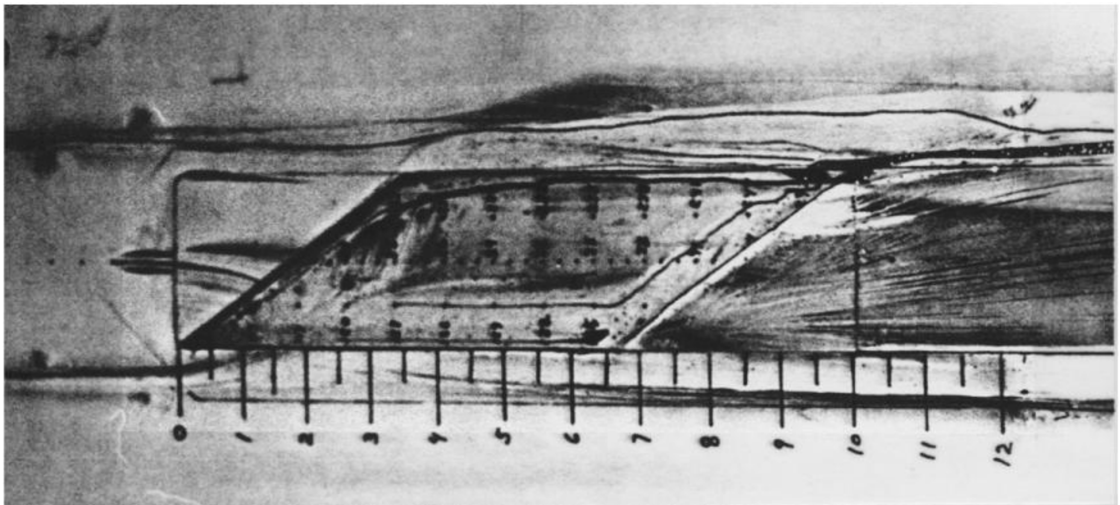

(j) l/h = 13.

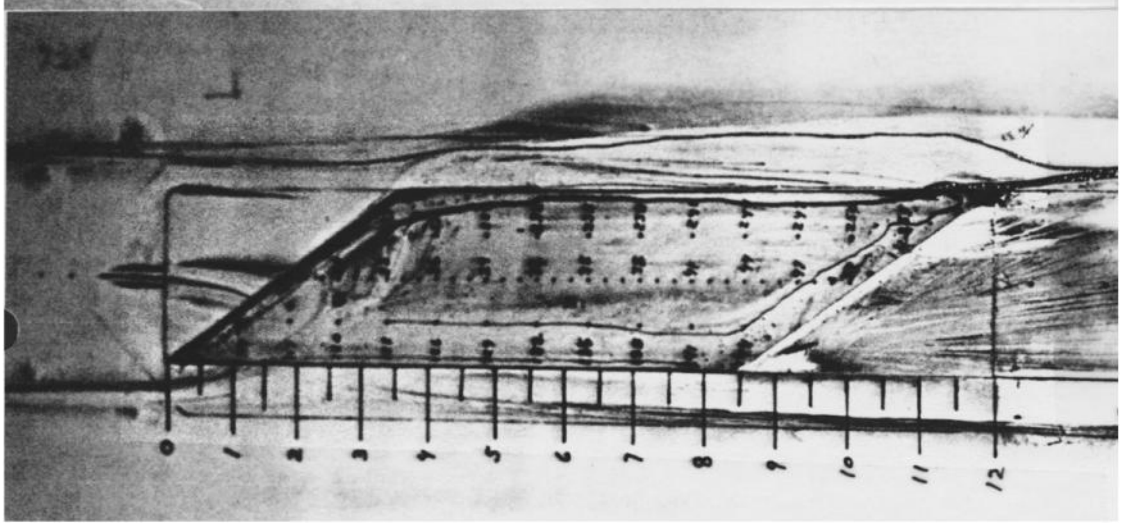

(k) l/h = 17.

Figure C-9. Concluded.

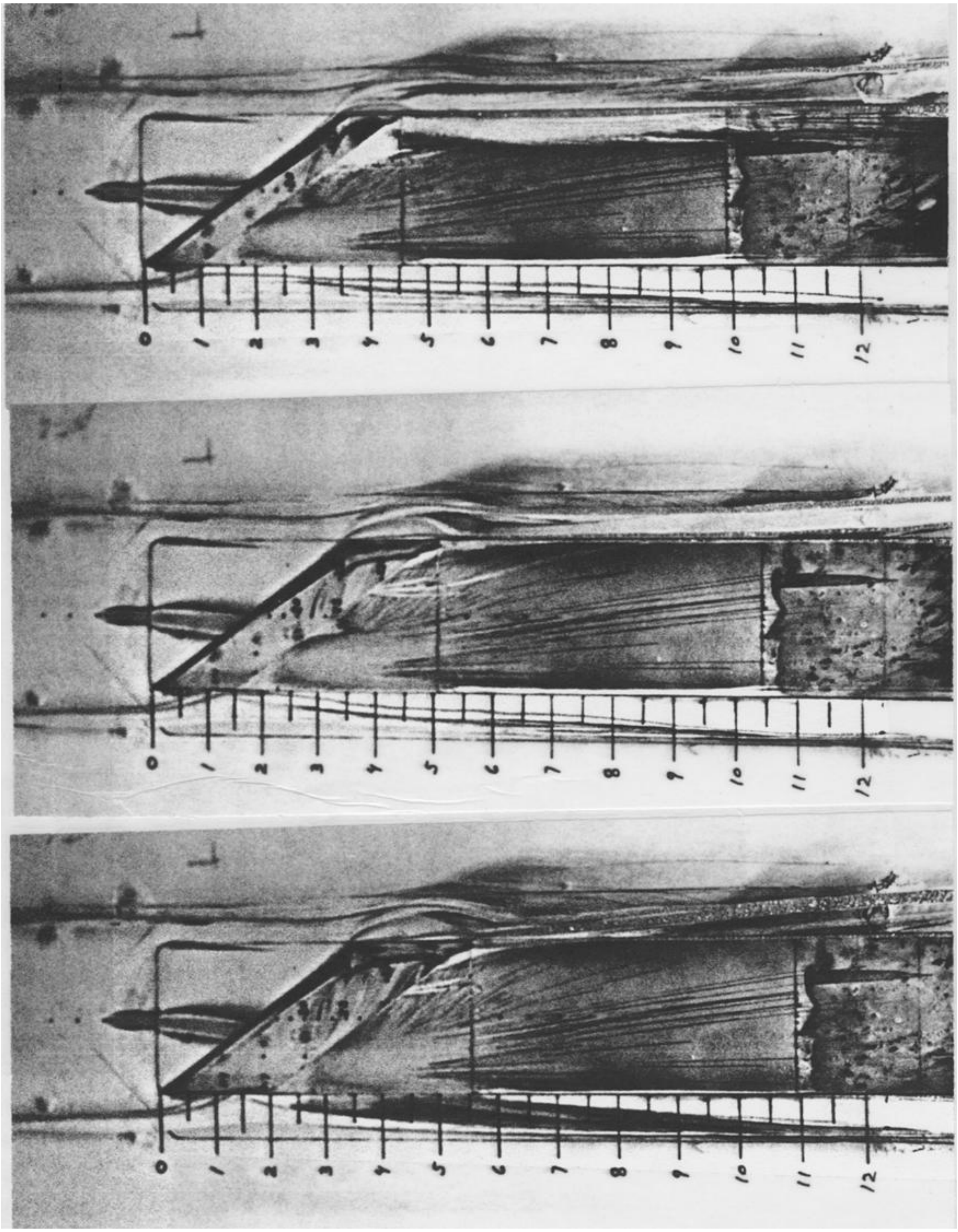

(a) $l/h = 2$.

(b) $l/h = 3$.

(c) $l/h = 4$.

Figure C-10. Surface water flow-visualization photographs for $\psi = 55°$ (configuration 2), $M = 0.4$.

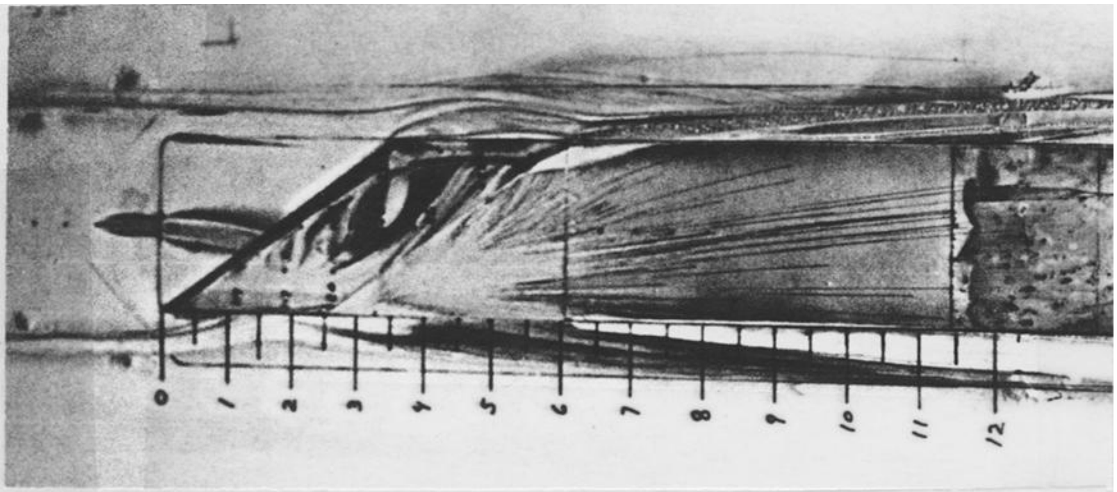

(d) l/h = 5.

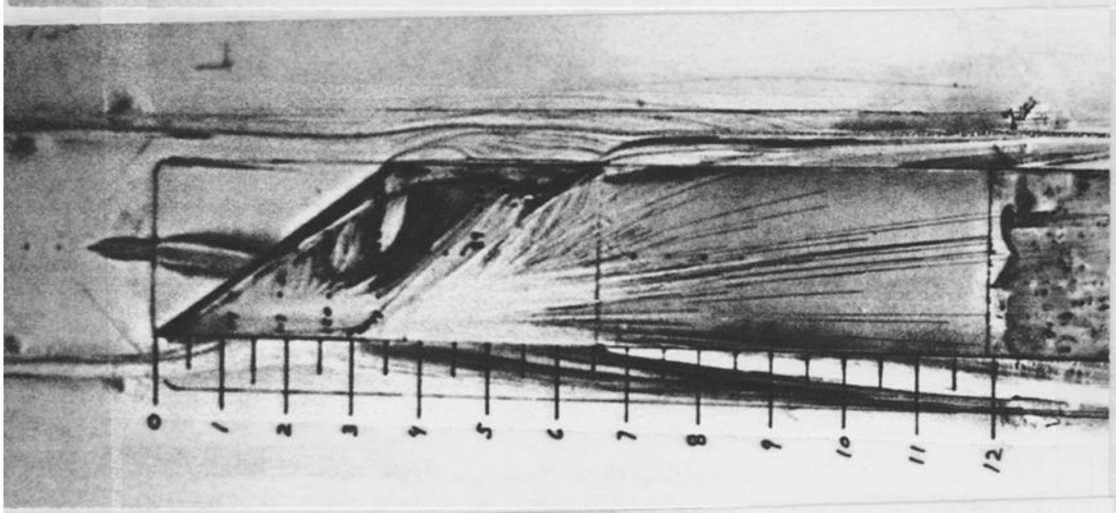

(e) l/h = 6.

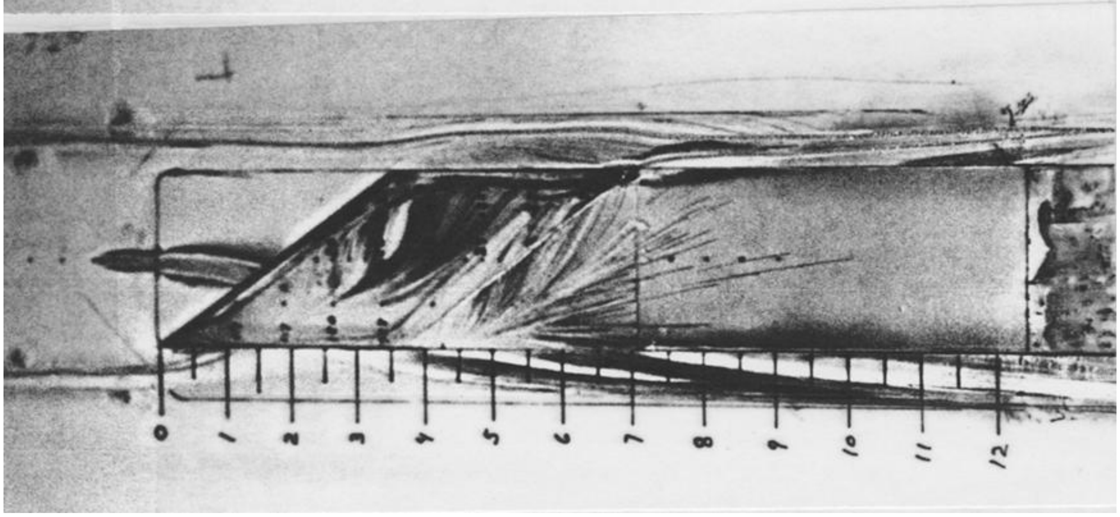

(f) l/h = 7.

Figure C-10. Continued.

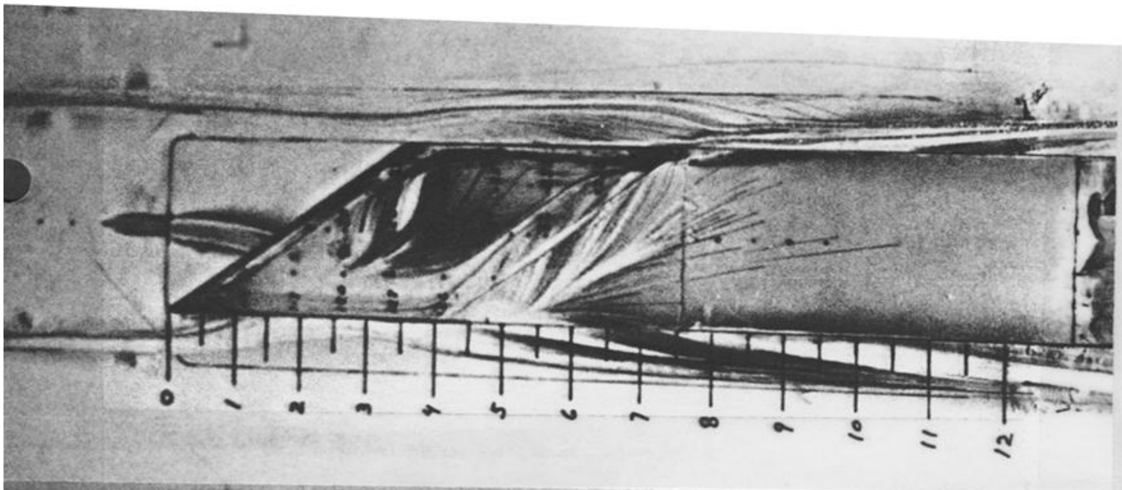

(g) l/h = 8.

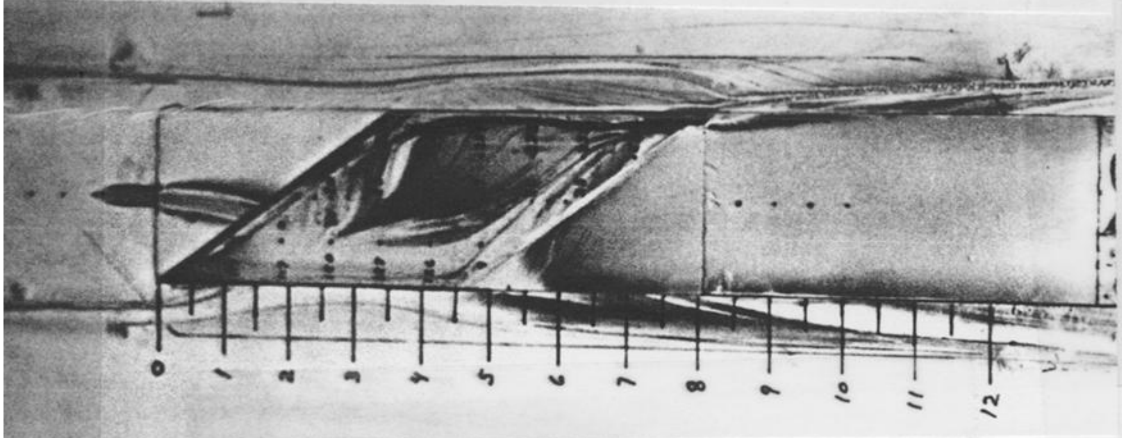

(h) l/h = 9.

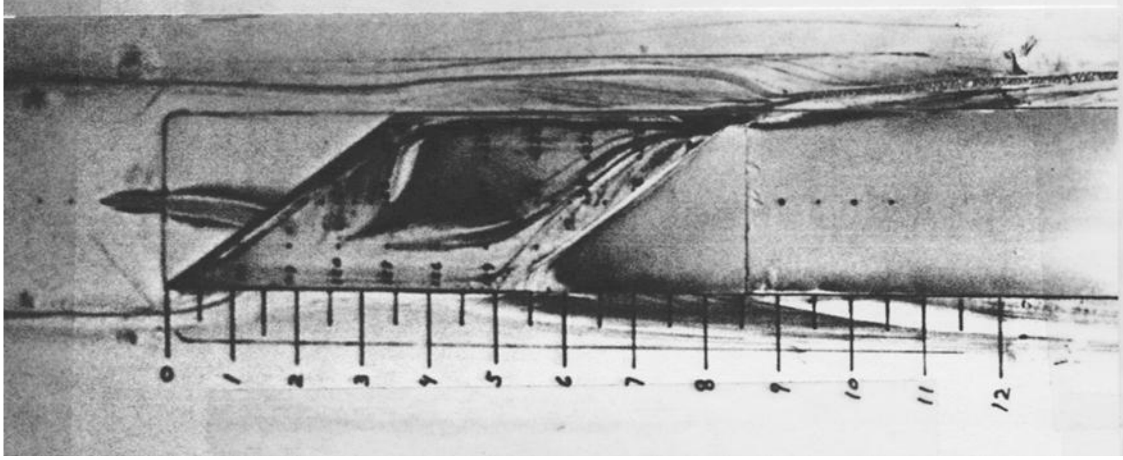

(i) l/h = 10.

Figure C-10. Continued.

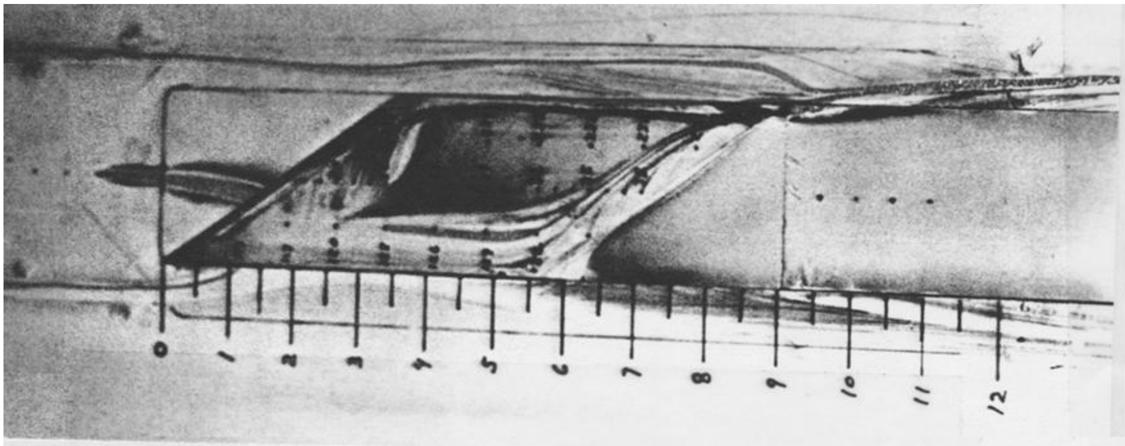

(j) $l/h = 11$.

Figure C-10. Concluded.

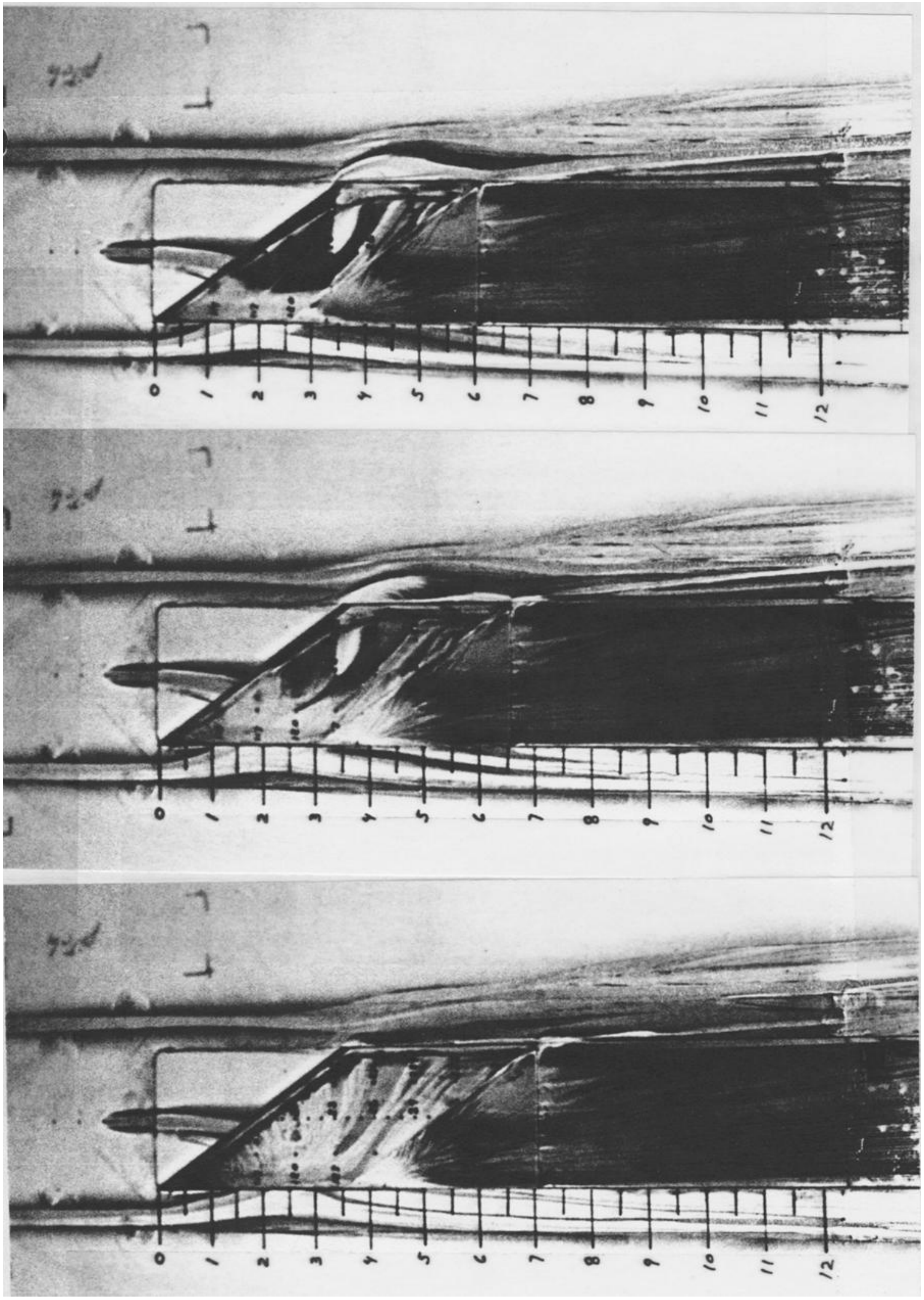

(a) $l/h = 5$.

(b) $l/h = 6$.

(c) $l/h = 7$.

Figure C-11. Surface water flow-visualization photographs for $\psi = 55°$ (configuration 2), $M = 0.6$.

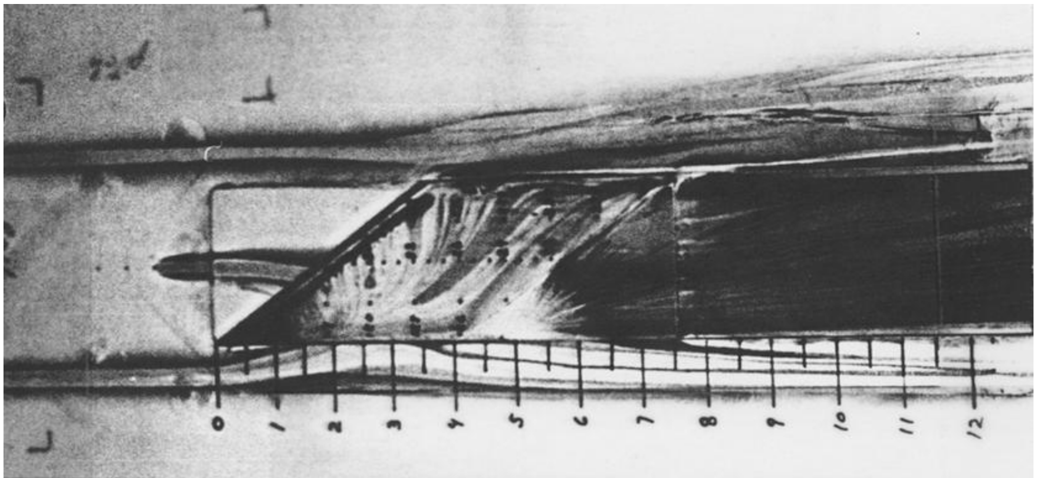

(d) l/h = 8.

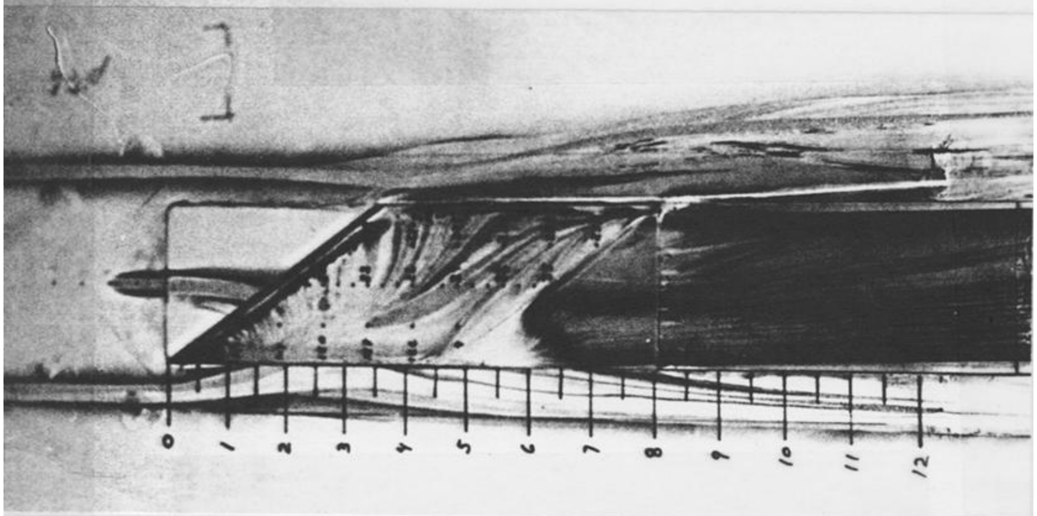

(e) l/h = 9.

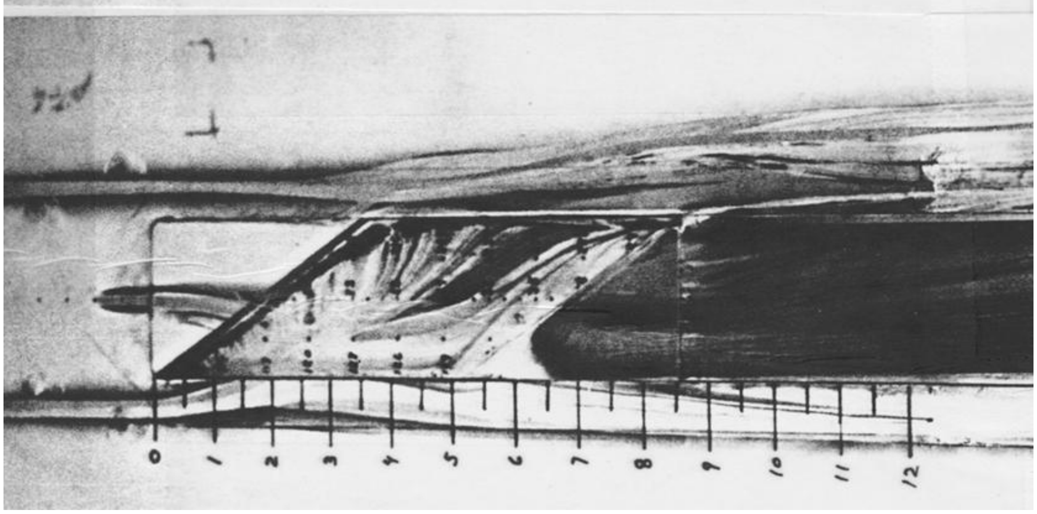

(f) l/h = 10.

Figure C-11. Continued.

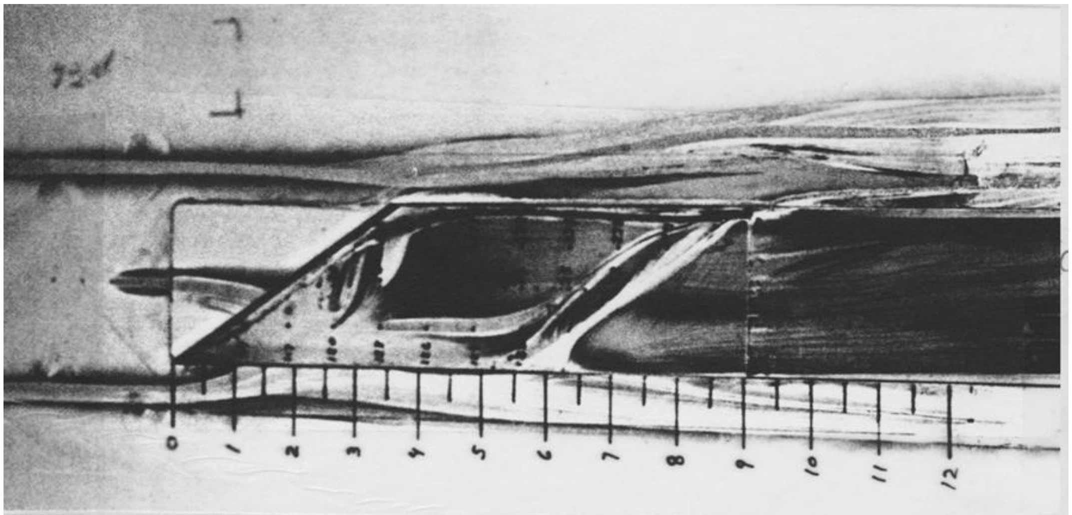

(g) l/h = 11.

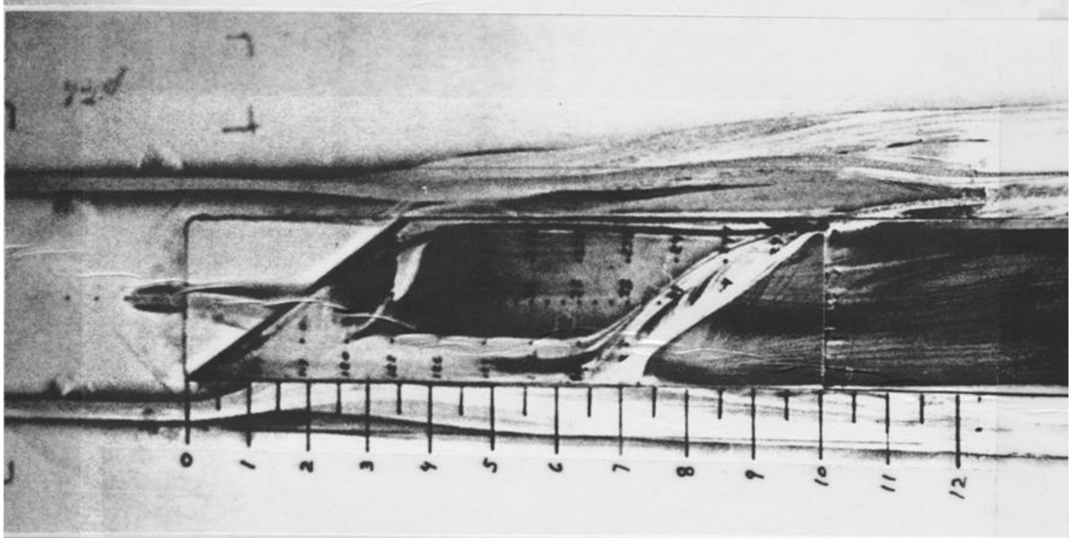

(h) l/h = 13.

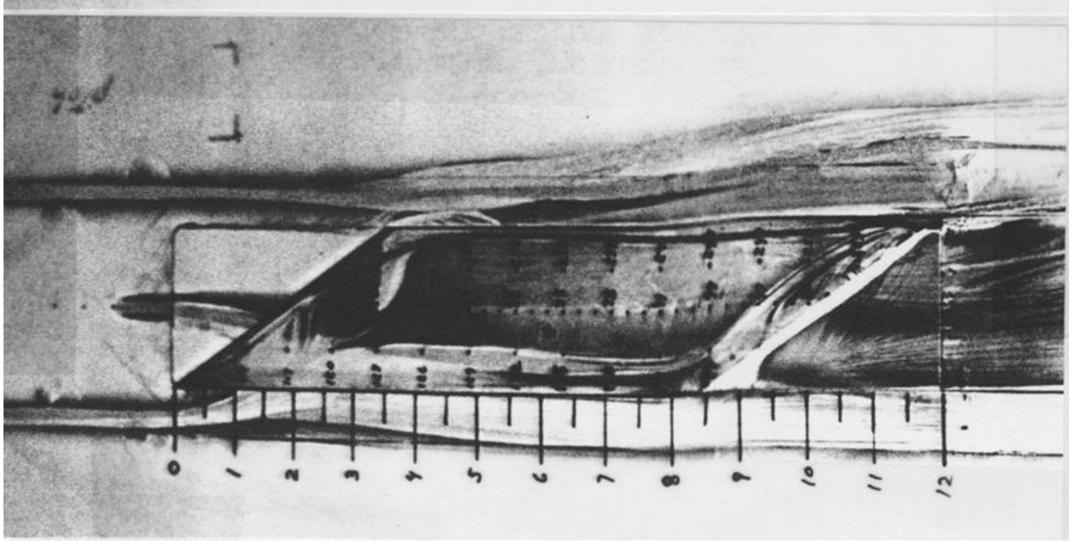

(i) l/h = 17.

Figure C-11. Concluded.

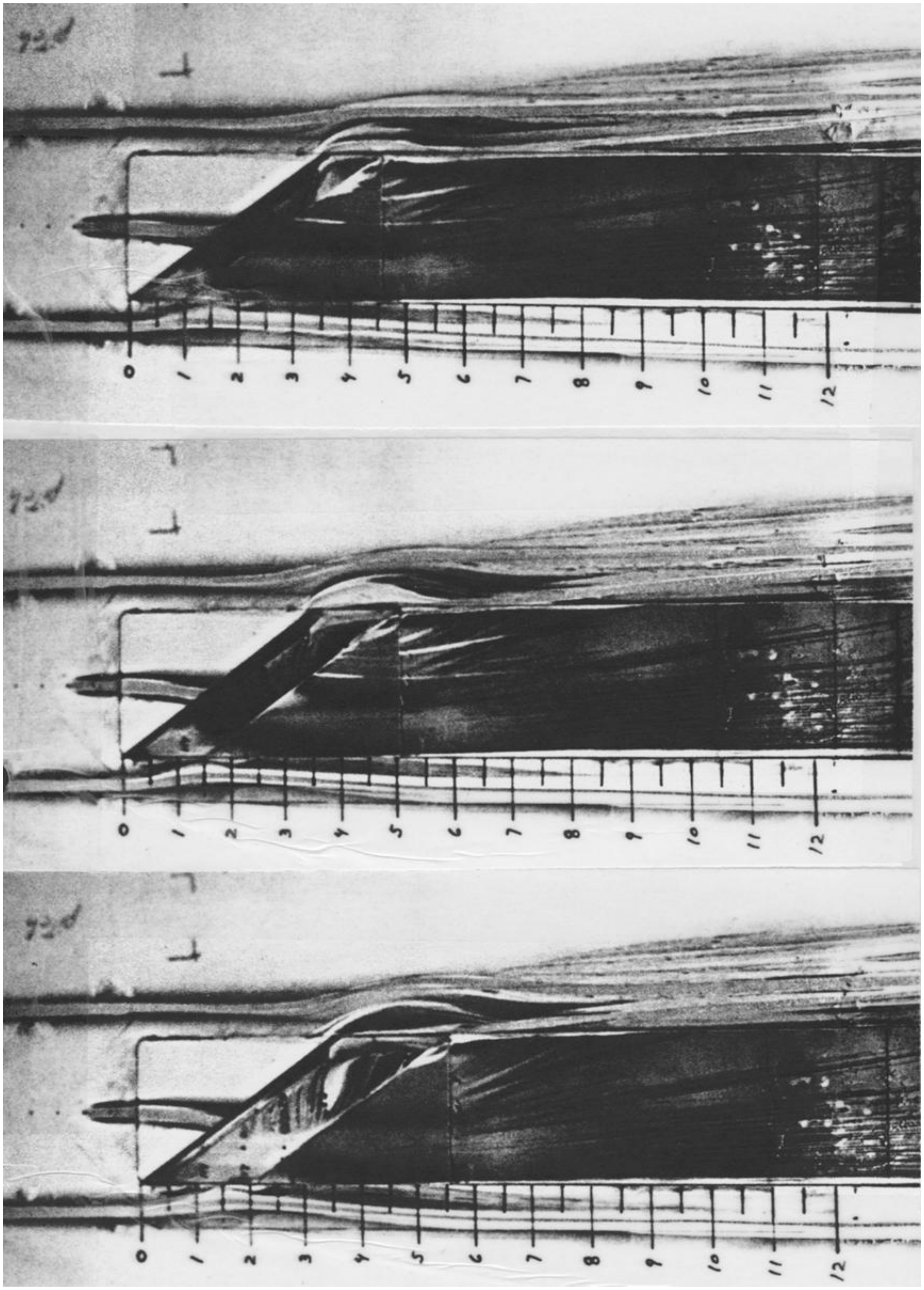

(a) *l*/*h* = 2.

(b) *l*/*h* = 3.

(c) *l*/*h* = 4.

Figure C-12. Surface water flow-visualization photographs for $\psi = 55°$ (configuration 2), $M = 0.8$.

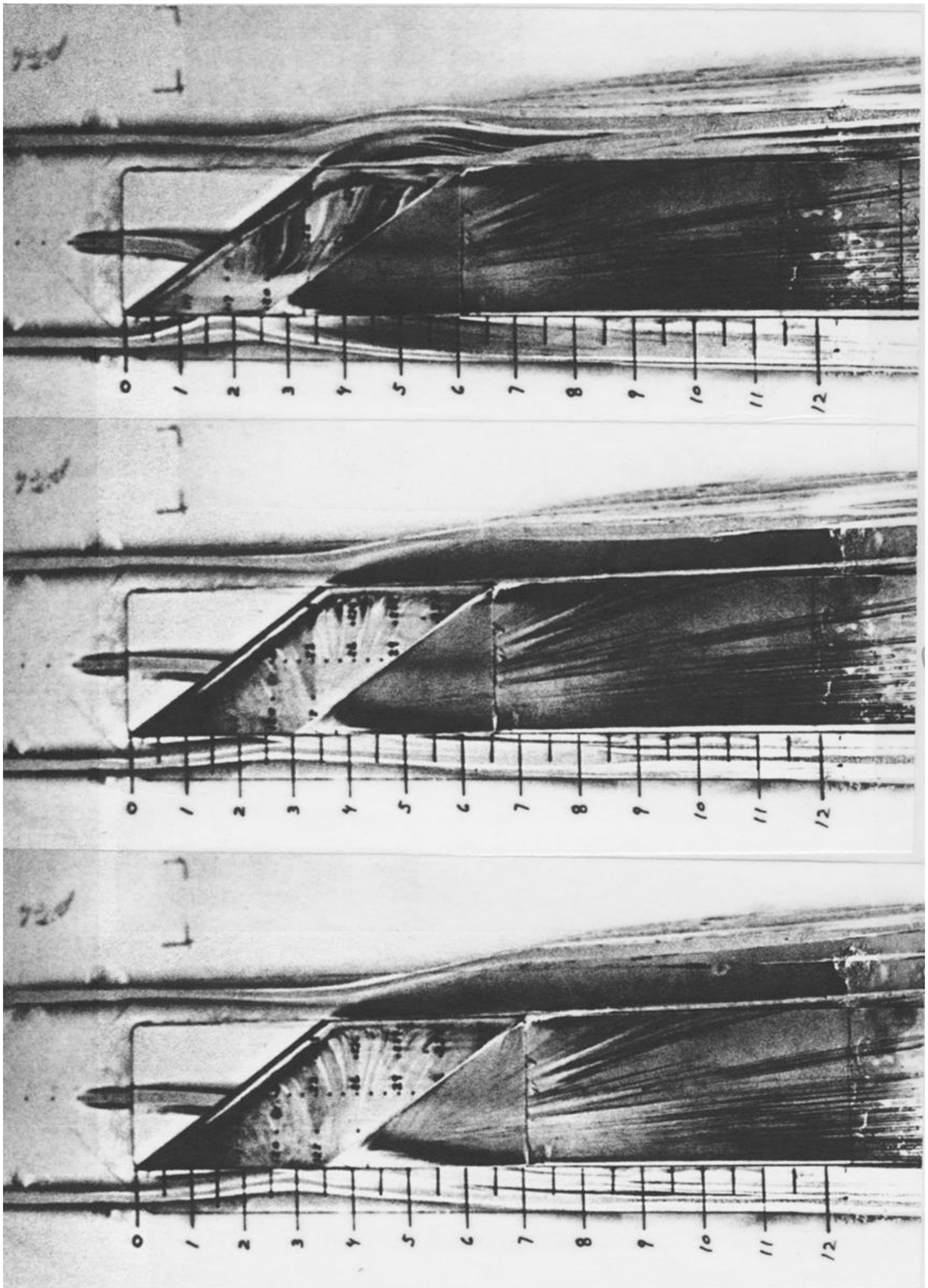

(d) l/h = 5.

(e) l/h = 6.

(f) l/h = 7.

Figure C-12. Continued.

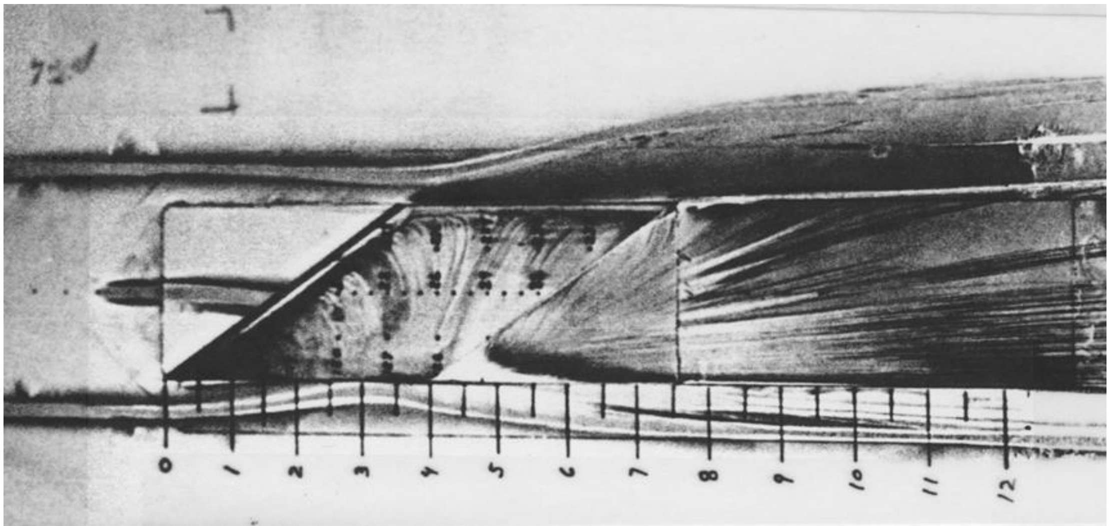

(g) *l*/*h* = 8.

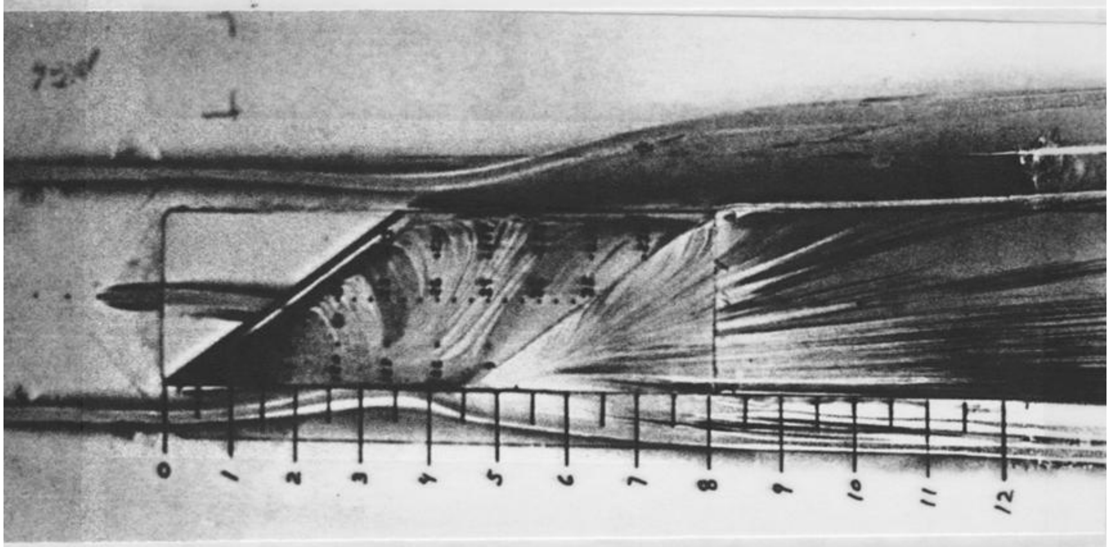

(h) *l*/*h* = 9.

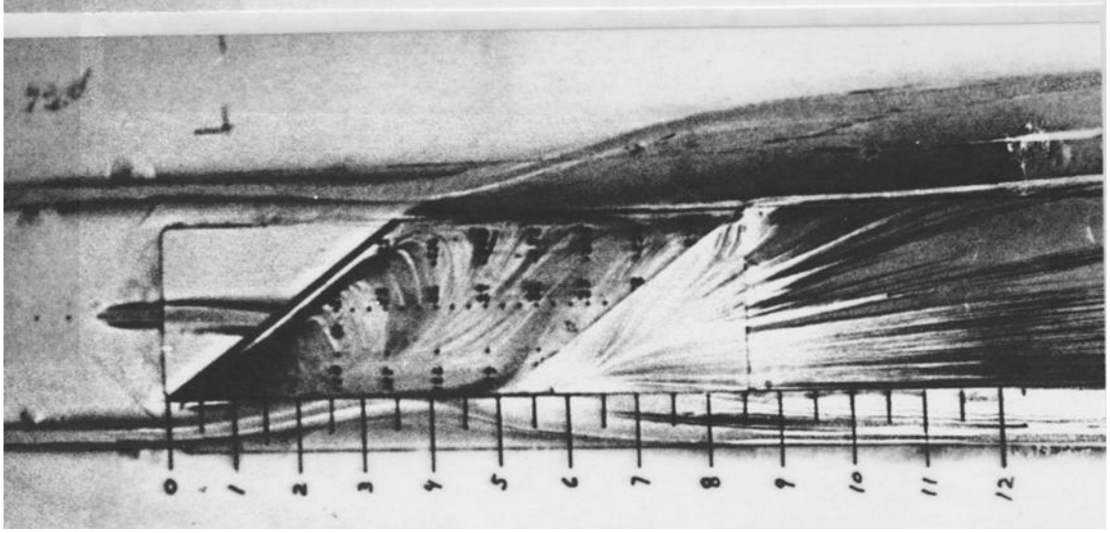

(i) *l*/*h* = 10.

Figure C-12. Continued.

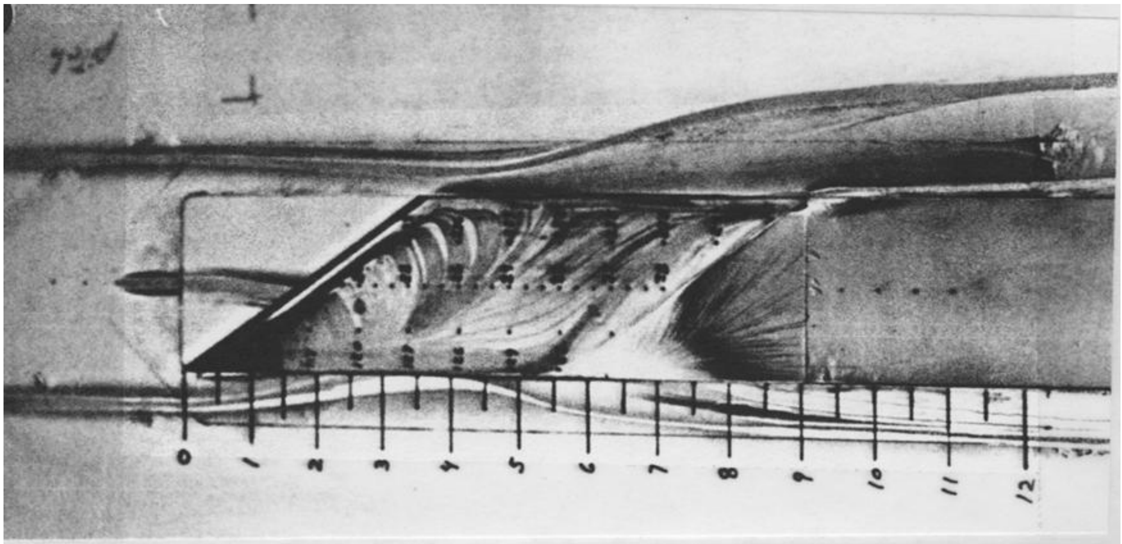

(j) *l*/*h* = 11.

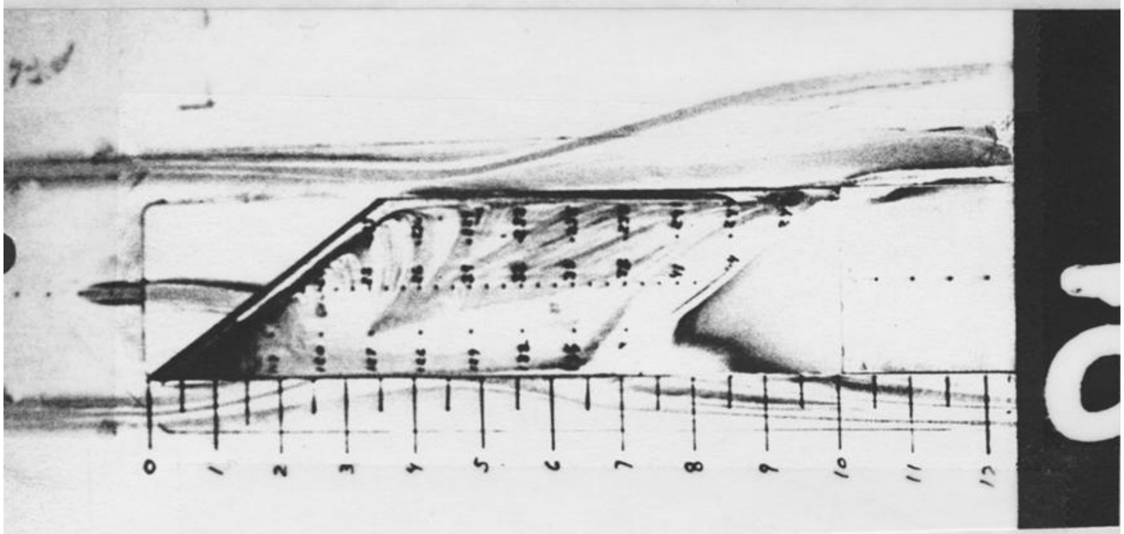

(k) *l*/*h* = 13.

Figure C-12. Concluded.

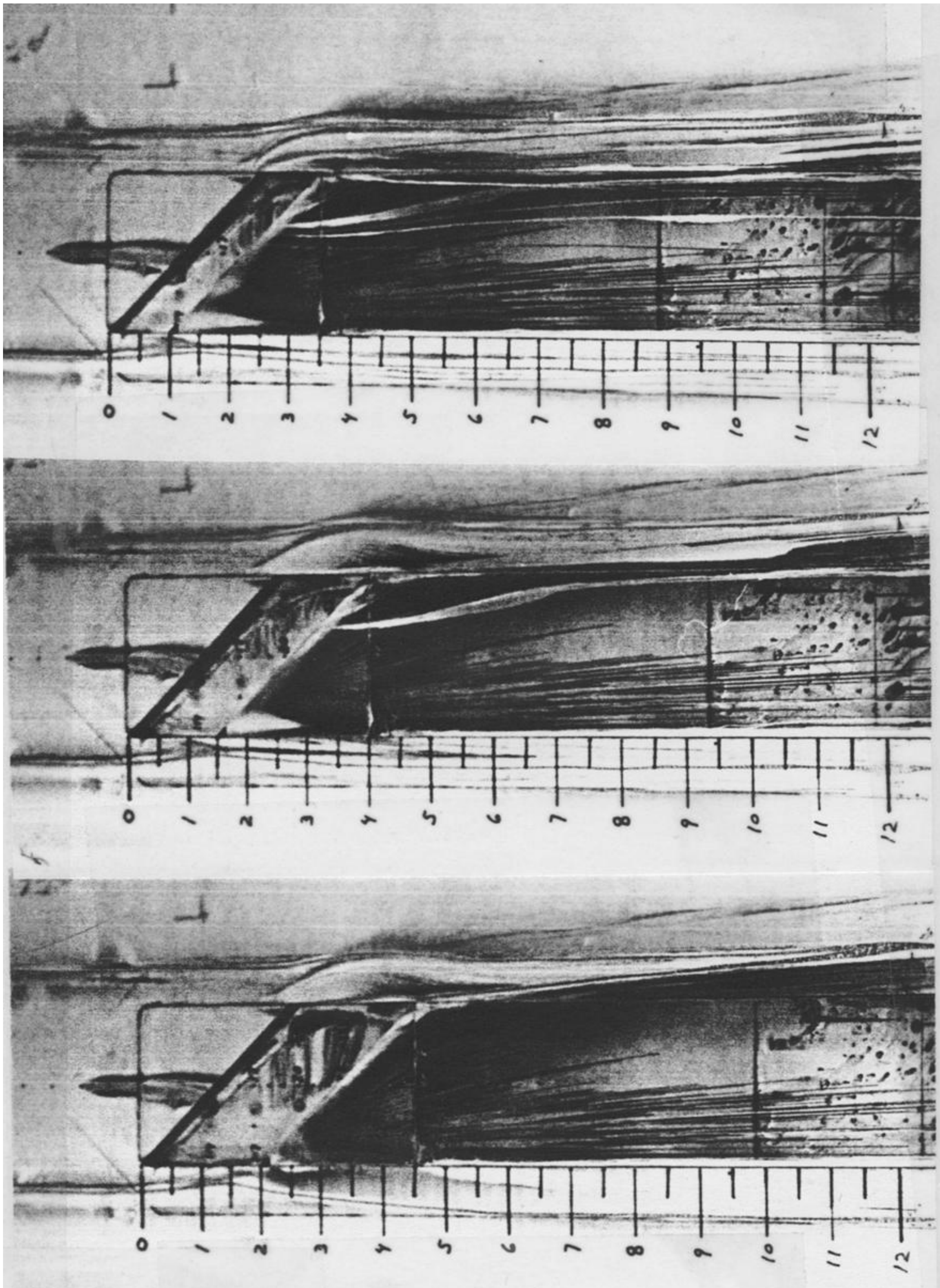

(a) l/h = 2.

(b) l/h = 3.

(c) l/h = 4.

Figure C-13. Surface water flow-visualization photographs for $\psi = 45°$ (configuration 3), $M = 0.4$.

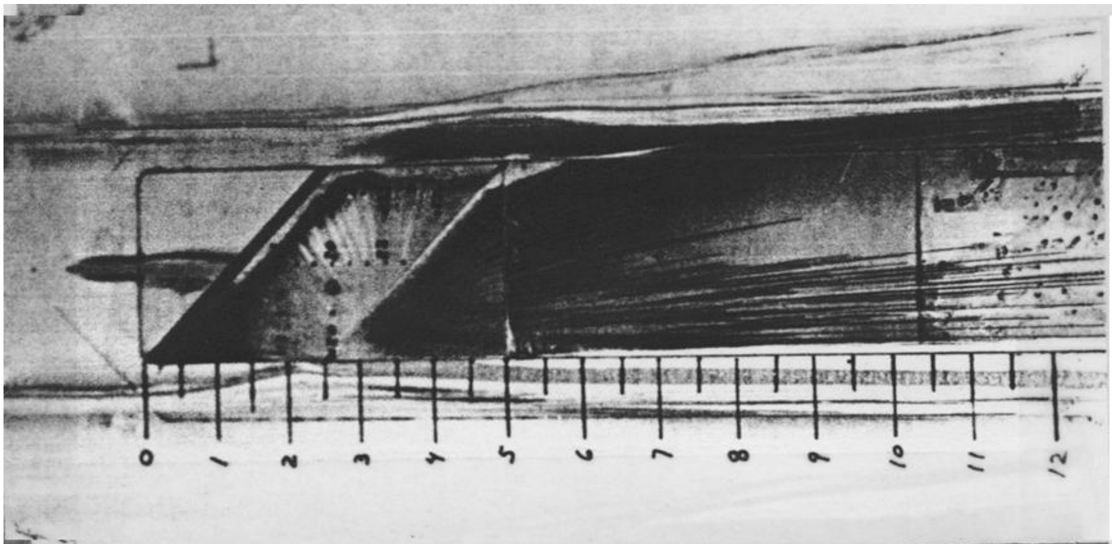

(d) l/h = 5.

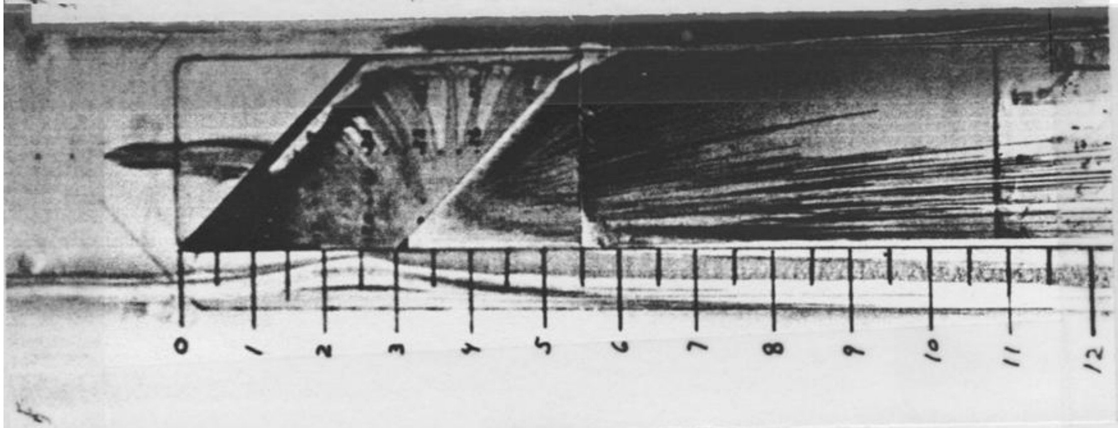

(e) l/h = 6.

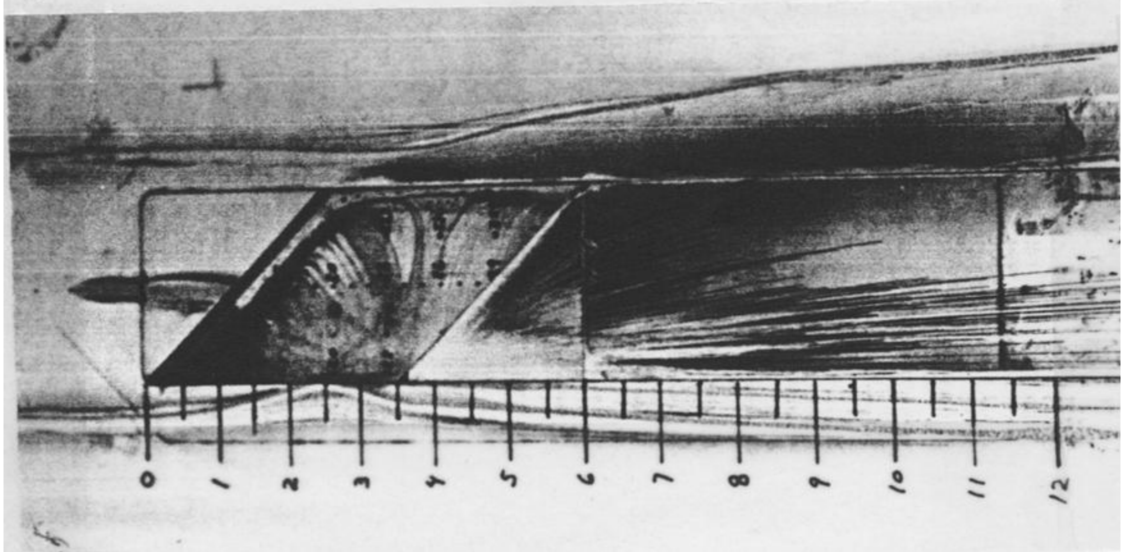

(f) l/h = 7.

Figure C-13. Continued.

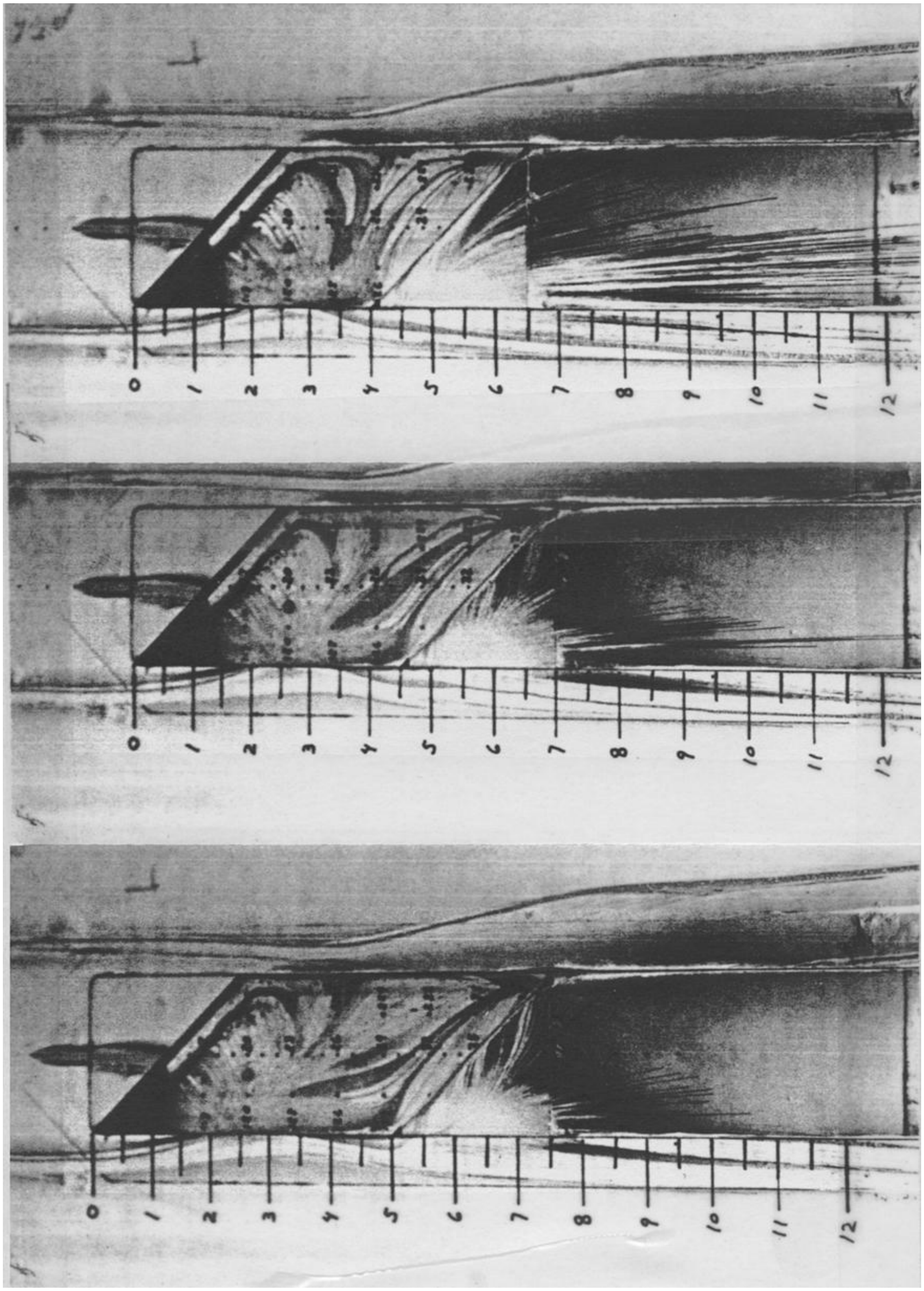

(g) $l/h = 8$.

(h) $l/h = 9$.

(i) $l/h = 10$.

Figure C-13. Continued.

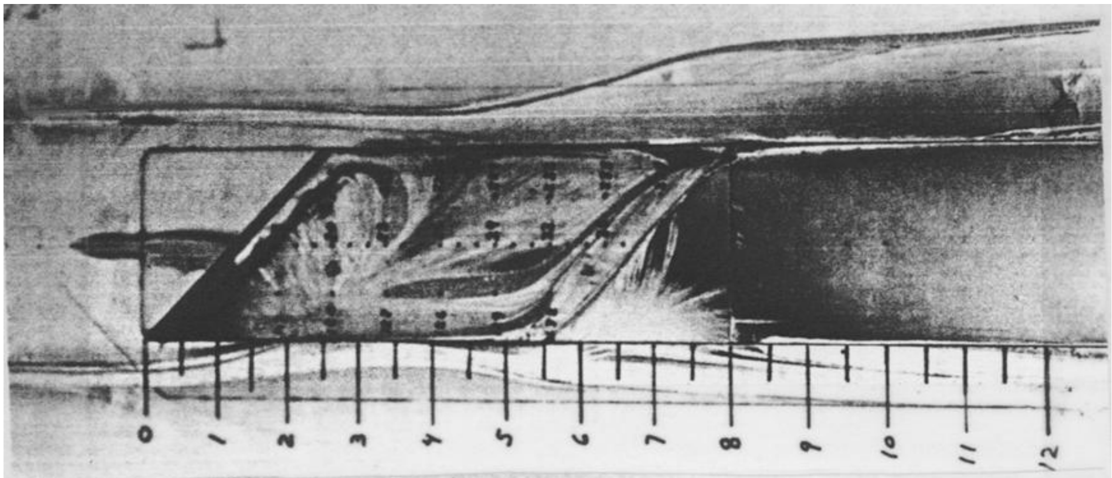

(j) l/h = 11.

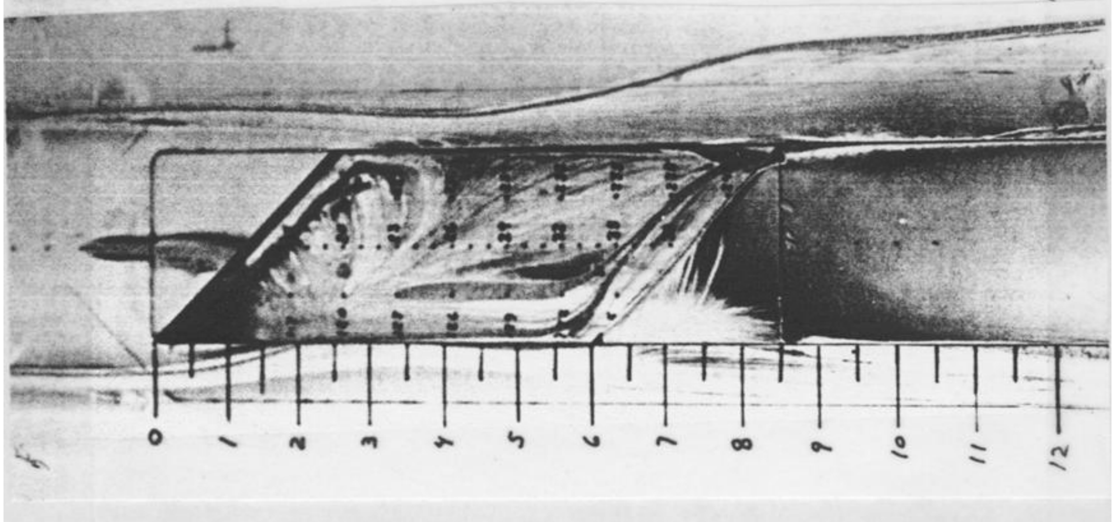

(k) l/h = 12.

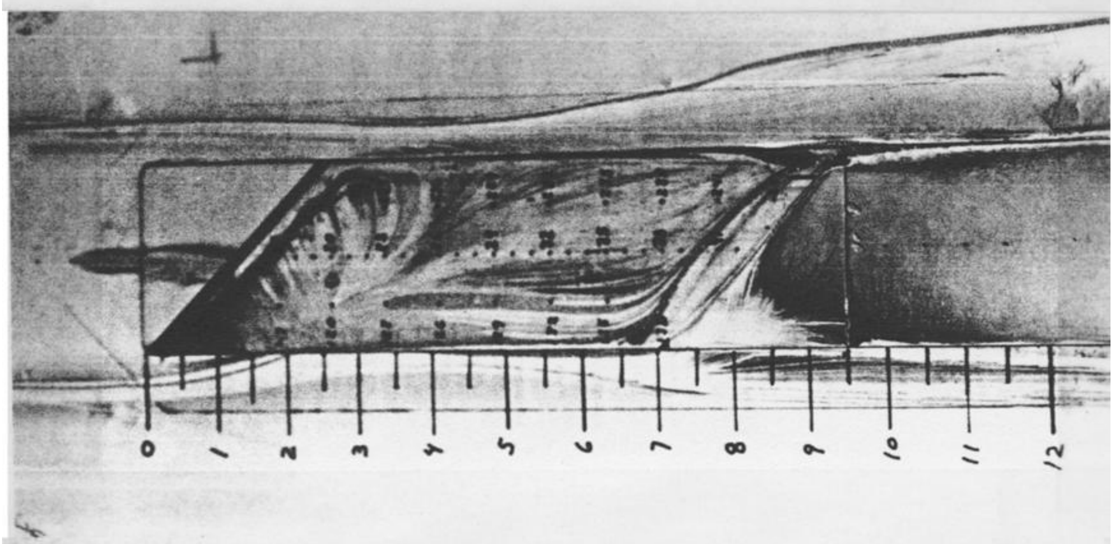

(l) l/h = 14.

Figure C-13. Continued.

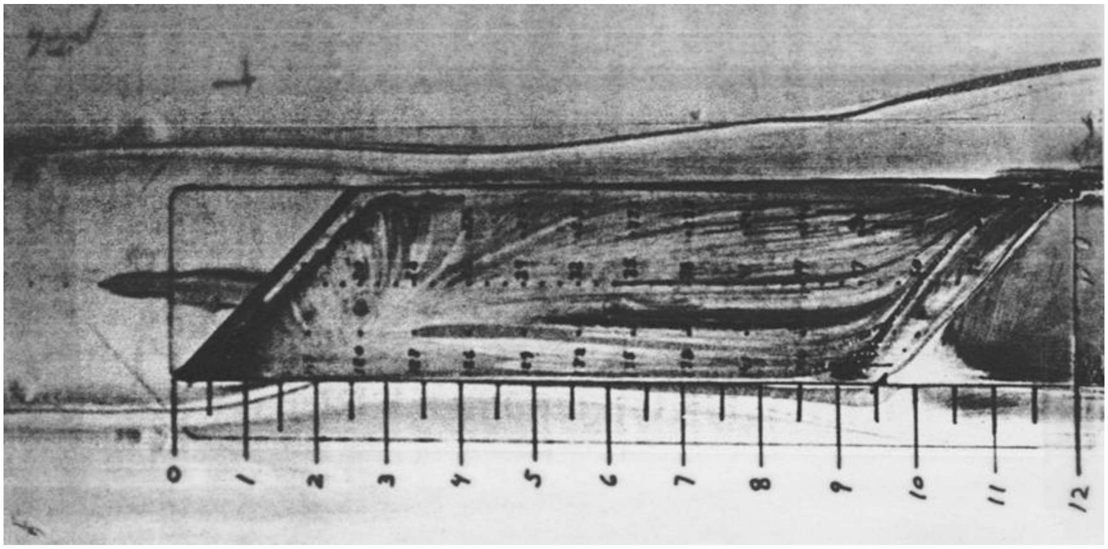

(m) l/h = 19.

Figure C-13. Concluded.

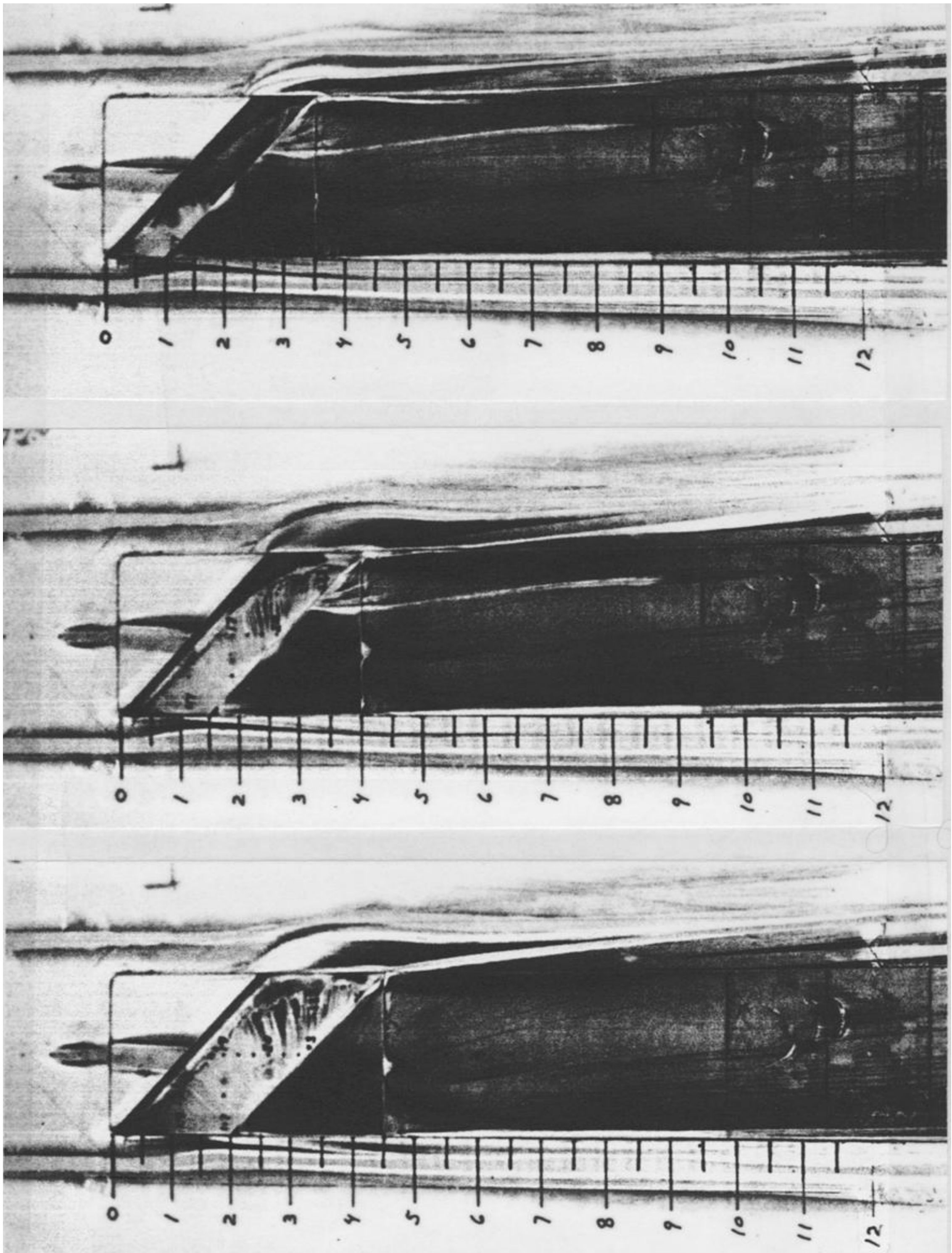

(a) $l/h = 2$.

(b) $l/h = 3$.

(c) $l/h = 4$.

Figure C-14. Surface water flow-visualization photographs for $\psi = 45°$ (configuration 3), $M = 0.6$.

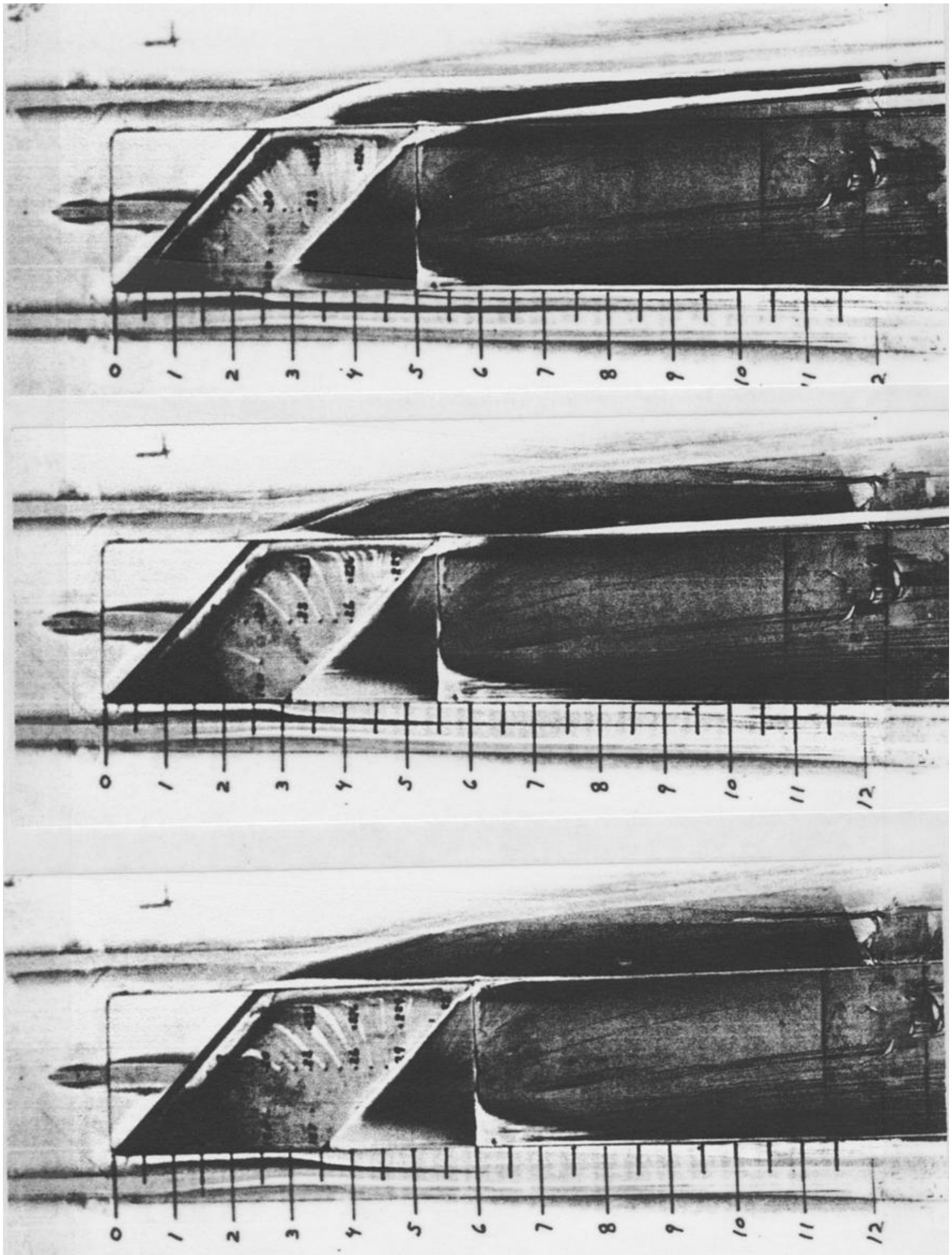

(d) $l/h = 5$.

(e) $l/h = 6$.

(f) $l/h = 7$.

Figure C-14. Continued.

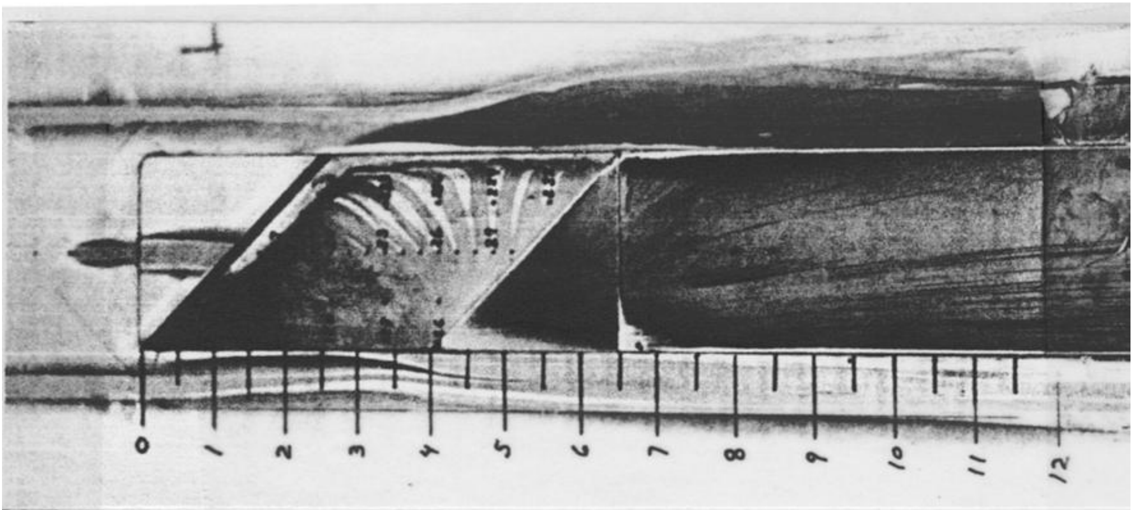

(g) l/h = 8.

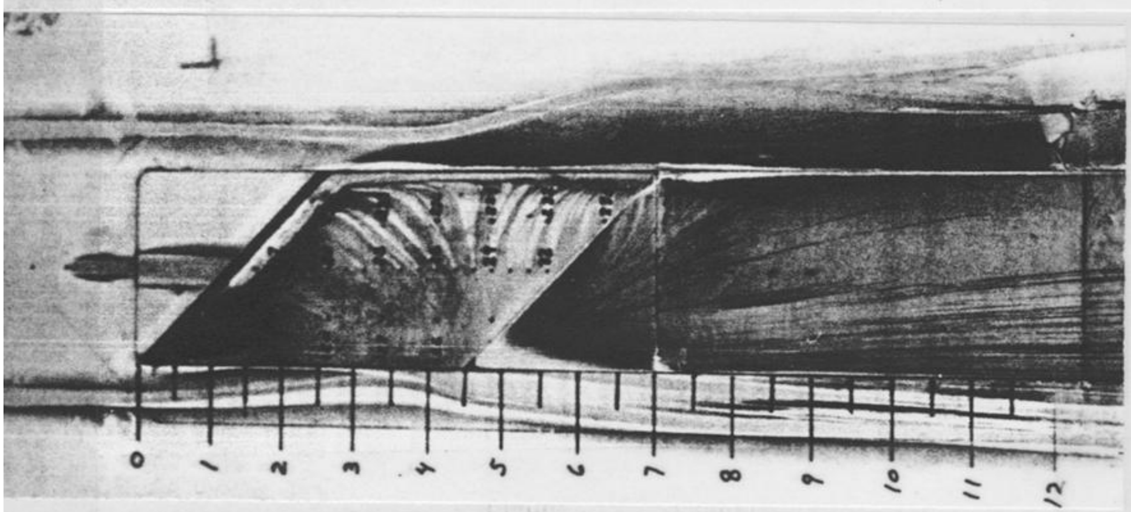

(h) l/h = 9.

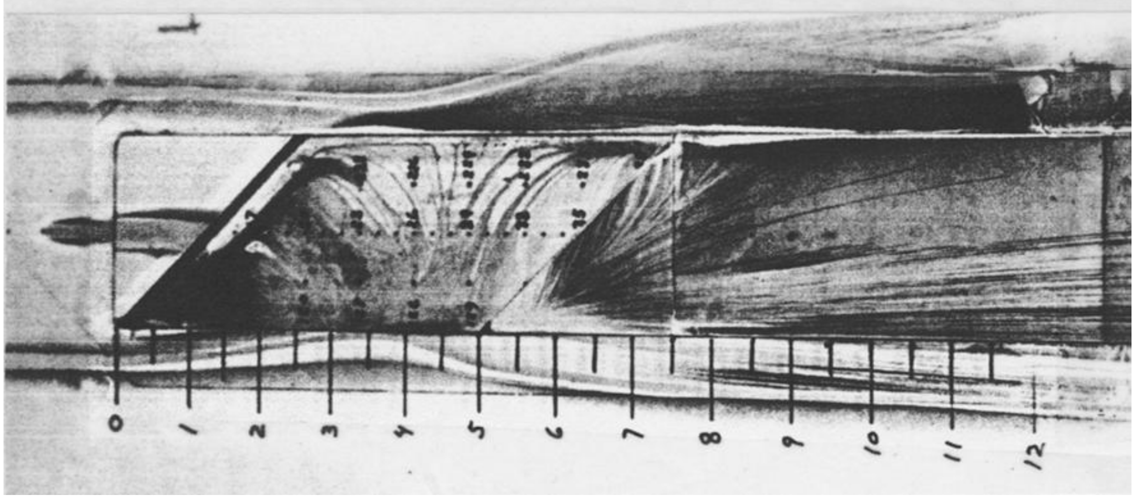

(i) l/h = 10.

Figure C-14. Continued.

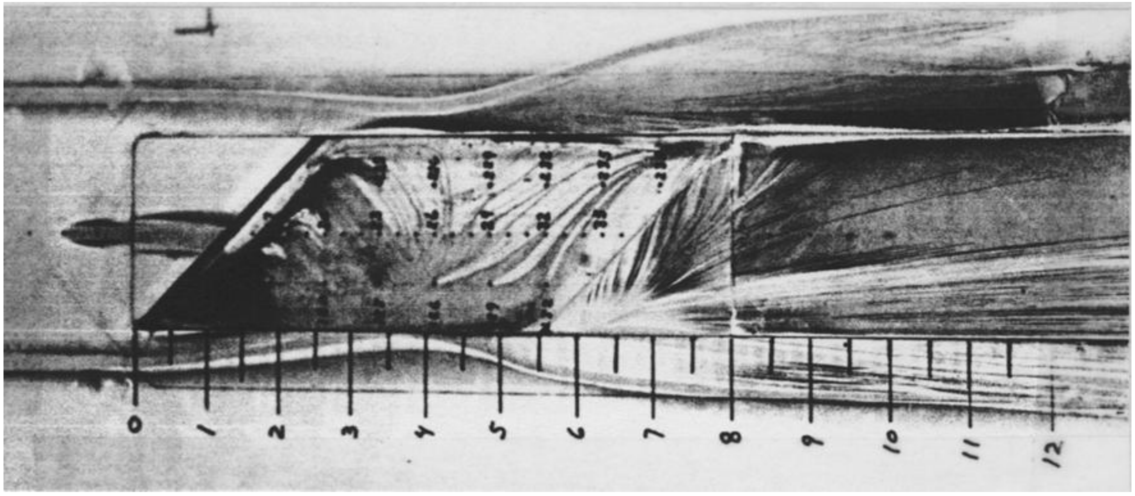

(j) l/h = 11.

Figure C-14. Concluded.

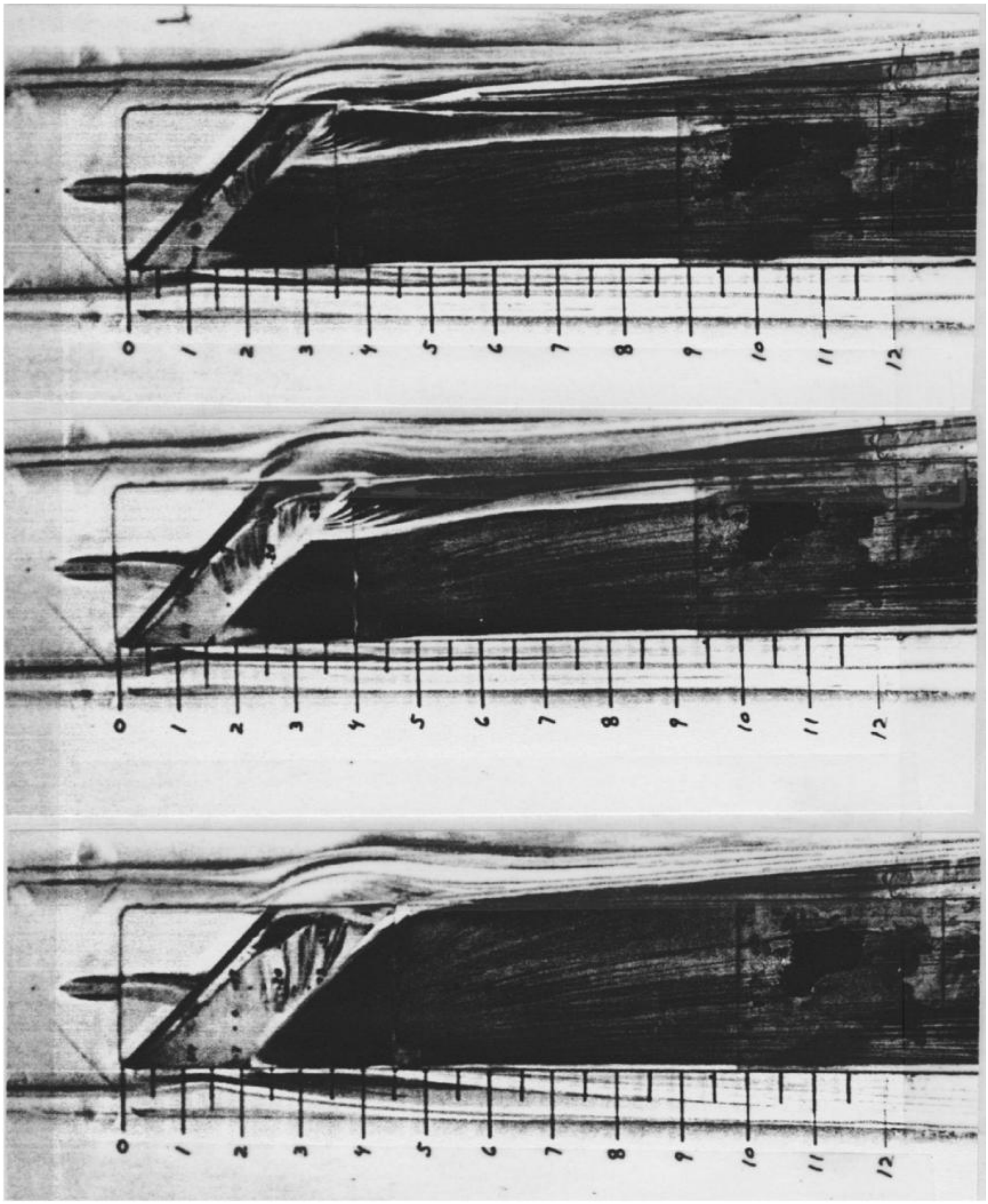

(a) l/h = 2.

(b) l/h = 3.

(c) l/h = 4.

Figure C-15. Surface water flow-visualization photographs for ψ = 45° (configuration 3), M = 0.8.

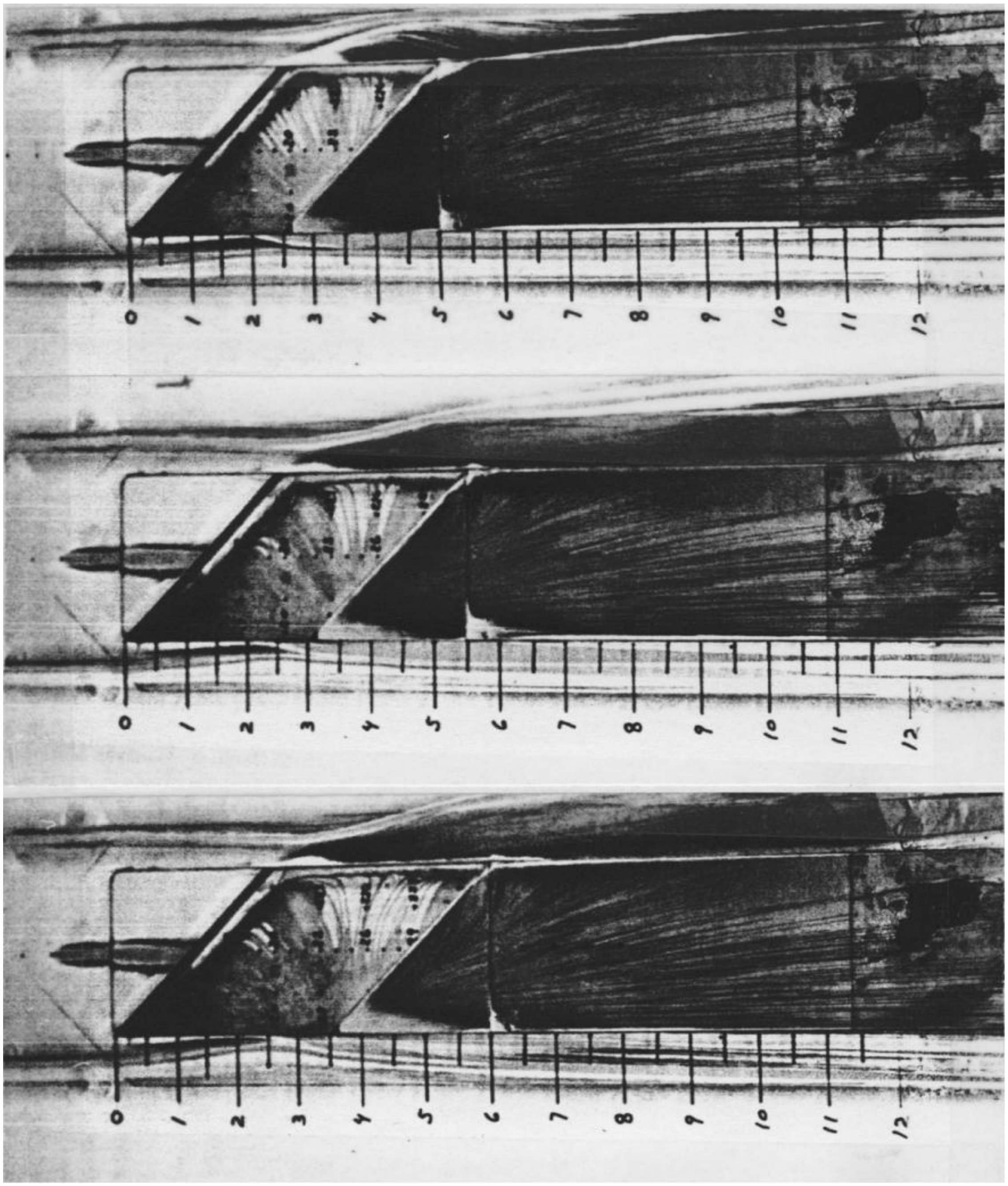

(d) l/h = 5.

(e) l/h = 6.

(f) l/h = 7.

Figure C-15. Continued.

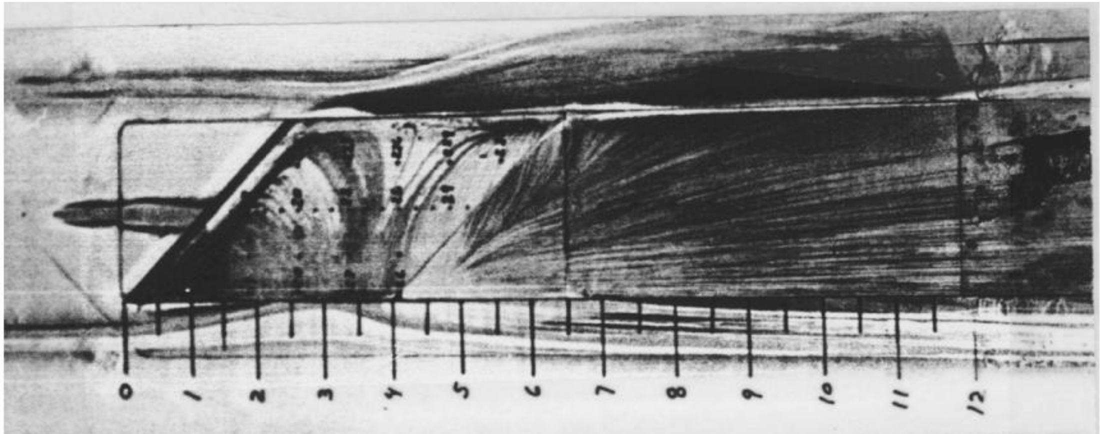

(g) l/h = 8.

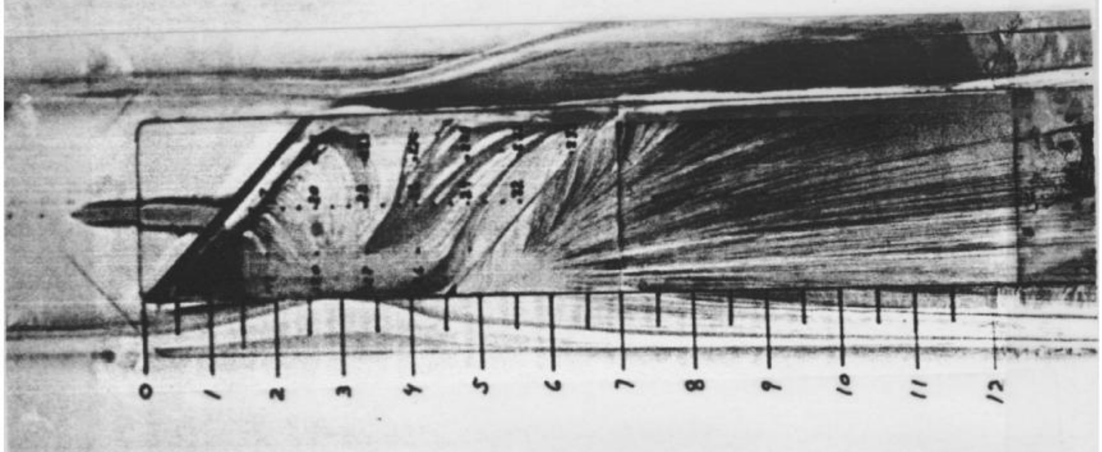

(h) l/h = 9.

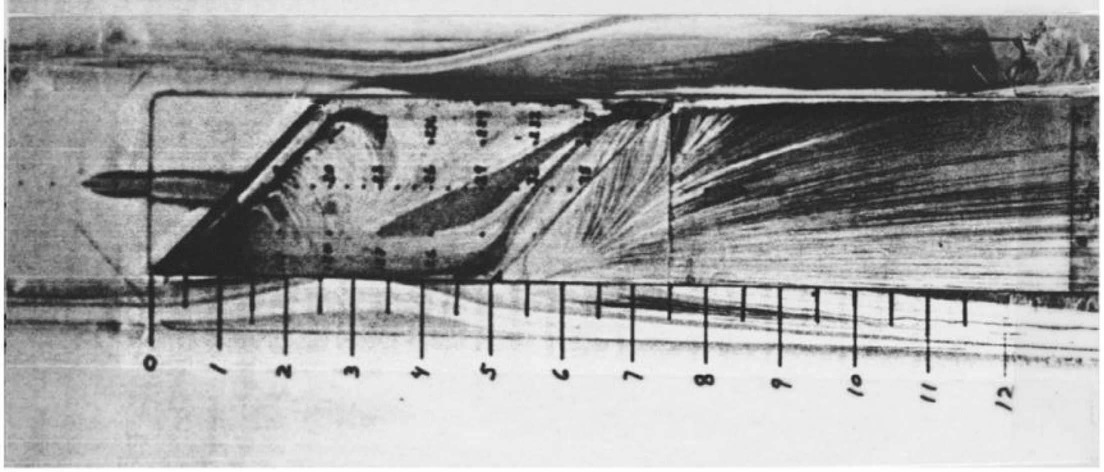

(i) l/h = 10.

Figure C-15. Continued.

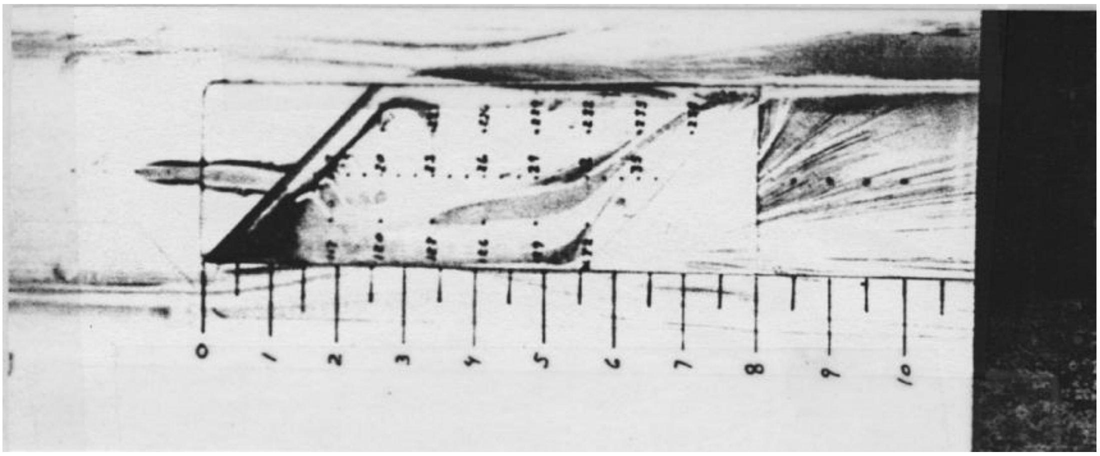

(j) *l*/*h* = 11.

Figure C-15. Concluded.

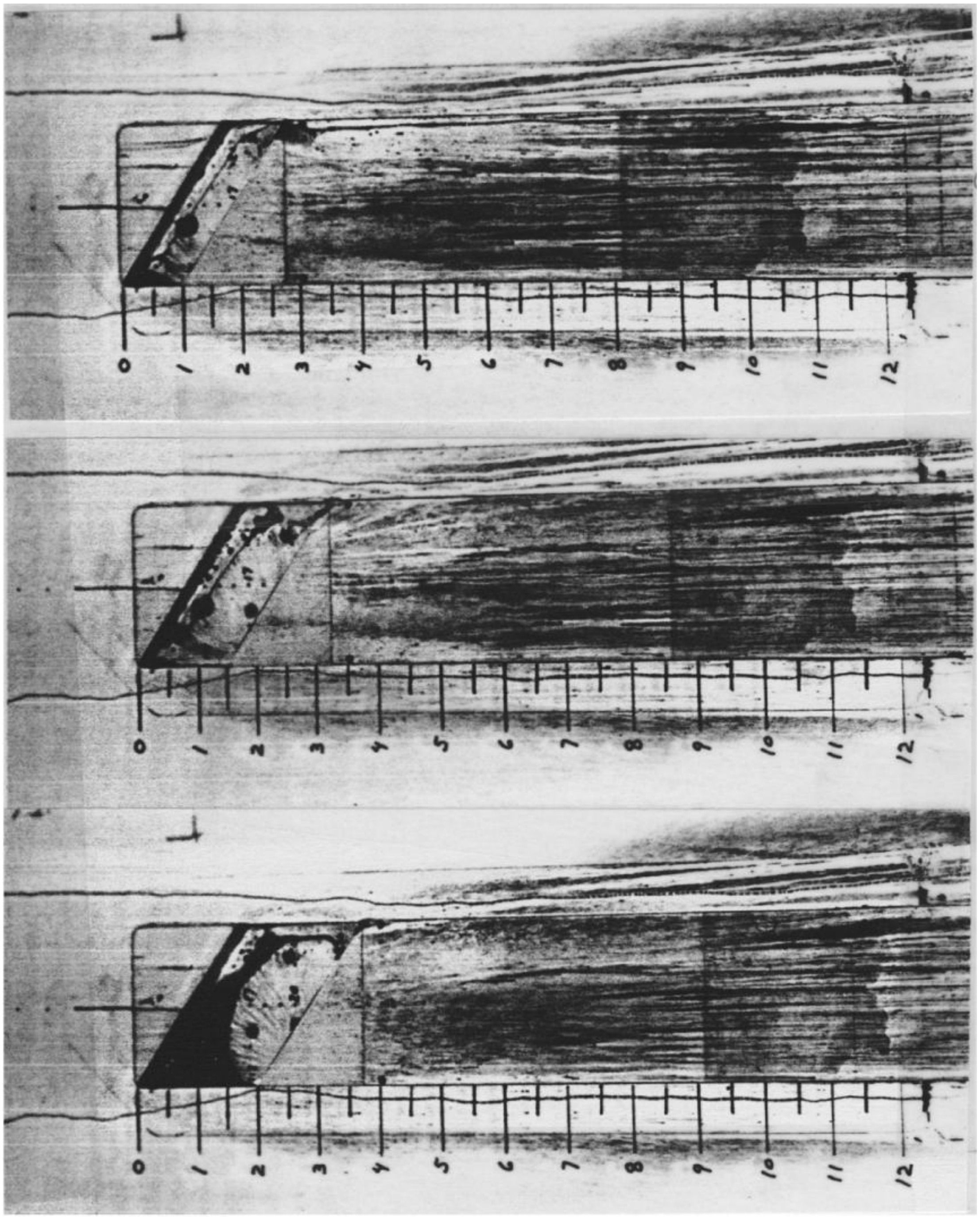

(a) l/h = 2.

(b) l/h = 3.

(c) l/h = 4.

Figure C-16. Surface water flow-visualization photographs for ψ = 35° (configuration 4), M = 0.2.

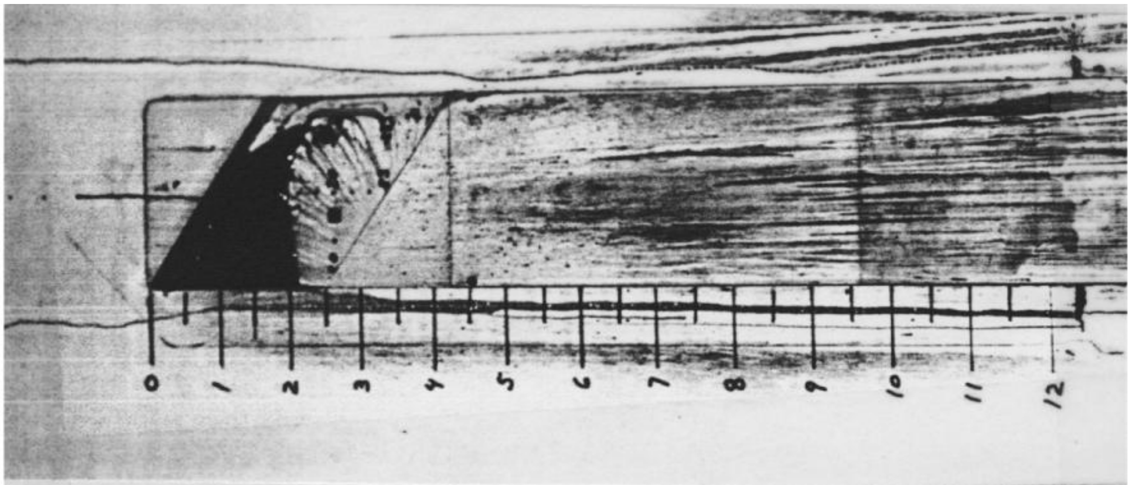

(d) l/h = 5.

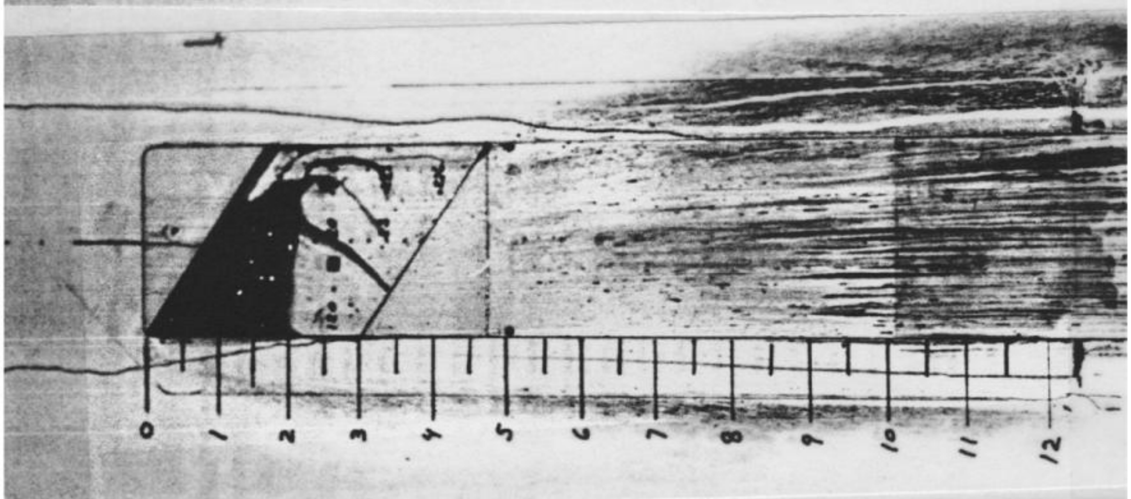

(e) l/h = 6.

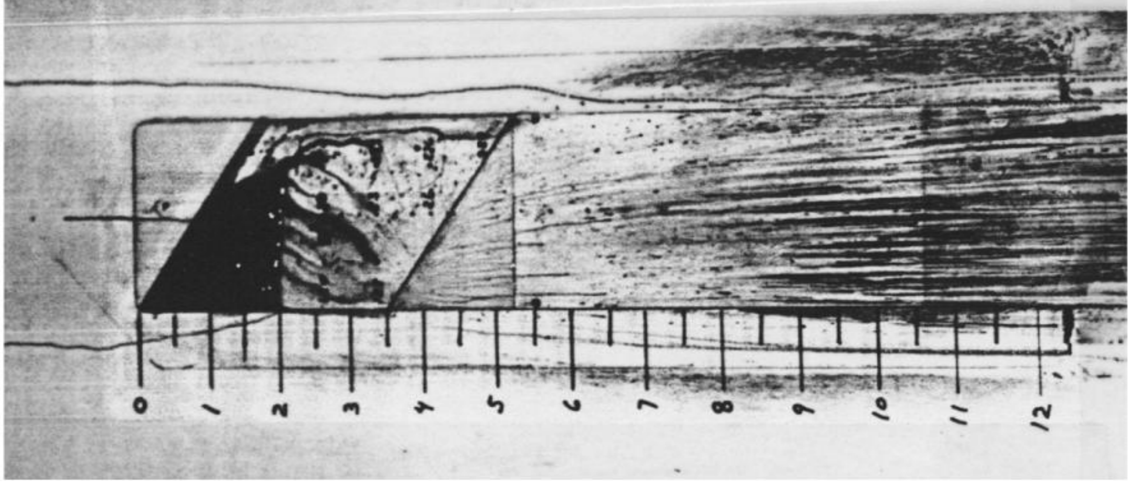

(f) l/h = 7.

Figure C-16. Continued.

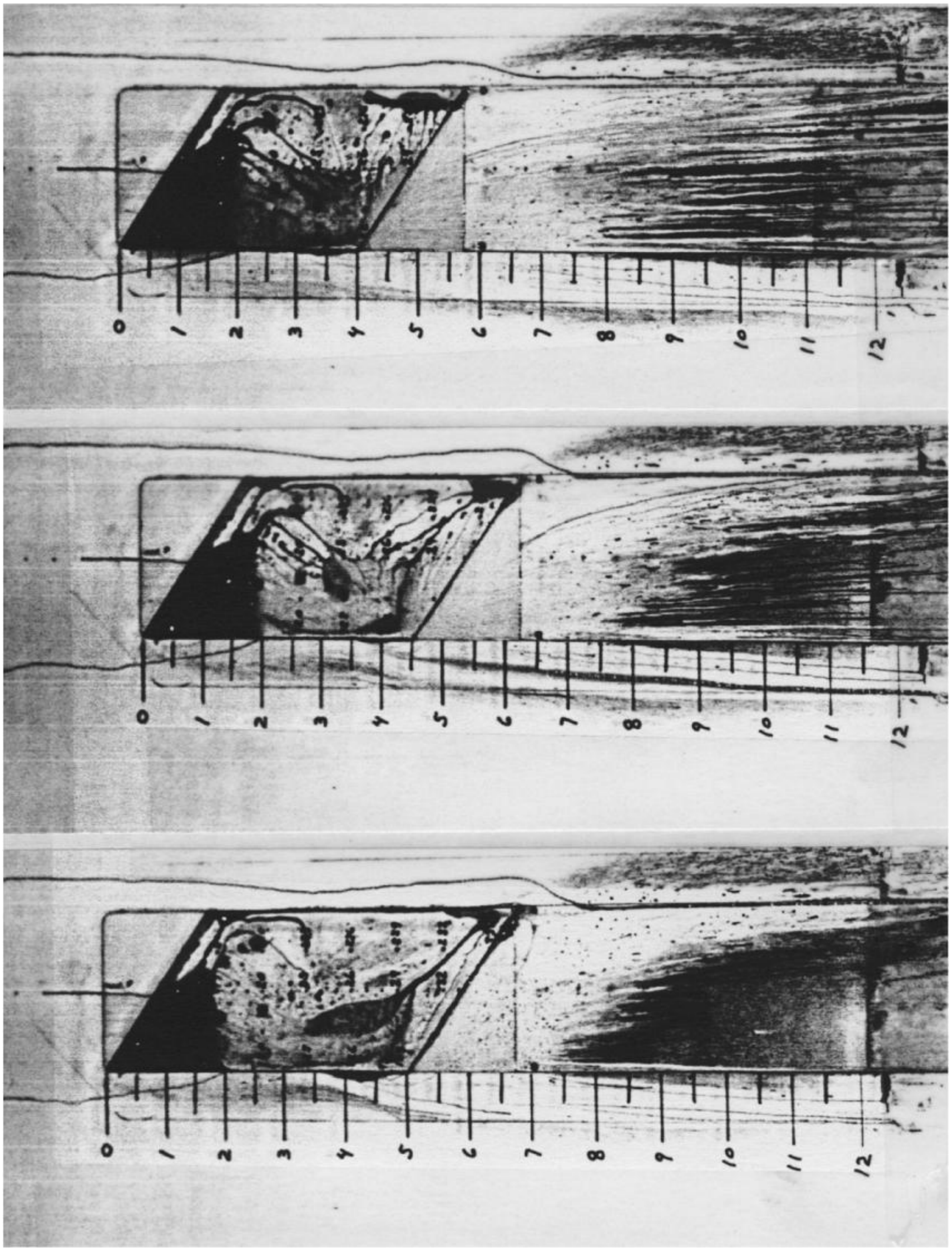

(g) $l/h = 8$.

(h) $l/h = 9$.

(i) $l/h = 10$.

Figure C-16. Continued.

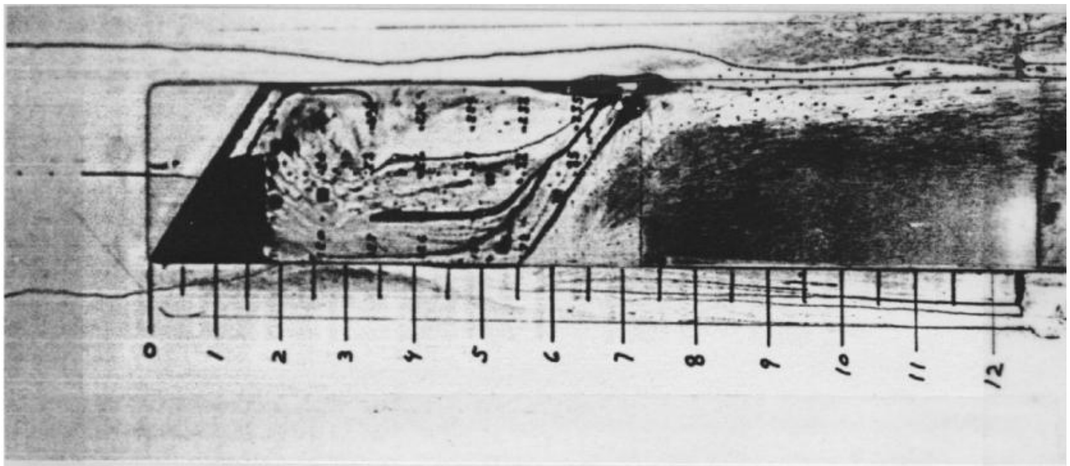

(j) l/h = 11.

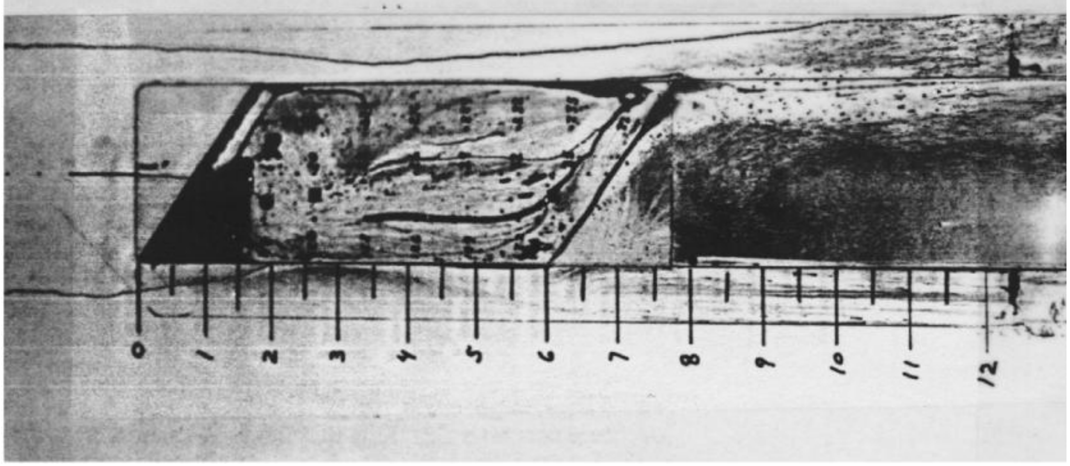

(k) l/h = 12.

Figure C-16. Concluded.

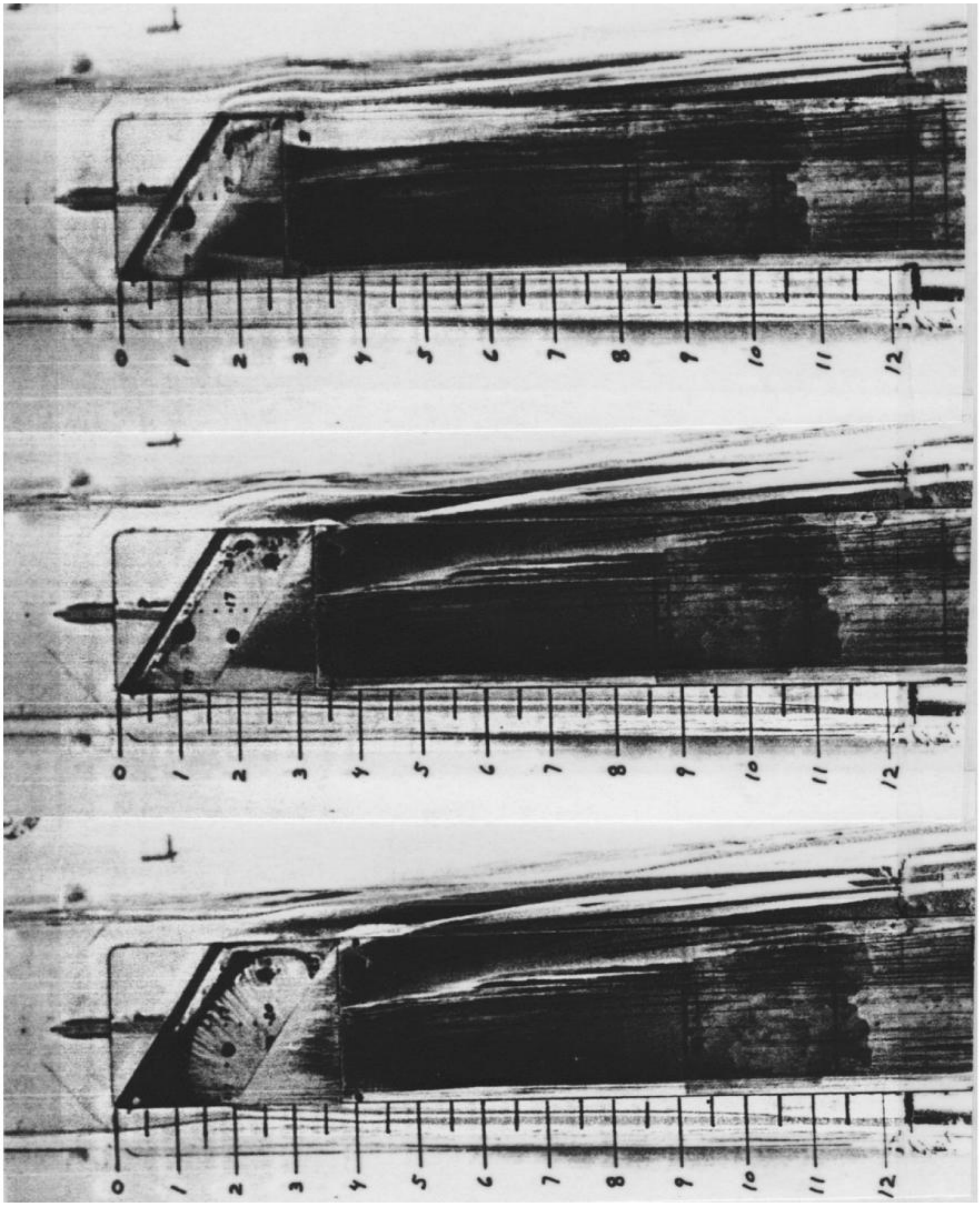

(a) $l/h = 2$.

(b) $l/h = 3$.

(c) $l/h = 4$.

Figure C-17. Surface water flow-visualization photographs for $\psi = 35°$ (configuration 4), $M = 0.4$.

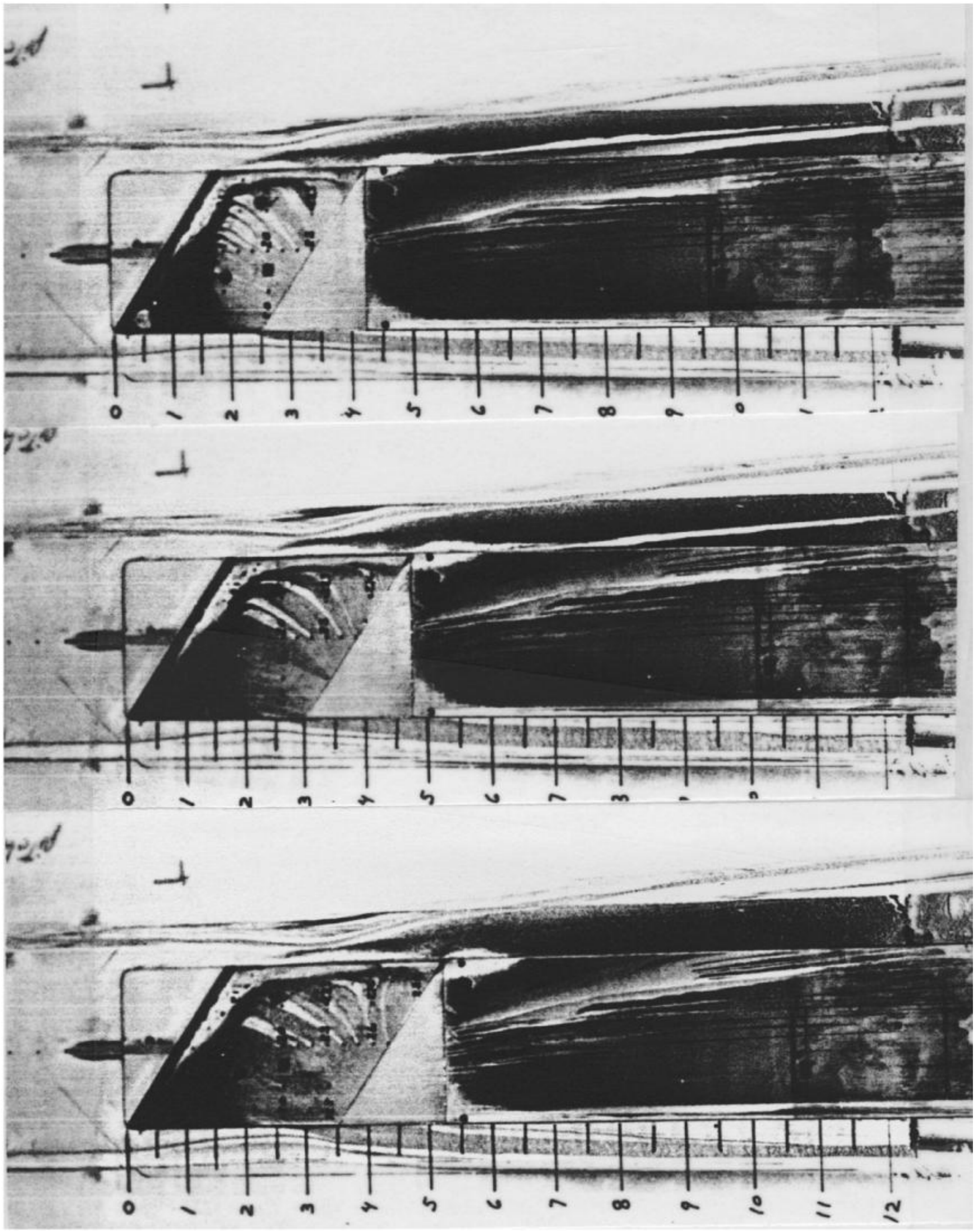

(d) l/h = 5.

(e) l/h = 6.

(f) l/h = 7.

Figure C-17. Continued.

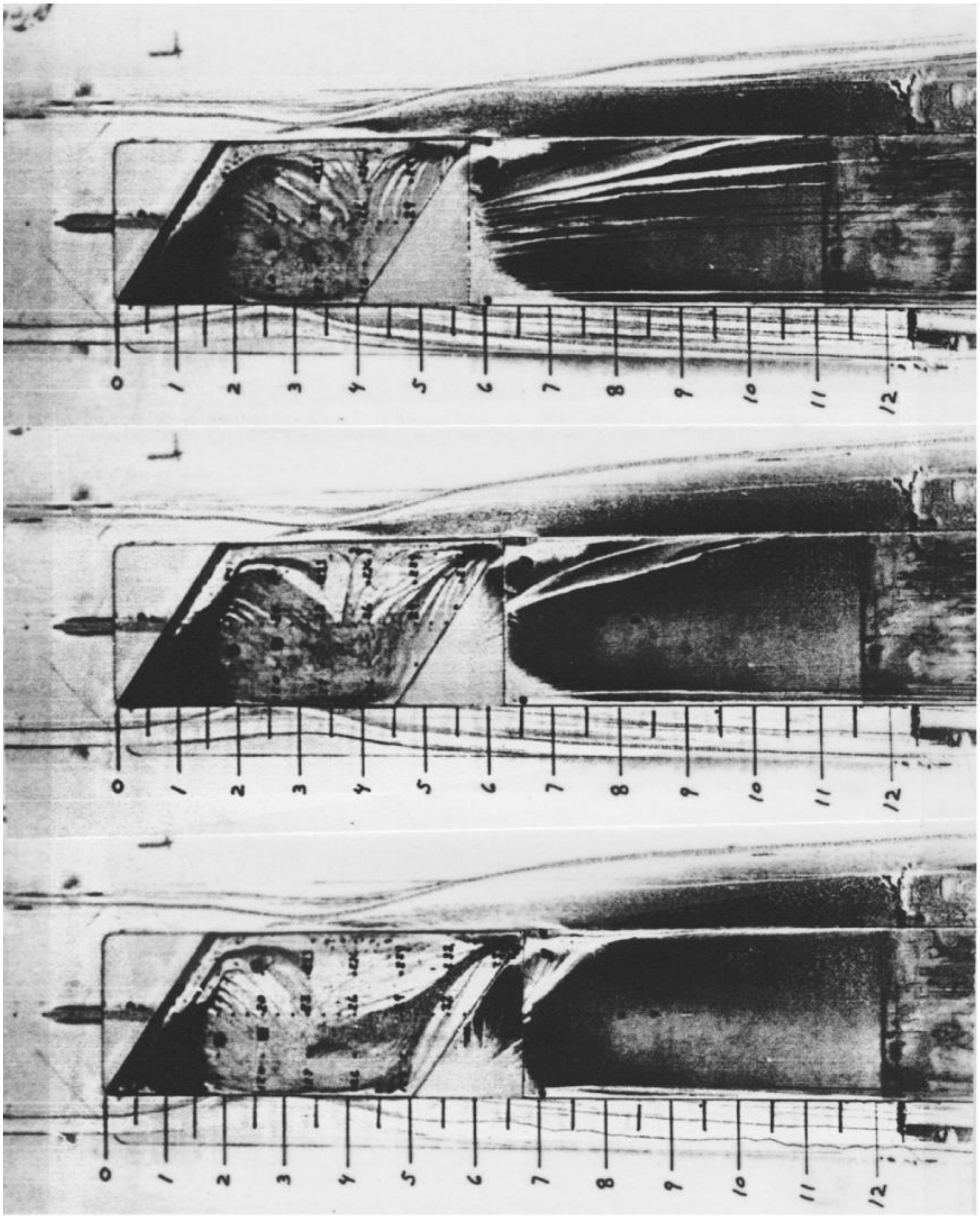

(g) $l/h = 8$.

(h) $l/h = 9$.

(i) $l/h = 10$.

Figure C-17. Continued.

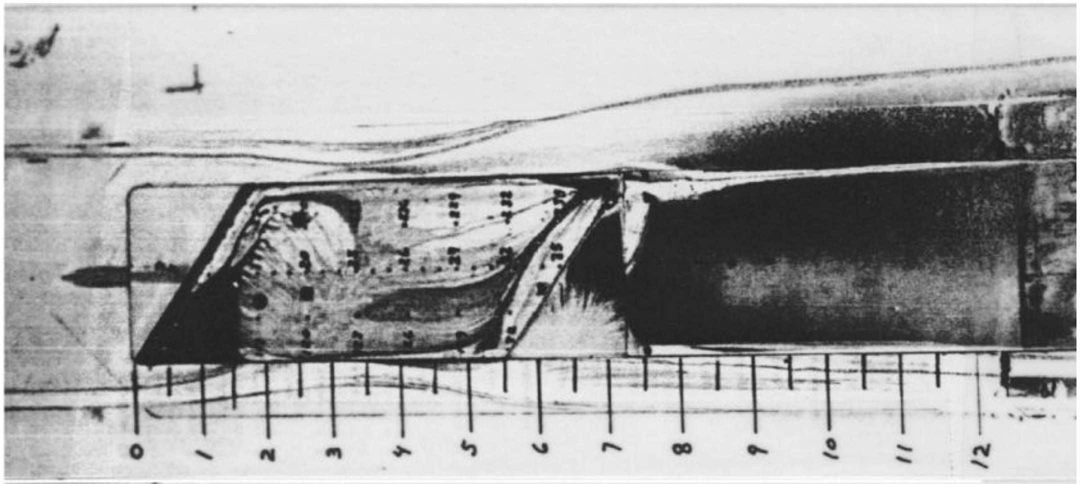

(j) *l*/*h* = 11.

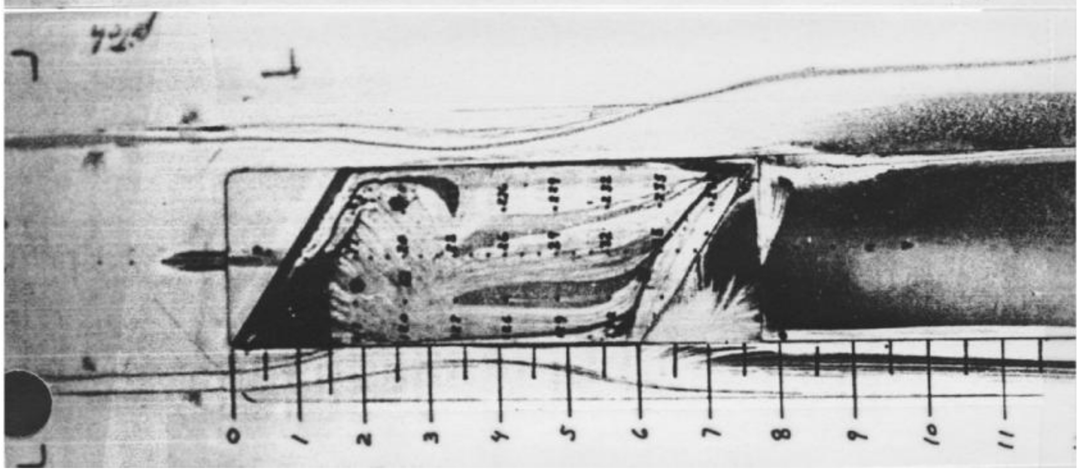

(k) *l*/*h* = 12.

Figure C-17. Concluded.

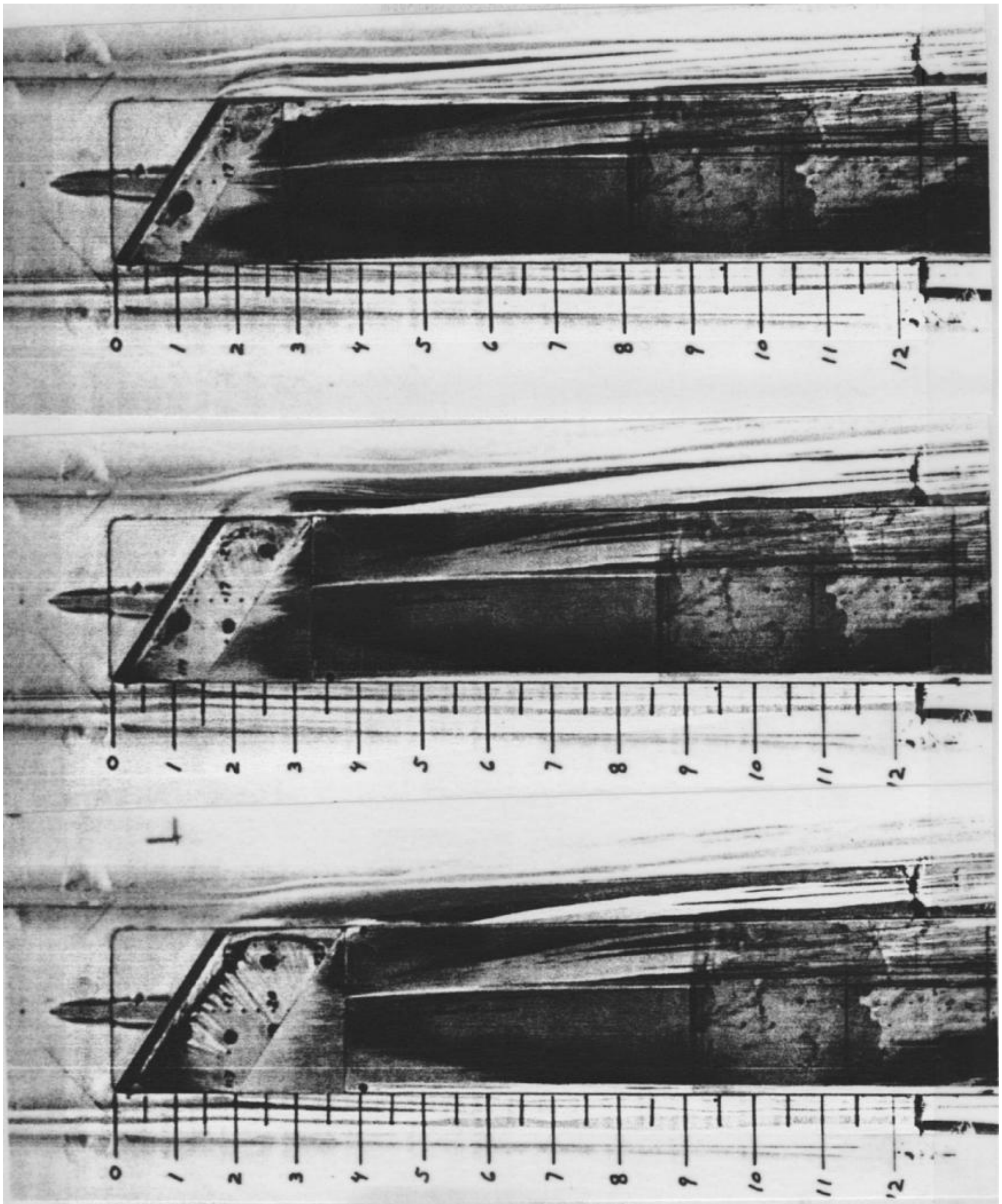

(a) l/h = 2.

(b) l/h = 3.

(c) l/h = 4.

Figure C-18. Surface water flow-visualization photographs for ψ = 35° (configuration 4), M = 0.6.

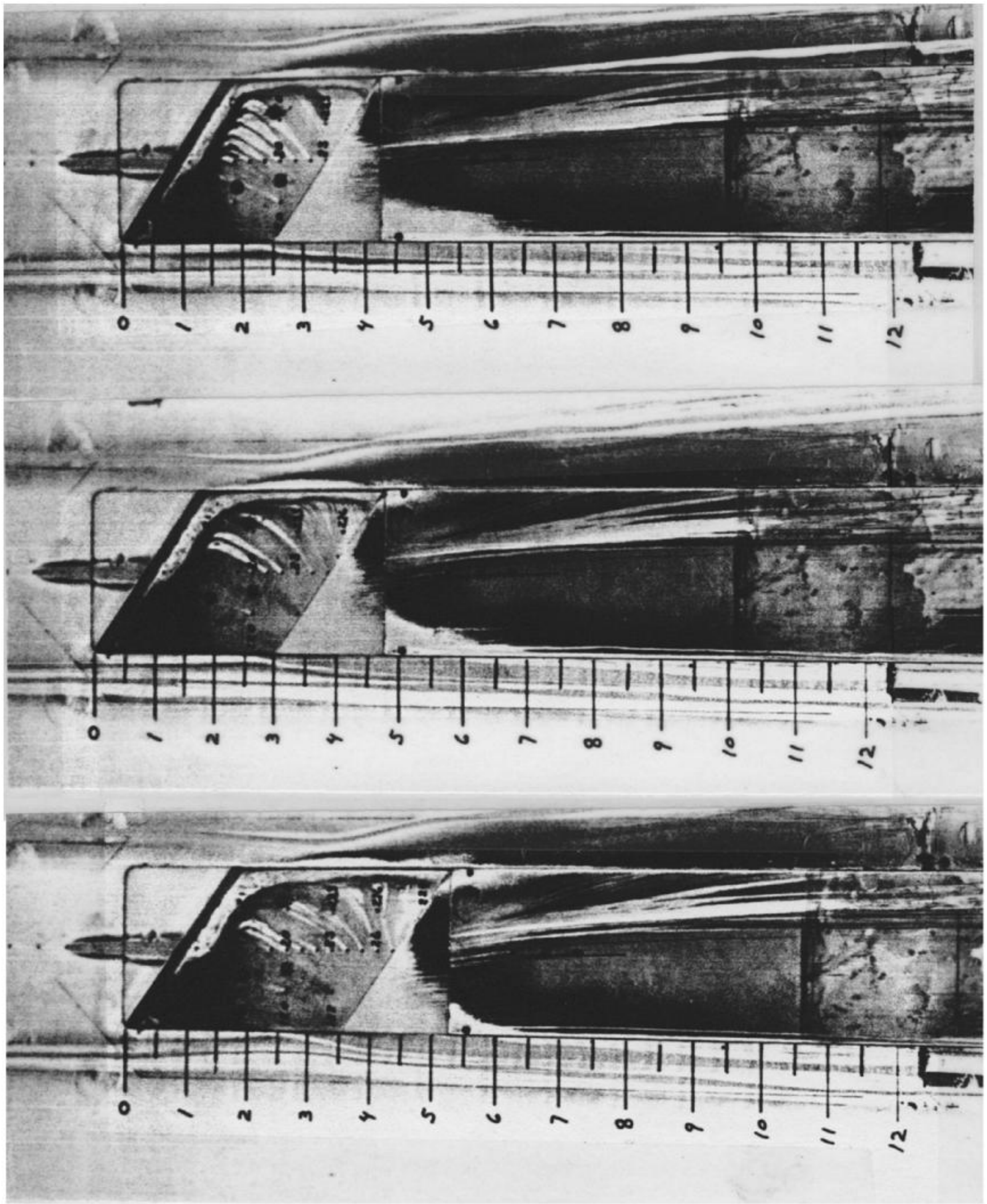

(d) l/h = 5.

(e) l/h = 6.

(f) l/h = 7.

Figure C-18. Continued.

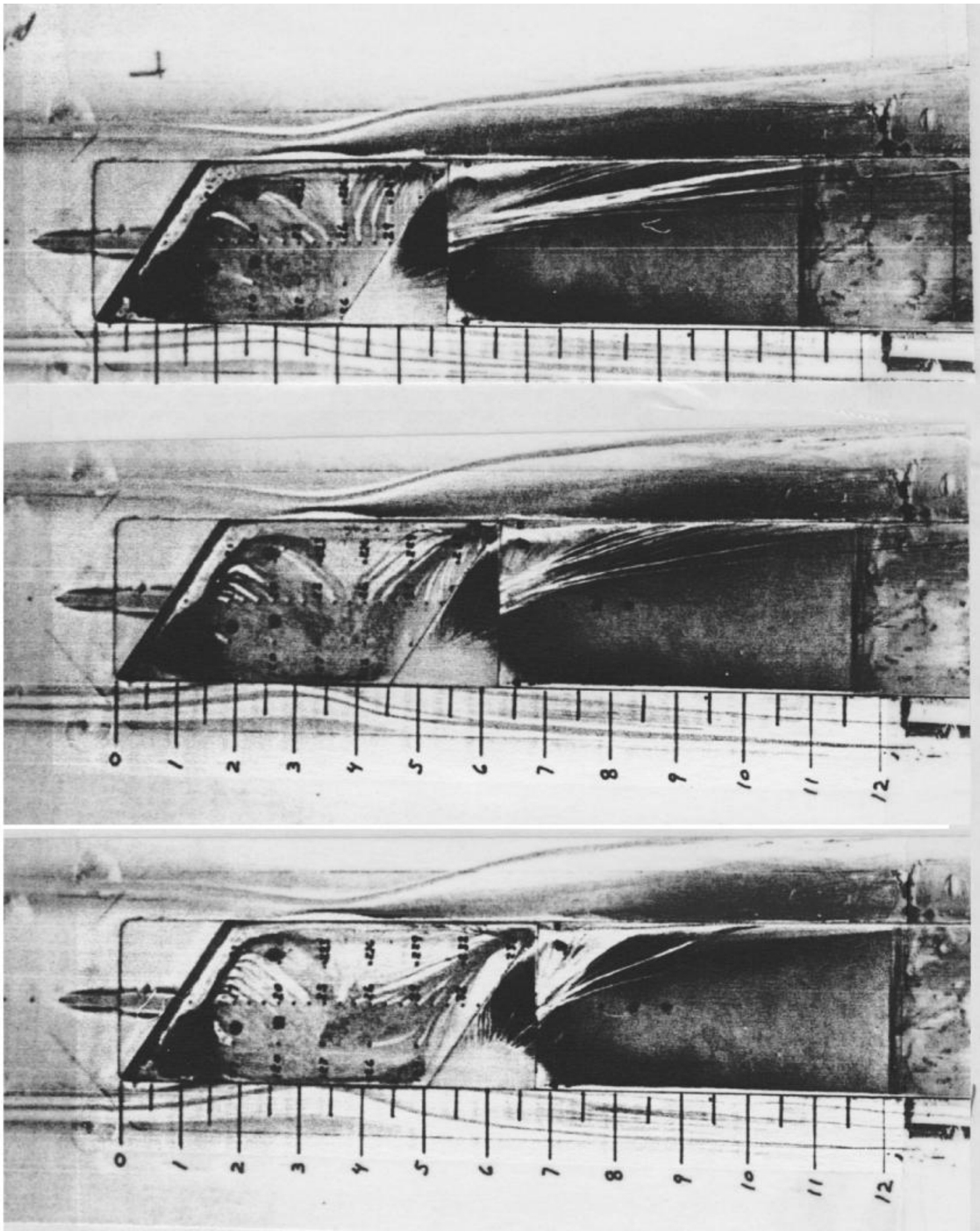

(g) l/h = 8.

(h) l/h = 9.

(i) l/h = 10.

Figure C-18. Continued.

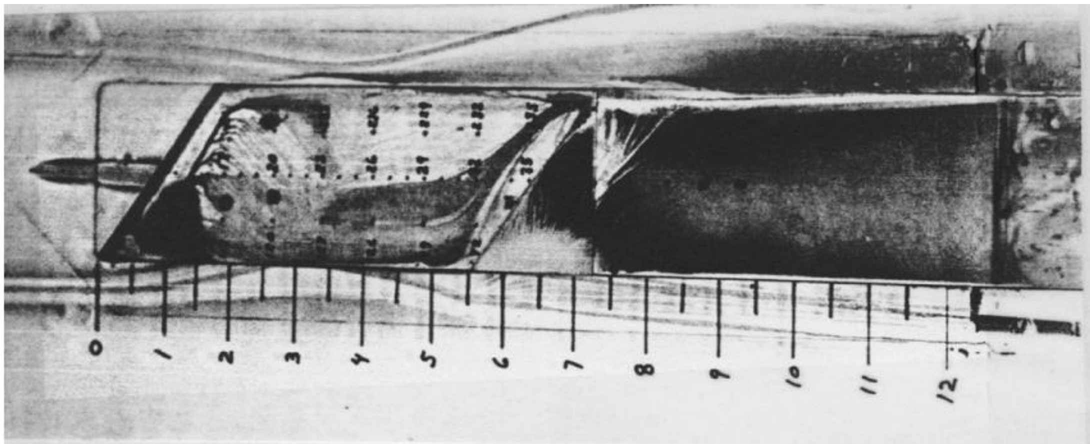

(j) l/h = 11.

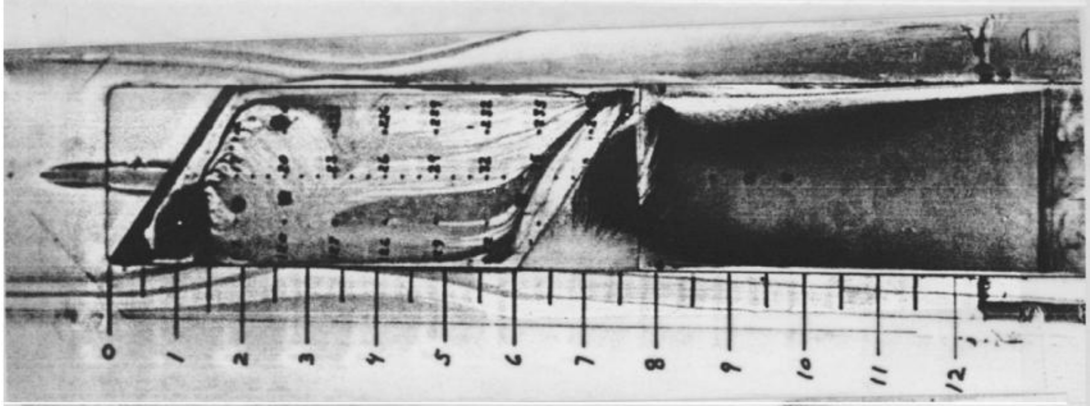

(k) l/h = 12.

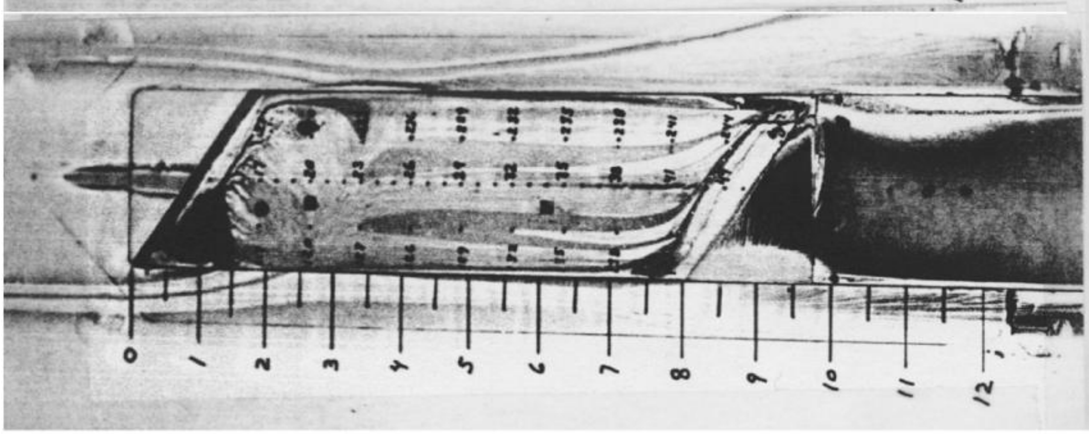

(l) l/h = 16.

Figure C-18. Concluded.

REPORT DOCUMENTATION PAGE	*Form Approved OMB No. 0704-0188*

1. REPORT DATE *(DD-MM-YYYY)*	**2. REPORT TYPE**	**3. DATES COVERED** *(From - To)*
01- 05 - 2012	Technical Memorandum	

4. TITLE AND SUBTITLE
Effect of Sweep on Cavity Flow Fields at Subsonic and Transonic Speeds

5a. CONTRACT NUMBER

5b. GRANT NUMBER

5c. PROGRAM ELEMENT NUMBER

6. AUTHOR(S)
Tracy, Maureen B.; Plentovich, Elizabeth B.; Hemsch, Michael J.; Wilcox, Floyd J., Jr.

5d. PROJECT NUMBER

5e. TASK NUMBER

5f. WORK UNIT NUMBER
984754.02.07.07.14.02

7. PERFORMING ORGANIZATION NAME(S) AND ADDRESS(ES)
NASA Langley Research Center
Hampton, VA 23681-2199

8. PERFORMING ORGANIZATION REPORT NUMBER
L-20047

9. SPONSORING/MONITORING AGENCY NAME(S) AND ADDRESS(ES)
National Aeronautics and Space Administration
Washington, DC 20546-0001

10. SPONSOR/MONITOR'S ACRONYM(S)
NASA

11. SPONSOR/MONITOR'S REPORT NUMBER(S)
NASA/TM-2012-217577

12. DISTRIBUTION/AVAILABILITY STATEMENT
Unclassified - Unlimited
Subject Category 02
Availability: NASA CASI (443) 757-5802

13. SUPPLEMENTARY NOTES

14. ABSTRACT
An experimental investigation was conducted in the NASA Langley 7 × 10-Foot High Speed Tunnel (HST) to study the effect of leading- and trailing-edge sweep on cavity flow fields for a range of cavity length-to-height (l/h) ratios. The free-stream Mach number was varied from 0.2 to 0.8. The cavity had a depth of 0.5 inches, a width of 2.5 inches, and a maximum length of 12.0 inches. The leading- and trailing-edge sweep was adjusted using block inserts to achieve leading edge sweep angles of 65 deg, 55 deg, 45 deg, 35 deg, and 0 deg. The fore and aft cavity walls were always parallel. The aft wall of the cavity was remotely positioned to achieve a range of length-to-depth ratios. Fluctuating- and static-pressure data were obtained on the floor of the cavity. The fluctuating pressure data were used to determine whether or not resonance occurred in the cavity rather than to provide a characterization of the fluctuating pressure field. Qualitative surface flow visualization was obtained using a technique in which colored water was introduced into the model through static-pressure orifices. A complete tabulation of the mean static-pressure data for the swept leading edge cavities is included.

15. SUBJECT TERMS
aerodynamics; cavity flow; cavity flow fields; static pressure measurements; swept cavity; transonic speeds

16. SECURITY CLASSIFICATION OF:			**17. LIMITATION OF ABSTRACT**	**18. NUMBER OF PAGES**	**19a. NAME OF RESPONSIBLE PERSON**
a. REPORT	**b. ABSTRACT**	**c. THIS PAGE**			STI Help Desk (email: help@sti.nasa.gov)
					19b. TELEPHONE NUMBER *(Include area code)*
U	U	U	UU	251	(443) 757-5802